Issues 1-4 2017 | Volume 13

The Journal on Advanced Studies in Theoretical and Experimental Physics, including Related Themes from Mathematics

PROGRESS IN PHYSICS

"All scientists shall have the right to present their scientific research results, in whole or in part, at relevant scientific conferences, and to publish the same in printed scientific journals, electronic archives, and any other media." — Declaration of Academic Freedom, Article 8

ISSN 1555-5534

The Journal on Advanced Studies in Theoretical and Experimental Physics, including Related Themes from Mathematics

PROGRESS IN PHYSICS

A quarterly issue scientific journal, registered with the Library of Congress (DC, USA). This journal is peer reviewed and included in the abstracting and indexing coverage of: Mathematical Reviews and MathSciNet (AMS, USA), DOAJ of Lund University (Sweden), Scientific Commons of the University of St. Gallen (Switzerland), Open-J-Gate (India), Referativnyi Zhurnal VINITI (Russia), etc.

Electronic version of this journal:
http://www.ptep-online.com

Postal Address

Department of Mathematics and Science,
University of New Mexico,
705 Gurley Ave., Gallup, NM 87301, USA

ISSN: 1555-5534 (print)
ISSN: 1555-5615 (online)

Standard Address Number: 297-5092
Printed in the United States of America

January 2017 **Vol. 13, Issue 1**

CONTENTS

Information for Authors

Progress in Physics has been created for rapid publications on advanced studies in theoretical and experimental physics, including related themes from mathematics and astronomy. All submitted papers should be professional, in good English, containing a brief review of a problem and obtained results.

All submissions should be designed in LaTeX format using *Progress in Physics* template. This template can be downloaded from *Progress in Physics* home page http://www.ptep-online.com

Preliminary, authors may submit papers in PDF format. If the paper is accepted, authors can manage LaTeXtyping. Do not send MS Word documents, please: we do not use this software, so unable to read this file format. Incorrectly formatted papers (i.e. not LaTeXwith the template) will not be accepted for publication. Those authors who are unable to prepare their submissions in LaTeXformat can apply to a third-party payable service for LaTeX typing. Our personnel work voluntarily. Authors must assist by conforming to this policy, to make the publication process as easy and fast as possible.

Abstract and the necessary information about author(s) should be included into the papers. To submit a paper, mail the file(s) to the Editor-in-Chief.

All submitted papers should be as brief as possible. Short articles are preferable. Large papers can also be considered. Letters related to the publications in the journal or to the events among the science community can be applied to the section *Letters to Progress in Physics*.

All that has been accepted for the online issue of *Progress in Physics* is printed in the paper version of the journal. To order printed issues, contact the Editors.

Authors retain their rights to use their papers published in *Progress in Physics* as a whole or any part of it in any other publications and in any way they see fit. This copyright agreement shall remain valid even if the authors transfer copyright of their published papers to another party.

Electronic copies of all papers published in *Progress in Physics* are available for free download, copying, and re-distribution, according to the copyright agreement printed on the titlepage of each issue of the journal. This copyright agreement follows the *Budapest Open Initiative* and the *Creative Commons Attribution-Noncommercial-No Derivative Works 2.5 License* declaring that electronic copies of such books and journals should always be accessed for reading, download, and copying for any person, and free of charge.

Consideration and review process does not require any payment from the side of the submitters. Nevertheless the authors of accepted papers are requested to pay the page charges. *Progress in Physics* is a non-profit/academic journal: money collected from the authors cover the cost of printing and distribution of the annual volumes of the journal along the major academic/university libraries of the world. (Look for the current author fee in the online version of *Progress in Physics*.)

An Explanation of De Broglie Matter Waves in Terms of the Electron Coupling to the Vacuum State

William C. Daywitt

National Institute for Standards and Technology (retired), Boulder, Colorado. E-mail: wcdaywitt@me.com

This paper examines the de Broglie wave theory derived by Synge who assumed that Hamilton's variational principle in three dimensions applies also to the four-dimensional Minkowski spacetime. Based on the Planck vacuum (PV) view of the electron coupling to the vacuum state, calculations here suggest that the Synge de Broglie waves exist and travel within the PV state.

1 Introduction

In the early part of the twentieth century when it was realized that the massless photon had *particle-like* properties, de Broglie figured therefor that the massive electron must have *wave-like* properties — and the de Broglie matter wave was born [1, p.55].

In circa 1954 Synge [2] published a study on the idea of 3-waves propagating in the 4-dimensional Minkowski spacetime. The study was based on the properties of a *medium-function* which the present author interprets as a vacuum medium. In the PV theory, the occurrence of 3-waves in a 4-dimensional spacetime is symptomatic of an invisible vacuum continuum interacting with a free-space particle.

What follows compares the Compton-(de Broglie) relations derived in the PV theory with the Synge ray-wave diagram in spacetime, and concludes that his de Broglie waves propagate within the vacuum state rather than free space.

2 Compton-(de Broglie) relations

In the PV theory the interaction of the electron with the vacuum state leads to the Compton-(de Broglie) relations [3]

$$r_c \cdot mc^2 = r_d \cdot cp = r_L \cdot E = r_* \cdot m_* c^2 = e_*^2 \ (= c\hbar) \qquad (1)$$

where e_* is the massless bare charge that is related to the electronic charge via $e = \alpha^{1/2} e_*$, and α and m_* are the fine structure constant and the Planck particle mass. The radii $r_c\,(= e_*^2/mc^2)$ and $r_*\,(= e_*^2/m_* c^2)$ are the electron and Planck-particle Compton radii respectively and m is the electron mass. The magnitudes of r_* and m_* are equal to the Planck length and mass respectively [4, p. 1234]. It is because $r_* \neq 0$ that the PV state is a quasi-continuum.

The de Broglie radii, r_L and r_d, are derived from r_c and the Lorentz invariance of the vanishing electron/PV coupling force (A1) at $r = r_c$

$$i\left(\frac{e_*^2}{r_c^2} - \frac{mc^2}{r_c}\right) = 0 \qquad (2)$$

and result in

$$r_L = \frac{r_c}{\gamma} \qquad \text{and} \qquad r_d = \frac{r_c}{\beta\gamma} \qquad (3)$$

where $\beta = v/c$ and $\gamma = 1/\sqrt{1-\beta^2}$. From (3) $\beta = r_L/r_d$ yields the relative velocity of the electron in the coupled electron/PV system. The relations in (1) also lead to the relativistic electron energy $E = \sqrt{m^2c^4 + c^2p^2}$.

The relativistic scaler wave equation is [5, p. 319]

$$\left(\frac{\hbar}{mc}\right)^2 \left(\nabla^2 - \frac{\partial^2}{c^2\partial t^2}\right)\psi = r_c^2 \left(\nabla^2 - \frac{\partial^2}{c^2\partial t^2}\right)\psi = \psi \qquad (4)$$

while its nonrelativistic counterpart reads

$$\left(\nabla^2 - \frac{\partial^2}{v^2\partial t^2}\right)\psi = 0 \qquad (5)$$

where $v \ll c$; so the electron radii in (1) and (4) are relativistic parameters.

The planewave solution ($\psi \propto \exp i\phi$) to (4) in the z-direction involves the phase

$$\phi = \frac{Et - pz}{\hbar} = \frac{Ect - cpz}{c\hbar} = \frac{Ect - cpz}{e_*^2}$$

$$\phi = \frac{ct}{r_L} - \frac{z}{r_d} \qquad (6)$$

where the relativistic energies $E\,(= m\gamma c^2)$ and $cp\,(= cm\gamma v)$ from (1) are used in the final expression. The normalization of ct and z by the de Broglie radii r_L and r_d is a characteristic of the PV model of the vacuum state, and is related to the Synge primitive (planewave) quantization of spacetime to be discussed below.

3 De Broglie waves

The Ray/3-Wave diagram that represents the Synge de Broglie wave propagation in spacetime [2, p. 106] is shown in Fig. 1, where the electron propagates upward at a uniform velocity v along the Ray. The vertical axis is ict and the horizontal axes are represented by (x, y, z). The need for quantizing the Synge vacuum waves (adding the parameters r_c, r_L, and r_d to Fig. 1) is explained in the following quote. "So far the [variational-principle] theory has been confined to the domain of geometrical mechanics. The de Broglie waves have no phase, no frequency, no wave-length. It is by *quantization*

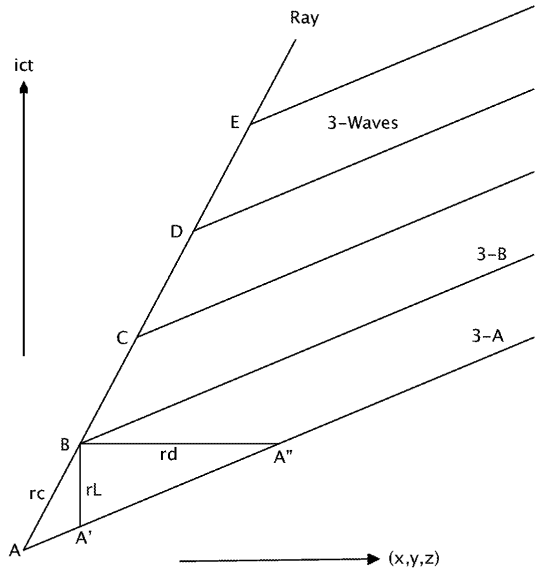

Fig. 1: Planewave quantization of de Broglie Waves in Spacetime. The figure consists of a single Ray and a partial picture of the corresponding 3-Waves propagating toward the upper left. The Ray and their 3-Waves are orthogonal in the 4-dimensional spacetime sense. The quantization consists of the normalization constants r_c, r_L, and r_d.

that these things are introduced, in much the same way as they are introduced in the transition from geometrical optics to physical optics" [2, p. 105].

The parameters in the figure correspond to rc = r_c, rL = r_L, and rd = r_d; the Compton and de Broglie radii from (1). In the quantization, the Synge theory utilizes the wavelengths $2\pi r_c$, $2\pi r_L$ and $2\pi r_d$. Thus there is a one-to-one correspondence between the electron/PV coupling radii from (1) and the Synge wave theory regarding Fig. 1. In the PV theory the electron radii (r_c, r_L, r_d) are parameters generated by the electron/PV interaction — thus it is reasonable to conclude that the de Broglie waves travel within the vacuum state.

Appendix A: Coupling force

In its rest frame, the coupling force the electron core $(-e_*, m)$ exerts on the PV quasi-continuum is [3]

$$i\left(\frac{e_*^2}{r^2} - \frac{mc^2}{r}\right) \tag{A1}$$

where the radius r begins at the electron core. The spacetime coordinates are denoted by

$$x_\mu = (x_0, x_1, x_2, x_2) = (ict, x, y, z) \tag{A2}$$

where $\mu = (0, 1, 2, 3)$ and $r = (x^2 + y^2 + z^2)^{1/2}$.

The force (A1) vanishes at the electron Compton radius r_c and leads to:

$$\frac{i}{r_c}\left(\frac{e_*^2}{r_c} - mc^2\right) = 0 \tag{A3}$$

in the electron rest frame; and when (A3) is Lorentz transformed it results in the two coupling forces

$$\frac{i}{r_L}\left(\frac{e_*^2}{r_c} - mc^2\right) = 0 \tag{A4}$$

and

$$\frac{1}{r_d}\left(\frac{e_*^2}{r_c} - mc^2\right) = 0 \tag{A5}$$

in the uniformly moving frame.

To complete the PV perspective, the space and time derivatives in the scaler wave equation

$$r_c^2\left(\nabla^2 - \frac{\partial^2}{c^2\partial t^2}\right)\psi = \psi \tag{A6}$$

and the Dirac electron equation [6, p. 74]

$$ic\hbar\left(\boldsymbol{\alpha}\cdot\nabla + \frac{\partial}{c\partial t}\right)\psi = mc^2\beta\psi$$

or

$$ir_c\left(\boldsymbol{\alpha}\cdot\nabla + \frac{\partial}{c\partial t}\right)\psi = \beta\psi \tag{A7}$$

are quantized (normalized, scaled) by the same constant r_c, where the 4×4 vector matrix $\boldsymbol{\alpha}$ accounts for electron spin. [The β in (A7) is a 4×4 matrix, not a relative velocity.]

Submitted on September 28, 2016 / Accepted on October 8, 2016

References

1. De Broglie L., Brillouin L. Selected Papers on Wave Mechanics. 1928, London and Glasgow, Blackie.
2. Synge J.L. Geometrical Mechanics and de Broglie Waves. 1954, Cambridge University Press.
3. Daywitt W.C. The de Broglie relations derived from the electron and proton coupling to the Planck vacuum state. *Progress in Physics*, 2015, v. 11, Issue 2 (April), 189. See also www.planckvacuum.com.
4. Carroll B.W. Ostlie D.A. An Introduction to Modern Astrophysics. 2007, Addison-Wesley, San Francisco—Toronto.
5. Schiff L.I. Quantum Mechanics. 1955, McGraw-Hill Book Co., Inc., Second Edition, New York.
6. Gingrich D.M. Practical Quantum Electrodynamics. 2006, CRC, The Taylor & Francis Group, Boca Raton, London, New York.

Beyond the Hubble's Law

Nilton Penha Silva
Departmento de Física (Retired Professor), Universidade Federal de Minas Gerais, Belo Horizonte, MG, Brazil.
Email: nilton.penha@gmail.com

Based on the Universe's scale factor introduced by Silva [1], we derive an expression for the receding velocities of arbitrary astronomical objects, which increase linearly up to the lookback distance of 2.1×10^3 Mpc and after that they increase in a positively accelerated way. The linear part corresponds to the Hubble'law.

1 Introduction

In a 2014 paper, Silva [1] introduced an expression for Universe's scale factor to describe the Universe's expansion,

$$a(t) = \exp\left(\frac{H_0 T_0}{\beta}\left(\left(\frac{t}{T_0}\right)^{\beta} - 1\right)\right), \tag{1}$$

where

$$\beta = 1 + H_0 T_0\left(-\frac{1}{2}\Omega_m(T_0) + \Omega_\Lambda(T_0) - 1\right), \tag{2}$$

H_0 is the Hubble constant, T_0 is the Universe current age, $\Omega_m(T_0)$ is the cosmic matter density parameter (baryonic + non-baryonic matter), $\Omega_\Lambda(T_0)$ is the cosmic dark energy density parameter [2].

In reference [1] matter and dark energy are treated as perfect fluids and it is shown that it very difficult to distinguish between closed ($k = 1$), flat ($k = 0$) and open ($k = -1$) universes. In this paper we intuitively adopt $k = 1$ and explore the Universe as being closed.

The spacetime metric for $k = 1$ according to Friedmann-Lemaitre-Robertson-Walker (FLRW) is [1, 3]

$$ds^2 = \mathfrak{R}^2(T_0)a^2(t)\left(d\psi^2 + \sin^2\psi\left(d\theta^2 + \sin^2\theta d\phi^2\right)\right) - c^2dt^2 \tag{3}$$

where ψ, θ and ϕ are the the comoving space coordinates ($0 \leqslant \psi \leqslant \pi$, $0 \leqslant \theta$ and $0 \leqslant \phi \leqslant 2\pi$); $\mathfrak{R}(T_0)$ is the current Universe's radius of curvature. This proper time t is the cosmic time.

It is known that at $t = 380,000$ yr $\simeq 10^{-4}$ Gyr, after the Big Bang, the Universe became transparent and the first microwave photons started traveling freely through it. They constitute what is called the Cosmic Microwave Background (CMB).

The observer (Earth) is assumed to occupy position $\psi = 0$ for any time t in the comoving reference system. To reach the observer at the Universe age T the CMB photons leave a specific position ψ_T ($t \simeq 10^{-4}$ Gyr). They follow a null geodesic.

It's time to make the following observation: since we will be dealing with large times values (some *giga* years) we have no loss if we treat $t \simeq 10^{-4}$ Gyr as $t \simeq 0$ Gyr for practical purposes.

For a null geodesic we have:

$$-\frac{c\,dt}{\mathfrak{R}(0)} = d\psi, \tag{4}$$

$$\psi_T = \frac{c}{\mathfrak{R}(0)}\int_0^T \frac{1}{a(t)}\,dt. \tag{5}$$

We have seen then that CMB photons emitted at ψ_{T_0} and $t = 0$ should arrive at the observer, $\psi = 0$ and T_0. Along their trajectory, other emitted photons, at later times, by astronomical objects that lie on the way, join the the photons troop and eventually reach the observer. They form the picture of the sky that the observer "sees". Certainly CMB photons emitted at $\psi > \psi_{T_0}$ will reach the observer at times latter than T_0.

2 The receding velocity

As the Universe expands, the streching distance between the observer and any astronomical object at time t is given by

$$\begin{aligned} d(t) &= \mathfrak{R}(0)\,a(t)\,(\psi_{T_0} - \psi_t) + ct \\ &= c\,a(t)\left(\int_0^{T_0}\frac{1}{a(t')}\,dt' - \int_0^{t}\frac{1}{a(t')}\,dt'\right) + ct \\ &= c\,a(t)\int_t^{T_0}\frac{1}{a(t')}\,dt + ct. \end{aligned} \tag{6}$$

The receding velocity of any astronomical object with respect to the observer is

$$\begin{aligned} v_{rec}(t) &= \dot{a}(t)\,c\int_t^{T_0}\frac{1}{a(t')}\,dt' \\ &= a(t)H(t)\,c\int_t^{T_0}\frac{1}{a(t')}\,dt', \end{aligned} \tag{7}$$

where we have used the fact that

$$\dot{a}(t) = a(t)H(t). \tag{8}$$

According to reference [1],

$$H(t) = H_0\left(\frac{t}{T_0}\right)^{\beta-1} \tag{9}$$

By performing the integration in equation (8) we have

$$v_{\mathrm{rec}}(t) = c\left(\frac{H_0T_0}{\beta}\right)^{1-\frac{1}{\beta}}\left(\frac{t}{T_0}\right)^{-1+\beta}\exp\left(\frac{H_0T_0}{\beta}\left(\frac{t}{T_0}\right)^{\beta}\right) \times\left(\Gamma\left(\frac{1}{\beta},\frac{H_0T_0}{\beta}\left(\frac{t}{T_0}\right)^{\beta}\right)-\Gamma\left(\frac{1}{\beta},\frac{H_0T_0}{\beta}\right)\right) \tag{10}$$

where $\Gamma(A,B)$ and $\Gamma(A,C)$ are incomplete Gamma Functions [4].

Taking into account that

$$\Gamma(A,B)-\Gamma(A,C)=\Gamma(A,B,C), \tag{11}$$

where $\Gamma(A,B,C)$ are generalized incomplete Gamma Functions [4], we have

$$v_{\mathrm{rec}}(t) = c\left(\frac{H_0T_0}{\beta}\right)^{1-\frac{1}{\beta}}\left(\frac{t}{T_0}\right)^{-1+\beta}\exp\left(\frac{H_0T_0}{\beta}\left(\frac{t}{T_0}\right)^{\beta}\right) \times\Gamma\left(\frac{1}{\beta},\frac{H_0T_0}{\beta}\left(\frac{t}{T_0}\right)^{\beta},\frac{H_0T_0}{\beta}\right). \tag{12}$$

3 Comparison to Hubble's law

By replacing t by $T_0 - d_{lb}/c$, where $d_{lb} = ct_{lb}$ is the so called lookback distance, t_{lb} being the lookback time:

$$v_{\mathrm{rec}}(d_{lb}) = c\left(\frac{H_0T_0}{\beta}\right)^{1-\frac{1}{\beta}}\left(1-\frac{d_{lb}}{cT_0}\right)^{-1+\beta} \times\exp\left(\frac{H_0T_0}{\beta}\left(1-\frac{d_{lb}}{cT_0}\right)^{\beta}\right) \times\Gamma\left(\frac{1}{\beta},\frac{H_0T_0}{\beta}\left(1-\frac{d_{lb}}{cT_0}\right)^{\beta},\frac{H_0T_0}{\beta}\right). \tag{13}$$

Figure 1 shows that the receding velocities increase as the lookback distance increases, initially in a linear way. Distant astronomical objects are seen to recede at much faster velocities than the nearest ones.

By expanding expression (13) in power series of d_{lb}, and retaining the lowest order term we get

$$v_{\mathrm{rec}}(d_{lb}) = H_0 v_{\mathrm{rec}}(d_{lb}) + \text{higher order terms}. \tag{14}$$

The Hubble's law,

$$v_{\mathrm{rec}}(d_{lb}) = H_0 v_{\mathrm{rec}}(d_{lb}), \tag{15}$$

is an approximation to our just obtained expression. According to the present work, Hubble's law holds up to ~ 7 Gly or, equivalently $\sim 2.1\times10^3$ Megaparsecs.

For this work, we have used the following experimental data [5]:

$$H_0 = 69.32\ \mathrm{kms^{-1}Mpc^{-1}} = 0.0709\ \mathrm{Gyr^{-1}},\quad T_0 = 13.772\ Gyr. \tag{16}$$

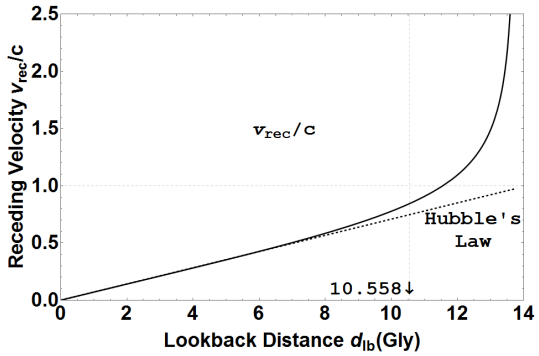

Fig. 1: Receding velocities as function of d_{lb}, the lookback distances from astronomical objects to the observer, on Earth.

As indicated by references [1, 6] the present scale factor predicts that the Universe goes from a matter era to a dark energy era at the age of $T_\star = 3.214$ Gyr. Before that matter dominated, and after that dark energy era dominates.

4 Conclusion

The Universe's scale factor $a(t) = \exp\left(\frac{H_0T_0}{\beta}\left(\left(\frac{t}{T_0}\right)^{\beta}-1\right)\right)$, with $\beta = 1 + H_0T_0\left(-\frac{1}{2}\Omega_m(T_0)+\Omega_\Lambda(T_0)-1\right)$ introduced by Silva [1] has been used to find an expression for the receding velocities of astronomical objects caused by the expansion of the Universe. The expression found, equation (13), is a generalization of Hubble's law. This later one should be valid up to $\sim 2.1\times10^3$ Megaparsecs.

After such very good results we feel very stimulated with the idea that expression (1) is a very good candidate for describing the geometrical evolution of our Universe.

Submitted on October 16, 2016 / Accepted on October 21, 2016

References

1. Silva N.P. A Model for the Expansion of the Universe. *Progress in Physics*, 2014, v. 10 (2), 93–97.
2. Silva N.P. The Universe's Expansion Factor and the Hubble's Law. *ResearchGate*, 2016, https://www.researchgate.net/publication/296060533.
3. Peebles P.J.E. The Large-scale Structure of the Universe. Princeton University Press, 1980.
4. Wolfram Research, Inc., Mathematica, Version 10, Champaign, IL, 2014.
5. Bennet C.L. et al. Nine-Year Wilkinson Microwave Anisotropy Probe (WMAP) Observations: Final Maps and Results. arXiv: astro-ph.CO. 2013.
6. Silva N.P. The Universe's Scale Factor: From Negative to Positive Acceleration of the Expansion. *ResearchGate*, 2016, https://doi.org/10.13140/RG.2.1.1540.3608.

Are Quazars White Holes?

Anatoly V. Belyakov

E-mail: belyakov.lih@gmail.com

Based on the mechanistic interpretation of J. Wheeler's geometrodynamic concept, which allows for transitions between distant regions of space, it was suggested that a quasar is a cosmological object, i.e. a white hole, where gravitational forces are replaced with dynamic ones with together the balance of electric and magnetic forces. Thus, a schematic model of a typical quasar was proposed. Its parameters (calculated on the basis of this model) are consistent with the observational data on quasars.

1 Quazars according to Wheeler's geometrodynamics

Quasars are still the most striking mystery of modern astrophysics. According to the most common hypothesis, a quasar is a distant active galaxy with a supermassive *black hole* in the centre. An alternative hypothesis belongs to V. Ambartsumyan. According to the latter, quasar nuclei are the place of matter transition from prestellar existence in the form of super-dense bodies to existence in the form of stars and rarefied interstellar medium, which are more common for astronomy. The transition can occur in the following sequence: super-dense state — kinetic energy — synchrotronic radiation. This process may be connected with formation of a *white hole*. Possibility of existence of white holes is also admitted by some other researchers [1, 2].

This approach is the closest to J. Wheeler's geometrodynamic concept allowing for drain-source transitions between distant regions of space ("wormholes"), thus ensuring circulation of matter along the *vortex tubes* (power lines) along some closed *contour*. The mechanistic interpretation of Wheeler's idea that only uses balances of main forces (electric, magnetic, gravitational and dynamic ones) makes it possible to build schematic models of cosmological objects and successfully determine some of their important parameters [3, 4]. In this case, there is no need to delve into the complex dynamics of phenomena and their mechanisms, which are the research subjects of specialised scientific disciplines. The same approach was used here to construct a schematic model of a quasar, assuming that it is a white hole.

Indeed, the most dramatic transition in the general circulation of matter is the transition, when the gravitational forces are replaced with dynamic ones (centrifugal forces in our case). In other words, it is the transition when interactions change their polarity. Probably, such a phase transition (inversion) occurs in quasars, where the super-dense state of matter transforms into radiation and diffused matter followed by its condensation. Under such a phase transition, the initially closed contour, which are based on the balance of gravitational and magnetic forces, break leaving unclosed vortex tubes with contradirectional currents. These currents carry charges of different polarity at the circuit break point. The charges are gradually destructing each other (not necessarily through annihilation). The reverse process occurs in black holes, respectively.

At the same time, the characteristic value of R_c (determined by the balance of electric and magnetic forces [3]) is preserved, since the same result is obtained from the balance of gravitational and magnetic forces, when the *evolutionary parameter* ε (characterises the difference of the material medium from vacuum) becomes numerically equal to the ratio of electric forces to gravitational ones. The R_c value is the geometric mean of linear values. They are the distance between the charges r and length l of the conductor (force line, current line or contour):

$$R_c = \sqrt{l\,r} = 7.52 \times 10^8 \text{ m}. \tag{1}$$

Assuming that the energy release in the quasar is due to mutual destruction of the charges with opposite polarity, the quasar may be schematically represented as a number of z charge unit contours or vortex thread concentrated to the maximum extent in the region with the radius R_c typical of the transition. Let us determine their number as follows:

$$z = \left(\frac{R_c}{r}\right)^3. \tag{2}$$

As the central mass, the quasar mass is determined by the following virial:

$$M = \frac{v^2 l}{\gamma}, \tag{3}$$

where v is the velocity of matter circulation in the contour, also known as peripheral speed and γ is the gravitational constant.

As the total mass of all the contours, the same mass is determined as follows:

$$M = z\varepsilon_0 l, \tag{4}$$

where ε_0 is linear density of the unit contour, which is equal to $m_e/r_e = 3.23 \times 10^{-16}$ kg/m^3.

It is clear that the evolutionary parameter of the general contour is increased proportionally to the number of unit counters, so $\varepsilon = z$.

Solving equations (1) to (4), we find the number of unit contours, distance between the charges, length of the contour

and quasar mass:

$$z = \frac{v^2}{\varepsilon_0 \gamma}, \tag{5}$$

$$r = \frac{R_c}{z^{1/3}}, \tag{6}$$

$$l = z^{1/3} R_c, \tag{7}$$

$$M = z^{4/3} \varepsilon_0 R_c. \tag{8}$$

Let us assume that the process of mutual destruction of charges occurs at the velocity of matter motion in the contour in all the individual contours simultaneously. Then the quasar's life time is:

$$\tau = \frac{l}{v}, \tag{9}$$

the average energy released by the quasar "burnout" is:

$$N = \frac{Mv^2}{\tau} = z\varepsilon_0 v^3, \tag{10}$$

and minimum radiation wavelength, referring to [3], is:

$$\lambda = \frac{\lambda_k c}{v}, \tag{11}$$

where λ_k is the Compton electron wavelength equal to 2.426 $\times 10^{-12}$ m.

Each contour has minimum reference length:

$$l_{min} = \frac{l}{z^{1/3}} = R_c, \tag{12}$$

then the minimum characteristic time interval for the quasar "burnout" or radiation will be:

$$\tau_{min} = \frac{R_c}{v}, \tag{13}$$

thus, the characteristic or standard mass converted into radiation during this time interval is:

$$M_{st} = \frac{M\tau_{min}}{\tau} = \frac{M}{z^{1/3}}, \tag{14}$$

and the number of standard masses in the mass of the quasar is:

$$n_{st} = \frac{M}{M_{st}} = z^{1/3}. \tag{15}$$

To some extent, the quasar inherits some super-dense state (microcosm) features, so the visible size of the quasar — its core l_0 — is determined by analogy with the Bohr atom, assuming that the core is $(an)^2$ times smaller than the contour size. Therefore:

$$l_0 = \frac{l}{(an)^2}, \tag{16}$$

where a is the reverse fine structure constant.

To determine the quasar's parameters, we need to know the velocity of matter circulation in the contour, i.e. the quantum number n. The main quantum number for a standard electronic contour [5] is:

$$n_s = \frac{c_0^{1/3}}{a} = 4.884, \tag{17}$$

and velocity is

$$v = \frac{c c_0^{1/3}}{(an_s)^2} = 4.48 \times 10^5 \text{ m/sec}, \tag{18}$$

with indication of $c_0 = c/[\text{m/sec}]$.

As shown by (4), (5), (17) and (18), the ratio of the quasar core linear density M/l_0 to the same of the electron m_e/r_e for such a standard quasar becomes the maximum possible and equal to the ratio of electric to the gravitational forces $f = c^2/\varepsilon_0\gamma = 4.17 \times 10^{42}$, i.e. $\varepsilon = f$. Moreover, as we see from the dependencies above, kinetic energy Mv^2 for a quasar contour is equal to electrostatic energy, provided that the number of individual charges placed along the length of the unit contour equals to l/r_e, and the distance between them is equal to the size of a standard contour. For a unit contour, this energy is equal to the following:

$$E_i = \frac{\varepsilon_0^{2/3} v^{8/3} R_c}{\gamma^{1/3}} = 1.03 \times 10^{17} \text{ J}. \tag{19}$$

2 The balance of electric and magnetic forces requires "stretching" charge contours of quasars to cosmic distances

Thus, the quasar model includes linear objects (force lines or vortex tubes) with the length of hundreds of light-years. This indicates the need for a mechanism of energy transfer from the quasar core to remote distances. Apparently, such extended formations are double radio sources. They often have a compact radio source between them, coinciding by its coordinates with the optical object — a quasar or a galaxy [6]. Notably, the outer edges of these structures are the brightest parts of the radio components. It is clear that in our model they are associated with the ends of quasar vortex tubes. The latter may be considered as super-charges, which are gradually destroying each other. Radiation comes from the peripheral part of the contours as charged particles move in the areas of the magnetic field's force lines with the greatest curvature, which are sources of synchrotron radiation.

Let us estimate the nature of the radiation emitted by such a contour. Continuing the analogy with the Bohr atom, we shall consider this contour as a super-atom. For a proton-electron contour, the wave range is within the range from 3.7×10^{-6} to 0.95×10^{-7} m under transitions within quantum numbers from n_s to 1. We suppose that, for the super-atom quasar, the wavelength increases in proportion to the ratio $r/(n_s^2 R_B)$. Then their range changes up to the range 1.05 m to 0.027 m (290 MHz to 11,000 MHz), which exactly covers most of the radio emission spectrum of typical galaxies and quasars.

Parameters	Values
Number of individual contours, z	9.33×10^{36}
Quasar mass M, kg	4.76×10^{42}
Total energy of the quasar E, J	9.61×10^{53}
Average radiation power N, W	2.72×10^{38}
Contour length or the maximum size of the quasar l, m	1.58×10^{21} (1.67×10^{5} light years)
Observed size of the quasar core l_0, m	$3.53 \times 10^{15} \ldots 1.26 \times 10^{11}$
Distance between charges r, m	3.57×10^{-4}
Minimum radiation wavelength λ, m	1.62×10^{-9}
Core pulsation period (minimum) τ_0, sec	70,400 (19.6 hours)
Periphery pulsation period (maximum) τ_{0_m}, sec	1.98×10^{9} (62.6 years)
Generalised pulse duration of the vortex tube τ_i, sec	117…5,440
Minimum light period τ_{min}, sec	1,675
Quasar life time τ, years	1.12×10^{8}
Standard "burnable" mass M_{st}, kg	2.26×10^{30}
Number of standard masses in the quasar n_{st}	2.10×10^{12}

Table 1.

Dual radio sources are relatively rare (it is possible due to that reason that we observe not the true size of a radio-source but its projection into the celestial sphere [8]) This implies that most of the long contours of the quasar are completely or partially spirally twisted forming a vortex structure or a tube immersed in the Y area (an extra dimension or a degree of freedom in relation to our world [8]). We can say that this vortex tube "is beaded" with future standard stellar masses convertible into radiation in respective portions (a sort of quanta).

Thus, the quasar as a phenomenon — on the much greater scale though — resembles the process of neutronisation [3], but occurs reversely, when the nominal one-dimensional vortex tube of the quasar is eventually transformed into a nominal two-dimensional disk spiral structure and further into a galaxy.

Some parameters of the quasar can be estimated using the most general equations obtained for stellar objects in the paper [3]. Thus, the core diameter is:

$$l_0 = M^j R_s \,, \tag{20}$$

where $j = 1 \ldots \frac{1}{3}$, the factor considering packing (the shape) of the object with the greatest value at $j = 1$ (a sphere) coinciding with the result of formula (16), and the lowest value at $j = \frac{1}{3}$ (a vortex tube) being close to the size of the Earth's orbit.

It is logical to assume that the quasar pulses relative to the symmetry axis, as do stellar objects, which is manifested in changing luminosity of the quasar. Thus, duration of the generalized momentum τ_i of a pulsar with the mass of a quasar as a vortex tube is:

$$\tau_i = 2.51\, M^{1/2 \ldots 1/4} \text{ sec}, \tag{21}$$

and pulsation periods of the core τ_0 and periphery τ_{0_m} of a stellar object with the mass of a quasar as a two-dimensional spiral object are:

$$\tau_0 = 2.51\, \frac{f}{\varepsilon} \left(\frac{M}{M_m} \right)^{2/3} \text{ sec}, \tag{22}$$

$$\tau_{0_m} = 2.51 \left(\frac{f}{\varepsilon} \right)^{3} \left(\frac{M}{M_m} \right)^{4/3} \text{ sec}, \tag{23}$$

where $M_m = 1.013 \times 10^{36}$ kg is the characteristic mass, determined by the formula (3) with $r = R_c$ and $v = c$. We may take $\varepsilon = f$ for the initial period of the quasar's life (the super-dense state). Then the periods determined by (22) and (23) are only dependent on the mass of the object.

Since the quasar pulsation periods vary depending on its form, the quasar emits at different frequencies. In addition, variability of radiation within different frequency ranges is asynchronous [9]. In particular, Seyfert galaxies — with a quasar presumably located in the centre of each — have a rapid high-amplitude radiation component (which are weeks and months) along with the slow low-amplitude radiation component (years), and the variability of radiation within different ranges is shifted in time. Thus, radio bursts can lag behind optical flares by years.

The state of a quasar in the form of a vortex tube may be observed as a *blazar*, which is believed to be an extremely compact quasar. It is characterised by rapid and considerable changes in luminance in all the spectrum ranges over a period of several days or even several hours [10].

It is understood that the quasar's parameters and its external appearance seen by the viewer will depend on the quantum number, density of packing of the charge pairs in the quasar volume, as well as on the quasar's age, pulsation phase, possible shape and orientation relative to the viewer. In general, the model estimates are consistent with the available data on quasars.

Calculated parameters of a standard quasar with $n_s = 4.884$ are shown in Table 1.

Indeed, the quasar mass estimated by the mass-luminance ratio should be about 10^{12} or more masses of the Sun; cumulative luminance throughout the spectrum may reach 10^{39} W to 10^{40} W; and energy contained in radio components alone may reach 10^{52} J. As for the quasar's life time, the analysis of the radio source observation data shows that energy emitted by the core as a result of a continuous (non-explosive) process may be emitted for 10^7 to 10^9 years [11–13].

The quasar's radiation is variable in all the wavelength ranges up to the X-ray and gamma radiation. The variability periods characteristic of quasars — months or even days — indicate that the generating area of the quasar radiation is not large, i.e. the linear dimensions of the emitting area (the quasar's core or active part) are fairly small — from one light year to the Solar System size [2, 10]. The shortest variation observed had a period of about one hour, which is within the range of the generalized pulse duration. This is consistent with the "burnout" time of the standard mass that corresponds to a typical stellar mass.

At the same time, the areas emitting within the radio range (double radio sources) are dozens and hundreds or more light-years away from the central optical object — a quasar or a galaxy [6, 7] — which is consistent with the length of the open contour. Their variability (months or years) may depend on the period of the quasar's outer cycle time (the periphery). As the quasar evolves, its evolutionary parameter ε decreases, but pulsation periods increase. We may assume that the initial configuration of the quasar is inherited in future, as matter condensates and stars form, and somehow "freezing" with a sharp decrease in the periphery spin velocity, it manifests itself in various forms of galaxies (elliptical or spiral).

3 Conclusion

It has been established by now that there were a lot more quasars at the earlier stages of the Universe evolution than there are now. Obviously, the quasar is the ancestor of other subsequent cosmological objects. In particular, this may explain the oddity of closeness of their energies of various origins, noted by astrophysics. Thus, we can conclude that quasars, their varieties and different types of galaxies (with quasars or black holes in the centre) are cosmological objects, gradually and naturally evolving from the white hole singularity to the black hole singularity.

Submitted on October 3, 2016 / Accepted on October 25, 2016

References

1. Retter A., Heller S. The revival of white holes as small bangs. arXiv: 1105.2776.:1105.2776
2. Narlikar J. Violent Phenomena in the Universe. Oxford University Press, 1984.
3. Belyakov A.V. Evolution of stellar objects according to J. Wheeler's geometrodynamic concept. *Progress in Physics*, 2013, v.1, 25–40.
4. Belyakov A.V. On some general regularities of formation of the planetary systems. *Progress in Physics*, 2014, v.10, 28–35.
5. Belyakov A.V. Charge of the electron, and the constants of radiation according to J. A. Wheeler's geometrodynamic model. *Progress in Physics*, 2010, v.4, 90–94.
6. Verkhanov O.V., Pariysky Yu.N. Radio Galaxies and Cosmology. Fizmatlit, Moscow, 2009.
7. Amirkhanyan V. R. Angular size — redshift: experiment and calculation. *Astrophysical Bulletin*, 2014, v. 69, no. 4, 383–389.
8. Belyakov A.V. Macro-analogies and gravitation in the micro-world: further elaboration of Wheeler's model of geometrodynamics. *Progress in Physics*, 2012, v.2, 47–57. *Nature*, v.379, issue 6563 (25 January 1996), 304.
9. Serjeant S., Rawlings S. Hidden quasars reddened by dust? Nature, v.379, issue 6563 (25 January 1996), 304.
10. Kantharia N. G. Decoding quasars: gravitationally redshifted spectral lines! arXiv: 1609.01593 [astro-ph.GA].
11. Shklovsky I.S. Radiogalaxies. *Soviet Uspekhi-Physics*, 1962, v.77, no. 5, 365–400.
12. Vorontsov-Velyaminov B.A. Extragalactic Astronomy. Revised and Exp. edition, Harwood Academic Publishers, 1987.
13. Pacholczyk A.G. Radiogalaxies. Pergamon Press, 1977.

Atom of Long-Range Action Instead of Counter-Productive Tachyon Phenomenology. Decisive Experiment of the New (Additional) Phenomenology Outside of the Light Cone

Boris M. Levin

Semenov Institute of Chemical Physics, Russ. Acad. Sci, Moscow (1964–1987)
In cooperation with Konstantinov Institute of Nuclear Physics, Russ. Acad. Sci., Gatchina (St. Petersburg) (1984–1987)
Ioffe Physical-Technical Institute, Russ. Acad. Sci., St. Petersburg (2005–2007)
E-mail: bormikhlev@yandex.ru

Limited, ultramicroscopic action radii of weak ($\sim 10^{-16}$ cm) and baryon ($\sim 10^{-13}$ cm) charges (interactions) against unlimited action radii of electrical and gravitational ones are the basis of phenomenology explaining the anomalies of positron annihilation in the "positron beta-decay Na-22 — neon (~9% Ne-22)" system established experimentally (1956–2003). A priori, it was impossible to imagine that the study of positron beta-decay positron annihilation (Na-22, Cu-64, and Ga-68) in noble gases would rise the issue of overcoming stagnation of fundamental physics (from mid-1970's) on the way to the expansion of the Standard Model and unification of physical interactions.

In noble (and any monoatomic) gases, slowing of positrons (e^+) under the positronium formation threshold (Ps; $E_{e^+} < E_0 = I - 6.8$ eV, where I is the atom ionization potential and 6.8 eV is the binding energy of Ps) is only possible through elastic collisions with atoms and may be observed, since: first, it is relatively long process (small parameter $\zeta = 2m_e/M$, where m_e is the positron mass and M is the atomic mass); and secondly, when the positron slows down to certain energy E_1 (determined by the inequalities $E_0 \gg E_1 \gg kT \cong 0.025$ eV) the positron annihilation rate rises more or less sharply, depending on the atomic number Z, as the positron polarize outermost electron shell of the atom. The combined effect of these two factors creates a non-exponential feature, the so-called *shoulder* in the time spectra of positron annihilation in inert gases (delayed $\gamma_n - \gamma_a$-coincidences; where γ_n is the nuclear gamma-quantum of the daughter nucleus after the β^+-decay of $^{22}\mathrm{Na} \xrightarrow{e^+_\beta + \nu} {}^{22*}\mathrm{Ne} \xrightarrow{E_{\gamma n} \cong 1.28\mathrm{MeV}} {}^{22}\mathrm{Ne}$)/"start", γ_a is one of the annihilation gamma-quanta/"stop"). The simplified theory of elastic slowing down says that the product of the shoulder length t_s and gas density (pressure, p) is the constant $t_s \times p$ for inert gas. In approximation of ideas gas, the constant is dependent on its parameters according to the following formula

$$(t_s \times p)_Z \cong \frac{\sqrt{2m_e}}{2.7 \times 10^{19}\, \sigma_e \zeta} \left(\frac{1}{\sqrt{E_1}} - \frac{1}{\sqrt{E_0}} \right),$$

where σ_e is the averaged cross section of elastic scattering of positrons [1].

When comparing lifetime charts of positrons of β^+-decay ^{22}Na for the entire range of noble gases, we cannot but notice the absence (or blurring) of the shoulder in neon [2]. Annihilation of *quasi-free positrons* after the shoulder with rate Λ depends on the number of electrons in the outermost shell of atom (Z_V). Value of Λ are shown in Table 1 [2]:

Table 1:

Noble gas	Λ, $\mu\mathrm{sec}^{-1} \times \mathrm{atm}^{-1}$	Z_V
Xenon (Xe)	26.3	8
Kripton (Kr)	5.78	8
Argon (Ar)	2.78	8
Neon (Ne)	0.661	8
Helium (He)	0.453	2

The chart $\Lambda/Z_V(Z)$ shown that neon falls out of the general monotonic dependence (Fig.1).

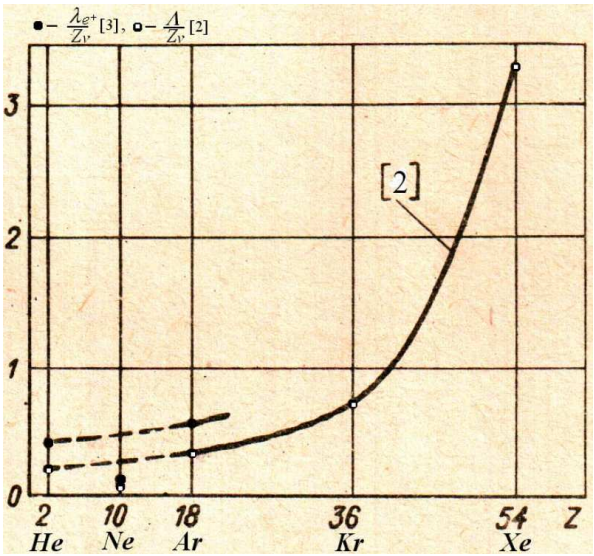

Fig. 1: Dependence of λ_{e^+}/Z_V [3] and Λ/Z_V [2] on Z (the atomic number of inert gas), where Z_V is the number of electrons in the outermost atomic shell.

Blurring of the shoulder in neon has been confirmed in other laboratories [3–7]. All these experiments showed different degrees of blurring. It should be noted in this regard that the shape of the shoulder is influenced by the orthopositronium ($o-$Ps, ^{T}Ps) component of the lifetime spectrum (I_2), following the component of annihilation of quasi-free positrons (e^+_β) on the time axis. Special features of neon individuating it in terms of measurements in the range of inert gases also include the following:

1. There is a big difference (twofold) in the data on the portion of positrons forming Ps in neon, obtained by the lifetime method with ^{22}Na as the source of positrons ($f = (28 \pm 3)\%$ [3] and $f = 26\%$ [8]) and by another method, i.e. according the energy spectrum of annihilation γ_a-quanta with ^{64}Cu as the source of positrons ($f = (55 \pm 6)\%$ [9]). This discrepancy between the results of independent experiments was noted in [7]. However, it was not discussed because of the lack of any basis for its explanation.
   In note [10], we have drawn attention to the fact that the start in the lifetime method is marked by the detection of the nuclear γ_n-quantum from transition of the excited daughter nucleus of ^{22*}Ne to the ground state of ^{22}Ne ($E_{\gamma_n} \cong 1.28$ MeV). This method usually provides high-precision measurements of the time spectra, since the lifetime of the excited state $^{22*}\mathrm{Ne}(E2)$ $\tau^* \cong 4 \times 10^{-12}$ s is considerably less than the resolving time of a spectrometer $\tau \sim 10^{-9}$ s.
   Hence, the question suggested itself in respect of the measurements in neon – whether the destiny of marker γ_n-quantum accompanying β^+-decay of ^{22}Na could be affected to some extent by high concentration of atoms with non-excited identical nuclei ($\sim 9\%$ ^{22}Ne)? In argon, where such a question is impossible, these different measurement methods provide consistent ($f = (30 \pm 3)\%$ [3] and $f = (36 \pm 6)\%$ [9]).
2. In contrast to helium and argon [7], there is large difference between experimental values of the constant characterizing the shoulder in neon $t_s \times p = 500 \div 900$ ns×atm [3] (see also [4,7]), $t_s \times p = 2200 \pm 6\%$ ns×atm [5] and $t_s \times p = 1700 \pm 200$ ns×atm [6]. The discrepancy between shoulder lengths may be an indication of the difference between neon samples in impurities of polyatomic gases. Nevertheless, authors characterized neon as *high purity* gas in all measurements. On the other hand, almost double the difference in shoulder length in measurements with the same sample of neon [3] (see also [4, 7]) also shows another uncontrollable cause of such a big difference in $t_s \times p$ neon in all measurements with ^{22}Na as the source of positrons [2–6].
3. There is also a strong discrepancy between the data on the cross section of elastic scattering of positrons under the threshold of formation of Ps obtained with beams of slow positrons using the lifetime method (with ^{22}Na as the positron source). Even the greatest of the values of the constant $t_s \times p$ in neon, obtained in work [5], is almost three times less than the estimated one, if we use the cross section of elastic scattering of positrons in neon are in full compliance with the theory and with results of beam experiments [11, 12].

All the experimental results of special manifestations of annihilation in the "β^+-decay ^{22}Na – neon ($\sim 9\%$ ^{22}Ne)" system were presented at the 7th Conference of Positron Annihilation (ICPA-7) [13].

A critical experiment (*falsification* by Karl Popper) was performed a decade after the publication of a proposal for experimental verification of the paradoxical idea of nuclear gamma-resonance in *gaseous* neon of natural isotopic compositions [10]. The successful experiment [14], which confirmed the paradoxical implementation of the Mössbauer Effect in gas in final state of β^+-decay $^{22}\mathrm{Na}(3^+) \xrightarrow{e^+_\beta+\nu} {}^{22*}\mathrm{Ne}(2^+)$ opened the prospect of building a phenomenology of extension of the Standard Model [15] in the suggestion that the limited four-dimensional space-time of the final state of β^+-decay of this type ($\Delta J^\pi = 1^\pi$) is topologically non-equivalent to the initial state (the *topological quantum transition*). With this in mind, let us denote the orthopositronium formed in the gas by the β^+-decay positron as β^+-orthopositronium: $^3(e^+_\beta e^-)_1$.

Since there is an *isolated virtual photon* $\widetilde{\gamma}$ in $o-$Ps dynamics, there is a possibility that the β^+-orthopositronium may overcome the *light barrier* due to quantum-mechanical oscillations. Hence we have sensing of four-dimensional space-time "on the outside" of the light cone and, consequently, an additional (single quantum) mode of annihilation involving a double-valued ($\pm$) space-like structure. The existence of the Planck mass $\pm M_{Pl} = \pm(\hbar c/G)^{1/2}$ opens a unique opportunity to represent a macroscopic space-like structure.

The phenomenology of physical nature of "resonance conditions" in the "β^+-decay ^{22}Na — neon ($\sim 9\%$ ^{22}Ne)" system formulated in [15]* leads to the conclusion that the uncontrollable factor in all neon measurements is the gas temperature (laboratory temperature). This means that deciding experiment aiming to confirm double resonance I_2 within the range ± 30°C (see below) is out of the question in Standard Model.

Theorists have been independently (for their own reasons) probing the possibility of going beyond the Standard Model:

*The Michigan group have renounced their results in the β^+-o-Ps self-annihilation rate by $(0.19 \pm 0.02 \div 0.14 \pm 0.023)$ percent over the theoretical value (*QED*) [16]. The findings of this work are most likely to be erroneous, since they were obtained by introducing an auxiliary electric field into the space of the measuring chamber. The field might "obscure" the effect. Fairly speaking, the work-2003 by the Michigan group has also played a constructive role. It destructive conclusions made it possible to detect and substantiate the fundamental link between gravity and electricity [17] — the cause of the erroneous nature of the conclusion made by the Michigan group, who did not have all the experimental data available by the time [14]. *A decisive experiment is needed.*

1. **Lev Landau** at the International Conference on High Energy Physics (Kiev, 1959) spoke about the limited perspective of the *Hamiltonian method* for strong interactions (the text of the presentation was included in the collection of articles in memory of **Wolfgang Pauli**, 1962) [18].
   Although quantum chromodynamics (QCD) was formulated in the framework of the *Hamiltonian method* in the 1960s–1970s, it did not solve the problem of strong interactions (the absence of fundamental justification of *confinement*), and the problem of the fundamental interactions unification (*Theory of Everything*) was complicated by mysterious nature of *dark matter* and *dark energy* (~ 95% of the Universe);

2. **R. F. Feynman [19]:** "At the suggestion of Gell-Mann I looked at the theory Yang-Mills with zero mass [...] it should been noticed by meson physicists who had been fooling around the Yang-Mills theory. They had not noticed it because they're practical, and the Yang-Mills theory with zero mass obviously does not exist, because a zero mass field would be obvious; it would come out of nuclei right away. So they didn't take the case of zero mass and no investigate it carefully";

3. **F. Hoyle and J. V. Narlikar** considered discrete scalar C-field with negative mass density [20]. This allowed presenting the final state of the topological quantum transition in β^+-decay of ^{22}Na (and the like) as a vacuum structure $U^{\pm}$, in which the space-like negative mass is balanced by the vacuum-like state of matter (an *atom of long-range action with a nucleus*). That is β^+-decay of $^{22}\mathrm{Na}(3^+) \xrightarrow{e^+_\beta+\nu} {}^{22}\mathrm{Ne}(2^+)$ under expansion of the Standard Model will be $^{22}\mathrm{Na}(3^+) \xrightarrow{e^+_\beta+\nu+U^{\pm}} {}^{22*}\mathrm{Ne}(2^+)$;

4. **E. B. Gliner [21]:** "The physical interpretation of some algebraic structures of the energy-momentum tensor allows us to suppose that there is a possible form of matter, called the μ-vacuum, which macroscopically possesses the properties of vacuum. [...] Because of the multiplicity of the comoving reference systems we cannot introduce the concept of localization of an element of μ-vacuum matter, and consequently cannot introduce the concepts of particle and of the number of particles of the μ-vacuum in a given volume, if we understand by a particle an object singled out in a classical sense relative to the remaining "part" of the matter. Similarly, one cannot introduce the classical concept of a photon".
   Views on β^+-decay of the type $\Delta J^{\pi} = 1^{\pi}$, $^{22}\mathrm{Na}(3^+) \rightarrow {}^{22}\mathrm{Ne}(2^+)$, $^{64}\mathrm{Cu}(1^+) \rightarrow {}^{64}\mathrm{Ni}(0^+)$, $^{64}\mathrm{Ga}(1^+) \rightarrow {}^{68}\mathrm{Zn}(0^+)$ in the Standard Model's expansion $^{22}\mathrm{Na}(3^+) \xrightarrow{e^+_\beta+\nu+U^{\pm}} {}^{22*}\mathrm{Ne}(2^+)$ (see item 3 above) was based on Gliner's cosmological ideas;

5. **V. I. Ogievetskii and I. V. Polubarinov** discussed the *notoph* in [22]: "...a massless particle with zero helicity, additional on the properties to photon. In interactions notoph, as well as photon, transfers spin 1".
   This makes possible to postulate an additional mode of annihilation of β^+-*o*-Ps by one notoph (γ°) $\beta^+ - {}^{\mathrm{T}}\mathrm{Ps} \rightarrow \gamma^{\circ} U^{\pm}$ (see items 3 and 4 above). Annihilation of *o*-Ps by one photon is prohibited in *QED* by the law of conservation of momentum;

6. **G. J. Iverson and G. Mack [23]** on the possibility of the space-like nature of some types of neutrinos;

7. **V. L. Lyuboshits and M. I. Podgoretskii** about the identity of elementary particles; the mirror world outside context of the P and CP violation [24].
   This opened the possibility of consideration of β^+-*o*-Ps oscillations in the mirror world, as Ps *initially is object of quantum electrodynamics* (electromagnetic interactions) preserving the P and CP symmetries, while the mirror was considered in the context of their violation under weak interactions;

8. **Yu. A. Golfand and E. P. Likhtman** discovered the mathematical structure of supersymmetry [25].
   Since the mid-1970s no common physical realization of supersymmetry has been found;

9. **S. W. Hawking and C. F. R. Ellis [26]:** "...the simultaneous creation of quanta of positive energy fields and of the negative energy C-field".
   This justifies the postulation of $U^{\pm}$ on an experimental basis [2–6, 9, 14, 15] (see item 3 above);

10. **J. L. Synge [27]:** "Anti-Compton scattering" — the idea that was not seen by the author as a physical concept — was developed in [28] to justify additional realization of supersymmetry (*superantipodal symmetry*) manifested in lifetime anomalies of β^+(^{22}Na)-*o*-Ps in neon;

11. **A. F. Andreev:** "Gravitational Interaction of Zero-Mass Particles", "Macroscopic Bodies with Zero Rest Mass" [29]; complete relativity, i.e. equivalence of "...all speeds (but speed of light)" [30].
   This was the first quantum-field justification of space-like fundamental structures previously postulated on the basis of general theory of relativity (the μ-vacuum concept, see item 4 above);

12. **P. Fayet and M. Mezard [31]:** Calculation of the probability of *o*-Ps annihilation by a single γ_a-quantum and a neutral supersymmetric gauge boson U with spin 1: $B(^{\mathrm{T}}\mathrm{Ps}) \rightarrow \gamma_a U = 3.5 \times 10^{-8}(1 - x^4)$, where $x = m_U/m_e \rightarrow 0$, m_e standing for the electron (positron) mass;

13. **P. Di Vecchia and V. Schuchhardt [32]:** complete degeneration of $N = 2$ para- and orthosuperpositronium.
   This has set a precedent of complete degeneration of para- and orthopositronium while maintaining superantipodal symmetry in the final state of β^+-decay ^{22}Na

and others. We know that conservation of full spin Ps is unequivocal law, not related to approximation. It follows from the CP-invariance of electromagnetic interactions, while the annihilation modes (the even number of γ_a-quanta for parapositronium ^{S}Ps and the odd number for ^{T}Ps) are determined by conservation of the charge parity (C) and the total angular momentum (the spin, as the ground states of Ps have no orbital angular momentum). Hence, the possibility in principle to justify the complete degeneration of the ground spin states of a superpositronium, taking into account the oscillations in the mirror world, may be associated with the relativistic transformation of the angular momentum. Indeed, if we postulate random mirror-world wandering in the three-dimensional space with velocity $|V| \sim c$ relative to the ground laboratory (observer) and if the relation between the walk step Δ (and the time Δ/c) and the ^{T}Ps$|^{T}$Ps$'$ (stroke indicates belonging to the mirror world) lifetime is favorable, the averaged (over this time interval) value of spin seen by the observer is $\langle(S = 0)\rangle = (S = 1)'(|V|^2/c^2)^{1/2}$ [33];

14. S. L. Glashow due to the presence of the isolated virtual photon $\widetilde{\gamma}$ in the dynamics of the orthopositronium, postulated (outside the context of the violation of P- and CP-symmetries) the possibility of o-Ps oscillations in the mirror world. The difference in understanding the nature of the mirror world discussed herein as past a new (additional) $G\hbar/ck$-physics and the *mirror Universe* by Glashow (the "mirror world"), rejected by himself in comparing the alleged consequences with the experimental data available at the time [34], is that the *energy* and *action* in the $G\hbar/ck$-mirror world of a new (additional) $G\hbar/ck$-physics have *negative sings*. In addition, the mirror world of $G\hbar/ck$-physics (with the negative sign) is realized *locally* (in the atom of long-range action) through the double-valued ($\pm$) Planck mass $M_\mu = M_{U^\pm} = \pm M_{Pl} = \pm(\hbar c/G)^{1/2}$ (development of Gliner's ideas);

15. A. D. Linde [35] earlier proposed an independent concept of antipodal symmetry of energy and action in the mirror world relative to the observable Universe. The $G\hbar/ck$-physics is substantiated by this concept. Expansion of the Standard Model includes the double-valued nature of the Planck's constant $\pm\hbar$;

16. L. B. Okun considered the possibility of "... the existence of many-particle states with anomalous permutation symmetry [...] in the relativistic case, it leads to non-positive energy or non-locality" (ferbons/parastatistic) [36];

17. G. A. Kotelnikov [37]: "It was shown that equations of electrodynamics are invariant with respect to the operation of changing the value the speed of light".
The double-valued nature of the speed of light $\pm c$ was realized in $G\hbar/ck$-physics. Two of the three superconstants of physics are double-valued $G, \pm\hbar, \pm c$.
We have noted the fact that $\pm\hbar$ and $\pm c$ are included in the structure of all quantum-relativistic physical constants with odd exponents, i.e. in the form of the positive-definite product of $(\pm\hbar)^{2k+1} \otimes (\pm c)^{2\kappa+1}$ (where k and κ are equal to 0 or an integer) as a phenomenon of the *antipodal cosmological invariance* (*ACI phenomenon*) *of the fundamental physical constants*: dimensionless constants of physical interaction — $\alpha = e^2/\hbar c$ (electromagnetic), $\alpha_g = Gm^2/\hbar c$ (gravitat.), $\alpha_W = G_F m^2/\hbar c$ (weak), Planck values — mass $M_{Pl} = (\hbar c/G)^{1/2}$, length $l_{Pl} = (\hbar G/c^3)^{1/2}$, time $t_{Pl} = (\hbar G/c^5)^{1/2}$ and all the rest. This means that mirror-world physics ("on the outside of the light cone") may be regarded as an extension of the Standard Model;

18. A. Yu. Andreev and D. A. Kirzhnits [38]: "Not quite simple and rather obscure relations between the concept of 'instability' and 'tachyons' are discussed".
This work has defined the physical status of the double-valued $\pm$ four-dimensional space-time "on the outside" of the light cone. At the time of publication, the authors could not give up the phenomenology and the term *tachyon*. The key word is *instability*. The only realization is the β^+-orthopositronium oscillating in the mirror world. In the final state of the topological quantum transition under the β^+-decay of ^{22}Na, β^+-o-Ps breaks the light barrier due to presence of the isolated virtual photon $\widetilde{\gamma}$ in its dynamics. An *atom of long-range action with a nucleus* takes over from the counterproductive phenomenology "tachyon".
The β^+-decay of $p \to n + e^+_\beta + \nu$ (in the atomic nucleus) in the earth laboratory (g = 981 cm/s^2) involves physical interactions of all types: *strong* — $p \to n$, *electromagnetic* — p, e^+_β, *weak* — ν (*electroweak*) and *gravitational* one. That is why "instability" in the context of the β^+-decay (of the $\Delta J^\pi = 1^\pi$ type) must be accompanied by a unified field reaction (generalized displacement current) ad modum the displacement current in electrodynamics.
The space-like structure of the unified field displacement current (an atom of long-range action with a nucleus) was postulated instead of the counterproductive phenomenology "tachyon";

19. L. B. Borissova and D. D. Rabounski [39]: Using the method of chronometric invariants (physical observable values, A.L. Zelmanov, 1956), "... the possibility of co-existence of short-range and long-range action has be studied" as an extension of GR.
Mathematical prediction of the existence of the third form of matter in the zero-space (zero particles) has given rise to construction of the phenomenology of the additional one notoph mode of β^+-o-Ps annihilation

(see items 5,7,10 above);

20. J. M. Fröhlich ("Planck's Hypercube" [40]): following the logic and intuition of **Max Planck** (1900/1906), reattributes Boltzmann's constant k to the status of the fundamental constants $c, G, \hbar$, which determined the *cube of physical theories* (G. Gamov, D. Ivanenko, L. Landau, M. P. Bronstein/1928, and A. Zelmanov/ 1967–1969), thus opening the opportunity of the *four-dimensional generalization of the cube*.
The formulation of the double resonance concept (Appendix in [15]) predicts dependence of intensity of β^+-o-Ps (I_2) on temperature in the "β^+-decay ^{22}Na — neon ($\sim$ 9% ^{22}Ne)" system to be studied in the range — $30°\text{C} < T < +30°\text{C}$.
This remind on lecture [40]. If there was destructive criticism of the Planck's Hypercube concept in [41], lecture [40] would hardly be noticed, as it was published in a non-peer-reviewed journal (it is absent in the Science Citation Index);

21. A. D. Sukhanov and O. N. Golubeva [42]: "We show that the quantum statistical mechanics (QSM) describing quantum and thermal properties of objects has only the sense of particular semiclassical approximation. We propose a more general (than QSM) microdescription of objects in a heat bath taking into account a vacuum as an object environment; we call it $\hbar$-k-dynamics";

22. L. V. Prokhorov [43]: "On Planck Distances Physics. Universe as a Net", "On Physics at the Planck Distance. Strings and Symmetries".

These ideas and results obtained by theoreticians (items 1 to 22) were included in the wording of the Standard Model extension phenomenology, as the isotope effect in neon (the increased β^+-orthopositronium component I_2 in the sample depleted by an isotope of ^{22}Ne [14]; 1.85 ± 0.1 factor) is on 6-7 order of magnitude greater than estimated in the Standard Model (by isotopic shift of atomic energy levels).

The main motives for extending the Standard Model to explain the anomalies in the "β^+-decay ^{22}Na – neon ($\sim$ 9% ^{22}Ne)" system [2–6, 9, 14, 15] are determined by three concepts — vacuum-like state of matter (see item 4 [19] above), complete relativity (see item 11 [29, 30] above) and development of the idea of β^+-o-Ps oscillations in the mirror world [15] ([34]).

It is surprising that, in the XIX century, the genius of Sir W. R. Hamilton (1806-1865) linked the Standard Model of physics of XX century (the Hamiltonian method) and its alleged expansion in XXI century, since quantitative harmonization of lifetime anomaly β^+-o-Ps in the "β^+-decay ^{22}Na — neon ($\sim$ 9% ^{22}Ne)" system is based on the phenomenology of the *atom of long-range action with nucleus*. This spacelike structure in the final state of β^+-decay is represented by bound Hamiltonian chains/cycles (paths contain each node of the graph once).

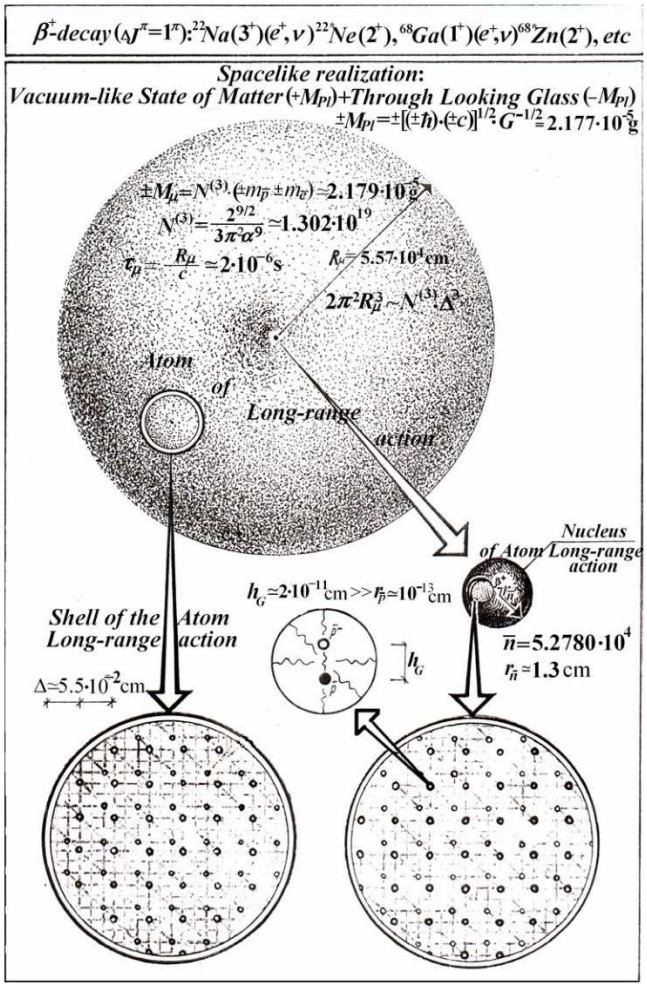

Fig. 2: "Microstructure" of the vacuum-like state of matter (*VSM/mirror world*); h_G is vertical displacement of double-valued sublattices $U^{\pm}$ in the gravitational field of the Earth.

The Planck mass $M_\mu = M_{U^\pm} = \pm M_{Pl} = \pm(\hbar c/G)^{1/2}$ g is regarded as a space-like structure (the number of nodes in *atom of long-range action* and radii is $N^{(3)} \cong 1.302 \times 10^{19}$, $R_\mu \cong 5.57 \times 10^4$ cm, in the nucleus $\bar{n} \cong 5.2780 \times 10^4$, $r_{\bar{n}} \cong 1.3$ cm). It is assumed that each node contains elementary charges of all physical interactions ($\bar{p}^+$, $\bar{p}^-$, $\bar{e}^-/\bar{e}^+$, $\bar{\nu}/\bar{\bar{\nu}}$ with their double-valued $\pm$ masses). In these assumptions, the Planck mass is calculated with high accuracy using the fine structure constant α [15].

Unlike the *gravitational* (G) and *electromagnetic* (α) *interactions* with infinitive ranges ($r_G, r_\alpha = \infty$), the ranges of the *weak* ($r_W = 10^{-16}$ cm) and *baryon* ($r_{str} = r_{\bar{p}} \sim 10^{-13}$ cm) *interactions* are *ultramicroscopically* small. Since $+M_{Pl}$ and $-M_{Pl}$ move in the gravitational field vertically and in opposite directions and diverge to a distance of $h_G = 2g\tau^2_{0-Ps}/2 = 2 \times 10^{-11}$ cm over the lifetime of β^+-o-Ps (up to 142 ns), the weak and baryon charges are decompensated (opened) in the nodes of *vacuum-like state of matter/VSM* ($+M_{Pl}$) as $h_G \gg r_W, r_{\bar{p}}$ (Fig. 2).

The rate of self-annihilation of β^+-*o*-Ps (in non-resonant conditions) is exceeded by $(0.19 \pm 0.02 \div 0.14 \pm 0.023)$ % (see footnote in Page 12) due to the amplification factor as result of β^+-*o*-Ps oscillations on $\bar{n} \cong 5.2780 \times 10^4$ nodes of the space-time structure of the *nucleus of atom of long-range action* [15] (parallel acts of annihilation)

$$B\left(\beta^+ - {}^{\mathrm{T}}\mathrm{Ps}\right)\bar{n} \to \gamma^{\circ} U^+ = 3.5 \times 10^{-8} \times 5.2780 \times 10^4 \cong 1.9 \times 10^{-3}(0.19)\%$$

(see item 12 above).

In the fourth dimension of space-time outside the light cone, the $+M_{Pl}$ lattice has the properties of an *absolutely rigid body*. Electrical charges in the nodes of $\bar{p}^+/\bar{p}^-$, $\bar{e}^-/\bar{e}^+$ lattices are balanced as a result of the infinite range (the Coulomb barrier is absent in the VSM nodes). Exchange of *quasiprotons* in the nodes of the *VSM* lattice with protons of the atomic nuclei of the gas surrounding the source of positrons becomes possible. In the case of neon, nuclear gamma-resonance (the Mössbauer Effect) is realized in the "β^+-decay ^{22}Na — neon ($\sim 9\%$ ^{22}Ne)" system.

Appearance of protons (quasi-particles $\bar{p}$) in each node of the $+M_{Pl}$ lattice and bonding of atoms with ^{22}Ne nuclei in the "β^+-decay ^{22}Na — neon ($\sim 9\%$ ^{22}Ne)" system is the response to β^+-decay ^{22}Na. This is similar to the displacement current, but having the space-like structure.

The difference between the masses of the neutron and proton $\Delta m_{np}c^2 = m_n c^2 - m_p c^2 = 1.2933317 \pm 0.0000005$ MeV is exceeding energy of the marker γ_n-quantum ("start": $^{22*}\mathrm{Ne} \xrightarrow{E_{\gamma n}=1.274577\,\mathrm{MeV}} {}^{22}\mathrm{Ne}$; $\Delta m_{np}c^2 - E_{\gamma_n} = 18.7547$ keV).

There was an idea to link the difference $\Delta m_{np}c^2 - E_{\gamma_n} = 18.7547$ keV with response energy resonance in the topological quantum transition under β^+-decay ^{22}Na, because the kinetic energy of neon atoms from gaseous phase "freeze" on the $+M_{Pl}$ lattice during the β^+-*o*-Ps lifetime, and the final-state neutrino also participates in "vertical" ($\updownarrow$) oscillations and gains the additional (topological) mass ($m^{\mathrm{eff}}_{\nu_e}$)

$$^{22}\mathrm{Na}(3^+) \to {}^{22*}\mathrm{Ne}(2^+) + e^+_{\beta} + \nu_e + U^{\pm}.$$

Then $\Delta m_{np}c^2$ exceeding E_{γ_n} may be presented as follows

$$\Delta m_{np}c^2 - E_{\gamma_n} = \frac{3}{2}\, k\, T\bar{n} + m^{\mathrm{eff}}_{\nu_e} = 18.7547\ \mathrm{keV},$$

where $\frac{3}{2} kT\bar{n} = 0.038 \times 5.2780 \times 10^4 \cong 2$ keV, $m^{\mathrm{eff}}_{\nu_e} \cong 16.75$ keV.

The effective mass of the neutrino $m^{\mathrm{eff}}_{\nu_e}$ is equal to the mass heavy 17-keV neutrino as a possible result of mixing "horizontal" generation of neutrinos (a brief review of the 17-keV neutrino problem is described in monograph [44]). The dramatic history of experimental studies of 17-keV neutrinos is similar to the history of the β^+-orthopositronium problem [44, 45].

All the anomalies in the "β^+-decay ^{22}Na — neon ($\sim 9\%$ ^{22}Ne)" system — blurred shoulder and variability of the observed β^+-orthopositronium intensity (I_2) (up to factor 2) [9, 14] — are explained by the assumption of existence of the temperature-dependent resonance I_2. The inert gas temperature (the laboratory temperature) was not monitored in lifetime spectra measurements [2–6, 14].

Submitted on October 5, 2016 / Accepted on October 19, 2016

References

1. Tao S.J., Green J.H., and Celitans G.J. *Proc. Phys. Soc.*, 1963, v.81, 1091.
2. Osmon P.E. *Phys. Rev.*, 1965, v.B138(1), 216.
3. Goldanskii V.I. & Levin B.M. Institute of Chemical Physics, Moscow (1967): in *Atomic Energy Review*, v.6, IAEA, Vienna, 1968; in *Table of Positron Annihilation Data*, Ed. By B. G. Hogg, C. M. Laidlaw, V. I. Goldanskii and V. P. Shantarovich, pages 154, 171, 183.
4. Canter K.F. and Roellig L.O. *Phys. Rev.*, 1975, v.A12(2), 386.
5. Mao A.C. and Paul D.A.L. *Canad. J. Phys.*, 1975, v.53(21), 2406.
6. Coleman P.G., Griffith T.C., Heyland G.R. and Killen T.L. *J. Phys.*, 1975, v.B8(10), 1734.
7. Griffith T.C. and Heyland G.R. *Phys. Rep.*, 1978, v.39(3), 170.
8. Coleman P.G., Griffith T.C., Heyland G.R. and Killen T.L. *J. Phys.*, 1975, v.B8(10), L185.
9. Marder S., Huges V.W., Wu C.S., and Bennett W. *Phys. Rev.*, 1956, v.103(5), 1258.
10. Levin B.M. and Shantarovich V.P. *Khim. Vys. Energ.* (*High Energy Chem. USSR*), 1977, no.11, 382.
11. Campeanu R.I., Dubau J. *J. Phys.*, 1978, v.B11, L567.
12. Levin B.M. *Sov. J. Nucl. Phys.*, 1981, v.34(6), 917.
13. Levin B.M., Shantarovich V.P. Anomalies of Positron Annihilation Lifetime Spectra in Gaseous Neon. *ICPA-7*, sect. D38, January 6–11, 1985, New Delhi, India.
14. Levin B.M., Kochenda L.M., Markov A.A., and Shantarovich V.P. *Sov. J. Nucl. Phys.*, 1987, v.45(6), 1119.
15. Levin B.M. About extension of the Standard Model of Physics; see Appendix: About physical nature "resonance conditions" in the lifetime annihilation spectra of the positron (orthopositronium) from β^+-decay ^{22}Na in gaseous neon. http://science.snauka.ru/2013/01/3279
16. Vallery R.S., Zitzewitz P.W., and Gidley D.W. Resolution of the Orthopositronium-Lifetime Puzzle. *Phys. Rev. Lett.*, 2003, v.90(20), 203402.
17. Kotov B.A., Levin B.M., and Sokolov V.I. Orthopositronium: On the possible relation of gravity to electricity. arXiv: quant-ph/0604171.
18. Landau L.D. Collected Papers, 1965, 800–802.
19. Feynman R. *Acta Phys. Pol.*, 1963, v.24, 697 (*Conference on Relativistic Theories of Gravitation*, July 1962).
20. Hoyle F., and Narlikar J.V. *Proc. Roy. Soc.*, 1964, v.A282, no.1389, 178.
21. Gliner E.B. *Sov. Phys. JETP–USSR*, 1966, v.22, 378.
22. Ogievetskii V.I., Polubarinov I.V. *Sov. J. Nucl. Phys.*, 1967, v.4, 156.
23. Iverson G.J., and Mack G. *Phys. Rev.*, 1970, v.D2(10), 2326; *Ann. Phys.*, 1971, v.B64(10), 211.
24. Lyuboshits V.L., Podgoretskii M.I. *Sov. Phys. JETP–USSR*, 1971, v.33(1), 5.
25. Golfand Yu.A., Likhtman E.P. *JETP Lett.*, 1971, v.13(8), 323.
26. Hawking S.W., Ellis G.F.R. The Large Scale Structure of Space-Time. Cambridge University Press, 1973.

27. Synge J.L. *Proc. Roy. Ir. Acad.*, 1974, v.A74(9), 67.
28. Levin B.M., Sokolov V.I. arXiv: quant-ph/0702063.
29. Andreev A.F. *JETP Lett.*, 1973, v.17(8), 303; *Sov. Phys. JETP–USSR*, 1974, v.38(4), 648.
30. Andreev A.F. *JETP Lett.*, 1982, v.36(3), 100.
31. Fayet P. and Mezard M. *Phys. Lett.*, 1981, v.B104(3), 226.
32. Di Vecchia P., Schuchhard V. *Phys. Lett.*, 1985, v.B155, 427.
33. Levin B.M. *Phys. At. Nucl.*, 1985, v.58(2), 332.
34. Glashow S.L. *Phys. Lett.*, 1986, v.B167, 35.
35. Linde A.D. *Phys. Lett.*, 1988, v.B200, 272.
36. Okun L.B. *Sov. J. Nucl. Phys.*, 1988, v.47(4), 752.
37. Kotelnikov G.A. *Izvestiya VUZov*, 1992, no.12, 69 (*in Russian*).
38. Andreev A.Yu., Kirzhnits D.A. *Phys. Usp.*, 1996, v.39(10), 1071.
39. Borissova L., Rabounski D. Fields, Vacuum, and the Mirror Universe. 2nd edition, Svenska fysikarkivet, Stockholm, 2009; Rabounski D., Borissova L. Particle Here and Beyond the Mirror. 3rd edition, American Research Press, Rehoboth (NM), 2012.
40. Fröhlich J. *Phys. Blätter*, 2001, B57(7/8), 53.
41. Okun L.B. On the Article of G.Gamov, D.Ivanenko, and L.Landau "World Constants and Limiting Transition". *Phys. At. Nucl.*, 2002, v.65(7), 1370; Cube or hypercube of natural units. arXiv: hep-ph/0112339; in: Michael Marinov memorial volume *Multiple Facets of Quantization and Supersymmetry*, Ed. by M. Olshanetsky, A. Vainshtein, World Scientific Publishing, 2002, 670–675.
42. Sukhanov A.D., Golubjeva O.N. *Physics of Elementary Particles and Atomic Nuclei*, 2010, v.41(7).
43. Prokhorov L.V. *Physics of Elementary Particles and Atomic Nuclei*, 2007, v.38(3), 696; 2012, v.43(1), 4.
44. Klapdor-Kleingrothhaus H.V., Staudt A. Teilchenphysik ohne Beschleunger. B. G. Teubner, Stutgart, 1995.
45. Levin B.M. arXiv: quant-ph/0303166.

Half-Century History of the Project of New (Additional) $G\hbar/ck$-Physics

Boris M. Levin

Semenov Institute of Chemical Physics, Russ. Acad. Sci, Moscow (1964–1987)
In cooperation with Konstantinov Institute of Nuclear Physics, Russ. Acad. Sci., Gatchina (St. Petersburg) (1984–1987)
Ioffe Physical-Technical Institute, Russ. Acad. Sci., St. Petersburg (2005–2007)
E-mail: bormikhlev@yandex.ru

The origins of fundamental knowledge, which were mentioned by the genius of Pushkin, are closed in the history of science like in lens focus. This paper survey the 50-years history of studying the orthopositronium anomaly, where the author spent decades on the substantial experiments and further analysis among the experiments made by other experimental groups in different countries throughout the world.

Oh, how much of wondrous discoveries
Enlightenment Spirit preparing for us
And Experience the son of difficult errors
And genius, the paradoxes' friend,
And Case — the got of all inventions.

A. S. Pushkin, 1829

. . . Enlightenment spirit. . .

A single (as one might think) yet fundamental (!) phenomenon — **the annihilation of positrons emitted by a ^{22}Na isotope (and the like) in positron beta decay in inert gases** — combines all the types of physical interactions, such as: **strong/nuclear** interaction (transformation of a *proton* into a *neutron* in a *neutron-deficient atomic nucleus* with emission of a *positron* and a *neutrino*); **electromagnetic** interaction (electrically charged *proton* and *positron* with magnetic moments); **weak** interaction (emission of *neutrino*); and **gravity** interaction, since experiments have only been made in *ground-based* laboratories so far.

Therefore, if we come to think of it, we should not exclude the special role of the half-century *observations of anomalies in neon* (1956–2003) in making a *unified description of physical interactions* (*unified field theory*). Furthermore, these observations are only possible with *monoatomic* gases, which are the closest to the ideal gas status [1].

This idea is relevant against the backdrop of stagnation in fundamental physics (since mid-1970s), as Standard Model (SM) formulated in the same period has led to development of idea started by Einstein (with no final success through) and for the first time worded by Faraday (in respect of then known gravity and electromagnetism) [2]. The idea was given an official status in the XX century. It was the idea of all the fundamental interactions (the Theory of Everything).

The constructive idea presented by the new (additional) $G\hbar/ck$-physics Project could not emerge a priori. The signs of *new physics* in the experimental data on the beta-decay positron annihilation in inert gases were recorded for the first time by experimentalists involved in solving the issues of orthopositronium/parapositronium with a chemical-physical (or physical-chemical) "pedigree".

However, it would be impossible to implement the idea without the results achieved by fundamentalist theoreticians in their independent efforts on expanding SM [1]. It is clear why the phenomenology of the $G\hbar/ck$-physics Project finalized among experimenters a decade ago cannot get through to implementation of the *Decisive Experiment Project* [4], despite being based on the giant effect exceeding the SM estimate by 6–7 orders of magnitude [3].

Nevertheless, there is another reason, which the prominent ethologist Konrad Lorenz described as one of "*the civilised man's eight deadly sins*". It is *indoctrinability of the "Big Science"* (susceptibility to fashion and stereotypes).

"...never before have the manipulators had at their disposal such clever advertising techniques or such impressive mass media as today. [...]

However, the worst effect of fashion ... can be observed in the realm of science. It is mistake to suppose that all professional scientists are free from the cultural diseases that are the subject of this treatise. [...] "Big Science" in no way implies a science concerned with the most important things on our planet, nor is it the science of the human psyche and intellect: it is exclusively that science which promises money, energy, or power... [...] The special danger of fashionably indoctrination in the field of science lies in the fact that it leads too many, though fortunately not all modern scientists, in a directions exactly opposite to that of the real aim of all human striving for truth — the aim for the better self-knowledge" [5].

In 1970s, K. Lorenz still retained hope for overcoming the "*mortal*" contradictions. In another essay of this, we can feel the spirit of the Rome Club ("*sustainable development*") founded in those years:

"I believe that we can see the true sings that self-consciousness begins to awaken in the cultural humanity, based on scientific knowledge. [...] **Until now, there has never been a rational self-study of human culture on our planet**, just like there was no objective, in our opinion, natural science before Galileo' s times. [...]

Of course, the position of mankind is now more dangerous than it has ever been in the past. However, thinking found by our culture due to its natural science potentially gives it a

change to escape death that befell all the high cultures in the past. This is the first time in world history" [6].

The first (and only so far) constructive response by theorists to the unique information on the positron (orthopositronium) annihilation anomalies, received by "quiet physics" (without accelerators of ultrahigh-energy particles) after they created the mathematical theory of the existence of the *third form of matter* [7], is that the experimental data was understood by the authors as subject for application of their fundamental theory [8]. Through paradoxical expansion of the general relativity, they "... studied the possibility of coexistence of short-range and long-range actions", using the method of chronometric invariants (physical observable values, A. L. Zelmanov, 1956). The theoretical (mathematical) prediction of the existence of the third form of matter (*zero-particles*) in the *zero-space* became an additional incentive for building the phenomenology of new (additional) $G\hbar/ck$-physics on the way to justifying the anomalies in neon.

And experience the son of difficult errors...

The start (1964) of assumption of a new range of time spectrometry (up to 200 ns) at the Department of Matter Structure of the Institute of Chemical Physics Academy of Sciences USSR/DMS IChP in Moscow (led by Professor V. I. Goldanskii) to study the annihilation of beta-decay positrons in physical media with the large void volume (gases or porous solids) coincided with the publication of a work by P. E. Osmon from Columbia University, New York, presenting comparative data on annihilation of quasi-free positrons (from the Na-22 isotope) in all inert gases at pressures of several atmospheres and room temperature [9].

Here is the abstract of this work:

"Positron lifetime spectra have been measured in helium, neon, argon, krypton, and xenon at pressures of a few atmospheres. The annihilation rates of the free positrons are found to be time-dependent. Physical reasons, based on the strong correlation between energy and age of a positron, are suggested for this time dependence. Three parameters describing the main features of the free-positron spectrum are separated from the data, for each gas, and tabulated".

Neither the abstract, nor the article itself contains any reference to the characteristic feature of *neon* lifetime diagrams. Lifetime diagrams show a nonexponential feature of this area of the lifetime spectra — the so-called *shoulder*. Its manifestation is generally enhancing from helium to xenon along with the increasing atomic number of gas Z. However, *neon* stands out — the shoulder in its diagrams is blurred or nonexistent at all.

It was decided to repeat the observation in the *helium-neon-argon* area to verify the said distinctive feature of neon. The blurring effect in the shoulder of neon was confirmed. The result were published (1967) in the departmental Newsletter of the Institute of Instrument Engineering, which provided time range converter into digital vernier type code up to 200 ns for lifetime spectrometer, and in Tables [10].

V.I.Goldanskii discussed the results at international meetings. Later on, several laboratories took up measurements with neon and confirmed the neon shoulder blur [11–14].

As we known, polyatomic impurities in inert gas influence the dynamics of positron moderation under the positronium formation threshold due to inelastic energy losses on the background of elastic moderation in inert (monoatomic) gas. Therefore, the difference in shoulder parameters between experimental data obtained in different laboratories could be attributed to differences in residual polyatomic impurities in neon samples used in the experiments [9–14], despite the fact that neon had the *ultra-high purity* grade in all the experiments.

However, an analysis of all the experimental data showed that this cannot explain the observed differences in shoulder parameters in neon. In our measurements, using *the same sample of neon* in a wide pressure range (16 atm to 32 atm), the product of the shoulder length t_s and the gas pressure p (the constant for ideal gas [1]) differ almost twofold (from 500 ns atm to 900 ns atm); in [10] these results are only represented by upper limit of 900 ns atm). The true result (500÷900) ns atm was reported by V. I. Goldanskii (see [11]*, [14]†). At the same time, according to our measurements, the shoulder lengths in helium and argon remain constant (with in the experimental errors) [10].

A decade after the shoulder blur in neon had been confirmed, a hypothesis was published that the marker gamma-quantum of lifetime spectrometer is collectivized under special conditions of the system described as "**beta-decay of a Na-22 isotope** $\xrightarrow{\text{positron+neutrino}}$ **excited Ne-22** (the source of the marker gamma-quantum of the lifetime spectrometer/ "start") **in gaseous neon with natural isotope composition (~9% of the Ne-22 isotope)**" [15].

Two decades later, a comparative critical experiment was made on separated neon isotopes [3]. The experiment confirmed the hypothesis and opened up the prospects for expanding SM and building the phenomenology of $G\hbar/ck$-physics.

The project of new $G\hbar/ck$-physics was surprisingly supported by the results of the Michigan group (University of Michigan, Ann Arbor) for absolute measurement of the lifetime (the reciprocal of the self-annihilation rate) of an orthopositronium (1982–1990). Two methods (with buffer gases and in vacuum) revealed that the self-annihilation rate of an orthopositronium is exceeded by ($0.19 \pm 0.02 \div 0.14 \pm$

*"Aside from the presence of the prompt component, it is very difficult to discern any nonexponential region of the spectrum. Goldanskii claims to see a shoulder in his room-temperature spectra, (ρt_s = 500–900 nsec amagat), but he states that it is considerably weaker than that which occurs in helium and is difficult to locate".

†"The only other evidence for the shoulder comes from the work Goldanskii and Levin reported by Hogg et al. [10] to have a width in the range 500–900 ns amagats".

0.023) percent compared with the calculated value (quantum electrodynamics/QED), which has reached the accuracy of $1.6 \times 10^{-4}\%$ by now. As we see, the deviation of the experimental data from the theory was recorded at the level of 10σ (standard deviation)!

These groups of H.M. Randal Laboratory at the University of Michigan led by Professor A. Rich (1937–1990) were the world leaders in the orthopositronium lifetime absolute precision measurements. The irony is that the article titled "*Resolution of the Orthopositronium-Lifetime Puzzle*" [16], published by the Michigan group in Phys. Rev. Lett., and disavowed the results of the group's previous measurements (1982–1990), which were in conflict with the theory, and thus "closed" the problem for the scientific community.

In the modified method, an auxiliary electric field was introduced *vertically* in the measurement chamber [16]. A sequential analysis, taking into account all the information available, showed that previously found discrepancy between the theory and the experiment would be preserved with a *horizontal* direction of the auxiliary electric field [17].

In all fairness, Work-2003 had a constructive role too. Its destructive conclusions made it possible to find and substantiate the manifestation of the fundamental connection between *gravity* and *electricity*, which was the cause of the wrong conclusion by the Michigan group, who did not have all the experimental data available by the time.

The shoulder shape is influenced by intensity of the orthopositronium component I_2, since the **orthopositronium component follows the component of annihilation of quasi-free positrons on the time axis** in lifetime spectra. This can cause the shoulder blurring and problems with anomalies of beta-decay positrons (from Na-22) annihilation in neon [3,9–13], because the **laboratory temperature was not taken into account in all of this measurements**.

It is also worth nothing that there is an abnormally high share of positrons forming a positronium in gaseous neon — $(55 \pm 6)\%$ — obtained on the energy spectrum of the annihilation gamma-quanta with Cu-64 as the source of positrons [18] in contrast to half the value — $(28 \pm 3)\%$ — obtained by a lifetime method with Na-22 as the source of positrons.

And genius, the paradoxes' friend...

The blatant paradox in the perspective of justification on the hypothesis of collectivization of Ne-22 nuclear excitation ($\cong$ 1.28 MeV) by nuclei of Ne-22 atoms with natural isotopic composition ($\sim$ 9%) in the macroscopic volume of the measuring chamber at the final stage of the beta-decay of Na-22 nucleus was confirmed by comparing the lifetime spectra of neon samples — a natural one and a sample depleted by Ne-22 isotope [15]. As said above, the effect of changing I_2 was 6–7 orders of magnitude higher than the estimate of SM.

Now we can exclude the general suggested version of the determining role of the residual polyatomic gas impurities.

The paradox is that, in experimental conditions [3], the Mössbauer effect (nuclear gamma-resonance) takes place for a sufficiently hard gamma-quantum ($\cong$ 1.28 MeV) of the excited daughter Ne-22 nucleus, located on the solid positron source, and nuclei of Ne-22 atoms staying in gas at room temperature. As we known, the Mössbauer Effect is possible in condensed media (solids: crystalline, amorphous, or powder one).

Most likely, this paradoxical formulation of the issue was due to the fact that two group of experimenters were working alongside at DMS IChP in Moscow (from beginning 1960s) led by V.I. Goldanskii — "positron group" (the group of Chemistry of New Atoms) and "Mössbauer group" (the Mössbauer Effect laboratory). The groups met at general workshops, making presentations and passively sharing information and ideas.

The concept of zero-space (zero-particles) as an extension of the *general relativity* [7] has set a framework for overcoming the paradox through introduction of the four-dimensional space-time on the *outside* of the light cone into fundamental physics.

But how shall we implement this program on a quantitative level, when compared with the experimental data?

The collective genius of famous and prominent theorists, who independently sought (each for their own reasons) to go beyond SM, determined the development of a phenomenology of new (additional) $G\hbar/ck$-physics [1]. The search for unique and rarely-cited works of theorists with high index of citing continued for two with half decades (1987–2012) following publication of the critical experiment results [3].

An analysis of the paradoxical experimental situation has led to the conclusion that the macroscopic volume of the double-valued ($\pm$) four-dimensional space-time of the final state of positron beta-decay of $\Delta J^{\pi} = 1^{\pi}$ type is filled with bonded Hamiltonian chains/cycles of the *nucleus* of the atom of long-range action (with a number of nodes $\bar{n} \cong 5.2790 \times 10^4$) and the *atom of long-range action* as a whole ($N^{(3)} = 1.302 \times 10^{19}$) [1].

Summing up this phenomenology, we can say that two fundamental (mathematical) abstractions — the *material point* (*inside* the light cone) and *absolutely rigid body* (*outside* the light cone) — will determine the relevant expansion of SM (the *unified quantum field theory*).

A decisive experiment in the study of the supposed temperature resonance I_2 in the range $-30^{\circ}\mathrm{C} < T < +30^{\circ}\mathrm{C}$ (see [4], Appendix) will finally clarify the issue of anomalies of positron (Na-22) annihilation in gaseous neon.

And case — the God of all inventions

One might think that the sacral line by Pushkin is a poetic paraphrase of a revelation from the New Testament, the Apostle Paul to the Romans 11:33, "*Oh, the depth of the riches and wisdom and knowledge of God! How unsearchable are*

His judgments and His ways!" The deep thought received a lapidary form — "*The ways of God are inscrutable*".

Fundamental physics is the search for Truth, for understanding of the basic of Existence — the space-time (quantitative criteria of cause-and-effect relationship, *experiment and theory*).

However, since the mid-1970s, physics suffers a profound crisis. At no time in history there was such a long stagnation of fundamental knowledge, when the issue was formulated (e.g. *How does the supersymmetry manifest itself? What is the nature of dark matter/dark energy? What is the mainstay of consciousness? And others???*), but they had no solutions. This breaks the formation of fundamentally new technologies. That cannot not have globally destructive social consequences.

There is a high measure of confidence, that crisis could be overcome for a long time. A decade before the physicists understood the heuristic importance of supersymmetry, there was made an experiment [9, 10], which laid the foundation for the study of anomalies in the system described as "**beta-decay of a Na-22 isotope $\xrightarrow{\text{positron+neutrino}}$ excited state of Ne-22 isotope (the source of the marker gamma-quantum of the lifetime spectrometer/"start") in gaseous neon with natural isotopic composition (~9% of Ne-22 isotope)** — "resonance conditions" [15]". Later on, this anomaly was linked to the anomaly of the positronium share in neon (55 ± 6)% under nonresonance conditions (with Cu-64 as the source of positrons) [16].

All of this have prepared the ground for the introduction of space-like object physics (i.e., on the outside of the light cone) in the fundamental context.

Physics is one, but the now prevailing stereotype — the increased interest in ultra-high energies as a prospect for overcoming stagnation — and neglect of the unique data received by "quiet physics", does not promise to overcome stagnation. The existence of the quantum-field resonance as a consequence of the existence of a *nucleus of the atom of long-range action* is possible, if energy $m_p \times \bar{n} \cong 50$ TeV (where m_p is proton mass), which is half order of magnitude greater than the energy of the colliding proton beams of the Large Hadron Collider. It is very distant, if not illusory prospect...

The core of the Project of New (Additional) $G\hbar/ck$-physics was the critical experiment [3]. It was the result of previous work in many laboratories [9–13], an independent breakthrough by theorists to the double-valued ($\pm$) four-dimensional space-time [7], which virtually legalized the results of independent theoretical searches for the way to go beyond Standard Model by the methods of the *general relativity* [19] and the *quantum field theory* ([20] and [21]).

Setting a decisive experiment promises a breakthrough to the *unified field theory* based on expansion of the Hamiltonian method by including the Hamiltonian chain/cycle [1].

Submitted on October 5, 2016 / Accepted on October 19, 2016

References

1. Levin B.M. *Progress in Physics*, 2017, v.13, issue 1, 11–17.
2. Faraday M. The Bakerian Lecture. *Philosophical Transactions*, 1851, 1.
3. Levin B.M., Kochenda L.M., Markov A.A., and Shantarovich V.P. *Sov. J. Nucl. Phys.*, 1987, v.45(6), 1119.
4. Levin B.M. http://science.snauka.ru/2013/01/3279 (Appendix).
5. Lorenz K. Die acht todsünden der zivilisierten Menshheit. R. Piper & Co., München, 1973.
6. Lorenz K. Die Rückerte des Spiegels: Versuch einer Naturgeschichte menschlichen Erkenners. R.Piper & Co., München, 1973.
7. Borissova L.B., Rabounski D.D. The theory of movement of particles in four-dimensional space-time. Lomonossov Workshop, Moscow, 1997 (*in Russian*); Rabounski D.D. Three form of existence of matter in four-dimensional space-time. Lomonossov Workshop, Moscow, 1997 (*in Russian*).
8. Borissova L., Rabounski D. Fields, Vacuum, and the Mirror Universe. 2nd edition, Svenska fysikarkivet, Stockholm, 2009; Rabounski D., Borissova L. Particle Here and Beyond the Mirror. 3rd edition, American Research Press, Rehoboth (NM), 2012.
9. Osmon P.E. *Phys. Rev.*, 1965, v.B138(1), 216.
10. Goldanskii V.I. & Levin B.M. Institute of Chemical Physics, Moscow (1967): in *Atomic Energy Review*, v.6, IAEA, Vienna, 1968; in *Table of Positron Annihilation Data*, Ed. By B. G. Hogg, C. M. Laidlaw, V. I. Goldanskii and V. P. Shantarovich, pages 154, 171, 183.
11. Canter K.F. and Roellig L.O. *Phys. Rev.*, 1975, v.A12(2), 386.
12. Mao A.C. and Paul D.A.L. *Canad. J. Phys.*, 1975, v.53(21), 2406.
13. Coleman P.G., Griffith T.C., Heyland G.R. and Killen T.L. *J. Phys.*, 1975, v.B8(10), 1734.
14. Griffith T.C. and Heyland G.R. *Phys. Rep.*, 1978, v.39(3), 170.
15. Levin B.M. and Shantarovich V.P. *Khim. Vys. Energ.* (*High Energy Chem. USSR*), 1977, no.11, 382.
16. Vallery R.S., Zitzewitz P.W., and Gidley D.W. Resolution of the Orthopositronium-Lifetime Puzzle. *Phys. Rev. Lett.*, 2003, v.90(20), 203402.
17. Levin B.M. arXiv: quant-ph/0303166.
18. Marder S., Huges V.W., Wu C.S., and Bennett W. *Phys. Rev.*, 1956, v.103(5), 1258.
19. Gliner E.B. *Sov. Phys. JETP–USSR*, 1966, v.22, 378.
20. Andreev A.F. *JETP Lett.*, 1973, v.17(8), 303; *Sov. Phys. JETP–USSR*, 1974, v.38(4), 648.
21. Glashow S.L. *Phys. Lett.*, 1986, v.B167, 35.

Probing Quantum Memory Effects in the Single Photon Regime

Carlos Belmonte[1], Frederik Vanden Berghe[1], Krassimir Panajotov[1,2], Thomas Durt[3*]

[1]B-Phot. Vrije Universiteit Brussel Pleinlaan 2, 1050 Brussel, Belgium.
[2]Institute of Solid State Physics, 72 Tzarigradsko Chaussee blvd., 1784 Sofia, Bulgaria.
[3]Aix Marseille Université, CNRS, Centrale Marseille, Institut Fresnel, UMR 7249, 13013 Marseille, France.
*Corresponding author: thomas.durt@centrale-marseille.fr

In this paper we study correlations present in experimental random series extracted from a Quantum Optical Random Number generator conceived and implemented in our lab. In particular we study the manifestations of inertia/memory effects. This study is realized in the single photon regime.

1 Introduction

We learn from classical and quantum physics that the future properties of a physical system are determined by its instantaneous, present state. This is reminiscent of the so-called Markov property in statistics, according to which* *"...the conditional probability distribution of future states of the process, given the present state and all past states, depends only upon the present state and not on any past states..."*

In previous papers (see [5] for a survey), one of us (T. D.) studied the possibility that quantum correlations exhibit non-Markovian features [4], in other words that quantum correlations would be endowed with an intrinsic, non-standard memory effect. Actually, several experiments were realized in the past, in different contexts, in order to test the possibility of such memory effects [2–4, 7]. These experiments aimed at testing hidden variable models (both local and non-local models [5]) which predicted the appearance of non-standard correlations between measurement outcomes collected at different times (different places in the case of non-local models [2]). We shall not enter in the detail of these experiments and models here, but instead we shall focus on the results of a statistical test that we developed in the past in order to characterize quantum random number generators that were developed at the Université Libre de Bruxelles (U.L.B.) and Vrije Universiteit Brussel (V.U.B.). We developed this test, from now on denoted the Histogram Inertia Indicator (H.I.I.) test in order to reveal whether histograms constituted from data measured at different times were correlated to each other.

Besides the aforementioned hidden variable models, we found inspiration in the idea of morphic resonance expressed and developed by Rupert Sheldrake [17] according to which the evolution of species and development of life in general are characterized by memory effects having as a consequence that new shapes/patterns tend to behave as attractors for other shapes/patterns. In a previous paper we showed that mixing Sheldrake's ideas and hidden variable models led to the prediction of observable non-standard memory effects (see [4] section 3: Sheldrake and Smolin's Models, and a Related Experimental Proposal).

*Quoted from Wiktionary.

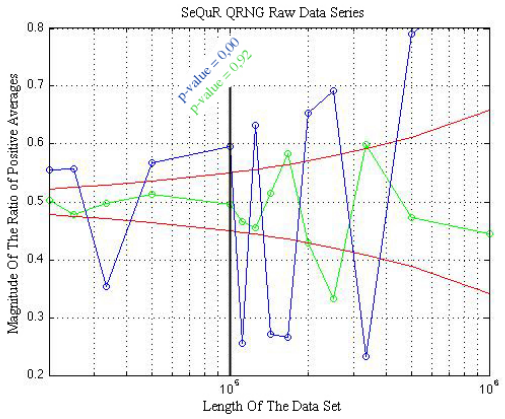

Fig. 1: SeQuR QRNG - Raw Data: A "near zone" effect is clearly present in the SeQuR data (blue graph). Successive histograms, each drawn from 1000 sequential random values, exhibit a manifest tendency to resemble each other. The green graph represents the same test on a Matlab pseudo-random series. The red lines represent the boundaries that are assigned to "perfect" random series. The plotted p-values confirm the results in graphical form. (quoted from [19])

Our main goal, when we developed the H.I.I. was to try and reveal whether quantum histograms would exhibit memory effects. It can be seen as an attempt to extrapolate the extent of validity of Sheldrake's ideas to the quantum realm.

A last source of inspiration was provided by the evidence for annual periodicity in decay data [9, 10] that has been revealed a few years ago. It has been suspected that this periodicity cannot be explained by environmental effects such as temperature, humidity, pressure, *etc* [11], nor is there a correlation with the Sun-Earth distance after re-analysation of the data [13].

All these observations suggest that there could exist some "regularity in randomness", some "hidden" pattern, a non-standard memory effect characterized by correlations between data collected at different times. This is a very upsetting and at the same time challenging idea which deserves to be considered seriously, from a foundational perspective [2–5, 7].

In particular we noticed the presence of an intriguing memory effect already some years ago [19], at the level of a random optical signal measured in the continuous counting

regime (see section 2.3). The data were delivered to us by colleagues from the U.L.B. developing a prototype of ultra-fast quantum optical random number generator [6]. Essentially, this device amplified fluctuations of the intensity delivered by a laser source. The results plotted at the level of Fig. 1 reveal for instance a clear deviation from the theoretical boundaries (in red) associated to a fully random process (without memory effect). We also checked in the same work [19] that Fourier filtering and/or Faraday filtering diminishes the effect, but does not suppress it totally. Our interpretation of these observations is that these correlations could be partially due to an external mechanism, and partially due to the internal memory of the device (here the light detector which is acting in the continuous (many photons) regime).

It was not clear however, uniquely on the basis of the observations, to decide whether the external source of the correlations had to be attributed solely to electromagnetic pollution (GSM devices, FM radio channels and so on) or whether it was necessary to resort to a universal memory effect in order to explain our observations.

Therefore we decided to test experimentally similar memory effects in the low intensity (single photon) regime, which was made possible by the development of quantum random number generators (QRNG) active in the low intensity (discrete counting) regime *in situ* in our labs and based on the random character of time delays between clicks collected with a single photon avalanche detector at the output of an attenuated laser source. The corresponding generator, the so-called Parity Quantum Optical Random Number (PQORN) generator has been described in a separate publication [6] and is briefly described in section 3.1 (see also Fig. 2).

As we shall describe in the present paper, we applied the H.I.I. test to the raw data generated with our PQORN generator. This program is triply challenging in our eyes because, as far as we know, nobody tested in the past the existence of memory effects by the same method, and *a fortiori* no such test has been achieved so far in the low intensity regime. Last but not least, if the memory effect revealed by the H.I.I. indicator is universal, its detection provides a criterion for discriminating physical randomness from pseudo-randomness which is a very challenging idea.

The paper is structured as follows. We describe in section 2 a new statistical test, the H.I.I. test, introduced in [19] aimed at measuring and/or revealing memory effects (section 2.1), as well as the corresponding p-value (section 2.2). Our methods are also relevant in the framework of random number generation because the H.I.I. test and the associated p-value are thus useful tools in order to characterize randomness.

Before scrutinizing (making use of the tests described in section 2) the existence of memory effects at the level of the PQORN generator (section 4), we investigated more in depth the correlations which appear in the high intensity regime at the level of our single photon detectors (section 3.2). These correlations are *a priori* not of quantum nature but they are induced by the dead time of the detector. As we show in section 4, in the high intensity regime, and only in this regime, the H.I. memory effect is present.

We also studied whether similar memory effects still exist beyond the near zone regime studied in section 4.1, and in particular whether non-local in space (section 4.2) and time (section 4.3) memory effects (previously denoted Spatial and Temporal Long Range Memory effects) can be measured at the level of our device. The last section is devoted to the conclusions and to the interpretation of the collected results.

2 The near-zone H.I.I. test

2.1 Qualitative test

In order to derive a statistical test aimed at revealing memory effects, we approached the problem as follows [19]: Each histogram of a given data sample – given it is not too large

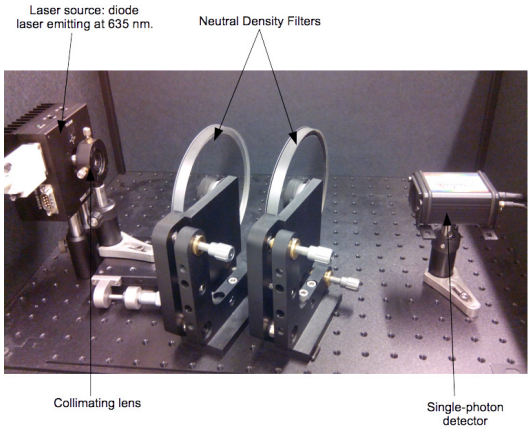

Fig. 2: Detailed setup for the near-zone experiment. It is composed of a laser source, two neutral density filters and a single photon detector. The same setup, supplemented with a nanosecond resolution clock constitutes the Parity QORNG.

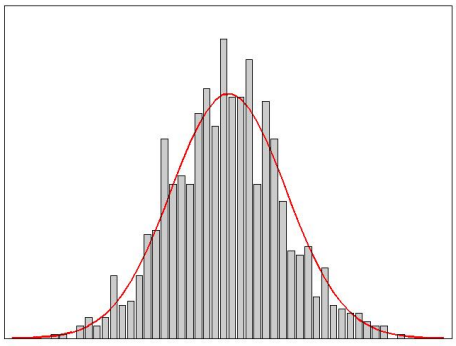

Fig. 3: Fluctuations of a sample histogram - constructed from 1 000 gaussian distributed random data values - around the line of the average histogram computed from a data sample of 10 000 000 gaussian distributed random values.

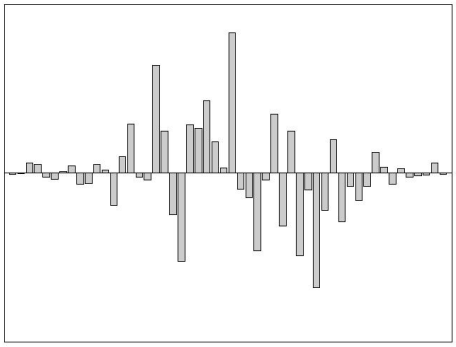

Fig. 4: The difference $\tilde{H}$ of a sample histogram H with the average histogram.

– fluctuates around the average histogram, which is obtained from a very large data sample, *cfr*. Fig. 3. For each histogram H we compute its difference with the mean histogram. This leaves us with a new normalized histogram $\tilde{H}$ in which each value can either have a positive of a negative value, depending whether that value is observed more or less often than in average, as shown in Fig. 4. Thereafter, we introduce a quantitative "resemblance" value r as follows. Consider $\tilde{H}_i$ and $\tilde{H}_j$ two neighboring histograms.

$$r_i = \sum_{\alpha} \tilde{H}_{i_\alpha} \tilde{H}_{j_\alpha} \quad \text{(with } j = i + 1\text{)} \tag{1}$$

with α the corresponding value of the histogram at this entry. Remark that we are working with histograms where values can be both positive and negative. Consequently, the inproduct r can be either positive or negative. The following interpretation can now be given to r:

- r **is large and negative**: Both histograms seem to be inverse of each other for most of the entries. The histograms have no near zone effect. Instead this suggests an anti- or complementary- "near-zone" effect.
- r **is close to zero**: Both histograms have approximately as much resemblance as difference. Again no "near zone" effect is observed.
- r **is large and positive**: Both histograms have the same shape for most of their entries. A "near zone" effect is then observed.

Considering that the random sequence of length n is divided in M data samples of length N, this analysis leaves us with $\lfloor \frac{N}{1000} \rfloor - 1$ values of r for each of the M samples, since we choose each histogram to be created from 1000 random values. Fig. 5 depicts graphical results after calculating all r-values.

This is only the first part of the investigation since, as one can deduce from Fig. 5, often, not much can visually be said about a possible "near-zone" effect. Therefore, it is appropriate to perform a statistical treatment of the data.

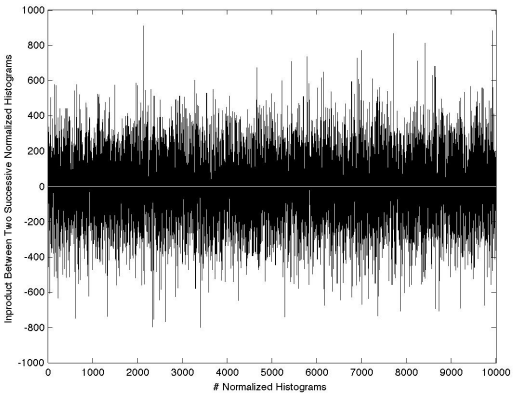

Fig. 5: Example graph of 9 999 inproducts between 10 000 successive histograms obtained from a data sample of $N = 10^7$ values.

Let us start by taking the average of all r inproducts:

$$\bar{r} = \frac{\sum_{i=1}^{\frac{N}{1000}-1} r_i}{\frac{N}{1000} - 1} . \tag{2}$$

Since the analysis is performed on M data samples of length N, each of the M samples now leaves us with one value of $\bar{r}$. These M average values $\bar{r}$ provide us with a qualitative indication of a "near zone" effect that we choose to express through the ratio of positive averages of $\bar{r}$, i.e.

$$\frac{\#\bar{r}_{pos}}{M} \tag{3}$$

with $\#\bar{r}_{pos}$ the amount of $\bar{r} \geq 0$. Note that the sign of $\bar{r}$ can be regarded as a Bernoulli process, or as a bit sequence with for example a bit value of 1 corresponding to a positive value and a bit value of 0 to a negative one. In a perfectly random process the ratio between them should be close to $1/2$ with a deviation depending on M, the amount of data samples. In order to determine the magnitude of this deviation we consider the law of large numbers to derive the boundaries:

$$\frac{\#\bar{r}_{pos}}{M} \sim \frac{1}{2} \pm \frac{\sigma_{bit}}{\sqrt{M}} = \frac{1}{2}\left(1 \pm \frac{1}{\sqrt{M}}\right) \tag{4}$$

with M the amount of data samples or the amount of values $\bar{r}$. For a data set of length n, $M = \lfloor \frac{n}{N} \rfloor$ so that the boundaries also depend on N.

It is expected for perfect random processes that the magnitude of the ratio of positive averages $\bar{r}$ will remain confined within the boundaries plotted in Fig. 6. One expects that sporadically $\bar{r}$ will be found outside the boundaries but in the case that it will remain persistently outside the boundaries we must suspect that the random sequence is biased. Considered so, we now have at our disposal a qualitative test aimed at testing the presence of the near zone effect. In the next section, we shall also derive a quantitative criterion, in the form of a p-value.

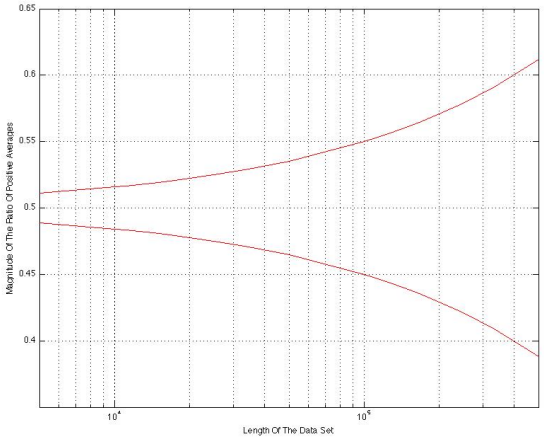

Fig. 6: Boundaries for the fluctuations of the ratio of positive averages $\bar{r}$ depending on M, the amount of data samples tested. Since a very large data sample is divided in M subsamples of length N, M decreases as N increases and consequently, the fluctuations also depend on the size N of the subsamples.

2.2 Derivation of a p-value for the near-zone H.I.I. test

The standard randomness tests (*e.g.* the NIST or Die Hard tests [12,16]) deliver their results through a so-called p-value. Typically, $p \in [0,1]$ is the probability of obtaining a test result at least as extreme as the one that was actually observed, assuming that the null hypothesis is true, *i.e.* the tested sequence is considered random. A p-value ≥ 0.01 indicates that the tested series of bits is random with a confidence interval of 99%. While the near-zone H.I.I. test described in the previous section is of qualitative nature and delivers its results in a graphical way, we shall now show how to connect a p-value to the different values in the graph of this near-zone H.I.I. test.

Recall that the value of $\bar{r}$ from (2) can be regarded as a Bernoulli process or conversely as a random walk if one considers a positive value of $\bar{r}$ as the value $+1$ and a negative value of $\bar{r}$ as -1. Consider the sequence $X = X_1, X_2, \ldots$ of values ± 1 in accordance to positive or negative values of $\bar{r}$. We define S_M as the sum

$$S_M = X_1 + X_2 + \ldots + X_M \tag{5}$$

with M the amount of values of $\bar{r}$ (see discussion at (2) and (3)). Compute the test statistics

$$Z = \frac{|S_M|}{\sqrt{2M}}\,. \tag{6}$$

Making use of the law of large numbers, the p-value can be shown [19] to be equal to

$$p\text{−value} = \operatorname{erfc}\left(\frac{Z}{\sqrt{2}}\right). \tag{7}$$

2.3 Near zone memory effect in the continuous counting regime

Some years ago [19], we investigated the existence of a memory effect at the level of an optical random number generator the SeQuR QRNG, acting in the continuous regime. Essentially, the device amplifies the fluctuations of the intensity delivered by a laser source [6]. We considered the decimal random data delivered by the detector. The tested results show clear similarities in the successive histograms from the data samples. This can be observed in Fig. 1, quoted from [19]. This analysis clearly indicates the presence of an inertia or memory effect in the signal. Let us now consider discrete data collected with single photon detectors.

3 Randomness in the low photon number regime

3.1 Parity QORNG

The *Parity QORNG* exploits the random nature of the distribution of clicks in a single photon detector. It is based on the parity of the time (in nanoseconds) for which the events (clicks) occur. If this time is even, the bit will be zero; if this time is odd, the bit will be one. The set-up to carry out this method consists of an attenuated laser source coupled to a single-photon detector (Fig. 2). The detector is coupled to a buffer via an acquisition card synchronized with a clock of high resolution (1 nanosecond).

As has been shown in [6], the principal advantages with this method are 1) that it requires to use only one photon-detector to generate a random number and 2) that even in the high intensity regime it delivers random series of very high quality*.

Before we characterize the H.I. effect, let us study the physical correlations exhibited by the single photon detectors of the parity QORNG.

3.2 Study of correlations due to dead-time of detectors

3.2.1 Successive clicks in one single-photon detector

In this section we will check the statistical properties of the data acquired in single-photon detectors in various regimes. These regimes are reached by modifying the attenuation of our two tunable attenuators (Fig. 2), from almost no attenuation at all to a high attenuation.

Before going further it is worth recalling that the single-photon detector is characterized by a dead time (that is to say the lapse of time during which the photon-detector will be off after detecting a photon) in the range of 45 to 50 ns. The resolution time of the acquisition card is 1 ns, therefore every 1 ns a datum will be acquired, while the maximum data that the acquisition card can memorize is 750 000 ns, after which the memory of the acquisition card is full.

*For instance bit series obtained from the PQORNG successfully pass [6] the NIST battery of standard randomness tests (frequency test, parity test, spectral test, entropy test and so on).

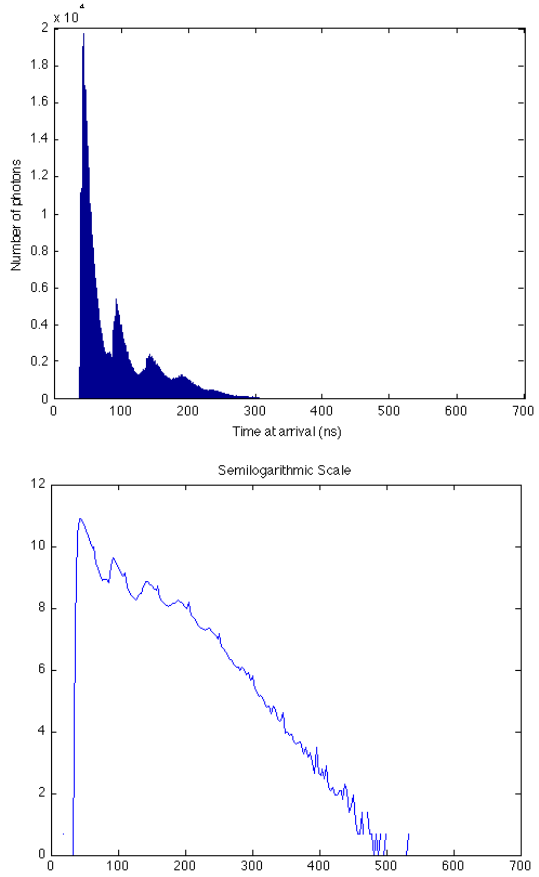

Fig. 7: Statistics of time arrival between photons in the high intensity regime. Average time between photons estimated to be more or less 36 ns.

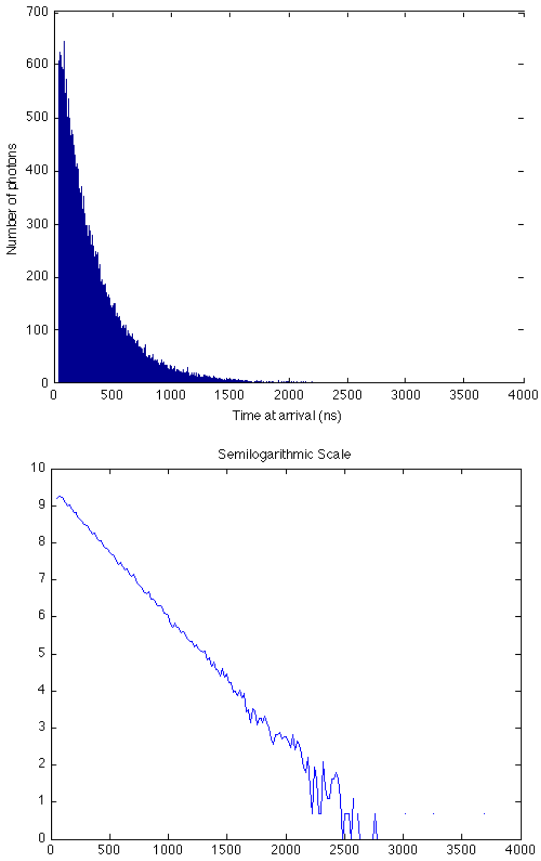

Fig. 8: Statistics of time arrival between photons in the low intensity regime. Average time between photons estimated to be more or less 294 ns.

Taking into account the specifications above, we performed a study of the time arrival between two photons in different regimes changing the attenuation. For instance, in the high intensity regime (low attenuation regime) we observe a distribution of delay times between clicks plotted in Fig. 7 which is contaminated by the correlations induced by the dead-time of the detector (as revealed by the presence of peaks separated by 45 ns). From the tail of the semi-logarithmic plot, we can infer the average time between two photons, which would be exactly the slope of the straight line if the distribution was Poissonian, which corresponds to a dead time equal to zero.

If in turn we work in a low intensity regime, for which the average time between two clicks is quite larger than the dead time of the detectors, we observe a nearly Poissonian distribution, as can be seen from Fig. 8. The single noticeable difference with a Poisson distribution is the null probability to measure successive clicks in a time smaller than the dead time (here 45 ns).

3.2.2 Simultaneous clicks in two single-photon detectors

In order to check the departure from the Poisson distribution, we estimated another parameter which is the number of simultaneous counts in two detectors placed at the output of a beamsplitter. When two photons arrive at the exact same time to the beamsplitter, there exist four possible scenarios (Fig. 9):

1. Both photons are detected by the photon-detector A.
2. Both photons are detected by the photon-detector B.
3. Photon A is detected by the photon-detector A and photon B is detected by the photon-detector B.
4. Photon A is detected by the photon-detector B and photon B is detected by the photon-detector A.

The probability of obtaining a single photon during a unit-period of time is (in case of a perfectly Poissonian distribu-

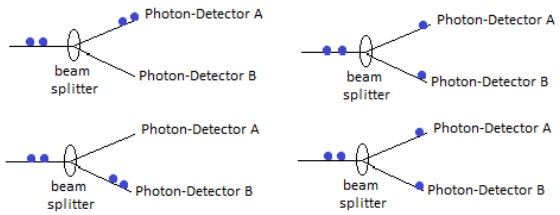

Fig. 9: Possibilities that two photons are detected by two photon-detectors.

tion):

$$P(\text{single}) = \frac{1}{\text{average time between photons}} \tag{8}$$

The probability of obtaining two photons at the input of the beamsplitter is then:

$$P(\text{pair}) = \left(\frac{1}{\text{average time between photons}}\right)^2 \frac{1}{2!} \tag{9}$$

Henceforth, the probability that two photons arrive during a same temporal window unity in the two photon-detectors can be calculated theoretically:

$$P(\text{double count}) = \left(\frac{1}{(\text{average time between photons})^2 \cdot 2!}\right)\frac{1}{2}$$

The average number of double clicks obeys therefore

$$N(\text{double counts}) = \left(\frac{\text{total number of photons}}{\text{average time between photons} \cdot 2!}\right)\frac{1}{2}$$

In the high intensity regime we found a significant departure from the Poisson distribution:

- Total number of photons $\approx 640\,000$.
- Average time between photons ≈ 21 ns.
- Simultaneous clicks in the 2 photon-detectors = 4 999.

$$\left(\frac{640\,000}{21 \cdot 2!}\right)\frac{1}{2} \approx 7\,619 \tag{10}$$

In the low intensity regime we found a better agreement:

- Total number of photons $\approx 184\,000$.
- Average time between photons ≈ 141 ns.
- Simultaneous clicks in the two photon-detectors = 272.

$$\left(\frac{184\,000}{141 \cdot 2!}\right)\frac{1}{2} \approx 326 \tag{11}$$

This confirms that when the dead time is small compared to the average time between two photons, the statistics of counts is Poissonian in good approximation, which fits with the standard quantum prediction for a coherently attenuated laser source. From this point of view, the limit of low intensities corresponds to the genuinely quantum regime, while in the high intensity regime (for which the dead time is comparable to the average time between two photons) quantumness is spoiled by correlations induced by the dead time mechanism of the detector.

Incidentally, our study also confirms that we nearly always operate in the single photon regime; the probability to have two photons or more in the same interval of acquisition (one nanosecond) being at most of the order of 10^{-2}, even in the "high" intensity regime.

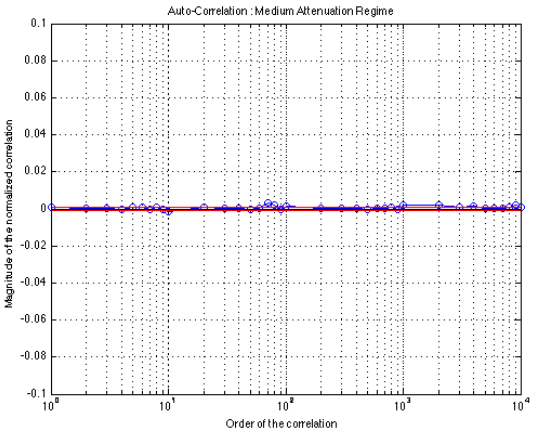

Fig. 10: Autocorrelation for the low intensity regime.

4 Characterization of the PQORN generator using the H.I.I. test

4.1 Near-zone temporal memory effect

The existence of a near-zone temporal memory effect would be revealed through the fact that similar histograms are significantly more probable to appear in the nearby (neighbouring) intervals of the time series of the results of measurements.

Using the setup in Fig. 2, we measured this effect in the two different regimes, the low intensity regime and the high intensity regime (they were defined in terms of the dead time at the end of the previous section).

To determine whether the effect is present, we make use of the H.I.I. test described in section 2, which delivers a p-value and a graph for a fast visual appreciation. We applied a level of significance of 0.01 for the p-value, hence if the p-value delivered is lower than the level of significance, we assumed that the presence of a significant memory effect gets confirmed by experimental data. Similarly, if the curve provided by the test remains outside the boundary curves, we assume that the existence of a memory effect is experimentally confirmed. We also used a standard auto-correlation test [6, 12, 16] to corroborate the results of the H.I.I. test.

4.1.1 Low intensity regime

We firstly measured the effect in the (highly attenuated) low intensity regime. We observed no correlation in this regime, as it is shown in Fig. 10. The H.I.I. test gives us the option to choose arbitrarily the sample length, which optimally ought to be of the order of the memory time of the H.I. effect. We selected four different sample lengths of 100, 300, 500 and 1000; and for each choice of a sample length, we tested the possible existence of a memory effect with the first, the second, the fifth and the tenth neighbour. For instance selecting 100 as a sample length, the reference sample runs from 1 to 100, the first neighbour sample from 101 to 200, the second neighbour one runs from 201 to 300, the fifth neighbour sam-

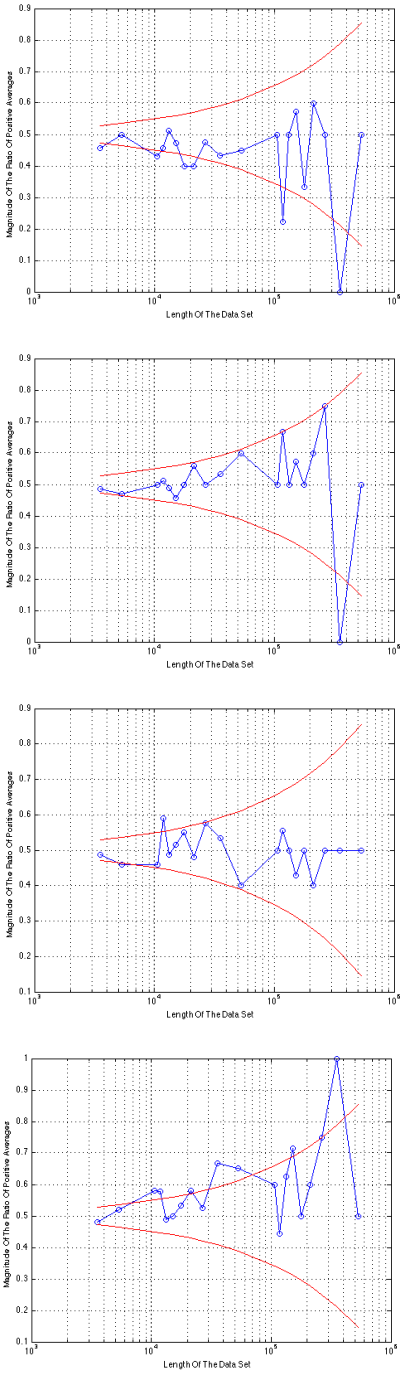

Fig. 11: Memory effect for the low attenuation regime with sample length of 100 for the first(a), the second (b), the fifth(c) and the tenth neighbour (d).

ple runs from 501 to 600 and so on. As is clear from Fig. 11, no memory effect is present in the low intensity regime. The result is also confirmed by similar plots obtained for sample lengths of 300, 500 and 1000 that we do not reproduce here in order not to overload the presentation. The corresponding p-values are gathered in Tab. 5. All the p-values are larger than

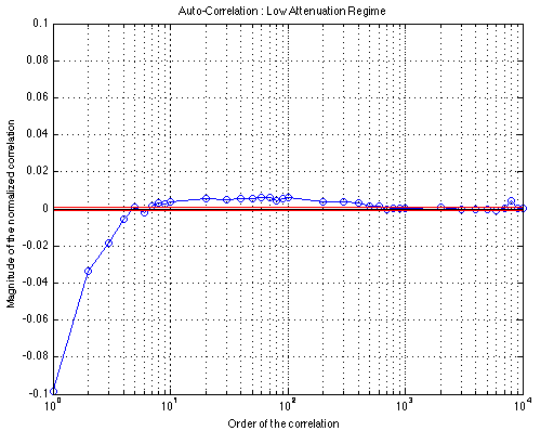

Fig. 12: Autocorrelation for the high intensity regime.

0.01, thus we can safely conclude that there is no memory effect in the low intensity regime, confirming the information provided by the graphics. These p-values are obtained by averaging all p-values associated to one "graphical" test.

4.1.2 High intensity regime

We measured again the correlations in the high intensity (weakly attenuated) regime and Fig. 12 shows that in this regime a strong auto-correlation prevails until the bit 600 approximately. We also measured the memory effect in the same way as for the low intensity regime, *i.e.* for different sample lengths (100, 300, 500 and 1000) and different neighbours (1^{st}, 2^{nd}, 5^{th} and 10^{th}). From Figs. 13, 14, 15 and 16, it can be seen that for a sample length of 100, the H.I. effect is present. On the other hand, for a sample length of 1000, the experimental curve stays inside the red boundaries most of the time. Actually, when two samples separated by less than say 1000 bits are compared, the memory effect is present, otherwise there is no H.I. effect. These results are corroborated by the auto-correlation (Fig. 12) which is strong until the bit 600 approximately. They also fit with the average p-values shown in Tab. 6.

4.2 Long range spatial H.I.-like correlations

In a previous paper [4], one of us (T. D.) predicted that similar histograms are highly probable to appear at different geographical points at the same time on the basis of a genuine quantum hidden variable model incorporating the morphic resonance concept of Sheldrake [17]. We conceived a new experiment in order to study this prediction, based on the setup of Fig. 17, which is composed of two sub-setups (sub-setup A and sub-setup B). Each sub-setup consists of one source, one neutral density filter and one photodetector and is equivalent to the set-up described in the previous section that we used for testing the near-zone effect. The two sources are launched at the same time. In a first time we implemented the same H.I.I.

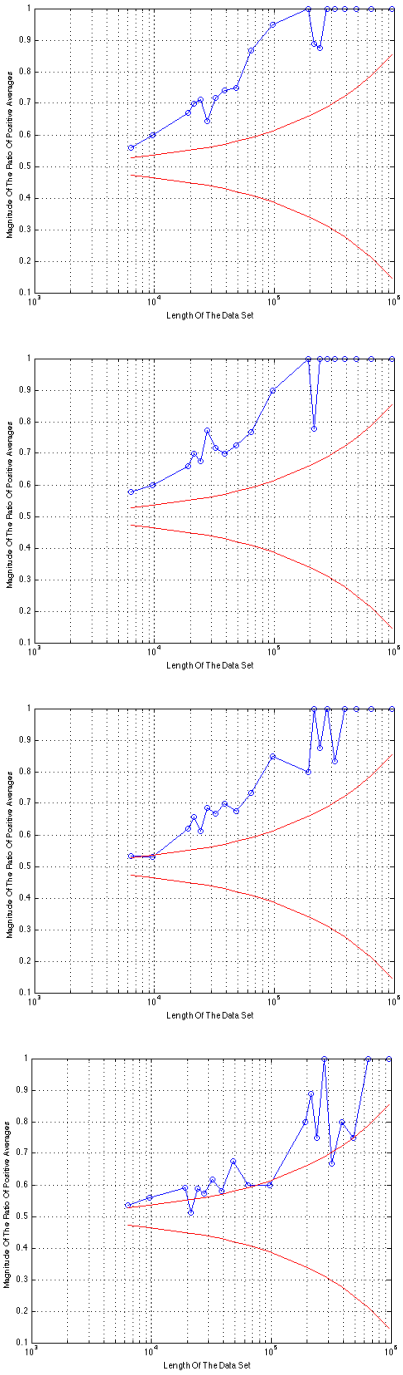

Fig. 13: Memory effect for the high intensity regime with sample length of 100 for the first (a), the second (b), the fifth (c) and the tenth neighbour (d).

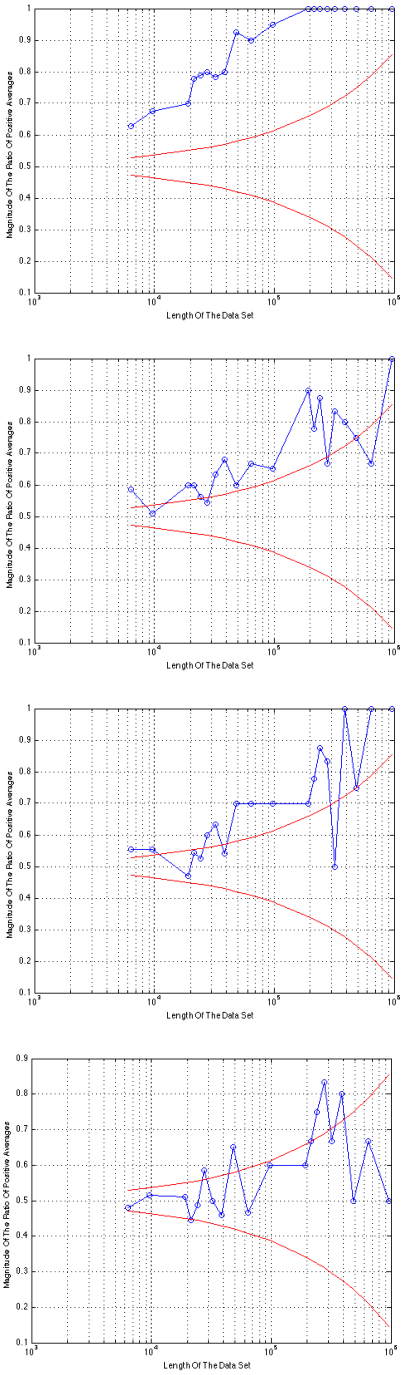

Fig. 14: Memory effect for the high intensity regime with sample length of 300 for the first (a), the second (b), the fifth (c) and the tenth neighbour (d).

test as in section 4.1 separately for each detector in order to check that each individual subset-up exhibits the near-zone memory effect. This can be seen for instance at the level of Tab. 1. The period of the near-zone memory effect is of the order of 500 clicks, as is corroborated by the auto-correlation tests in Figs. 18a and 18b.

In a second time, we adapted the H.I.I. test in order to be able to detect H.I.-like correlations between the two subset-ups. We have thus to compare the random series of time delays obtained in one photodetector (series A) with the random series obtained in the other photodetector (series B). Comparing both of them will determine whether the histograms are

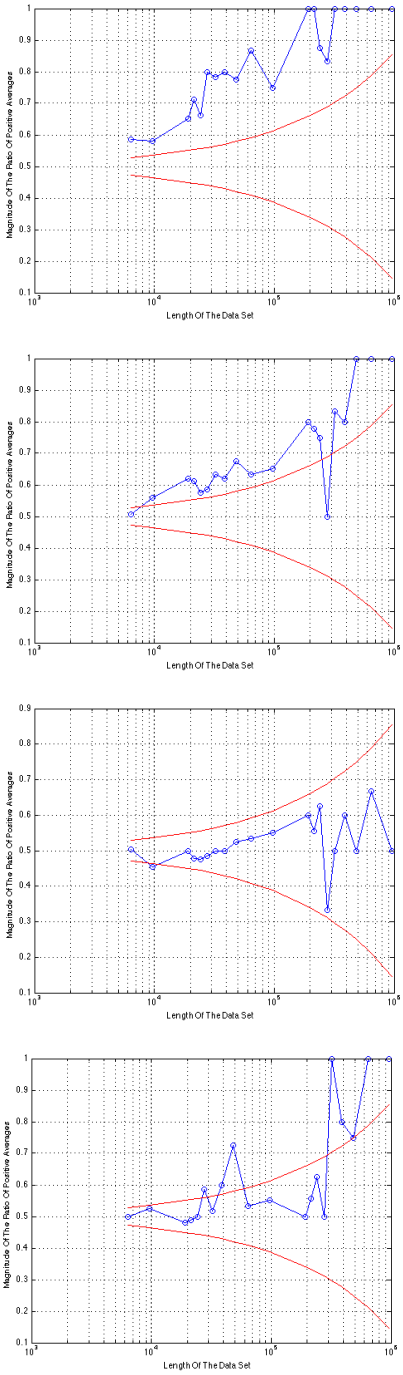

Fig. 15: Memory effect for the high intensity regime with sample length of 500 for the first (a), the second (b), the fifth (c) and the tenth neighbour (d).

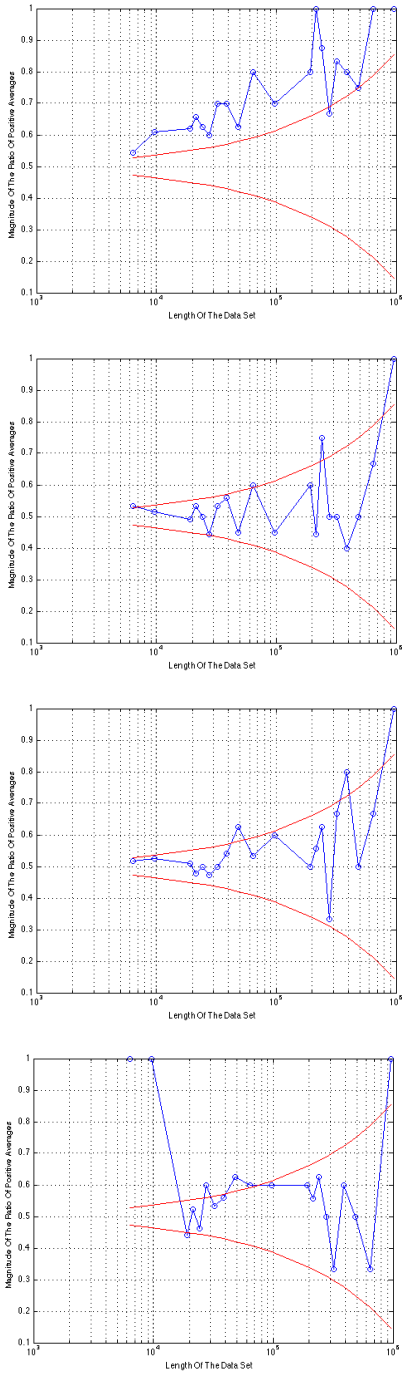

Fig. 16: Memory effect for the high intensity regime with sample length of 1000 for the first (a), the second (b), the fifth (c) and the tenth neighbour (d).

similar or not. In order to do so, a fixed sample length is selected (in our case, 100, 300, 500 and 1000) and we compare the histogram built from samples of this length extracted from series A with the corresponding histograms from series B, *i.e.* sample 1-100 of series A with the sample 1-100 of series B. We also compared neighbour histograms, like we did in section 4. This time we compare one histogram of series A with the neighbours of series B, *i.e.* for the first neighbour, sample 1-100 of series A with sample 101-200 of series B. We extended this procedure for the second, third, fifth, tenth and twentieth neighbour too. The results are encapsulated in Tab. 7. The average p-values are always quite larger than

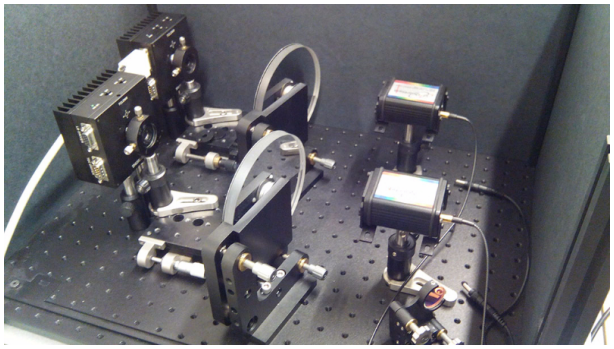

Fig. 17: Double set-up for detecting long range spatial H.I.-like correlations.

0.01, for all the cases, which shows that no observable spatial H.I.-like effect is present at the level of our experimental setup, even in the high intensity regime where individual setups exhibit a near zone memory effect. We checked by similar methods that in the low intensity regime no spatial H.I.-like effect is present. In both regimes we also scrutinized the graphical presentations of the test results (that we do not reproduce here in order not to overload the presentation), which confirmed the conclusions already drawn from the estimate of the p-values.

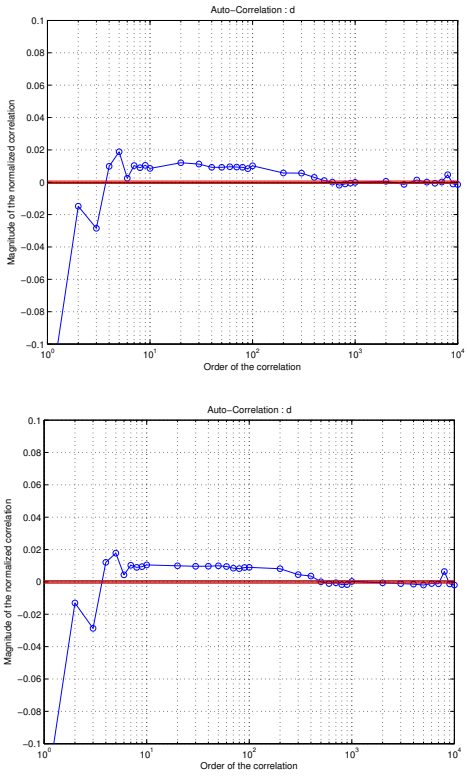

Fig. 18: Correlation for the data obtained in the two different photondetectors. Fig. (a) and Fig. (b) present a strong correlation.

Sample Length: 100	A	B
1 neighbor	0.0036	0.0033
2 neighbor	0.0071	0.0036
3 neighbor	0.0367	0.0094
5 neighbor	0.4984	0.3224
10 neighbor	0.4746	0.3269
20 neighbor	0.3191	0.3168

Tab. 1: p-values for the two sub-setups with a sample length of 100 bits for different neighbours (first, second, third, fifth, tenth and twentieth.

4.3 Long range temporal memory effects

The aforementioned periodic modulation of radio-active emission with a period of about 365 days [9, 10], suggests that the phenomenon has a cosmophysical origin. We therefore investigated the possibility to generalize these observations in the case of a quantum signal. We focused on the 24-hour period experiment due to the large amount of time that we would have spent in tracking yearly memory effects. The 24-hour period would be an indication of the existence of an external agent that influences the object of study, most probably the rotation of the Earth. Our aim was to probe the existence of this effect at the level of the quantum signal obtained from our QRNG. For our experiment we used the same setup as in the near-zone experiment in section 4. It consists again of a laser source, a collimating lens, two neutral density filters and one avalanche photo-diode.

In February 2015, we realized a series of experiments, after having synchronized our computer clock with an atomic clock from the nist.gov website* in such a way that all the measurements were automatized. Then, the runs were performed at exactly the same time every day for three consecutive days and we performed 20 different experimental runs with an interval of 20 second between each of them†.

We estimated, based on the slope of the semi-logarithmic plot of the histogram of delay times, the average time delay and we found that the drift was small, with average times comprised in the interval 45-52 ns. Thereafter we estimated the individual H.I.I. p-values which measure the cross-correlations between the samples of days 1 and 2, of days 2 and 3, and of days 1 and 3. The results are encapsulated in Tab. 2.

*The procedure for doing so is available on the website http://www.nist.gov/pml/div688/grp40/its.cfm

† We learn from wikipedia that... *"A synodic day is the period it takes for a planet to rotate once in relation to the body it is orbiting. For Earth, the synodic day is known as a solar day, and is about 24 hours long. The synodic day is distinguished from the sidereal day, which is one complete rotation in relation to distant stars. A synodic day may be "sunrise to sunrise" whereas a sidereal day can be from the rise of any star to the rise of the same star on the next day. These two quantities are not equal because of the body's movement around its parent"...* Henceforth we expect a difference between the sidereal and synodic (solar) day to be of the order of 24x3600/365 second, more or less 240 second. Our measurements cover 400 second, which allows us to address at the same time the synodic and sidereal periods

Total number of p-values: 3380
Day 1 Day 2
Number p-values < 0.01 = 272
Number p-values < 0.1 = 978
Day 2 Day 3
Number p-values < 0.01 = 284
Number p-values < 0.1 = 980
Day 1 Day 3
Number p-values < 0.01 = 221
Number p-values < 0.1 = 988

Tab. 2: Statistics of "pathological" p-values, from consecutive random series separated by 24 or 48 hours.

Total number of p-values: 8000
Day 1 Day 2
Number p-values < 0.01 = 123
Number p-values < 0.1 = 1195
Day 2 – Day 3
Number p-values < 0.01 = 152
Number p-values < 0.1 = 1201
Day 1 – Day 3
Number p-values < 0.01 = 104
Number p-values < 0.1 = 1185

Tab. 3: Statistics of "pathological" p-values, from pseudo-random series.

There were 13 runs each day and from each pair of runs we extracted twenty p-values (each of these values is associated to a point on a graph similar to, for instance, the plots in Fig. 11). By doing so, for each pair of days, we were able to estimate 13 times 13 times 20 = 3380 p-values from the cross-correlations between samples extracted at different days.

In order to properly calibrate the statistical distribution of p-values we did two things:

A) we generated sixty runs of Poisson distributed time series characterized by an average time of the order of 50 ns. The duration of each series was the same as the duration of each experimental run. We arbitrarily assigned a day to each of them, according to the rule 1-20 → day 1, 21-40 → day 2, 41-60 → day 3. Then we considered the 400 (20 times 20) cross-correlations between the data "extracted at different days" and estimated the corresponding p-values, following the same algorithm already used for establishing Tab. 2. The results are encapsulated in Tab. 3.

B) We also estimated through the same method the H.I. cross-correlation between samples that were measured in June 2014 and those measured in February 2015. Here again there were three runs of 13 samples, measured at different days, after a period of the order of 24 hours each time, and also in the high intensity regime, but the timing of the data collected in June 2014 was not automated. We estimated correlations between data measured in days 1, 2 and 3 in June 2014 and those measured in days 1, 2 and 3 in 2015. The results are summarized in Tab. 4.

Total number of p-values: 3380
Day 1 in June 2014 Day 1 in February 2015
Number p-values < 0.01 = 112
Number p-values < 0.1 = 578
Day 2 in June 2014 Day 1 in February 2015
Number p-values < 0.01 = 82
Number p-values < 0.1 = 526
Day 1 in June 2014 Day 3 in February 2015
Number p-values < 0.01 = 91
Number p-values < 0.1 = 521

Tab. 4: Statistics of "pathological" p-values, from consecutive random series measured in June 2014 and February 2015.

For obvious reasons, we consider that the statistical distribution of "pathological" p-values which appears in Tabs. 3 and 4 is representative of uncorrelated data. Indeed, pseudo-random series do not exhibit any memory effect, and we do not expect that data measured in June 2014 and February 2015 are correlated. This is confirmed by a comparison of those tables: if we consider the occurrence of p-values smaller than 0.1, we find a probability of the order of 0.15 in each case*.

On the contrary, in Tab. 2 the occurrence of p-values smaller than 0.1 is of the order of 0.29, twice more, which reveals the existence of a systematic memory effect, persisting after 24 hours. We consider therefore that our observations confirm the existence of long range temporal H.I.-like correlations of periodicity of the order of 24 hours, which appears, at least in our eyes, to be a very surprising result.

5 Conclusions and discussions

In this paper we studied the H.I. effect, which, roughly, would manifest itself through a tendency of random series to present analogous departures from their mean statistical behaviour. This tendency would possibly characterize data collected in the same temporal interval (what we denoted the near zone memory effect) but could present non-local features (non-local in time and/or space), what we denoted the long range temporal (resp. spatial) memory effect.

Our main goal was to study experimentally whether or not a memory effect of the H.I. type was present in the single photon regime. We developed a new, self-cooked algorithm, described in section 2 in order to realize this objective.

*At first sight we ought to expect 0.1 instead of 0.15, but we must have in mind that the p-value derived by us corresponds to a situation where the sign of the parameter r defined at the level of (1) was negative in exactly fifty percent of the cases and positive in fifty percent of the cases, which is of course an assumption that is not always strictly verified. From this point of view, the p-value defined by (7) ought not to be considered as an exact p-value but still plays the role of a valuable indicator.

Sample Length	1^{st} Neighbor	2^{nd} Neighbor	5^{th} Neighbor	10^{th} Neighbor
100	0.4762	0.6031	0.6048	0.3997
300	0.4515	0.5647	0.4537	0.5269
500	0.5323	0.3049	0.4101	0.4614
1000	0.4105	0.4745	0.5121	0.2665

Tab. 5: p-values extracted from the H.I. test for the low intensity regime for different sample lengths and different neighbours.

Sample Length	1^{st} Neighbor	2^{nd} Neighbor	5^{th} Neighbor	10^{th} Neighbor
100	0.0037	0.0043	0.0219	0.1005
300	0.0033	0.1100	0.1489	0.4066
500	0.0042	0.1098	0.6511	0.4410
1000	0.0304	0.4866	0.4876	0.3305

Tab. 6: Parity Method: Results of the file generated with the Split Method applying the NIST test battery.

Sample length	0^{th} neighbour	1^{st} neighbour	2^{nd} neighbour	3^{rd} neighbour	5^{th} neighbour	10^{th} neighbour
100	0.4330	0.5725	0.4067	0.4844	0.4530	0.5348
300	0.4608	0.5303	0.2870	0.2363	0.3765	0.3965
500	0.4508	0.4930	0.5378	0.4623	0.3572	0.0361
1000	0.5029	0.4965	0.4373	0.3953	0.2483	0.1399

Tab. 7: p-values when series A and B are compared for different sample length (100, 300, 500 and 1000 bits) for different neighbours (first, second, third, fifth, tenth and twentieth.

Our conclusions are the following:

A) The near-zone H.I. memory effect is well present in the single photon regime, but only in the high intensity regime (for which the dead time is comparable to the average time between two photons). As we discussed in section 3.2, the limit of low intensities (when the dead time is quite larger than the average time between two photons) corresponds to the genuinely quantum regime, and in this regime no memory effect is present. This goes in the sense of the conclusion [19] drawn from the study of the SeQuR QORNG, for which the H.I. effect could be explained in terms of external electromagnetic pollution, combined with an internal memory time (inertia) of the photodetector. The persistence of H.I.-like correlations after 24 hours (that we address below) is however more difficult to explain. Anyhow, we can safely conclude from our experiments and our analysis that "pure" quantum random series, collected in the low intensity single photon regime do not exhibit any kind of observable H.I.-like correlation.

B) We were unable to observe manifestations of a long range spatial memory effect but detected a systematic tendency indicating the possible presence of the long range temporal memory effect, even after 24 hours. Our preliminary result ought to be of course confirmed by supplementary studies. The door remains thus open for what concerns the "daily" effect. It is worth noting that, even if this effect gets definitively confirmed, its interpretation is not straightforward. It is well-known for instance that some noises in nature (and in particular at the surface of our planet) exhibit a 24 hours period. It could be that the daily memory effect merely reveals this feature.

In any case, we hope that, beside contributing to a better understanding of fundamental aspects of quantum randomness*, our study also brings new tools aimed at characterizing randomness in general. We actually consider that the H.I.I. test provides a new statistical test, complementary to the standard NIST tests, and in particular to the auto-correlation test.

As we have shown (*e.g.* in section 4.1.2), at the level of physical random number generators, when auto-correlation is present, the H.I. effect is most often present too, which is already remarkable in itself and suggests the existence of a universal memory effect.

Moreover, as shown in section 4.3, the long range temporal H.I. effect provide an example where the H.I.I. test reveals a systematic tendency, even in absence of auto-correlation (we checked for instance that the auto-correlation between data collected at different days (1,2,3) was uniformly flat).

We are still far away from one of our initial motivations, which was to be able to discriminate between physical randomness and pseudo-randomness thanks to the H.I.I. test†,

*In particular the main motivation of one of us (T. D.) was to investigate possible memory effects at the level of the quantum statistics, and finds its place in a series of works centered around this question [2–5, 7]

†In certain cases, pseudo-randomness can be revealed by measuring the

and the low intensity case provides a counterexample to the mere possibility of doing so in general, but at least, our measurements confirmed that the H.I. effect is present in nature in various regimes. In particular it is weakened but still present after a delay of 24 hours, which is very amazing. Therefore we are intimately convinced that it is important to pursue these investigations. For instance it would be interesting in the future to compare results obtained with our algorithm and those obtained by Shnoll and coworkers, making use of a quite different algorithm [8,14,18], and applying it to noise [15], not to quantum signal as we did, which addressed relatively short series of data (of the order of 30 clicks only), contrary to ours, where we systematically made use of the law of large numbers in order to estimate p-values.

Last but not least, it would be interesting to study the appearance of the H.I.-effect at various temporal and spatial scales, the present work constituting only a first probe in this direction.

Acknowledgements

Support from the B-Phot team, to his leader Hugo Thienpont, and the ICT Impulse Program of the Brussels Capital Region (Project Cryptasc) is acknowledged. Sincere thanks to Marco Bischof for drawing attention of one of us (T.D.) on Shnoll's work, some years ago.

Submitted on August 16, 2016 / Accepted on October 9, 2016

References

1. Calude C. S., Dinneen M. J., Dumitrescu M., and Svozil K. Experimental Evidence of Quantum Randomness Incomputability. *Physical Review A*, 2010, v. 82 (022102).
2. Durt T. About the Possibility of Supraluminal Transmission of Information in the Bohm-Bub Theory. *Helvetica Physica Acta*, 1999, v. 72, 356.
3. Durt T. Do Dice Remember? *International Journal of Theoretical Physics*, 1999, v. 38, 457.
4. Durt T. Quantum Mechanics and the Role of Time: Are Quantum Systems Markovian? *International Journal of Modern Physics B*, 2012, v. 26 (27&28), 1243005.
5. Durt T. Do Quantum Dice Remember? in Aerts D., Aerts S., and de Ronde C., eds. Probing the Meaning of Quantum Mechanics. World Scientific, Singapore, 2014, 1–24.
6. Durt T., Belmonte C., Lamoureux L-P., Panajotov K., Vanden Berghe F., and Thienpont H. Fast Quantum-Optical Random-Number Generators. *Physical Review A*, 2013, v. 87, 022339.
7. Durt T., Mathevet R., Robert J., and Viaris de Lesegno B. Memory Effects in Atomic Interferometry: A Negative Result, in Aerts D., Czachor M., Durt T., eds. Entanglement, Non-linearity, Quantum Structures and New Experiments, 2000, 165–204.
8. Fedorov M. V., Belousov L. V., Voeikov V. L., Zenchenko T. A., Zenchenko K. I., Pozharskii E. V., Konradov A. A., and Shnoll S. E. Synchronous Changes in Dark Current Fluctuations in Two Separate Photomultipliers in Relation to Earth Rotation. *Astrophysics and Space Science*, 2003, v. 283, 3–10.
9. Fischbach E., Buncher J. B., Gruenwald J. T., Jenkins J. H., Krause D. E., Mattes J. J., and Newport J. R. Time-Dependent Nuclear Decay Parameters: New Evidence for New Forces? *Space Science Review*, 2009, v. 145, 285–335.
10. Jenkins J. H., Fischbach E., Buncher J.B., Gruenwald J. T., Krause D. E., and Mattes J. J. Evidence of Correlations Between Nuclear Decay Rates and Earth-Sun Distance. *Astroparticle Physics*, 2009, v. 32, 42–46.
11. Jenkins J.H., Mundy D.W., and Fischbach E. Analysis of Environmental Influences in Nuclear Half-Life Measurements Exhibiting Time-Dependent Decay Rates. *Nuclear Instruments and Methods A*, 2010, v. 620 (2–3), 332–342.
12. Marsaglia G. The Marsaglia Random Number CDROM Including the Diehard Battery of Tests of Randomness, 1995, http://www.stat.fsu.edu/pub/diehard/.
13. Norman E. B., Browne E., Shugart H. A., Joshi T. H., and Firestone R. B. Evidence Against Correlations Between Nuclear Decay Rates and Earth-Sun Distance. *Astroparticles Physics*, 2009, v. 31, 135–137.
14. Panchelyuga V. A., Kolombet V. A., Panchelyuga M. S., and Shnoll S. E. Local-Time Effect on Small Space-Time Scale. arXiv: physics/0610137.
15. Rabounski D. and Borissova L. General Relativity Theory Explains the Shnoll Effect and Makes Possible Forecasting Earthquakes and Weather Cataclysms. *Letters to Progress in Physics*, 2014, v. 10 (2), 63–70.
16. Rukhin A., Soto J., Nechvatal J., Smid M., Barker E., Leigh S., Levenson M., Vangel M., Banks D., Heckert A., Dray J., and Vo S. Statistical Test Suite for Random and Pseudorandom Number Generators for Cryptographic Applications. NIST Special Publication, 2001, v. 800-22.
17. Sheldrake R. Une nouvelle science de la vie. Eds. du Rocher, Monaco, 1985.
18. Shnoll S. E., Colombet V. A., Pozharskii E. V., Zenchenko T. A., Zvereva I. M., and Konradov A. A. Realization of Discrete States During Fluctuations in Macroscopic Processes, *Physics-Uspekhi*, 1998, v. 43 (2), 1025–1035.
19. Vanden Berghe F. Quantum Aspects of Cryptography: From Qutrit Symmetric Informationally Complete Projective Operator Valued Measure Key Encryption to Randomness Quality Control. Ph.D. thesis, Vrije Universiteit, Brussels, 2011.

algorithmic complexity of a pseudo-random series, which delivers by then a criterion for discriminating quantum randomness from pseudo-randomness because, as has been shown elsewhere [1], quantum random series are incompressible.

Relativity and the Luminal Structure of Matter

Andrew Laidlaw

Calle Cuesta de los Cubos 17, Velez de Benaudalla, 18670, Spain

It is shown that Lorentz Invariance is a wave phenomenon. The relativistic mass, length contraction and time dilation all follow from the assumption that energy-momentum is constrained to propagate at the speed of light, c, in all contexts, matter as well as radiation. Lorentz Transformations, and both of the usual postulates, then follow upon adopting Einstein clock synchronisation. The wave interpretation proposed here is paradox free and it is compatible with quantum nonlocality.

1 Introduction

> *"But the division into matter and field is, after the recognition of the equivalence of mass and energy, something artificial and not clearly defined. Could we not reject the concept of matter and build a pure field physics? What impresses our senses as matter is really a great concentration of energy into a comparatively small space. We could regard matter as the regions in space where the field is extremely strong. In this way a new philosophical background could be created."* — Einstein & Infeld [1].

Modern Physics relies heavily on relativistic wave equations, especially the d'Alembert, Helmholtz and Dirac [2] equations, that feature either propagation at the characteristic velocity, c, or a velocity operator of constant modulus equal to c [3]. There are also many Lorentz covariant classical field theories in the literature, including nonlinear theories with subluminal soliton solutions that serve as candidate models for the fermions. [4–10] are just a few to illustrate the diverse range of approaches. This Article shows that the first, necessary step towards achieving Einstein's dream of a pure field physics is to recognise that, whether it appears as radiation or as matter, energy is a propagative phenomenon.

We shall consider the basic mechanics of luminal wave systems, *i.e.* systems of waves that propagate at c. Adapting the Newtonian momentum equation, $p = mv$, for use with constant speed luminal waves and then applying universally accepted basic principles of mechanics to luminal waves leads to a general structural analysis of luminal wave systems that is inherently relativistic without asserting any principle of relativity. The usual relativistic mechanics of matter can thus be interpreted as the basic mechanics of subluminally moving systems constructed entirely from luminal waves.

The proposed luminal wave ontology provides new perspectives on many issues including the Dirac velocity operator, angular momentum quantisation, the structure of Electromagnetics [11], gravity [12], the existence of nonlocal relations between observables, and interference phenomena in matter beams. The plan of the Article is as follows:

Section 2 defines the basic principles of mechanics that are regarded as universally accepted and identifies the simple general relationship that governs the connection between inertial frames for systems of luminal wave momenta. Section 3 shows that the usual relativistic momentum equation for particles applies to systems of luminal wave momenta. Section 4 derives the (forward) relativistic transformation of wave momenta in a form that is useful for analysing wave systems as a whole. Section 5 extends the results to any kind of luminal wave system, provided a wave vector in the direction of propagation can be defined, linear momentum is locally conserved, and propagation is luminal. In particular, linear superposition is not required so the method is applicable to nonlinear wave systems with subluminal soliton solutions.

For luminal waves the speed of propagation is, by definition, fixed and any luminal wave model of a subluminal massive particle is immediately subject to the kinematic constraint that, when the speed of the particle changes, the speed of its constituent wave components does not. Sections 6 and 7 show that length contraction and time dilation are the consequences of this kinematic constraint, so luminal systems display all the usual relativistic phenomena.

Section 8 addresses the question how the physical phenomena of length contraction and time dilation constrain the coordinate transformations. Selleri [13, 14] has shown that, subject mainly to the use of Einstein clock synchronisation, Lorentz Transformations follow directly from length contraction and time dilation, which are derived here from the basic principles of mechanics without making any further assumptions. As discussed in Subsection 8.2, the proposed wave interpretation is also equipped with a readily observable preferred frame, eliminating the paradoxes associated with the usual, relativist interpretation.

It remains only to point out, in Section 9, that any form of non-luminal structure for the massive particles is implausible, hence the conclusion reached is that the relativistic phenomena imply the luminal structure. Finally, Section 10 outlines the reasons why Lorentz Invariance does not preclude nonlocal relations between observables in this pure field context.

2 Basic physics of luminal waves

2.1 The basic principles of Mechanics

The usual classical field approach to mechanics in wave systems begins by choosing wave or field equations. Any analy-

sis is immediately limited to the mechanics of one particular kind of wave system. We would identify various solutions to the chosen equations, which are in general expressed as spatial distributions of some field variables. Field energy and momentum densities must be induced from these field variables. After evaluating the spatial integrals of the energy and momentum densities we would arrive at expressions for the momenta and energies of the wave solutions and we could begin the mechanics.

Unfortunately, in many circumstances we do not know what equations to use, much less their solutions. Moreover, the great variety of Lorentz covariant wave equations suggests that relativistic mechanics is a general feature that many wave systems have in common. What kind of wave systems? As mentioned in the introduction, the leading relativistic wave equations feature the characteristic velocity, suggesting that, when the field energy-momentum in a wave system is constrained to propagate at c (i.e. luminally), then the system displays the usual relativistic mechanics.

Therefore, instead of taking the usual fields approach to mechanics let us take a *mechanics* approach to *fields*, applying the basic principles of mechanics directly to a field energy-momentum density that propagates at c. The universally accepted principles to rely upon can be stated as follows:

1. The momentum of an object is defined as the product of its inertia times its velocity. Similarly, field momentum density is the product of inertia density and velocity.
2. Momentum is conserved. Field momentum is locally conserved.
3. The principle of local action means that wave objects, as defined below, may interact with each other only in regions of space where they overlap.
4. The force acting on an object is equal to its rate of change of momentum.
5. The resulting change in the energy of the object is given by the work integral.
6. Energy is conserved. Field energy is locally conserved.

Here 'wave object' means: some set of functions on a 3-space*, which together induce a field momentum density, $\vec{\rho_p}(x, y, z, t)$, that propagates luminally according to a unique unit wave vector, $\hat{\mathbf{k}}(x, y, z, t)$ and whose spatial integral, $\int\int\int_{-\infty}^{+\infty} \vec{\rho_p}(x, y, z, t)\, dxdydz$, is finite.†,‡,§

*That is, spatial distributions of field variables.

†In addition to inducing the field momentum density, the space functions that define wave objects in a nonlinear field theory may also act as sufficient causes for any interactions that there may be.

‡Note that infinite plane waves are not wave objects.

§Neither the propagation of the space functions nor their relation to the linear momentum density are specified here. This allows for wave objects with intrinsic field angular momentum and, more generally, the definition accommodates two kinds of internal evolution, via the internal movements of an otherwise invariant set of functions and via their individual time evolutions.

We are interested in the mechanics of systems that comprise multiple wave objects. This begins with non-interacting systems, where the wave objects are not presently interacting with each other. The next Subsection focusses on the case where each object's unit wave vector, $\hat{\mathbf{k}}(x, y, z, t)$, is a constant vector, independent of x, y, z and t. The momentum density distribution of such wave objects moves through space in a self similar form at c. We shall refer to this special kind of wave object as a light flash.

2.2 Application to light

Consider a source that simultaneously emits a set of N light flashes in various directions. The development here can be applied to any kind of light flashes, including individual photons, short segments of laser beams, or collimated beams in general, monochromatic or not. We require only that each flash propagates at c, carrying a finite linear momentum in a well-defined direction in space.

Let the i^{th} light flash carry linear momentum $\mathbf{p}_i$. According to the first basic principle, momentum equals the product of inertia and velocity and the wave inertia of the i^{th} light flash is therefore defined as $m_i = p_i/c$, where $p_i = |\mathbf{p}_i|$ is the magnitude of the momentum of the i^{th} light flash, also called the 'scalar momentum':

$$p_i = m_i\, c\,. \tag{1}$$

This Article is essentially a consistent application of the basic mechanics principles, using (1) in place of the familiar $p = mv$, where the speed v is a variable. Note that, *prima facie*, the inertia, m_i, of a wave propagating in a well-defined direction in space has nothing to do with the mass of a particle. However, we use the symbol m_i because, unless they ALL propagate in the same direction, the total inertia of a set of N waves will be found to correspond to the usual, relativistic particle mass. The time differential of (1) is:

$$\frac{dp_i}{dt} = c\,\frac{dm_i}{dt}\,. \tag{2}$$

Having fixed the propagation speed, c, changes of the scalar momentum are thus associated with changes of the wave inertia. It will become clear in Sect. 8 that the inertia changes we will be discussing throughout this Article are in fact frequency changes. Such changes may be due to a change of observer or they may be physical changes due to any forces that are acting on the wavefield.

In general, if a force acts on a light flash then, since (2) is the force component parallel to the light flash's motion, the work integral is:

$$W = \int_{p_s}^{p_f} \frac{d\mathbf{p}}{dt}\cdot d\mathbf{s} = \int_{m_s}^{m_f} c\,\frac{dm}{dt}\,cdt = (m_f - m_s)\,c^2\,, \tag{3}$$

where subscripts s and f refer to the words 'start' and 'finish'. The radiation reaction force that acts on a light flash

reflected by a moving mirror is an example that highlights the role of the work integral in a basic mechanics calculation*. According to the fifth basic principle, the work done equals the energy change, and we may assume that a light flash that has zero momentum requires zero energy, so the energy of the i^{th} flash is:

$$E_i = m_i c^2 = c p_i . \quad (4)$$

According to the second basic principle, momentum is conserved so the total momentum of a set of N wave objects is given by the vector sum over their momenta:

$$\mathbf{P} = \sum_{i=1}^{N} \mathbf{p}_i . \quad (5)$$

Suppressing the summation range henceforth, we write the total inertia as $m_e = \sum_i m_i$. The total energy of the set is then:

$$E = \sum_i c p_i = m_e c^2 . \quad (6)$$

According to the (first and second) basic principles, the velocity of the centre of inertia of a system of objects is the inertia weighted average velocity, $\mathbf{V} = \sum_i m_i \mathbf{v}_i / \sum_i m_i$, so that:

$$\mathbf{V} = \frac{\sum_i \mathbf{p}_i}{m_e} \Rightarrow \mathbf{P} = m_e \mathbf{V} . \quad (7)$$

For a relativistic analysis, these basic Equations (1) - (7) must be good for any observer, however, since we intend *inter alia* to show it, no principle of relativity will be asserted *a priori*. Consider an incremental change that affects the system of light flashes as a whole. For example, an incremental change in the condition of motion of the observer would alter all his observations of the $\mathbf{p}_i$. Similarly, a single observer considering light flashes emitted by otherwise identical sources that are in different conditions of motion will find different values for the $\mathbf{p}_i$. Since these two cases are not *a priori* assumed equivalent, consider the latter one, and consider, specifically, two otherwise identical sources moving at velocities $\mathbf{v}$ and $\mathbf{v} + d\mathbf{v}$ in the inertial frame of a single inertial observer.

This scenario closely corresponds to applying a Lorentz boost to a system of wave momenta. We may write the momenta of the light flashes as $\mathbf{p}_i$ and $\mathbf{p}_i + d\mathbf{p}_i$ respectively and their totals as $\mathbf{P}$ and $\mathbf{P} + d\mathbf{P}$. We are interested in how the $d\mathbf{p}_i$ are related to $d\mathbf{P}$. As shown in Appendix 2, this is determined by the relevant known facts, the relativistic Doppler shift and aberration phenomena, which together imply:

$$d\mathbf{p}_i = \frac{p_i}{m_e c} d\mathbf{P} . \quad (8)$$

We are assuming neither Special Relativity nor the relativity principle by referring to these phenomena. Indeed, while Lorentz Transformations correctly imply each of them, there exist other coordinate transformations [13] that also correctly predict these observables [15]. Because (8) is a direct consequence of the phenomena themselves, it necessarily applies to any theory that correctly accounts for them†.

It is nonetheless relevant to consider what, if anything, the facts here are introducing over and above the basic principles stated above. If our coordinate transformations are to be linear and homogeneous, as is usually assumed, then $d\mathbf{p}_i$ will be linear in p_i. Similarly, when considering the case of a single light flash, (the case $N = 1$), $d\mathbf{p}_i$ should be linear in, and parallel to, any incremental change of momentum of the light source, $d\mathbf{P}_{LS}$, prior to emission. Since the same applies to each of the light flashes in our system it follows that $d\mathbf{p}_i \propto d\mathbf{P}$ and we can safely assume that: $d\mathbf{p}_i = \alpha_i p_i \, d\mathbf{P}$.

Eq. (8) means that all the weights, α_i, are the same, $\alpha_i = \alpha$. Summing over i gives $\alpha = 1/m_e c$ (since $\sum_i d\mathbf{p}_i = d\mathbf{P}$). In particular, under an incremental momentum boost of the whole system, the momentum shifts, $d\mathbf{p}_i$, applied to the various wave momenta, $\mathbf{p}_i$, depend linearly on their energies but not on their directions of propagation, $\hat{\mathbf{k}}_i$.

The next two sections show how (8) governs the connection between inertial frames for systems of luminal wave momenta. In order to avoid asserting the relativity principle, the boost will not presently be associated with a change of observer. It will turn out to work relativistically, but for the present purposes the incremental momentum boost, (8), has only the restricted meaning of an incremental change $d\mathbf{v}$ in the velocity of a light source, the result of which is to add $d\mathbf{P}$ to the total wave momentum by adding wave momentum $d\mathbf{p}_i$ to each of the N constituent light flashes‡.

3 The relativistic momentum

This section shows that systems of luminal wave momenta that are connected by incremental momentum boosts obey the usual relativistic momentum equation for particles.

In subsection 2.2, the incremental change in the scalar momentum of the i^{th} light flash, dp_i, is given by the component of $\mathbf{dp}_i$ parallel to $\mathbf{p}_i$, which is:

$$dp_i = d\mathbf{p}_i \cdot \frac{\mathbf{p}_i}{p_i} .$$

Substituting (8) in this gives $m_e c \, dp_i = \mathbf{p}_i \cdot d\mathbf{P}$. Noting that $\sum dp_i = c \, dm_e$, summing over i gives $c^2 m_e dm_e = \mathbf{P} \cdot d\mathbf{P}$, and integrating this we obtain the common expression for the invariance of the 4-momentum:

$$m_e^2 c^2 = P^2 + m_0^2 c^2 , \quad (9)$$

*See Appendix 1, which shows that the ratio of reflected and incident momenta is the square of the relativistic doppler shift.

†When Appendix 1 is generalised to the case of non-normal incidence, the result is the product of the two relativistic Doppler shift and aberration operations involved. The basic principles are thus arguably sufficient to derive (8) by themselves, although the analysis is tedious.

‡Note that we do not need to assume that $d\mathbf{V} = d\mathbf{v}$

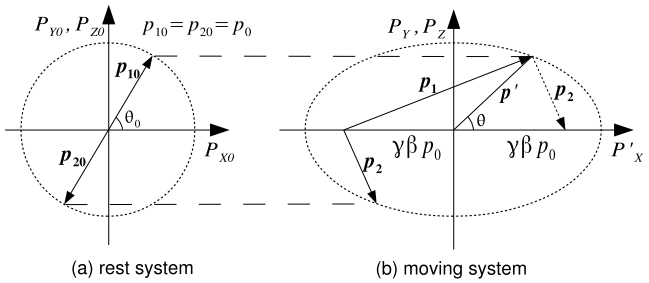

Fig. 1: Binary light flash systems whose centers of inertia are (a) at rest (b) moving at speed $V = \beta c$.

where m_0 is the value of m_e for $P = 0$. Let $\beta = V/c$ as usual so β is a +ve real number in the interval $[0, 1]$. The basic equations of relativistic mechanics, $\mathbf{P} = \gamma m_0 \mathbf{V}$ and $m_e = \gamma m_0$, where $\gamma = 1/\sqrt{1-\beta^2}$, follow upon substituting (7) into (9).

4 Wave system transformations in momentum space

In this section we show how the momenta of individual wave objects in a multi-object wave system transform under the action of (8).

By analogy to the usual comoving frame for massive particles, let us define the rest frame of a multi-object wave system as the (unique) inertial frame for which the right hand side of (5) vanishes. This definition is convenient, but not essential. Given the definition, let us now adopt the perspective of a single inertial observer who compares systems of light flashes emitted by two otherwise identical sources in different conditions of motion such that he considers one system's centre of inertia to be at rest, i.e. $\mathbf{P} = 0$ in (5) and $\mathbf{V} = 0$ in (7), and the other's to be moving at speed V in the x-direction, so that, from Section 3, $P = \gamma m_0 V$.

Let us refer to these two systems of light flashes as the 'rest system' and the 'moving system' respectively. We shall use a 0 subscript to refer to rest system momenta, so $\mathbf{P}_0 = \sum_i \mathbf{p}_{i0} = 0$. The analysis is expressed in momentum coordinates and it does not involve anything about spatial relations between the waves until Section 6.

The simplest case of a compound wave system where $\mathbf{P}_0 = 0$ consists of 2 light flashes of equal scalar momentum, $p_{10} = p_{20} = p_0$, propagating in opposite directions, as shown in Fig. 1a. The moving system is shown in Fig. 1b, where the x-components of the wave momenta, $\mathbf{p}_{10}$ and $\mathbf{p}_{20}$, have been modified in accordance with (8) so that the centre of inertia moves at speed V in the x-direction.

In Fig. 1a, $m_0 = (p_{10} + p_{20})/c = 2p_0/c$. Recalling from Section 3 that $m_e = \gamma m_0$, the sum of scalar momenta in the moving system of Fig. 1b is:

$$p_1 + p_2 = m_e c = 2\gamma p_0 \,, \tag{10}$$

whilst the total momentum, $\mathbf{P} = m_e \mathbf{V}$, is the vector sum of momenta:

$$\mathbf{P} = \mathbf{p}_1 + \mathbf{p}_2 = \frac{2\gamma p_0}{c}\mathbf{V} = 2\gamma\beta p_0 \,\hat{\mathbf{i}} \,.$$

Consider the vector $\mathbf{p}'$ in Fig. 1b, where $\mathbf{p}_1 = \mathbf{P}/2 + \mathbf{p}'$ and $\mathbf{p}_2 = \mathbf{P}/2 - \mathbf{p}'$. Using the law of cosines, its magnitude, p', is such that:

$$p_1^2 = p'^2 + (\gamma\beta p_0)^2 + 2\gamma\beta p_0 p' \cos\theta \tag{11}$$

$$p_2^2 = p'^2 + (\gamma\beta p_0)^2 - 2\gamma\beta p_0 p' \cos\theta \,, \tag{12}$$

where θ is the angle $\mathbf{p}'$ makes with the x-axis. Upon eliminating p_1 and p_2 from (10)-(12) we find that $p' = p'(\theta)$ is the ellipsoid:

$$p'(\theta) = \frac{p_0}{\sqrt{1-\beta^2\cos^2\theta}} \,. \tag{13}$$

Writing the momenta in component form as $\{p_{ij}\}_{i=1,2\,;\,j=x,y,z}$, (13) is then the ellipsoid:

$$(p'_x/\gamma)^2 + p_{iy0}^2 + p_{iz0}^2 = p_{i0}^2 \,,$$

where $p'_x = p_{1x} - \gamma\beta p_{10} = -(p_{2x} - \gamma\beta p_{20})$, so that the moving system momenta satisfy the following equation:

$$\left(\frac{p_{ix} - \gamma\beta p_{i0}}{\gamma}\right)^2 + p_{iy0}^2 + p_{iz0}^2 = p_{i0}^2 \,. \tag{14}$$

Eq. (14) is here derived only for the case N=2, however this equation also covers the general case, as we shall now show. Consider as initial condition an arbitrary system of light flashes, comprising a number $N \geqslant 2$ of wave momenta of scalar momentum p_{i0}, whose directions of propagation are distributed in space such that $\mathbf{P}_0 = \sum_i \mathbf{p}_{i0} = 0$ and $\sum_i p_{i0} = m_0 c$. In the rest system components are such that:

$$p_{ix0}^2 + p_{iy0}^2 + p_{iz0}^2 = p_{i0}^2 \,. \tag{15}$$

The example for $N = 2$ above suggests that after (8) acts on the set, bringing the total momentum to $\mathbf{P} = \gamma m_0 V \,\hat{\mathbf{i}}$, then (14) applies to the moving system momenta. Fig. 2 shows the moving system momenta when all the rest system scalar momenta are the same, i.e. $p_{i0} = p_0$ for all i. Differentiating (14) with respect to β gives:

$$\frac{dp_{ix}}{d\beta} = \gamma\,(p_{i0} + \gamma\beta p_{ix}) \,. \tag{16}$$

Expanding the first term in (14) and using $\gamma^2\beta^2 = \gamma^2 - 1$ gives:

$$p_i = \frac{p_{i0} + \gamma\beta p_{ix}}{\gamma} \,. \tag{17}$$

From $P_x = \gamma m_0 V$, we also have $dP_x = \gamma^3 m_0\, dV$, so that:

$$dp_{ix} = \frac{dp_{ix}}{dV} dV = \frac{dp_{ix}}{d\beta}\frac{dP_x}{\gamma^3 m_0\, c} \,. \tag{18}$$

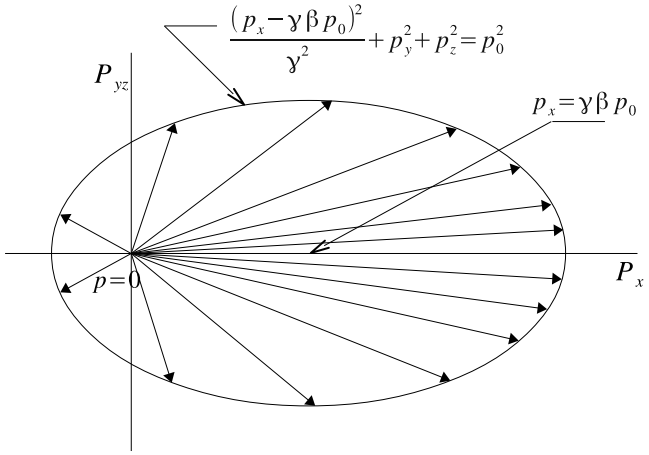

Fig. 2: Individual momenta in an isotropic wave system modified such that $V = \beta c$.

Finally, substituting (16) and (17) in (18):

$$dp_{ix} = \frac{p_i}{\gamma m_0 c} dP_x ,$$

which is the x-component of (8). Due to the choice of coordinates, the y and z components of momentum were unaffected, so the ellipsoidally modified distribution (14) is generated by the action of (8) on our arbitrary initial condition as expected. Comparing (14) and (15), the components of the moving system wave momenta are:

$$p_{ix} = \gamma(p_{ix0} + \beta p_{i0}) \;\; ; \;\; p_{iy} = p_{iy0} \;\; ; \;\; p_{iz} = p_{iz0} . \qquad (19)$$

Note that these physical transformations due to changes in the condition of motion of a light source are identical to Lorentz Transformations of wave momenta between different reference frames in standard configuration. However, as we are not asserting the Principle of Relativity there is no guarantee (so far) that our analysis works relativistically, and (19) corresponds only to the forward transformations of wave momenta in relativity theory.

We can now calculate the relative velocity of the i^{th} light flash, which is to say its velocity relative to the centre of inertia of the system, which our observer considers to be moving at V in the x-direction. The total velocity of the i^{th} flash has components $\{v_{ij} = c p_{ij}/p_i\}_{i=1..N\,;\,j=x,y,z}$. Using $\gamma^2\beta^2 = \gamma^2 - 1$ with (17) and (19), it is readily shown that the relative velocity, $\mathbf{v}_{ri}$, has components*:

$$v_{rix} = v_{ix} - V = \frac{c p_{ix0}}{\gamma p_i} \; ; \; v_{riy} = v_{iy} = \frac{c p_{iy0}}{p_i} \; ; \; v_{riz} = v_{iz} = \frac{c p_{iz0}}{p_i} .$$

If $\mathbf{v}_{ri}$ makes the angle ϑ_i with the x-axis, then:

$$\tan\vartheta_i = \frac{\sqrt{v_{riy}^2 + v_{riz}^2}}{v_{rix}} = \gamma \tan\vartheta_{i0} , \qquad (20)$$

*Since $\mathbf{V}$, $\mathbf{v}_i$ and $\mathbf{v}_{ri}$ are all referred to the same observer

where ϑ_{i0} is the corresponding angle in the rest system. Sect. 6 shows how this basic kinematic relationship leads to length contraction in 'pure field' models of the massive particles where all the field energy propagates luminally. Such models are discussed in the next section.

5 Luminal wave models of matter

Up to this point the analysis has dealt with systems of light flashes emitted by identical sources in different conditions of motion. No functional description of the light flashes was required, neither as photons nor as solutions to any particular wave equation. The fact that these systems obey the usual relativistic momentum equation for particles strongly suggests that the massive particles should also be thought of as luminally propagating field systems. This Section shows how the basic mechanics principles can be applied quite generally to compound, interacting systems of wave objects that are commensurate with modelling subluminally moving systems.

5.1 Compound wave systems

At any point in a system of disjoint light flashes (*i.e.* whose momentum densities do not overlap), there is a single field momentum density associated to a well defined unit wave vector. In principle, this field momentum density could be induced from a set of space functions in accordance with the definition of a wave object, so the entire system can be thought of as a single wave object, but there are also wave systems that cannot be represented as single wave objects.

Consider instead a system of N light flashes that propagate towards each other. When the field momentum densities of the various light flashes meet and overlap, the physical situation is inevitably such that there are multiple waves coexisting at the same place, propagating in different directions†. Since the set of space functions that comprises a wave object only induces a single momentum density at each point, when wave objects collide the luminal wave description necessarily involves multiple wave objects coexisting at the same place and time.

We shall now see that interactions between these distinct entities are required in order to construct luminal wave models of subluminally moving matter.

5.2 Forces, field variables and superposition

The force operating on a wave object is, by definition, equal to its rate of change of momentum, which is to say the space integral of the rate of change of its momentum density‡. Momentum is locally conserved, so forces necessarily manifest

†Note that the vector addition of two non-collinear luminal wave vectors is not a luminal wave vector because there is no wave actually propagating at c in the direction of the resultant vector.

‡There is also generally a rate of change of a wave object's momentum density at every fixed point due to the movement of the object, but the space integral of such changes obviously vanishes.

as reciprocal local exchanges of momentum between the momentum densities of the participating wave objects. These exchanges necessarily sum to zero locally as well as globally, so 'local action' can only mean that the objects' momentum densities must overlap. Now, when the momentum density distribution of a wave object changes then so must the field variables that induce it, so the essential nature of forces in a wave theory is to modify wave objects.

In a compound wave system formed by intersecting light flashes, if there were no forces between wave objects, then the momentum distributions pertaining to each object would not change as they move through each other, the same space functions could be retained for each wave object throughout the encounter and it is reasonable to think of each object's field variables as being the same as if it were by itself. A linear field theory is then appropriate. In Electromagnetics, for example, the wavefields interact with charges but not with each other. The chosen field variables, **E** and **H**, are force fields defined by the force that the wavefield exerts on a standard reference system, a 1 coulomb point charge. The global values of these field variables are given as linear superpositions of the *disjoint* values pertaining to individual wavefields.

In linear field theory, wave components evolve independently of each other, there are no interactions amongst the waves and any superposition must dissipate unless all of the wave vectors are parallel, in which case the motion of the centre of inertia of the wave group is $V = c$. Electromagnetic field models of subluminal massive particles are thus excluded. The idea that a finite subluminal image can be formed as an interference pattern can also be excluded as it requires infinite wave trains, which requires infinite energy. Therefore, the construction of luminal wave models for the massive particles requires multiple distinct wavefields that share the same space and interact with each other to form bounded systems, which is to say they form wave solitons.

When the wavefields in a model do interact with each other, the forces that are actually operating on a given wave object still superpose (by definition). However, as mentioned above, the definition of force also implies that wave objects are distorted under interaction. If the wave object is defined by force field variables, as in Electromagnetics, then its force fields (which are propensities to exchange momentum as opposed to actual forces) are not the same under interaction as would be the case if it had been disjoint. Furthermore, if a wave object in an interacting system persists in a self-similar form then that form depends in an essential way on the forces that are operating on it. It is obviously counterfactual to consider such an object as if it were disjoint from the others that are actually present. If they were not present, it would be a different object.

Overall, once we include interactions between wave objects, the global values of field variables cannot be expressed as a linear superposition of disjoint values so a nonlinear theory is required. If the chosen field variables are force fields, then global values are by definition still given as a linear superposition, but this is a linear superposition of *conjoint* values that correspond to actual transfers of wave momentum from one object to another.

Of course one might choose other field variables besides force fields. With water waves for example the vertical displacement of the water surface is commonly used as a field variable. Such alternatives also do not generally superpose linearly. Whatever field variables we may choose and however they may induce it, the field momentum density is locally conserved. As we shall see in the next two sections, the field momentum density is also the physical basis for any mechanical quantities that we may observe including not just momenta but also lengths and times.

5.3 Wave trajectories

Whereas a field variables description immediately confronts us with some unknown nonlinearity, we can focus directly on the inherently linear field momentum density by considering a wave trajectories description. This kind of description is often useful in Electromagnetics, where it arises from the field variables description as follows. Electromagnetic waves in a vacuum obey the well known d'Alembert wave equation:

$$\left\{\nabla^2 - \frac{1}{c^2}\frac{\partial^2}{\partial t^2}\right\}\psi = 0\,, \tag{21}$$

where $\psi(x, y, z, t)$ may be any component of either the Electric field **E** or the Magnetic field **H**. Electromagnetic waves involve both Electric and Magnetic fields and the linear momentum density is $\vec{\rho}_p = \mathbf{S}/c^2$, where the Poynting vector $\mathbf{S} = \mathbf{E}\times\mathbf{H}$ is aligned with the wave vector, **k** (which by definition points in the direction of propagation). The field lines of the wave vector trace out well defined trajectories at the ray velocity $v_{ray} = c$ (in vacuo) [16,17], and the linear momentum carried by the Electromagnetic wave propagates along these trajectories at the characteristic velocity.

Any luminal wave theory, linear or nonlinear, has a wave vector pointing in the direction of propagation, and once we have a wave vector, the wave trajectories description works as in Electromagnetics.

5.4 Closed wave systems

Whether we consider a subatomic particle or some macroscopic object, it is a basic premise that the energy that constitutes a persistent subluminally moving system must remain in the same general vicinity as the object. From the perspective of a luminal wave model where the energy is moving at c, any trajectory of the wave vector will remain bound to the system because any wave trajectory that leaves the system bleeds energy from it. Therefore, when considering luminal wave models for matter, we shall restrict our attention to closed trajectory systems, where the trajectories may or may not form closed loops, but any given trajectory remains within some finite distance of the centre of inertia of the system.

5.5 Towards coordinate transformations

In order for wave trajectories to remain bound to a subluminally moving centre of inertia they must be curved. Therefore, the unit wave vector for any given wave object in a closed system must be position dependent and may in general also be time dependent. Consequently, space functions that describe light flashes, where the unit wave vector is constant (see for example [18–20]), are unsuitable for describing closed systems, so we cannot think that the massive particles are constructed of light flashes. Therefore, we now require the incremental momentum boosts to operate directly on the momentum densities.

Eqs. (1) - (7) can be rewritten in terms of momentum densities, however it is more convenient to preserve the notation by converting momentum densities into momenta as follows. Let the entire space be divided into small regions of dimension $\delta x = \delta y = \delta z = \delta l$, where δl is sufficiently small that any of the momentum densities, $\overrightarrow{\rho}_{pi}(x, y, z, t)$, can be considered constant within each region so that $\overrightarrow{\rho}_{pi}(x, y, z, t)\,\delta l^3$ is a linear momentum propagating at c in a definite direction in space. Introducing a new subscript, k, to label the regions, we write the linear momentum of the i^{th} field in the k^{th} region as $\mathbf{p}_{ik}(t) = \overrightarrow{\rho}_{pi}(\mathbf{r}_k, t)\,\delta l^3$, where $\mathbf{r}_k$ is the position vector to the centre of the k^{th} region. Since the space integral of the momentum boost must recover (8) for all possible light flashes, the incremental momentum boost operating on the $\mathbf{p}_{ik}$ can only be:

$$d\mathbf{p}_{ik} = \frac{p_{ik}}{m_e c} d\mathbf{P}\,, \tag{22}$$

where $\mathbf{P} = \sum_k \sum_i \mathbf{p}_{ik}$, $p_{ik} = |\mathbf{p}_{ik}|$ and $m_e = \frac{1}{c}\sum_k \sum_i p_{ik}$, and the rest goes through as before.

The rest system in Sect. 4 could be a particle or any macroscopic system that is comoving with the observer. The moving system's internal momenta, $\mathbf{p}_{ik}$, are related to the $\mathbf{p}_{ik0}$ by (19), with an additional k subscript inserted. The system's momentum is $\mathbf{P} = \gamma m_0 \mathbf{V}$, where the velocity of the centre of inertia of the wavegroup, $\mathbf{V}$, is simply the observed velocity of the system. The relative velocity we developed at the end of the last section, $\mathbf{v}_{rik} = \mathbf{v}_{ik} - \mathbf{V}$, describes the internal movements of the system as seen by an observer who considers it to be moving at $\mathbf{V}$.

Since internal movements obviously change in response to changes in the observed velocity, neither the shape nor the internal evolution of a subluminally moving wave system can be assumed to be velocity independent so that, in order to determine coordinate transformations, we must first calculate the impacts this has on rulers and clocks constructed from luminal wave energy.

Before moving onto the analysis of length contraction and time dilation in luminal wave models let us contrast (22) with the Newtonian concept of a force field acting on a point-like massive particle. According to the fourth basic principle, the force acting on an interacting field is, by definition, equal to its rate of change of momentum*. It might appear at first blush that:

$$\frac{d\mathbf{p}_{ik}}{dt} = \frac{p_{ik}}{m_e c}\frac{d\mathbf{P}}{dt} \tag{23}$$

and the left hand side of (23) should be interpreted as the force acting on the i^{th} wave object in the k^{th} region when the total externally applied force acting on the particle is $\mathbf{F} = d\mathbf{P}/dt$. Such a dynamic interpretation requires making unreasonable extraneous assumptions, including not least a uniform applied field. This is unnecessary for our analysis, for which (22) applies to the relationship between systems in steady state conditions, before and after (but not necessarily during) some physical process that results in an incremental boost to the system's momentum. A one-to-one correspondence between the momentum densities of rest and moving systems is assumed, but without such an assumption no inherently relativistic structure would be possible because we could never equate a boost with a change of observer.

6 The Lorentz-Fitzgerald contraction

This section shows that closed wave trajectory systems contract in the direction of motion. This is easily understood by considering the special case of a rest system where the wave vector is transverse to the direction to the centre of inertia so that the system evolves under rotations and any wave trajectory exists on the surface of a sphere. Such systems are of particular interest because the usual interpretation [21] of the little group of transformations that preserves the linear momentum of a particle in Special Relativity is that rest particles evolve under the action of elements of the rotations group.

Consider a system of concentric spherical surfaces constructed about the rest system's centre of inertia, which we shall assume is at the origin. Given the abovementioned condition, all rest system wave trajectories through a given point, $\mathbf{r}_{k0}$, lie instantaneously in the tangent plane at that point to the sphere of radius r_{k0}. Without loss of generality, let us consider the trajectories passing through a point in the xy plane where the tangent plane makes the angle θ_0 with the x-axis, as shown in the top left of Fig. 3. The wave momentum along a trajectory lying in this plane has components in the form $p_{x0} = p_0 \cos\theta_0 \cos\phi_0$, $p_{y0} = p_0 \sin\theta_0 \cos\phi_0$, $p_{z0} = p_0 \sin\phi_0$, where ϕ_0 is the angle the trajectory makes with the xy plane. Note that this is just the component form of any of the $\mathbf{p}_{ik0}$. The i and k subscripts can be omitted without ambiguity: p_{x0} means p_{ikx0} and so on. Using (19), the components of the corresponding wave momentum in the moving system are:

$$p_x = p_0\gamma(\cos\theta_0 \cos\phi_0 + \beta)\ ;\ p_y = p_{y0}\ ;\ p_z = p_{z0}\,.$$

The moving system momenta for different values of ϕ_0 are not coplanar. As shown in the top right of Fig. 3, they lie on

*Donev and Tashkova [20] have also developed this within a field variables approach to luminally propagating bivector fields.

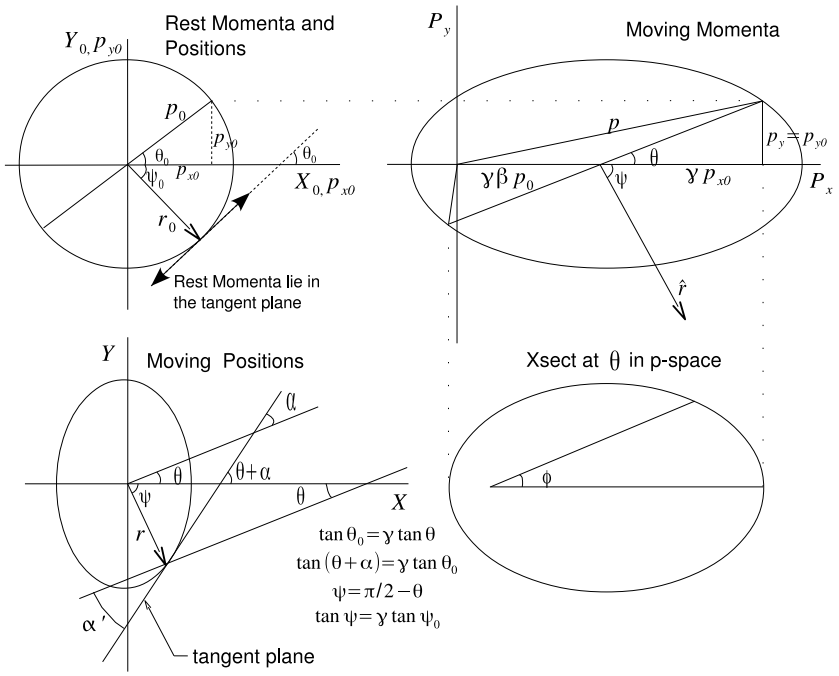

Fig. 3: Momenta and Positions in Rest and Moving Luminal Wave Particle Models.

a conical surface whose vertex is at the origin of momentum coordinates, and whose base is the intersection of the plane at angle θ, where $\tan\theta = \tan\theta_0/\gamma$, with the moving system momentum distribution. This elliptical intersection is shown in the bottom right of Fig. 3.

The (total) velocity for each of these momenta has components of the form $\{v_j = cp_j/p\}_{j=x,y,z}$, where p is given by (17):

$$p = \frac{p_0 + \gamma\beta p_x}{\gamma} = \frac{p_0}{\gamma}\left(1 + \gamma^2\beta(\cos\theta_0\cos\phi_0 + \beta)\right). \quad (24)$$

The group velocity is $V\hat{\mathbf{i}}$, so using (24) the relative velocity components are:

$$v_{rx} = \frac{cp_x - pV}{p} = \frac{cp_0\cos\theta_0\cos\phi_0}{\gamma p},$$

$$v_{ry} = \frac{cp_0\sin\theta_0\cos\phi_0}{p} \text{ and } v_{rz} = \frac{cp_0\sin\phi_0}{p}.$$

The ratio $v_{ry}/v_{rx} = \gamma\tan\theta_0$ is independent of ϕ_0 (and ϕ), so the velocities that lay in a given tangent plane in the rest system transform into relative velocities lying in a corresponding moving plane, tangent to the moving trajectory system*. Let α be the angle between the plane at θ and the tangent plane, as shown in the bottom left of Fig. 3. The moving system tangent plane makes the angle $\alpha + \theta$ with the x-axis, where $\tan(\theta+\alpha) = v_{ry}/v_{rx} = \gamma\tan\theta_0 = \gamma^2\tan\theta$. Using the angle sum trigonometric relations we obtain:

$$\tan\alpha = \frac{\beta^2\sin\theta\cos\theta}{1 - \beta^2\cos^2\theta}. \quad (25)$$

The set of all tangent planes defines the surface up to a scale factor. Due to rotational symmetry we can anticipate being able to write the equation describing this surface in the form $r = r(\psi)$, where ψ is the angle from the position vector to the x-axis. For any function $r(\psi)$ the angle between the tangent plane and the plane transverse to the radius vector is:

$$\tan\alpha' = \frac{1}{r}\frac{dr}{d\psi}. \quad (26)$$

Consider as trial function the ellipsoid:

$$r(\psi) = \frac{\lambda}{\sqrt{1 - \beta^2\sin^2\psi}}, \quad (27)$$

for which

$$\tan\alpha' = \frac{\beta^2\cos\psi\sin\psi}{1 - \beta^2\sin^2\psi}, \quad (28)$$

independent of the scale parameter λ. With $\psi = \pi/2 - \theta$, this is identical to (25), which therefore describes an ellipsoid of revolution (27), such that the plane at θ is transverse to the position vector, $\mathbf{r}$, shown in the bottom left of Fig. 3.

*Recall that we showed in Section 4 that the relative velocity of any trajectory is rotated by the kinematic relation $\tan\vartheta = \gamma\tan\vartheta_0$, where ϑ was the angle $\mathbf{v}_r$ makes with the x-axis. We now see the consequence of the little group: Locally flat surfaces formed by sets of trajectories at a given point in the rest system transform into locally flat moving surfaces, rotated so that the tangent of the angle the moving surface makes with the x-axis is $\gamma\tan\theta_0$, where θ_0 is the angle the rest system surface makes with the x-axis.

The scale factor, λ, is readily found by inspection. The moving system equatorial plane is the plane $x = Vt$ and $\psi = \pi/2$. The tangent plane at any point in the equatorial plane is parallel to the x-axis so the $d\mathbf{p}_{ik}$ at these points lie in the tangent plane. Therefore the equatorial tangent planes are not altered by the action of (22). Therefore the radius of a circumferential trajectory in the equatorial plane is invariant under the dimensional transformation (27), and $\lambda = r_0/\gamma$, where r_0 is the radius of the spherical surface in the rest system.

The result is that, for our rest observer, any wave trajectory in the moving system lies on the surface of an ellipsoid moving along the x-axis at speed V and of the form:

$$r(\psi) = \frac{r_0}{\gamma\sqrt{1-\beta^2\sin^2\psi}}\,. \tag{29}$$

The moving system wave trajectories are thus compressed by the factor γ in the direction of motion. Let us now consider general wave trajectories that are not confined to the surfaces of spheres in the rest system. The analysis above shows that any short segment of the general trajectory is rotated so that the ratio of its dimensions parallel and transverse to V is suppressed by γ. Since this applies to every segment it applies to entire trajectories and since we have already identified specific trajectories whose transverse dimensions are invariant, the same scale factor applies to the general case.

Closed luminal wave trajectory systems are thus physically compressed by the factor γ in the direction of motion so that any macroscopic physical objects, including rulers, that are constructed entirely from luminal wave energy undergo the usual Lorentz-Fitzgerald length contraction.

7 Time dilation

It can be seen from (7) and Fig. 2 that any movement of a closed luminal wave system through space is the result of correlations amongst the directions of propagation of the internal momenta, $\hat{\mathbf{k}}_i(x, y, z, t)$. On the other hand, if all the trajectories of a wave system were exactly parallel the spatial configuration of the system would not change and there would be no internal evolution. Just as correlations are necessary for movement in space, decorrelations are necessary for evolution in time. There is a direct tradeoff involved, so some form of time dilation is an inevitable consequence of constructing variable speed particles from fixed speed waves.

We shall now show that internal processes in wave systems slow down according to $dt/dt_0 = 1/\gamma$. The analysis is similar to the standard analysis of a light clock.

With respect to the rest system's wave trajectory system, consider any closed trajectory formed by n segments, where the i^{th} segment has length l_{i0} and makes the angle θ_{i0} with the x-axis. The speed on all segments is $v_0 = c$ so the period around the closed trajectory is $T_0 = \frac{1}{c}\sum_{i=1}^{n} l_{i0}$, where T_0 is the time elapsed on a clock in the rest frame to traverse the trajectory in the rest system. Lengths in the rest system may be written in component form such that:

$$l_{i0}^2 = l_{ix0}^2 + l_{iy0}^2 + l_{iz0}^2\,.$$

Let the trajectory system now move in the x-direction at speed V. Given the length contraction, x-components contract by the factor γ and the corresponding relationship is:

$$l_i^2 = \frac{l_{ix0}^2}{\gamma^2} + l_{iy0}^2 + l_{iz0}^2\,.$$

It is readily shown that:

$$l_i^2 = l_{i0}^2(1-\beta^2\cos^2\theta_{i0})\,. \tag{30}$$

The moving and rest system angles are related by $\tan\theta_i = \gamma\tan\theta_{i0}$, from which it is easily shown that:

$$\frac{\cos\theta_i}{\cos\theta_{i0}} = \sqrt{1-\beta^2\sin^2\theta_i}\,. \tag{31}$$

The relative velocity on the i^{th} segment in the moving system, v_{ri}, is constrained by:

$$(v_{ri}\cos\theta_i + V)^2 + v_{ri}^2\sin^2\theta_i = c^2\,, \tag{32}$$

which leads to: $v_{ri} + V\cos\theta_i = c\sqrt{1-\beta^2\sin^2\theta_i}$, from which, using (31):

$$v_{ri} = \frac{l_{ix0}\,c\,(1-\beta\cos\theta_{i0})}{\gamma l_i\cos\theta_{i0}}\,.$$

The time taken to traverse the i^{th} segment in the moving system is $l_i/v_{ri} = l_i^2/v_{ri}l_i$, so, using (30), we may write the period elapsed on clocks in the rest system for traversals around the Lorentz contracted moving system trajectory as:

$$T_0^V = \sum_{i=1}^{n}\frac{l_i^2}{v_{ri}l_i} = \frac{\gamma}{c}\sum_{i=1}^{n} l_{i0}(1+\beta\cos\theta_{i0})\,.$$

Since $\sum_i l_{i0}\cos\theta_{i0} = 0$ it follows that $T_0^V = \gamma T_0$. It might be argued that trajectories need not form closed loops, but a path that crosses a given plane transverse to $\mathbf{V}$ must eventually either recross the same plane or become confined to a smaller region, in which it must either routinely recross a transverse plane or become confined to an even smaller region and so on. In steady state, the trajectories can only be transverse or regularly recross a transverse plane. The analysis above also covers open paths between points in the same transverse plane, for which the condition $\sum_i l_{i0}\cos\theta_{i0} = 0$ is also fullfilled. The time between such crossing points dilates by γ. We conclude that the internal processes of a luminal wave system slow down by the factor γ. The argument from internal processes to real world clocks is well established [23], and tested [24–26], so moving clocks will run slow according to the usual relation $dt/dt_0 = 1/\gamma$.

A similar tradeoff occurs in the Dirac Equation. Consider the equation for the time dependence of the velocity operator in the Heisenberg representation of the Dirac theory [22]:

$$\overrightarrow{\alpha}(\mathrm{t}) = \left(\overrightarrow{\alpha}(0) - \frac{\mathbf{p}}{\mathrm{H}}\right)\exp\left(-2i\mathrm{H}t\right) + \frac{\mathbf{p}}{\mathrm{H}}\,, \qquad (33)$$

where $\mathbf{p}$ and H are both constants, $c = 1$ and the group velocity is $\mathbf{p}/\mathrm{H} = \mathbf{v}_g = const.$. The first term on the right is routinely interpreted to represent the internal movements of the electron, the 'Zitterbewegung'. Since $\overrightarrow{\alpha}$ has real eigenvalues, its quantum mechanical expectation, $< \Psi \mid (\overrightarrow{\alpha}(0) - \mathbf{v}_g) \mid \Psi > / < \Psi \mid \Psi >$, varies with v_g as $\sqrt{1 - v_g^2}$. In other words, the Zitterbewegung slows down by a Lorentz factor as the group velocity increases.

Whilst we can now write down a constant overall rate of spatiotemporal evolution for a single observer as $c^2dt^2 = c^2dt_0^2 - d\mathbf{x}_0^2$, Lorentz Transformations do involve an additional ingredient, Einstein clock synchronisation, which will be the focus of the next Section.

8 Coordinate transformations

We have shown length contraction and time dilation as physical effects in luminal wave models subject to the basic mechanics Eqs. (1) - (7) and the incremental momentum boost generator (22). The analyses were constructed from the perspective of a single observer so the principle of relativity, covariance, coordinate independence, and coordinate transformations were *all* irrelevant.

Let us now focus on the question of how these physical phenomena of length contraction and time dilation constrain the coordinate transformations. Selleri has studied this question in some detail [13, 14]. He considered three assumptions, namely: length contraction, time dilation and constancy of the 2-way velocity of light. He showed that any two of these assumptions both implies the third and constrains the coordinate transformations between a preferred rest frame, $S_0 = (x_0, y_0, z_0, t_0)$ and a frame $S = (x, y, z, t)$ in standard configuration moving with speed v to the following form:

$$x = \frac{(x_0 - \beta c t_0)}{\sqrt{1-\beta^2}}\,;\; y = y_0\,;\; z = z_0\,;$$

$$t = \sqrt{1-\beta^2}\; t_0 + e_1(x_0 - \beta c t_0)\,,$$

where $\beta = v/c$ and e_1 is a synchronisation parameter.

Setting $e_1 = -\beta/(c\sqrt{1-\beta^2})$ corresponds to the usual Einstein clock synchronisation convention and reduces this to the Lorentz Transformation. Our coordinate transformations are therefore Lorentz Transformations and the relativity principle and the constant speed of light for all observers are therefore results, not postulates. It is also now finally clear that the wave inertia changes we have analysed are frequency changes corresponding to the relativistic Doppler shift, as opposed to, say, amplitude changes.

8.1 Other synchronisation protocols

Selleri also discusses alternative clock synchronisation protocols, especially the case $e_1 = 0$ which corresponds to using Einstein synchronisation in a preferred rest frame, and setting clocks in the moving frame to coincide with nearby clocks in the rest frame at $t = 0$. Both sets of observers agree that clocks in the moving system run slow, and they also agree on the simultaneity of spatially separated events. The transformations in this case, known as the inertial transformations, were first found by Tangherlini [27]. The empirical consequences of inertial transformations have been shown to comply with experimental evidence in a wide variety of situations [28]. As far as the present article is concerned, Appendix 2 derives (8) from the relativistic Doppler shift and aberration results, which apply equally well to inertial transformations [15], and therefore so do the structural consequences developed above.

Selleri and others have advanced various arguments in favour of absolute simultaneity [29–34] (notably a simplified analysis on the rotating platform), but nothing that questions the Lorentz form within the domain of inertial frames. Inertial transformations do not preserve the line element, $ds^2 = c^2dt^2 - dx^2 - dy^2 - dz^2$, the physical laws are frame dependent, the inverse transformation is different, the relative velocity of the origin of S as seen by S_0 does not equal the relative velocity of S_0 as seen by S and the inertial transformations do not form a group [14]. In short, they fail to deliver elegant and simple analysis in most physical situations.

The conventional nature of the Einstein protocol has, of course, always been stipulated in relativity theory but Selleri has shown something important: Like the choice between Cartesian and Spherical coordinates, the choice of a clock synchronisation protocol really is only a matter of convenience. Provided they use it consistently, physicists solving problems on a rotating platform and engineers developing GPS satellite networks (which use an inertial clock synchronisation protocol) can use whatever protocol is most effective.

The self-evident fact remains that the events that happen in the world cannot depend on the coordinate systems we use to describe them. Coordinate independence is one of the most powerful practical tools for the development of new physics. Other coordinate transformations may be empirically adequate, but special status is rightly afforded to Lorentz Transformations on the basis of symmetry and utility, not uniqueness, and what we have shown is that their 'natural habitat' is field theory.

8.2 Objective simultaneity and the preferred frame

An immediate consequence of the Einstein synchronisation protocol is that observers in relative motion find themselves in disagreement over intrinsically objective facts such as the rates of their respective clocks and the temporal ordering of spacelike separated events.

Philosophical relativism sought to leave these conflicts unresolved on the basis, ultimately, that a preferred frame cannot be observed. This approach induces numerous paradoxes that have been criticised for over a century [35]. More recently, Hardy [32] and Percival [33, 34] have each shown that relativity of simultaneity when combined with quantum nonlocality leads to more than just conflicts between different observers. It leads to manifest contradictions for individual observers.

Percival's double Bell paradox, for example, considers two EPR/Bell experiments in relative motion. According to relativity of simultaneity, a temporal loop can be constructed by using the measurement results in one arm of each experiment to select the measurement axis in the corresponding arm of the other experiment. Given the quantum predictions for individual EPR/Bell experiments, he showed that an observable measurement result is, on at least some occasions, inverted by the loop becoming equal to its own opposite which is a manifest contradiction.

The long standing loopholes [36] in EPR experiments finally having been closed [37], it can no longer be argued that the quantum predictions are somehow "wrong" when they correctly predict the experimental outcomes. Instead, one must simply admit what good sense always demanded: When two observers disagree about an objective fact, they cannot both be right. The temporal loop relativistically assumes that each observer's view of the temporal order of the relevant events is indeed "true", which is impossible because their views are mutually exclusive.

Therefore, we must admit a distinction between the real physical state of affairs and how things appear to a given observer. Two different concepts of simultaneity, apparent and objective, arise. Apparent simultaneity is what appears to observers using a given clock synchronisation protocol. Provided the protocol corresponds to a definite value for the synchronisation parameter, e_1, apparent simultaneity is sufficient for making valid predictions — an essential consideration since Physics expresses itself in terms of observable quantities*. Relativistic simultaneity is just the apparent simultaneity for observers who use the Einstein protocol and there is no need to assert the truth value of this clock synchronisation protocol (which would imply that the forbidden double-Bell temporal loop is real).

As far as objective simultaneity is concerned, the foregoing wave analyses have shown that motion induces objective changes in clocks and rulers that are constructed entirely from luminal waves. A unique preferred frame, in which these devices are undistorted, can now be identified in two different ways, because an observer's velocity relative to either (a) the medium in which waves propagate or (b) the universe as a whole can be determined from Doppler effects in the wave interpretation.

Of course, the nett observed Doppler shift for a given source and detector depends only on their relative velocity and the direction to the source, so that we cannot isolate the detector's velocity. However, with a large number of sources lying in different, random directions whose individual masses and conditions of motion are independent of the direction in space, we can determine the detector velocity relative to the centre of mass of the group as a whole. Similarly, measurements on an *a priori* isotropic radiation bath are sufficient [38] to determine the detector velocity relative to the rest frame of the bath, as defined in Section 4.

As discussed in [12] and references therein, two important cases have already been studied, namely the anisotropies of (1) the Cosmic Microwave Background Radiation (CMBR) [38, 39], which gives Earth's velocity relative to the medium and (2) the angular number density of observable astronomical objects [40], which gives Earth's velocity relative to the rest of the universe. In both cases, an identical velocity dipole of magnitude ~ 350 km/sec is observed!

It is anticipated that future observations on other isotropic radiation baths will show the same anisotropy and the same velocity dipole. Variations in the average red shift of distant galaxies as a function of the direction in space constitute a further example that can be tested in the future to confirm this prediction. Note that these results are at odds with the relativist interpretation.

Within the wave interpretation of Lorentz Invariance, we see from Section 2 that the momentum density distribution of a system whose centre of inertia has zero velocity relative to the medium has no bias in any given direction, and, with Sections 6 and 7, we can now safely state that clocks in this condition of motion really do run faster, rulers really are longer and so on. The existence of this preferred frame is implied by the wave analysis and its observability provides the essential empirical basis for asserting at last that objective simultaneity coincides with the Einstein simultaneity of observers at rest in the CMBR frame. The wave interpretation presented here has therefore eliminated all the paradoxes associated with Special Relativity without sacrificing any of the practical benefits of Lorentz symmetry, whilst also covering a wider range of observables.

However, this interpretation assumes a wave ontology, with energy constrained to propagate at c. The idea of matter as constructed from some form of energy that does not propagate at c is considered, and rejected, in the next Section.

9 Non-luminal structures

It is of course possible that wave propagation slows down or stops altogether under interaction, so that the wave energy is transformed into some ill-defined notion of 'substance'. Nothing prevents applying the same basic mechanics principles to such non-luminal structures, however once we intro-

*Note that the quantum predictions for EPR experiments are insenstitive to the temporal order of the Bell measurements, so they cause no difficulty.

duce entities that do not move at c, an immediate casualty is the work integral connection between momentum and energy. We would have no choice but to re-define inertia as being fundamentally velocity dependent.

Such a flexible approach to so pivotal a definition might raise eyebrows if it were not for the fact that this particular step is an integral part of Special Relativity. So, let us assume that we could somehow make sense of the relativistic inertia in its own right, as we have done in this Article but on some other grounds that are also independent of Special Relativity.

As far as the structure of particles is concerned, without the concept of internal movements it would not seem possible to provide any account of internal processes (such as muon decay for example). Likewise, the fact that the massive particles possess angular momentum implies the existence of internal movements*. Let us consider internal movements at speeds other than c. To illustrate the difficulties this causes, we shall also assume that we can somehow produce Lorentz contracted moving system trajectories on other grounds that are also independent of Special Relativity.

We must still use (32), with v_i^2 replacing c^2 on the RHS, to connect the total and relative velocities on the i^{th} segment (as both are referred to the same observer). If v_i were the same in the moving and rest systems, then clearly the periods would not dilate by γ, and yet we know that for any physical system, not just luminal systems, periods must dilate by γ under Lorentz Transformations.

The resolution is most easily seen from Special Relativity. If the total speed, v_{i0}, on the i^{th} segment as seen by a comoving observer is such that $v_{i0} \neq c$, then for observers in other frames, $v_i \neq v_{i0}$ and must in general be calculated according to the relativistic composition of velocities:

$$\mathbf{v}_i = \frac{\mathbf{V} + \mathbf{v}_{i0\parallel} + \sqrt{1-\beta^2}\,\mathbf{v}_{i0\perp}}{1 + \frac{\mathbf{V}\cdot\mathbf{v}_{i0}}{c^2}} .$$

Now as we Lorentz boost a particle in the frame of a single observer, there are two possibilities. If $v_{i0} = c$, then $v_i = c$ for all i independent of the condition of motion of the particle, and structural models incorporating length contraction and the relativistic momentum are readily available. Sect. 8 showed that these phenomena imply Lorentz Transformations, whose elegance and simplicity therefore has a coherent explanation based on the very definition of momentum as inertia times velocity, $p = mc$.

Alternatively, if $v_{i0} \neq c$ the total velocities of internal movements, $\mathbf{v}_i$, must depend on both the particle velocity and the orientation of individual segments in the above complicated manner. Why? The elegance and simplicity of Lorentz Transformations then has at its very foundations an implausibly inelegant, complex structure. We are left reasoning in a circle from Lorentz Transformations to the composition of velocities to the proposition that such complex structures are necessary as the basis for our simple coordinate transformations and we have no physical basis for either length contraction or the relativistic momentum. Ockham's razor insists that we reject nonluminal structures.

Therefore, we must conclude that, in the comoving frame, Lorentz invariant structural models of the massive particles should have internal movements at, and only at, c.

10 Does local action imply retarded interaction?

Local action is the single most basic, self-evident principle in Physics — interaction requires colocation. Both Newton and Einstein agreed. This section considers the logic of interaction at a distance, subject to local action, but from a pure field perspective where mass energy propagates luminally.

In Classical Physics it was taken for granted that matter emits field, leading to the idea that the far fields of a particle propagate away from it at c. It then follows that long-range interactions between particles are retarded and the unavoidable consequence is that there can be no causal relations between space-like separated events. On the other hand, Quantum Mechanics predicts instant causal correlations at a distance and experiments replicate these predictions [41–43]. However, if matter and field are one and the same, as Einstein suggested, then the idea that matter emits field is meaningless. We need to consider whether or not the far fields propagate away from the centre of inertia in a pure field particle model.

Section 6 considered a rest system that evolves under rotations, corresponding to Special Relativity's little group. Note that the radius of the rest system sphere was not relevant — the analysis applies to any radius, and there is no good reason, neither in our analysis nor in Special Relativity, to distinguish between the near and far fields of a particle. The distinction in Electromagnetics between the 'attached' field [44] and the 'body' of the particle is arguably incompatible with Special Relativity because it implicitly introduces (radial) field movements that contravene the little group.

Consistent with Einstein's view that relativity theory renders the division into matter and field 'artificial', our luminal wave structure implies that particles are unbounded with far fields that propagate transverse to the radius† rather than radially away from a 'body'. There is then no good reason to presume that local action implies retarded interaction.

The long range interaction between two particles, A and B, depends on the colocation of their respective fields. It is an integral over all space, dominated by terms close to the two centres, but any far fields of A that become colocated with the B particle's centre of inertia did not travel there from A's centre of inertia. They are part of the extended wave system that is comoving, as a whole, with the A centre of inertia so one

*The quantisation of angular momenta is also readily explicable as a wave phenomenon [12, 20].

†As is also consistent with Electromagnetics' radial Coulomb field because $\mathbf{E}$ and $\mathbf{H}$ are each transverse to the momentum density $\mathbf{S}/c^2$, whilst $\mathbf{H}$ fields cancel in the rest particle due to balanced movements.

might anticipate that the direct impact of A's far fields on the observed location of the B particle would be instantaneous, while the reaction impact on the observed location of the A particle might be retarded.

However, it is more apposite simply to observe that field theory problems are usually formulated and solved on whole regions evolving subject to local action at all points in parallel. The idea of a local realist wave ontology is inherently Lorentz invariant, but waves are inherently distributed. They run on correlations at a distance sustained by strictly local actions. Distributed interactions between distributed waves can have distributed impacts, occurring simultaneously in different places. Waves exemplify Redhead's conclusion that ontological locality does not rule out instant relations between observables [45]. Trajectories in local realist wave systems display entanglement as shown in [16], where a Madelung decomposition of the Helmholtz wave equation shows that it contains Bohmian mechanics' nonlocal quantum potential within it. Therefore, quantum nonlocality and entanglement can perhaps be interpreted as locally realistic wave phenomena. With specific reference to the EPR paradox [46], the Bell Inequalities [47] depend on a causality analysis that uses light cones emanating from point events [48], presuming a one to one correspondence with point-like 'beables' [49], but for inherently distributed systems like waves neither beables nor events can be presumed to be point-like.

11 Discussion

Since massive particles have finite energy, the volume integral of the field energy density must not diverge as $r \to \infty$. The $1/r^2$ long range force fields for the charged particles imply a $1/r^4$ energy density asymptote for both charged and neutral particles in luminal wave models [12]. The energy density integral does not then diverge as $r \to \infty$ so finite but unbounded luminal wave structures are compatible with the usual basic physics. They appear as pointlike particles because the field energy is highly concentrated near the centre. For example, according to a $1/r^4$ energy density asymptote the maximum energy density for a particle with the mass of an electron, at the radius $r \sim 4 \times 10^{-13} m$, is $\sim 400,000$ times greater than that at a radius of 0.1 Angstrom unit.

Unlike Electromagnetics, nothing prevents the method in this Article from applying to the fermions. A wide range of candidate models for the massive particles, in the form of subluminal soliton solutions found in typically nonlinear field theories, have been reported in the literature. The appearance of Lorentz covariance in so many disparate field models is no coincidence as they are all subject to the same basic kinematic constraints used in Sects. 2 - 7 to show that Lorentz invariance is the consequence of constructing subluminally moving particles from fields that are constrained to propagate luminally.

While the constraints are simple, the structures of soliton solutions are generally not simple. For example, evolution under rotations does not imply spherical symmetry and nor does it imply that the particle rotates as a whole in a simple manner, like a solid ball. Due to the kinematic constraint, trajectories at different radii necessarily evolve at different angular rates and, similarly, wave trajectories at various points on the same spherical surface in the rest system generally rotate about different axes.

12 Conclusions

This Article has developed a particularly simple hypothesis: Energy-momentum propagates at c. It has shown why subluminally moving physical systems, including observers' measuring devices, then display time dilation and length contraction, so that an underlying luminal wave reality, although objective, presents a Lorentz covariant "spacetime" to its observers. Neither the Relativity Principle nor the invariance of the observed speed of light were assumed. These two cornerstones of relativity theory were shown as results, not put in as postulates.

This 3D+t reality also entails a preferred frame that has been observed in practice in at least two independent ways, providing a natural definition of objective simultaneity. All the paradoxes formerly associated with Special Relativity's subjective notions of reality are thus removed, and, unlike Special Relativity, the proposed luminal wave interpretation of Lorentz invariance is consistent with all the relevant facts.

Although the Lorentz covariance of luminal wave systems was perhaps already familiar, the basic mechanics underlying Lorentz symmetry remained unnoticed for over a century. The discovery of this direct link between wave systems and relativistic mechanics has wide ranging implications for the interpretation and unification of modern physics.

Rather than replacing Newtonian Mechanics, Einstein's relativistic mechanics is the natural step accompanying the shift in our founding physical ideas from particle to wave concepts. The wave packet is reformed by giving explicit recognition to the conservation of momentum between wave components and particles, which can now be seen as widely distributed systems with instantly correlated far fields. Quantum nonlocality can be understood within this framework whilst general covariance is readily incorporated, conceptually and analytically, with a refractive medium approach to gravity [12] that produces the relevant phenomena without the raft of problems flowing from the usual field equations.

Hopefully, this article has highlighted the absence of any good reason to presume that any non-propagative form of mass-energy exists. It's not so much the introduction of a new hypothesis, as the removal of an old one — the idea of matter as a distinct ontological class in its own right.

Submitted on November 18, 2016 / Accepted on November 21, 2016

References

1. Einstein A., Infeld L. Evolution of physics: The growth of ideas from early concepts to relativity and quanta. 1961, Simon and Schuster, New York, 242-243.
2. Dirac P.A.M. The theory of the electron (parts 1 and 2). *Proceedings of the Royal Society in London A*, 1928, v. 117, 610 and v. 118, 351.
3. Breit G. An interpretation of Dirac's Theory of the electron. *Proceedings of the National Academy of Sciences USA*, 1928, v. 14, 553.
4. Bellazini J., Benci V., Bonanno C., Micheletti A.M. Solitons for the nonlinear Klein-Gordon equation. 2007, arXiv: math.AP/0712.1103v1.
5. Finkelstein R.J. A Field Theory of knotted solitons. 2007, arXiv: hep-th/0701124v2.
6. Radu E., Volkov M.S., Existence of stationary, non-radiating ring solitons in field theory: knots and vortons. 2008, arXiv: hep-th/0804.1357v1.
7. Moret-Bailly J. Electromagnetic solitons and de Broglie's "double solution". *J. of Theoretics*, 2003, v. 5-5, 11. arXiv: math-ph/0201002v1.
8. Borisyuk D., Faber M., Kobushkin A. Electromagnetic waves within a model for charged solitons. *J. Phys. A: Math. Gen.*, 2007, v. 40, 525–531. arXiv: hep-th/0708.3173v1.
9. Diaz-Alonso J., Rubiera-Garcia D. Generalized gauge field theories with non-topological soliton solutions. 2007, arXiv: hep-th/0708.0636v1.
10. Blas H., Carrion H.L. Solitons, kinks and extended hadron model based on the generalized sine-Gordon theory. *JHEP*, 2007, 0701, 027. arXiv: hep-th/0610107v2, 2006.
11. Cui H.Y. Direction adaptation nature of Coulomb's force and gravitational force in 4-Dimensional spacetime. 2001, arXiv: physics/0102073.
12. Laidlaw A. On the Electromagnetic basis for gravity. *Apeiron*, 2004, v. 11, 3.
13. Selleri F. Remarks on the transformations of space and time. *Apeiron*, 1997, v. 9(4), 116–120.
14. Selleri F. Non-invariant one-way speed of light. *Found. Phys.*, 1996, v. 26, 641.
15. Puccini G., Selleri F. Doppler effect and aberration from the point of view of absolute motion. *Nuovo Cim. B*, 2002, v. 117, 283.
16. Orefice A., Giovanelli R., Ditto D. Complete Hamiltonian Description of wave-like features in Classical and Quantum Physics. *Found. Phys.*, 2009, v. 39, 256.
17. Orefice A., Giovanelli R., Ditto D. Helmholtz wave trajectories in Classical and Quantum Physics. 2011, ArXiv: 1105.4973.
18. Donev S., Tashkova M. On the structure of the nonlinear vacuum solutions in extended Electrodynamics. 2002, arXiv: hep-th/0204217.
19. Donev S. Screw photon-like (3+1)-solitons in extended Electrodynamics. 2001, arXiv: hep-th/0104088.
20. Donev S., Tashkova M. From Maxwell stresses to nonlinear field equations. 2006, arXiv: physics/0604021v6.
21. Kim Y.S. Internal space-time symmetries of massive and massless particles and their unification. *Nucl.Phys.Proc.Suppl.*, 2001, v. 102, 369–376. arXiv: hep-th/0104051.
22. Messiah A. Quantum Mechanics. Vol 2. 1965, Ch XX, 922-925, North Holland Publishing Company.
23. Bohm D. The Special Theory of Relativity. 1965, 23–25, W.A. Benjamin New York.
24. Hafele J., Keating R. Around-the-world atomic clocks: predicted relativistic time gains. *Science*, 1972, v. 177, 166.
25. Kundig W. Measurement of the transverse Doppler effect in an accelerated system. *Phys Rev.*, 1963, v. 129, 2371.
26. Ives H., Stillwell G. An experimental study of the rate of a moving atomic clock. *Journal of the Optical Society of America*, 1938, v. 28, 215–226 and 1941, v. 31, 369.
27. Tangherlini F.R. On energy momentum tensor of gravitational field. *Supl. Nuov. Cim.*, 1961, v. 20, 351–367, (2^{nd} Trimestre 1961).
28. Rizzi G., Ruggiero M.L., Serafini A. Synchronization gauges and the principles of Special Relativity. *Found. Phys.*, 2005, v. 34, 1885.
29. Selleri F. Superluminal signals and causality. *Annales de la Fondation Louis de Broglie*, 2003, v. 28, 3–4.
30. Goy F. Derivation of three-dimensional inertial transformations. 1997, arXiv: gr-qc/9707004.
31. Goy F., Selleri F. Time on a rotating platform. 1997, arXiv: gr-qc/9702055v2.
32. Hardy L. Quantum Mechanics, local realistic theories, and Lorentz-invariant realistic theories. *Phys. Rev. Lett.*, 1992, v. 68, 2981–1284.
33. Percival I. Quantum transfer functions, weak nonlocality and relativity. *Physical Letters A*, 1998, v. 244(6), 495–501. arXiv: quant-ph/9803044.
34. Percival I. Quantum measurement breaks Lorentz symmetry. 1999, arXiv: quant-ph/9906005.
35. Selleri F. Weak relativity - The Physics of space and time without paradoxes. 2009, C. Roy Keys Inc.
36. Clauser J., Horne M. Detector inefficiencies in the Einstein-Podolsky-Rosen experiment. *Phys. Rev. D*, 1987, v. 35(12), 3831–3835.
37. Hensen B. et al. Experimental loophole-free violation of a Bell inequality using entangled electron spins separated by 1.3 km. *Nature*, 2015, v. 526, 682–686. arXiv: 1508.05949.
38. Peebles P.J.E., Wilkinson D.T. Comment on the anisotropy of the primeval fireball. *Phys. Rev.*, 1968, v. 174, 2168.
39. Smoot G. Detection of anisotropy in the cosmic blackbody radiation. *Physical Review Letters*, 1977, v. 39(14), 898.
40. Blake C., Wall J. A velocity dipole in the distribution of radio galaxies. *Nature*, 2002, v. 416, 180–182.
41. Aspect A., Grangier P., Roger B. Experimental realization of EPR-Bohm gedankenexperiment: A new violation of Bell's inequalities. *Phys. Rev. Lett.*, 1982, v. 49, 1804–1807.
42. Scarani V., Tittel W., Zbinden H., Gisin N. The speed of quantum information and the preferred frame: Analysis of experimental data. *Phys. Lett. A*, 2000, v. 276, 1–7. arXiv: quant-ph/0007008.
43. Ou Z.Y., Pereira S.F., Kimble H.J., Peng K.C. Realization of the Einstein-Podolsky-Rosen paradox for continuous variables. *Phys. Rev. Lett.*, 1992, v. 68, 3663.
44. Konopinski E.J. Electromagnetic Fields and relativistic particles. 1981, Mcgraw Hill.
45. Redhead M. Incompleteness, nonlocality and realism. 1987, Oxford University Press.
46. Einstein A., Podolsky B., Rosen N. Can Quantum-mechanical description of physical reality be considered complete? *Phys. Rev.*, 1935, v. 47, 777.
47. Bell J.S. On the Einstein Podolsky Rosen Paradox. *Physics*, 1965, v. 1, 195–200.
48. Norsen T. J.S. Bell's Concept of local causality. 2007, arXiv: 0707.0401v3.
49. Bell J.S. Speakable and unspeakable in Quantum Mechanics: Collected papers on quantum philosophy. 2004, Cambridge University Press.

Appendix 1

Consider a constant momentum density $\vec{\rho}_{pi}$ in a region of transverse crossectional area A and length l_i. The total momentum is $\mathbf{p}_i = Al_i\rho_{pi}\hat{\mathbf{k}}$. Let this be normally incident on

a mirror that is moving with velocity $\mathbf{v} = -v\hat{\mathbf{k}}$. Let the reflection begin at $t = 0$. It then ends at $\Delta t = l_{\rm i}/(c+v)$, after which there is a reflected wave with momentum density $\vec{\rho}_{pr}$ that occupies a region of length $l_{\rm r} = (c-v)\Delta t$ and crossectional area A, so the momentum of the reflected light flash is $\mathbf{p}_{\rm r} = -Al_{\rm r}\rho_{pr}\hat{\mathbf{k}}$.

During the reflection, the rates of change of momentum for the incident and reflected waves are $\dot{\mathbf{p}}_i = -(c+v)A\vec{\rho}_{\rm pi}$ and $\dot{\mathbf{p}}_{\rm r} = (c-v)A\vec{\rho}_{\rm pr}$ respectively, where a dot over a variable indicates the time differential. The total rate of change of momentum is:

$$\dot{\mathbf{p}} = \dot{\mathbf{p}}_{\rm i} + \dot{\mathbf{p}}_{\rm r} = -A((c+v)\rho_{pi} + (c-v)\rho_{pr})\hat{\mathbf{k}}\,,$$

where $\rho_{pi} = |\vec{\rho_{pi}}|$ and $\rho_{pr} = |\vec{\rho_{pr}}|$. As far as scalar momentum is concerned, for the incident wave $\dot{p}_{\rm i} = c\dot{m}_{\rm i} = -A(c+v)\rho_{pi}$, for the reflected wave $\dot{p}_{\rm r} = c\dot{m}_{\rm r} = A(c-v)\rho_{\rm pr}$ and the total is:

$$\dot{p} = c\dot{m} = c\dot{m}_{\rm r} + c\dot{m}_{\rm i} = A((c-v)\rho_{pr} - (c+v)\rho_{pi})\,.$$

The work done by the mirror on the incident and reflected waves is: $\int \dot{\mathbf{p}}_{\rm i}\cdot d\mathbf{s}_{\rm i} = -\int_0^{\Delta t} A(c+v)\rho_{\rm pi}\ cdt$ and $\int \dot{\mathbf{p}}_{\rm r}\cdot d\mathbf{s}_{\rm r} = \int_0^{\Delta t} A(c-v)\rho_{pr}\ cdt$ respectively, where $d\mathbf{s}_{\rm i}$ and $d\mathbf{s}_{\rm r}$ are the incremental movements of the incident and reflected waves, in the directions $\hat{\mathbf{k}}$ and $-\hat{\mathbf{k}}$ respectively. The total work done is just $W = \int_0^{\Delta t} c\,\dot{m}c\,dt = (m_{\rm r} - m_{\rm i})c^2$.

The energy change of the light flash is of course equal and opposite to the work done by the radiation pressure force on the mirror, so $(m_{\rm r} - m_{\rm i})c^2 = -(-\dot{\mathbf{p}})(-v)\Delta t$, and it is easily shown that $p_{\rm r}/p_{\rm i} = (c+v)/(c-v)$, from which we may infer the momentum shift factor for light emitted by a source moving towards an observer as $\sqrt{(c+v)/(c-v)}$, in agreement with the usual relativistic doppler shift.

Appendix 2

With respect to the system of light flashes in Subsect. 2.2, let us impose the condition in some inertial frame that $\mathbf{P}_0 = \sum_i \mathbf{p}_{i0} = 0$. The momentum of the i^{th} light flash, referred to this frame, is then:

$$\mathbf{p}_{i0} = p_{i0}\left(\cos\theta_{i0}\,\hat{\mathbf{i}} + \sin\theta_{i0}\cos\phi_{i0}\,\hat{\mathbf{j}} + \sin\theta_{i0}\sin\phi_{i0}\,\hat{\mathbf{k}}\right)\,,$$

where θ_{i0} is the angle with the x-axis and $\sum_i p_{i0}\cos\theta_{i0} = \sum_i p_{i0}\sin\theta_{i0}\cos\phi_{i0} = \sum_i p_{i0}\sin\theta_{i0}\sin\phi_{i0} = 0$.

Let an observer move relative to this frame with velocity $\mathbf{v} = -\beta c\hat{\mathbf{i}}$. Since $p_i/p_{i0} = f_i/f_{i0}$, the standard relativistic doppler shift and aberration formulae (with the observer moving towards the source at speed v) give, respectively:

$$p_i = p_{i0}\gamma\left(1 + \frac{v}{c}\cos\theta_{i0}\right) \text{ and } \cos\theta_i = \frac{\cos\theta_{i0} + \dfrac{v}{c}}{1 + \dfrac{v}{c}\cos\theta_{i0}}\,.$$

Note that the same result also holds for non-monochromatic light flashes. The scalar momentum of the i^{th} flash in the observer frame is:

$$p_i = p_{i0}\gamma(1 + \beta\cos\theta_{i0})\,.$$

Summing over i, the total energy, $m_e c^2 = \gamma c\sum_i p_{i0} = \gamma m_0 c^2$, where m_e and m_0 are as defined in subsection 2.2 and Section 3 respectively. The (vector) momentum of the i^{th} flash is:

$$\mathbf{p}_i = p_{i0}(\gamma(\beta + \cos\theta_{i0})\,\hat{\mathbf{i}} + \sin\theta_{i0}\cos\phi_{i0}\,\hat{\mathbf{j}} + \sin\theta_{i0}\sin\phi_{i0}\,\hat{\mathbf{k}})\,.$$

Summing over i, the total momentum is $\mathbf{P} = \gamma\beta\sum_i p_{i0}\,\hat{\mathbf{i}}$. Differentiating each of the two previous equations with respect to β, we get $d\mathbf{p}_i/d\beta = \gamma^2 p_i\,\hat{\mathbf{i}}$ and $d\mathbf{P}/d\beta = \gamma^2 m_e c\,\hat{\mathbf{i}}$, so that:

$$\frac{d\mathbf{p}_i}{d\beta} = \frac{d\mathbf{P}}{d\beta}\frac{p_i}{\sum_j p_j} = \frac{d\mathbf{P}}{d\beta}\frac{p_i}{m_e c}\,.$$

Finally, since the above expressions for $\mathbf{p}_i$ and $\mathbf{P}$ are functions of β alone, the incremental changes can be written as $d\mathbf{p}_i = (d\mathbf{p}_i/d\beta)\,d\beta$ and $d\mathbf{P} = (d\mathbf{P}/d\beta)\,d\beta$, upon which:

$$d\mathbf{p}_i = \frac{p_i}{m_e c}d\mathbf{P}\,.$$

Therefore (8) holds for a collinear incremental boost. For transverse boosts, consider as initial condition a system with a centre of inertia that is moving in the y-direction at speed V, so $m_e = \gamma(V)m_0$. We may repeat the above analysis for an observer moving at speed v_x in the x-direction with $\beta = v_x/c$ and $\sum_i p_{i0}\sin\theta_{i0}\cos\phi_{i0} \neq 0$. Evaluating the resulting expression for $d\mathbf{P}/d\beta$ at $v_x = 0$, then yields the same result, $d\mathbf{p}_i = p_i\,d\mathbf{P}/m_e c$, for an incremental transverse boost. In Special Relativity, the general boost decomposes into a collinear boost, a transverse boost and a rotation (a Thomas precession). As the latter has no impact on linear momenta, (8) is generally valid for incremental boosts of systems of luminal wave momenta.

Occurrence and Properties of Low Spin Identical Bands in Normal-Deformed Even-Even Nuclei

A. M. Khalaf, M. D. Okasha[1] and K. M. Abdelbased
Physics Department, Faculty of Science, Al-Azhar University, Cairo, Egypt

[1]Physics Department, Faculty of Science (Girls branch), Al-Azhar University, Cairo, Egypt. E-mail: mady200315@yahoo.com

The identical bands (IB's) phenomenon in normally deformed rare-earth nuclei has been studied theoretically at low spins. Six neighboring even-even isotopes ($N = 92$) and the isotopes ^{166,168,170}Hf are proposed that may represent favorable cases for observation of this phenomenon. A first step has been done by extracting the smoothed excitation energies of the yrast rotational bands in these nuclei using the variable moment of inertia (VMI) model. The optimized parameters of the model have been deduced by using a computer simulated search programm in order to obtain a minimum root mean square deviation between the calculated theoretical excitation energies and the experimental ones. Most of the identical parameters are extracted. It is observed that the nuclei having N_pN_n/Δ values exhibit identical excitation energies and energy ratio R(4/2), R(6/4) in their ground-state rotational bands, N_p and N_n are the valence proton and neutron number counted as particles or holes from the nearest spherical shell or spherical subshell closure and Δ is the average pairing gap. The nuclear kinematic and dynamic moments of inertia for the ground state rotational bands have been calculated, a smooth gradual increase in both moments of inertia as function of rotational frequency was seen. The study indicates that each pair of conjugate nuclei have moments of inertia nearly identical.

1 Introduction

One of the most remarkable properties so far discovered of rotational bands in superdeformed (SD) nuclei is the extremely close coincidence in the energies of the deexciting γ-ray transitions or rotational frequencies between certain pairs of rotational bands in adjacent even and odd nuclei with different mass number [1–5]. In a considerable number of nuclei in the Dy region as well as in the Hg region one has found different in transition energies E_γ of only 1-3 KeV, i.e there exist sequence of bands in neighboring nuclei, which are virtually identical $\Delta E_\gamma/E_\gamma \sim 10^{-3}$. This means that the rotational frequencies of the two bands are very similar because the rotational frequency (dE/dI) is approximately half the transition energy, and also implies that the dynamical moments of inertia are almost equal. Several groups have tried to understand the phenomenon of SD identical bands (IB's) or twin bands [5–10] assuming the occurrence of such IB's to be a specific property of the SD states of nuclei.

Shortly afterwards, low spin IB's were found in the ground state rotational bands of normally deformed (ND) nuclei [11–14], which showed that the occurrence of IB's is not restricted to the phenomenon of superdeformation and high-spin states. Since then, a vast amount of IB's have been observed both in SD and ND nuclei, and there have been a lot of theoretical works presented based on various nuclear models [15–18]. All explantation to IB's in SD nuclei differing by one or two particle numbers factor to the odd-even difference in the moments of inertia, namely the pair force, is substantially weakened for high-spin SD states. However, these outlines would fail to explain IB's at low spin, where the blocking of the pairing contributions of the odd nucleon is predicted to reduce the nuclear superfluidity, there by increasing the moment of inertia of the odd-A nucleus. Because of the known spins, configurations and excitations energies of the ND bands, the systematic analysis of IB's in ND nuclei would be useful in investigation of the origin of IB's.

It is the purpose of this paper to point out that existence of low-spin IB's in the well deformed rare-earth region is a manifestation of a more general property of nuclear excitation mechanism in this region, i.e, almost linear dependence of the moment of inertia on a simple function of the valence proton and neutron number. The properties of rotational bands in our selected normal deformed nuclei have been systematically analyzed by using the variables moment of inertia (VIM) model [19, 20].

2 Description of VMI model

The excitation energy of the rotational level with angular moment I for an axially symmetric deformed nucleus is given by

$$E(I) = \frac{\hbar^2}{2J} I(I+1), \tag{1}$$

with J being the rigid moment of inertia. This rigid rotor formula violated at high angular momenta. Bohr and Mottelson [21] introduced a correction term

$$\Delta E(I) = -B\,[I\,(I+1)]^2 \tag{2}$$

which is attributed to rotation-vibration interaction where J and B are the model parameters.

In the variable moment of inertia (VMI) model [19] the level energy is given by

$$E\left(I,J,J_0,c\right)=\frac{\hbar^2}{2J}I\left(I+1\right)+\frac{c}{2}\left(J-J_{00}\right)^2 \tag{3}$$

where J_0 is the ground-state moment of inertia. The second term represents the harmonic term with c in the stiffness parameter. The moment of inertia J is a function of the spin $I(J(I))$.

The equiblirium condition

$$\frac{\partial E}{\partial J}=0 \tag{4}$$

determines the values of the variable moment of inertia J_I, one obtains

$$J_I^3-J_0J_I^2=\frac{1}{2c}I\left(I+1\right). \tag{5}$$

This equation has one real root for any finite positive value of J_0 and c can be solved algebraically to yield

$$\begin{aligned}J(J_0,c,I)&=\frac{J_0}{3}\\&+\left\{\frac{1}{2}\frac{I(I+1)}{2C}+\frac{J_0^3}{27}+\left[\frac{1}{4}\frac{I^2(I+1)^2}{4c^2}+\frac{J_0^3}{27}\frac{I(I+1)}{2c}\right]^{\frac{1}{2}}\right\}^{\frac{1}{3}}\\&+\left\{\frac{1}{2}\frac{I(I+1)}{2c}+\frac{J_0^3}{27}-\left[\frac{1}{4}\frac{(I+1)^2}{4c^2}+\frac{J_0^3}{27}\frac{I(I+1)}{2c}\right]^{\frac{1}{2}}\right\}^{\frac{1}{3}}.\end{aligned} \tag{6}$$

A softness parameter σ was introduced, which measures the relative initial variation of J with respect to I. This quantity is obtained from the equation (3)

$$\sigma=\frac{1}{J}\frac{dJ}{dI}\mid_{I=0}=\frac{1}{2cJ_0^3}. \tag{7}$$

To find the rotational frequency $\hbar\omega$, the kinematic $J^{(1)}$ and dynamic $J^{(2)}$ moments of inertia for VMI model, let $\hat{I}=[I(I+1)]^{\frac{1}{2}}$. Equations (3,5) can be written in the form

$$E=\frac{\hbar^2}{2J}\hat{I}^2+\frac{c}{2}\left(J-J_0\right)^2, \tag{8}$$

$$J^3-J_0J^2-\frac{\hat{I}^2}{2c}=0. \tag{9}$$

Differentiating these two equations with respect to $\hat{I}$ and using the chain rule, we get

$$\frac{dE}{d\hat{I}}=\frac{\hat{I}}{J}+\left[c\left(J-J_0\right)-\frac{\hat{I}^2}{2J^2}\right]\frac{dJ}{d\hat{I}}, \tag{10}$$

$$\begin{aligned}\frac{d^2E}{d\hat{I}^2}=&\frac{1}{J}-\frac{2\hat{I}}{J^2}\frac{dJ}{d\hat{I}}+\left(c+\frac{\hat{I}^2}{J^3}\right)\left(\frac{dJ}{d\hat{I}}^2\right)\\&+\left[c\left(J-J_0\right)-\frac{\hat{J}^2}{2J^2}\right]\frac{d^2J}{d\hat{I}^2},\end{aligned} \tag{11}$$

$$\frac{dJ}{d\hat{I}}=\frac{\hat{I}}{cJ(3J-2J_0)}, \tag{12}$$

$$\frac{d^2J}{d\hat{I}^2}=\frac{1-2c(3J-J_0)}{cJ(3J-2J_0)}\left(\frac{dJ}{d\hat{I}}\right)^2. \tag{13}$$

Using the above differentiations, we can extract $\hbar\omega$, $J^{(1)}$ and $J^{(2)}$ from their definitions:

$$\hbar\omega=\frac{dE}{d\hat{I}}, \tag{14}$$

$$J^{(1)}=\hbar^2\hat{I}\left(\frac{dE}{d\hat{I}^2}\right)^{-1}\simeq\frac{2I-1}{E_\gamma(I\rightarrow I-2)}, \tag{15}$$

$$J^{(2)}=\hbar^2\left(\frac{d^2E}{d\hat{I}^2}\right)^{-1}\simeq\frac{4}{E_\gamma(I+2\rightarrow I)-E_\gamma(I\rightarrow I-2)}. \tag{16}$$

The $J^{(1)}$ moment of inertia is a direct measure of the transition energies while $J^{(2)}$ is obtained from differences in transitions energies (relative change in transition energies).

3 Identical bands parameters

In the concept of F-spin [22], the N_π proton bosons and N_ν neutron bosons are assigned intrinsic quantum number called F-spin $F=\frac{1}{2}$, with projection $F_0=+\frac{1}{2}$ for proton bosons and $F_0=-\frac{1}{2}$ for neutrons bosons.

Therefore, a given nucleus is then characterized by two quantum numbers $F=\sum_i F_i=\frac{1}{2}(N_\pi+N_\nu)=\frac{1}{4}(N_p+N_n)$ and it's projection $F_0=\frac{1}{2}(N_\pi-N_\nu)=\frac{1}{4}(N_p-N_n)$. Squaring and subtracting, yield $4(F^2-F_0^2)=4N_\pi N_\nu=N_pN_n$.

That is any pairs of conjugate nuclei with the same F-spin and $\pm F_0$ values in any F-spin multiplet have identical N_pN_n values [23]. The product N_pN_n was used in classification the changes occur in nuclear structure of transitional region [13, 24].

It was assumed that [14], the moment of inertia J has a simple dependence on the product of valence proton and neutron numbers (N_pN_n) written in the form

$$J\propto SF\cdot SP \tag{17}$$

where SF and SP are called the structure factor and saturation parameter given by

$$SF=N_pN_n(N_p+N_n), \tag{18}$$

$$SP=\left[1+\frac{SF}{(SF)_{\max}}\right]^{-1}. \tag{19}$$

Computing by taking

$$N_p = \min\left[(\mathrm{Z}-50),(82-\mathrm{Z})\right], \tag{20}$$

$$N_n = \min\left[(\mathrm{N}-82),(126-\mathrm{N})\right], \tag{21}$$

it was found that the low spin dynamical moment of inertia defined as

$$J^{(2)}(I=2) = \frac{4}{E_\gamma(4^+ \to 2^+) - E_\gamma(2^+ \to 0^+)} \tag{22}$$

shows an approximate dependence on SF

$$J^{(2)}(I=2) \propto (SF)^{\frac{1}{2}}. \tag{23}$$

Since the nuclei having identical N_pN_n and $|N_p - N_n|$ values are found to have identical moment of inertia, the structure factor SF is related not only to the absolute value of ground state moment of inertia but also to its angular momentum dependence.

Also it was shown [11, 25, 26] that the development of collectivity and deformation in medium and heavy nuclei is very smoothly parameterized by the p-factor defined as

$$P = \frac{N_pN_n}{N_p + N_n}. \tag{24}$$

The p-factor can be viewed as the ratio of the number of valence p-n residual interaction to the number of valence like-nucleon-pairing interaction, or, if the p-n and pairing interactions are orbit independent, then p is proportional to the ratio of the integrated p-n interaction strength.

Observables such as $E(4_1^+)/E(2_1^+)$ or $B(E_2, 0_1^+ \to 2_1^+)$ that are associated with the mean field vary smoothly with p-factor.

The square of deformation parameter β^2 is invariant under rotations of the coordinate system fixed in the space. In the SU(3) limit of the interacting boson model (IBM) [27], the matrix elements of β^2 in a state with angular momenta I are given by

$$\langle\beta^2\rangle_I = \frac{1}{6(2N-1)}\left[I(I+1) + 8N^2 + 22N - 15\right] \tag{25}$$

where N is the total number of the valence bosons For the expectations value of β^2 in the ground state $I = 0$, yielding

$$\langle\beta^2\rangle_{I=0} = \frac{1}{6(2N-1)}\left[8N^2 + 22N - 15\right] \tag{26}$$

which is increasing function of N.

In order to determine β from equation (26) to a given rotational region or grouped of isotopes, one should normalize it, then

$$\beta_0 = \alpha\left[\frac{8N^2 + 22N - 15}{6(2N-1)}\right]^{\frac{1}{2}} \tag{27}$$

where α is the normalization constant ($\alpha = 0.101$ for rare earth nuclei.)

Table 1: The simulated adopted best VMI parameters used in the calculations for the identical bands in normal deformed even-even ^{158}Dy, ^{160}Er, ^{162}Yb and $^{166-170}$Hf nuclei. σ denoting the softness parameter of the VMI model. We also list the total percent root mean square deviation.

Nucleus	J_0 ($\hbar^2$ MeV^{-1})	c (10^{-1}MeV^3)	$\sigma = 1/2cJ_0^3$ (10^{-1})	% rmsd
^{158}Dy	28.8866	2.37364	8.7372	0.57
^{170}Hf	29.9116	1.93836	9.6386	0.87
^{160}Er	22.7538	2.65536	15.9839	0.86
^{168}Hf	22.8761	2.48160	16.8303	0.70
^{162}Yb	16.8587	2.83884	36.7584	0.60
^{166}Hf	17.6941	2.76559	32.6359	0.82

4 Results and discussion

A fitting procedure has been applied to all measured values of excitation energies $E(I)$ in a given band. The parameters J_0, c and σ of the VMI model results from the fitting procedure for our selected three pairs IB's are listed in Table 1. The percentage root mean square (rms) deviation of the calculated from the experimental level energies is also given in the Table and is within a fraction of 1%. To illustrate the quantitative agreement obtained from the excitation energies, we present in Table 2 the theoretical values of energies, transition energies, rotational frequencies kinematic $J^{(1)}$ and dynamic $J^{(2)}$ moments of inertia and the variable moment of inertia J_{VMI} as a function of spin for our three pairs of IB's which each pair has identical $N_p\,N_n$ product. The calculated kinematic $J^{(1)}$ and dynamic $J^{(2)}$ moments of inertia are plotted against rotational frequency $\hbar\omega$ in Figure 1.

The similarities are striking, although the frequency range covered in each two IB's is smaller than that observed in the

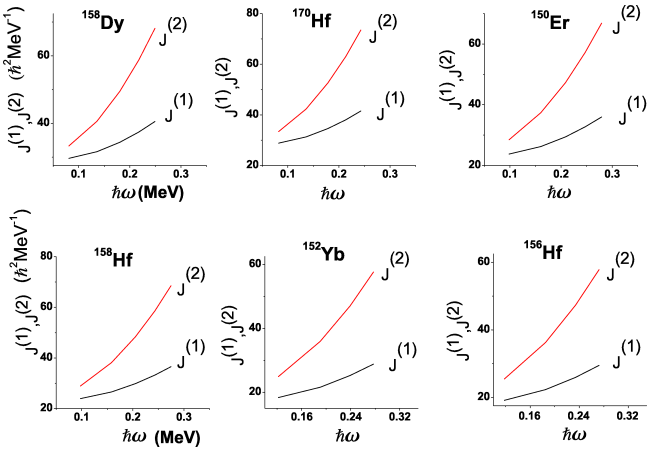

Fig. 1: Plot of the calculated kinematic $J^{(1)}$ and dynamic $J^{(2)}$ moments of inertia versus the rotational frequency $\hbar\omega$ for the low lying states in the conjugate pairs (^{158}Dy, ^{170}Hf), (^{160}Er, ^{168}Hf) and (^{162}Yb, ^{166}Hf).

Table 2: Theoretical calculations to outline the properties of our selected even rare-earth nuclei in framework of VMI model for each nucleus we list the energy E(I), the gamma ray transition energy $E_\gamma(I \to I-2)$, the rotational frequency $\hbar\omega$, the dynamic moment of inertia $J^{(2)}$, the kinematic moment of inertia $J^{(1)}$ and the variable moment of inertia J_{VMI}

$E_{exp}(I)$ (keV)	I^π ($\hbar$)	$E_{cal}(I)$ (keV)	$E_{\gamma(I\to I-2)}$ keV	$\hbar\omega$ (MeV)	$J^{(2)}$ ($\hbar^2$ MeV^{-1})	$J^{(1)}$ ($\hbar^2$ MeV^{-1})	J_{VMI} ($\hbar^2$ MeV^{-1})
			$^{158}Dy_{92}$				
99	2^+	101.379	101.379	0.0807	33.2515	29.5919	30
317	4^+	323.053	221.674	0.1354	40.5724	31.5779	33
638	6^+	643.316	320.263	0.1803	49.4620	34.3467	36
1044	8^+	1044.449	401.133	0.2175	58.8001	37.3940	39
1520	10^+	1513.609	469.160	0.2492	68.1419	40.4979	42
2050	12^+	2041.470	527.861			43.5720	45
			$^{170}Hf_{92}$				
100.8	2^+	104.135	104.135	0.0820	33.3828	28.8087	30
321.99	4^+	328.092	223.957	0.1356	42.2275	31.2560	33
642.9	6^+	646.774	318.682	0.1783	52.5513	34.5171	36
1043.3	8^+	1041.572	394.798	0.2132	63.1123	37.9941	40
1505.5	10^+	1499.749	458.177	0.2426	73.5077	41.4686	43
2016.4	12^+	2012.342	512.593			44.8699	47
			$^{160}Er_{68}$				
126	2^+	126.476	126.476	0.0983	28.4620	23.7199	25
390	4^+	393.490	267.014	0.1603	37.3148	26.2158	28
765	6^+	767.700	374.210	0.2082	47.2533	29.3452	31
1229	8^+	1226.560	458.860	0.2469	57.1845	32.6897	34
1761	10^+	1755.369	528.809	0.2793	66.8337	35.9297	37
2340	12^+	2344.028	588.659			39.0718	41
			$^{168}Hf_{96}$				
124	2^+	125.554	125.544	0.0974	28.8591	23.8941	25
386	4^+	389.712	264.158	0.1583	38.0709	26.4992	28
757	6^+	758.937	369.225	0.2052	48.3412	29.7921	31
1214	8^+	1210.907	451.970	0.2430	58.5677	33.1880	35
1736	10^+	1731.174	520.267	0.2747	68.4802	36.5194	38
2306	12^+	2309.582	578.678			39.7457	41
			$^{162}Yb_{92}$				
166	2^+	163.728	163.728	0.1220	24.9036	18.3230	20
487	4^+	488.075	324.347	0.1900	35.9266	21.5818	23
923	6^+	923.760	435.685	0.2390	47.0494	25.2475	27
1445	8^+	1444.462	520.702	0.2777	57.6036	28.8072	30
2023	10^+	2034.604	590.142			32.1936	34
			$^{166}Hf_{94}$				
159	2^+	157.173	157.173	0.1179	25.4281	19.0872	20
470	4^+	471.652	314.479	0.1848	36.2236	22.2590	24
897	6^+	896.556	424.904	0.2336	47.2768	25.8882	28
1406	8^+	1406.068	509.512	0.2720	57.8285	29.4399	31
1970	10^+	1984.750	578.682			32.8332	34

SD nuclei. The $J^{(2)}$ is significantly larger than $J^{(1)}$ over a large rotational frequency range.For our three IB pairs, the IB parameters are listed in Table 3.

5 Conclusion

The problem of identical bands(IB's) in normal deformed nuclei is treated. We investigated three pairs of conjugate normal deformed nuclei in rare-earth region (^{158}Dy,^{170}Hf), (^{160}Er, ^{168}Hf) and (^{162}Yb, ^{166}Hf) with the same F spin and projections $\pm F_0$ values have identical product of valence proton and neutron numbers N_pN_n values. Also the values of dynamical moment of inertia $J^{(2)}$ for each IB pair are approximately the same. We extracted all the IB symmetry parameters like p-factor, saturation factor SF, structure factor SP etc. which all depending on the valence proton and neutron numbers. By using the VMI model, we find agreement between experimental excitation energies and theoretical ones.

The optimized model free parameters for each nucleus have been deduced by using a computer simulation search programm to fit the calculated theoretical excitation energies with the experimental energies.

Submitted on October 17, 2016 / Accepted on October 24, 2016

Table 3: The calculated correlation factors for selected three pairs of even-even rare-earth nuclei having nearly identical bands.

	^{158}Dy	^{170}Hf	^{160}Er	^{168}Hf	^{162}Yb	^{166}Hf
(N_π, N_ν)	(8,5)	(5,8)	(7,5)	(5,7)	(6,5)	(5,6)
N_pN_n	160	160	140	140	120	120
F	6.5	6.5	6	6	5.5	5.5
F_0	1.5	-1.5	1	-1	0.5	-0.5
P	6.1538	6.1538	5.8333	5.8333	5.4545	5.4545
SF	4160	4160	3360	3360	2640	2640
SP	0.6176	0.6176	0.666	0.666	0.7179	0.7179
$J^{(2)}_{SF}$	32.2643	32.2645	28.9966	28.9966	25.7027	25.7027
$E^{(2)}_{SF}$	103.0160	103.0160	127.5437	127.5437	162.3283	162.3283
R(4/2)	3.2060	3.1943	3.0993	3.1096	2.9230	2.9671
R(6/2)	6.4468	6.3771	6.0866	6.1040	5.5430	5.6586
β_0	0.3322	0.3322	0.3218	0.3218	0.3110	0.3110
Δ	0.9546	0.9203	0.9486	0.9258	0.9428	0.9313
N_pN_n/Δ	167.6094	173.8563	147.5859	151.2205	127.2804	128.8521

References

1. Byrski T., Beck F.A., Curien D., Schuck C., Fallon P., Alderson A., Ali I., Bentley M.A., Bruce A.M., Forsyth P.D., Howe D., Roberts J.W., Sharpey-Schafer J.F., Smith G., and Twin P.J. Observation of identical superdeformed bands in N=86 nuclei. *Phys. Rev. Lett.* 1990, v. 64, 1650.
2. Janssens R.V.F. and Khoo T.L. Superdeformed Nuclei. *An. Rev. Nucl. Part. Sci.*, 1991, v. 41, 321.
3. Baktash C., Nazarewics W. and Wayss R. On the question of spin fitting and quantized alignment in rotational bands. *Nucl. Phys. A*, 1993, v. 555, 375.
4. Stephens F.S. Spin alignment in superdeformed Hg nuclei. *Phys. Rev. Lett.*, 1990, v. 64, 2623, and v. 65, 301.
5. Nazarewics W., Twin P.J., Fallon P. and Garrett J.D. Natural-parity states in superdeformed bands and pseudo SU(3) symmetry at extreme conditions. *Phys. Rev. Lett.*, 1990, v. 64, 1654.
6. Ragnarason I. Transition energies in superdeformed bands: Dependence on orbital and deformation. *Nucl. Phys. A*, 1990, v. 520, 76.
7. Chen B.Q. Observation of identical bands in superdeformed nuclei with the cranked Hartree-Fock method. *Phys. Rev. C*, 1992, v. 46, R1582.
8. Khalaf A., Sirag M. and Taha M. Spin assignment and behavior of superdeformed bands in A∼ 150 mass region. *Turkish Tournal of Physics*, 2013, v. 37, 49.
9. Khalaf A. and Okasha M.D. Properties of Nuclear Superdeformed Rotational Bands in A∼190 Mass. *Progress in Physics*, 2014, v. 10,246.
10. Khalaf A., Abdelmaged K. and Sirag M. Description of the yrast superdeformed bands in even-even nuclei in A∼190 region using the nuclear softness model. *Turkish Journal of Physics*, 2015, v. 39, 178.
11. Ahmad I., Carpenter M.P., Chasman R.R., Janssens R.V.F. and Khoo T.L. Rotational bands with identical transition energies in actinide nuclei. *Phys. Rev. C*, 1992, v. 44, 1204.
12. Baktash C., Garrett J.D. , Winchell D.F. and Smith A. Low-spin indentical bands in neighboring odd-A and even-even nuclei: A challenge to mean-field theories. *Phys. Rev. Lett.*, 1992, v. 69, 1500.
13. Casten R.F., Zamfir N.V., von Brentano P., and Chou W.-T. Identical bands in widely dispersed nuclei. *Phys. Rev. C*, 1992, v. 45, R1413.
14. Saha M. and Sen S. Low-spin identical bands in the NpNn scheme. *Phys. Rev. C*, 1992, v. 46, R1587.
15. Baktash C., Hass B. and Nazarewics W. Identical Bands in Deformed and Superdeformed Nuclei, *Annual Review of Nuclear and Particle Science*, 1992, v. 45, 485.
16. Zeng J.Y., Liu S.X., Lei Y.A. and Yu L. Microscopic mechanism of normally deformed identical bands at low spin in the rare-earth nuclei. *Phys. Rev. C*, 2001, v. 63, 024305.
17. Baktash C., Winchell D.F., Garrett J.D., Smith A. Low-spin identical bands in neighboring odd-A and even-even nuclei. *Nucl. Phys. A*, 1993, v. 557, 145.
18. Saha M. and Sen S. Simple phenomenology for the ground-state bands of even-even nuclei. *Phys. Rev. C*, 1994, v. 50, 2794.
19. Mariscotti M.A.J., Schaf G., Goldhaber G. and Buck B. Phenomenological Analysis of Ground-State Bands in Even-Even Nuclei. *Phys. Rev.*, 1969, v. 198, 1864.
20. Scharf G., Dover C.B. and Goodmann A.L. The Variable Moment of Inertia (VMI) Model and Theories of Nuclear Collective Motion. *Ann. Rev. Sci.*, 1976, v. 26, 239.
21. Bohr A. and Mottelson B. Nuclear structure. Vol. 2, Nuclear deformations. Benjamin (London), 1975.
22. Otsuka T., Arima A., Iachello F., Talmi I. Shell model description of interacting bosons. *Phys. Lett. B*, 1978, v. 76, 139.
23. Mittal H.M. and Devi V. Search for low-spin identical bands in light Xe-Gd nuclei. *Int. J. Nucl. Energy Sci. Techn.*, 2011, v. 6, 224.
24. Casten R.F. A simple approach to nuclear transition regions. *Phys. Lett. B*, 1985, v. 152, 145.
25. Zhang J.-Y., Casten R.F., Chou W.-T., Brenner D.S., Zamfir N.V. and von Brentano P. Identical bands and the varieties of rotational behavior. *Phys. Rev. Lett.*, 1992, v. 69, 1160.
26. Foy B.D., Casten R.F., Zamfir N.V. and Brenner D.S. Correlation between ε/Δ and the P factor. *Phys. Rev. C*, 1994, v. 49, 1224.
27. Iachello F. and Arima A. The Interacting Boson Model. Cambridge Univ. Press, Cambridge, 1987.

The Journal on Advanced Studies in Theoretical and Experimental Physics, including Related Themes from Mathematics

PROGRESS IN PHYSICS

A quarterly issue scientific journal, registered with the Library of Congress (DC, USA). This journal is peer reviewed and included in the abstracting and indexing coverage of: Mathematical Reviews and MathSciNet (AMS, USA), DOAJ of Lund University (Sweden), Scientific Commons of the University of St. Gallen (Switzerland), Open-J-Gate (India), Referativnyi Zhurnal VINITI (Russia), etc.

Electronic version of this journal:
http://www.ptep-online.com

Postal Address

Department of Mathematics and Science,
University of New Mexico,
705 Gurley Ave., Gallup, NM 87301, USA

ISSN: 1555-5534 (print)
ISSN: 1555-5615 (online)

Standard Address Number: 297-5092
Printed in the United States of America

April 2017 **Vol. 13, Issue 2**

CONTENTS

Information for Authors

Progress in Physics has been created for rapid publications on advanced studies in theoretical and experimental physics, including related themes from mathematics and astronomy. All submitted papers should be professional, in good English, containing a brief review of a problem and obtained results.

All submissions should be designed in LaTeX format using *Progress in Physics* template. This template can be downloaded from *Progress in Physics* home page http://www.ptep-online.com

Preliminary, authors may submit papers in PDF format. If the paper is accepted, authors can manage LaTeXtyping. Do not send MS Word documents, please: we do not use this software, so unable to read this file format. Incorrectly formatted papers (i.e. not LaTeXwith the template) will not be accepted for publication. Those authors who are unable to prepare their submissions in LaTeXformat can apply to a third-party payable service for LaTeX typing. Our personnel work voluntarily. Authors must assist by conforming to this policy, to make the publication process as easy and fast as possible.

Abstract and the necessary information about author(s) should be included into the papers. To submit a paper, mail the file(s) to the Editor-in-Chief.

All submitted papers should be as brief as possible. Short articles are preferable. Large papers can also be considered. Letters related to the publications in the journal or to the events among the science community can be applied to the section *Letters to Progress in Physics*.

All that has been accepted for the online issue of *Progress in Physics* is printed in the paper version of the journal. To order printed issues, contact the Editors.

Consideration and review process does not require any payment from the side of the submitters. Nevertheless the authors of accepted papers are requested to pay the page charges. *Progress in Physics* is a non-profit/academic journal: money collected from the authors cover the cost of printing and distribution of the annual volumes of the journal along the major academic/university libraries of the world. (Look for the current author fee in the online version of *Progress in Physics*.)

A Telemetric Multispace Formulation of Riemannian Geometry, General Relativity, and Cosmology: Implications for Relativistic Cosmology and the True Reality of Time

Larissa Borissova
E-mail: borissova@ptep-online.com

This thesis reveals an extended world-picture of Riemannian geometry as a telemetric multispace model of real space on the cosmological scale: certain new aspects of General Relativity are presented in terms of a fundamental membrane-transition picture of the deeper reality of time. We refer to this as "telemetric multispace formulation of General Relativity", a world-system with heavy emphasis on Riemannian geometry "per se" (in light of a particular set of extensive, purely geometric techniques), without all the usual historical-artificial restrictions imposed on it. This seminal model gives the purely geometric realization of instantaneous long-range action in the whole space-time of General Relativity whose sub-structure is extended to include an intrinsic, degenerate gravitational-rotational zero-space hosting zero-particles. The mathematical basis of modern cosmology is the four-dimensional pseudo-Riemannian space which is the curved space-time of General Relativity. The additional restrictions pre-imposed on space-time due to so-called "physical reasons" are, regularly: the signature conditions, the prohibition of super-luminal velocities, and the strictly uni-directional flow of time. We here study the peculiar conditions by which the observable time 1) is stopped; 2) flows from the future to the past. Our world and the world wherein time flows oppositely to us are considered as spaces such that they are "mirror images" of each other. The space wherein time stops (the present) is the "mirror" reflecting the future and the past. Then we consider the interaction between a sphere of incompressible liquid (the Schwarzschild bubble) and the de Sitter bubble filled with physical vacuum: this is an example of the interaction between the future and the past through the state of the present.

1 Riemannian geometry as a mathematical model of the real world

A brief historical background is at hand, followed by a critical mathematical repraisal. As known, the mathematical basis of modern cosmology is the four-dimensional pseudo-Riemannian space — the curved space-time of General Relativity. It belongs to the whole spectrum of Riemannian spaces obtained by Bernhard Riemann as a generalization of Carl Gauss' work on curved surfaces. Riemannian spaces possess any number dimension n. The numerical value of n is determined by a maximal number of independent basis vectors (general basis, in the collective sense) of the Riemannian space V_n [1]. The basis of the V_n is introduced at every point of the flat space E_n which is tangent to the V_n at this point. If the basis vectors are linearly dependent, the dimension of the V_n is less than that of the space wherein the basis vectors are independent of each other. There exist two types of basis vectors possessing: 1) the positive square of the length (a real vector); 2) the negative square of the length (an imaginary vector). As familiar, if all the basis vectors of the space are real or imaginary, it is known as the *Riemannian space*. If some of the basis vectors are real while other ones are imaginary, the space is known as the *pseudo-Riemannian space*. Flat Riemannian spaces, where all the basis vectors possess unit or imaginary unit lengths, are known as the *Euclidean spaces* E_n. For example, the E_3 is the ordinary flat three-dimensional space where the unitary system of Cartesian coordinates can be introduced. Flat Riemannian spaces where some basis vectors are real and other ones are imaginary, are known as the *pseudo-Euclidean spaces*. The four-dimensional pseudo-Euclidean space E_4, which possesses one imaginary basis vector along with three real ones, is known as the *Minkowski space* (German Minkowski introduced time as the fourth coordinate $x^0 = ct$, where t is the coordinate time while c is the light velocity). The pseudo-Euclidean space E_4 is of course the basic space (space-time) of Special Relativity. The pseudo-Riemannian (curved) four-dimensional space V_4 with the same set of the basis vectors is the basic space (space-time) of General Relativity. The idea of applying the four-dimensional pseudo-Riemannian space to the description of the real world was suggested Marcel Grossman, a close mathematician friend of Albert Einstein. Einstein agreed with him, because the metrical properties of Riemannian spaces are simplest in comparison to the properties of other metric spaces. The point is that Riemannian metrics are invariant relative to transformations of coordinates. It implies that the square of the elementary

infinitesimal vector dx^α conserves its length:

$$ds^2 = g_{\alpha\beta}dx^\alpha dx^\beta, \quad \alpha,\beta = 0,1,2,3, \tag{1}$$

where the contraction by indices α,β denotes the summation.

Metrics of Riemannian spaces are symmetric ($g_{\alpha\beta} = g_{\beta\alpha}$) and non-degenerate ($g = \det\|g_{\alpha\beta}\| \neq 0$), while the elementary four-dimensional interval is invariant relative to any reference system ($ds^2 = const$). The invariance of the ds^2 is a very important argument on behalf of Riemannian geometry as the mathematical basis of General Relativity.

The metric coefficients are of course the cosines of the angles between the basis vectors in the locally flat tangent space. This is because ds^2 is the scalar product of dx^α with itself. The dimension of the flat tangent space and the correlation between the imaginary and real basis vectors are the same as in the corresponding Riemannian space. A system of basis vectors $\mathbf{e}_\alpha$ can be introduced at any point of the locally tangent space. The $\mathbf{e}_\alpha$ are tangent to the coordinate lines x^α. The fundamental metric tensor can be expressed through the basis vectors $\mathbf{e}_\alpha$ as [2]:

$$g_{\alpha\beta} = e_\alpha e_\beta \cos\left(\widehat{x^\alpha, x^\beta}\right), \tag{2}$$

where e_α is the length of the $\mathbf{e}_\alpha$. Assume here the temporal basis vector $\mathbf{e}_0$ to be real, while, correspondingly, the basis spatial vectors $\mathbf{e}_i$ ($i = 1,2,3$) are imaginary.

We recall that the interval ds^2 can be positive, negative, or null. The value ds is used as the parameter along trajectories of particles (world-lines of particles). These lines can be: 1) real by $ds^2 > 0$, 2) imaginary by $ds^2 < 0$, 3) zero by $ds^2 = 0$. The value ds is used as the global parameter along world-lines. Real mass-bearing particles (the rest-mass $m_0 \neq 0$, the relativistic mass $m = \frac{m_0}{\sqrt{1-V^2/c^2}}$ is real) move along the non-isotropic lines ($ds \neq 0$) at sub-luminal velocities $V < c$; imaginary mass-bearing particles or hypothetical *tachyons* (the rest-mass $m_0 \neq 0$, the relativistic mass $m = \frac{im_0}{\sqrt{1-V^2/c^2}}$ is imaginary) move along non-isotropic lines ($ds \neq 0$) at super-luminal velocities $V > c$; massless particles (the rest-mass $m_0 = 0$, the relativistic mass $m \neq 0$) move along isotropic lines ($ds = 0$) at light velocity $V = c$. Thus, for example, photons are actual light-like particles.

The description of the world is to be linked with the real reference frame of a real observer who actually defines both geometrical and mechanical properties of the space of reference he inhabits. The reference frame is a reference body where coordinate nets are spanned and clocks are installed at the every point of the reference's body. The profound problem of the introduction of physically observable quantities in the whole inhomogeneous, anisotropic curved space of General Relativity is to determine which components of the every four-dimensional quantity are the physically observable quantities. This problem was solved decisively and comprehensively by A. Zelmanov [2]. He introduced chronometric invariants (chr.-inv.) as physically observable geometric quantities in General Relativity. These fundamental quantities are linked to the reference body which can, in general, gravitate, rotate, and deform. The three-dimensional observable space (the reference space) can be both curved and flat. The reference body is considered as a set of real coordinate systems, to which the observer compares all results of his measurements. Therefore the physically observable quantities are constructed as the result of fundamentally (in a unified, simultaneous geometrical-mechanical fashion) projecting four-dimensional quantities on the lines of time and on the three-dimensional space.

The chr.-inv. form of the four-dimensional interval ds^2 is [2]

$$\begin{aligned} &ds^2 = c^2d\tau^2 - d\sigma^2, \quad d\tau = \left(1 - \frac{\mathrm{w}}{c^2}\right)dt - \frac{v_i dx^i}{c^2}, \\ &d\sigma^2 = h_{ik}dx^i dx^k, \quad h_{ik} = -g_{ik} + \frac{v_i v_k}{c^2}, \quad i,k = 1,2,3, \end{aligned} \tag{3}$$

where $d\tau$ is the interval of the observable time, $d\sigma^2$ is the observable spatial interval, $\mathrm{w} = c^2(1 - \sqrt{g_{00}})$ is the three-dimensional gravitational potential, $v_i = -\frac{cg_{0i}}{\sqrt{g_{00}}}$ is the linear velocity of the space rotation, h_{ik} is the three-dimensional fundamental metric tensor. The expression (3) may be rewritten in the form

$$ds^2 = c^2d\tau^2\left(1 - \frac{V^2}{c^2}\right), \quad V^i = \frac{dx^i}{d\tau}, \quad V^2 = h_{ik}V^iV^k, \tag{4}$$

where V^i is the observable three-dimensional velocity.

It follows from (4) that ds is: 1) real if $V < c$, 2) imaginary if $V > c$, 3) zero if $V = c$. The condition $ds = 0$ has the form

$$cd\tau = \pm d\sigma, \tag{5}$$

which is of course the equation of the elementary light cone. The term *elementary* means that this cone can be introduced only at every point of the space-time, but not into the whole space. The elements of the cone are trajectories of massless particles moving along null geodesic lines.

As follows from (4, 5), photons are at rest within the space-time ($ds = 0$) itself, but they move at light velocity ($V = c$) along three-dimensional trajectories ($cd\tau = d\sigma$) within the three-dimensional observable space. The light cone is known as the "light barrier" which "prohibits" motions at super-luminal velocities. Really, this restriction means that mass-bearing particles, both real ones and tachyons, cannot move at light velocity. The zero-particles penetrating the light cone are considered in detail in [3]. These particles are essentially thinner structures than light, because their relativistic masses m are zeroes. Zero-particles possess non-zero gravitational-rotational masses $M = \frac{m}{1-(\mathrm{w}+v_iu^i)/c^2}$, where $u^i = \frac{dx^i}{dt}$. Zero-particles transfer instantly ($d\tau = 0$) along three-dimensional null trajectories ($d\sigma = 0$). The light cone is therefore transparent for zero-particles and non-transparent for mass-bearing real particles

and tachyons. As such, we may call it a "membrane". Thus the apparatus of General Relativity allows the existence of long-range action as truly instantaneous-transfer zero-particles. Moreover, this fundamental transfer unifies the worlds of both real particles and tachyons. As for the other new aspects of General Relativity, we shall introduce them in the next sections.

2 The past and the future as the mirror reflections each other

Most contemporary scientists presuppose that time flows only in a single direction — from the past to the future. The mathematical apparatus of General Relativity does not prohibit the reverse flow of time, i.e. from the future to the past. Nevertheless, the reverse flow of time is not introduced in contemporary physics and cosmology, partly because modern scientists refer to Hans Reichenbach's "arrow of time", which is directed always to the future. However, upon further analysis, Reichenbach, speaking about a unidirectional flow of time, implied a rather limited world-process of evolution (transfer mechanism of energy). He wrote: "Super-time has not a direction, but only an order. Super-time itself, however, contains local sections, each of whom has a direction, while the directions change from one section to another" [4]. Contemporary scientists consider the light cone of Minkowski space as a mathematical illustration of the time arrow: the lower half of the cone means the *past*, while the upper half — the *future*. The past automatically turns into the future at the point $t = 0$, meaning the *present*. But such an automatic transfer is due to the fact that the Minkowski space of Special Relativity is de facto empty. Besides, it does not at all include both gravitation and rotation (in addition to deformation and the whole curvature), therefore the ideal, uniformly flowing time of Special Relativity does not (and can not) depend on gravitation and rotation. In other words, this transfer does not require fundamental transformations of matter. In fact, in this picture, photons flow continuously from the lower half of the cone to the upper one. However the "real space" perceived by us as the "present" is ultimately penetrated by gravitation. Besides, the objects of the said space, ranging from electrons to galaxies and their clusters, do rotate around their centers of gravitational attraction. The problem is therefore to describe, in the framework of General Relativity, the fundamental interaction between the future and the past as a proper energetic transfer through the present state. Such description of the future-past transfer is a more exact approximation, than in the self-limited Minkowski space, because the observable time τ essentially depends on both gravitation and rotation: see (3, 5). The expressions $d\tau = 0$, $d\sigma = 0$ describe the *membrane*, which is situated between the past and the future. These expressions can be rewritten in the form [3]:

$$\mathrm{w} + v_i u^i = c^2, \quad h_{ik} dx^i dx^k = 0, \quad u^i = \frac{dx^i}{dt}. \qquad (6)$$

As the metric form $d\sigma^2$ is positively determined, the condition $d\sigma^2 = 0$ means that it is degenerated: $h = \det \|h_{ik}\| = 0$. The determinants of the matrices $g = \det \|g_{\alpha\beta}\|$ and h are linked by the relation $\sqrt{-g} = \sqrt{g_{00} h}$ [2], therefore the four-dimensional matrix $\|g_{\alpha\beta}\|$ is degenerated: $g = \det \|g_{\alpha\beta}\| = 0$. The condition of the membrane transition can be written in the form [3]:

$$\mathrm{w} + v_i u^i = c^2, \quad d\mu^2 = g_{ik} dx^i dx^k = \left(1 - \frac{\mathrm{w}}{c^2}\right)^2 c^2 dt^2, \qquad (7)$$

where the first expression characterizes the condition of the *stopped time*, the second expression describes the geometry of the hyper-surface, where events of the present are realized.

The conditions (7) describe the zero-space, where, from a viewpoint of a real observer, zero-particles extend instantly ($d\tau = 0$) along three-dimensional null lines ($d\sigma = 0$) [3]. The instant transfer of zero-particles means the **long-range-action**. We conclude that the **future-past transfer is realized instantaneously**, i.e. it is the long-range-action. Note, the coordinate length $d\mu = \left(1 - \frac{\mathrm{w}}{c^2}\right) cdt$ depends, in part, on the gravitational potential w, wherein $d\mu = 0$ by the collapse condition: $\mathrm{w} = c^2$. Thus the metric on the hyper-surface is, in general, not a Riemannian one, because its interval $d\mu$ is not invariant (yet it is invariant by the collapse, as in this case $d\mu^2 = 0$). The region of space-time, which is located between the spaces of the past and the future, is perceptible by a real observer as the present. It is the hyper-surface where all events are realized at the same moment of observable time $\tau_0 = const$, i. e. such events are *synchronized*. The momentary interaction (the long-range-action) is transferred by particles of a special kind — *zero-particles*. They possess zero rest-mass m_0, zero relativistic mass m, and non-zero gravitational-rotational mass M. This quantity is determined in the generalized space-time where the condition $g = 0$ is satisfied. The mass M in the generalized space has the form [3]

$$M = \frac{mc^2}{c^2 - (\mathrm{w} + v_i u^i)}.$$

Thus the elements of the elementary curved light cone (the so-called "light barrier") are indeed penetrable for zero-particles. As follows from (5), trajectories of photons belong to both the space and time, because they extend along null four-dimensional trajectories $ds = 0$. The three-dimensional body of the real observer can thus move at pre-light velocity in the three-dimensional space, but it is always rigidly attached to the moment of time, which is perceptible as the present.

A brief philosophical digression: transfers both in the past and in the future are possible, so far, only mentally. The typical human mind does remember the past (not always clearly) and does predict the future (not always exactly). It is possible to say that the past and the future are virtual, because only the human consciousness moves in these virtual spaces, but the

physical body is strictly in the present ("reality"). Studying the past of the Earth and remembering our own past, we see a recurrence of some events, both planetary and individual. We know what happened with the Earth in the past due to mainly the tales of our ancestors, if not historians. Events (three-dimensional points, as well as threads extended in time) are ordered in a determined sequence in time. Comparing similar events from different intervals of time, we can say that the past and the future are similar, being mirror reflections of one other. The object of the three-dimensional space and its mirror reflection differ only by the notions of "left" and "right" possessing the opposite sense for every one of them. The intervals of both coordinate time and observable time are linked by the formula [3]

$$\frac{dt}{d\tau} = \frac{\frac{v_i V^i}{c^2} \pm 1}{\sqrt{g_{00}}}. \tag{8}$$

The expression (8) was studied in [3] by the condition $\sqrt{g_{00}} > 0$. It means that we did not consider in [3] the reverse of time while simultaneously taking into account the state of collapse $g_{00} = 0$. As follows from (8), the coordinate time t: 1) is stopped ($dt = 0$) if $v_i V^i = \mp c^2$; 2) possesses direct flow ($dt > 0$) if $v_i V^i > \mp c^2$; 3) possesses reverse flow ($dt < 0$) if $v_i V^i < \mp c^2$. Thus the spaces with direct and the reverse flows of coordinate time t are divided by a fundamental surface of rotation, where the vectors v_i and V^i are linked by the relation, see (2, 3):

$$v_i V^i = \mp c^2 |v_i||V^i| \cos\left(\widehat{v_i, V^i}\right) = \mp c^2 |e_i||V^i| \cos\left(\widehat{e_i V^i}\right),$$

where e_i is the spatial basis vector in the tangent Minkowski space. It is evident that this relation is realized for two cases:

1) the vectors v_i and V^i are co-directed, $|v_i| = |V^i| = c$;

2) the vectors v_i and V^i are anti-directed, $|v_i| = |V^i| = c$.

Since the vector v_i means the linear velocity of space rotation, we conclude that the very surface dividing the spaces with direct and reverse flow of coordinate time rotates at light velocity. The rotation is either left or right.

A real observer measures that the time τ coincides completely with the coordinate time t only in the case wherein the reference space does not rotate ($v_i = 0$) nor gravitate ($w = 0$): see (3). If $w \neq 0$ or $v_i \neq 0$, the τ, in contrast to t, depends essentially on gravitation and rotation. Because we live in the real world, where gravitation and rotation do exist, we will further consider the *observable time*.

The observable Universe, which is a part of the Infinite Whole, can belong to one of the aforementioned spaces (either possessing positive or negative flow of coordinate time). Let the flow of coordinate time in the region, where the observer is situated, be positive: $dt > 0$. The observable time is divided by the consciousness of a real observer into the "past", the "present" and the "future": time flows from the past to the future through the present. The problem stated in the beginning of this paper is to study the future-past transfer from the point of view of a real observer, who is located in the world of positive flow of coordinate time $dt > 0$. This problem is essentially simplified in the case where the reference space does not rotate. Then the expression (8) can be rewritten in the form

$$d\tau = \pm\sqrt{g_{00}}\, dt = \pm\left(1 - \frac{w}{c^2}\right) dt. \tag{9}$$

Taking into account the collapse condition $\sqrt{g_{00}}$, we shall study the direction of observable time flow in the gravitational field. It follows from (9) that the observable time τ: 1) possesses positive direction if $\sqrt{g_{00}} > 0$, 2) possesses negative direction if $\sqrt{g_{00}} < 0$, 3) stops if $\sqrt{g_{00}} = 0$. Because the condition $g_{00} = 0$ is the collapse condition, the **surface of the collapsar is the mirror separating the spaces with both positive and negative flow of the observable time**. The observable time is perceptible by human consciousness as flowing from the past to the future, therefore we call the space of such direct flow of time the "space of the past". Then the space of reverse flow of observable time is necessarily the "space of the future". The present space is situated between these spaces. The concrete spaces reflecting from the surface of the collapsar, as from the mirror, will be studied in detail in the next section.

3 The interaction between the Schwarzschild and de Sitter bubbles as instantaneous transfer

All objects in the Universe consist of the same fluid substance being at different stages of cosmic evolution. Many cosmic bodies (planets, stars, ...) are spheroids, namely spinning, deforming spheres. Probably the physical body of the Universe has the same form. The problem is to introduce the space-time (gravitational field) created by a liquid incompressible sphere. A similar model was introduced earlier by the German astronomer Karl Schwarzschild [5]. He solved the field equations (Einstein equations) for the sphere by the assumption that the solution must be everywhere regular. In other words, Schwarzschild ruled out the existence of singularities. Meanwhile the problem of singularities is very actual for astrophysics and cosmology. The more general, allowing singularities, solution of the Einstein equations for the sphere filled by ideal incompressible liquid was obtained in [6]. The substance filling the sphere is described by the energy-impulse tensor

$$T^{\alpha\beta} = \left(\rho + \frac{p}{c^2}\right) b^\alpha b^\beta - \frac{p}{c^2} g^{\alpha\beta}, \tag{10}$$

where $\rho = const$ is the density of substance, p is the pressure, $b^\alpha = \frac{dx^\alpha}{ds}$ is the four-dimensional unit velocity vector: $g_{\alpha\beta} b^\alpha b^\beta = 1$.

The solution allowing singulary states of the space-time has the form [6]

$$ds^2 = \frac{1}{4}\left(3\sqrt{1-\frac{\varkappa\rho a^2}{3}} - \sqrt{1-\frac{\varkappa\rho r^2}{3}}\right)^2 c^2dt^2 - \frac{dr^2}{1-\frac{\varkappa\rho r^2}{3}} - r^2(d\theta^2+\sin^2\theta d\varphi^2), \quad (11)$$

where $\varkappa = \frac{8\pi G}{c^2}$ is the Einstein gravitational constant, G is the Newton gravitational constant, a is its radius, r, θ, φ are the spherical coordinates.

The gravitational field described by (11) has two singularities [6]:

1) it collapses if

$$3\sqrt{1-\frac{\varkappa\rho a^2}{3}} = \sqrt{1-\frac{\varkappa\rho r^2}{3}};$$

2) it breaks the space if

$$\frac{\varkappa\rho r^2}{3} = 1.$$

The radius of the collapsar r_c and the radius of the breaking space r_{br} have the forms, respectively:

$$r_c = \sqrt{9a^2 - \frac{24}{\varkappa\rho}} = \sqrt{9a^2 - 8r_{br}{}^2}, \quad (12)$$

where the breaking radius $r_{br} = \sqrt{\frac{3}{\varkappa\rho}} = \frac{4\times10^{13}}{\sqrt{\rho}}$ cm.

It follows from (12) that the incompressible liquid sphere collapses if $a > \sqrt{\frac{8}{9}}\, r_{br} = 0.94\, r_{br}$. (Because by $a = \sqrt{\frac{8}{9}r_{br}}$ the collapsing object transforms into the point $r_c = 0$, we do not consider this case non-sense in the physical meaning). If $\rho = 10^{-29}$ g/cm^3 (the assumed value of the density of matter in the observable Universe), then the sphere collapses by $a > 1.2\times10^{28}$ cm and breaks the surrounding space by $a = 1.3\times10^{28}$ cm. If the density of matter inside the sphere is $\rho = 10^{14}$ g/cm^3 (as inside the atomic nucleus), then $a > 3.8\times10^6$ cm and $r_{br} = 4\times10^6$ cm. The density of matter inside a typical neutron star is regularly assumed to be the same as the nuclear density, while its radius is about a dozen kilometers. With these, larger-sized neutron stars may be non-observable, because they are gravitational collapsars. Estimate now the minimal value of the mass of the neutron star by the assumption that it collapses. If $a = 3.8\times10^6$ cm, then the mass $M = \frac{4\pi a^3\rho}{3} = 23\times10^{33}$ g $= 11.5M_\odot$, where $M_\odot$ is the mass of the Sun. Assuming $\rho = 1$ g/cm^3 (the density of hydrodynamical fluid), we find $r_{br} = 4\times10^{13}$ cm. It means, such a fluid sphere collapses if its radius is $a > 4\times10^{13}$ cm.

A sphere of incompressible liquid with a constant volume and a constant density, which is situated in the state of weightlessness, is a kind of *condensed matter*. The planets, rotating around the Sun, as well as the stars, rotating around the center of the Galaxy, are in the state of weightlessness [6]. Assume that stationary stars consist of condensed matter. For example, consider the Sun as an actual sphere of condensed matter. The density of the Sun is $\rho_\odot = 1.4$ g/cm^3, and its radius is $a = 7\times10^7$ cm. We find $r_{br} = 3.4\times10^{13}$ cm. It follows from (12) that the collapse of the Sun is impossible in this state of matter, because r_c has an imaginary value. It is interesting to note that the surface of breaking of the Sun is at the distance r_{br}=2.3 AU, where the *Astronomical Unit* (AU) is the average distance between the the Sun and the Earth: 1 AU = 1.49×10^{13} cm. So we obtain that the surface of breaking (curvature discontinuity), created by the Sun, is actually situated inside the asteroid strip region, very close to the orbit of the maximal concentration of asteroids: 2.5 AU from the Sun [6]. (As known, the asteroid strip's distance from the Sun is within the limit of 2.1 to 4.3 AU).

Let's now study the simultaneous mechanical and geometrical properties of the metric (11). As shown in [2], the three-dimensional observable space (the reference space) is characterized by the three mechanical characteristics and one geometrical. The mechanical characteristics are: the vector of the gravitational inertial force F_i, the tensor of the angular velocity of rotation A_{ik}, and the tensor of the rate of deformation D_{ik}:

$$F_i = \frac{c^2}{c^2-\mathrm{w}}\left(\frac{\partial \mathrm{w}}{\partial x^i} - \frac{\partial v_i}{\partial t}\right), \quad D_{ik} = \frac{1}{2}\frac{{}^*\partial h_{ik}}{\partial t},$$

$$A_{ik} = \frac{1}{2}\left(\frac{\partial v_k}{\partial x^i} - \frac{\partial v_i}{\partial v_k}\right) + \frac{1}{c^2}(F_i v_k - F_k v_i),$$

where $\frac{{}^*\partial}{\partial t} = \frac{1}{\sqrt{g_{00}}}\frac{\partial}{\partial t}$ is the chr.-inv. operator of differentiation along the temporal coordinate.

We find that the reference space of the metric (11) does not rotate ($A_{ik} = 0$) and deform ($D_{ik} = 0$), but it gravitates. The gravitational inertial force F_i has the only non-zero component [6]

$$F_1 = -\frac{\varkappa\rho c^2}{3}\frac{r}{\left(3\sqrt{1-\frac{\varkappa\rho a^2}{3}} - \sqrt{1-\frac{\varkappa\rho r^2}{3}}\right)\sqrt{1-\frac{\varkappa\rho r^2}{3}}} \quad (13)$$

$F_1 < 0$.

Thus the quantity F_i is the non-Newtonian force of attraction. Then $F_1 \to \infty$ both by the collapse and the breaking of space [6].

The pressure of the ideal liquid p is determined from the conservation law [6]. It has the form

$$p = \rho c^2 \frac{\sqrt{1-\frac{\varkappa\rho r^2}{3}} - \sqrt{1-\frac{\varkappa\rho a^2}{3}}}{3\sqrt{1-\frac{\varkappa\rho a^2}{3}} - \sqrt{1-\frac{\varkappa\rho r^2}{3}}} > 0. \quad (14)$$

It follows from (14) that $p \to \infty$ by the collapse and $p = -\frac{\rho c^2}{3}$ at the surface of break.

The geometric characteristic of the reference space is the chr.-inv. three-dimensional tensor of curvature C_{ijkl} [2] possessing all the algebraic properties of the Riemann-Christoffel four-dimensional tensor of curvature $R_{\alpha\beta\gamma\delta}$. The C_{ijkl} has the form [2]:

$$C_{ijkl} = \frac{1}{4}(H_{ijkl} + H_{ljki} - H_{jilk} + H_{kilj}), \tag{15}$$

where H_{ijkl} is the chr.-inv. close analog of the Schouten tensor in the theory of non-holonomic manifolds

$$H^{\cdots l}_{ijk\cdot} = \frac{{}^*\partial\Delta^l_{ik}}{\partial x^j} - \frac{{}^*\partial\Delta^l_{ij}}{\partial x^k} + \Delta^m_{ik}\Delta^l_{jm} - \Delta^m_{ij}\Delta^l_{km}, \tag{16}$$

where

$$\Delta^k_{ij} = h^{km}\Delta_{ij,m}, \quad \Delta_{ij,m} = \frac{1}{2}\left(\frac{{}^*\partial h_{im}}{\partial x^j} + \frac{{}^*\partial h_{jm}}{\partial x^i} - \frac{{}^*\partial h_{ij}}{\partial x^m}\right) \tag{17}$$

are the chr.-inv. Christoffel symbols of the second and first kind, respectively, $\frac{{}^*\partial}{\partial x^i} = \frac{\partial}{\partial x^i} + \frac{v_i}{c^2}\frac{{}^*\partial}{\partial t}$ is the chr.-inv.operator of differentiation along spatial coordinates [2].

The tensors H_{ijkl} and C_{iklj} are linked by the relation [2]

$$H_{ijkl} = C_{ijkl} + \frac{1}{c^2}\Big(2A_{jk}D_{li} + A_{ik}D_{jl} + A_{lj}D_{ik} + A_{il}D_{jk} + A_{lj}D_{ki}\Big). \tag{18}$$

It is evident, therefore, that $C_{lkij} = H_{lkij}$ if $A_{ik} = 0$ or $D_{ik} = 0$. Calculating the Christoffel symbols of the second kind, we obtain for the non-zero components:

$$\begin{aligned}
&\Delta^1_{11} = \frac{\varkappa\rho r}{3}\frac{1}{1-\frac{\varkappa\rho r^2}{3}},\\
&\Delta^1_{22} = \frac{\Delta^1_{33}}{\sin^2\theta} = -r\left(1-\frac{\varkappa\rho r^2}{3}\right),\\
&\Delta^2_{12} = \Delta^3_{13} = \frac{1}{r}, \quad \Delta^2_{33} = -\sin\theta\cos\theta,\\
&\Delta^3_{23} = \cot\theta.
\end{aligned} \tag{19}$$

Substituting (19) into (16) and lowering the upper indices, we find the non-zero components C_{iklj} for the space-time described by the metric (11)

$$\begin{aligned}
&C_{1212} = \frac{C_{1313}}{\sin^2\theta} = \frac{\varkappa\rho r^2}{3}\frac{1}{1-\frac{\varkappa\rho r^2}{3}},\\
&C_{2323} = \frac{\varkappa\rho r^4}{3}\sin^2\theta.
\end{aligned} \tag{20}$$

The components $C_{ik} = h^{mn}C_{imkn}$ and the three-dimensional scalar $C = h^{ik}C_{ik}$ have the form [7]

$$\begin{aligned}
&C_{11} = \frac{2\varkappa\rho}{3}\frac{1}{1-\frac{\varkappa\rho r^2}{3}}, \quad C_{22} = \frac{C_{33}}{\sin^2\theta} = \frac{2\varkappa\rho r^2}{3},\\
&C = 2\varkappa\rho > 0.
\end{aligned} \tag{21}$$

The three-dimensional reference space satisfies the condition

$$C_{ijkl} = q(h_{ik}h_{jl} - h_{jk}h_{il}), \quad q = \frac{\varkappa\rho}{3} = const, \tag{22}$$

therefore it is the space of constant positive curvature, where q is the Gaussian curvature of the three-dimensional reference space. It follows from (12) that the radius of curvature is $\frac{1}{q} = r_{br} = \sqrt{\frac{3}{\varkappa\rho}}$. It is necessary to note that the *Gaussian curvature and, consequently, the radius of space breaking depend on the density of incompressible liquid*.

Thus we have found that the three-dimensional reference space of the space-time (11) is the space of constant positive curvature. Study now the geometric properties of the four-dimensional space (11). As is well-known, the geometric properties of every curved (Riemannian) space are described by the Riemann tensor

$$\begin{aligned}
R_{\alpha\beta\gamma\delta} = &\frac{1}{2}(\partial_{\beta\gamma}g_{\alpha\delta} + \partial_{\alpha\delta}g_{\beta\gamma} - \partial_{\alpha\gamma}g_{\beta\delta} - \partial_{\beta\delta}g_{\alpha\gamma}) +\\
&+g^{\sigma\tau}(\Gamma_{\alpha\delta,\sigma}\Gamma_{\beta\gamma,\tau} - \Gamma_{\beta\delta,\sigma}\Gamma_{\alpha\gamma,\tau}),
\end{aligned} \tag{23}$$

where $\Gamma_{\alpha\beta,\sigma}$ are the Christoffel symbols of the first kind

$$\Gamma_{\alpha\beta,\sigma} = \frac{1}{2}(\partial_\alpha g_{\beta\sigma} + \partial_\beta g_{\alpha\sigma} - \partial_\sigma g_{\alpha\beta}). \tag{24}$$

Calculating the values $\Gamma_{\alpha\beta,\sigma}$ for the metric (11) we obtain

$$\begin{aligned}
&\Gamma_{01,0} = -\Gamma_{00,1} = \frac{\varkappa\rho r}{12}\frac{3\sqrt{1-\frac{\varkappa\rho a^2}{3}} - \sqrt{1-\frac{\varkappa\rho r^2}{3}}}{\sqrt{1-\frac{\varkappa\rho r^2}{3}}},\\
&\Gamma_{11,1} = -\frac{\varkappa\rho r}{3}\frac{1}{\left(1-\frac{\varkappa\rho r^2}{3}\right)^2},\\
&\Gamma_{22,1} = -\Gamma_{12,2} = r,\\
&\Gamma_{33,1} = -\Gamma_{13,3} = r\sin^2\theta,\\
&\Gamma_{33,2} = -\Gamma_{23,3} = r^2\sin\theta\,\cos\theta.
\end{aligned} \tag{25}$$

Calculating the components of Riemann tensor (23) for the metric (11) we find

$$\begin{aligned}
&R_{0101} = -\frac{1}{4r^2_{br}}\frac{3\sqrt{1-\frac{a^2}{r^2_{br}}} - \sqrt{1-\frac{r^2}{r^2_{br}}}}{\sqrt{1-\frac{r^2}{r^2_{br}}}},\\
&R_{0202} = -\frac{r^2}{4r^2_{br}}\left(3\sqrt{1-\frac{a^2}{r^2_{br}}} - \sqrt{1-\frac{r^2}{r^2_{br}}}\right)\sqrt{1-\frac{r^2}{r^2_{br}}},\\
&R_{1212} = -\frac{r^2}{r^2_{br}}\frac{1}{1-\frac{r^2}{r^2_{br}}}, \quad R_{2323} = -\frac{r^4}{r^2_{br}}\sin^2\theta,\\
&R_{0303} = R_{0202}\sin^2\theta, \quad R_{1313} = R_{1212}\sin^2\theta,
\end{aligned} \tag{26}$$

where $r_{br}^2 = \frac{1}{q} = \frac{3}{\varkappa\rho}$.

The space-time is therefore not a constant-curvature space, because the components R_{0i0k} of the Riemann tensor do not satisfy the condition

$$R_{\alpha\beta\gamma\delta} = K(g_{\alpha\gamma}g_{\beta\delta} - g_{\beta\gamma}g_{\alpha\delta}), \quad K = const, \tag{27}$$

which is a necessary and sufficient condition that the space-time possesses constant curvature. Note that the spatial components R_{ijkl} satisfy (27), while the mixed components R_{oijk} are zeroes. It means, due the structure of the components R_{0i0k}, the space-time (11) does not possess constant curvature.

So forth, study the geometric properties of the space-time (11) in terms of Zelmanov's theory of physically observable quantities. Zelmanov selected three groups of all independent curvature components $R_{\alpha\beta\gamma\delta}$ — the projections on time, the projections on space, and the mixed projections [2]:

$$X^{ik} = -c^2\frac{R^{\cdot i\cdot k}_{0\cdot 0\cdot}}{g_{00}}, \quad Y^{ijk} = c\frac{R^{\cdot ijk}_{0\cdot\cdot\cdot}}{\sqrt{g_{00}}}, \quad Z^{iklj} = c^2R^{iklj}.$$

Here we have only interest in the components X^{ik}. Calculating these components, we obtain

$$\begin{aligned} X_{11} &= \frac{c^2}{r_{br}^2}\frac{1}{\left(3\sqrt{1-\frac{a^2}{r_{br}^2}} - \sqrt{1-\frac{r^2}{r_{br}^2}}\right)\sqrt{1-\frac{r^2}{r_{br}^2}}} > 0, \\ X_{22} &= \frac{X_{33}}{\sin^2\theta} = \frac{c^2r^2}{r_{br}^2}\frac{\sqrt{1-\frac{r^2}{r_{br}^2}}}{3\sqrt{1-\frac{a^2}{r_{br}^2}} - \sqrt{1-\frac{r^2}{r_{br}^2}}} > 0. \end{aligned} \tag{28}$$

All components $X_{ik} \to \infty$ in the state of collapse. Besides, if the breaking of space takes place, the $X_{11} \to \infty$ and $X_{22} = X_{33}$ are zeroes. Comparing (13) and (28), we find that the gravitational inertial force F_1 and the radial projection of the Riemann tensor on time X_{11} are linked by the relation

$$F_1 = -rX_{11}. \tag{29}$$

It means that the sign of the r-directed force is opposite to the sign of the temporal projection of the Riemannian tensor (the "curvature of the time") in this direction: the **negative non-Newtonian force of attraction is due to the positive curvature of time.**

The partial case of the collapse of the incompressible liquid sphere $r_c = r_{br} = a$ is studied in detail in [7]. As follows from (12), in this case the surface of the sphere is simultaneously both the surface of the collapsar and the surface of the breaking of the space. Remember that $a = \frac{1}{\sqrt{q}}$ is also the radius of curvature of the sphere of condensed matter, where q is the Gaussian curvature of the reference space. Assuming $a = r_{br} = \sqrt{\frac{3}{\varkappa\rho}}$ and substituting this expression in (11), we obtain the de Sitter metric

$$ds^2 = \frac{1}{4}\left(1 - \frac{r^2}{a^2}\right)c^2dt^2 - \frac{dr^2}{1-\frac{r^2}{a^2}} - r^2(d\theta^2 + \sin^2\theta d\varphi^2). \tag{30}$$

The space-time described by the metric (30) satisfies the Einstein equations

$$R_{\alpha\beta} - \frac{1}{2}g_{\alpha\beta}R = \lambda g_{\alpha\beta}, \tag{31}$$

where the cosmological constant $\lambda = \frac{3}{a^2}$.

The term $\lambda g_{\alpha\beta}$ can be expressed in the form [7]

$$\lambda g_{\alpha\beta} = \varkappa\widetilde{T}_{\alpha\beta}. \tag{32}$$

Thus the λ-field generating the de Sitter space (30) is equivalent to the substance described by the energy-impulse tensor

$$\widetilde{T}_{\alpha\beta} = \frac{\lambda}{\varkappa}g_{\alpha\beta}. \tag{33}$$

Calculating the physically observable components of the energy-impulse tensor (33) [2], we find

$$\begin{aligned} \rho_0 &= \frac{\widetilde{T}_{00}}{g_{00}} = \frac{\lambda}{\varkappa}, \quad J_0^i = \frac{c\widetilde{T}_0^i}{\sqrt{g_{00}}} = 0, \\ U_0^{ik} &= c^2\widetilde{T}^{ik} = -\frac{\lambda c^2}{\varkappa}, \end{aligned} \tag{34}$$

where ρ_0, J_0^i and U_0^{ik} are the chr.-inv. density of matter, the (vector) density of impulse, and the tensor of stress, respectively.

As seen, the expression (10) transforms into (33) if the condition is

$$p = -\rho_0c^2 = -\frac{\lambda c^2}{\varkappa}, \tag{35}$$

i.e. it describes matter in the state of inflation.

Thus the energy-impulse tensor (33) describes substance with positive constant density $\rho_0 = \frac{\lambda}{\varkappa}$ and negative constant pressure $p_0 = -\rho_0c^2$. The flow of energy is given as $q_0 = J_0c^2 = 0$. This substance is called *physical vacuum*. We conclude that *the collapsing sphere of ideal incompressible liquid transforms into a de Sitter vacuum bubble by the special case of collapse, when the radius of the sphere a equals the breaking radius* r_{br}

$$a = r_{br} = \sqrt{\frac{3}{\varkappa\rho}} = r_c, \tag{36}$$

where the radius of the collapsar r_c coincides with the radius of the sphere and the breaking radius.

The physical vacuum is an actual substance, possessing positive density and negative pressure. Because the bubble is stationary, the negative pressure, which inflates the bubble, must be balanced by attraction, thereby compressing it. To solve the problem of stability of inflation collapsar, it is necessary to find this compressing factor. Study the physical and geometrical characteristics of the de Sitter bubble and compare them with the corresponding characteristics of the liquid bubble. This comparison allows us to consider the process of transformation of the gravitational collapsar ("black hole") into the inflational collapsar ("white hole").

The physical and geometrical properties of the de Sitter bubble, described by the metric (30), are studied in detail in [7]. The local reference space does not rotate and deform. The gravitational inertial force has the form

$$F_1 = \frac{c^2 r}{a^2 - r^2} > 0, \quad F^1 = \frac{c^2 r}{a^2} > 0, \tag{37}$$

i.e. is the force of repulsion. As seen, the formula (13) transforms into (37) by the condition (36). Thus the gravitational inertial force of attraction (13), acting inside the liquid bubble, transforms into a force of repulsion, acting inside the vacuum bubble. Using the collapse condition (36), rewrite (37) in the form

$$F^1 = \frac{\varkappa \rho_0 c^2 r}{3} = -\frac{\varkappa p r}{3} > 0. \tag{38}$$

It is easy to see that **both the positive density and the negative pressure both inflate the vacuum bubble**. As known, the generally accepted viewpoint consists in that the stability of the de Sitter vacuum bubble is due to the action of two opposite factors: 1) compression due to the positive density; 2) inflation due to the negative pressure. As follows from (38), the positive density and negative pressure effects are identical, consequently it is necessary to find the factor, which causes the compression of the bubble.

Studying the physical and geometrical characteristics of the Schwarzschild liquid bubble, we have found that the force of attraction (13) is balanced by the value $-rX_{11}$, which possesses the dimension of acceleration: see (29). The quantity $X_{11} > 0$ is the observable projection of the Riemann tensor component R_{0101} on time — the "curvature of time in the radial direction". Thus the non-Newtonian force of attraction, which is proportional to the radial distance r, is balanced by the action of the "positive curvature of the time" (the term rX_{11}).

Consider the problem of the stability of the vacuum bubble. Calculating the Riemann tensor (23) for the metric (30), we find

$$\begin{aligned} &R_{0101} = \frac{1}{4a^2}, \quad R_{0202} = \frac{R_{0303}}{\sin^2\theta} = \frac{r^2(a^2 - r^2)}{4a^4}, \\ &R_{1212} = \frac{R_{1313}}{\sin^2\theta} = -\frac{r^2}{a^2 - r^2}, \quad R_{2323} = -\frac{r^4 \sin^2\theta}{a^2}. \end{aligned} \tag{39}$$

It is easy to see that the components (26) transform into (39) by the condition $a = r_{br}$. The components (39) satisfy the condition (27), where the four-dimensional constant curvature is negative: $K = -\frac{1}{a^2}$.

The quantities C_{ijkl}, C_{ik} and C (20–21) of the reference space (30) then take the form

$$\begin{aligned} &C_{1212} = \frac{C_{1313}}{\sin^2\theta} = \frac{r^2}{a^2 - r^2}, \quad C_{2323} = \frac{r^4 \sin^2\theta}{a^2}, \\ &C_{11} = \frac{2}{a^2 - r^2}, \quad C_{22} = \frac{C_{33}}{\sin^2\theta} = \frac{2r^2}{a^2}, \\ &C = \frac{6}{a^2} > 0. \end{aligned} \tag{40}$$

The components C_{ijkl} (40) satisfy the condition (22), where the three-dimensional Gaussian curvature is $q = \frac{1}{a^2}$, consequently the reference space of the vacuum bubble is a three-dimensional sphere of the real radius $a = \frac{1}{\sqrt{q}}$. We have shown above that the de Sitter space (30) possesses negative four-dimensional Gaussian curvature $K = -\frac{1}{a^2} = -q$, consequently it is a four-dimensional sphere with the imaginary radius $\Re = iq$.

Comparing the obtained results with the analogical ones for the liquid sphere (11), we find that both reference spaces possess positive constant curvature, but the four-dimensional de Sitter space possesses constant negative curvature. Calculating the physically observable components of the Riemann-Christoffel tensor X_{ik} (28) for the de Sitter vacuum bubble, we find

$$X_{11} = -\frac{c^2}{a^2 - r^2} < 0, \quad X_{22} = \frac{X_{33}}{\sin^2\theta} = -\frac{c^2 r^2}{a^2} < 0. \tag{41}$$

We conclude therefore that the sign of curvature of the de Sitter vacuum bubble coincides with the signs of the $R_{\alpha\beta\gamma\delta}$ projections onto time (the "negative curvature of time").

Comparing the component X_{11} (41) with the expression of the gravitational inertial force (37), we find that these quantities satisfy the condition (29), i.e. the signs of the F_1 and X_{11} are opposite. We conclude that **the non-Newtonian force of attraction inside the liquid sphere (11) is due to the positive curvature of time, the force of repulsion inside the vacuum bubble (30) is due to the negative curvature of time.**

These results are connected with the geometric structure of the physically observable curvature components X_{ik}. Generally speaking, they depend on the deformation, rotation, and gravitation of the reference space [2]. If locally the space does not deform and rotate, the components X_{ik} take the form

$$X_{ik} = \frac{1}{2}({}^*\nabla_i F_k + {}^*\nabla_k F_i) - \frac{1}{c^2} F_i F_k, \tag{42}$$

where ${}^*\nabla_i$ is the chr.-inv. operator of covariant differentiation [2].

We have thus shown that the collapsing liquid bubble (11) transforms instantly into the vacuum bubble (30) by the special case of collapse: $a = r_{br}$. The surface $r = a$ in this case is simultaneously: 1) the breaking surface; 2) the surface of the inflation collapsar.

Calculating the elementary observable interval of time for the metrics (11) and (30), we find, respectively:

1) the Schwarzschild liquid bubble

$$d\tau_l = \pm\frac{1}{2}\left(3\sqrt{1-\frac{\varkappa\rho a^2}{3}} - \sqrt{1-\frac{\varkappa\rho r^2}{3}}\right)dt; \qquad (43)$$

2) the de Sitter vacuum bubble

$$d\tau_v = \pm\frac{1}{2}\left(\sqrt{1-\frac{r^2}{a^2}}\right)dt. \qquad (44)$$

Assuming in (43) $a = \sqrt{\frac{3}{\varkappa\rho}} = r_{br}$, we obtain

$$d\tau_l = \mp\frac{1}{2}\left(\sqrt{1-\frac{r^2}{a^2}}\right)dt. \qquad (45)$$

We have obtained as a result that the observable time τ inside these bubbles flows in the opposite direction. We consider usually the observable time as flowing in the positive direction — from the past to the future. In order to determine one of the two signs in the formulaes (43–44), it is necessary to ask, which of the two bubbles is more applicable as the model of the observed Universe: the Schwarzschild liquid bubble or the de Sitter vacuum bubble? This question will be studied in detail in the next section.

4 The de Sitter bubble as a proposed cosmological model

Consider the Schwarzschild and de Sitter bubbles as the two possible cosmological models. The choice of such a model must be in accordance with astronomical data. The most important criterion for the choice is the observed red-shift. In other words, the model, which allows the red-shift, can be chosen as the cosmological model. The effect of the spectral line displacement is calculated exactly for every gravitational field configuration.

As known, the world-lines of light-like particles (null geodesic lines) are described by the equations of the parallel transfer of the isotropic (null) four-dimensional wave vector K^α

$$\begin{gathered}\frac{dK^\alpha}{d\sigma} + \Gamma^\alpha_{\mu\nu}K^\mu\frac{dx^\alpha}{d\sigma} = 0, \quad K^\alpha = \frac{\omega}{c}\frac{dx^\alpha}{d\sigma} = 0,\\ K_\alpha K^\alpha = 0,\end{gathered} \qquad (46)$$

where ω is the cyclic frequency, $\Gamma^\alpha_{\mu\nu}$ is the Christoffel symbols of the second kind, σ is the parameter of differentiation, $\frac{dx^\alpha}{d\sigma}$ is the isotropic (null) vector of the 4-velocity, which is tangent to the world-lines ($g_{\alpha\beta}\frac{dx^\alpha}{d\sigma}\frac{dx^\beta}{d\sigma} = 0$).

These equations have the form in terms of the physically observable quantities (viz. the theory of chronometric invariants) [9]

$$\frac{1}{\omega}\frac{d\omega}{d\tau} + \frac{1}{c^2}D_{ik}\frac{dx^i}{d\tau}\frac{dx^k}{d\tau} - \frac{1}{c^2}F_i\frac{dx^i}{d\tau} = 0, \qquad (47)$$

$$\begin{gathered}\frac{d}{d\tau}\left(\omega\frac{dx^i}{d\tau}\right) + 2\omega(D^i_k + A^{\cdot i}_{k\cdot})\frac{dx^k}{d\tau} -\\ -\omega F^i + \omega\Delta^i_{nk}\frac{dx^n}{d\tau}\frac{dx^k}{d\tau} = 0,\end{gathered} \qquad (48)$$

$$h_{ik}\frac{dx^i}{d\tau}\frac{dx^k}{d\tau} = c^2. \qquad (49)$$

The system of equations (47–49) is the chr.-inv. form of the parallel transfer equations of the four-dimensional wave vector $K^\alpha = \frac{\omega}{c}\frac{dx^\alpha}{d\sigma}$, where the equations (47–48) are linked by the relation (49). Solving the system for every metric, we find the frequency of the photon and the associted spatial trajectory in the given space-time.

If the reference space does not rotate and deform, the equations (47–48) take the form

$$\frac{1}{\omega}\frac{d\omega}{d\tau} - \frac{1}{c^2}F_i\frac{dx^i}{d\tau} = 0, \qquad (50)$$

$$\frac{1}{\omega}\frac{d}{d\tau}\left(\omega\frac{dx^i}{d\tau}\right) - F^i + \Delta^i_{nk}\frac{dx^n}{d\tau}\frac{dx^k}{d\tau} = 0. \qquad (51)$$

Substituting into (50) the expressions for gravitational inertial force F_1 (13) and (40), we obtain the equations describing the behaviour of the cyclic frequency inside both the condensed matter and physical vacuum bubbles, respectively:

1) the Schwarzschild bubble

$$\frac{1}{\omega}\frac{d\omega}{d\tau} = -\frac{\varkappa\rho c^2}{3}\frac{r}{\left(3\sqrt{1-\frac{\varkappa\rho a^2}{3}} - \sqrt{1-\frac{\varkappa\rho r^2}{3}}\right)\sqrt{1-\frac{\varkappa\rho r^2}{3}}}\frac{dr}{d\tau}; \qquad (52)$$

2) the de Sitter bubble

$$\frac{1}{\omega}\frac{d\omega}{d\tau} = \frac{r}{a^2 - r^2}\frac{dr}{d\tau}. \qquad (53)$$

Integrating (52–53), we obtain, respectively:

1) the Schwarzschild bubble

$$\omega = \frac{P}{3\sqrt{1-\frac{\varkappa\rho a^2}{3}} - \sqrt{1-\frac{\varkappa\rho r^2}{3}}}, \quad P = const; \qquad (54)$$

2) the de Sitter bubble

$$\omega = \frac{Q}{\sqrt{1-\frac{r^2}{a^2}}}, \quad Q = const, \qquad (55)$$

where P and Q are integration constants.

Cosmologists have introduced the quantity z — the relative variation of the frequency

$$z = \frac{\omega_{em} - \omega_{obs}}{\omega_{obs}}, \tag{56}$$

where ω_{em} is the frequency, emitted by the source, located at the radial distance r_{em} relative to the observer, ω_{obs} is the observable (observed, registered) frequency of this source at the place, where the observer is located: r_{obs}. The condition $z < 0$ means that the observable frequency is more than the emitted, consequently the observable light seems shifted more towards the blue than the emitted one (the phenomenon of blue-shift). The condition $z > 0$ implies a red-shift, because in this case the observable frequency is less than the emitted one.

Calculating the value z for the expressions (54–55), we obtain

1) the Schwarzschild bubble

$$z = \frac{\sqrt{1 - \dfrac{\varkappa\rho r_{em}^2}{3}} - \sqrt{1 - \dfrac{\varkappa\rho r_{obs}^2}{3}}}{3\sqrt{1 - \dfrac{\varkappa\rho a^2}{3}} - \sqrt{1 - \dfrac{\varkappa\rho r_{em}^2}{3}}} < 0; \tag{57}$$

2) the de Sitter bubble

$$z = \frac{\sqrt{a^2 - r_{obs}^2} - \sqrt{a^2 - r_{em}^2}}{\sqrt{a^2 - r_{em}^2}} > 0. \tag{58}$$

It follows from (58) that the red-shift takes place inside the de Sitter bubble, therefore namely this space-time can be considered as a cosmological model.

Let us study more exactly the behavior of the frequency of photons emitted by distant sources. Assume that the photons from the source move to the observer in the radial r-direction. Then (49) takes the form

$$\frac{a^2}{a^2 - r^2}\left(\frac{dr}{d\tau}\right)^2 = c^2. \tag{59}$$

Taking the root of (59), we obtain

$$\frac{dr}{\sqrt{a^2 - r^2}} = \pm\frac{c}{a}d\tau = \pm H d\tau, \tag{60}$$

where H is the Hubble constant. Assuming $H = 75\,\text{Mps/sec} = 2.3 \times 10^{-18}\text{sec}^{-1}$, we find $a = 1.3 \times 10^{28}$ cm.

Choose the sign + or −, respectively, if the distance between the observer and the source is taken into account: 1) from the observer to the source; 2) from the source to the observer. Integrating (60) from r (the distance from the source) until $r = 0$ (the location of the observer), we find

$$\int_r^0 \frac{dr}{\sqrt{a^2 - r^2}} = -\arcsin\frac{r}{a} = -H\tau, \tag{61}$$

where τ is the observable time, in the course that the signal from the source comes to the observer. It follows from (61) the expression for r:

$$r = a\sin H\tau, \tag{62}$$

i.e. the photometric distance is harmonic (sinusoidal) oscillation with the amplitude a and the period $T = \frac{2\pi}{H}$. The amplitude a is the maximal distance from any observer — the so called "event horizon". It is easy to find that the three-dimensional observable vector of the light velocity $c^1 = \frac{dr}{d\tau}$ has the form

$$c^1 = \frac{dr}{d\tau} = aH\cos H\tau = c\cos H\tau, \tag{63}$$

where

$$h_{11}c^1c^1 = \frac{a^2}{a^2 - r^2}\left(\frac{dr}{d\tau}\right)^2 = c^2.$$

This formula means that the radial component of the vector of the light velocity oscillates with a frequency H and an amplitude c. This oscillation is shifted for $\frac{\pi}{2}$ with respect to the oscillation of the radial distance r (62).

Substituting (63) into (55), we obtain

$$\omega = \frac{Q}{\cos H\tau}, \quad 0 \leqq \tau \leqq \frac{\pi}{2H}. \tag{64}$$

As seen, $\omega \to \infty$ if $\tau \to \frac{\pi}{2H}$, i.e. by $r \to a$. It follows from (58) that the value of z increases infinitely by $r \to a$. This effect takes place from the viewpoint of the real observer, because the observable time depends on the photometric distance r from the event horizon:

$$d\tau = \frac{1}{2}\left(\sqrt{1 - \frac{r^2}{a^2}}\right)dt. \tag{65}$$

Thus the tempo of the observable time decreases by $r \to a$, and the observable time is stopped at the event horizon. Therefore the observable cyclic frequency of photons increases infinitely by $r \to a$.

It was shown above, the coordinate (photometric) distance r is the sinusoidal (harmonic) oscillation (wave) with the amplitude a and the cyclic frequency $H = \frac{2\pi}{T}$. The quantity $T = \frac{2\pi}{H}$ is the full period of the oscillation, the maximal value a (amplitude) is the event horizon. Taking into account only the positive values of r, we are restricted only to the semi-period of the oscillation. The maximal value of $r = a$ takes place at $\tau = \frac{\pi}{2H} = \frac{T}{4}$. Introducing the used-in-contemporary cosmology value $H = 2.3 \times 10^{-18}\text{sec}^{-1}$, we find $T_a = \frac{\pi}{2H} = 21.6 \times 10^9$ years — the time of passing of the light signal from the event horizon to the observer. Contemporary cosmologists calculate the time of the life of the Universe as the interval of time after the Big Bang. They obtained the age of the Universe approximately 13.75×10^9

years. If we'll introduce H as the ordinary (not the cyclic) frequency $H = \frac{H_c}{2\pi} = \frac{1}{T}$, we find $T = 13.74 \times 10^9$ years.

As is well known, the mathematical basis of contemporary relativistic cosmology is the theory of a non-stationary (extending) universe. It is founded on Friedman's cosmological models, which belong to a particular class of solutions to Einstein's field equation, obtained by the imposing condition that the space of the observable Universe is homogeneous and isotropic. This class of solutions is described by the metric

$$ds^2 = c^2dt^2 - R^2(t)\frac{dx^2 + dy^2 + dz^2}{\left[1 + \frac{k}{4}(x^2 + y^2 + z^2)\right]^2}, \quad k = 0, \pm 1, \quad (66)$$

where $R(t)$ is the scale factor: $\frac{1}{R}\frac{dR}{dt} = H$. In accordance with the value k of the three-dimensional space: 1) is flat ($k = 0$); 2) has negative curvature ($k = -1$); 3) has positive curvature ($k = +1$). Models with $k = 0, -1$ are called open, and models with $k = +1$ are closed ones. Friedman's spaces are both empty ($T_{\alpha\beta} = 0$) and filled by ideal liquid described by (10).

The special reference space (68) does not rotate and gravitate, but it does deform. The tensor of the rate of deformation is described by the formula $D_{ik} = R\frac{dR}{dt}$. The observable time flows uniformly: $d\tau = dt$, in particular, it does not depend on the photometric distance r in contrast to the interval of the observable time in the de Sitter bubble. Friedman's models are: 1) extending; 2) compressing; 3) oscillating; 4) stationary [2]. The cosmological term λ can be: 1) positive, 2) negative, 3) zero. Cosmologists explain the observable red-shift by the Doppler effect which is due to the expansion of the space of the Universe. The generally accepted model of the non-stationary (extending) Universe is the Standard Cosmological Model. The age of the Universe is determined by means of extrapolation of the uniformly flowing time from the present to the past — the beginning of the Universe caused by the Big Bang. The age of the observable Universe, according to Friedman's theory, is determined approximately as 13×10^9 years — the interval of the time from the Big Bang of the initial singularity (the "point" consisting of super-compact initial substance).

Now we come to the essential question: What cosmological model is more applicable for the description of the observable Universe: the stationary de Sitter space or the extending Friedman's space? The criterium of the choice must be the results of astronomical observations. It follows from the observations of spectra of galaxies that the observable red-shift is linear for more near galaxies and it rapidly increases for the most distant objects. Most cosmologists explain this result as the accelerated expansion of space, while routinely avoiding some principal weaknesses. The correct theoretical explanation of this fact has not been obtained until now. Moreover, contemporary cosmologists do not calculate variations of frequencies as exact solutions to the general relativistic equation of motion of null geodesic lines. The observable phenomena of the red-shift is explained by the temporal variations of the scale factor $R(t)$. It is necessary to note that the exact solution(s) to the equations (47–49) can be found only for concrete metrics. In particular, the expression of the cyclic frequency ω for Friedman's metric can be obtained only if the exact expression for $R(t)$ is known and the value of k is chosen. In other words, in order to study variations of frequencies of cosmic objects, it is necessary before hand to assign the function $R(t)$, which determines the kind of deformation, and the value of k, which determines the geometry of the reference space.

The exact value of the frequency (55) is obtained here as the solution to equation of motion of null geodesic lines (47–49). It follows from (55, 59) that the observable frequency ω and the quantity z increase infinitely while approaching the event horizon. If $r \ll a$, the quantity z can be transformed as

$$z \approx \frac{r_{em}^2 - r_{obs}^2}{2a^2}. \quad (67)$$

It means that the red-shift in the spectra of near-to-the observer objects ($r \ll a$) is subject to the parabolic law. In other words, the linear red-shift cannot be explained in the de Sitter space. The gravitational inertial force of repulsion inside the de Sitter bubble causes the parabolic red-shift for near sources and the infinite increase at the maximal distance from the observer — the event horizon. Thus the red-shift in the de Sitter bubble is due to the non-Newtonian force of repulsion, which is proportional to the radial (photometric) distance r.

We conclude: neither the Friedman expansion, which is caused by the deformation of the reference space, nor the de Sitter force of repulsion can explain simultaneously both the linear red-shift for near sources and the sharp, non-linear increase for most distant sources. Probably, this problem can be solved in frames of a generalized metric which includes both Friedman's expansion and the de Sitter repulsion. It is possible that the de Sitter space is applicable near the event horizon ($r \backsim a$), while the Friedman extending space correctly describes more near-to-the observer regions ($r \ll a$).

5 The past, the present, and the future are three multispace aspects of the observable time

Now, let us consider in detail the collapse mechanism of the liquid bubble into the vacuum bubble. We have obtained above the key rôle in the very process the condition (36) plays. If such a state is realized, then the interval of the observable time interior to Schwarzschild's liquid bubble $d\tau_{\text{l}}$ transforms into the interval of the observable time inside de Sitter's vacuum bubble $d\tau_{\text{v}}$; moreover, each of these intervals possesses the opposite sign:

$$d\tau_{\text{l}} = -d\tau_{\text{v}}.$$

It means that the observable time inside the vacuum de Sitter bubble flows in the opposite direction. We have assumed in the previous section that once the de Sitter bubble is

applicable as a cosmological model, the flow of the τ in this space is positive: the observable time flows from the past to the future. Then the observable time inside the Schwarzschild liquid bubble flows from the future to the past, and its interval has the form:

$$d\tau_{\rm l} = -\frac{1}{2}\left(3\sqrt{1-\frac{a^2}{r_{br}^2}} - \sqrt{1-\frac{r^2}{r_{br}^2}}\right)dt < 0. \qquad (68)$$

If $a = r_{br}$, then (70) transforms into the expression

$$d\tau_{\rm v} = \frac{1}{2}\left(\sqrt{1-\frac{r^2}{a^2}}\right)dt > 0, \qquad (69)$$

which is the interval of the observable time inside the de Sitter bubble.

Thus the surface $a = \sqrt{\frac{3}{\varkappa\rho}} = r_{br}$ is the mirror dividing two worlds — the space of the future and the space of the past. It means, this surface is the space of the present. As was shown above, the surface a is singular. It means, the present is the *instantaneous state* between the future and the past, where the *future transforms into the past by means of passing through the singulary state*. The space of the future is here the vacuum de Sitter liquid bubble, where the observable time flows from the future to the present: that is, the future "goes to us". The future, after the passage through the said singulary surface, becomes the past: the present "leaves us". Thus the singular surface is not only a mirror (a reflecting surface). It is simultaneously a membrane: a telemetric, multispace membrane connecting the worlds of the past and the future. The future penetrates into the inflation collapsar namely through this "mirror-like membrane" — the *interior layer* between the past and the future. This situation can be illustrated in terms of the well-known description of the interaction between a light beam and some incident surface (as the light beam falls upon the surface). This beam splits into three beams: 1) the reflected; 2) the refracted; 3) the absorbed. The light beam within the framework of General Relativity is the trajectory of photons — the world-line of the null four-dimensional length $ds = 0$, where here every individual photon is said to be the event itself. The world-lines with $ds \neq 0$ also consist of four-dimensional world-points. It is possible to say therefore that the light beam of events, falling onto the singular surface, splits into: 1) the reflected light beam (returned into the space of the future); 2) the refracted light beam (directed into the space of the past); 3) the absorbed light beam, by the said singularity surface. The first light beam describes those events, which cannot be realized (*materialized*) in the present (for example, using analogy with daily life, certain ideas or epochs which are far too advanced for the time). The second light beam describes those events, which could be realized in principle, but they can not actually be realized (in part, these are not readily perceived by the bulk human consciousness). Finally, those events in the likeness of the absorbed light-beam represent the world of the present, which is uniquely perceived by our consciousness (taking into account varying internal degrees of consciousness) as "reality". The said non-realized (for a while) events can be called *virtual events*.

An event in General Relativity is the four-dimensional point of the space-time V_4 — the three-dimensional point, which is expanded into a "thread". This thread is the four-dimensional trajectory of the event — the world-line. These lines can be: 1) non-null (trajectories of mass-bearing particles, both real and imaginary); 2) null (trajectories of light-like particles; in particular, photons). Interlacing of these threads creates the "material of the space". Because we assume here fundamental interactions between the past, the present, and the future, we must introduce a "medium", which realizes these interactions. We will consider in this paper only null world-lines, i.e. we will study events of the "life of photons".

It is evident that those particles, which realize the transfer of energies between the future into the past, must penetrate the singularity surface. As known, regular photons cannot pass through the singularity surface, but this surface is penetrable for *zero-particles*, introduced in [3]. These particles exist in the generalized space-time $\widetilde{V}_4$, which is determined as an immediate generalization of the Riemannian space-time V_4 of General Relativity (both at the differential-geometric manifold and sub-manifold levels): $\widetilde{V}_4 = V_4 \cup Z$, where Z is the *zero-space*. Zero-particles have zero rest-mass m_0, zero relativistic mass m, and non-zero gravitational-rotational mass M, which is described in the $\widetilde{V}_4$ as

$$M = \frac{m}{1-\dfrac{\mathrm{w}+v_i u^i}{c^2}}, \quad u^i = \frac{dx^i}{dt}. \qquad (70)$$

The four-dimensional metric of $\widetilde{V}_4$ satisfies the condition $g = \det|g_{\alpha\beta}| \leqslant 0$, i.e. it allows the versatile degeneration of the metric. The manifold $\widetilde{V}_4$ is the ordinary space-time V_4 by $g < 0$ and it is the zero-space Z by $g = 0$. Zero-particles transfer instantaneously ($d\tau = 0$), from the viewpoint of a real observer, along three-dimensional lines of null observable length ($d\sigma = 0$), i.e. they are mediums for the *long-range-action*. Zero-particles can be considered as the *more tenuous and thinner structures* than the photon. The condition (5) takes for zero-particles the form $d\sigma = d\tau = 0$.

The four-dimensional null wave vector K^α of the $\widetilde{V}_4$ can be expressed both in the corpuscular form and in the wave form

$$K^\alpha = \frac{\omega}{c}\frac{dx^\alpha}{d\sigma}, \quad K_\alpha = \frac{\partial\psi}{\partial x^\alpha}, \qquad (71)$$

where ψ is the phase of the wave (the eikonal).

The physically observable characteristics of K^α are [3]

$$\frac{K_0}{\sqrt{g_{00}}} = \pm\omega = \frac{{}^*\partial\psi}{\partial t}, \quad K^i = \frac{\omega}{c^2}\frac{dx^i}{d\tau} = -h^{ik}\frac{{}^*\partial\psi}{\partial x^k}, \qquad (72)$$

where

$$\frac{{}^*\partial}{\partial t} = \frac{1}{\sqrt{g_{00}}}\frac{\partial}{\partial t}, \quad \frac{{}^*\partial}{\partial x^i} = \frac{1}{\sqrt{g_{00}}}\frac{\partial}{\partial x^i} + \frac{v_i}{c^2}\frac{{}^*\partial}{\partial t}$$

are the chr.-inv. operators of differentiation along the temporal and spatial coordinates, respectively [2]. The signs (+) and (−) are related to the spaces possessing the direct and reverse flow of time, respectively.

The wave form of the condition $K_\alpha K^\alpha = 0$ is the well-known eikonal equation

$$g^{\alpha\beta}\frac{\partial\psi}{\partial x^\alpha}\frac{\partial\psi}{\partial x^\beta} = 0. \tag{73}$$

Expressing (73) in terms of physically observable values, we obtain

$$\frac{1}{c^2}\left(\frac{{}^*\partial\psi}{\partial t}\right)^2 - h^{ik}\frac{{}^*\partial\psi}{\partial x^i}\frac{{}^*\partial\psi}{\partial x^k} = 0. \tag{74}$$

The cyclic frequency of zero-particles is $\omega = 0$, consequently the equation (74) takes the form of the standing wave [3]

$$h^{ik}\frac{{}^*\partial\psi}{\partial x^i}\frac{{}^*\partial\psi}{\partial x^k} = 0, \tag{75}$$

which can certainly be interpreted as a hologram, i.e., a standing wave of the extended space-time. Thus the present, in the sense of geometric optics, is a **holographic picture perceived by our consciousness as the material (real) world.**

We conclude therefore that zero-particles are the **mediums of the long-range-action** in the space of the present — the boundary between the spaces of the future and the past. Zero-particles can be considered as a result of the fundamental interaction between the photons themselves, moving in time in the two above-mentioned opposite directions and possessing certain cyclic frequencies of the opposite signs. In other words, the standing wave can be interpreted as a result of the summarization of the two waves ψ_+ and ψ_-, directed from the past to the future and from the future to the past, respectively. Let photons, moving in the space of the past, possess positive frequencies ω_+, and photons moving in the space of the future, possess negative frequencies ω_-, respectively. The interaction between the ψ-waves, oppositely oriented in time, generates information, which is transmitted instantaneously by means of zero-particles. This information creates a hologram (the unique "reality" of the present moment), which exists during the infinitely small interval of time as well as after it is substituted by the next hologram. By analogy, the perception of the continuity (and solidity) of the present is due to the fact that the successive frames of a movie are substituted very quickly.

We do not consider here the whole unique process of the chain of sequential materializations: zero-particles → photons → mass-bearing particles, because this problem is very difficult and impractical to be considered in further detail. We introduce here instead the problem of observation of cosmic objects. Consider the information which comes to us from stars and galaxies in the form of light beams. Because the cosmic objects are distant from us, we register the photons later than they were first emitted. It means, the observer, registering the electromagnetic radiation of the source, studies the **past state of this cosmic object**. This state corresponds to the moment of radiation of the electromagnetic signal. The information about the present state of the object can be obtained by means of registration of zero-particles, emitted by the source at the moment of observation. But the observer does not perceive it, because he does not use corresponding intermediary instruments. Contemporary astronomers use instruments, which can register only different ranges of electromagnetic radiation transferring at the light velocity.

6 Newtonian and non-Newtonian forces in the Universe

We have studied until now only non-Newtonian forces:

1) the force of attraction (13), created by the homogeneous liquid sphere (11);

2) the force of repulsion (37), created by the vacuum bubble (30);

3) the values of these forces are proportional to the radial coordinate r;

4) both forces are connected to the observable components of the Riemann tensor by the correlation (29).

The metrics (11) and (30) describe the gravitational fields created by the continuous bodies (bubbles). It is necessary to note that the force of attraction (13) transforms into the force of repulsion (37) as a result of the collapse of the liquid bubble, and both forces are non-Newtonian. The force of attraction (13) is created by the liquid sphere, which was initially introduced by Schwarzschild for the description of the Sun. On the other hand, the Sun as an attracting body is described by the well-known Schwarzschild metric of a single mass (mass-point) in emptiness ($R_{\alpha\beta} = 0$) [8]. This metric has the form

$$\begin{aligned} ds^2 &= \left(1-\frac{r_g}{r}\right)c^2dt^2 - \frac{dr^2}{1-\dfrac{r_g}{r}} - r^2(d\theta^2+\sin^2\theta d\varphi^2), \\ r_g &= \frac{2GM}{c^2} \end{aligned} \tag{76}$$

where r_g is the gravitational (Hilbert) radius and M is the mass of the gravitating mass-point.

The space-time (76) collapses by the condition $r = r_g$, and the surface $r = r_g$ is called the *Schwarzschild surface*. Besides this, the space experiences breakage by the same condition. Thus the mass-point stops the time and breaks the space by $r = r_g = r_{br}$.

The metric (76) is applied for the description of the gravitational field of the Sun and the motion of the planets of the Solar System. It allows the post-Newtonian approximation, consequently it must include Newtonian gravitation. Let us study in detail the physical and geometrical characteristics

of the gravitational field of the mass-point in order to compare the obtained results with the analogous results for the metric (11), which describes the continuous body — a liquid sphere. This approach allows us to determine the problem of the connection between the local geometry of space-time and the character of attractive forces therein.

We have obtained for the metric (11) that the radial non-Newtonian force of attraction (13) is linked to the radial projection of the "curvature of time" (28) by the correlation (29). As follows from (29), the force of attraction is due to the positive curvature of time. Let us study the connection between the observable components of the Riemann tensor and the gravitational inertial force for the space-time (76).

The reference space described by (76) does not rotate and deform, but it gravitates. Calculating the gravitational inertial force F_i by the formula $F_i = \frac{c^2}{c^2-\mathrm{w}}\frac{\partial \mathrm{w}}{\partial x^i}$, we obtain

$$F_1 = -\frac{c^2 r_g}{2r^2}\frac{1}{1-\dfrac{r_g}{r}}, \quad F^1 = -\frac{c^2 r_g}{2r^2}. \tag{77}$$

Substituting into the expression for F^1 the value $r_g = \frac{2GM}{c^2}$, we rewrite (77) in the form

$$F_1 = -\frac{GM}{r^2}\frac{1}{1-\dfrac{2GM}{c^2 r}}, \quad F^1 = -\frac{GM}{r^2}. \tag{78}$$

We see that the component F^1 is the ordinary Newtonian force of attraction. Calculating the observable components of the Riemann tensor X_{11} by the formula (42), we find

$$X_{11} = -\frac{c^2 r_g}{r^3}\frac{1}{1-\dfrac{r_g}{r}} < 0. \tag{79}$$

It follows from (78–79) the relation between the force of attraction and the "curvature of time" in the radial direction:

$$F_1 = \frac{r}{2}X_{11}. \tag{80}$$

The signs of F_1 and X_{11} coincide in contrast to the analogous relation (29), which is satisfied for both the de Sitter and Schwarzschild bubbles. It means that the Newtonian force of attraction is due to the "negative curvature of time". The point is that the Non-Newtonian and Newtonian gravitational forces of attraction are originated by different sources. As shown earlier, the non-Newtonian force of attraction is connected to the *continuous body* (the liquid sphere). The Newtonian force is connected usually to the mass, which is *concentrated inside a small volume*, so called a " mass-point" [8]. Meanwhile, it is evident that continuous bodies possess the said Newtonian force, because they attract bodies with smaller masses. Therefore, it is necessary to state correctly the criterium, which will determine what kind of cosmic bodies must be described as "continuous bodies" and what kind — as "mass-points".

The gravitational field of the mass-point is described by the Schwarzschild metric (76), which includes Newtonian gravitation (as well as the post-Newtonian approximation). The motion of cosmic bodies, which move around the attracting center (mass-point), is usually studied in either the framework of Newtonian gravitation or that of the post-Newtonian theory of gravitation. In the second case, the motion of cosmic objects is calculated in the Schwarzschild mass-point field by the condition $r_g \ll r$. This condition means that the Hilbert radius is very small in comparison to the distance between the attracting center and the object moving around the center. This approach is applicable both to the Sun and to the planets, asteroids, etc. On the other hand, continuous bodies also possess gravitational attraction. In part, the gravitational inertial force of attraction in the reference space of the homogeneous liquid sphere is described by (13). The question now arises: what are the conditions, by which the Newtonian force of attraction is the partial case of the non-Newtonian force (13)?

It follows from (77–78) that the gravitational inertial force coincides with the Newtonian force of attraction if $r_g \ll r$. Because the Newtonian theory of gravitation is constructed in the flat three-dimensional (Eucledian) space, we can assume that the homogeneous gravitating mass M has the form

$$M = \rho V, \quad V = \frac{4\pi a^3 \rho}{3}, \tag{81}$$

where V is the volume of the mass, a is its radius, $\rho = const$ is the density of mass. This assumption is admissible also for any homogeneous sphere. Using (81), we can rewrite the expression (13) in the form

$$F_1 = -\frac{c^2 r_g}{a^3}\frac{r}{\left(3\sqrt{1-\dfrac{r_g}{a}} - \sqrt{1-\dfrac{r_g r^2}{a^3}}\right)\sqrt{1-\dfrac{r_g r^2}{a^3}}}. \tag{82}$$

Let $r_g \ll r \leqq a$. Expressing the value $\sqrt{1-\frac{r_g r^2}{a^3}}$ into series, neglecting the members of the second kind and assuming $\sqrt{1-\frac{r_g}{a}} \approx 1-\frac{r_g}{2a}$, we obtain, after transformations, the expression for the F_1 in the form

$$F_1 \approx -\frac{c^2 r_g r}{2a^3} = -\frac{GMr}{a^3}. \tag{83}$$

If $r = a$, then (83) transforms into the expression for the Newtonian force of attraction, created by the sphere of radius a

$$F_1 = -\frac{GM}{a^2}. \tag{84}$$

The expression (84) coincides completely with (78) by $r_g \ll r = a$. Thus the Newtonian gravitational force is the

partial case of the non-Newtonian force of gravitation (82) by the condition $r_g \ll r = a$. But this fact does not mean that we must use the Newtonian theory of gravitation for the description of the gravitational field of the single body, whose Hilbert radius is small in comparison with its radius. The point is that the application of the relativistic mass-point metric (76) allows us to calculate the well-known effects (e.g. the perihelion motion of Mercury, the gravitational shift of light beams, the gravitational shift of spectral lines). It is possible that many other effects, unknown until now, will be explained by means of this metric.

We have studied until now only the case $r_g \ll r = a$. This condition corresponds to a single body, whose Hilbert radius r_g is negligible in comparison with its geometrical radius a. Consider now the case $r_g \ll r$, where the radial coordinate r can possess any values. Then the value $\frac{\varkappa\rho r^2}{3} = \frac{r_g r^2}{a^3}$ is not infinitely small for $r \gg a$. It follows from (11) that the condition $\frac{\varkappa\rho r^2}{3} = 1$ is the *condition of space breaking*, consequently the quantity $r_{br} = \sqrt{\frac{3}{\varkappa\rho}}$ is the breaking radius. Using the expressions for the r_g and r_{br}, we can rewrite (13) in the form

$$F_1 = -\frac{2GM}{c^2 a^3} \frac{r}{\left(3\sqrt{1-\dfrac{2GM}{c^2 a}} - \sqrt{1-\dfrac{r^2}{r_{br}^2}}\right)\sqrt{1-\dfrac{r^2}{r_{br}^2}}}. \quad (85)$$

The formula (85) describes the gravitational inertial force of the liquid sphere, whose Hilbert radius is small in comparison with the radius of the sphere ($\frac{r_g}{a} \ll 1$) and the sphere of space breaking $r = r_{br}$ is outside the liquid sphere ($r_{br} > a$). It follows from (85) that the force $F_1 \to \infty$ by $r \to r_{br}$. It is evident that the force (85) is the non-Newtonian force of attraction, manifesting a curvature dicontinuity in the environment.

The condition of space breaking was initially studied in [6]. The Sun was introduced as a liquid homogeneous sphere. It was shown that the Sun would break the surrounding space, with the breaking radius $r_{br} = 3.43\times10^{13}$ cm = 2.3 AU (1 AU = 1.49×10^{13} cm), where 1 AU is the distance between the Sun and the Earth. Thus the breaking (curvature discontinuity) of the Sun's space is located inside the asteroid strip, i.e. outside the gravitating body (the Sun). The Hilbert radius of the Sun is $r_g = 2.9 \times 10^5$ cm, the proper radius being $a = 6.95 \times 10^{10}$ cm. It is easy to calculate $\frac{r_g}{a} = 4.2 \times 10^{-6} \ll 1$, and $\frac{r_{br}}{a} = 4.9 \times 10^2$. It is possible that this non-Newtonian force creates the additional effect on the motion of the bodies in the Solar System. In partial, those bodies, which recede from the Sun in the radial direction, must possess additional negative (directed to the Sun) acceleration.

Analogous calculations were realized for all the planets of the Solar System [6]. It is important to note that the breaking spheres of the Earth, Mars, and Jupiter intersect with the asteroid strip near the hypothetical planet Phaeton, according to the Titus-Bode law at $r = 2.8$ AU. It is possible that the breaking of the Solar System space by the Sun and the mentioned planets plays an important rôle in the very formation of the Solar System itself. It means that not only the Sun, but also other planets of the Solar System exert an effect on the motion of different objects, including artificial satellites, moving in the orthogonal direction with respect to the orbits of planets. The additional non-Newtonian force of attraction is proportional to the radial distance r, and the Newtonian force decreases as $\frac{1}{r^2}$. It means that the more distant the body moves away from the center of attraction, the more appreciable the effect of the non-Newtonian part of the force is. It is possible that the Pioneer anomaly can be explained by the existence of non-Newtonian forces: this effect is registered near the boundary of the Solar System, because Newtonian attraction here decreases (with radial distance), and non-Newtonian attraction increases.

Thus the gravitational field of a single mass, whose Hilbert radius is considerably smaller than its radius, can be described by the Schwarzschild mass-point metric (76) by way of performing calculations of the orbital motions of the test bodies. The analogical field must be described by the metric of a continuous body (such as the simplest metric of the homogeneous liquid sphere), i.e. if we consider the radial motion of the moving test body.

Consider now a cosmic body whose Hilbert radius is comparable with its proper radius: $r_g \sim a$. A model of the observable Universe whose whole radius matches the Hilbert radius was first suggested by Stanyukovich [10]. He studied some geometric properties of the liquid body in the state of gravitational collapse, but he did not introduce the concrete metric. Stanyukovich assumed that the space of the Universe was a collapsar, whose Hilbert radius r_g was equal to the distance up to horizon of events a. According to this concept, the mass of the Universe could be calculated by the formula $M = \frac{ac^2}{2G}$. Assuming $a = 1.3\times10^{28}$ cm (the maximal observed distance), we should find $M = 8.78 \times 10^{55}$ g. This value coincides approximately with estimates obtained by way of other sorts of reasoning.

The average value of the density of the liquid substance is $\rho = \frac{M}{V}$. Calculating the value of the density of the mass-point collapsar $M = \frac{ac^2}{2G}$ by the assumption $V = \frac{4\pi a^3}{3}$, we obtain

$$\rho = \frac{3c^2}{8\pi G a^2} = \frac{3H^2}{8\pi G} = 9.5 \times 10^{-30} \frac{\text{g}}{\text{cm}^3}, \quad H = \frac{c}{a}. \quad (86)$$

This value corresponds to the range of values obtained from observational data. Moreover, it corresponds to the theoretical value of the critical density ρ_{cr} by the condition $H = 2.3 \times 10^{-18}$ sec^{-1}.

It is necessary to note that the critical density is determined in standard cosmology as the density of the Friedman model (66), whose three-dimensional space is flat: $k = 0$. It is evident that this space-time is not a collapsar, because the observable time τ coincides with the coordinate time t: $d\tau = dt$,

consequently $g_{00} = 1$. (Recall that the collapse condition is $\sqrt{g_{00}} = 0$). Calculating the volume of the gravitational collapsar by the formula $V = \frac{4\pi a^3}{3}$, we have assumed in fact that the space inside the collapsar is flat. Let us study this problem in detail below.

Recall once again that Stanyukovich considered the Universe as the result of the collapse of the space-time (76), created in emptiness by the mass-point, because he actually used the Hilbert radius r_g [10]. We have introduced in this paper the collapse of a specific continuous body — a homogeneous liquid sphere (liquid bubble). It follows from (12) that the radius of the liquid sphere (11) in the collapse condition r_c equals its proper radius a and the breaking radius r_{br}, if

$$r_c = a = r_{br} = \sqrt{\frac{3}{\varkappa\rho}}. \tag{87}$$

Substituting into (87) $\varkappa = \frac{8\pi G}{c^2}$ and $\rho = \frac{3M}{4\pi a^3}$, we find, after elementary transformations,

$$r_c = a = r_{br} = r_g = \frac{2GM}{c^2}, \tag{88}$$

where M is the mass of both the liquid and vacuum bubbles, because the liquid bubble in the state of collapse is precisely the vacuum bubble.

We have interpreted above that the liquid and vacuum bubbles are the spaces of the future and the past, respectively. This is partly how we geometrize the reality of time in terms of its flows (successive states) and in a cosmological framework. Then the space of the present must: 1) belong to these states simultaneously; 2) be situated between the future and past spaces. Of special interest, the singular surface $r = a$ (the event horizon) satisfies both conditions. Firstly, the event horizon belongs to the gravitational and inflation collapsars; secondly, it is between the future and the past, since the observable time at the surface of the collapsar is stopped.

Since the event horizon is the characteristic surface of both the gravitational and inflation collapsars, it is simultaneously the surface of both the "white" and "black" holes. The collapsing liquid bubble transforms **instantaneously** into the de Sitter vacuum bubble — the **inflation collapsar**. Besides, the space inside the inflation collapsar (the "white hole") is simultaneously also the space inside the gravitational collapsar (the "black hole"). The white and black holes possess the generic surface $r = a$, which is simultaneously: 1) the radius of the liquid sphere and its breaking radius; 2) the event horizon itself and the radius of curvature of the vacuum bubble; 3) the Hilbert radius of the whole mass-point, which equals both the masses of the liquid and vacuum bubbles. The transformation of the liquid into the vacuum is accompanied by the inversion of the observable time: the **flow of time changes the direction by way of transformation**. Let us consider the causes of this transformation in detail. The question is: where, in the reality of time, is the mass M? The answer is: the liquid and vacuum bubbles are reflections of one other, where the mirror is the singular surface, therefore the mass is in the very present state of time, i.e. at the singular surface. Thus the materialization of the present ("reality") is the transfer of time flows through the said singularity.

Let us return for a moment to the "black-and-white" model of the Universe. This object is the result of some transformations: 1) the liquid substance transforms **instantly** into the physical vacuum in the state of inflation; 2) the "curvature of time" changes its sign; 3) the Non-Newtonian force of attraction transforms into the force of repulsion. In fact, the liquid sphere overturns itself in time. This overturning is similar to the transfer of a time flow from one side of the Möbius strip onto the other side where the respective time on each of these sides flows in the opposite direction (compared to the other). We know that the Möbius strip is a two-dimensional one-sided surface which can be included (embedded) in three-dimensional Eucledian space E_3 (otherwise, it is generally non-orientable).

It is possible to say, therefore, that the observable time has three dimensions: the past, the present, the future. Time is perceived by human consciousness as one-dimensional and directed from the past to the future. Meanwhile, similar events are repeated for different epochs, demonstrating that the past and the future are mirror images of one other, where the mirror is the present. But these events are not identical. It is possible to say that the spaces of the past and the future are created from "different cosmic substances", which depends on the time of creation of each space. Thus the past, present, and future are the three dimensions of the temporal volume, and these dimensions are different in principle. The past contains the consequence of holograms — physically realized (materialized) events. Besides, it also contains non-realized events. The future is virtual, because it contains only non-materialized events. Some events will be physically realized, others will be virtual. Such materialized events create the hologram (standing-wave picture) of the events, which is perceived by human consciousness as the (present) "reality".

As such, our Universe transforms the space of the future through the singular surface (the present) into the space of the past, consequently the *following materialization is none other than time transfer through the pertinent singularity — the event horizon*. This singular surface is the place of interaction of two opposite forces — attraction and repulsion. The energy of physical vacuum creates the force of attraction, appearing as the "scattering of galaxies". It can be called "radiant energy". The energy of compression, which is due to the force of attraction, can be called "dark energy". These two types of energy are divided and connected at the same time by said singular surface, which transforms the future into the past. When the course of the future reaches an end, the radiant energy will not develop, and the observable Universe will be compressed into the state of initial singularity. The cos-

mos will exist the way it does at present until it transforms all the virtual realities of the future time (as it flows from the future to the past). When this mechanism is exhausted, the observable Universe will compress itself into a Schwarzschild black hole, namely the initial singularity. It is possible that the mass of the singularity itself is the hypothetical "hidden mass", which exerts a definite effect on the motion of stars and galaxies.

Let us now calculate the values r_{br} and r_g for the Earth, the Galaxy, and the observable Universe: see Table 1. Besides, let us include into Table 1 the relative values r_{br}/a and r_g/a for the mentioned objects. It follows from the Table that the physical-geometric properties of the Universe differ in principle from the analogous properties of other objects (the Earth, the Sun, the Milky Way). In reality, only the Universe is simultaneously both a white hole and a black hole, because its Hilbert radius r_g equals the radius of the inflation collapsar a. These values coincide completely with the radius of space breaking in the curvature of time. It is possible to say that the forces of attraction and repulsion in the cosmos are in the state of equilibrium. It is evident that the observable Universe must be described as a stretched meta-body filled with matter (physical vacuum in the given case).

The other objects (the Earth, the Sun, the Milky Way) contain black holes, whose Hilbert radiuses r_g are very small in comparison to their radiuses a. In addition, these objects break the surrounding space, and the respective spheres of spatial discontinuities are located out of the bodies (sources), far away from them. Since the Hilbert radius $r_g \ll a$ depends only on the mass of the body, we will consider these bodies as mass-points, for example, by studying test bodies motion in their gravitational fields. But if we want to study this case in detail, we must consider the sources as stretched bodies filled with matter. This approach applied in [6] to the Solar System allows us to study the coupling between them. It is easily obtained from the formula (12), that the Earth, the Sun, and the Galaxy cannot be "white holes", since the value r_c is imaginary. Therefore, these objects include Hilbert "black holes" inside their spaces, but the resepctive space breakings are outside of them.

7 Conclusion

The seminal process of time-transfer transformation of the future into the past has been considered in this paper. The future and past spaces are introduced geometrically as two telemetric spheres (bubbles), filled with ideal substances — liquid vacuum and physical vacuum respectively. These bubbles are mirror reflections of each other, where the mirror is the singular surface. It means that the transfer of time from the future to the past is realized through the singular state — the very space of the present. The singular surface is simultaneously the surface of both the gravitational and inflation collapsar, which can be called the dual "black-white hole". Thus, the present is the result of the collapse of the future space, where the singular surface (the present) is the event horizon. The collapsar is in the state of equilibrium, because the two oppositely directed forces equalize each other. They are 1) the gravitational force of attraction; 2) the force of repulsion, which can be called the "force of anti-gravitation". The present is stable, until these forces neutralize one other. If the force of attraction is greater than the force of repulsion, the event horizon approaches the observer in space-time: the space of the observable Universe "compresses". If the force repulsion is greater than the force of attraction, the event horizon recedes from the observer: the space of the Universe observable "expands".

We have obtained that observable time flows in the opposite directions inside the liquid and vacuum bubbles. As was shown in [3], spaces with the opposite directions of time are mirror reflections of each other. In essence, the very term the "mirror space" is linked immediately to the "arrow of time". The widely accepted opinion is that the "arrow of time" can be directed only from the past to the future. The mathematical apparatus of General Relativity does not prohibit the reverse flow of time, i.e. from the future to the past. Nevertheless the reverse flow of time is not introduced in contemporary physics and cosmology, because modern scientists refer to Hans Reichenbach's "arrow of time", which is directed always to the future [4]. However, Reichenbach stipulating unidirectional time also implied a world process of evolution (transfer of energy). In particular, in the geometric framework of General Relativity, time can be stopped (as light can also be frozen) or be directed to the past or the future. Setting free cosmology from the unidirectional time concept gives us a definite advantage as to introduce the pontentially revolutionary Mirror Universe into General Relativity.

It is therefore more correct to introduce time as an ultimate kind of energy, although formally time is one of the coordinates of the four-dimensional Riemannian manifold — the space-time of General Relativity. But the three spatial coordinates are measured by lines, while time is measured by clocks, consequently space and time are two aspects of the indivisible manifold — the space-time. Clearly speaking, space-time can be considered as *material* (space), which is filled with time (time-energy). Time-filled spaces exists only in pseudo-Riemannian spaces, because the principal difference between coordinates exists, namely in spaces where the basis vectors possess both real and imaginary lengths.

It is necessary to mention "rulers" of a special kind, which are used in contemporary astronomy and cosmology, namely light rays. Because light transfers at the finite velocity c, observation of electromagnetic radiation ensuing from cosmic objects allows us to study only the past states of these objects. It is evident that the present states of these cosmic objects could be studied by means of instruments, which could register a long-range action. The unfortunate negation of a long-range action allows us to consider only the past states

of the Universe. In reality, our telescopes perceive only those light rays from stars and galaxies, emitted in the past. But if we'd only virtually reflect on the very boundaries of the observable Universe, that the present exists simultaneously in the whole space of the Universe, we might be able to build a space-time apparatus capable of registering the momentary (present) action of cosmic objects. (For example, such apparatuses have been constructed and tested by Nikolai Kozyrev). It is well-known that the consensual opinion exists that General Relativity prohibits a long-range action due to the "light barrier". This opinion is fundamentally incorrect: only the typical human consciousness produces this imaginary barrier. In fact, the mathematical apparatus of General Relativity allows the existence of zero-particles possessed of instantenous transfer. The rejection of the notion of the "light barrier" allows us to construct, in principle, instruments for the registration of zero-particles.

All the innovative techniques in this paper are substantially based on Riemannian geometry only. The usual imaginary prohibitions (e.g., the speed of light barrier) by way of consensus in the field of General Relativity retard the development of General Relativity and science as a whole on the furthest horizon, which is a way to negate General Relativity as a whole. Clearly, those typical conditions restricting Special Relativity (as in the usual particle physics) do not ultimately exist in General Relativity as a whole by way of the vastness and versatility of the underlying Riemannian geometry (in our extensive case as shown in [3], the basic Riemannian geometry of General Relativity is extended at the sub-manifold level by the presence of degenerate, generally rotating zero-spaces and zero-particles). Meanwhile, in principle, the fundamental elements of Riemannian geometry allow for the existence of both the long-range action and the reverse flow of time: the long-range action is realized by null-particles, while the reverse flow of time is due to gravitation and rotation. It is necessary to note that these results are obtained by the condition that gravitation and rotation are rather strong. Meanwhile, most specialists in General Relativity consider gravitation and rotation as weak factors. For example, the gravitational potential w and the linear velocity of rotation v_i from the expression of $d\tau$ (3) are taken into account by the usual problem of the synchronization of clocks as merely small corrections. Moreover, contemporary cosmologists assume that the reality of time of the Universe is the same in the whole space (being limited usually by the Hubble volume), since the observable time in the Friedman cosmological model flows uniformly: $d\tau = dt$. But, as shown here, even using very simple non-rotating model of the gravitating Universe (the de Sitter bubble) as a start, we have seen that gravitation causes the accelerated extension of the space of the Universe near the event horizon.

All that has been said above is similar to the observation of a thunderstorm: we first see a lightning flash, only then the thunderpeal is registered by our ears. This is because light and sound travel at different speeds. A blind observer will, however, perceive only the thunderpeal. Moreover, having not a visual connection to the source of this sound (which is the lightning flash), he will be unable to determine the distance to the lightning. (A normal, sighted observer merely multiplies the sound speed in the air by the duration between the observed lightning and the heard thunderpeal, thus calculating the distance to the lightning.) Most astronomers may now be compared to the previous blind researcher of the thunderstorm: the instruments they use in their astronomical observations register only electromagnetic radiations of different sorts (visible light, radio-waves, x-rays, etc.), while all these radiations travel at the speed of light (in vacuum) or even slower than light (if travelling in a medium); their current instruments are not able to register real cosmic signals which are faster than light. In other words, those astronomers merely focus on the registration of the "short-range action" (transferred by photons, in particular). They do not take the possibility of the "long-range action" (instantaneous geometric interactions) into account. The key role in this primitive approach is played by the psychological wall erected against superluminal (and instantaneous) interactions. There is an easily popular bias that this prohibition is due to Einstein, whose prior postulate of the Special Theory of Relativity stipulated that signals travelling faster than light was practically impossible. This is, however, not true in the bigger picture. Einstein claimed this postulate in his early "positivistic" publication prior to General Relativity, in the framework of his theory of observable phenomena registered by means of signals of light: superluminal (and instant) signals were naturally out-of-access for such an observer. However, the geometric (if not hypergeometric) structure of the four-dimensional pseudo-Riemannian space (which is the basic space-time of Einstein's General Theory of Relativity, being geometrically more complete, vast, and versatile in comparison to the Special Theory of Relativity) allows more diverse paths along which particles (signals) of different kinds may travel. For instance, particles bearing non-zero rest-mass/energy inhabit the sub-light speed region of the space-time (located "inside" the light cone); meanwhile, particles bearing imaginary masses and energies inhabit the superluminal space-time region (located "outside" the light cone); subsequently, there exist light-like particles bearing zero rest-mass (they are always in motion), while their relativistic masses and energies ("kinetic" masses and energies of motion) are non-zero, as they travel along space-time trajectories located along the light cone. There are also the so-called "zero-particles": they are the ultimate case of light-like particles, and travel along the fully degenerate light-like trajectories which seem to have zero length and duration to an external observer; as a result zero-particles seem to be travelled instantaneously, thus transferring long-range action such as that in the case of the geometric non-quantum teleportation as shown in [3].

Object	Mass, gram	Proper radius, cm	Density, g/cm^3	Space breaking radius, cm	Hilbert radius, cm	r_g/a	r_{br}/a
Earth	5.97×10^{27}	6.38×10^{8}	5.52	1.64×10^{13}	0.88	1.4×10^{-9}	2.6×10^{4}
Sun	1.98×10^{33}	6.95×10^{10}	1.41	3.43×10^{13}	2.9×10^{5}	4.2×10^{-6}	4.9×10^{2}
Milky Way	6.0×10^{45}	4.5×10^{22}	6.58×10^{-23}	4.95×10^{25}	8.9×10^{17}	2.0×10^{-5}	1.1×10^{3}
Universe	8.8×10^{55}	1.3×10^{28}	9.5×10^{-30}	1.3×10^{28}	1.3×10^{28}	1.0	1.0

A real observing human whose body is made of regular substance such as atoms and molecules cannot travel at the speed of light. At the same time, he perceives light by his physical organs and the other (artificial) instruments of observation: there is not a barrier dividing him and light. In analogy to this case, instruments registering zero-particles (which seem to be travelling instantaneously) may be invented. All that the innovative engineers need to do it is set themselves free of the psychological prohibition and limitation in traveling at the light speed, as to be professionally equipped with the full extent of the General Theory of Relativity which has already theoretically predicted zero-particles carrying the long-range action (geometric non-quantum teleportation).

Again, there are unfortunately many popular biases about Einstein's General Theory of Relativity. Most of them originated in the non-technically equipped reporters of pop-science, or the pop-science authors themselves whose knowledge in this field is limited with those "first-grade" rudimentary textbooks on the the Theory of Relativity. Such books present Einstein's theory rather very shallowly, paying attention to mostly the native examples based on Einstein's early postulates revolving around his theory of exchanging light signals. The greater true meaning of Einstein's theory — the deeper picture of space-time geometry as the basis of all the physical world — is regularly out-of-scope in such books due to the psychological threshold of the need to master Riemannian geometry and tensor calculus at a certain great level of mathematical and physical depth (which is not a trivial task for a beginner and indeed most would-be specialists, with the exception of very few gifted and versatile ones). As a result, we have such a popular bias (not based on geometry) as the above-mentioned aforementioned myth about the insurpassable nature of the light speed limit, and also the myth about the irreversibility of the arrow of time (which naturally depends on the physical conditions of observation in different space-time regions). There is also another myth saying that the General Theory of Relativity can result in only small corrections to Classical Mechanics and Electrodynamics (this is not true on cosmological scales where the effects of General Relativity greatly rule), and many other biases concerning Einstein's theory.

Setting ourselves free from these popular, primitive, anti-progressive biases, and following the deeper versatile trajectory (geometry) of the theory of space-time-matter established by Albert Einstein, no doubt certain researchers could arrive at new instruments of observation based on the geometric resurgence of the long-range action (in parallel with certain gravitational and gauge field instantons of the Plebanski type). These new developments, based on completely different principles than the usual electromagnetic interactions, could lead to certain cosmic engines allowing for (geometric) non-quantum teleportation, as well as other new exotic technologies in order to carry the human species to an unprecedented Golden Age in the cosmos.

Submitted on September 30, 2012 / Accepted on October 10, 2012

References

1. Raschewski P. K. Riemannische Geometrie und Tensoranalysis. Deutscher Verlag der Wissenschaften, Berlin, 1959 (translated by W.Richter); reprinted by Verlag Harri Deutsch, Frankfurt am Main, 1993.
2. Zelmanov A. Chronometric invariants. Dissertation, 1944. American Research Press, Rehoboth (NM), 2006.
3. Borissova L. and Rabounski D. Fields, Vacuum and the Mirror Universe. 2nd edition, Svenska fysikarkivet, Stockholm, 2009. Also, in parallel, see: Rabounski D. and Borissova L., Particles Here and Beyond the Mirror. 2nd edition, Svenska fysikarkivet, Stockholm, 2008.
4. Reichenbach H. The Direction of Time. University of California Press, Berkeley (CA), 1956.
5. Schwarzschild K. Über das Gravitationsfeld einer Kugel aus inkompressibler Flüssigkeit nach der Einsteinischen Theorie. *Sitzungberichte der Königlich Preussischen Akademie der Wissenschaft*, 1916, 426–435.
6. Borissova L. The Gravitational Field of a Condensed Matter Model of the Sun: the Space Breaking Meets the asteroid Strip. *The Abraham Zelmanov Journal*, 2009, vol.2, 224–260.
7. Borissiva L. De Sitter Bubble as a Model of the Observable Universe. *The Abraham Zelmanov Journal*, 2010, vol.2, 208–223.
8. Schwarzschild K. Über das Gravitationsfeld eines Massenpunktes nach der Einsteinischen Theorie. *Sitzungberichte der Königlich Preussischen Akademie der Wissenschaft*, 1916, 189–196.
9. Zelmanov A. On the relativistic theory of an anisotropic inhomogeneous universe. The Abraham Zelmanov Journal, 2008, vol. 1, 33–63 (originally presented at the 6th Soviet Meeting on cosmogony, Moscow, 1959).
10. Stanyukovich K. On the Problem of the Existence of Stable Particles in the Metagalaxy. *The Abraham Zelmanov Journal*, 2008, vol. 1, 99–110.

A Single Big Bang and Innumerable Similar Finite Observable Universes

Nilton Penha Silva
Departamento de Física (Retired Professor), Universidade Federal de Minas Gerais, Belo Horizonte, MG, Brazil.
E-mail: nilton.penha@gmail.com

Gravity dominated Universe until it was 3.214 Gyr old and, after that, dark energy dominates leading to an eternal expansion, no matter if the Universe is closed, flat or open. That is the prediction of the expansion factor recently proposed by Silva [2]. It is also shown that there is an upper limit for the size of the Observable Universe *relative radial comoving coordinate*, beyond which nothing is observed by our fundamental observer, on Earth. Our Observable Universe may be only a tiny portion of a much bigger Universe most of it unobservable to us. This leads to the idea that an endless number of other fundamental observers may live on equal number of Observable Universes similar to ours. An unique Big Bang originated an unique Universe, only part of it observable to us.

1 Introduction

Since 1929, with Hubble [1], we learned that our Observable Universe has been continuously expanding. Nearly all galaxies are moving away from us, the further they are, the faster they move away. If the galaxies are moving apart today, they certainly were closer together when the Universe was younger. This led to the idea of the Big Bang theory, which is the most accepted theory for the explanation on how the Universe began. According to it, all started from a physical singularity where all Universe matter-energy-space were extremely concentrated with temperature well above 10^{32} K, when a cataclismic expansion ocurred and the size of it went from a Planck's length to some Gigayears (Gyrs) in an extremely tiny fraction of a second.

According to the theory, as the Universe cooled, the first building blocks of matter, quarks and electrons, were formed, followed by the production of protons and neutrons. In minutes protons and neutrons aggregated to produce nuclei.

Around 380,000 years after the Big Bang, there was the so called recombination era in which matter cooled enough to allow formation of atoms transforming the Universe into a transparent eletrically neutral gas. The first photons that managed to be traveling freely through the Universe constitute the so called Cosmic Microwave Background (CMB) which are detected today. This "afterglow light" study is very important because they show how was the the Primeval Universe. Next step is the formation of the structure which gave rise to the astronomical objects [4–10].

Today the Universe keeps expanding, but since 1998 we learned that it has a positive acceleration rate. This indicates that there is something overcoming the gravity and that has been called dark energy. A completely characterization of the dark energy is not done yet. Most researchers think it comes from the vacuum.

In previous papers [2, 3], we have succeeded in obtaining an expression for the Universe scale factor or the Universe expansion factor as you may well call it too:

$$\begin{aligned} a(t) &= \exp\left(\frac{H_0T_0}{\beta}\left(\left(\frac{t}{T_0}\right)^{\beta}-1\right)\right), \\ \beta &= 1+H_0T_0\left(-\frac{1}{2}\Omega_m(T_0)+\Omega_\Lambda(T_0)-1\right) \end{aligned} \tag{1}$$

and H_0 is the so called Hubble constant, the value of the Hubble parameter $H(t)$ at $t = T_0$, the current age of the Universe. Expression (1) is supposed to be describing the expansion of the Universe from the beginning of the so called *matter era* ($t \approx 10^{-4}$ Gyr, after the Big Bang). Right before that the Universe went through the so called *radiation era*. Only the role of the matter (baryonic and non-baryonic) and the dark energy, both treated as perfect fluids are considered. In our work the dark energy was associated to an *a priori* time dependent $\Lambda(t)$ (cosmological "constant").

Figure 1 shows the expansion factor $a(t)$ as function of the Universe age. In Figure 2 the behaviour of the expansion factor acceleration, $\ddot{a}(t)$, is reproduced. Before $t = T_\star = 3.214$ Gyr, acceleration was negative, and after that, acceleration is positive. To perform the numerical calculations we

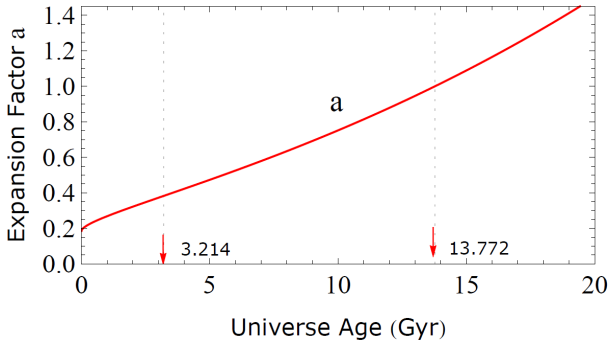

Fig. 1: $a(t) = \exp\left(\frac{H_0T_0}{\beta}\left(\left(\frac{t}{T_0}\right)^{\beta}-1\right)\right)$.

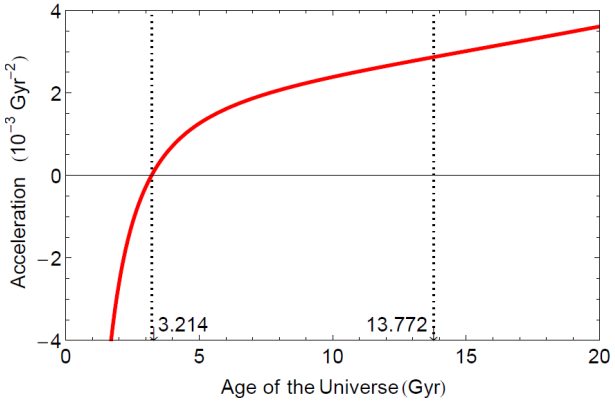

Fig. 2: $\ddot{a}(t) = a(t)\left(H_0\left(\frac{t}{T_0}\right)^{\beta} - (1-\beta)\frac{1}{t}\right)H_0\left(\frac{t}{T_0}\right)^{\beta-1}$.

have used the following values [11]:

$$\begin{aligned} H_0 &= 69.32\ \text{kms}^{-1}\text{Mpc}^{-1} \\ &= 0.0709\ \text{Gyr}^{-1}, \\ T_0 &= 13.772\ \text{Gyr}, \\ \Omega_m(T_0) &= 0.2865, \\ \Omega_\Lambda(T_0) &= 0.7135. \end{aligned} \tag{2}$$

In reference [2], some properties such as Gaussian curvature $K(t)$, Ricci scalar curvature $R(t)$, matter and dark energy density parameters $(\Omega_m, \Omega_\lambda)$, matter and dark energy densities (ρ_m, ρ_λ), were calculated and plotted against the age of the Universe, for $k = +1, 0, -1$. It was found that the current curvature radius $\mathfrak{R}(T_0)$ has to be larger than 100 Gly, for $k = \pm 1$. Obviously, for $k = 0$, $\mathfrak{R} = \infty$. So, arbitrarily [2], we have chosen $\mathfrak{R}(T_0) = 102$ Gly. None of the results were sufficient to decide which value of k is more appropriate for the Universe. The bigger the radius of curvature, the less we can distinguish which should be the right k among the three possible values. Considering that, we pick the most intuitive geometry, at least in our view, we work here with the closed Universe version.

2 Closed Universe

The closed Universe Friedmann - Lemaitre - Robertson - Walker (FLRW) spacetime metric is given by [4–10]:

$$\begin{aligned} ds^2 &= \mathfrak{R}^2(t)\left(d\psi^2 + \sin^2\psi\left(d\theta^2 + \sin^2\theta d\phi^2\right)\right) - c^2dt^2 \\ &= \mathfrak{R}^2(T_0)\,a^2(t)\left(d\psi^2 + \sin^2\psi\left(d\theta^2 + \sin^2\theta d\phi^2\right)\right) \\ &\quad - c^2dt^2, \end{aligned} \tag{3}$$

where ψ, θ and ϕ are comoving space coordinates ($0 \le \psi \le \pi$, $0 \le \theta \le \pi$ and, $0 \le \phi \le 2\pi$), t is the time shown by any observer clock in the comoving system. $\mathfrak{R}(t)$ is the scale factor in units of distance; actually it is *radius of curvature* of the Universe as already said in previous section. The time t is also known as the cosmic time. The function $a(t)$ is the usual expansion factor

$$a(t) = \frac{\mathfrak{R}(t)}{\mathfrak{R}(T_0)}, \tag{4}$$

here assumed to be that of Equation 1.

The FLRW metric embodies the so called Cosmological Principle which says that the Universe is spatially homogeneous and isotropic in suficient large scales.

We have to set that our "fundamental" observer (on Earth) occupies the $\psi = 0$ position in the comoving reference system. To reach him(her) at cosmic time T, the CMB photons spend time T since their emission at time $t \approx 380,000$ yr, after the Big Bang, at a specific value of the comoving coordinate ψ. Let us call ψ_T this specific value of ψ. We are admitting that the emission of the CMB photons occured simultaneously for all possible values of ψ. Although that happened at $t \approx 380,000$ yr, for purposes of integrations ahead it is assumed to be $t \approx 0$ with no considerable loss.

Having said that, we can write, for the trajectory followed by a CMB photon ($ds^2 = 0, d\phi = d\theta = 0$), the following:

$$-\frac{cdt}{\mathfrak{R}(t)} = d\psi, \tag{5}$$

$$-\int_0^T \frac{c}{\mathfrak{R}(t)}dt = \int_{\psi_T}^0 d\psi, \tag{6}$$

$$\psi_T = \frac{c}{\mathfrak{R}(T_0)}\int_0^T \frac{1}{a(t)}dt, \tag{7}$$

The events ($\psi = 0$, $t = T$) and ($\psi = \psi_T$, $t = 0$) are connected by a null geodesics. The first event is relative to the fundamental Observer, while the second event refers to the emission of the CMB photons at $t \approx 0$ as explained above. ψ_T gets bigger as T increases which means that *the older the Universe gets, the further the referred Observer sees from the CMB*.

The comoving coordinate which corresponds to the current "edge" (horizon) of our Observable Universe is

$$\begin{aligned} \psi_{T_0} &= \frac{c}{\mathfrak{R}(T_0)}\int_0^{T_0}\frac{1}{a(t)}dt \\ &= \frac{c}{\mathfrak{R}(T_0)}\int_0^{T_0}\exp\left(\frac{H_0T_0}{\beta}\left(1-\left(\frac{t}{T_0}\right)^{\beta}\right)\right)dt \\ &= 0.275\ \text{Radians} = 15.7\ \text{Degrees}. \end{aligned} \tag{8}$$

where, again, $\mathfrak{R}(T_0)$ is assumed to be 102 Gly for the reason exposed in reference [2] ($\mathfrak{R}(T_0) > 100$ Gly). Very much probably $\mathfrak{R}(T_0)$ should be much greater than that. The value of the current curvature radius is crucial in the sense of determining the coordinate ψ_{T_0}.

So CMB photons emitted at ψ_{T_0} and $t = 0$ should arrive at $\psi = 0$ and $t = T_0$, the current age. Along their

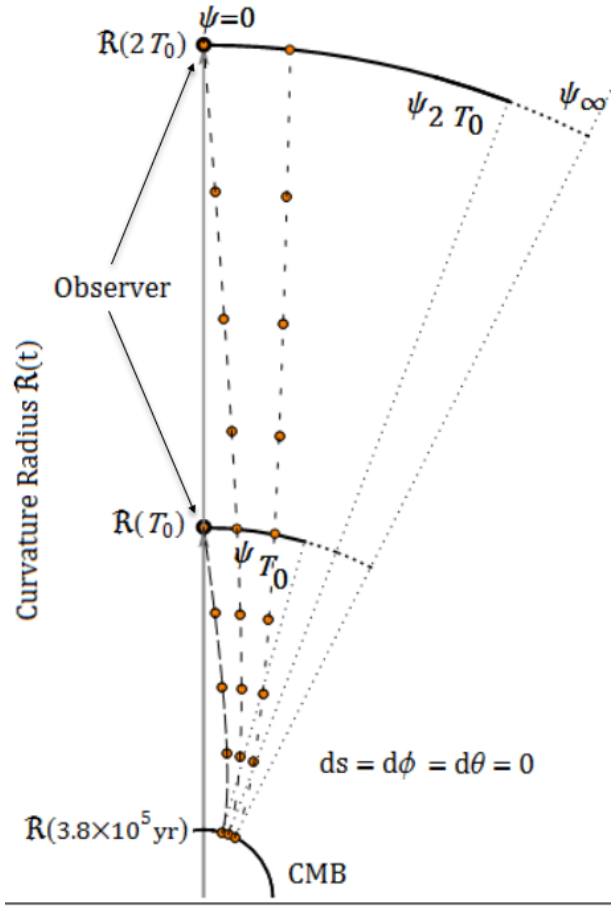

Fig. 3: The null geodesics connecting two events: $(\psi_{T_0},\ t \approx 0)$ and $(\psi = 0, t = T_0)$; $(\psi_{2T_0},\ t \approx 0)$ and $(\psi = 0,\ t = 2T_0)$. The null geodesic between $(\psi_\infty = 1.697\ \psi_{T_0},\ t \approx 0)$ and $(\psi = 0,\ t = \infty)$ will never be accomplished. $\mathfrak{R}(T)$ is radius of curvature at age T.

whole trajectory, other photons emitted, at later times, by astronomical objects that lie on the way, join the troop before reaching the fundamental observer. So he(she) while looking outwards deep into the sky, may see all the information 'collected' along the trajectory of primordial *CMB* photons. Other photons emitted at the same time $t \approx 0$, at a comoving position $\psi > \psi_{T_0}$ will reach $\psi = 0$ at $t > T_0$, together with the other photons provenient from astronomical objects along the way. As the Universe gets older, its "edge" becomes more distant and its size gets bigger. See Figure 3.

The current value for ψ_{T_0} should actually be smaller than 0.275 Radians, because, as we said above, $\mathfrak{R}(T_0)$ should be greater than the assumed value (102 Gly).

To get rid of such dependence on $\mathfrak{R}(T_0)$, we find convenient to work with the ratio r

$$r \equiv \frac{\psi}{\psi_{T_0}}, \tag{9}$$

which we shall call the *relative radial comoving coordinate*.

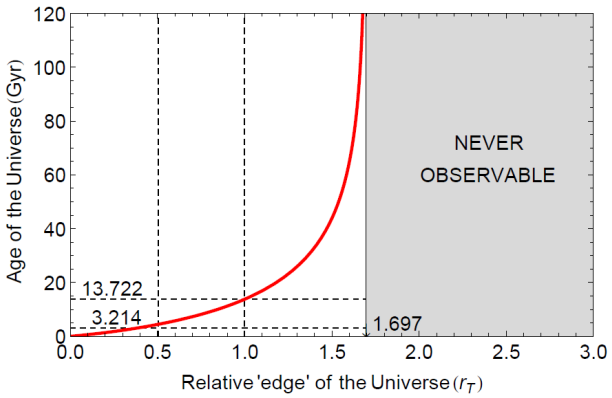

Fig. 4: $r_T = \int_0^T \frac{1}{a(t)}dt \Big/ \int_0^{T_0} \frac{1}{a(t)}dt$. The relative radial comoving coordinate r_T, from which *CMB* photons leave, at $(t \approx 0)$, and reach relative comoving coordinate $r = 0$ at age $t = T$ gives the relative position of the "edge" of the Observable Universe $(r_{T\to\infty} \to 1.697)$. (Axes were switched.)

Obviously, at age T, r_T is the *relative* measure of the "edge" position with respect to the fundamental observer $(\psi = 0)$

$$r_T = \int_0^T \frac{1}{a(t)}dt \Big/ \int_0^{T_0} \frac{1}{a(t)}dt, \tag{10}$$

and $r_{T_0} = 1$. For a plot of r_T see Figure 4.

3 Observable Universes

One question that should come out of the mind of the fundamental observer is: "Is there a maximum value for the relative comoving coordinate r?" What would be the value of r_∞?

By calculating r_∞, we get

$$r_\infty = \int_0^\infty \frac{1}{a(t)}dt \Big/ \int_0^{T_0} \frac{1}{a(t)}dt = 1.697. \tag{11}$$

To our fundamental observer (Earth), there is an upper limit for the relative comoving coordinate $r = r_\infty = 1.697$, beyond that no astronomical object can *ever* be seen by such fundamental observer.

This should raise a very interesting point under consideration.

Any other fundamental observer placed at a relative comoving coordinate $r > 2r_\infty$ $(\psi > 2\psi_\infty)$, with respect to ours, will never be able to see what is meant to be our Observable Universe. He (she) will be in the middle of another visible portion of the same whole Universe; He (she) will be thinking that he (she) lives in an Observable Universe, just like ours. Everything we have been debating here should equally be applicable to such an 'other' Observable Universe.

The maximum possible value of ψ is π (Equation 3), then the maximum value of r should be at least 11.43. Just recall that $r = 1$ when $\psi = \psi_{T_0}$. This ψ_{T_0} was overevaluated as being 0.275 Radians = 15.7 Degrees, in equation (8)

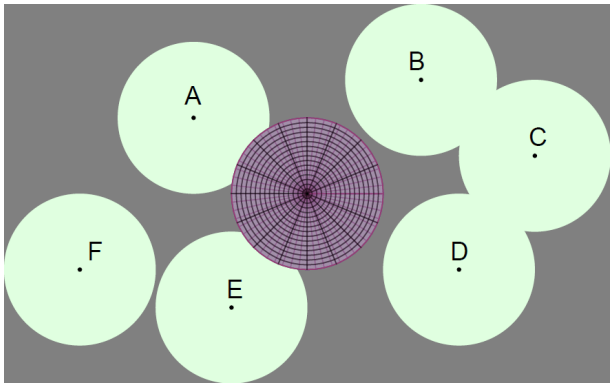

Fig. 5: This illustration tries to show schematically a hypersurface at time T with our Observable Universe surrounded by other similar Observable Universes, arbitrarily positioned, some of them overlapping.

when considering the current radius of curvature as $\Re(T_0) =$ 102 Gly. As found in reference [2] $\Re(T_0)$ should be bigger than that, not smaller. Consequently the real ψ_{T_0} should be smaller than 0.275 Radians = 15.7 Degrees, not bigger. One direct consequence of this is that there is room for the ocurrence of a large number of isolated similar *Observable Universes* just like ours.

We may say that the Big Bang gave birth to a large Universe, of which our current Observable Universe is part, perhaps a tiny part. The rest is unobservable to us and an endless number of portions just the size of our Observable Universe certainly exist, each one with their fundamental observer, very much probably discussing the same Physics as us.

Of course, we have to consider also the cases of overlapping Observable Universes.

One important thing is that we are talking about **one Universe**, originated from **one Big Bang**, which is not observable as a whole, and that may contain **many** other Observable Universes **similar** to ours. Would it be a *Multiverse*? See Figure 5.

4 Conclusion

The expansion factor $a(t) = exp\left(\frac{H_0 T_0}{\beta}\left(\left(\frac{t}{T_0}\right)^{\beta} - 1\right)\right)$, where $\beta = 1 + H_0 T_0\left(-\frac{1}{2}\Omega_m(T_0) + \Omega_\Lambda(T_0) - 1\right) = 0.5804$ [2], is applied to our Universe, here treated as being closed ($k = +1$). Some very interesting conclusions were drawn. One of them is that the radial relative comoving coordinate r, measured from the fundamental observer, $r = 0$ (on Earth), to the "edge" (horizon) of our Observable Universe has an upper limit. We found that $r \to 1.697$ when $T \to \infty$. Therefore all astronomical objects which lie beyond such limit would never be observed by our fundamental observer ($r = 0$). On the other hand any other fundamental observer that might exist at $r > 2 \times 1.697$ would be in the middle of another Observable Universe, just like ours; he (she) would never be able to observe our Universe. Perhaps he (she) might be thinking that his (her) Observable Universe is the only one to exist. An endless number of other fundamental observers and an equal number of Observable Universes similar to ours may clearly exist. Situations in which overlapping Universes should exist too. See Figure 5.

The fact is that the Big Bang originated a big Universe. A tiny portion of that is what we call our Observable Universe. The rest is unobservable to our fundamental observer (Earth). Equal portions of the rest may be called also Observable Universes by each of their fundamental observers if they exist. So we may speak about many Observable Universes - a Multiverse - or about only one Universe, a small part of it is observable to the fundamental observer.

By using the expansion factor here discussed we have also succeeded in finding a generalization of Hubble's Law, which may be found in reference [13].

The expansion factor, Equation 1, proposed in reference [2] has been shown to be a very good candidate to be describing the expansion of the Universe.

Submitted on January 2, 2017 / Accepted on January 4, 2017

References

1. Hubble E. A relation between distance and radial velocity among extragalactic nebulae, *Proceedings of the National Academy of Sciences of the United States of America*, 1929, v. 15(3), 168–173.
2. Silva N.P. A Model for the Expansion of the Universe. *Progress in Physics*, 2014, v. 10(2), 93–97.
3. Silva N.P. A Closed Universe Expanding Forever. *Progress in Physics*, 2014, v. 10(3), 191–195.
4. Raine D. An Introduction to the Science Of Cosmology. Institute of Physics Publishing Ltd, 2001.
5. Peacock J.A. Cosmological Physics. Cambridge University Press, 1999.
6. Harrison E.R. Cosmology: The Science of the Universe. Cambridge University Press, 2^{nd} ed., 2000.
7. Islam J.N. An Introduction to Mathematical Cosmology. Cambridge University Press, 2002.
8. Ellis G.F.R. Relativistic Cosmology. Cambridge University Press, 2012.
9. Springel V., Frenk C.S. and White S.D. The Large-scale Structure of the Universe. *Nature*, 2006, v. 440(7088), 1137–1144.
10. Luminet J.P. Cosmic Topology: Twenty Years After. *Gravitation and Cosmology*, 2014, v. 20(1), 15–20.
11. Bennett C.L. et al. Nine-Year Wilkinson Microwave Anisotropy Probe (WMAP) Observations: Final Maps and Results. arXiv: astro-ph.CO. 2013.
12. Peebles P.J.E. The Large-scale Structure of the Universe. Princeton university press, 1980.
13. Silva N.P. Beyond the Hubble's Law. *Progress in Physics*, 2017, v. 13(1), 5–6.

Physical Properties of Stars and Stellar Dynamics

Yuri Heymann

3 rue Chandieu, 1202 Geneva, Switzerland. E-mail: y.heymann@yahoo.com

The present study is an investigation of stellar physics based on observables such as mass, luminosity, radius, and photosphere temperature. We collected a dataset of these characteristics for 360 stars, and diagramed the relationships between their characteristics and their type (white dwarf, red dwarf, main sequence star, giant, supergiant, hypergiant, Wolf-Rayet, carbon star, etc.). For stars dominated by radiation pressure in the photosphere which follow the Eddington luminosity, we computed the opacity and cross section to photon flux per hydrogen nuclei in the photosphere. We considered the Sun as an example of star dominated by gas pressure in the photosphere, and estimated the density of the solar photosphere using limb darkening and assuming the adiabatic gradient of a monoatomic gas. We then estimated the cross section per hydrogen nuclei in the plasma of the solar photosphere, which we found to be about 2.66×10^{-28} m^2, whereas the cross section of neutral hydrogen as given by the Bohr model is 8.82×10^{-21} m^2. This result suggests that the electrons and protons in the plasma are virtually detached. Hence, a hydrogen plasma may be represented as a gas mixture of electrons and protons. If the stellar photosphere was made of large hydrogen atoms or ions such as the ones we find in gases, its surface would evaporate due to the high temperatures.

1 Introduction

The present study is an investigation of stellar physics based on characteristics such as mass, luminosity, radius, and photosphere temperature. We analysed a set of 360 stars for which we collected available data from the literature. The set included white dwarfs, red dwarfs, main sequence stars, giant stars, Wolf-Rayet stars, carbon stars, etc. Let us introduce the basics to get a sense of how stars regulate fusion reactions and the basic principles of stellar dynamics.

We can easily infer that stellar equilibrium is driven by hydrostatic pressure. The internal pressure of a star is determined by the radiation pressure and gas pressure, which counterbalance the hydrostatatic pressure from gravitation and prevent the star from collapsing. Radiation pressure and gas pressure are temperature dependent. When a star cools, it experiences a drop in internal pressure that causes the star to contract. This contraction will cause an increase in the hydrostatic pressure within the star. The gravitational force exerted by the inner mass of the star on a particule at a given radius is $F_g = \frac{GM_r m_p}{r^2}$, where r is the radius, M_r the interior mass of the star up to radius r, m_p the mass of the particule, and G the gravitational constant. Therefore, the more the star contracts, the higher the hydrostatic pressure. The increase in hydrostatic pressure increases the rate of fusion, which produces excess heat. In return, this excess heat increases the gas and radiation pressure in the star causing the star to expand. This process repeats until the star reaches a certain equilibrium.

Nuclear fusion, therefore, is driven by the hydrostatic pressure in stars. There are three possible mechanisms by which hydrostatic pressure could affect the fusion power of stars:

- Assuming that a minimum pressure or temperature is required to sustain fusion, the volume of the fusing core increases as hydrostatic pressure increases. According to the Arrhenius equation, reaction kinetics are highly dependent on temperature. Note that the Arrhenius equation assumes the Maxwell-Boltzmann distribution, and the relationship would be different for a Fermi gas.
- The density in the core of the star increases as hydrostatic pressure increases. Hence, a larger quantity of matter would be subject to fusion in the core of the star.
- The kinetic rate of fusion (i.e. the reaction rate or speed) may increase as pressure increases.

These are the mechanisms we propose regulate a star. In some instances the volume and luminosity of the star oscillates. These are the so-called variable stars. A notable example of variable stars are the Cepheid variables. They are known for a method to measure distances based on the period of their oscillation. As there is a relationship between the period of the star's oscillations and its luminosity, one can infer the intrinsic luminosity and compute the distance. Several different theories explain the oscillations of variable stars. We enumerate some possible mechanisms below:

- The κ-mechanism or Eddington valve is the most popular theory explaining variable Cepheids [1]. According to this theory, doubly ionized helium is more opaque than single ionized helium. As helium in the star heats, it becomes more ionized and less transparent so that the heat is retained longer. As the star expands, it cools and its helium becomes less ionized and hence more transparent, allowing the heat to escape. Then the star contracts again and the process repeats.

- Another mechanism would be a change in the regime of the fusion reactions for certain thresholds in the hydrostatic pressure of the star. For example, fusion of heavier elements in the core of large stars could ignite at a certain temperature threshold and produce large temperature spikes causing the star to oscillate. This theory would be applicable to massive stars where fusion of heavy elements in the core occurs.
- The ageing model of the core could also explain variable stars. Let us consider a star fusing hydrogen into helium when the star has too low a mass to ignite helium fusion. As the star ages, the helium core grows, and the shell of fusing hydrogen around the core thins. Let us say the hydrogen shell heats the core, making it expand and push the hydrogen shell to the exterior; the temperature of the shell would fall below the ignition point, and switch off hydrogen fusion. Then the core would cool, returning the hydrogen shell to the ignition point and switching hydrogen fusion on again. This pattern would repeat in cycles. This theory would apply to stars with small cores and explain the type II Cepheids, which have about half the mass of the Sun and therefore are not massive enough to fuse helium.
- Temperature driven kinetics for fusion reactions may also induce stellar oscillations. If the kinetic rate of fusion increases as temperature increases, a small increase in temperature at the core would cause large temperature spikes. Then the star would expand over a long period of time before cooling and contracting again. Note that this process would cause stars to be unstable. The fact that the Sun is stable with very low oscillations of order 0.1 % of its luminosity would be a counter example of temperature driven fusion kinetics, unless the sensitivity of the fusion-kinetic rate with respect to temperature is very small.

When a star has exhausted the nuclear supply at its core, it will cool. This will eventually trigger a gravitational collapse. When the star contracts, the depleted nuclear fusion at its core would not be able to counterbalance the hydrostatic pressure. As the radius of the star diminishes, the gravitational force acting on the particles of the star increases proportionally to $\frac{1}{r^2}$. The gravitational collapse of the star can lead to the formation of a black hole on one extreme or a supernova at the other. The latter occurs if at a certain point during the collapse the pressure is so high that it triggers fusion reactions in series at a very fast rate, causing the star to explode and leading to the formation of up to the heaviest elements of the Mendeleev table such as uranium. A black hole would form if fusion does not halt the gravitational collapse. In some instances gravitational collapse stops before the formation of a black hole, producing a neutron star or white dwarf. These are intermediary stages before the formation of a black hole. White dwarfs are less dense than neutron stars, at an earlier stage of matter compression than neutron stars. Neutron stars are composed of neutronium, a compact pack of neutrons, and have densities around 4×10^{17} kg/m^3. White dwarfs have densities around 10^7 to 10^{10} kg/m^3. Electron degeneracy pressure is the mechanism which supposedly prevents the further collapse of white dwarfs. Degeneracy of matter from gravitational collapse starts at the core of the star. Sometimes the core of the star collapses into a neutron star or a black hole while the outer shell of the star explodes into a supernova. Red giants of masses comparable to the Sun generally blow out their outer layer at the end of their life to form planetary nebulae, leaving a white dwarf in the core.

We find that stellar photosphere dynamics are crucial in the determination of the power of stars as measured by their luminosity. We cannot miss the notable work of Arthur Eddington on the dynamics of stars dominated by radiation pressure in the photosphere, according to which, the luminosity of such stars is proportional to their mass. Using data from stars dominated by radiation pressure in their photosphere, we can estimate the opacity parameter. We also discuss models and factors which may affect opacity, as this is a preponderant parameter for radiative heat transfer, a key component of stellar models. For stellar models we also need boundary conditions such as the density of the photosphere. We show how to estimate the density of the solar photosphere using limb darkening. According to the standard solar model, there is a layer at the surface of the Sun where radiative heat transfer is not efficient enough and convection takes place. The photosphere can be viewed as a plasma surface; hence using a model of the surface we can compute the cross section per hydrogen nuclei in the photosphere. We computed the cross section per hydrogen nuclei from radiation pressure and gas pressure, and found that both values match closely. From the cross section per hydrogen nuclei we obtained, we can infer that in stellar plasma the electrons and nuclei are virually detached. Therefore, stellar plasma may be represented as a gas mixture of electrons and nuclei. We discuss the modelling implications of this representation of stellar plasma.

2 Overview of stellar data

Stars form a very heterogeneous group having various luminosities, masses, temperatures, and densitities. In the below diagrams we show the relationships between these characteristics for the stars in our catalog. In section 2.1 we introduce the classification of stars we used for the diagrams. Section 2.2 shows the stellar diagrams we obtained with a emphasise on their interpretation.

2.1 Classification of stars

Stars can be classified according to their spectra, color, and size. Stellar spectra provide precious information about their atmospheric composition by analyzing their spectral lines, and surface temperature from Planck's law of black-body

spectrum. We divided the stars in our catalog according to the below groups:

- White dwarfs are degenerated stars which are very dense and composed mostly of electron-degenerate matter. They have masses comparable to that of the Sun, volumes comparable to that of Earth, and are very faint. Some white dwarfs are classified as helium stars as they have very strong helium lines and weak hydrogen lines [2].
- Brown dwarfs have masses comprised in the range of 13 to 80 Jupiter masses. Their mass is below the threshold needed to fuse hydrogen, but enough to fuse deuterium.
- Red dwarfs have masses in the range of 0.075 to 0.6 solar masses, and surface temperatures below 4,000 K. A count the stars nearest to earth, it was estimated that red dwarfs comprise about 80% of the stars in the Milky Way.
- Yellow dwarfs are main-sequence stars of comparable mass to the Sun, with a surface temperature between 5,300 and 6,000 K. We created a broader group that we called yellow main sequence stars to include all stars with masses between 0.6 and 1.7 solar masses, and a temperature between 4,200 and 7,200 K.
- A-type stars are main-sequence stars of spectral type A of 1.4 to 2.1 solar masses, and a surface temperature between 7,600 and 11,500 K. Their spectra have strong hydrogen Balmer absorption lines.
- B-type stars are main-sequence stars of 2 to 16 solar masses, and a surface temperature between 10,000 and 30,000 K. Their spectra have non-ionized helium lines.
- Subgiants are stars at an intermediary stage of evolution before becoming giants. These stars are brighter than main-sequence stars but not as bright as giants.
- Red giants are evolved stars of 0.8 to 8 solar masses which have exhausted the hydrogen supply in their core and are fusing helium into carbon. They have high luminosities compared to their main-sequence peers, and inflated atmospheres making their radii large, resulting in low surface temperatures between 3,200 and 4,000 K. Orange giants are distinguished from red giants by their temperature, which ranges from 4,000 to 5,500 K.
- Carbon stars are red giants whose atmosphere contains more carbon than oxygen.
- S-type stars are giant stars with approximately equal quantities of carbon and oxygen. These are intermediaries between giants and carbon stars.
- Blue giants are hot giant stars with masses in the range of ten to hundreds of solar masses, and surface temperatures between 22,000 and 45,000 K.
- Supergiants are stars with luminosities between those of the giants and hypergiants on the Hertzsprung-Russell diagram. They are divided into red supergiants, orange supergiants, and blue supergiants according to their surface temperatures. The red ones have surface temperatures between 3,200 and 4,000 K, the orange ones between 4,000 and 7,000 K, and the blue ones between 7,000 and 50,000 K.
- Hypergiants are stars with tremendous luminosities on the high end of the Hertzsprung-Russell diagram. They are divided into red hypergiants, yellow hypergiants, and blue hypergiants according to their surface temperatures. The temperature ranges are the same as for supergiants with the yellow group replacing the orange stars of the supergiant category.
- Wolf-Rayet stars are evolved massive stars which are fusing helium or heavier elements in the core. They have spectra showing broad emission lines of highly ionized helium and nitrogen or carbon. Most Wolf-Rayet stars have lost their outer hydrogen and have an atmosphere predominantly made of helium. Their surface temperature ranges between 30,000 and 200,000 K. A subgroup of Wolf-Rayet stars referred to as WO stars have strong oxygen emission lines, indicating the star is on the oxygen sequence.

2.2 Stellar diagrams

In the current section we display several diagrams showing the relationship among the characteristics of stars along with their classification. Figure 1 shows the relationship between the luminosity and mass of stars, Figure 2 the relationship between the volume and the luminosity of stars, and Figure 3 the relationship between the average density of stars and temperature of the photosphere.

Figure 1 shows that red giants are much more luminous than their main-sequence star counterparts for the same mass. As red giants are evolved stars which fuse helium in the core, we can infer that the fusion of helium into carbon is much more exothermic than the fusion of hydrogen into helium. Red giants are also less dense than their main-sequence counterparts, meaning that helium fusion occurs in a domain at lower pressure than hydrogen fusion and produces more heat. In Figure 2, we see that main sequence stars expand when shifting on the helium burning sequence to form red giants, and contract when shifting from the main-sequence branch to Wolf Rayet stars. For Wolf-Rayet stars which fuse helium or heavier elements in the core, fusion occurs in a domain at higher pressure than their counterparts. This is especially pronounced for OW Wolf-Rayet stars on the oxygen sequence, where the fusion pressure domain is clearly higher than for helium fusion.

There are also mass threadshods for fusion to occur. For example, red giants of mass less than 0.9 solar mass are never

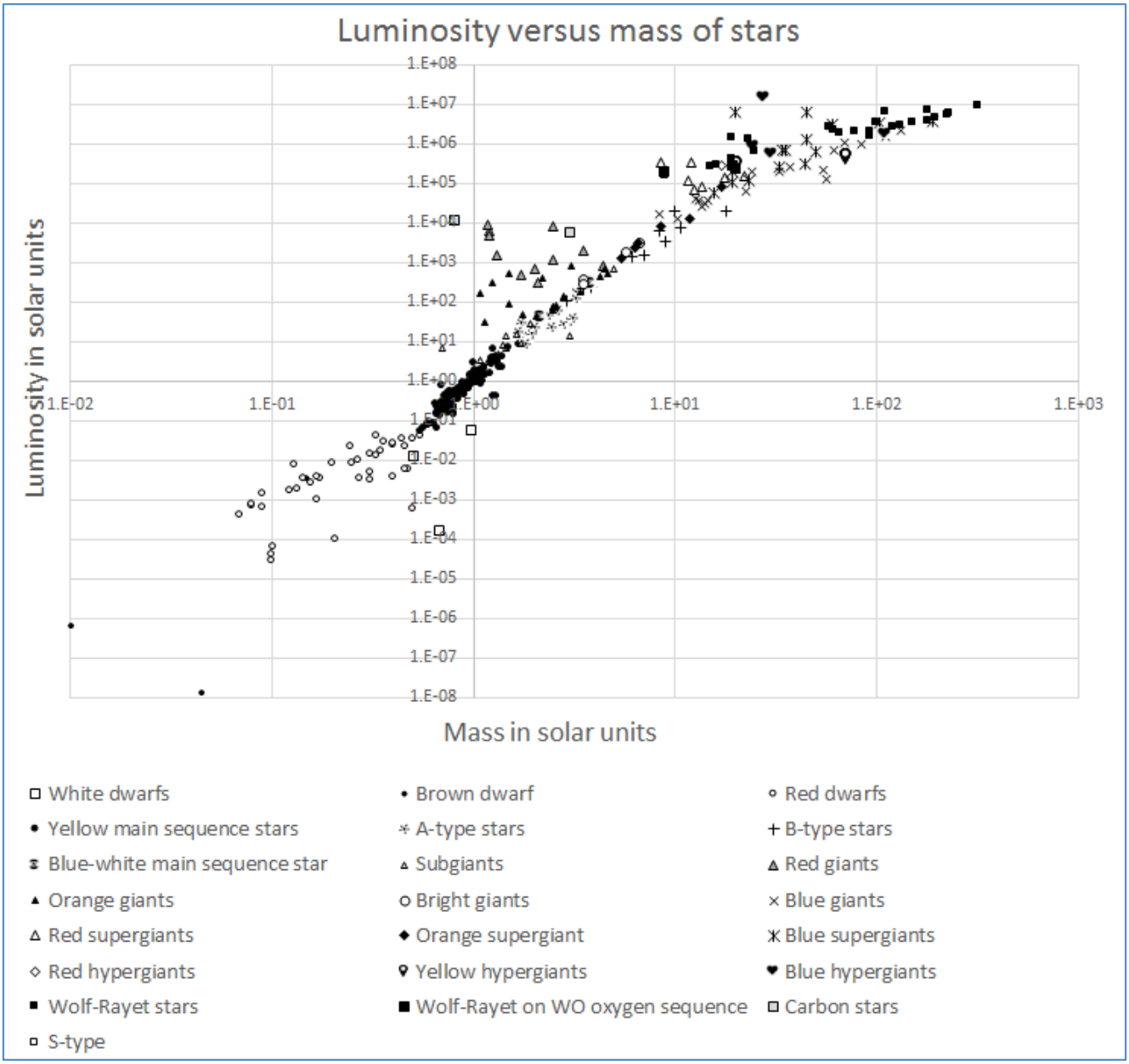

Fig. 1: Luminosity versus mass of stars. Mass and luminosity are in solar units.

observed. This limit is commonly attributed to the age of the universe, because low mass main-sequence stars take longer to fuse the hydrogen in their core, and therefore it is hypothesized that stars below 0.9 solar masses did not have sufficient time to become red giants. However, this limit could also represent the minimum mass required to obtain the necessary conditions for helium fusion. Similarly, Wolf-Rayet stars have masses above the 8.0-9.0 solar mass limit. Thefore, low mass stars do have the necessary conditions to fuse elements heavier than helium in the core.

The red dwarfs in Figure 1, show a distribution in their luminosities. This might be due to ageing, as red dwarfs haven't sufficient mass to fuse the helium accumulating in their core. As a star exhausts its hydrogen supply and accumulates helium in its core, the core cools and contracts. As the core contracts, a new shell of fresh hydrogen fuel is formed at the periphery of the core. Fusion of this hydrogen shell maintains the temperature of the core, preventing it from contracting further. The fact that the atomic mass of helium is greater than that of hydrogen also plays a role.

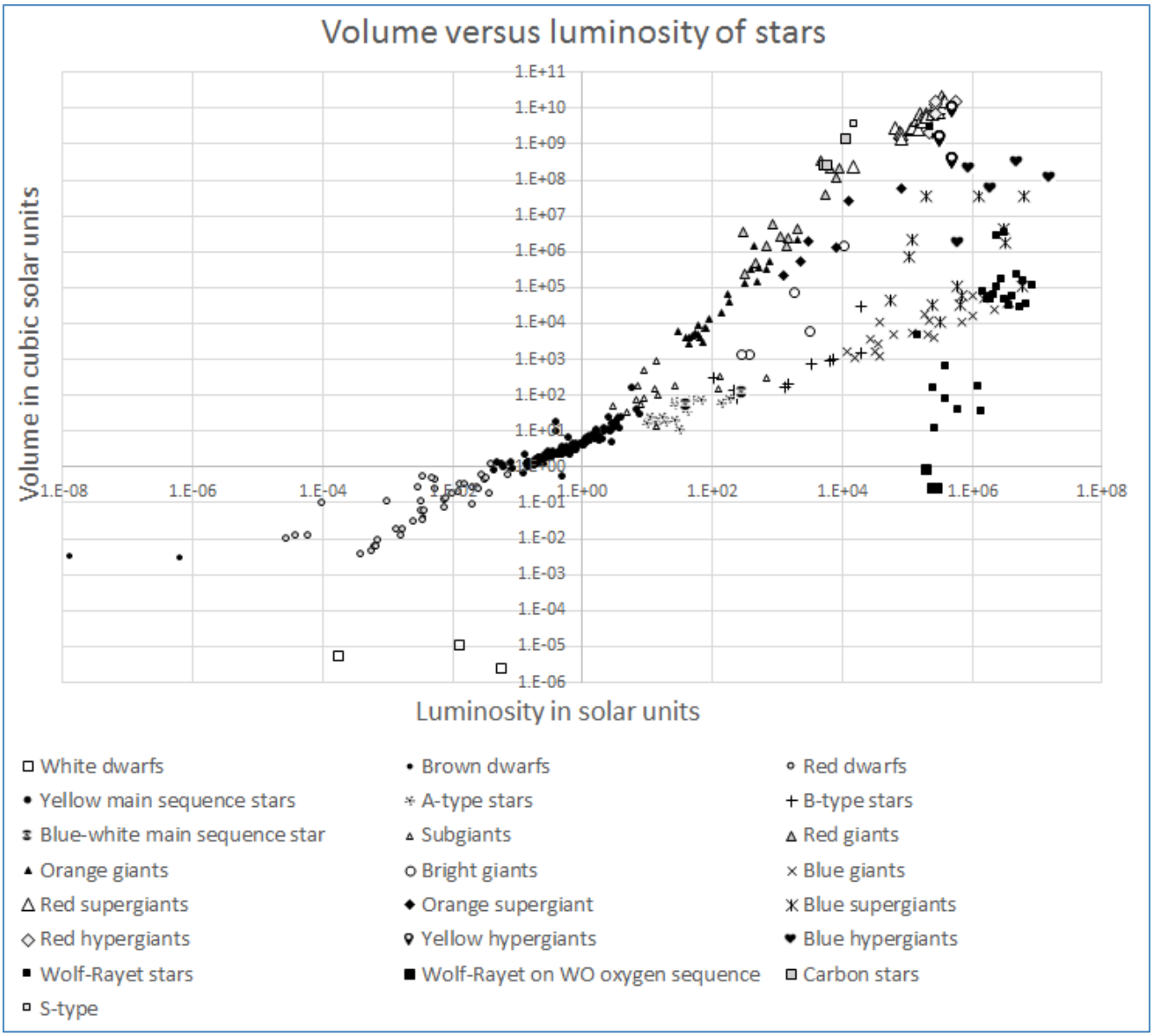

Fig. 2: Volume versus luminosity of stars. Volume and luminosity are in solar units.

Helium nuclei are formed of four nucleons (two protons and two neutrons). Therefore, there is four times more mass in a helium gas than in a hydrogen gas at a given pressure, provided they obey the ideal gas law. As the star gets older, the core shrinks and grows ever denser by accumulating helium. Therefore, as red dwarfs age, they should become denser and less luminous. Common stellar age-dating methods, based on the main-sequence turnoff, are focused on main-sequence stars that become red giants. Such age calculation methods do not yield stellar ages older than about 15 billion years, perhaps because this is when a solar type main-sequence star becomes a red giant. No methods have been developed so far to estimate the age of red dwarfs, which could possibly be much older. Using stellar models would be an approach for age-datating of red dwarfs.

3 Stars dominated by radiation pressure in the photosphere

3.1 Eddington luminosity

Inside a star, the internal pressure acting against the hydrostatic pressure is the sum of the radiation pressure and gas pressure, hence:

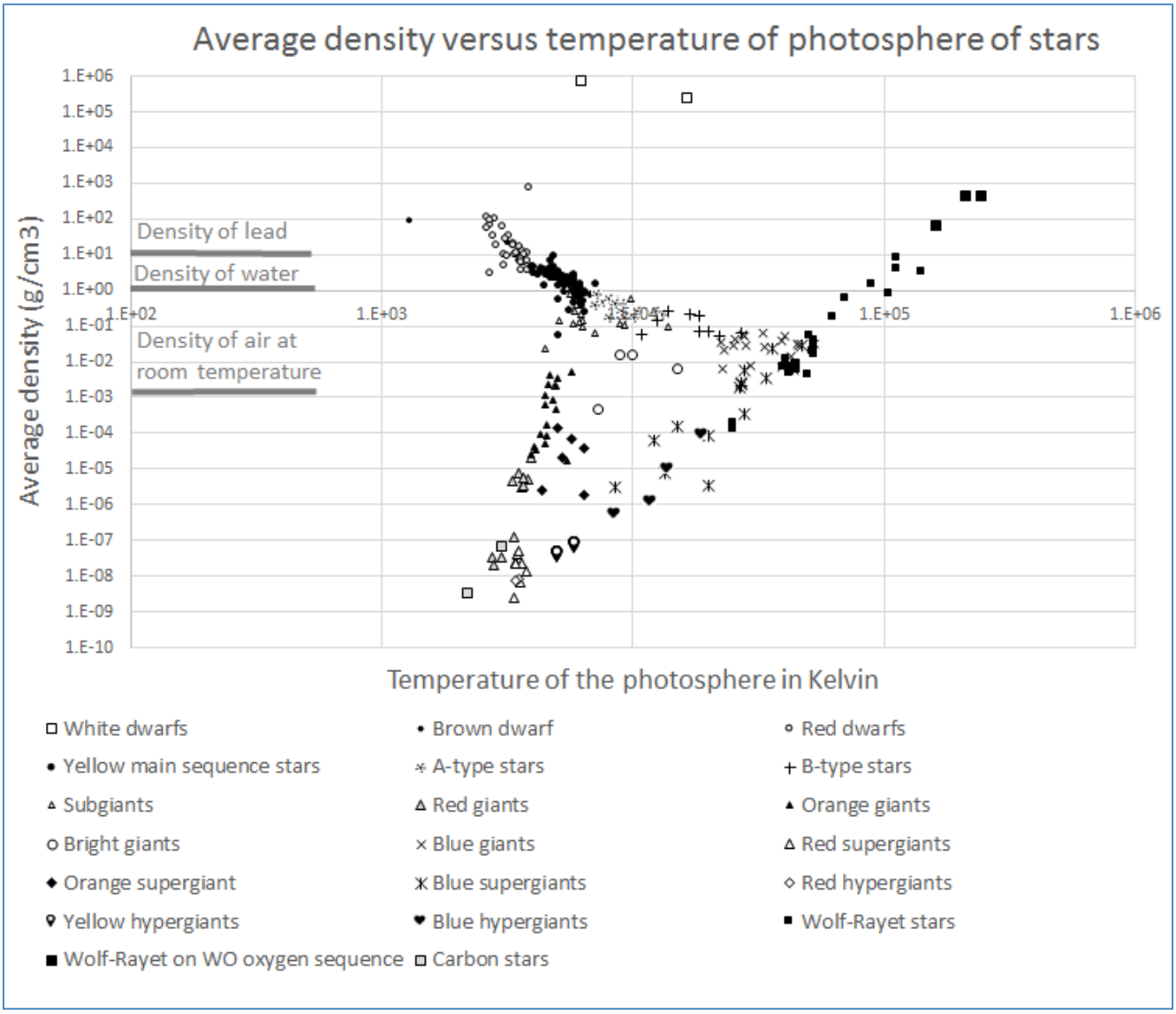

Fig. 3: Average density versus temperature of the photosphere of stars. Density is given in g/cm^3, and temperature in Kelvin.

$$P = \rho_n kT + \frac{1}{3}aT^4 , \tag{1}$$

where $\rho_n = \frac{N}{V}$, N is the number of molecules in the gas, V is the volume, $a = \frac{4\sigma}{c}$ is the radiation constant, k is the Boltzmann constant, σ is the Stefan-Boltzmann constant, T is the temperature, and c the speed of light.

When the radiation pressure is considerably higher than the gas pressure, the gas pressure term can be neglected, therefore we get:

$$\frac{\partial P_r}{\partial T} = \frac{4}{3}aT^3 , \tag{2}$$

The equation for radiative heat transfer is expressed as follows:

$$\frac{\partial T}{\partial r} = -\frac{3}{4}\frac{1}{ac}\frac{\kappa\rho}{T^3}\frac{L}{4\pi r^2} , \tag{3}$$

where κ is the opacity, L is the luminosity, T is the temperature, r is the radius, ρ is the density, c is the speed of light, and a the radiation constant.

Rewriting (2), we get:

$$\frac{\partial P_r}{\partial r}\frac{\partial r}{\partial T} = \frac{4}{3}aT^3 , \tag{4}$$

Combining (3) and (4) we get:

$$\frac{\partial P_r}{\partial r} = -\frac{\kappa\rho}{c}\frac{L}{4\pi r^2}\,, \tag{5}$$

From hydrostatic equilibrium:

$$\frac{\partial P}{\partial r} = -\frac{GM_r\rho}{r^2}\,, \tag{6}$$

where G is the gravitational constant, M_r is the interior mass of the star at radius r, and ρ is the density.

By combining (5) and (6) we get:

$$L = \frac{4\pi cG}{\kappa}M\,, \tag{7}$$

which is the Eddington luminosity. Stars dominated by radiation pressure in their photosphere are fully determined by the photosphere, meaning that their luminosities will adjust to match the Eddington luminosity. For such stars luminosity is proportional to mass as shown by the Eddington luminosity equation. Should excess heat be generated, the star will lose matter through its photosphere, which may explain why many Wolf-Rayet stars have lost their outer hydrogen layer.

We can also express this equation in terms of temperature using Stefan-Boltzmann as:

$$Flux = \frac{L}{4\pi r^2} = \sigma T^4\,. \tag{8}$$

Hence, combining (7) and (8), we get:

$$T = \left(\frac{cG}{\kappa\sigma}\right)^{1/4}\frac{M^{1/4}}{R^{1/2}}\,. \tag{9}$$

3.2 Cross section of an hydrogen ion from photon flux

There are two different methods to calculate the cross section of an ion exposed to photon flux in the photosphere; these are known respectively as the optical and the radiation pressure cross section approaches.

The optical cross section calculation considers the obscuration of a radiative flux travelling in an isotropic medium. Let us consider an isotropic gas with a radiative flux going through a surface A in the x-direction orthogonal to the surface. The flux at step $x + dx$ is equal to the flux at step x multiplied by one minus the proportion of the area that is obscured by the cross section of the atoms in the volume Adx. The number of atoms in the volume Adx is $\rho_n Adx$. We multiply the number of atoms in the volume by the cross section of the atom σ_p to give the total area obscured by the gas. Hence, we get:

$$F(x + dx) = F(x)\left(1 - \sigma_p\rho_n dx\right)\,, \tag{10}$$

where $F(x)$ is the flux at step x, $F(x + dx)$ is the flux at step $x + dx$, ρ_n is the density in number of particles per volume, and σ_p is the cross section per particle.

As $dF = F(x + dx) - F(x)$, we get:

$$\frac{dF}{F} = -\sigma_p\rho_n dx\,. \tag{11}$$

We integrate (11) to obtain:

$$F(x) = F_0\exp(-\sigma_p\rho_n x)\,. \tag{12}$$

The opacity is defined from the attenuation of radiation intensity through a medium and is given by $I(x) = I_0\exp(-\kappa\rho x)$, where I is the intensity, therefore:

$$\kappa = \frac{\sigma_p}{m_p}\,, \tag{13}$$

where κ is the opacity, σ_p is the cross section of a particle, and m_p is the mass of a particle.

The radiation pressure cross section considers an ion above the surface of a star. Let us assume that the ion is in equilibrium, meaning that the gravitational force exerted by the star on the atom is equal to the radiation pressure from the radiation flux coming from the surface of the star times the cross section of the ion. Therefore, we get:

$$\frac{GMm_p}{R^2} = \sigma_p\frac{1}{3}aT^4\,, \tag{14}$$

where G is the gravitational constant, M the mass of the star, R the radius of the star, m_p the mass of an ion, σ_p the cross section of an ion, T the temperature, and a the radiative constant.

Note that the radiation pressure just above the surface is the same as the radiation pressure below the surface. This can be proven but is outside scope of our discussion.

Combining (9) and (14) we get:

$$\kappa = \frac{4}{3}\frac{\sigma_p}{m_p}\,. \tag{15}$$

This equation differs slightly from (13) due to factors introduced in the derivation of the radiative heat transfer equation (3). The factor 3/4 in equation (3) comes from the fact that a collimated radiation flux was used to compute the radiation pressure dependency on the flux [3]. The two cross section calculation approaches provide a consistency check across the different models. We see that the optical and radiation pressure cross sections mean the same thing; it is the cross section of an ion exposed to photon flux.

3.3 Opacity and cross-section calculations

Now let us confront the model for stars dominated by radiation pressure in the photosphere with actual data. The stars dominated by radiation pressure must be those with low average densities and high photosphere temperatures and include the most massive stars. We included in this group blue giants, carbon stars, all the supergiants and hyper giants (red to blue), and all the Wolf-Rayets. Then we did a linear regression of

photosphere temperature against $M^{1/4}R^{-1/2}$, where temperature is in Kelvin, mass M in kilograms, and radius R in meters (see figure 4). We obtained a linear equation with slope $\alpha = 35.87$ [K kg$^{-1/4}$ m$^{1/2}$] and determination coefficient R^2 standing at 93%. Using the formalism of equation (14), we obtain the below cross section to particle mass ratio function of the slope α:

$$\frac{\sigma_p}{m_p} = \frac{3G}{a\alpha^4} . \tag{16}$$

The cross section σ_p expresses the surface of the ion exposed to photon flux.

By considering a hydrogen ion having a mass $m_p = 1.67\times 10^{-27}$ kg, we obtain a cross section $\sigma_p = 2.67 \times 10^{-28}$ m^2. This cross section is equal to four times the Thomson cross section for the scattering of a free electron by radiation. The Thomson cross section of free electron scattering is expressed as follows:

$$\sigma_T = \frac{8\pi}{3}\left(\frac{q^2}{4\pi\epsilon_0 mc^2}\right)^2 = 6.65 \times 10^{-29}\,\mathrm{m}^2 , \tag{17}$$

where q is the charge of the electron, ϵ_0 is the permittivity of free space , m is the mass of the electron, and c is the speed of light.

For comparison purpose, the radius of a proton is about 8.8×10^{-16} m, which works out to a cross section of 2.43×10^{-30} m^2, which is about hundred times less than the cross section we computed. The radius of a hydrogen atom from the Bohr model is about 5.3×10^{-11} m, or a cross section of 8.82×10^{-21} m^2, which is about 33 million times larger than the cross section we computed. In contrast, the cross section of hydrogen ion exposed to photon flux we computed is four times the Thomson cross section for the scattering of free electrons.

The corresponding opacity κ is 0.160 m^2 kg^{-1} given (13) or 0.213 m^2 kg^{-1} given (15). Opacity remains fairly consistent across the range of photosphere temperatures (2,200 K to 245,000 K), and photosphere compositions (different hydrogen to helium ratio) for the stars in our sample. Wolf-Rayet stars generally exhibit strong helium lines in their atmosphere. For example, Wolf-Rayet star WR136 which is among our sample set was determined to have an atmospheric composition of 86.5% helium, 12% hydrogen and 1.5% nitrogen by mass based on analysis of its spectra [4]. The red hypergiant star WOH G64 has a broad number of emission lines in its spectrum including Hα , $H\beta$, [O I], [N I], [S II], [N II], and [O III] [5]. Despite the limited data available on helium to hydrogen ratio estimates for these stars, the variability of stellar spectra in our sample would suggest that opacity is not sensitive to the composition of the photosphere, unless all of these stars have lost their outer hydrogen layer. For example, if the ratio $\frac{\sigma_p}{m_p}$ is higher for hydrogen than for helium, according to (14), stars dominated by radiation pressure in the photosphere would preferentially lose hydrogen through their surface while retaining their helium.

Ionisation supposedly depends on temperature. However, the wide range of photosphere temperatures in the sample would suggest that the degree of ionisation is not relevent. This could be indicative of the process contributing to radiative opacity in the photosphere. For bound-free transitions which consist of the absorption of radiation by an electron bound to an ion, and free-free transitions which consist of the absorption of a photon by an unbound electron moving in the field of an ion, the Rosseland opacity is a function of the temperature and hydrogen fraction, and exhibits the dependency with temperature $\kappa \propto \rho T^{-7/2}$ as per Kramers' law. This is quite unexpected as the data do not show such a dependency; otherwise, the regression in Figure 4 would not be linear. Instead, temperature would be proportional to the square of $M^{1/4}R^{-1/2}$. As this is not the case, these opacity models do not seem to adequately describe stellar photosphere plasma.

4 Stars dominated by gas pressure in the photosphere

4.1 Estimation of the density in the solar photosphere

The density of the photosphere is an important parameter required to solve the heat transfer equation for stars. A way to probe the density of the photosphere of the Sun is by using limb darkening. Limb darkening is the observation of the center part of a star appearing brighter than the edge or limb of the luminous disk. This effect is due to the thermal gradient and transparency of the photosphere. The intensity of light at the center of the disk corresponds to the black-body spectrum at an optical depth of 2/3 because of the transparency of the photosphere. The intensity of light at the edge of the disk corresponds to the black-body spectrum at the surface of the photosphere, which is cooler than the temperature at an optical depth of 2/3. The intensity of light travelling through a semi-transparent medium is expressed as follows:

$$I(x) = I_0 \exp(-\kappa\rho x) , \tag{18}$$

where κ is the opacity, ρ the density, and x the depth of the medium.

Therefore, the distance from the surface at an optical depth of 2/3 corresponding to 1/3 of the intensity going through is expressed as follows:

$$l = -\frac{\ln(1/3)}{\kappa\rho} . \tag{19}$$

Let us say T_0 is the temperature at the limb which is the surface of the photosphere, and $T_{2/3}$ is the temperature at the center of the disk or an optical depth of 2/3. Hence, the temperature gradient is expressed as follows:

$$\frac{dT}{dr} = \frac{T_0 - T_{2/3}}{l} , \tag{20}$$

where l is given by (19).

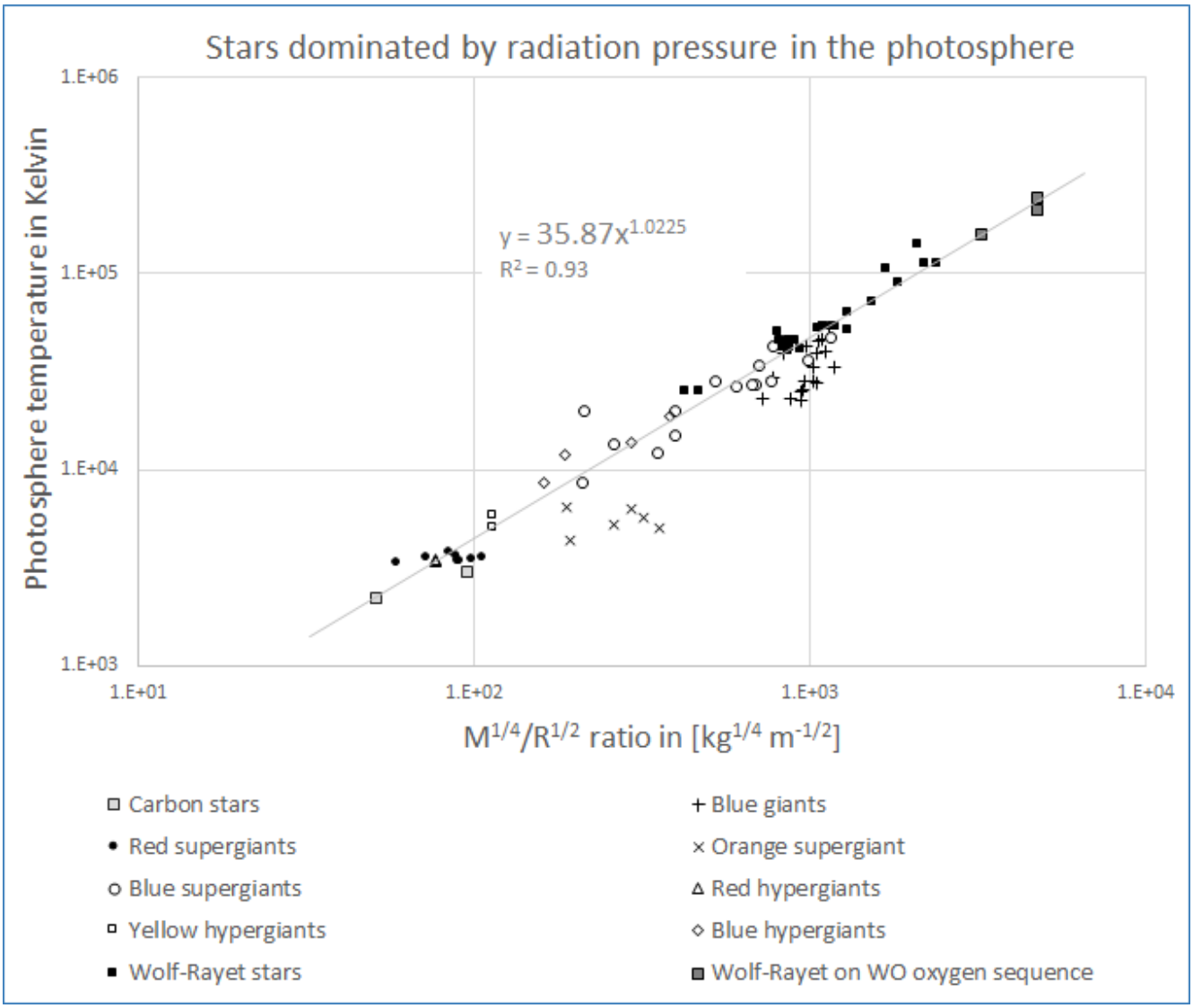

Fig. 4: Photosphere's temperature versus $M^{1/4}R^{-1/2}$ ratio for stars dominated by radiation pressure in the photosphere.

Within a star heat transfer is dominated by the process having the lowest thermal gradient. We know that for the external layer of the Sun, the temperature is too low for radiative heat transfer to be efficient, and convective heat transfer dominates. The thermal gradient of convective heat transfer in a gas is the adiabatic gradient. From limb darkening we get T_0 and $T_{2/3}$. Therefore, using (19) and (20), we can estimate the density of the photosphere.

The ratio of the intensity at an angle θ to intensity at the center of the star from limb darkening is expressed as follows [6]:

$$\frac{I(\theta)}{I(0)} = \frac{2}{5} + \frac{3}{5}\cos(\theta)\,. \tag{21}$$

The intensity at the limb is the intensity at an angle $\theta = \frac{\pi}{2}$. Therefore, the ratio of the intensity at the limb to the intensity at the center of the star is 0.4. From Stefan-Boltzmann law, we get the ratio of the temperature at the limb to the temperature at the center:

$$\frac{T_0}{T_{2/3}} = 0.4^{1/4}\,. \tag{22}$$

The average temperature of the solar photosphere is about 5,800 K. Let us say the temperature at the center of the disk is $T_{2/3}$ = 6,300 K. Hence, the temperature at the limb is T_0= 5,010 K.

The adiabatic gradient is the temperature gradient obtained for a gas parcel as it rises, assuming an ideal gas. For an ideal gas we have $P = (R/\mu)\rho T$, where R is the ideal gas constant and μ the molar weight. As we move a gas parcel

upwards an infinitesimal distance, the variation in pressure is given by:

$$\frac{dP}{dr} = \frac{R}{\mu}\left(\rho\frac{dT}{dr} + T\frac{d\rho}{dr}\right) = \frac{P}{T}\frac{dT}{dr} + \frac{P}{\rho}\frac{d\rho}{dr}\,. \tag{23}$$

For an adiabatic gas, we also have $P = K\rho^{\gamma}$, hence:

$$\frac{dP}{dr} = K\gamma\rho^{\gamma-1}\frac{d\rho}{dr} = \gamma\frac{P}{\rho}\frac{d\rho}{dr}\,. \tag{24}$$

Combining (23) and (24) we get:

$$\frac{dT}{dr} = (\gamma-1)\,\frac{T}{P}\frac{P}{\rho}\frac{d\rho}{dr} = \left(\frac{\gamma-1}{\gamma}\right)\frac{T}{P}\frac{dP}{dr}\,. \tag{25}$$

From hydrostatic pressure, we have:

$$\frac{dP}{dr} = -\frac{GM}{R^2}\rho\,. \tag{26}$$

Combining (25) and (26) with $P = \frac{\rho}{m_p}kT$ we get:

$$\frac{dT}{dr} = -\left(\frac{\gamma-1}{\gamma}\right)\frac{GM}{R^2}\frac{m_p}{k}\,, \tag{27}$$

which is the adiabatic gradient at the stellar surface, where k is the Boltzmann constant, G the gravitational constant, M the mass of the star, R the radius of the star, m_p the mass of a gas molecule.

For a monoatomic gas $\gamma = \frac{5}{3}$. Hence, the adiabatic gradient at the surface of the sun is 0.013 K/m. In contrast, the standard solar model uses an adiabatic gradient of 0.010 K/m.

Hence, the density of the photosphere of the Sun from (19) and (20) is:

$$\rho = -\frac{1}{\kappa}\frac{\ln(1/3)}{(T_{2/3} - T_0)}\frac{dT}{dr}\,, \tag{28}$$

which yields a density of 6.92×10^{-5} kg/m^3, whereas the standard solar model uses a photosphere density of about 10^{-6} kg/m^3 [7]. For the calculation, we used the opacity obtained in section 3.3.

4.2 Calculation of the cross section per hydrogen nuclei from gas pressure

Let us consider an ion above the stellar surface. A condition to have a stable surface is that the gravitational force exerted by the star on the ion is offset by the repulsive force due to gas pressure. Assuming an ideal gas, we get:

$$\frac{GMm_p}{R^2} = \sigma_{ef}\frac{\rho\,k\,T}{m_p}\,, \tag{29}$$

where σ_{ef} is the effective cross section, m_p is the mass per hydrogen nuclei, M is the mass of the star, G is the gravitational constant, R is the radius of the star, ρ is the mass density in the photosphere, k is the Boltzmann comstant, and T is the temperature.

Although the photosphere is about 500 km thick, modelling the photosphere as a surface makes sense. As shown in figure 5, we can see a clear surface of dense plasma at the photosphere of the Sun. Note that in equation (29) we did not consider the electromagnetic forces. Because free electrons are lighter than the protons, they should tend to escape the surface much easier. However, the plasma may have mechanisms in place to keep its neutrality. For example, a positively charged surface would retain the electrons while pushing out the protons. Equation (29) provides a net cross section from gravity alone and does not model such an effect.

The gas pressure due to molecular collisions is somehow different than radiation pressure. When a photon collides with a surface, the momentum vector is applied in the direction of the trajectory of the photon. For molecular gas collisions, it is like playing pool. Considering molecules of spherical shape, the momentum vector is normal to the sphere, meaning it is applied along the axis between the point of impact of the collision and the center of the sphere. Therefore, we need to introduce a shape coefficient to relate the effective cross section to the geometrical cross section of the molecule.

Let us consider a force f exerted on a sphere of radius r. The surface element is $dS = r^2\sin(\theta)\,d\theta\,d\varphi$. The projection of the force f on the z-axis is $f_z = f\cos(\theta)$, where θ is the angle between the z-direction and and the vector f. The effective force is the average of f_z over the half sphere. Hence, the effective force is computed as follows:

$$f_{ef} = \frac{1}{2\pi r^2}\int_{\varphi=0}^{2\pi}\int_{\theta=0}^{\pi/2} f\cos(\theta)r^2\sin(\theta)\,d\theta\,d\varphi\,. \tag{30}$$

Because $\sin(\theta)\cos(\theta) = \frac{\sin(2\theta)}{2}$, we get:

$$f_{ef} = \frac{f}{4\pi}\int_{\varphi=0}^{2\pi}\int_{\theta=0}^{\pi/2}\sin(2\theta)\,d\theta\,d\varphi\,. \tag{31}$$

We get:

$$f_{ef} = \frac{f}{2}\,. \tag{32}$$

Therefore, the geometric cross section is twice the effective cross section from gas pressure: $\sigma_g = 2\sigma_{ef}$, where σ_g is the geometric cross section and σ_{ef} the effective cross section.

From (29) and the density we obtained in section 4.1, we get an effective cross section of 1.33×10^{-28} m^2 or a geometric cross section of 2.66×10^{-28} m^2. In section 3.3, we obtained a cross section to photon flux of 2.67×10^{-28} m^2. Hence, in the plasma the cross section per hydrogen nuclei from gas pressure is virtually the same as the cross section from radiation pressure.

Neutral hydrogen atoms in the Bohr model are represented with the nucleus at the center and an electron in orbit around the nucleus. The Bohr model yields a radius of

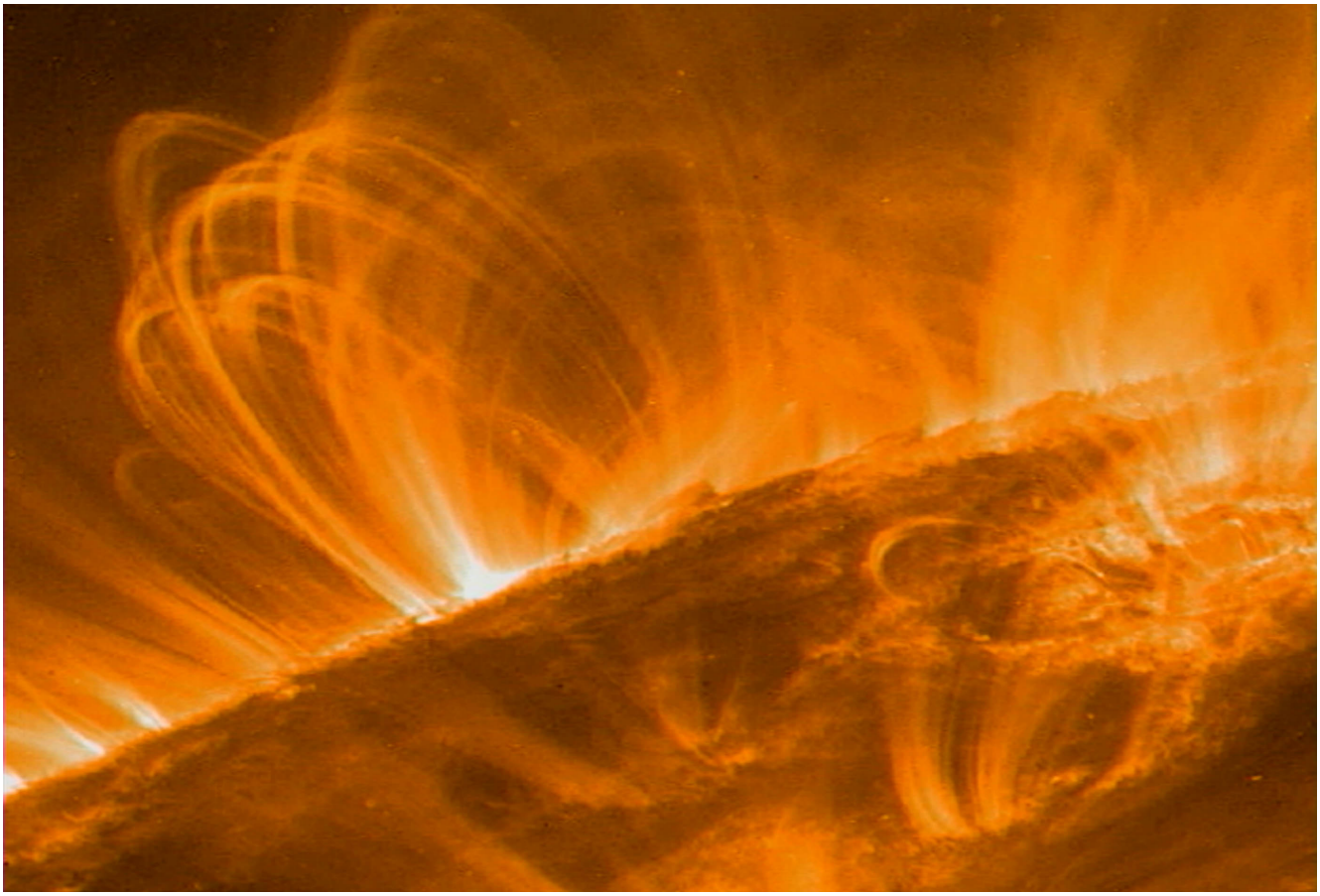

Fig. 5: Image of the solar surface. Credit: NASA/GSFC (December 2000)

5.3×10^{-11} m for the hydrogen atom with a corresponding cross section of 8.82×10^{-21} m^2. Hydrogen cross sections have been obtained from electron collisions yielding cross sections on the order of 10^{-21} m^2 for ionized hydrogen [8]. A precise value was measured by [9], who obtained a cross section of 3.86×10^{-21} m^2 using photodetachment of negatively charged hydrogen ions H^-, that is in close agreement with the Bohr model. The fact that we obtained a much smaller cross section per hydrogen nuclei suggests that in a plasma, the electrons are virtually detached from the nuclei. Therefore, a hydrogen plasma may be represented as a gas mixture of electrons and protons. Hence, the total pressure would be equal to the sum of the partial pressure of the electrons and protons.

Assuming that the electrons and protons are at the same temperature, the adiabatic gradient we computed with eq. (27) should be divided by two, and the density in the photosphere would be half the estimate we obtained, leaving the cross section unchanged. For the proton and electron temperatures to equilibrate, the Coulomb collision rates would need to dominate to allow energy transfer between the electrons and protons. Most plasmas are considered weakly collisional, which means that the Coulomb collision rates are negligible compared to other processes that control the velocity distributions. Therefore, if we assume that the temperature of the electrons is much lower than the temperature of the protons, we can neglect the electron pressure; and if it is the reverse, then we can neglect the proton pressure, provided that both particles are on the ideal gas domain.

Electrons and protons are fermions, meaning they are modelled as a Fermi gas. Fermions are particles described by the Fermi-Dirac distribution thus obeying the Pauli exclusion principle. Whenever the average interparticular separation is much larger than the average de Broglie wavelength of the particules, the Fermi-Dirac distribution can be approximated by the Maxwell-Boltzmann distribution, and the Fermi gas behaves similarly to an ideal gas [10]:

$$\bar{R} \gg \frac{h}{\sqrt{3mkT}}\,, \tag{33}$$

where $\bar{R}$ is the average interparticle separation, h the Planck's constant, m the mass of the particle, k the Boltzmann constant, and T the temperature.

This condition is satisfied in the solar photosphere for

both the electrons and protons, hence we can use the ideal gas equation as an approximation in the photosphere.

Note that if the particles in the plasma of the solar photosphere were made of large ions or atoms such as the ones we find in gases, according to (29), the surface of the Sun would evaporate due to the high temperatures.

5 Conclusion

In the present study we collected stellar data (mass, radius, luminosity and surface temperature) for a set of 360 stars. From stars dominated by radiation pressure in the photosphere, we estimated the opacity, a key parameter for radiative heat transfer. As radiative heat transfer is no longer efficient in the solar convective zone where heat transfer occurs by convection, we assumed the adiabatic gradient of a monoatomic gas for the solar photosphere. We then estimated the density in the photosphere of the Sun using limb darkening. Photosphere density is a boundary parameter required for the solar model. We also considered that the stellar photosphere can be modelled as a surface. Hence, for an hydrogen ion in equilibrium in the photosphere, the force exerted by the gravitation of the star on the ion should be offset by the radiation and gas pressure. Therefore, we computed the cross section per hydrogen nuclei from radiation pressure for stars dominated by radiation pressure in the photosphere, and from gas pressure for stars dominated by gas pressure in the photosphere. We found that the cross section per hydrogen nuclei in stellar plasma is about 2.66×10^{-28} m^2 from both radiation and gas pressure. The cross section of neutral hydrogen as given by the Bohr model for an electron in orbit around the nucleus is 8.82×10^{-21} m^2, which suggests that the electrons and protons in the plasma are virtually detached. Hence, a hydrogen plasma may be represented as a gas mixture of electrons and protons. If the stellar photosphere was made of large hydrogen atoms or ions such as the ones we find in gases, the surface of the photosphere would evaporate due to the high temperatures. This result could impact stellar models as we would have to add together the partial pressures of the electrons and the protons in the plasma.

Submitted on January 10, 2017 / Accepted on January 14, 2017

References

1. Smith D.H. Eddington's Valve and Cepheid Pulsations. *Sky and Telescope*, 1984, v. 68, no. 6, 519.
2. Liebert J., Bergeron P., Eisenstein D., Harris H.C., Kleinman S.J., Nitta A., and Krzesinski J. A Helium White Dwarf of Extremely Low Mass. *The Astrophysical Journal*, 2004, v. 606, L147.
3. Salaris M., and Cassisi S. Evolution of Stars and Stellar Populations. John Wiley & Sons Ltd., 2005, p. 53.
4. Hamann W.-R., Wessolowski U., and Koesterke L. Non-LTE spectral analyses of Wolf-Rayet stars: The nitrogen spectrum of the WN6 prototype HD 192163 (WR136). *Astronomy and Astrophysics*, 1994, v. 281, no. 1, 184–198.
5. Levesque E.M., Massey P., Plez B., and Olsen K.A.G. The Physical Properties of the Red Supergiant WOH G64: The Largest Star Known? *Preprint arXiv:0903.2260*, 2009.
6. Carroll B.W., and Ostlie D.A. An Introduction to Modern Astrophysics Addison-Wesley Publishing Co, Inc., 1996, p. 292.
7. Eddy J.A. A New Sun. The Solar Results from Skylab. *Ed. Rein Ise*, 1979, p. 37.
8. Yoon J.-S., Song M.-Y., Han J.-M., Hwang S.H., Chang W.-S., Lee B., and Itikawa Y. Cross Sections for Electron Collisions with Hydrogen Molecules. *Journal of Physical and Chemical Reference Data*, 2008, v. 37, 913.
9. Frolov A.M. Photodetachment cross-section of negatively charged hydrogen ion *Preprint arXiv:1510.04766*, 2015.
10. Reif F. Fundamentals of Statistical and Thermal Physics. *Levant Books*, 2010, p. 247.

Flyby Anomaly via Least Action

Arto Annila
Department of Physics, University of Helsinki, Gustaf Hällströmin katu 2 FI-00014, Helsinki, Finland.
E-mail: arto.annila@helsinki.fi

The observed but unexpected changes in velocity during spacecraft flybys of Earth are examined using the principle of least action in its original dissipative form. In general, the spacecraft's momentum will change when it travels through an energy density gradient of space that is enfolding a gravitating, orbiting and rotating body. When space is understood as a physical substance that embodies quanta of actions, rather than being modeled by a mere metric, it becomes apparent that the changes in momentum couple with flux of quanta from the local system of bodies to the universal surroundings or vice versa. In this way the original least-action principle accounts also for the 'anomalous' change in velocity by an equation of motion which complies with the empirical relation that has been deduced from Earth-flybys.

1 Introduction

Even a slight deviation from a common rule may entail an error in the very rule. Here, in the context of flyby anomaly, the rule – perhaps at stake – is conservation of momentum. It is a corner stone of physics, whence the flyby anomaly is worth attention.

The law of conservation of momentum asserts, for example, that when a spacecraft is passing by a planet, it will gain momentum as much as the planet will lose momentum. The momentum transfer is a minute drop for the massive planet but a giant boost for the tiny spacecraft. The spacecraft's velocity v will change relative to the Sun as much as its flight direction will change relative to orbital velocity u of the planet [1–3]. The gain can be at most $2u$ when the planet is moving straight at the spacecraft which will subsequently swing a full U-turn around the planet. Curiously though, it seems as if spacecraft had acquired more speed during certain flybys than the planet's orbital momentum could possibly grant them [4, 5]. The origin of this anomaly is unknown.

However, it has been inferred from meticulously monitored flybys of Earth [6–10] that the anomalous change in velocity Δv complies closely with relation [5]

$$\frac{\Delta v}{v} = \frac{2\omega_\oplus R_\oplus}{c}(\cos\delta_i - \cos\delta_o), \qquad (1)$$

where c is the speed of light, $R_\oplus$ is Earth's radius and $\omega_\oplus$ angular velocity of rotation, δ_i is the spacecraft's inbound and δ_o outbound declination, so that $2\omega_\oplus R_\oplus/c = 0.49\times10^{-6}$. The relationship (Eq. 1) implies that the anomalous gain Δv in the spacecraft's velocity stems from Earth's angular velocity $\omega_\oplus$ depending on how the spacecraft's inbound and outbound asymptotes align relative to the axis of rotation. Yet, the effect of Earth's gravito-magnetic field on the spacecraft's velocity has been calculated to be many orders of magnitude smaller than the measured anomaly [11, 12]. Other explanations have also been considered [13–17] and found feasible [18], but there is currently no consensus what exactly underlies the phenomenon. Also the general validity of Eq. 1 has been questioned [19–22]. Moreover, it should be noted that anomalies, when without radar monitoring, are difficult to detect along flybys of other planetary bodies.

As long as the case is open there ought to be room for attempts to explain the measurements. Thus, we would like to contribute to the puzzle of flyby anomaly by maintaining that the spacecraft does move along a geodesic, i.e., a path of least action, also when it is subject to the unknown force that causes the unaccounted change in momentum. So, it should be possible to infer the cause of anomaly from the principle of least action. However, the familiar Lagrangian form when without dissipation applies only to closed stationary orbits such as ellipses or to ideal paths with symmetrical inbound and outbound trajectories. In contrast, the general form of the least action principle by Maupertuis [23–25] accounts also for open paths, most notably for hyperbolic flyby trajectories that are asymmetric relative to the planet's rotation. Furthermore, we are motivated to apply this general principle that distinguishes itself from particular models of celestial mechanics, because it has already accounted for anomalous perihelion precession [26], rotation of galaxies [27], geodetic and frame dragging drift rates [28] as well as for frequency shifts and bending of light [29], as well as for propagation of cosmic rays [30] and the thrust of electromagnetic drive [31]. Thus, our examination of the flyby anomaly using the universal principle is not a standalone study. It can be seen as a further test of our approach yet in another physical situation.

2 The least-action principle

The spacecraft is customarily pictured to move along a hyperbolic path as if it was coming from a distant asymptotic state of free space and returning via periapsis back to the asymptotic state. Per definition this ideal, i.e., fully reversible passage cannot accommodate any net change in momentum in the planet's frame of reference, because the initial and final asymptotic states are taken as indistinguishable from

each other in energetic terms. In other words, the Lagrangian having only kinetic and potential energy terms does not allow for any change in the total energy, i.e., dissipation. But in reality the unaccounted increase (or decrease) in kinetic energy reveals that during the flyby the spacecraft does descend down (or move up) along a potential energy gradient, so that the initial and final states are not equal in energetic terms. Therefore, to account for the flyby anomaly as a non-conserved phenomenon we will use Mauperutuis's rather than Lagrange's principle of least action. Then it remains for us to identify among conceivable gradients in energy, the one that lies asymmetrically with respect to the spacecraft's inbound and outbound trajectories, and hence is responsible for the net change in energy.

In all cases, the spacecraft treks at least through the gravitational potential of free space. The all-embracing vacuum potential energy $GM^2/R = Mc^2$ totals from the mass M of all bodies in the Universe within Hubble's radius $R = cT$ at its current age $T = 13.8$ billion years where G is the gravitational constant [32]. In terms of geometry the free space energy density is characterized by the universal L^2-norm [33] that manifest itself in the quadratic form c^2. Physically speaking, the norm means that in the free space there is no shorter path than that taken by light. Thus, the energy density of free space, on the order of one nJ/m^3, is the ultimate reference for any other energy density.

A local potential energy, known as the local gravitational potential energy is in balance with the bound energy density of a body, for example, a planet, just as the universal gravitational potential is energy is in balance with all bodies in the Universe [34]. Thus, the spacecraft when moving past by the planet, will be subject to energy density gradients, i.e., forces that will show as changes in its momentum. We acknowledge that general relativity accounts for the space without energy density due to the gravitational field itself. General relativity expresses gravity in terms of the geometrical properties of spacetime through the Einstein field equations. This mathematical model is excellent for many data, but when without dissipation, it does not account accurately for irreversible changes in momentum, for instance, for the spacecraft anomalous gain in momentum during the flyby.

To work out the energy density gradient responsible for the dissipative change in momentum we will express the local energy density at a distance r from the body relative to the universal energy density by the ratio of light's universal velocity to its local velocity $n = c/v$. The index n has been used earlier to describe the gravitational potential in terms of an optical medium [35] consistently with the fact that gravity and electromagnetism share the same functional forms [34, 36]. The local excess in energy density is miniscule in the vicinity of an ordinary celestial body. This is to say that when light is grazing the planet Earth, its speed $v \leq c$ will hardly deviate from c. Therefore, light will experience only a minute change in momentum that will manifest itself as a tiny blue shift and next-to-negligible bending.

However, the spacecraft with velocity $v \ll c$ will be subject to a marked change in its momentum during its passage through the local potential of space imposed by the gravitating, orbiting and rotating Earth. This is to say that the spacecraft will gain momentum when inbound and conversely it will lose momentum when outbound. The inbound gain and outbound loss will sum up to zero in the case the open hyperbolic trajectory through a spherically symmetric field. A net change in momentum will accrue only if the flight path is open asymmetric relative to energy density gradients of space due to the planet's orbital and rotational motion.

In general the index n for a locus of space can be obtained from the least action principle in its original form by Maupertuis. The principle [23, 25–27, 29] equates a change in kinetic energy $d_t 2K$ with changes in scalar potential energy $\partial_t U$ and vector potential energy $\partial_t Q$,

$$d_t 2K = -\partial_t U + i\partial_t Q, \tag{2}$$

where we emphasize, although self-evidently, the orthogonal relationship between the gradients of scalar and vector potential energy by the imaginary quotient i. The equation of motion (Eq. 2) containing both real and imaginary parts ensures that any (formal) solution is non-conserved. Moreover, orthogonality is familiar from electrodynamics, for instance, as defined by Poynting theorem. Accordingly, when the spacecraft accelerates in the gravitational field of a planet, the quanta will dissipate to the surrounding free space from the local gravitational potential orthogonally to the acceleration.

The equation for the dissipative changes in energy [25,31] (Eq. 2) corresponds to Newton's second law of motion for a change in momentum $\mathbf{p} = m\mathbf{v}$ when multiplied with velocity $\mathbf{v}$, i.e.,

$$\begin{aligned} \mathbf{F} &= d_t \mathbf{v} \quad | \cdot \mathbf{v} \\ \mathbf{F} \cdot \mathbf{v} &= d_t(m\mathbf{v}) \cdot \mathbf{v} = \mathbf{v} \cdot m\mathbf{a} + v^2 \partial_t m \\ d_t 2K &= -\mathbf{v} \cdot \nabla U + i\partial_t Q, \end{aligned} \tag{3}$$

where kinetic energy, i.e., vis viva is $2K = mv^2$, and where the spatial gradient of U relates to the familiar term $m\mathbf{a}$ of acceleration and the change in mass $dm = dE/c^2$ equals dissipation $n^2 d_t Q = d_t E$ to the free space. As usual, the mass-energy equivalence converts mass-bound energy to energy E of freely propagating photons in the vacuum. In short, Eqs. 2 and 3 simply state that at any position along the spacecraft's least-time path the momentum will follow the force $\mathbf{F} = -\nabla U + i\nabla Q$, where the energy density gradient subsumes both the scalar and vector components. In this way our account on gravity is physical rather than merely mathematical and consistent with electromagnetism. However, in what follows, the orthogonality of the two components remains only implicit when we work out only the magnitude of the total

potential energy in any given position along the spacecraft's path.

3 Passages through gradients

The general principle of least action in its original form allows us to examine the flyby trajectories by specifying the energy density of space by the index n at a particular position r of space from the center of a gravitating body with mass $M_\oplus$. Also earlier the gravitational field has been described in terms of an optical medium [35], but we do not model space by an explicit metric, instead present it in energetic terms. When approximating the total potential energy U only with the local gravitational potential energy $GmM_\oplus/r$, Eq. 3 can be solved for the index of space

$$\begin{aligned} d_t(mv^2) &= -\partial_t \frac{GmM_\oplus}{r} + i\partial_t mc^2 \\ n^2 = \frac{c^2}{v^2} &= \left(1 - \frac{GM_\oplus}{c^2 r}\right)^{-1} \approx 1 + \frac{GM_\oplus}{c^2 r} = 1 + \varphi_\oplus \end{aligned} \tag{4}$$

at a locus r. The squared index sums the universal density (unity) and the local excess $\varphi_\oplus$ as experienced by a test body of vanishing mass, i.e., a photon. The first order approximation means that n^2 does not differ much from the asymptotic ($r \to r_\infty$) unity of free space. Explicitly, a ray of light will bend hardly at all even when grazing the Earth of radius $R_\oplus$, since $\varphi_\oplus = GM_\oplus/c^2 R_\oplus \approx 0.7 \times 10^{-9}$.

However, the spacecraft with its minute velocity v relative to the speed of light, i.e., $v^2/c^2 \ll 1$, will accelerate considerably when traversing through the gradient $d(n^2)/dr = \nabla\varphi_\oplus = -GM_\oplus \mathbf{r}_o/c^2 r^2$ where the unit vector $\mathbf{r}_o = \mathbf{r}/r$ points to the center of mass. According to Eqs. 2 and 3 the spacecraft will fly past by the planet when $\mathbf{v} \cdot d_t\mathbf{p}/c^2 > -\mathbf{v} \cdot \nabla\varphi_\oplus$. Conversely, when $\mathbf{v} \cdot d_t\mathbf{p}/c^2 < -\mathbf{v} \cdot \nabla\varphi_\oplus$, the spacecraft will spiral down to a crash on the planet. Eventually, when $\mathbf{v} \cdot d_t\mathbf{p}/c^2 = -\mathbf{v} \cdot \nabla\varphi_\oplus$, Eq. 2 can be integrated to a closed form. Then the net flux from to the system to its surroundings vanishes $d_t Q = 0$, and hence the integration yields the familiar stationary condition $2K + U = 0$, i.e., the virial theorem. This is to say, the spacecraft has settled on a stable Keplerian orbit about the planet.

When the planet is not only gravitating but both orbiting and rotating, then the excess in energy density of space at r is in balance also with energy that is bound in both the orbital and rotational motion as much as $\mathbf{r}_o$ aligns along the planet's orbital u and rotational $\mathbf{w}_\oplus = \omega_\oplus R_\oplus$ velocities, denoted by $u_r = \mathbf{u} \cdot \mathbf{r}_o$ and $w_r = \|\mathbf{w}_\oplus \times \mathbf{r}_o\|$, i.e.,

$$\begin{aligned} n^2 = \frac{c^2}{v^2} &= \left(1 - \frac{GM_\oplus}{c^2 r} - \frac{u_r^2 R_\oplus}{c^2 r} - \frac{w_r^2 R_\oplus}{c^2 r}\right)^{-1} \\ &\approx 1 + \varphi_\oplus + \varphi_u + \varphi_w. \end{aligned} \tag{5}$$

Again the first order approximation means that n^2 does not differ much from the free space unity. Explicitly when setting for the Earth with $r \approx R_\oplus$ and $u_r = u_\oplus$, the orbital $\varphi_u = u_\oplus^2/c^2 \approx 10^{-8}$ and rotational $\varphi_w = w_\oplus^2/c^2 \approx 0.6 \times 10^{-13}$ contributions are tiny. This means that the Earth hardly drags the vacuum along with its orbital and rotational motion.

However, the spacecraft with velocity $v^2/c^2 \ll 1$ will acquire momentum markedly during its way through the gradient $\nabla\varphi$. The gain in momentum from the orbital motion is the well-known gravity assist. Obviously this gravitational slingshot cannot be used when the spacecraft moves too slowly to catch the planet, i.e., $\mathbf{v} \cdot d_t\mathbf{p}/c^2 < -\mathbf{v} \cdot \nabla\varphi_u$. Eventually, when $\mathbf{v} \cdot d_t\mathbf{p}/c^2 = -\mathbf{v} \cdot \nabla\varphi_u$, dissipation vanishes, and hence Eq. 2 can be integrated to the stationary state condition $2K + U = 0$. It means that the spacecraft has settled on a stable Lagrangian point where it is coorbiting Sun along with Earth.

In addition to the gain in momentum from the planet's orbital motion, the spacecraft may gain a detectable amount of momentum when traversing through the gradient $\nabla\varphi_w$ due to the planet's rotation about its axis. Obviously this velocity excess will be deemed as anomalous when left unaccounted. Conversely, when the gradients along the inbound and outbound trajectories are opposite and equal, i.e., symmetric about the planet's rotation, there is no net dissipation and no net change in momentum. Eventually, when dissipation vanishes, $\mathbf{v} \cdot d_t\mathbf{p}/c^2 = -\mathbf{v} \cdot \nabla\varphi_w$, and hence Eq. 2 reduces to the steady-state condition $2K + U = 0$. It means that the spacecraft has settled on a geostationary orbit. When the spacecraft is in synchrony with the planet's rotation, obviously it will not be exposed to any energy density gradients due to the rotation.

4 Anomalous change in velocity

The above classification of spatial energy density in the gravitational, orbital and rotational terms (Eq. 5) serves us to specify the equation for the "anomalous" gain in velocity Δv. It accrues during the flyby through the energy density gradient of space $\nabla\varphi_w$ imposed by the rotating planet. In general the change in the spacecraft's momentum at any point along the trajectory is, according to Eq. 3, equal to the force $\mathbf{F} = d_t\mathbf{p} = d_t(m\mathbf{v}) = mc^2\nabla\varphi_w$. When the minute change in mass dm is neglected, the anomalous gain in velocity Δv due to the gradient ∂_w of rotational contribution φ_w can be obtained by summing up the changes in velocity dv

$$\begin{aligned} \Delta v &= \int_{v_i}^{v_o} \partial_w \varphi_w dv = \int_{\theta_i}^{\theta_o} v \frac{\partial(\omega_\oplus R_\oplus \cos\delta/c)^2}{\partial(\omega_\oplus R_\oplus \sin\delta/c)} \frac{R_\oplus}{r} d\delta \\ &= \int_{\delta_i}^{\delta_o} v \frac{2\omega_\oplus R_\oplus \sin\delta}{c} \frac{R_\oplus}{r} d\delta \\ &\approx v \frac{2\omega_\oplus R_\oplus}{c} (\cos\delta_i - \cos\delta_o) \end{aligned} \tag{6}$$

along the flight path from the inbound asymptotic velocity v_i to the outbound asymptotic velocity v_o. The equation 6 integrates the gradient ∂_w of the rotational contribution φ_w

given by Eq. 5 from the inbound asymptote with declination δ_i to the outbound asymptote with declination δ_o along the spacecraft's path. The gain in velocity will accrue only when the inbound and outbound trajectories through the energy gradients due to the planet's rotation are asymmetric. The trigonometric form of the energy density gradient $\partial_w = \partial/\partial(\omega_\oplus R_\oplus \sin\delta/c)$, where δ denotes declination (Figure 1), for the integration of declination from the inbound to outbound asymptote has been derived earlier [16]. It is easy to check by inspecting the following two points. At the Equatorial plane $\delta = 0$, where the quadratic factor $(\omega_\oplus R_\oplus \cos\delta/c)^2$ of φ_w peaks, the energy density gradient vanishes. Conversely, at poles $\delta = \pm\pi/2$, where φ_w in turn vanishes, the gradient in space due to the planet's rotation peaks. In addition to the declination by $\sin\delta$, the gradient depends on the angular velocity $\omega_\oplus$ and radius $R_\oplus$ relative to c. The product form of the three factors ensures the obvious fact that if any one of them vanishes, the gradient does not exist. The transformation from one variable of integration to another $dv = vd\delta$ follows from $vdt = rd\delta$, e.g., defining $dv = adt$ via acceleration $a = v^2/r$.

We motivate the approximation $R_\oplus/r \approx 1$ in Eq. 6 to recognize the empirical equation (Eq. 1) because the radial gradient of φ falls as $1/r^2$, and hence most of Δv accumulates when the spacecraft is near the periapsis whereas contribution from the long opposite inbound and outbound legs is negligible. The polar coordinate representation $R_\oplus/r = 1/2(1-R_\oplus/C+\cos\theta)/(1-R_\oplus/2C)$ reveals the decreasing contribution of a path position r in the sum (Eq. 6) as a function of increasing polar angle θ. The distance from the center of mass to the intersection of the inbound and outbound asymptotes of the hyperbola is denoted with C. Specifically, Eq. 6 yields the maximum change $\Delta v/v = 2\omega_\oplus R_\oplus/c$ for the flight along the rectangular hyperbola from the inbound arm $\delta_i = \pi$ to the outbound arm $\delta_o = -\pi/2$ via the periapsis at $\delta_a = \pi/4$ for a low altitude $r \to R_\oplus$ passage. Conversely, for a high altitude path, such as that of Rosetta's last flyby, the approximation $r \to R_\oplus$ underlying the empirical equation is less motivated, and hence the anomaly is negligible.

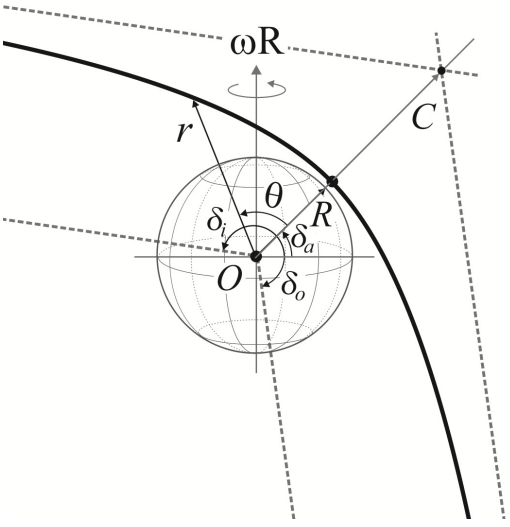

Fig. 1: Equatorial view of a grazing flyby trajectory. The hyperbolic flight path is defined by the planet's radius R extending nearly to the periapsis (solid dot) at declination δ_a and the distance C from the center of mass at the origin O to the intersection of inbound and outbound asymptotes (dashed lines) with declinations δ_i and δ_o. The path's radial coordinate is given by r and polar angle by θ as measured from δ_a. The planet's axis of rotation with angular velocity ωR stands upright.

Obviously the derived formula (Eq. 6) is not only an explicit approximation by $R_\oplus/r \approx 1$, but also implicit in modeling the planet as a rigid homogenous sphere. Moreover, the derivation also neglects apparent forces that are imposed on the spacecraft, such as a drag due to atmospheric friction. However, our study does not aim at producing a formula to calculate Δv due to the atmospheric drag or planet's geoid, instead it targets by the derivation of $\Delta v/v$ to explain the phenomenological formula (Eq. 1) and to identify the anomalous gain in momentum to result from the spacecraft traversing through the energy density gradient of space imposed by the rotation of the planet. Undoubtedly, when more flyby data accumulates, the empirical formula (Eq. 1) will be verified or falsified, thereby giving also a verdict on this study.

5 Discussion

The mathematical correspondence between the empirical relationship (Eq. 1) and the derived formula (Eq. 6) is reassuring, but not alone an explanation for the anomalous gain in velocity. Namely, the obtained consistency in energetic terms is by itself not a tangible explanation, because energy as such does not exist but it is an attribute of its carrier. Thus, the profound question is: What is the carrier substance that embodies the universal density of space and local gravitational potentials that the spacecraft is subject to during its flyby? Of course, this query is not relevant when general relativity is used as a mathematical model for measurements. But when one is after the cause, i.e., the force responsible for the flyby anomaly, the physical form of space must be considered.

The carrier of gravitational force has been sought for long. Nonetheless the graviton of quantum field theory remains a hypothetical elementary particle. In the past the photon was considered as the carrier, because gravity and electromagnetism share similar functional forms [34, 36, 38] as well as because the squared speed of light in the vacuum relates to the absolute electromagnetic characteristics of free space via $c^2 = 1/\varepsilon_o\mu_o$. Also the free space gauge $\partial_t\phi + c^2\nabla\cdot\mathbf{A} = 0$ implies physical existence of scalar ϕ and vector $\mathbf{A}$ potentials, so that ϕ will decrease with time when quanta move down

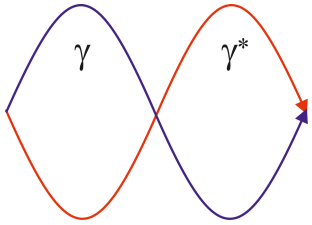

Fig. 2: The photon γ (blue) is the undividable quantum of action whose momentum resides on its wavelength, and equivalently, whose energy is within its period of time. The photon with opposite polarization (red) is the antiphoton γ^*. When γ and γ^* copropagate, the net electromagnetic force will vanish, but the compound boson continues to carry momentum and energy. These compound actions embody space universally and locally. Thus, the associated energy density appears as the universal gravitational potential energy, known as the vacuum density, which is in balance with all bodies. Likewise, a local potential energy is in balance with a local gravitating, orbiting and rotating body.

along the gradient of **A** or vice versa. Recently the old tenet of photon-embodied space has been revived so that the photons are considered to propagate in pairs of opposite polarization, and hence the pairs are without electromagnetic forces [28, 31, 39]. This destructive interference is, of course, familiar from diffraction. By the same token, Aharonov-Bohm experiment demonstrates how an applied vector potential will increase the energy density without introducing fields along the path [40]. According to this percept the two quanta of light do not vanish for nothing when interfering destructively, instead they continue in copropagation with opposite phases, and hence continue in carrying energy and momentum (Figure 2).

Our portrayal of the physical vacuum reminds of de Broglie's theory [41] about a spatially extended, particle centered pilot wave [42]. This view of the physical vacuum, as ours, makes sense of quantum mechanical phenomena without conceptual challenges [43]. In view of that, it has been understood also earlier that c, ε_o and μ_o are not constants, but properties when the vacuum has been considered to embody continuously appearing and disappearing fermion pairs [44, 45]. Instead of accounting for the vacuum's electromagnetic properties by transiently appearing paired charges we reason that when a charge appears in the vacuum, a corresponding force will appear. The force will move the paired photons away from the out-of-phase relation, and hence an electromagnetic field will appear around the charge. Thus, when an atom ionizes, the photons of the electromagnetic field will not appear out of the blue, but they have been around all the time, however in the out-of-phase configuration that manifests itself only as energy density.

The photon-embodied vacuum is understood to emerge from various processes, such as annihilation, where constituents of matter with opposite charge transform to mere radiation. For example, the annihilation of electron with positron will yield, in addition to the two readily observable photons of opposite polarization and directions of propagation, also pairs of co-propagating photons. Conversely, the photon-embodied vacuum is the source of quanta for pair production [37,39,46]. Likewise, electron capture where a proton turns to a neutron, pairs of co-propagating photons will emerge from annihilation of the constituents with opposite charges. When the space is understood to embody the oppositely paired photons, it is easy to envision that space around a body of high energy density houses a radially decreasing energy density, known as the local gravitational potential energy. In this way gravity can be understood as force, like any other force, to result from the energy density difference over a distance, i.e., from a gradient. Ensuing motions consume the free energy in least time. This evolution is expressed by the principle of least action in its original form (Eq. 2). Namely, all bodies move from one state to another along geodesics to diminish density gradients in the least time.

The least-time imperative means that the two bodies will move toward each other when the surrounding universal space is sparse enough to accept the paired quanta that are released from the dense gravitational potential of the bodies to the surrounding free space along the paths of least time. For example, an object falls straight down on the ground, i.e., along the least-time path, to consume the energy density difference between the local gravitational potential and the sparse surrounding vacuum. When the body is falling down, the oppositely paired photons are released from the local gravitational potential to the surrounding universal vacuum also along their paths of least time. Conversely, the two bodies will move away from each other when the surrounding potential is rich enough to grant paired quanta with energy to the local potential about the bodies.

In the same manner it is inescapable that it takes some form of free energy, ultimately carried by the photons that have been acquired from insolation, to lift up the fallen object from the ground back up on its initial height. So, the logic of reversibility says that the photons that were absorbed when the object was lifted up must have been emitted when the object was falling down. Thus, gravity is a dissipative phenomenon. When the bodies move toward each other, there is an efflux of quanta with energy to the surroundings, and conversely when the bodies move away from each other, there is an influx of quanta with energy from the surroundings. Manifestly, there is no net flux, i.e., no net dissipation from the system of bodies at a stationary state corresponding to an energetic balance with its surroundings.

This insight to gravity allows us to describe the spacecraft's flyby as an energy transfer process where quanta move from the local system of bodies to the surrounding space or vice versa. Flyby mission data show temporary maxima and minima in energy transfer that moderate toward the space-

craft's asymptotic courses [4]. We remind that oscillations are characteristics of least-time transitions from one state to another [47]. The oscillations are pronounced when the rate of energy transfer is rapid compared with the bound energy.

With this insight to gravity as a dissipative phenomenon, let us first consider the flight past a gravitating spherical body. The spacecraft treks along its inbound trajectory through an increasing energy density of space, i.e., the $1/r^2$-force field when the distance r closes toward the body. The increase in the spatial potential energy is balanced, according to Eqs. 2 and 3, by an increase in kinetic energy as well as by efflux of the oppositely paired quanta from the local gravitational potential comprising the body and the spacecraft to the universal gravitational potential due to all bodies in the Universe. The flux of quanta is often overlooked because the oppositely paired quanta without net electromagnetic field cannot be detected readily. However, the dissipation can be inferred recalling that the total gravitational potential energy of the body and the spacecraft at the periapsis is not exactly equal to the total potential energy when the spacecraft is at a point on the arm of hyperbola. The emission of quanta will cease, i.e., dissipation will vanish $d_t Q = 0$ momentarily, when the spacecraft arrives at the periapsis, where kinetic energy $2K$ matches the scalar potential energy U. Thereafter, along the outbound asymptote $2K$ will exceed U, and hence the paired quanta will be acquired from the surrounding vacuum to the local gravitational potential so that the balance with the surrounding density will be eventually regained far away from the planet. Since the passage from the inbound asymptotic state via the periapsis to the outbound asymptotic state is symmetric, the emission of quanta from the local system and the absorption to the local system match perfectly, and hence the net dissipation vanishes. Thus, the momentum of the two-body system is conserved.

Next, let us consider the flight past by an orbiting body. Along the inbound trajectory the spacecraft travels through the energy density of space that increases more rapidly than in the case of the merely gravitating body, namely at the rate that the planet orbits straight at the spacecraft. This more rapid increase in the potential energy is balanced, just as reasoned above, by a more rapid increase in kinetic energy concurrently with dissipation of the oppositely paired quanta to the surrounding space. First when at the periapsis, where the spacecraft moves orthogonal to the planetary orbit, dissipation vanishes momentarily. Thereafter, along the outbound asymptote $2K$ will exceed U, and hence quanta will be acquired from the surrounding vacuum to the local gravitational potential energy comprising the body and the spacecraft to regain the balance eventually when far away. Clearly the flyby about the approaching planet and the flyby about the departing planet differ from each by the rates of momentum and energy transfer from the system to the surrounding space. Thus, the spacecraft will pick up momentum in the former case and it will lose momentum in the latter case. The formula for the spacecraft's change in velocity can be derived in the same manner as Eq. 6 was derived. Consistently, also the (very slightly) perturbed planet will regain a stable orbit by processes where the paired quanta carry energy from the surroundings to the local potential and vice versa until the free energy minimum state has been attained.

Finally, let us consider the flight past a rotating planet that imposes an axially symmetric energy density gradient on the surrounding space. When the gradient along the inbound trajectory is equal in magnitude to the gradient along the outbound trajectory but of opposite sign, the emission and absorption of quanta from the system comprising the body and the spacecraft to the surrounding vacuum are equal. Thus, in that case the momentum is conserved, and hence no anomalous gain or loss in velocity will detected. Conversely, when the emission of quanta along the inbound trajectory and the absorption of quanta along the outbound trajectory do not cancel each other exactly, the spacecraft will either pick up or lose momentum depending on the sign of net dissipation. Likewise the concurrent (minute) perturbation of the planet's rotational momentum will damp down toward a stable state of spinning by energy transfer processes from the systemic potential to the surroundings and vice versa until the net dissipation finally vanishes at the free energy minimum state. Perhaps our account on gravity summons up the old abandoned idea of luminiferous ether [48]. Therefore, it is worth emphasizing that the proposed physical vacuum is not a medium that supports propagation of light, instead the photons constitute space. The paired photons without net polarization do not couple in electromagnetic terms, and hence the space is dark, but not illusive or only a mathematical metric. It reacts to every act. Any change in momentum is met with resistance, known as inertia, since the spatial energy density redistributes to regain balance among perturbed bodies [31].

6 Conclusions

We conclude that the flyby anomaly only appears as an odd phenomenon when not all components of force are included in its explanation. Specifically, we maintain that the law of conservation of momentum holds when the system of bodies associated with local potentials of space will in total neither lose nor gain quanta from the surrounding systems. The ultimate surroundings for any local system is the universal free space. It must be taken into account in the explanation of flyby anomaly.

We resort to the old idea that the vacuum is embodied by the quanta of light which pair in opposite polarization. Hence space is dark but it holds an energy density [32] on the order of one nJ/m^3. The non-zero energy density displays itself also in the Aharanov-Bohm experiment [40] and as the Casimir effect [49]. So in any closed system the conservation of momentum is a solid law. In fact, the law may seem universal, since the Universe as a whole may by definition seem like

a closed system. However, the quanta of light, that embody the space both in pairs of opposite polarization and solo, are open actions (Figure 2), whose momentum $\mathbf{p}$ may decrease concomitantly with increasing wavelength λ or vice versa so that the measure, known as Planck's constant, $h = \mathbf{p} \cdot \lambda$ remains invariant. Equivalently stated, a decrease in energy E is counterbalanced by an increase in time t, so that $h = Et$ is constant. Indeed, astronomical observations imply that the total energy density of the Universe is decreasing with increasing time. The photon that emerged from the nascent energy-dense Universe has shifted down in frequency $f = 1/t$ when adapting to ever more sparse surrounding densities on its way to us and eventually terminating at absorption to our detector. Conversely, when insisting on that energy is conserved, i.e., by applying a theory that conserves a symmetry, the ensuing interpretation of supernovae data will require an ad hoc patching, for instance, by dark energy [26].

Rules and regularities that are so apparent across scales of nature, are rightfully related to conservation laws. However, to avoid assigning phenomena as anomalous, it is necessary to include everything in an explanation. To this end among the laws of nature the truly superior and solid one is the conservation of the total number of quantized actions in the whole Universe.

Acknowledgements

I thank Dr. Pekka Teerikorpi for valuable comments.

Submitted on January 9, 2017 / Accepted on January 15, 2017

References

1. Flandro G.A. Fast Reconnaissance Missions to the Outer Solar System Utilizing Energy Derived from the Gravitational Field of Jupiter. *Astronautica Acta*, 1966, v. 12 329–337.
2. Wiesel W.E. Space flight Dynamics. McGraw-Hill, New York, NY, 1989.
3. Nieto M.M., Anderson J.D. Earth flyby anomalies. *Physics Today* 2009, v. 62 76–77.
4. Anderson J.D., Campbell J.K., Nieto M.M. The energy transfer process in planetary flybys. *New Astronomy*, 2007, v. 12 383–397.
5. Anderson J.D. et al. Anomalous Orbital-Energy Changes Observed during Spacecraft Flybys of Earth. *Physical Review Letters*, 2008, v. 100 091102.
6. Antreasian P.G., Guinn J.R. AIAA Paper No. 98-4287 presented at the AIAA/AAS Astrodynamics Specialist Conference and Exhibit, Boston, August 10-12, 1998. http://www2.aiaa.org/citations/mp-search.cfm.
7. Edwards C., Anderson J., Beyer P., Bhaskaran S., Nicholson F., Ottenhoff T., Stevens S. Tracking Gali-leo at Earth-2 perigee using the tracking and data relay satellite system. *Adv. Astron. Sci.*, 1994, v. 85 1609–1621.
8. Guman M.D., Roth D.C., Ionasescu R., Goodson T.D., Taylor A.H., Jones J.B. Cassini Orbit Determina-tion from First Venus Flyby to Earth Flyby. *Advances in Astronautical Sciences*, 2000, v. 105 1053–1072.
9. Morley T., Budnik F. Rosetta Navigation at its First Earth-Swingby. *Proceedings of the International Symposium on Space Technology and Science*, 2006, v. 25 59.
10. Williams B., Taylor A., Carranza E., Miller J., Stanbridge D., Page B., Cotter D., Efron L., Farquhar R., McAdams J., Dunham D. Early navigation results for NASA's Messenger mission to Mercury. *Advances in the Astronautical Sciences*, 2005, v. 120 1233–1250.
11. Iorio L. The Effect of General Relativity on Hyper-bolic Orbits and Its Application to the Flyby Anomaly. *Scholarly Research Exchange*, 2009, 807695, arXiv:0811.3924.
12. Acedo L. The flyby anomaly: A case for strong gravitomagnetism? *Advances in Space Research*, 2014, v. 54 788–796.
13. Cahill R.T. Resolving Spacecraft Earth-Flyby Anom-alies with Measured Light Speed Anisotropy. *Progress in Physics*, 2008, v. 3 9–15.
14. Adler S.L. Can the flyby anomaly be attributed to Earth-bound dark matter? *Physical Review D*, 2009, v. 79 023505.
15. Mbelek J.P. Special relativity may account for the spacecraft flyby anomalies. 2009, arXiv:0809.1888v3.
16. Hafele J.C. Causal Version of Newtonian Theory by Time–Retardation of the Gravitational Field Explains the Flyby Anomalies. *Progress in Physics*, 2013, v. 2 3–8.
17. Tajmar M., Assis A.K.T. Influence of Rotation on the Weight of Gyroscopes as an Explanation for Flyby Anomalies. *Journal of Advances in Physics*, 2016, v. 5 176–179.
18. McCulloch M.E. Modelling the flyby anomalies using a modification of inertia. *Monthly Notices of the Royal Astronomical Society*, 2008, v. 389 L57–L60.
19. Pinheiro M.J. Effect of TTC on Satellite Orbital Mechanics. *Physical Letters A*, 2014, v. 378 3007–3011.
20. Iorio L. A flyby anomaly for Juno? Not from stand-ard physics. *Advances in Space Research*, 2014, v. 54 2441–2445. arXiv:1311.4218.
21. Acedo L. The Flyby Anomaly in an Extended White-head's Theory. *Galaxies*, 2015, v. 3 113–128.
22. Pinheiro M.J. Some effects of topological torsion currents on spacecraft dynamics and the flyby anomaly. *Monthly Notices of the Royal Astronomical Society*, 2016, v. 461 3948–3953.
23. De Maupertuis P.-L.M. Les loix du mouvement et du repos déduites d'un principe metaphysique. *Histoire de l'Académie Royale des Sciences et des Belles-Lettres de Berlin*, 1746, 267–294.
24. Sharma V., Annila A. Natural process – Natural selection. *Biophysical Chemistry*, 2007, v. 127 123–128.
25. Tuisku P., Pernu T.K., Annila A. In the light of time. *Proceedings of Royal Society of London A*, 2009, v. 465 1173–1198.
26. Koskela M., Annila A. Least-time perihelion precession. *Monthly Notices of the Royal Astronomical Society*, 2011, v. 417 1742–1746.
27. Annila A. Rotation of galaxies within gravity of the Universe. *Entropy*, 2016, v. 18 191–205.
28. Annila A. Probing Mach's principle. *Monthly Notices of the Royal Astronomical Society*, 2012, v. 423 1973–1977.
29. Annila A. Least-time paths of light. *Monthly Notices of the Royal Astronomical Society*, 2011, v. 416 2944–2948.
30. Annila A. Cosmic rays reports from the structure of space. *Advances in Astronomy*, 2015, 135025.
31. Grahn P., Annila A., Kolehmainen E. On the exhaust of EM-drive. *AIP Advances*, 2016, v. 6 065205.
32. Feynman R.P., Morinigo F.B., Wagner W.G., Hatfield B. Feynman Lectures on Gravitation. Addison-Wesley, Reading, MA, 1995.
33. Bourbaki N. Topological vector spaces. Springer, Berlin, 1987. ISBN 3-540-13627-4.
34. Sciama D.W. On the origin of inertia. *Monthly Notices of the Royal Astronomical Society*, 1953, v. 113 34–42.
35. Evans J., Kamal K.N., Anwarul I. The Optical-Mechanical Analogy in General Relativity: Exact Newtonian Forms for the Equations of Motion of Particles and Photons. *General Relativity and Gravitation*, 1996, v. 28 413–439.

36. Heaviside O. A gravitational and electromagnetic analogy, Part I. *The Electrician*, 1893, v. 31 281–282.
37. Annila A. Natural thermodynamics. *Physica A*, 2016, v. 444 843–852.
38. Newton I. Opticks (1704) Excerpts of Queries 29 and 30 of Book III. Dover, New York, NY, 1979.
39. Annila A. The meaning of mass. *International Journal of Theoretical and Mathematical Physics*, 2012, v. 2 67–78.
40. Aharonov Y., Bohm D. Significance of electromag-netic potentials in quantum theory. *Physical Review*, 1959, v. 115 485–491.
41. De Broglie L. La mécanique ondulatoire et la structure atomique de la matière et du rayonnement. *Journal de Physique et Le Radium*, 1927, v. 8 225–241.
42. Bush J.W.M. The new wave of pilot-wave theory. *Physics Today*, 2015, v. 68 47–53.
43. Boyer T.H. Any classical description of nature requires classical electromagnetic zero-point radiation. *American Journal of Physics*, 2011, v. 79 1163–1167.
44. Urban M., Couchot F., Sarazin X., Djannati-Atai A. The quantum vacuum as the origin of the speed of light. *The European Physical Journal*, 2013, v. 31 281–282.
45. Leuchs G., Villar A.S., Sánchez-Soto L.L. The quantum vacuum at the foundations of classical electrodynamics. *Applied Physics B*, 2010, v. 100 9–13.
46. Annila A. All in action. *Entropy*, 2010, v. 12 2333–2358.
47. Mäkelä T., Annila A. Natural patterns of energy dis-persal. *Physics of Life Reviews*, 2010, v. 7 477–498.
48. Michelson A.A., Morley E.W. On the Relative Mo-tion of the Earth and the Luminiferous Ether. *American Journal of Science*, 1887, v. 34 333–345.
49. Casimir H.B.G., Polder D. The influence of retarda-tion on the London-van der Waals forces. *Physical Review*, 1948, v. 73 360–372.

The Proton Radius Anomaly from the Sheltering of Unruh Radiation

Michael Edward McCulloch

Plymouth University, Drake Circus, Plymouth, PL4 8AA, UK. E-mail: mike.mcculloch@plymouth.ac.uk

It has been found that in muonic hydrogen either the proton radius is 4% smaller than usual (a 7σ anomaly) or an unexplained extra binding energy of 320 μeV is present. Here it is shown that 55% of this extra energy can be explained if Unruh radiation seen by the orbiting muon can push on it, and is being asymmetrically blocked by the proton.

1 Introduction

The proton radius has been measured for many years to be 0.88 fm, with experiments using electron-proton scattering and by using atomic spectoscopy to look at the Lamb shift seen by an orbiting electron, a shift which depends on the proton radius [1].

More recently, it was realised that a more accurate proton radius could be obtained by replacing the electron in the atom with its heavier twin: the muon, but when this was done, the, more accurate, proton radius was found to be 0.84 fm, 4% smaller and a difference seven times larger than the uncertainty in the original measurement [2]. This was confirmed in 2013 [3] and has also been confirmed using a muon orbiting a deuterium nucleus [4].

The standard model has no mechanism that allows the proton to change size in the proximity of a muon as opposed to an electron, so this is a crucial finding. Another possibility however, is that the proton size is not changing but that a new binding energy equal to 320 μeV is appearing [1]. It is the contention of this paper that this extra binding energy comes from sheltering by the hypothesised Unruh radiation.

[5] suggested that black hole event horizons can separate pairs of particles in the zero point field, swallowing one and allowing the other to escape as a real particle, thus allowing black holes to radiate. [6], [7] and [8] then suggested that the same thing may occur when objects accelerate since then a horizon appears, and may similarly seperate paired virtual particles making half of them real. This is now called Unruh radiation.

[9] and [10] suggested that inertia is caused by Unruh radiation: the acceleration of an object causes a Rindler horizon to form on the side opposite to the acceleration vector and this damps Unruh radiation on that side of the object, causing a net imblance in Unruh radiation pressure that pushes it back against the original acceleration. This new process predicts inertial mass [10] and [11] and also predicts deviations from the standard inertial mass that explains the galaxy rotation problem without the need for dark matter [12] and also cosmic acceleration [13]. The crucial point here is that Unruh radiation is taken to exist and to be able to push on particles.

In this paper it is argued that the usually isotropic Unruh radiation seen by the orbiting muon is blocked by the central proton, which subtends a much larger solid angle at the close-orbiting muon than at the distantly-orbiting electron. It is shown that this sheltering effect on Unruh radiation can account for about half of the proton radius anomaly in muonic hydrogen.

2 Method and Results

Let us imagine a muon orbiting around a proton as shown in Figure 1.

In quantum mechanics of course it is not possible to specify an exact orbital speed for the muon, but one can estimate the probable speed: $v \sim \alpha c$ where α is the fine structure constant and c is the speed of light. The acceleration of the muon as it orbits at a radius R is then

$$a = \frac{v^2}{R} = \frac{(\alpha c)^2}{R} \tag{1}$$

where $\alpha \sim 1/137$. The wavelength of Unruh radiation seen by the muon while orbiting can be found using Wien's law for the wavelength emitted by a body of temperature T, $\lambda = \beta hc/kT$ where $\beta = 0.2$, h is Planck's constant, c is the speed

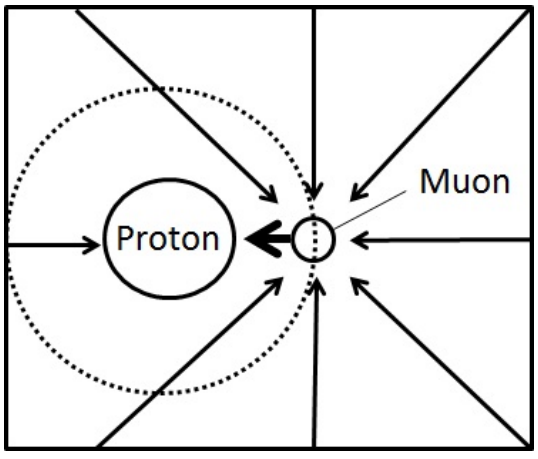

Fig. 1: Schematic showing a muon (the small right hand circle) orbiting close to a proton (the large left hand circle). The muon is pushed by the Unruh radiation associated with its acceleration (the arrows) from all directions except from the direction of the blocking proton (the truncated arrow). So there is a new net force pushing the muon towards the proton. The size of this force produces 55% of the proton radius anomaly.

of light and k is Boltzmann's constant, and combining it with the temperature of Unruh radiation seen at an acceleration a: $T = \hbar a/2\pi ck$, so that

$$\lambda_U \sim \frac{8c^2}{a}. \quad (2)$$

The de Broglie energy associated with this wavelength is

$$E = \frac{hc}{\lambda_U}. \quad (3)$$

Using (2) we get

$$E \sim \frac{ha}{8c} \quad (4)$$

and using (1) we get

$$E \sim \frac{h\alpha^2 c}{8R}. \quad (5)$$

This is the energy in the Unruh radiation field at the muon, which usually strikes the muon isotropically so does not push it in any net direction. However, we shall assume that the proton, as seen from the muon, blocks all the Unruh radiation coming from that direction (Fig. 1). The amount will be proportional to the solid angle of the proton as seen by the muon, which is $\pi r_P^2/2\pi R^2 = 5.7\times10^{-6}$, where r_P is the proton radius and R is the muon-proton distance. Note that we are only looking at one side of the muon, to work out the energy asymmetry that pushes on the muon, so it is the half-sphere we consider.

As energy is being blocked on the side of the muon closer to the proton, this represents a new source of energy pushing the muon towards the proton, and adding to its boundedness. The specific amount of energy is

$$E \sim \frac{h\alpha^2 c}{8R} \times \frac{\pi r_P^2}{2\pi R^2} = 2.8 \times 10^{-23}\text{J}. \quad (6)$$

The extra binding energy required to account for the observed proton radius anomaly is 320μeV or 5.1×10^{-23} J. Therefore a sheltering of Unruh radiation by the proton predicts roughly 55% or 180 μeV of the energy needed to explain the observed proton radius anomaly for muonic hydrogen.

This extra Unruh binding energy is far smaller in the case of the electron. Electrons orbit the proton about 200 times further out than the muon and so the solid angle of the proton at the electron is much smaller. The energy released in the electron case would be

$$E \sim \frac{h\alpha^2 c}{8R} \times \frac{\pi r_P^2}{2\pi R^2} = 7.1 \times 10^{-28}\text{J} \quad (7)$$

or about 5 orders of magnitude smaller than for the muon. So there is no anomaly for normal hydrogen. When the electron is replaced by a muon there is a difference of roughly 180 μeV, or 55% of the observed anomaly.

3 Conclusion

It has been observed that the radius of the proton, as determined by the Lamb shift, is apparently 4% less when measured using an orbiting muon instead of an electron. This can be interpreted as an anomalous increase in the proton-muon binding energy of 320 μeV.

Assuming that Unruh radiation is able to push on particles, and that the proton can block it, predicts an extra proton-muon binding energy of 180 μeV, about 55% of the observed anomaly.

Submitted on January 5, 2017 / Accepted on January 19, 2017

References

1. Carlson C.E. The proton radius puzzle. 2015, arxiv: 1502.05314.
2. Pohl R., et al. *Nature*, 2010, v. 466, 213.
3. Antognini A. et al. *Science*, 2013, v. 339, 417.
4. Pohl R., et al. Laser spectroscopy of muonic deuterium. *Science*, 2016, v. 353, 6300.
5. Hawking S.W. Particle creation by black holes. *Commun. Math. Phys.*, 1975, v. 43, 199.
6. Fulling S.A. *Phys. Rev. D.*, 1973, v. 7(10), 2850.
7. Davies P.C.W. Scalar production in Schwarzschild and Rindler metrics. *J. Physics*, 1975, v. 8(4), 609.
8. Unruh W.G. Notes on black hole explosions. *Phys. Rev. D.*, 1976, v. 14, 870.
9. McCulloch M.E. Modelling the Pioneer anomaly as modified inertia. *MNRAS*, 2007, v. 376, 338–342.
10. McCulloch M.E. Inertia from an asymmetric Casimir effect. *EPL*, 2013, v. 101, 59001.
11. Gine J., McCulloch M.E. Inertial mass from Unruh temperatures. *MPL-A*, 2016, v. 31(17), 1650107.
12. McCulloch M.E. Testing quantised inertia on galactic scales. *ApSS*, 2012, v. 342(2), 575–578.
13. McCulloch M.E. Minimum accelerations from quantised inertia. *EPL*, 2010, v. 90, 29001.

Energy is the Expansion

Jacques Consiglio

52 Chemin de Labarthe, 31600 Labastidette, France
E-mail: Jacques.Consiglio@gmail.com

Here, using Mach's principle we symmetrize the Schwarzschild solution. It enables to compute the universe densities of baryonic matter, dark matter, and dark energy as distinct effects of the same unique source and the time invariance of the theory naturally gives an inflation period (or its illusion). The theory does not change GR equations but its classical limit is a MOND theory which parameter is predicted. Hence we claim the discovery of a natural law.

1 Introduction

In relativity and cosmology, the mystery of the time is the nature of dark matter and dark energy. Dark matter is inferred from the anomalous galaxies rotation curves and dark energy from the universe accelerated expansion. The debate is long open between dark matter particles and modified gravity; the nature of the dark energy field is unknown. On the other hand of physical theories, quantum gravity which cannot be renormalized and gives absurd predictions.

The purpose of this paper is to provide with a natural solution to the first issue without modifying GR, firstly by computing the amount of matter, dark matter and dark energy from elementary symmetry considerations; thus uncovering a fundamental law of nature. It addresses in the most general manner the long expected rule of energy and metric formation — namely space-time and everything therein. We also show that the classical approximation is a MOND-type theory and compute its parameter. Concerning quantum gravity, it shows why a different approach is needed.

Note that all masses, densities and accelerations in this paper are computed using as input the universe age T given by the Planck mission and two natural constants G, and c. The other ΛCDM parameters output of this mission are only used for comparison.

2 Theory

Theoretical physics works by the study of symmetry; for any variation, compensation exists. The universe expands, therefore compensation exists and then symmetry. Take the Einstein field equation:

$$R_{\mu\nu} - \frac{1}{2}\, R\, g_{\mu\nu} = \frac{8\pi G}{c^4}\, T_{\mu\nu} - \Lambda\, g_{\mu\nu}\,, \tag{1}$$

where the term Λ is experimentally justified and is a constant scalar; meaning its density is constant in space. It leads to results which are unique in physics: two kinds of energies do not transform in each other and, as we know from phenomenology, it eventually requires a third kind with the same property, namely dark matter. This is the problem we shall discuss.

On the other hand the ΛCDM model is well verified and it gives no reason to doubt the Friedman-Lemaitre-Robertson-Walker (FRLW) cosmology. Therefore we shall neither modify gravity nor implement ad-hoc fields, but instead discuss energy formation; masses, the scalar Λ, and their relation with G. For this we shall take the problem by the other end and use the standard short distance case with central mass M. The Schwarzschild spherical solution reads:

$$c^2\, d\tau^2 = \left(1 - \frac{R_s}{r}\right) c^2 dt^2 - \left(1 - \frac{R_s}{r}\right)^{-1} dr^2 - r^2\,(d\theta^2 + sin^2\theta\, d\phi^2)\,. \tag{2}$$

This "local" solution does not admit a scalar Λ; it is not appropriate but we shall make direct use of this defect. If we properly instantiate Mach's principle therein we should get a nice correction, because by definition it should includes all effects. The symmetry in (2) is unbalanced since two of the quantities are not geometrical, namely G and M. Then in an attempt to symmetrize the Schwarzschild solution we write:

$$\frac{R_s}{r} = \frac{R_U\, M}{M_S\, r} \rightarrow \frac{2G}{c^2} = \frac{R_U}{M_S}\,, \tag{3}$$

where M_S and R_U represent respectively the scalar field energy and the distance to the event horizon ($R_U = c\,T$). Note that this equation instantiates Mach's principle in the most trivial manner. Now compute:

$$M_S = \frac{R_U\, c^2}{2\, G} = 8.790 \times 10^{52}\,\text{kg}. \tag{4}$$

It looks to the observer like an energy contained in a 3-sphere, but it is actually a conic 4-dimensional structure intersecting the present, the surface of the 4-sphere. Then consider the constancy of Λ: with respect to the 4-sphere volume, and in order to reduce to its surface, we divide M_S by the 4-sphere surface coefficient, namely $2\,\pi^2$; we get:

$$M_V = \frac{M_S}{2\,\pi^2} = 4.453 \times 10^{51}\,\text{kg}, \tag{5}$$

which corresponds to 4.82% of the total mass and density:

$$M_{total} = M_S + M_V = 9.236 \times 10^{52}\,\text{kg}, \tag{6}$$

$$D_{total} = \frac{3\,(M_S + M_V)}{4\,\pi\, R_U^3} = 9.91 \times 10^{-27}\,\text{kg/m}^3. \tag{7}$$

All numerical results above are in great agreement with the Planck mission outputs [1] even though we get a single dark field M_S summing dark energy and dark matter.

The Planck mission also gave $H_0 = 67.74\,(46)$ km/s/Mpc and we use $H = 1/T = 71.10$ km/s/Mpc to compute the distance to the event horizon. Then compare:

$$\frac{M_S + M_V}{M_S} = 1 + \frac{1}{2\pi^2} = 1.0507\,, \tag{8}$$

with:

$$\frac{1}{H_0\,T} = 1.0496\,. \tag{9}$$

This utterly stunning not only for the right orders of magnitude, but for getting also the first two or three decimals right and multiple coincidences — seemingly coherent — which, in principle, address independent quantities. Considering also that from (3) M_S is the critical density, it suggests that the mass terms are linked to G by geometry in a manner that is consistent with GR; possibly a fundamental law of nature ruling the universe formation. Now the equation (4) also reads:

$$2M_S\,c^2 = P_p\,T = \frac{P_p\,R_U}{c}, \tag{10}$$

where $P_p = c^5/G$ is the Planck power. It looks as though a 4-sphere at the surface of which observable energy lies is either inflated or heated by a constant feed; in other words, it replaces the big bang singularity by a constant power and the correlation is such that we must conjecture the following identification: *energy is the expansion*; meaning that M_S and M_V increase linearly in time. Expansion is observed, and then we shall discuss the conjecture as a new theory which is embodied by the equation (3) and the following premises:

P1: The scalar Λ is a constant of nature.

P2: The matter field (all particles) is the surface of a 4-sphere.

P3: A feed mechanism exists inflating the sphere and expanding its inner metric; both effects are simultaneous.

P4: The inner metric expansion is the product of inflation of the sphere radius by the reduction of particles wavelengths; both effects have identical coefficients.

Essentially, we states that M_S is the critical density, that the matter field M_V has no effect on the course of the universe expansion, and that the source terms of the Einstein field equation (1) are not identified for what they are. In the following sections we analyze what the new theory predicts.

3 Predictions

3.1 Inflation

Considering P3 and P4 the wavelength of massive particles reduce in time while the 4-sphere expands, the product of this reduction by this expansion gives a linear increase of the universe radius.

But this is considering constant energy; since the wavelengths reduce the relative rate of time is not constant between distinct epochs and reaches zero at the origin. Therefore the theory requires an inflation period; the global curve is a straight line if expressed in "constant" time T, but a logarithmic law if expressed in proper time.

3.2 The dark matter effect

Let us study the effects at different heights in the gravitational pit of a central mass M (the basic test case) and assume the system far away from other gravitational sources. With respect to (2), M_S is variable in time but constant in space ($M_S \sim T$). At the opposite since gravitation is a retarded interaction, the metric in r is retarded and the equation (3) must be modified accordingly. Hence, using P3-P4, since r and M (or R_s) expand, we write:

$$\frac{R_s}{r} \to \frac{R_s}{r} \times \sqrt{\frac{1 - Hr/c}{1 + Hr/c}}\,, \tag{11}$$

which second order limited development yields:

$$\frac{2\,G\,M}{r\,c^2} \to \frac{2\,G\,M}{r\,c^2} - \frac{M}{M_S} + \frac{M\,r}{M_S\,R_U}. \tag{12}$$

Now examine this expression:

- The first term is nominal.
- The middle term cannot be seen negligible since it addresses identically all masses of the universe. Hence it must be identified to the contribution of M_S to the mass M, and then integrated to M_S, giving -1 *which is the flat metric*. Finding the flat metric here may look stunning but it is coherent with its production.
- Therefore the right hand term must also be integrated to M_S giving $H\,r\,c$ of unit squared velocity, and a cosmological term $H\,c$ with unit of acceleration; it comes from the expansion but its effect in the gravitational field is not trivial.

Still, we know that this value is in the range of the anomalous acceleration at galaxies borders. Then let us discuss angular momentum.

Quantum gravity is usually expected to work from the same principles as any other field. But this assumption holds a fundamental contradiction with the spirit of GR and even more with the theory we discuss, because here gravitation defines *entirely* the context in which the rest of physics lives. In this way, the position of M_S at the denominator of (3) is quite evident since like GR it scales the matter field — but globally. Still, the theory is compatible with the SM fields. The bottom line is scale-independence and all SM couplings constants are unitless including mass ratios.

Now on angular momentum, consider simply the Bohr radius for the simplest but most general case:

$$a_0 = \frac{\hbar}{m_e\,c\,\alpha} = \frac{1}{2\,\pi} \times \frac{\lambda_e}{\alpha}\,. \tag{13}$$

We know that the fine structure constant α did not change during many billion years; then with a linear increase of m_e, the electron wavelength and the Bohr radius decrease together and coherently; but when considering only lengths like in (13) the orbit radius scaling factor is $1/2\,\pi$.

Expressing this simply, when the electron mass increases in time, the Bohr radius and the first Bohr orbit reduce like:

$$\frac{da_0}{dt} = \frac{d\lambda_e}{\alpha\, dt} \times \frac{1}{2\pi} \to \frac{\alpha\, da_0}{d\lambda_e} = \frac{1}{2\pi}\,. \tag{14}$$

But this contraction is universal. It addresses all phenomena ruled by quantum physics (rulers, clocks, etc...); *it is not measurable where only quantum physics rules*.

But there is a neat difference with gravitation: with quantum fields, angular momentum quantizes distances as the inverse of mass, but gravity cannot since its classical force is a product of masses. With the product of two masses increasing simultaneously, we get a square and only half the effect is non-measurable. *Hence in the gravitational field a residual term $H\,c/2\pi$ gives measurable effects*.

3.3 Dark matter and dark energy

In the spirit of the coincidence in (4), GR (or the ΛCDM model) splits the scalar energy M_S into a massive dark matter field and the scalar field Λ, and we have a compression factor which derivative is $H\,c$ applied on any piece of the matter field M_V. But for *any* scalar field X having this double effect, and for any R and $H_R = c/R$, its compression energy M_{Co} (dark matter) at any place is given by:

$$\frac{M_{Co}}{M_X} = \frac{1}{2}\int_0^R \frac{4\pi\rho_X\, r^2}{M_X\, c^2}\,(H_R\, c\, r)\, dr = \frac{3}{8} = 0.375\,, \tag{15}$$

where in the integral energy is given by acceleration, then kinetic energy $p^2/2m$; thus the factor $1/2$. The kinetic impact of X has effect of pressure and its energy is calculable. Obviously, the Planck mission gave the same result:

$$\frac{\Omega_C}{\Omega_{DE}} = \frac{0.2589}{0.6911} = 0.3746. \tag{16}$$

From this equation the sum $\Omega_C + \Omega_{DE} = \Omega_S$ is not a split but a unique field giving distinct effects ruled by geometry, a consequence of which is M_S:

$$\Omega_S = 2\pi^2\,\Omega_V = \frac{11}{8}\,\Omega_{DE} = \frac{11}{3}\,\Omega_C\,. \tag{17}$$

This is not unification of distinct fields, this is unity. In GR:

- Ω_{DE} provides with negative pressure, a repelling force;
- Ω_C is seen as mass but here it must be seen as counterpart, an isotropic stress *and* a positive pressure applied to massive particles by the same repelling force; in the equation (1), stress is part of the stress-energy tensor.
- Ω_V the matter density is the proportion of their sum at the 4-sphere surface.

Here there is no contradiction with (1) nor with the FLRW universe; but the concept appears to imply that dark matter is pressure and that mass is compression work.

3.4 The Hubble paramater

Let a photon be emitted in A at date t_1 with observable energy m, the transit time to the receptor in B is t, and then $t_1 + t = T$. It has no mass, but it takes away a part of the emitter mass m, and then the full energy it transfers includes its share of M_S and corresponds to $m\,(2\pi^2 + 1)$.

During the transfer, its wavelength increases of a factor $\sqrt{(t_1 + t)/t_1}$. Hence:

$$m_{\text{transfer}} = \frac{(2\pi^2 + 1)\,\sqrt{t_1}}{\sqrt{t_1 + t}}\, m\,.$$

But during the time t, the mass of the receptor evolved by a factor $\sqrt{t_1} \to \sqrt{t_1 + t}$. Therefore the energy transferred by the photon to the receptor, before it reconstitutes mass in B evolves like:

$$\frac{m_{\text{transfer}}}{m_{\text{receptor}}} \sim (2\pi^2 + 1)\,\frac{t_1}{t_1 + t}\,.$$

Once the photon is absorbed, it gives:

$$\frac{m_{\text{absorbed}}}{m_{\text{receptor}}} \sim 1 - Ht\,, \tag{18}$$

which is standard red-shift for a universe of age T expanding at constant rate c for which $H\,T = 1$. It fits with observation of type 1A supernova with accelerated expansion due to the scalar field Λ. On the other hand, consider a field of photons created at the origin (not emitted by mass); the term $(2\pi^2 + 1)$ is not present at emission, meaning in facts that the field M_S has decayed of a factor $(1 + 1/2\pi^2)^{-1}$ with mass creation; hence the equation (9). So the theory predicts a discrepancy between measurements of the Hubble parameter from the CMB and type 1A supernovas:

$$H^0_{1A} = \frac{1}{T} = H^0_{CMB}\left(1 + \frac{1}{2\pi^2}\right). \tag{19}$$

This equation is in range of the discrepancy given by the Hubble space telescope measurements in [5], which is currently valid at $\sim 3\sigma$, as compared to the Planck mission. Older data is also compatible with the prediction.

3.5 The classical limit

The limited development in (12) also applies in the classical theory provided a retarded field. (Even though we would obtain $M_S \to 2\,M_S$ with a classical equation in place of (3) and the same reasoning.) According to (14), the cosmological term to apply is is:

$$S_{HC} = \frac{H\,c}{2\,\pi} = 1.10 \times 10^{-10}\text{m/s}^2, \tag{20}$$

where Milgrom's limit is $a_0 = 1.20\,(\pm 0.2) \times 10^{-10}\text{m/s}^2$; so we shall compare with MOND.

But here S_{HC} is a derivative that scales the gravitational field and it cannot be independent of the "normal" acceleration. In a classical manner we need to discuss forces with the following substitution:

$$\frac{G\,m\,M}{r^2} \to \frac{G\,m\,M}{r^2} + m\,S_{HC}\,,$$

which, on circular orbit, corresponds to the Newton acceleration at a distance R such that:

$$\frac{G\,M}{R^2} = \frac{G\,M}{r^2} + S_{HC}\,.$$

Then multiplying this expression by $R^2\,r^2$, using $A = G\,M/r^2$ we get:

$$R^2 = r^2\Big(1 + \frac{S_{HC}}{A}\Big)^{-1}\,.$$

Now this result is the exact opposite of MOND interpolation. This is perfect since we work in forces while MOND modifies the dynamics, namely the effective acceleration a but preserves the Newton force. Then reversing the correction, that is conserving the Newton force in r, using MOND concept that is an anomalous acceleration a and notations with $a_0 = S_{HC}$, we get:

$$\mathbf{F} = m\,\mathbf{a}\Big(1 + \frac{a_0}{a}\Big)^{-1}\,, \tag{21}$$

which is the so called "simple" MOND interpolation function. Hence the classical approximation is MOND [4], which is important considering the wide range of effects it predicts that agree with observation.

It shows, rather stunningly, that MOND and GR as it is are not incompatible, but that the former comes naturally as the classical approximation of the latter if we replace the big bang energy emission by a constant feed. Here again there is no need to choose between modified gravity and dark matter particles; we find that both are irrelevant.

3.6 Other consequences

Firstly the theory does not need dark matter particles nor does it accept any. Considering the "energy feed" a good candidate is a continuous scalar field propagating at light speed — and quantum physics live therein; importantly, the existence of such a field is opposite to the very notion of isolated particle. Secondly, all fields known to particles physics take energy at the same source and they do so permanently; unity is there but theories are not unified. Hence, even though it requires an intuitive leap, the consequence is that all parameters of the SM of particle physics reduce to geometry; a geometry which is scale-independent and fits locally and globally with the new theory. Those parameters need to be natural.

4 Conclusions

It is well known that Einstein was influenced by Mach's principle when designing general relativity. In this article, the principle is expressed in the most trivial manner and leads to an extended theory enabling to compute the densities of the matter, dark matter, and dark energy fields of the ΛCDM model. Its classical approximation is MOND which parameter and equation are predicted; it shows that the ΛCDM and MOND are discussing the same physics. This is an enlightening surprise for it shows the irrelevance of discussing modified gravity and dark matter particles. The theory is also instructive as to the structure of space-time and imposes constraints to its evolution, but also to its nature and origin. It refutes the existence of a big bang as a huge and final energy emission — the very first issue in cosmology; instead it provides with a first step toward unity.

Hence, considering those results, we claim the discovery of law of nature that rules gravity and the universe formation, including metric and energy.

A first note [6] on this theory was previously published by the same author. With respect to this note the present paper was written based on minimal hypothesis.

5 Addendum

The new theory implies that an almost empty galaxy will be understood as made of close to 100% dark matter. Here, with an estimate of 98% dark matter, the observations of Dragonfly 44 recently reported by Van Dokkum & al. [2] is an important test because it will be systematic. A similar ratio will be found in any galaxy of this type; in a general manner, the lesser the baryonic mass the higher the ratio of dark matter given by the standard theory.

Submitted on January 24, 2017 / Accepted on January 26, 2017

References

1. The Plank Collaboration. Planck 2015 results. I. Overview of products and scientific results. arXiv: 1502.01582.
2. Van Dokkum, Pieter et al. A High Stellar Velocity Dispersion and ~100 Globular Clusters For The Ultra-Diffuse Galaxy Dragonfly 44. *The Astrophysical Journal Letters*, 2016, v. 828, no. 1.
3. Milgrom M. A modification of the Newtonian dynamics as a possible alternative to the hidden mass hypothesis. *Astrophysical Journal*, 1983, v. 270, 365–370.
4. Milgrom M. MOND theory. (2014), arXiv: 1404.7661v2.
5. Riess A.G., Macri L.M., Hoffmann S.L., Scolnic D., Casertano S., Filippenko A.V., Tucker B.E., Reid M.J., Jones D.O. A 2.4% Determination of the Local Value of the Hubble Constant. (2016), arXiv: 1604.01424.
6. Consiglio J. On the Absorber in Gravitation. *Progress in Physics*, 2016, v. 12(1), 20–25.

On a 4th Rank Tensor Gravitational Field Theory

Patrick Marquet

18 avenue du Président Wilson, 62100 Calais, France
E-mail: patrick.marquet6@wanadoo.fr

In an earlier publication, we showed that a slightly varying cosmological term is a necessary ingredient to restore the true tensor nature of the gravitational field produced by neutral matter. As a result, this term induces a background field filling the entire vacuum. The global energy-momentum tensor of matter and its gravity field is proved to be intrinsically conserved like the Einstein tensor, once it has been identified with the Rosenfeld-Belinfante symmetric tensor. Within the GR representation in the absence of matter, the remnant field never vanishes and we showed that it represents the lower horizon state of the Lorentzian space-time vacuum. In what follows, we work out a 4th rank tensor theory of gravity which formally leads to have the background field superimposed onto the large scale structure of space-time classically described by the de Sitter Universe with a cosmological constant. Our 4th rank tensor theory thus substantiates the recent investigations which would adopt the de Sitter Space-time as a mathematical frame more general that the Minkowski space.

Introduction

By introducing a space-time variable term Ξ that supersedes the so-called cosmological constant Λ in Einstein's field equations, we formally showed that the gravity field of a (neutral) massive source is no longer described by an *ill-defined pseudo-tensor*, but it is represented by a *true canonical tensor* [1]. As a result, the physical space should be always filled with a *homogeneous vacuum background field* [2] which is described by a tensor on the r.h.s. of the Einstein's "source free" equations. Inspection shows that the matter-gravity tensor must be identified with the *Rosenfeld-Belinfante symmetric tensor* [3, 4], thus complying with the intrinsic conservation property of the *Einstein tensor* as it should be. Regarding the *vacuum background field*, it was shown to be a *space-time contraction* unveiling a low horizon state, arising from the geodesics incompleteness postulate [5]. Conversely, it is desirable to analyze the background field nature in the larger scale. To this effect, we suggest here a 4th rank tensor theory based on the full Riemann curvature, and which suitably generalizes the Einstein-Ricci 2nd rank tensor formulation. Unlike many attempts of the kind, our mathematical approach does not trivially entail Einstein GR theory. In fact, due to its peculiar formulation, it leads to view the usual Einstein equations as merely initial conditions following the Cauchy problem.

As will turn out, such a broader theory clearly grants the background field a sound macroscopic meaning. When matter is absent, it closely follows the pattern of the *constant curvature space-time* described by the de Sitter metric when the term Ξ is reduced to the cosmological constant Λ.

In this way, the vacuum background field may be regarded as an intrinsic property of the basic physical structure of our Universe.

Notations

Space-time Greek indices run from $\alpha = \beta$: 0, 1, 2, 3, while spatial Latin indices run from $a = b$: 1, 2, 3. The space-time signature is -2. In the present text, $\varkappa$ is Einstein's constant $8\pi G/c^4 = 8\pi G$ with $c = 1$.

1 The background field and the gravitational field tensor (reminder)

In a pseudo-Riemannian manifold V_4, let us first set the following tensor densities

$$\mathfrak{g}^{\alpha\beta} = \sqrt{-g}\, g^{\alpha\beta}\,, \tag{1.1}$$

$$\mathfrak{G}^{\alpha\beta} = \sqrt{-g}\, G^{\alpha\beta} \ \text{(Einstein tensor density)}, \tag{1.2}$$

$$\mathfrak{G}^{\alpha}_{\beta} = \sqrt{-g}\, G^{\alpha}_{\beta}\,, \tag{1.2bis}$$

$$\mathfrak{R}^{\alpha\beta} = \sqrt{-g}\, R^{\alpha\beta} \ \text{(Ricci tensor density)}. \tag{1.2ter}$$

In density notations, the usual field equations with a massive source then read

$$\mathfrak{G}^{\alpha\beta} = \mathfrak{R}^{\alpha\beta} - \frac{1}{2}\, g^{\alpha\beta}\mathfrak{R} - g^{\alpha\beta}\Lambda\sqrt{-g} = \varkappa\, \mathfrak{T}^{\alpha\beta}, \tag{1.3}$$

where

$$\mathfrak{T}^{\alpha\beta} = \sqrt{-g}\, T^{\alpha\beta}$$

while Λ is the so-called cosmological constant.

However, unlike the Einstein tensor $G^{\alpha\beta}$ which is *conceptually conserved*, the conditions

$$\partial_\alpha \mathfrak{T}^{\alpha}_{\beta} = 0 \tag{1.4}$$

are never satisfied in a general coordinates system [6]. To cure this problem, we have demonstrated once more the conservation condition

$$\partial_\alpha \left[(\mathfrak{T}^{\alpha}_{\beta})_{\text{matter}} + (\mathfrak{t}^{\beta}_{\alpha})_{\text{gravity}} \right] = 0\,, \tag{1.5}$$

but where $(\mathfrak{t}_\alpha^\beta)_{\text{gravity}}$ is no longer a pseudo-tensor density.

To achieve this, we introduced a space-time varying term Ξ in place of the cosmological constant Λ, and whose scalar density is denoted by

$$\zeta = \Xi\sqrt{-g}\,. \tag{1.6}$$

Its variation is given by

$$\zeta = \sqrt{-g}\,\nabla_a\kappa^a = \partial_a\left(\sqrt{-g}\,\kappa^a\right) \tag{1.7}$$

and the term

$$\zeta = \sqrt{-g}\,\nabla_a\kappa^a \tag{1.8}$$

is related to the *vacuum volume expansion scalar* $\theta = \nabla_a\theta^a$ (see [7] for detail).

Such a form allows to maintain the original *Einstein Lagrangian density* as

$$\mathfrak{L}_E = \sqrt{-g}\,g^{\alpha\beta}\left[\left\{{}^{\nu}_{\alpha\beta}\right\}\left\{{}^{\lambda}_{\lambda\nu}\right\} - \left\{{}^{\lambda}_{\alpha\nu}\right\}\left\{{}^{\nu}_{\beta\lambda}\right\}\right], \tag{1.9}$$

the latter expression being used to derive the new canonical gravity tensor attached to a mass:

$$(\mathfrak{t}_\beta^\alpha)_{\text{gravity}} = \frac{1}{2\varkappa}\Big[\left\{{}^{\alpha}_{\gamma\mu}\right\}\partial_\beta\mathfrak{g}^{\gamma\mu} - \\ - \left\{{}^{\gamma}_{\gamma\mu}\right\}\partial_\beta\mathfrak{g}^{\mu\alpha} - \delta^\alpha_\beta(\mathfrak{L}_E - \zeta)\Big], \tag{1.10}$$

ζ can be regarded as a *Lagrangian density* characterizing a specific *vacuum background field* which pre-exists in the absence of matter. Close inspection of equation (1.10) shows that local gravitational field of matter is just a mere "excited state" of the background field. Sufficiently far from the massive source, $(\mathfrak{t}_\beta^\alpha)_{\text{gravity}} \to (\mathfrak{t}_\beta^\alpha)_{\text{background}}$.

2 Symmetrization of the gravity tensor

The tensor density (1.10) includes the *Einstein-Dirac pseudo-tensor density* [8] which is not symmetric.

Symmetrizing the canonical tensor $(\Theta_\beta^\alpha)_{\text{gravity}}$ extracted from $(\mathfrak{t}_\beta^\alpha)_{\text{gravity}} = \sqrt{-g}\,(\Theta_\beta^\alpha)_{\text{gravity}}$ is equivalent to identifying it with the *Belinfante-Rosenfeld tensor*:

$$(t^{\gamma\beta})_{\text{gravity}} = (\Theta^{\gamma\beta})_{\text{gravity}} + \nabla_\alpha\,\Upsilon^{\gamma\beta\alpha} \tag{2.1}$$

with

$$\Upsilon^{\gamma\beta\alpha} = \frac{1}{2}\left(S^{\gamma\beta\alpha} + S^{\beta\gamma\alpha} - S^{\alpha\beta\gamma}\right), \tag{2.2}$$

where the antisymmetric tensor $S^{\alpha\beta\gamma}$ is the contribution of the *intrinsic angular momentum*. Now, we check that:

$$\nabla_\alpha(\Theta_\beta^\alpha)_{\text{gravity}} = \nabla_\alpha(t_\beta^\alpha)_{\text{gravity}} = 0\,. \tag{2.3}$$

Far from matter $(t^{\alpha\beta})_{\text{gravity}} \to (t^{\alpha\beta})_{\text{background}}$ and $\Upsilon^{\alpha\beta\gamma} = 0$. By essence, $(t^{\alpha\beta})_{\text{background}}$ is thus symmetric.

The field equations with a (neutral) massive source together with its gravity tensor can now be explicitly written down

$$G^{\alpha\beta} = R^{\alpha\beta} - \frac{1}{2}\,g^{\alpha\beta}R = \varkappa(T^{\alpha\beta})_{\text{global}}\,, \tag{2.4}$$

where

$$(T^{\alpha\beta})_{\text{global}} = (T^{\alpha\beta})_{\text{matter}} + (t^{\alpha\beta})_{\text{gravity}} \tag{2.5}$$

with, for example $(T^{\alpha\beta})_{\text{matter}} = \rho u^\alpha u^\beta$ (here ρ is the homogeneous mass density).

3 The 4th rank theory of the gravitational field

3.1 The new field equations

We now state that the *true gravitational field equations with a source* are the 4th rank tensor equations

$$G_{\beta\gamma\ \mu}^{\ \alpha} = \varkappa\,T_{\beta\gamma\ \mu}^{\ \alpha}\,, \tag{3.1}$$

where

$$G_{\beta\gamma\ \mu}^{\ \alpha} = R_{\beta\gamma\ \mu}^{\ \alpha} - \frac{1}{2}\,R\left(\delta^\alpha_\gamma g_{\beta\mu} - \delta^\alpha_\mu g_{\beta\gamma}\right) \tag{3.1bis}$$

and

$$T_{\beta\gamma\ \mu}^{\ \alpha} = \delta^\alpha_\gamma(T_{\beta\mu})_{\text{global}} - \delta^\alpha_\mu(T_{\beta\gamma})_{\text{global}} \tag{3.2}$$

is the generalized energy-momentum tensor.

Our assumption can be legitimized by the following considerations. From Bianchi's second identities [9]

$$(s)_{\alpha\beta\gamma}\nabla_\alpha R_{\beta\gamma\lambda\mu} = 0\,, \tag{3.3}$$

where (s) denotes the cyclic sum, we easily infer [10]

$$\nabla_\alpha R_{\beta\gamma\ \mu}^{\ \alpha} = \nabla_\gamma R_{\beta\mu} - \nabla_\mu R_{\beta\gamma}\,, \tag{3.4}$$

hence

$$\nabla_\alpha G_{\beta\gamma\ \mu}^{\ \alpha} = \nabla_\gamma R_{\beta\mu} - \nabla_\mu R_{\beta\gamma} - \frac{1}{2}\,\nabla_\alpha R\left(\delta^\alpha_\gamma g_{\beta\mu} - \delta^\alpha_\mu g_{\beta\gamma}\right) \tag{3.5}$$

i.e.

$$\nabla_\alpha G_{\beta\gamma\ \mu}^{\ \alpha} = \nabla_\gamma R_{\beta\mu} - \nabla_\mu R_{\beta\gamma} - \frac{1}{2}\,\nabla_\gamma R g_{\beta\mu} + \frac{1}{2}\,\nabla_\mu R g_{\beta\gamma}\,. \tag{3.5bis}$$

The right hand side equation is obviously zero, therefore:

$$\nabla_\alpha G_{\beta\gamma\ \mu}^{\ \alpha} = 0\,. \tag{3.6}$$

The tensor

$$G_{\beta\gamma\ \mu}^{\ \alpha} = \delta^\alpha_\gamma R_{\beta\mu} - \delta^\alpha_\mu R_{\beta\gamma} - \frac{1}{2}\,R\left(\delta^\alpha_\gamma g_{\beta\mu} - \delta^\alpha_\mu g_{\beta\gamma}\right) \tag{3.6bis}$$

is thus intrinsically conserved as is the case for the Einstein-Ricci tensor $G_{\beta\mu}$, and we call it the *Einstein 4th rank tensor*.

In addition, we also have:

$$\nabla_\alpha\,T_{\beta\gamma\ \mu}^{\ \alpha} = \nabla_\alpha\left[\delta^\alpha_\gamma(T_{\beta\mu})_{\text{global}} - \delta^\alpha_\mu(T_{\beta\gamma})_{\text{global}}\right] = 0\,. \tag{3.7}$$

Proof:

$$\delta^\alpha_\gamma(T_{\beta\mu})_{\text{global}} = \delta^\nu_\gamma g_{\beta\nu}(T^\alpha_\mu)_{\text{global}} = g_{\beta\gamma}(T^\alpha_\mu)_{\text{global}} \tag{3.8}$$

and since $\nabla_\alpha\,(T^\alpha_\mu)_{\text{global}} = 0$ according to our initial demonstration, then $\nabla_\alpha\left[\delta^\alpha_\gamma(T_{\beta\mu})_{\text{global}}\right] = 0$. The same reasoning holds for $\delta^\alpha_\mu(T_{\beta\gamma})_{\text{global}}$

$$\delta^\alpha_\mu(T_{\beta\gamma})_{\text{global}} = \delta^\nu_\mu g_{\beta\nu}(T^\alpha_\gamma)_{\text{global}} = g_{\beta\mu}(T^\alpha_\gamma)_{\text{global}} \tag{3.8bis}$$

which finally yields (3.7).

Equations (3.6) and (3.7) tell us that the conservation conditions are fully satisfied by the system:

$$G_{\beta\gamma\ \mu}^{\ \ \alpha} = \varkappa\, T_{\beta\gamma\ \mu}^{\ \ \alpha}\,. \tag{3.9}$$

Hence, $T_{\beta\gamma\ \mu}^{\ \ \alpha}$ is confirmed to be the appropriate generalization of the energy-momentum 2nd rank tensor $(T_{\gamma\mu})_{\text{global}}$.

How do the Einstein second rank tensor equations fit in the theory?

3.2 Some hypothesis on the Cauchy problem

Let us consider again (3.1bis) and (3.2)

$$G_{\beta\gamma\ \mu}^{\ \ \alpha} = \delta^\alpha_\gamma R_{\beta\mu} - \delta^\alpha_\mu R_{\beta\gamma} - \frac{1}{2}\, R\left(\delta^\alpha_\gamma g_{\beta\mu} - \delta^\alpha_\mu g_{\beta\gamma}\right),$$

$$T_{\beta\gamma\ \mu}^{\ \ \alpha} = \delta^\alpha_\gamma (T_{\beta\mu})_{\text{global}} - \delta^\alpha_\mu (T_{\beta\gamma})_{\text{global}}\,,$$

and by subtraction we have:

$$\delta^\alpha_\gamma \left[G_{\beta\mu} - \varkappa (T_{\beta\mu})_{\text{global}}\right] - \delta^\alpha_\mu \left[G_{\beta\gamma} - \varkappa (T_{\beta\gamma})_{\text{global}}\right] = 0 \tag{3.10}$$

i.e.

$$P_{\beta\mu} - P_{\beta\gamma} = 0\,. \tag{3.10bis}$$

where $\boldsymbol{P} = \boldsymbol{G} - \varkappa \boldsymbol{T} = 0$ are the Einstein equations with a source which read in mixed indices as:

$$P^\alpha_\beta = 0\,. \tag{3.11}$$

Both relations (3.10bis) and (3.11) then strongly suggest that the Einstein equations $\boldsymbol{P} = 0$ can be regarded as mere initial conditions on a spacelike hypersurface Σ defined on V_4. To see this, consider Σ on which is given $P^\alpha_\beta = 0$, we must show that upon the above conditions, $\boldsymbol{P} = 0$ also holds beyond Σ [11].

For $\beta = 0$ and α reduced to spatial indices $i, k = 1, 2, 3$, equation (3.10bis) can be expressed by

$$P_{0\mu} = P_{0\gamma} \tag{3.12}$$

and (3.11) becomes:

$$g_{00} P^{i0} = -2 g^{i0} P_{00} - g^{ik} P_{k0} \tag{3.12bis}$$

Now, if the hypersurface Σ admits the local equation $x^0 = 0$, we have $g_{00} \neq 0$ which means that $\boldsymbol{P} = 0$ would also hold beyond Σ.

On the hypersurface Σ, the zero initial data require that the system (3.12)–(3.12bis) admits nothing but the zero solution leading to $\boldsymbol{P} = 0$ as well. This is what we wanted to show.

In relation with (3.12), one may regard the equations

$$G_{\beta 0\ \mu}^{\ \ \alpha} - \varkappa \left[\delta^\alpha_0 (T_{\beta\mu})_{\text{global}} - \delta^\alpha_\mu (T_{\beta 0})_{\text{global}}\right] = 0 \tag{3.13}$$

as *constraint equations for the initial data at the time* $x^0 = 0$ which are usually set in the Cauchy problem. For a particular example see [12].

3.3 Newton's law

Let us consider the massive tensor classically expressed by

$$(T^{\alpha\beta})_{\text{global}} = \rho u^\alpha u^\beta + (t^{\alpha\beta})_{\text{gravity}} \tag{3.14}$$

which becomes here

$$T_{\beta\gamma\ \mu}^{\ \ \alpha} = \delta^\alpha_\gamma \left[\rho u_\beta u_\mu + (t_{\beta\mu})_{\text{gravity}}\right] - \\ - \delta^\alpha_\mu \left[\rho u_\beta u_\gamma + (t_{\beta\gamma})_{\text{gravity}}\right]. \tag{3.15}$$

When the spatial 3-velocities are low and the gravitational field is weak, the static case corresponds to the Newton's law for which $u_0 = 1$ in an orthonormal basis. In the framework of our theory, this translates to:

$$G_{0i\ 0}^{\ \ i} = \varkappa\, T_{0i\ 0}^{\ \ i} \tag{3.16}$$

Explicitly: the left hand side is easily shown to reduce to:

$$G_{0i\ 0}^{\ \ i} = R_{00} - \frac{1}{2}\, R g_{00}\,. \tag{3.17}$$

In the same way, the right hand side of (3.16) reduces to:

$$T_{0i\ 0}^{\ \ i} = (\rho + t_{\text{gravity}}). \tag{3.17bis}$$

As usual, we can re-write the field equations as

$$R^0_0 = \varkappa \left[(\rho + t_{\text{gravity}}) - \frac{1}{2}\, \delta^0_0 (\rho + t_{\text{gravity}})\right] \tag{3.18}$$

which eventually yields with the explicit value of the Einstein's constant

$$R^0_0 = 4\pi G (\rho + t_{\text{gravity}})\,, \tag{3.19}$$

where G is Newton's constant.

We then retrieve the *Poisson equation* which is also expressed by:

$$\Delta\psi = 4\pi G \rho'. \tag{3.19bis}$$

We have set: $\rho' = \rho + t_{\text{gravity}}$ because we consider a stationary gravity field (in a general case, the gravity field is "dragged" along with the mass and $\rho' = \rho + t_{\text{gravity}}$ no longer holds). With the metric approximation:

$$g_{00} = 1 + 2\psi\,, \tag{3.20}$$

where ψ is the Newton's gravitational potential

$$\psi = -G \int \frac{\rho'}{R}\, dV\,, \tag{3.21}$$

while R is here the distance from the observer to the volume element dV. Integration is performed over a volume V which comprises both the bare mass and its (stationary) gravitational field.

4 The background field in our Universe

We now come to the persistent field appearing in the 2nd rank tensor field equations when matter is absent. These are

$$G^{\beta\gamma} = R^{\beta\gamma} - \frac{1}{2}\, g^{\beta\gamma} R = \varkappa (t^{\beta\gamma})_{\text{background}} \tag{4.1}$$

with

$$(t_{\alpha\beta})_{\text{background}} = \frac{\Xi}{2\varkappa}\, g_{\alpha\beta}\,. \tag{4.2}$$

Expressed in the framework of the 4th rank tensor theory, this yields:

$$G_{\beta\gamma\ \mu}^{\ \ \alpha} = R_{\beta\gamma\ \mu}^{\ \ \alpha} - \frac{1}{2}\, R\left(\delta^\alpha_\gamma g_{\beta\mu} - \delta^\alpha_\mu g_{\beta\gamma}\right) = \\ = \frac{\Xi}{2}\left(\delta^\alpha_\gamma g_{\beta\mu} - \delta^\alpha_\mu g_{\beta\gamma}\right). \tag{4.3}$$

In virtue of $\nabla_\alpha G_{\beta\gamma\ \mu}^{\ \ \alpha} = 0$, the r.h.s. is conserved:

$$\nabla_\alpha \left[\frac{\Xi}{2}\left(\delta^\alpha_\gamma g_{\beta\mu} - \delta^\alpha_\mu g_{\beta\gamma}\right)\right] = 0\,. \tag{4.3bis}$$

The latter equation is worthy of attention, for the term Ξ never happens to be a constant as could be (ambiguously) the case for $\nabla_\alpha G^{\alpha\beta} = \nabla_\alpha \frac{\Xi}{2} g^{\alpha\beta}$.

This lends support to the fact that only a 4th rank tensor theory can strictly describe a metric with a variable cosmological term. Therefore, after interchanging α with β, we find:

$$G_{\alpha\beta\gamma\mu} = \frac{\Xi}{2}\left(g_{\alpha\gamma} g_{\beta\mu} - g_{\alpha\mu} g_{\beta\gamma}\right). \tag{4.4}$$

The latter equations constitute here the *4th rank tensor background field equations* which characterize the *fundamental structure of physical space-time*.

They adequately generalize the Einstein space endowed with the cosmological constant Λ defined as:

$$G_{\beta\gamma} = R_{\beta\gamma} = \Lambda\, g_{\beta\gamma}\,. \tag{4.5}$$

For a specific value of Ξ, we retrieve the space-time of constant curvature [13], which characterizes the de Sitter Universe when $3\Lambda = R$ [14]:

$$R_{\alpha\beta\gamma\mu} = \frac{R}{12}\left(g_{\alpha\gamma} g_{\beta\mu} - g_{\alpha\mu} g_{\beta\gamma}\right). \tag{4.6}$$

Finally, let us emphasize a major point. In a Universe devoid of matter described by equations (4.4), the Weyl conformal trace-free tensor $C_{\alpha\beta\gamma\mu}$ never vanishes, in contrast to the de Sitter model equipped with curvature (4.6). However, the Weyl tensor being that part of the curvature which is not determined locally by the matter distribution, there is no reason why it should disappear in an "empty" model of space-time. Hence, our approach of a Universe with a pervasive background field proves to be physically consistent for it preserves the Weyl tensor, whatever its content.

So, as expected from our 2nd rank tensor field equations (4.1), the case $G^\alpha_{\beta\gamma\ \mu} = 0$ will never occur.

Conclusion

Our 4 th rank tensor gravitational field theory appears to be the appropriate extension of the 2nd order Einstein-Ricci formulation.

However, it should be noted that the presented theory does not use the well-known *Bel-Robinson tensor* [15] which gave birth to the very thorough paper of *R. Debever* on *Super Energy* [16].

The presented remarkably simple theory is partly inspired from a lecture given by *A. Lichnérowicz* in a Paris seminar dedicated to linearized field quantization solutions prior to their global formulation [17]. We have however substantially modified this theory allowing for a clearer physical significance of the vacuum background field on the very large scale structure of space-time.

Indeed, when matter is absent, the intrinsic curvature of space-time is modeled by the background field through its variable term Ξ, just as de Sitter's empty Universe does with its cosmological constant Λ arbitrarily introduced.

Such a close similarity with the de Sitter curvature should not come as a surprise. The de Sitter metric recently saw some revived interest among several physicists [18–20]. They conjectured that the laws of physics are invariant under the symmetry group of de Sitter space (*maximally symmetric* space-time), rather than the Poincaré group of special relativity. The full Poincare group is the semi-direct product of translations $\mathbf{T}$ with the Lorentz group $\mathbf{L} = \mathrm{SO}(3,1)$: $\mathbf{P} = \mathbf{L} \otimes \mathbf{T}$. The latter acts transitively on the *Minkowski space* $\mathbf{M}$ which is homogeneous under $\mathbf{P}$.

In the framework of a generalized group where translations mix up non trivially with rotations, the requirements of homogeneity and isotropy lead ipso facto to the de Sitter Universe with a uniform scalar curvature. More specifically, the de Sitter space whose metric is induced from the pseudo-Euclidean metric $(+1,-1,-1,-1,-1)$ has a specific group of motion which is the pseudo-orthogonal group SO(4, 1) [21]. Then, de Sitter group obviously involves an additional length parameter l which is related to the (positive) cosmological term by:

$$\Lambda = \frac{3}{l^2}\,.$$

The *Poincaré group* "contracts" to the *Galilean group* for low velocities.

Analogously the *de Sitter group* "contracts" to the *Poincaré group* for short distance kinematics, when the order of magnitude of all translations are small compared to the de Sitter radius. (See: Wigner and Inönü, for the group contraction concept [22]). These distances are probed by high energies meaning that quantum effects must be taken into account. In that case, when we have $\Lambda \to \infty$, this would correspond to $\Lambda_P = 3/l_P^2$, where l_P is the Planck length. If $\Lambda \to 0$, however, the underlying space-time would reduce to the Minkowski space.

From the fundamental vacuum field equations (4.4), the variable term Ξ would represent a fluctuation between two appropriate values of Λ wherein the de Sitter space-time can be fully represented. In this view, the 4th rank tensor field equations are to the de Sitter space-time, what the 2nd rank tensor field equations are to the Minkowski space.

Submitted on January 20, 2017 / Accepted on January 25, 2017

References

1. Marquet P. The gravitational field: a new approach. *Progress in Physics*, 2013, v. 9, issue 3, 62–66.
2. Marquet P. Vacuum background field in General Relativity. *Progress in Physics*, 2016, v. 12, issue 4, 314–316.
3. Belinfante J. *Physica*, 1939, v. 6, 887.
4. Rosenfeld L. Sur le tenseur d'Impulsion-Energie. *Acad. Roy. de Belgique* (*Mémoires de Classes de Sciences* 18), 1940.
5. Marquet P. Some insights on the nature of the vacuum background field in General Relativity. *Progress in Physics*, v. 12, issue 4, 366–367.
6. Landau L. and Lifshitz E. The Classical Theory of Fields. Addison-Wesley, Reading (Massachusetts), 1962, p. 402 (French translation).
7. Straumann N. General Relativity and Relativistic Astrophysics. Springer-Verlag (Berlin), 1984, p. 159.
8. Dirac P.A.M. General Theory of Relativity. Princeton University Press, 2nd edition, 1975, p. 61.
9. Hawking S.W., Ellis G.F.R. The Large Scale Structure of Space time. Cambridge University Press, 1987, p. 62.
10. Lapiedra R. Sur les équations d'ordre supérieur du champ gravitationnel. *Annales de l'IHP*, section A, 1969, t. 11, 277–307.
11. Lichnérowicz A. Propagateurs. Quantification du Champ. *Séminaire Janet*, 1960, no. 4, 3ème année.
12. Choquet-Bruhat Y., York J.W. Jr. Well posed reduced systems for the Einstein equations. arXiv: gr-qc/9606001.
13. Kramer D., Stephani H., Hertl E., MacCallum M. Exact Solutions of Einstein's Field Equations. Cambridge University Press, 1979, p.101.
14. de Sitter W. On the curvature of space. *Proc. Roy. Acad. Sci. Amsterd.*, 1917, v. 20, 229–243.
15. Bel L. Introduction d'un tenseur du 4ème ordre. *Comptes rendus hebdomadaires des Séances de l'Académie des Sciences*, 1956, t. 248, 1297.
16. Debever R. Super-energy in General Relativity. *Bull. Soc. Math. Belg.*, 1958, v. 10, 112–147.
17. Lichnérowicz A. Propagateurs et commutateurs en Relativité Générale. *Institut des Hautes Etudes Scientifiques*, *Publications mathématiques*, 1961, no. 10.
18. Aldrovani R., Beltran Almeida J.P., Pereira J.G. Some implications of the cosmological constant to fundamental physics. arXiv: gr-gc/0702065.
19. Bacry H., Levy-Leblond J.M. *Journal of Mathematical Physics*, 1968, v. 9(10), 1605.
20. Lev F.M. de Sitter symmetry and quantum theory. arXiv: 1110.0240.
21. Aldrovani R., Beltran Almeida J.P., Pereira J.G. de Sitter special relativity. arXiv: gr-gc/0606122.
22. Inönü E., Wigner E.P. *Proc. Natl. Acad. Scien.*, 1953, v. 39, 510.

Optimizing the Teflon Thickness for Fast Neutron Detection Using a Ge Detector

Sylvian Kahane[1] and Raymond Moreh[2]

[1]P.O. Box 1630, 84965, Omer, Israel. E-mail: sylviankahane@gmail.com
[2]Department of Physics, Ben-Gurion University, 84120, Beer-Sheva, Israel. E-mail: moreh@bgu.ac.il

The optimum Teflon $(C_2F_4)_n$ thickness for fast neutron detection through the ^{19}F(n,α)^{16}N reaction was calculated and found to be $\approx$ 5.0 cm. Here, the 6.13 MeV γ ray emitted by ^{16}N is assumed to be detected by a Ge diode. The geometry of the system is discussed and the γ line intensity was found to vary weakly with Teflon thickness.

1 Introduction

Several methods are used in the literature for fast neutron detection. Among those methods are: (1) the detection of protons recoiling from the impinging neutrons [1], (2) the use of plastic and liquid scintillators [2], (3) the use of Gd-loaded liquid scintillators [3], (4) ^{3}He gas-filled detectors can be used for both neutron detection and spectroscopy measurements [4], (5) Semiconductor-based neutron detectors [5]. In other methods the neutrons are first moderated to thermal velocities then captured using BF_3 detectors via the ^{10}B(n,α)^{7}Li reaction [6]. In addition, fast neutron detection often relies on neutron induced nuclear reaction.

The topic of the present work is the use the ^{19}F(n,α)^{16}N reaction [7] to detect fast neutrons with energies $E_n > 3$ MeV. This may be done by holding Teflon $(C_2F_4)_n$ in close vicinity to a Ge gamma detector. When the Teflon is hit by fast neutrons it forms ^{16}N; it is a β emitter (τ = 7.2 s) proceeding to an excited state in ^{16}O (68%) which emits a 6.13 MeV photon. This can readily be measured using a Ge detector. Teflon is a combination of 24.0% C and 76.0% F (by weight), with a density of 2.2 g/cc [8]. Note that because of the high gamma energy emitted by ^{16}O, it is easily visible above background and may be viewed as an excellent finger print of fast neutrons. The ^{19}F(n,α)^{16}N reaction is endothermic with $Q = -1.52$ MeV and because of the Coulomb barrier viewed by the emitted α–particles, a non-zero yield is obtained only for $E_n > 3$ MeV.

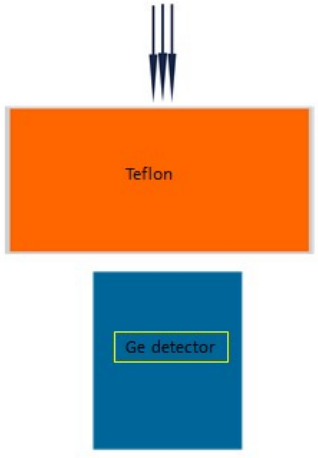

Fig. 1: A pencil neutron beam is hitting few cm thick Teflon absorber, at 5.0 mm above a ϕ 64×90 mm Ge coaxial detector, placed in a 1 mm thick Aluminum case (not shown).

In the past, this reaction was discussed in some detail for the detection of fast neutrons [7] where a Teflon cup covering a 30 cc Ge(Li) diode was used to detect the 6.13 MeV photon. Our interest here is to calculate the optimum thickness of the Teflon covering a pure Ge detector.

We use the simple geometry described in Fig. 1. The present calculation includes two representative Ge detector volumes: 100 cc, and 300 cc. In Fig. 1 the neutron beam is assumed to be mono-energetic with E_n = 5 to 11 MeV, hitting the Teflon in a normal direction (shown by the arrows), or embedded in a neutron field of uniform flux. Results were obtained also for a fission neutron spectrum having a Watt shape.

2 Simulations

The goal of the simulations is to "measure" the response of a Ge detector to the gamma rays induced by incoming neutrons on a Teflon shield, 5 mm above the detector, placed in an Aluminum cover, Fig. 1. This is calculated as a function of the Teflon thickness. We are especially interested in the β decaying ^{16}N nuclei proceeding to the excited level in ^{16}O emitting the 6.13 MeV γ line. The incoming neutron undergoes nuclear reactions with the Fluorine nuclei producing ^{16}N by ^{19}F(n,α) and ^{15}N by ^{19}F(n,α+n) respectively. ^{15}N is stable with no further decays or γ rays. The respective cross sections, from Janis [9], are shown in Fig. 2.

It can be seen that the first reaction has a non-zero cross section at a threshold of 3 MeV while the threshold of the second is 5 MeV. The simulations proceed in two steps, one for neutrons and one for gammas. The neutron simulation "measures" the production yield of the ^{16}N nuclei in Teflon cylinders of different thicknesses. The gamma simulations "measure" the actual detector response to the 6.13 MeV γ produced in the same Teflon cylinders. A convolution of the two results produces the response of the detector, per neutron, as a function of the Teflon thickness.

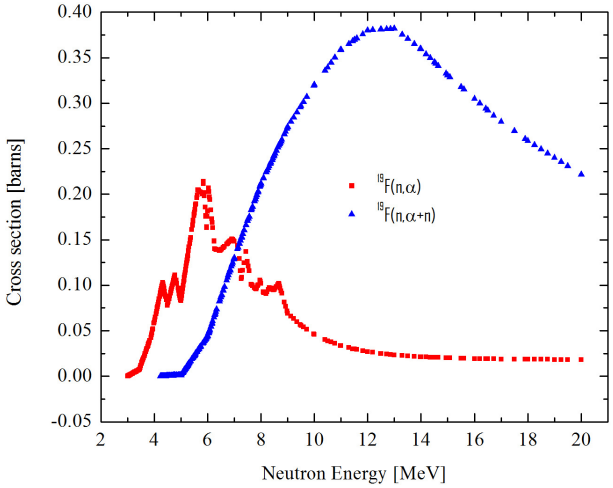

Fig. 2: The cross sections of the ^{19}F(n,α) and ^{19}F(n,α+n) reactions taken from the Japanese cross sections library JENDL-4.0.

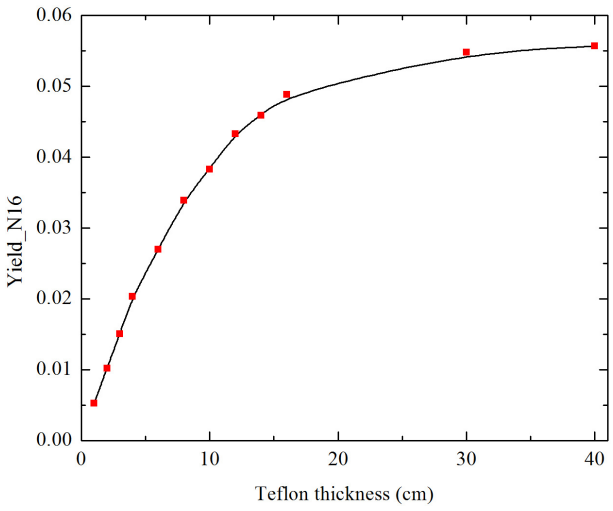

Fig. 3: Calculated yield of ^{16}N nuclei as a function of Teflon thickness obtained by assuming a neutron pencil beam of E_n = 5 MeV. The line is only a guide to the eye.

2.1 Neutrons

Two different geometries were employed: in one a monoenergetic and monodirectional pencil beam of neutrons impinges on a cylindrical Teflon sheet placed above the Ge detector, Fig. 1; in the second, the same Teflon cylinder, is placed in a "bath" of monoenergetic neutrons, simulating a uniform neutron field. The number of ^{16}N nuclei produced is counted and normalized to the number of neutrons used in the simulation. For the present purpose this quantity is called *Yield–^{16}N* which is the γ–source of interest. It increases with Teflon thickness reaching a saturation which depends on the extent of neutron absorption (Fig. 3). The statistical error in this Monte Carlo calculations is less than 1%, using 10^6 neutrons

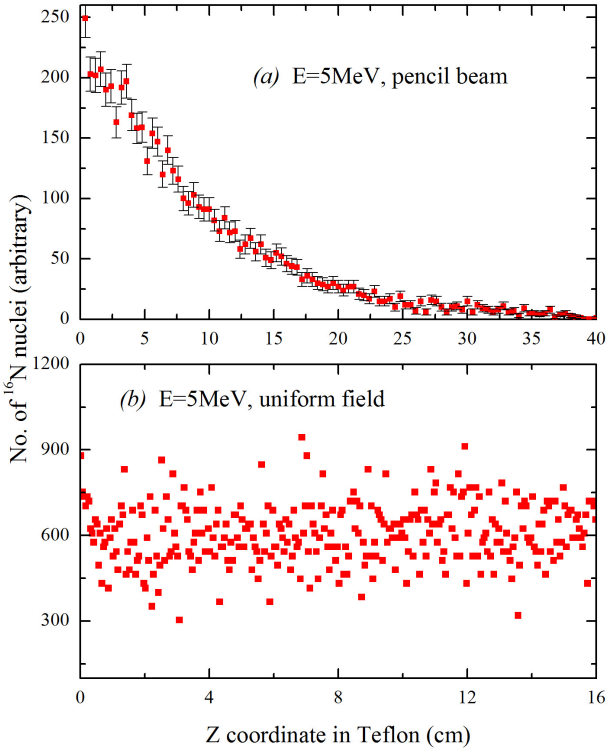

Fig. 4: The distribution of the ^{16}N nuclei along the z axis of the Teflon cylinder for two cases: (a) pencil beam and (b) uniform flux. In the second case the standard deviation is larger (17%) but the distribution is undoubtedly uniform.

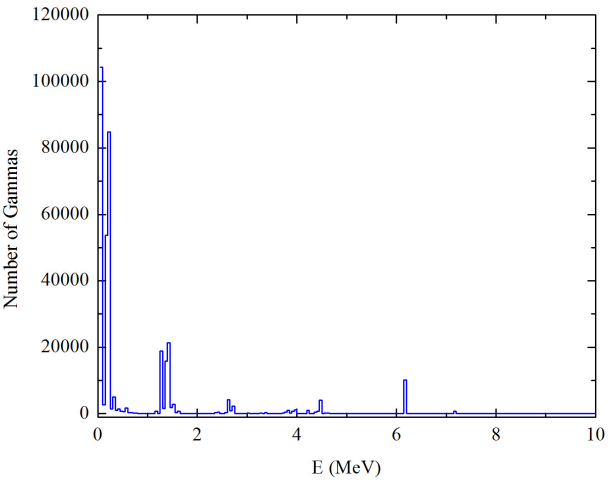

Fig. 5: Energies of the gammas produced in Teflon by 5 MeV neutrons. The gammas at 6.13 MeV are free of any interference.

for the case of a pencil beam and 4×10^6 for an uniform flux of neutrons.

Additionally, we calculated the distribution of the ^{16}N nuclei along the z axis of the Teflon cylinders (taken to be along the direction of the normal). Obviously, in the case of a uni-

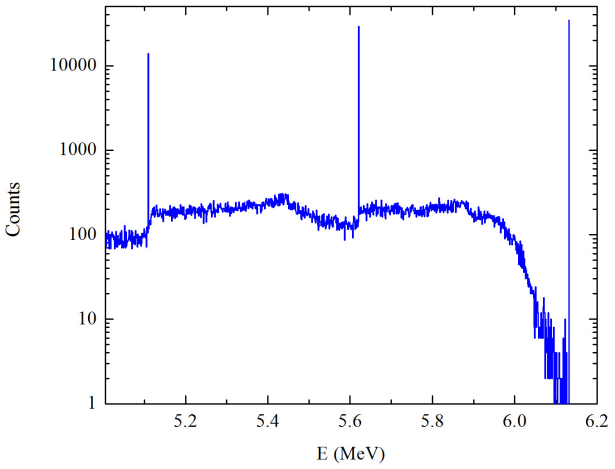

Fig. 6: Calculated spectrum in the 300 cc detector from a Teflon shield of 5cm.

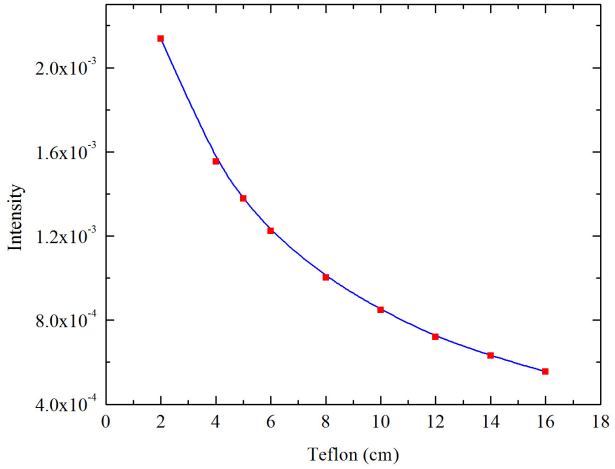

Fig. 7: Photopeak (6.13 MeV) intensity as a function of the Teflon thickness, calculated for the 100 cc detector.

form neutron field this distribution is also uniform, but in the case of a pencil beam the nuclei density is highest at the beam entrance, Fig. 4.

2.2 Technical details

The neutron simulations were performed with Geant4 [10]. This platform was chosen because it produces a plethora of ions in Teflon, both by nuclear reactions and by radioactive decay. An example is given in Tab. 1.

The kinetic energies of the *C*- and *F*–ions appearing in the table are acquired via elastic and inelastic neutron scattering. The number of α's is equal to the sum of ^{15}N and ^{16}N ions. The total number of gammas (1.4×10^6) is far larger than the ones at 6.13 MeV (4×10^4), but most of the gammas have low energies < 0.3 MeV (Fig. 5) and do not interfere with the measurements. The Geant4 system offers many options concerning the exact physics to be used in the simulations. We borrowed the detailed physics which appears in the example Hadr06 (/examples/extended/hadronic) found in its distribution. It employs high precision (HP) neutron physics i.e. uses actual neutron cross sections, for neutrons under 20 MeV, and not models, standard electromagnetic physics, radioactive decay and ion physics based on the internal models used by Geant4. Furthermore, the new neutron cross sections, developed by Mendoza and Cano-Ott [11], based on ENDF-VII, were adopted.

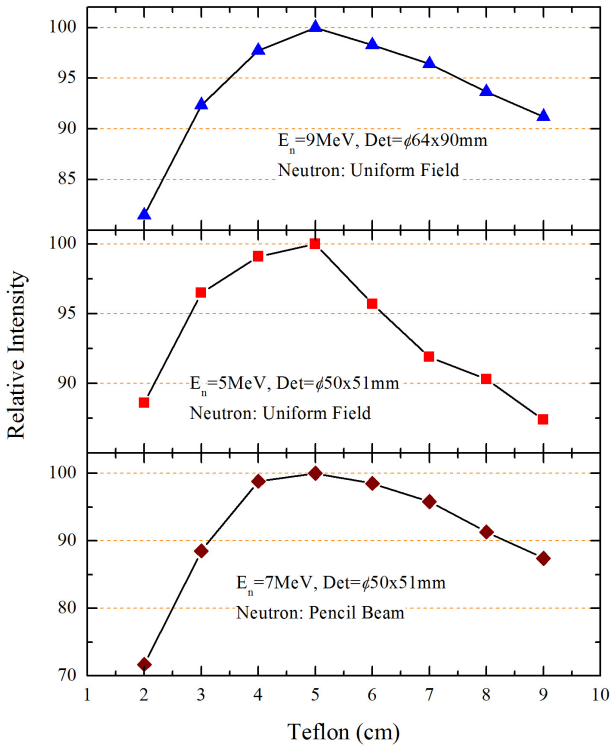

Fig. 8: Relative intensities versus Teflon thickness for various neutron energies and different Ge volumes. Some input data are listed in the figures.

2.3 Gammas

Here, the Teflon cylinder acts as a volume source. The exact departing point of each gamma is sampled in this volume, uniformly in the radial direction, and according to the distributions of Fig. 4 in the z direction. The statistical error is negligible. The simulations were carried out for two detector volumes: 100 cc (ϕ 50×51 mm), and 300 cc (ϕ 64×90 mm). These dimensions correspond to one of our detectors (100 cc) or taken from the ORTEC catalog (300 cc). The spectrum of the energy deposition is calculated by assuming no broadening, i.e. with zero energy resolution, in 1 keV bins (Fig. 6). This is because we did not compare to an actual measured spectrum but are interested only in the relative peak intensities.

Table 1: Number of ions produced in Teflon by a uniform neutron field of 5 MeV (4×10^6 neutrons). The numbers in square brackets are the energies of excited levels in keV, i.e. ^{19}F [1554.0] stands for the 1554.0 keV level of ^{19}F.

Ion	Numbers produced	Mean Energy
^{12}C	559603	436.0 keV
^{13}C	5907	404.1 keV
^{19}F	1414198	267.8 keV
^{19}F [109.9]	46	60.9 eV
^{19}F [1554.0]	1033	217.1 eV
^{19}F [197.1]	1884	224.2 eV
^{19}F [2779.9]	1	72.1 eV
^{19}F [4377.7]	1	11.2 eV
^{20}F	77	188.3 keV
^{15}N	294	535.9 keV
^{16}N	60366	891.2 keV
^{20}Ne	77	71.7 eV
^{20}Ne [1633.7]	77	487.1 eV
^{16}O	60364	1.6 keV
^{16}O [6049.4]	9	387.2 eV
^{16}O [6129.9]	40378	427.6 eV
^{16}O [6917.1]	22	128.20 eV
^{16}O [7116.9]	3037	260.8 eV
^{16}O [8871.9]	614	70.9 eV
^{19}O	2025	294.2 keV
α	60660	2.38 MeV
anti-ν_e	62466	3.14 MeV
e+	2786	2.00 MeV
e-	2030049	186.6 keV
γ	1416604	707.0 keV
Neutron	564213	2.72 MeV
Proton	2025	673.2 keV

The peak intensities are normalized per one gamma at source. As a function of the Teflon thickness it is a descending plot (less Teflon, less absorption) – Fig. 7. In order to obtain the intensities per neutron one has to multiply by the number of gammas found at a given Teflon thickness, this is what we called *Yield-*^{16}N, in Fig. 3. One of the graphs is going up (Fig. 3) and one is going down (Fig. 7), hence a maximum appears at a point corresponding to the optimum thickness – Fig. 8.

We sought the optimum with a resolution of 1 cm. We obtained a thickness of 5 cm for this optimum, for both detectors, for both neutron fields and for all the energies studied (between 5 to 11 MeV).

Fig. 8 presents the obtained intensities as percentage points where the optimum is 100%. Data come from the first escape (FE) peak in the case of the 100 cc detector and from the photopeak in the case of the 300 cc detector. While the optimum is well defined it is not very sharp, Fig. 8 shows that there are additional values, for the Teflon thickness, which differ from the optimum by only few percent. An interesting point in the results of the calculations is that the optimum thickness is sensitive neither to the incident neutron energy (in the energy range of our calculations) nor to the size of the detector. It may be seen that by varying the Teflon thickness between 4 to 6 cm, the counting rate of the detector varies by few percent only. In general, it can be said that the range 4–6 cm for Teflon will provide equally good counting results in an actual measurement. Even when using a much thinner Teflon of 2 cm we are within 15% from the optimum (in the uniform field case).

2.4 Fission like neutron spectrum

In the vicinity of nuclear reactors or a ccelerators there are non monoenergetic neutron fields. For nuclear reactors one can assume a fission like uniform Watt spectrum:

$$f(E) = \exp(-E/0.965) \times \sinh(2.29 \times E). \quad (1)$$

With the parameters taken from the defaults given in the MCNP manual [12] (the units are MeV for the first parameter and MeV^{-1} for the second). Obviously, because we obtained a flat value of 5 cm for all the energies of interest in the Watt spectrum, the optimum value for a reactor spectrum will be also 5 cm.

2.5 Other details

The simulations for the gammas were done with the MCNP program [12]. In principle, they can be done also by using Geant4 but with greater effort. Geant4 is a library and the user has to possess considerable programming skills in order to build a running program. MCNP is a closed, tested program and the user has to provide only the input data.

3 Conclusions

As may be seen from the above, the Teflon thickness yielding the optimum intensity of the 6.13 MeV γ line is $\approx$ 5.0 cm. It is surprising to see that this thickness is almost independent on the volume of the Ge detector, on the incident neutron energy (in the range studied) and on the direction of incidence of the neutrons.

Acknowledgements

One of us (R.M.) would like to thank Y. Ben-Galim for help in the initial stages of this work.

Submitted on February 11, 2017 / A ccepted on February 17, 2017

References

1. Shultis J. K., McGregor D. S. Efficiencies of coated and perforated semiconductor neutron detectors. *IEEE Trans. Nucl. Sci.*, 2006, v. 53, 1659.
2. Knoll G. F. Radiation Detection and Measurement. John Wiley & Sons, New York, 2010.

3. Kapoor S. S., Ramamurthy V. S. Nuclear Radiation Detectors. New Age International, New Delhi, 1986.
4. Tsoulfanidis N., Landsberger S. Measurement and Detection of Radiation, 4th Edition. CRC Press, Boca Raton, 2015.
5. Hussein E. M. Handbook on Radiation Probing, Gauging, Imaging and Analysis: Volume I. Kluwer Academic Publishers, New York, 2004.
6. Ben-Galim Y., Wengrowicz U., Moreh R., Orion I., Raveh A., Using the Doppler broadened γ line of the ^{10}B(n,$\alpha\gamma$)^{7}Li reaction for thermal neutron detection. *Nucl. Inst. Meth. Phys. Res. A*, 2016, v. 810, 140–143.
7. Wolf A., Moreh R., Utilization of Teflon covered Ge(Li) diodes for fast neutrons detection. *Nucl. Inst. Meth.*, 1978, v. 148, 195–197.
8. http://physics.nist.gov/cgi-bin/Star/compos.pl?matno=227.
9. https://www.oecd-nea.org/janis.
10. Agostinelli S. *et al*. Geant4 — a simulation toolkit. *Nuc. Inst. Meth. Phys. Res. A*, 2003, v. 506, 250–303.
11. https://www-nds.iaea.org/geant4.
12. Briesmeister J. F. MCNP-A General Monte Carlo N-Particle Transport Code. Technical Report LA-13 709-M, Los Alamos National Laboratory, NM, USA, 2001.

The Newtonian Constant G and the Einstein Equations

Bernard G. Colenbrander and Willem S. Hulscher

E-mail: b.g.colenbrander@gmail.com

The measurement of the Newtonian constant of gravitation G is in an impasse because most results deviate from the average value more than 10 times their estimated measurements uncertainties. Via the Einstein field equations G is related to the cosmological constant Λ and because normal matter, dark matter and dark energy must add up to 100%, Λ is a measure for dark energy. So it follows that G is related to dark matter. The density of the dark matter halo around the earth is influenced by the gravitational attraction of the earth and because the earth is not a perfect sphere, the halo varies along the surface. So we expect a variation of dark matter density with the gravitational acceleration g. These variations in dark matter affect G and indeed we have found a correlation between the constant G and the local value of the gravitational acceleration g.

1 Introduction

The gravitational constant G is commonly measured by using a torsion balance suspended by a wire as has been introduced by Cavendish. The plane of the rotating masses is positioned exactly horizontal and therefore the influence of local gravity variations is supposed to be negligible. However, the horizontal attraction force between the test masses in the apparatus is not only governed by these masses and their distance, but also by the local density of dark matter. We accept that gravitational attraction forces are influenced by dark matter and the local density of dark matter will vary with the local mass variations of the earth. So we expect a correlation between G and the gravitational acceleration g.

2 The correlation between G and g

In the following analyses 16 values of G recommended by CODATA in the period 1999-2014 [1, 2, 3] are represented, as they were measured by 9 institutes. The values of the gravitational acceleration g at 8 different locations are calculated by the website Wolfram Alpha. This calculation method is based on the Earth Gravitational Model, EGM 2008. It is noted that Uci-14 has not been measured at Irvine, California but near Handford, Washington [4].Therefore the value of g is calculated for the nearby city Richland.

Furthermore, the g value of Florence was measured in situ with the Atom Interferometer by the group of Tino [5, 6].

The analysis results in the following table and Figure 1.

G is the gravitational constant in 10^{-11} $m^3kg^{-1}s^{-2}$ and the last column in the table shows the standard uncertainty u of the measured value of G.

The graph shows a correlation of the gravitational constant G with the gravitational acceleration g according to the best-fit linear regression line, having a slope of 0.1371 and the coefficient of determination $R^2 = 0.6323$.

Obviously this effect also results in a dependency of G on the geographical latitude on the earth, as shown in Figure 2.

From 1999 onwards the measured values of G seem to be more reliable than before, so we have included only the values from the year 1999 and after. Where CODATA replaces old measured values by later measurements from the same institute, we have included all values measured in the named

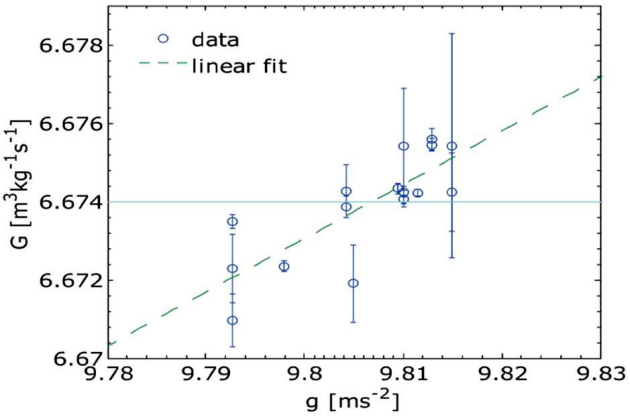

Fig. 1: Correlation of the gravitational constant G with the gravitational acceleration g. G = 0.1371 g + 5.328; R^2=0.6323.

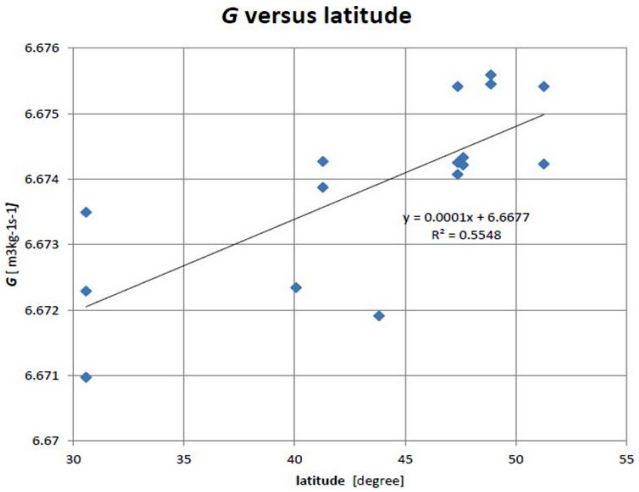

Fig. 2: Dependency of G on the geographical latitude.

Table 1: The 16 values of G recommended by CODATA in the period 1999-2014.

g -	G $\times 10^{-11}$	Institute -	Location -	Latitude Degree	std $\times 10^{-11}$
9.7927	6.67097	hust 99	Wuhan	30.58	0.00067
9.7927	6.67229	hust 05	Wuhan	30.58	0.00087
9.7927	6.67349	hust 09	Wuhan	30.58	0.00018
9.79795	6.67234	jila 010	Boulder	40.07	0.00014
9.80422	6.67427	msl 99	New Zeland	41.28	0.00067
9.80422	6.67387	msl 03	New Zeland	41.28	0.00027
9.80492	6.67191	lens 14	Florence	43.82	0.00099
9.80943	6.67433	uci 14	Richland	47.62	0.00013
9.81007	6.67542	uzur 99	Zurich	47.37	0.00147
9.81007	6.67407	uzur 02	Zurich	47.37	0.00022
9.81007	6.67425	uzur 06	Zurich	47.37	0.00013
9.81145	6.67422	uwash 00	Seattle	47.62	0.00009
9.81289	6.67559	bipm 01	Paris	48.87	0.00027
9.81289	6.67545	bipm 13	Paris	48.87	0.00016
9.81498	6.67542	uwup 99	Wuppertal	51.26	0.00287
9.81498	6.67423	uwup 02	Wuppertal	51.26	0.00100

period. The horizontal line in the graph at G = 6.674×10^{-11} $m^3kg^{-1}s^{-1}$ represents the average value calculated by CODATA in the year 2010. However, the correlation between G and g as we have found, renders it not useful to calculate an average value for G.

3 Further measurements

It has been raised by Quinn [7] that the Newtonian constant may be too difficult to measure, as the measured values spread 10 times more than the uncertainties of most measurements. However, we maintain that the problem is not the difficulty of the measurement but ignorance about the correlation of G and g.

Further compelling evidence for the named correlation can be obtained by doing several measurements with one and the same apparatus at different locations. Then the measured values can be compared better, because their accuracy is the same and no differences occur due to different measuring methods and different devices. It is also necessary to measure g in situ instead of calculating that value. More clarity can be obtained by taking additional measurements at places where g has an extreme value, for instance far away from the equator (e.g. at Helsinki) and nearby (e.g. at Quito). The group of Tino [5, 6] has developed a small apparatus based on atom interferometry. Such apparatus would be quite suitable for measuring both G and g.

4 Conclusion

Our analysis shows a correlation between G and g. This correlation suggests that the value of G depends on the place where it is measured, and thus G is not a universal constant of nature.

5 Appendix

The original Einstein field equations are:

$$R_{\mu\nu} - \frac{1}{2}Rg_{\mu\nu} = \frac{8\pi G}{c^4}T_{\mu\nu}.$$

The right hand part of the equation is the energy/momentum tensor and governs the curvature of space-time. The left hand part describes the measure of this curvature.

This set of equations generates no stationary solution, and therefore Einstein made a correction by adding an extra term with the cosmological constant Λ. The corrected field equations are:

$$R_{\mu\nu} - \frac{1}{2}Rg_{\mu\nu} + \Lambda g_{\mu\nu} = \frac{8\pi G}{c^4}T_{\mu\nu}$$

which can generate a stationary solution by inserting a suitable value for Λ.

At the end of the 20th century dark matter and dark energy were introduced in order to understand the uneven expansion of the universe and since then Λ is considered to be a measure of dark energy. When dark energy dominates dark matter, there is an accelerated expansion of the universe, and when dark matter dominates, the expansion is decelerated.

The cosmological constant Λ is linked to the gravitational constant G by the corrected field equations of Einstein. At the same time dark energy, dark matter and normal matter must add up to 100%. So dark energy and dark matter are dependent. In the field equations Λ and G are dependent as well. This means that we can rewrite the corrected field equations in the original form, without Λ, realizing that G depends on place and time. The field equations then become:

$$R_{\mu\nu} - \frac{1}{2}Rg_{\mu\nu} = \frac{8\pi G(r,t)}{c^4}T_{\mu\nu}.$$

Submitted on January 27, 2017 / Accepted on January 27, 2017

References

1. Mohr P.J. and Taylor B.N. CODATA recommended values of the fundamental physical constants: 2002.
2. Mohr P.J., Taylor B.N. and Newell D.B. CODATA recommended values of the fundamental physical constants: 2006.
3. Mohr P.J., Taylor B.N. and Newell D.B. CODATA Recommended Values of the Fundamental Physical Constants. arXiv: 1203.5425v1 [physics, atom-ph] 24 Mar 2012.
4. Schlamminger S., Gundlach J.H. and Newman R.D. Recent measurements of the gravitational constant as a function of time. *Phys. Rev. D*, 2015, v. 91, 121101(R).
5. Rosi G., Sorrentino F., Cacciapuoti L., Prevedelli M. and Tino G.M. *Nature*, 2014, v. 510, 518–521.
6. De Angelis M., Greco F., Pistorio A., Poli N., Prevedelli M., Saccorotti G., Sorrentino F. and Tino G.M. *Eur. Phys. J. Plus*, 2012, v. 127, 27.
7. Quin T. and Speake C. The Newtonian constant of gravitation - a constant too difficult to measure? An introduction. *Phil. Trans. R. Soc. A*, 2014, v. 372, 20140253.

Null Result for Cahill's 3-Space Gravitational Wave Experiment with Zener Diode Detectors

Wolfgang Baer[1], Eric Reiter[2], Harry Jabs[3]

[1]Nascent Systems Inc., 380 W Carmel Valley Rd., Carmel Valley, CA 93924 , USA, wolf@NascentInc.com
[2]Unquantum Lab, 251 Nelson Avenue, Pacifica, CA 94044, USA, unquant@yahoo.com
[3]Institute for Frontier Science, 6114 LaSalle Avenue, no. 605, Oakland, CA 94611, USA, harryjabs@yahoo.com

Zener diode detectors have been reported to show correlated current output related to the absolute motion of the earth through space [1–4]. Such reports are of utmost importance since it would contradict the Michelson-Morely experiments, the basis of Special Relativity, and connect the randomness of quantum theory with gravitation. Experiments designed to reproduce the reported effects have not seen the reported wave form output or any correlation between Zener diode detectors. Instead we found no detectable signal could be discerned above the noise floor of the digital storage scopes themselves. This does not mean the Cahill's space flow effect does not exist, however the methods reported in the literature do not describe equipment that reproduced the reported measurements.

1 Introduction

Experimental detection of space inhomogeneities flowing at approximately 500 km/sec in the direction of the constellation Vega has been reported [1–3]. Two Zener Diode detectors were oriented in inertial space so that the flow passing first through one detector and subsequently the second detector would produce correlated current output.

A diagram showing a single detector and its circuit diagram copied from reference [1] is shown in Figure 1. The voltage V across the resistor is used to determine the turbulent space flow driven fluctuating tunneling through the Zener diodes. Two such detectors are placed next to each other as shown in Figure 2.

At the bottom of the detector boxes a coaxial cable is shown which in the original experiment connected to a LeCroy Waverunner 6051A 500 MHz, 2 channel 5 Gs/sec Digital Storage Oscilloscope (DSO), which was used to record and display the two resistor voltage measurements. Correlated voltage from the two collocated detectors reported in reference [1] and [2] are shown in Fig 3.

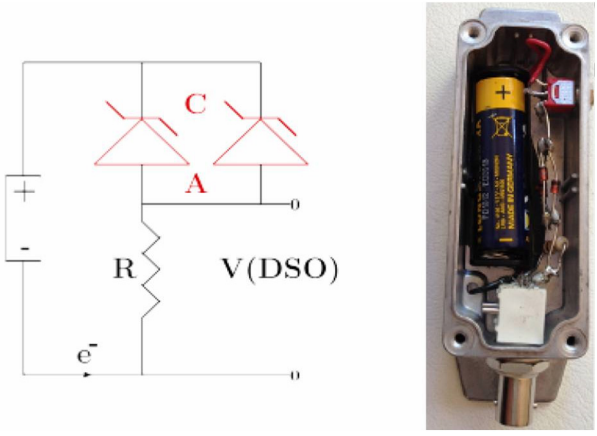

Fig. 1: Left: Circuit of Zener Diode Space Flow Detector, showing a 1.5 V AA battery, two 1N4728A Zener diodes operating in reverse bias mode, having a Zener voltage of 3.3 V, and resistor R=10 kΩ [2].

A clear correlation is indicated by the wave forms of approximately 200 MHz along with some noise. A similar diagram with the two wave forms 180° out of phase was reported when the alignment of the two detectors was reversed so that one coaxial lead came out the top while the second one came out the bottom.

The correlation presumed by R. Cahill is due to structure in the flow which passed through each diode in the detectors. When the detectors were separated by 25 cm and aligned in direction RA=5 h, Dec=-80 deg similar correlation diagrams were shown but required a delay of 0.48 μs to compensate for the flow speed estimated to be 520 km/s from these measurements.

The simplicity of the detectors and the obvious correlated wave forms along with the enormous significance of these

Fig. 2: Two collocated detectors.

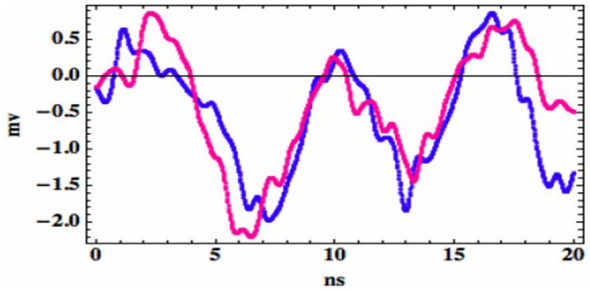

Fig. 3: Correlated current fluctuations as indicated by voltage across resistor R and with DSO operated with 1 MΩ AC input, and no Filters.

reported experiments encouraged us to attempt a verification experiment.

2 Initial verification experiment

The straight forward verification of the Space Flow Detectors was a simple experiment which consisted of building two Space Flow Detectors, connect their two channels to a DSO, move the detectors around a Southerly direction and watch the sum and difference signals on the screen. A qualitative indicator of signal correlation would show a small difference reading for the difference display and relatively large amplitudes in the sum display. Such oscilloscope comparisons are easy to make, and if seen would be the initial indicator that the equipment was functioning properly and the hoped for space flow could be measured.

The initial work was done in E. Reiter's lab. Figure 4 shows the two detectors. Each one has two Zener Diodes closely packed together. The bottom metal square shows the coaxial cable connection. In the left corner the metal shielding tube can be seen. In operation the detectors are completely encased in metal shielding so any external electromagnetic signals would be attenuated all the way to the DSO's two input channels. The initial correlation search experiment was run over many trials, days, orientations, and separation distances.

We also built detectors with more diodes packed in a cluster. A side view of a single detector with 5 z-diodes, in front of the LeCroy Waverunner LT344 500 MHz, 4 channel, 500 Ms/sec DSO, is seen in Figure 5.

No evidence of correlation could be detected. A typical screen shot of the DSO front panel showing Channels 1 and 2, at the first and fourth trace, is shown in Figure 6.

The second and third traces shows an amplified difference and sum trace. These traces show noise without discernible amplitude differences we would expect if correlations were present.

Using the storage facility of the DSO, E. Reiter searched for signals. A typical report reads: "I'm looking at diode noise for 10 div × 20 sec × 1412 sweeps = 282400 s = 3.2

Fig. 4: Two Zener diode detectors.

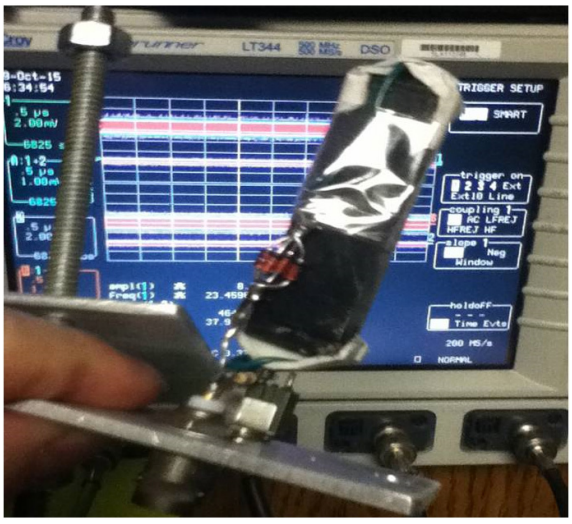

Fig. 5: Detector in front of DSO.

days. It is just non-interesting noise. Trigger is at 0.32 millivolts. I also searched with the trigger at 1 mV to see if there were periodicities; there were none."

We had not seen any indication of either a correlated signal or a periodic wave form as reported in the literature. We must assume something was wrong with our equipment or technique. To get to the bottom of the problem we contacted Prof. Cahill, who helped us diagnose our experimental setup.

3 Configuration refinement

The details of the actual phenomena had to be examined to determine whether any features could be detected. The earth is moving at roughly 500 km/s toward the direction RA=5 h, Dec=-80 deg. Figure 7 shows a space flow coming from the southerly direction. In this orientation the flow past our detectors should be in parallel so that no time delay would be encountered. However if the orientation to the South Sidereal Pole is offset by θ degrees when the spacing between the detector clusters is "d"centimeters then the time delay is

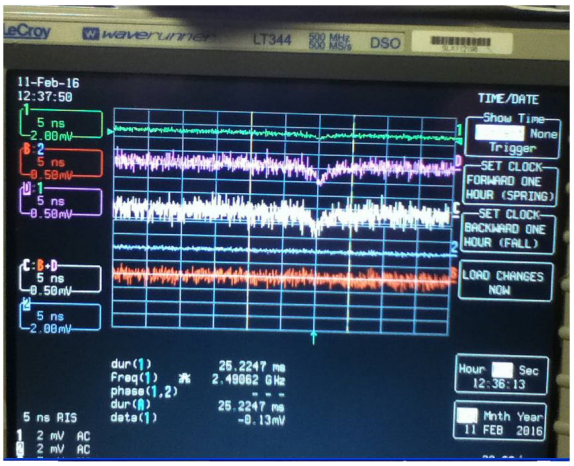

Fig. 6: Typical DSO trace.

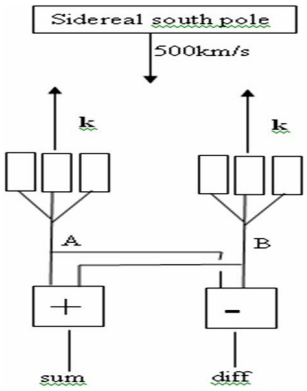

Fig. 7: Detector configuration.

calculated by

$$t = \frac{d\ \sin(\theta)}{500\ \text{km/sec}}. \qquad (1)$$

For a typical spacing of d=5 cm between side by side shielded detectors with an angle of $\theta = 30°$, the delay is 50 ns. The delay time for a 25 cm spacing would be on the order of 250 ns at 30° angle and 500 ns at 90°. This time delay of 0.5 μs corresponds to side by side direction pointing to the Sidereal South Pole and was also calculated in reference [3, Fig. 28].

Wave features similar to those shown in Figure 3 above where published showing wave features with approximate periodicities, of 10 ns in reference [1] Fig. 5, of 100 ns in references [2] Fig. 5, of 6 ns reference [1] Fig. 4, and 200 to 300 ns in reference [3] Fig. 28.

From this analysis it can be concluded that with a 500 Msamples/sec scope all but the highest frequency features reported would be adequately sampled to allow simple correlation. The time delay issue is more critical. Features with a structure on the order of 10 ns can only be convincingly correlated using our sum-difference strategy when the delay between the signals A and B in Fig. 7 is on the order of 1 ns. Using eq. 1 and assuming that the packaging distance "d" is limited to 2 cm the alignment angle must be controlled to,

$$1.4° = \arcsin\left(\frac{1\ \text{ns} \cdot 500\ \text{km/s}}{2\ \text{cm}}\right). \qquad (2)$$

This is not only a difficult orientation tolerance to maintain but the 1.4° angle at 2 cm spacing corresponds to 1.4 mm linear distance by which the diodes must be aligned with each other in a cluster. If the packaging could be reduced to half a centimeter and the time delay restriction relaxed to 2 ns we would get an angular tolerance of 11.5°. This is an orientation tolerance that could be met with fairly primitive equipment.

During our communications with Prof. Cahill many additional possible error sources were discussed. Improper cabling allowing EM radiation from external sources could explain sinusoidal wave forms. This possibility was soundly rejected by Prof. Cahill. Whether additional data processing was used to searched for correlations in oder to achieve the results was also denied. Cherry picking of accidental correlations to show in the reported papers was also denied. Prof. Cahill claimed to have observed consistent and reproducible correlation measurements many times.

We explored the possibility of borrowing the detectors to explore any differences in construction but such an exchange was rejected as time consuming due to the requirements of export regulations. This left some additional theoretical questions. We wondered about the size of the features in both time and space that were predicted. Since correlations were found between well separated detectors after time delay adjustment and time features of between 5 and 200 ns were routinely measured by Prof. Cahill. This could not be a problem.

Could the earth mass between the detector location and the Sidereal South pole attenuate the space flow signals more in the northern hemisphere than the south? A mass shielding effect was not considered likely from Cahills theory and because measurements of the effect were reported involving random number generators in Europe. Therefore the improvement in the three design features discussed above were left to consider when designing a follow on experiment.

4 Follow on experiment design

A repetition of the experiment was planned with the following changes:

1. Collocated detector design with minimum Zener Diode distances
2. careful alignment of the diode cluster to less than 1 mm
3. Less than 10° orientation with the direction of the expected velocity vector.

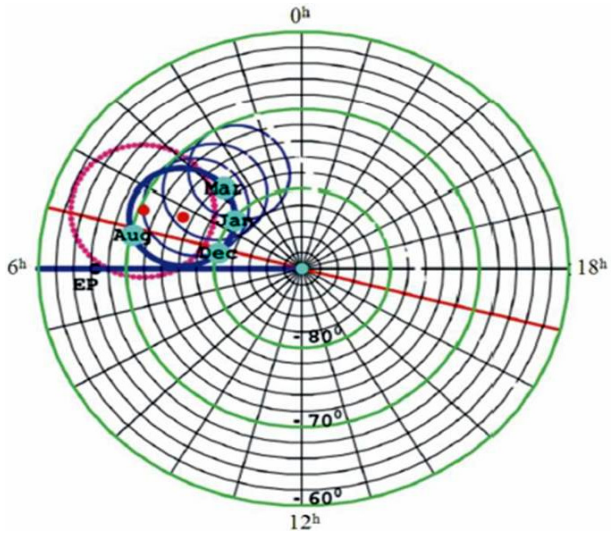

Fig. 8: Earth motion directions [3].

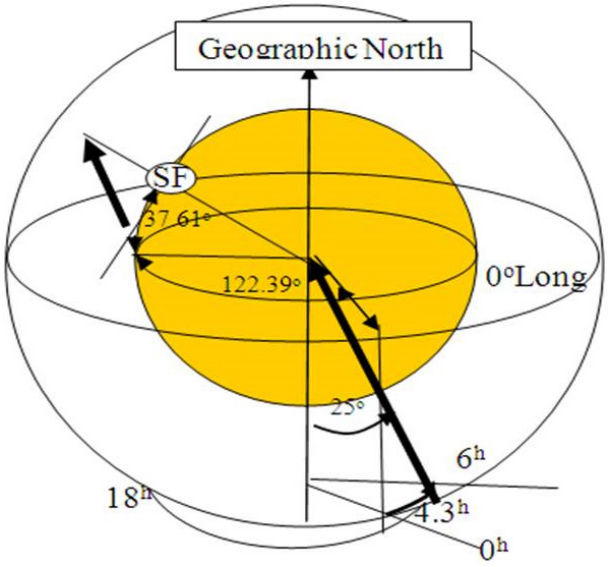

Fig. 9: Sidereal geography.

4.1 Orientation in inertial space

Fig. 8 shows the Sidereal South pole region. The right dot (red) at RA=4.3 h, Dec=75°S is the direction of motion of the solar system through space with a speed of 486 km/s as determined from NASA spacecraft earth-flyby Doppler shifts. The thick circle centered on this direction is the observed velocity direction for different days of the year. Relative to the earth location of the San Francisco Airport is 37.61 latitude and -122.39 longitude.

Figure 9 shows the Earth with San Francisco (SF) on the left edge. The local time in San Fransisco is 3.8 h AM and the Greenwich Meridian 122.39° toward the East is at 0 h. The Sidereal south pole is 4.3 h or 64.5° further east and 75° south latitude. The bold arrow shows the direction of the earth motion pointing toward the center of the earth. The parallel velocity vector at that time will point down toward an elliptic path.

4.2 Detector configuration

A stand placed flat on the ground aligned to geographic North, with a beam pointing down toward the ellipse marked by local time of day shows the direction of the Sidereal South Pole from San Francisco.

A dual detector is aligned so the Zener diodes clusters are correctly aligned to intercept the Flow vector as nearly perpendicular as possible.

The dual detector assembly was constructed with two single Zener diodes, mounted in a sealed metal box to eliminate external noise so that the entire assembly could be oriented perpendicular to the presumed space flow. A variable battery voltage supply was introduced to allow us to adjust the voltage close to the reverse bias breakdown voltage and thereby maximize the expected noise output. Dip switch jumpers

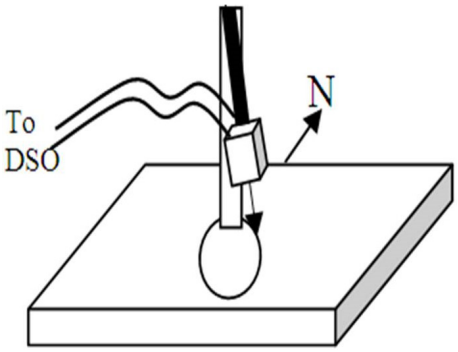

Fig. 10: Detector stand.

were added to allow multiple circuit configurations of the circuit shown in Figure 11.

With this new detector we began calibrating the variable battery voltage to determine the optimum noise output before attempting space flow alignment.

4.3 Experimental result

To our surprise we could not determine any sensitivity of output noise level. The noise level remained the same even when the battery power was completely turned off. In fact after first disconnecting the battery and then disconnecting the Detector from the DSO and replacing the cables with terminators placed directly on the oscilloscope input connector no difference in noise level showed. We had all along been attempting to find correlations between internally generated DSO noise.

Could Dr. Cahill have used a white noise amplifier [5] in his circuit and simply failed to mention the fact? He claimed no amplifier was used but did acknowledge that he had dis-

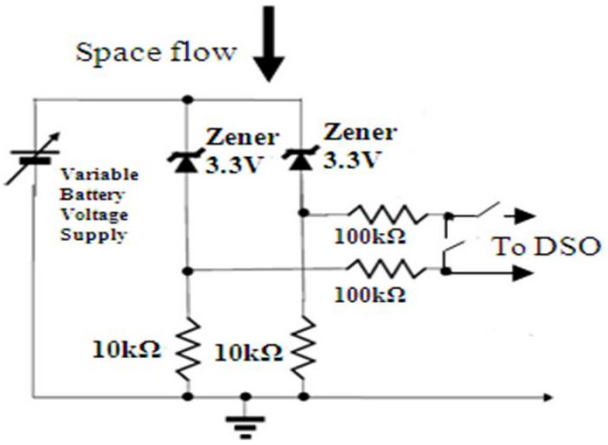

Fig. 11: Dual detector.

covered a space flow correlation simply between DSO devices and sent us the article [6]. We separately tested a second available DSO to verify the noise output when

(a) no detector was attached,

(b) no battery was in the detector, and

(c) everything was connected as described in the literature.

We performed sum and difference signal testing on the two input channels to see if any correlation between the noise sources existed. These experiments also showed nothing. FFT analysis of the signals only showed power at frequencies corresponding to wi-fi routers. Leakage from these high frequency signals were surprisingly difficult to eliminate but clearly not due to Zener diode noise.

5 Conclusion

We have attempted to verify the space flow detector experiment reported by Dr. Cahill which reported an effect that is consistent with the absolute motion of the earth through inertial space. Our conclusions are:

1. Zener Diode circuits without a white noise amplifier could not provide the signal levels reported in the literature as duplicated here in Figure 3.
2. Nothing in any signals produced by Zener diodes in reverse bias mode contains substantial power at frequencies whether of the 7ns periods or any others published by Dr. Cahill.
3. Internal Noise by Zener Diodes or other components in DSO equipment may be the source of the signals reported by Dr. Cahill.
4. There is no indication any signals generated by equipment reported by Dr. Cahill in the literature contains correlations that can support the space flow hypothesis.

No statement is made here regarding the theory of space flow as proposed by R. Cahill. There are other experiments supporting similar theoretical results [7] are also controversial [8]. Only the ability to detect space flow with the Zener diode detector design reported by Cahill in the literature has been tested.

In order to further explore the possibility that a Cahill type space flow disturbance may exist and may have a detectable effect on quantum devices it will be necessary to repeat Dr. Cahill's correlation experiments augmented by white noise amplifiers, statistical correlation software, and adequate shielding tested to eliminate any possibility of local signal corruption.

Submitted on February 4, 2017 / Accepted on February 19, 2017

References

1. Cahill R.T. Quantum Gravity Experiments. *Progress in Physics*, 2015 v. 11, 317–320.
2. Cahill R.T. Gravitational Wave Experiments with Zener Diode Quantum Detecors: Fractal Dynamical Space and Universe Expansion with Inflation Epoch. *Progress in Physics*, 2014 v. 10, 131–138.
3. Cahill R.T. Review of Gravitational Wave Detections: Dynamical Space. *Physics International*, 2014 v. 5(1), 49–86.
4. Cahill R.T. Process Physics: Emergent Unified Dynamical 3-Space, Quantum and Gravity-a Review. *Physics International*, 2015 v. 6(2), 51–67.
5. Application note, Building a Low-Cost White Noise Generator, Electronics Sep-Oct 2004: http://www.maximintegrated.com/en/app-notes/index.mvp/id/3469
6. Cahill R.T. Nanotechnology Quantum Detectors for Gravitational Waves: Adelaide to London Correlations Observed. *Progress in Physics*, 2013, v. 4, 57–62.
7. Silvertooth E.W. and Whitney C.K. A New Michelson-Morley Experiment. *Physics Essays*, 1992, v. 5, 1, 82–88.
8. Marett D. A Replication of the Silvertooth Experiment (2012) http://www.conspiracyoflight.com/Silvertooth/Silvertooth.pdf

LETTERS TO PROGRESS IN PHYSICS

Calculating the Parameters of the Tetraneutron

Anatoly V. Belyakov
E-mail: belyakov.lih@gmail.com

A large international group of theorists, using the high precision nucleon-nucleon interaction between neutrons, issued the theoretical estimates of the four-neutron (4n) system resonance state energy and its lifetime. For this purpose numerous calculations using supercomputers have been made and obtained the values of 0.84 MeV and 5×10^{-22} seconds. The same results were obtained with much less efforts based on the mechanistic interpretation of John Wheeler's geometrodynamic idea.

1 Introduction

In the Japanese RIKEN Institute as a result of experiments by the decay of 8He nuclei (alpha particle and four neutrons) some events managed to allocate, which are interpreted as short-lived resonance state of the tetraneutron. In a recent article, published in Physical Review Letters [1], according to calculations the tetraneutron resonance energy is estimated at 0.84 MeV, and its lifetime is about 5×10^{-22} seconds, which is consistent with the Japanese experimental data.

According to the first author of the article Andrey Shirokov (MSU: Lomonosov Moscow State University), "*... theoretical approach has been carefully designed and numerous calculations using supercomputers were made...*". For the calculation of only a few parameters characterizing tetraneutron scientific forces of the various institutes and organizations were involved in the work process and the expensive computing resources based on international scientific cooperation were expended. As stated in the original, "*Computational resources were provided by NERSC, which is supported by the U.S. Department of Energy under Contract No. DE-AC02-05CH11231 and by Lawrence Livermore National Laboratory (LLNL) institutional Computing Grand Challenge program under Contract No. DEAC52-07NA27344*".

There is a great regret for the efforts and the lack of other physical paradigms that could have given the same result with much less expenses. The same is confirmed by the authors themselves: "*More recent state-of-the-art theoretical calculations have concluded that without altering fundamental characteristics of the nuclear forces, the tetraneutron should not be bound. More theoretical calculations were performed, all of them agreeing that a bound tetraneutron is not supported by theory*".

2 Calculation of the tetraneutron parameters

The basis for one of the alternative theories could be a model based on the use of the elementary *mechanistic interpretation of J. Wheeler's geometrodynamic concept* where the charges are seen as singular points on the three-dimensional surface, connected "wormholes" or current tubes by drain-source type through an extra dimension, forming in general a closed *contour*. It is assumed the existence of common or similar natural laws, which are reproduced at different scale levels of matter. Earlier, on the basis of this model the binding energy of the deuteron, triton and alpha particle have been determined [2], as well as many other parameters for both micro- and macrocosm [3–6].

We now determine the binding energy for the tetraneutron. Let us recall that the contour or vortex thread having a radius r_e and the linear density m_e/r_e, along which some medium with velocity v circulates, a vortex thread with radius r fills a spiral manner. The vortex thread can be regarded as completely "stretched", i.e. elongated proportional to r_e/r or, on the contrary, extremely "compressed", i.e. shortened proportional to r_e/r and filling all the vortex tube of radius r_e.

In papers [3, 4], proceeding from the conditions of conservation of charge and constancy of the linear density when contour's changing, parameters of the vortex thread v, r for an arbitrary plus-minus contour is defined as a proportion of the light speed and electron radius as:

$$v = \frac{c_0^{1/3}}{(an)^2}, \tag{1}$$

$$r = \frac{c_0^{2/3}}{(an)^4}, \tag{2}$$

where n is the own quantum number for the microparticles, a is the inverse fine structure constant, c_0 is the dimensionless velocity of light, $c/[\text{m}/\text{sec}]$. For the proton

$$n = \left(\frac{2c_0}{a^5}\right)^{1/4} = 0.3338, \tag{3}$$

and of the above formulas it follows: $v = 0.320$, $r = 0.102$.

Assume that neutrons, surrounding an alpha particle before decay of 8He, is polarized the same as in the alpha-particle (1, −2/3, and 1/3). Let the four polarized neutrons disposed symmetrically like the nucleons in the alpha particle, as shown in the figure. Charge radius neutrons r_n is assumed to be the radius of the proton, plus 3% (since on this

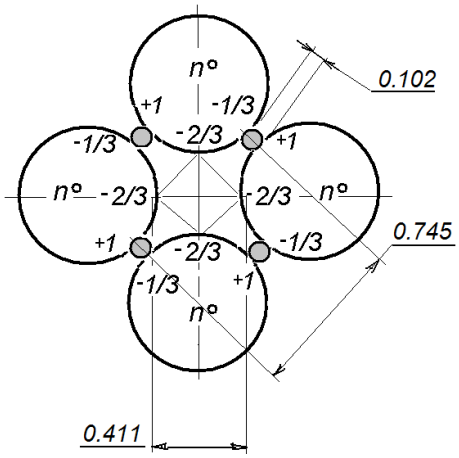

value the radius of the neutron magnetic moment distribution is increased in comparison with that of a proton), then

$$r_n = 0.322\ (\text{or } 9.07) \times 10^{-16}\ \text{m}. \tag{4}$$

There are taken into account four interactions between charges of $+1$ and $-1/3$ (attraction) at a distance $r = 0.102$, and six interactions between charges of $-2/3$ (repulsion), i.e. their projections on the sides of the square and along the diagonals at distances determined from geometrical considerations (0.291 and 0.411). The minimum distance between the charges made equal to the transverse dimension of the nucleon vortex tube (thread) $r = 0.102$. This characteristic size has also been adopted by reason that for the magneto-gravitational equilibrium with given parameter and charges of $+1$ and $-1/3$ the product of the quark masses, involved in the circulation contour, found to be equal to the value of 84.3. Thus, the average mass of the quarks $(84.3)^{1/2} = 9.18$ is nearly the mass of two neutron quarks $(8.6\, m_e)$, defined on the basis of entirely different reasons earlier [4].

The tetraneutron bonds form a closed system, so one can assume that the tetraneutron binding energy is the averaged binding energy of a link, since at destruction of a link the particle splits as a whole (as the alpha particle). Having in mind the accepted scheme of charges arrangement, tetraneutron geometry, and specified dimensions, we can write the final formula for the binding energy as the average energy per bond. For single charges in units of MeV, and in a proportion of r_e we have:

$$E = \frac{0.511}{r}\,. \tag{5}$$

In our case by substituting the data we obtain:

$$E = \frac{0.511}{4} \times \left(\frac{4 \times 1 \times \frac{1}{3}}{0.102} - \frac{4 \times \frac{2}{3} \times \frac{2}{3} \times \cos 45^\circ}{0.291} - \right.$$
$$\left. - \frac{2 \times \frac{2}{3} \times \frac{2}{3}}{0.411} \right) = 0.835. \tag{6}$$

Note, that if the charges of the polarized neutron is $(+2/3, -1/3$, and $1/3)$, and in this case the binding energy is approximately the same amount.

Tetraneutron instability can be explained by the fact that kinetic energy of the tetraneutron quarks (having a total mass m_k and rotating on the same radius r at speed v), is comparable to the binding energy. Let's equate these energies. At the units of MeV we have:

$$m_k\, m_e\, (vc)^2 = 0.835\ \text{MeV}. \tag{7}$$

Since $m_e c^2 = 0.511$ MeV, then from (7), by substituting the values of v, we have $m_k = 16.0$. That is, the value, which is close to the total two neutron quark mass involved in the circulation counter, creates the inertia repulsive forces that can destroy, at least, one bond of the tetraneutron.

The lifetime of the tetraneutron τ is determined from the reason of the duration of existence of four neutrons in a bound state, which should at least be sufficient for one circulation of medium flow along the contour having some diameter d. Suppose that it is equal to the distance between the centers of neutrons, $d = 0.745$.

Then, taking into account the "stretching" (i.e. elongation of the vortex thread is a multiple of $1/r$ and decreasing in the flow velocity is a multiple of v), and substituting the data we obtain:

$$\tau = \frac{\pi\, d\, r_e}{c} \times \frac{1}{vr} = 6.73 \times 10^{-22}\ \text{sec}. \tag{8}$$

3 Conclusion

Thus, the calculated parameters of the tetraneutron are consistent with those obtained in the experiments of RIKEN and coincide to those declared in [1] that once again proves the validity of the proposed model.

Submitted on January 22, 2017 / Accepted on January 25, 2017

References

1. Shirokov A. M., Papadimitriou G., Mazur A. I., Mazur I. A., Roth R., Vary J. P. Prediction for a four-neutron resonance. *Phys. Rev. Lett.*, 2016, v. 117, 182502; arXiv: 1607.05631 [nucl-th].
2. Belyakov A. V. Nuclear power and the structure of a nucleus according to J. Wheeler's geometrodynamic concept. *Progress in Physics*, 2015, v. 11, issue 1, 89–98.
3. Belyakov A. V. Charge of the electron, and the constants of radiation according to J. A. Wheeler's geometrodynamic model. *Progress in Physics*, 2010, v. 4, 90–94.
4. Belyakov A. V. Macro-analogies and gravitation in the micro-world: further elaboration of Wheeler's model of geometrodynamics. *Progress in Physics*, 2012, v. 2, 47–57.
5. Belyakov A. V. Determination of the neutrino mass. *Progress in Physics*, 2016, v. 12, issue 1, 34–38.
6. Belyakov A. V. Evolution of stellar objects according to J. Wheeler's geometrodynamic concept. *Progress in Physics*, 2013, v. 1, 25–40.

Harmonic Orbital Resonances and Orbital Long-Range Order of the TRAPPIST-1 Exoplanetary System

Felix Scholkmann
Research Office for Complex Physical and Biological Systems (ROCoS),
Mutschellenstr. 179, 8038 Zurich, Switzerland. E-mail: felix.scholkmann@gmail.com

Recently, seven exoplanets orbiting the ultra-cool dwarf star TRAPPIST-1 were reported. The present paper explores whether (i) the sequence of semi-major axis values of the planets shows a long-range order, and whether (ii) the values can be described by harmonic orbital resonances. The analysis showed that orbits of the planets follow (i) a long-range order, and (ii) a quantization in accordance with harmonic orbital resonances. The study supports the view that planetary systems are best viewed as self-organizing systems with attractor states of the planet orbits being related to resonance effects.

1 Introduction

A paper [1] was recently published on the discovery and description of an extrasolar planetary system with seven planets (TRAPPIST-1b, c, d, e, f, g and h) orbiting an ultra-cool dwarf star (TRAPPIST-1, 2MASS J23062928-0502285; apparent magnitude: $V = 18.80$) in the constellation Aquarius (RA = $23^{\mathrm{h}}\,06^{\mathrm{m}}\,29.28^{\mathrm{s}}$, dec = $-05^{\circ}\,02'\,28.5''$).

This discovery was the result of an intensive observation program using space- and earth-based telescopes comprising the TRAPPIST (TRansiting Planets and PlanetsIsimals Small Telescope) North system (Chile), the TRAPPIST-North telescope (Morocco), the Himalayan Chandra Telescope (India), the Very Large Telescope (Chile), the UK Infrared Telescope (Hawaii), the Spitzer Space Telescope, the William Herschel and Liverpool telescopes (La Palma, Spain), as well as the South African Astronomical Observatory telescope [1, 2].

The orbital parameters of the TRAPPIST-1 planetary system exhibit a non-random behaviour, i.e., "the six inner planets form the longest known near-resonant chain of exoplanets, with the ratios of the orbital periods (P) $P_{\mathrm{c}}/P_{\mathrm{b}}$, $P_{\mathrm{d}}/P_{\mathrm{c}}$, $P_{\mathrm{e}}/P_{\mathrm{d}}$, $P_{\mathrm{f}}/P_{\mathrm{e}}$ and $P_{\mathrm{g}}/P_{\mathrm{f}}$ being close to the ratios of small integers, namely 8/5, 5/3, 3/2, 3/2 and 4/3, respectively", as noted in the recent *Nature* publication [1]. A property that is associated with an *orbital resonance*, or a mean-motion orbital resonance, in particular. Other examples of planetary systems where the *orbital periods* are in a specific resonance-like relationship include the exoplanetary systems Kepler-223 [3], Kepler-80 [4], GJ 876 [5] and HD 82943 [6]. If the orbital *periods* show this resonance phenomenon, then also the orbital *spacing* of a planetary system follows the same pattern – a direct consequence of Kepler's third law linking the orbital spacing (given as the semi-major axis, (a)) with the period of an planet orbiting a star, $P^2 \propto a^3$, leading to the relationships $a \propto P^{2/3}$ and $P \propto a^{3/2}$.

The orbital resonances can be analysed by examining the orbital spacings locally and separately, or by analysing the whole planetary system orbital spacing *in toto*. Foundational work on this second approach was conducted by J. Bohr and K. Olsen [9, 10] who showed that the orbital spacing of the planets of our solar system follows long-range order on a logarithmic scale, i.e., the logarithmic positions of the planets are correlated and follow a periodic pattern (a kind of "quantization") [9]. This long-range order of the orbital spacing was also detected in the exoplanetary system HD 10180 [10]. Stimulated by this work, I showed in 2013 that the orbital spacing of the exoplanetary system Kepler-62 exhibits a long-range order too and I predicted an additional planet (which has not been detected yet, however) based on this analysis [7].

The discovery of the TRAPPIST-1 planetary system [1] triggered the question of whether the orbital spacing of this system also follows a long-range order, and how the orbital structure of the planetary system can be described based on approach of orbital resonances. The aim of the present work was therefore to investigate these two asepcts in detail.

2 Materials and methods

2.1 Data

The parameter values of the TRAPPIST-1's exoplanets were obtained from Gillon et al. [1]. In the present work, two parameters were selected for analysis: the semi-major axis (a) and the radius (r) of each planet (see Table 1).

2.2 Analysis of the orbital long-range order

To analyse the TRAPPIST-1 system, the same approach as already employed for the previously published analysis of the Kepler-62 system [7] was used. In particular, the semi-major axis values a (given in units of 10^6 km) of each exoplanet were first divided by 10^6 km, then logarithmized ($\hat{a}_i = \ln(a_i/10^6\,\mathrm{km})$) and according to these values a multimodal probability distribution function (PDF) $p(\hat{a})$ was calculated by

$$p(\hat{a}) = \sum_{i=1}^{N} \alpha_i \, e^{-\beta}, \tag{1}$$

Planet	i	a [AU]	a [km]	r [$R_\oplus$]	r [km]	$\hat{a}$
b	1	0.01111 ± 0.00034	$1.6621\times 10^6 \pm 5.0864 \times 10^4$	1.086 ± 0.035	6926.508 ± 223.23	0.5081
c	2	0.01521 ± 0.00047	$2.2754 \times 10^6 \pm 7.0312 \times 10^4$	1.056 ± 0.035	6735.168 ± 223.23	0.8222
d	3	$0.02144^{+0.00066}_{-0.00063}$	$3.2074 \times 10^6\ ^{+9.8736\times 10^4}_{-9.4248\times 10^4}$	0.772 ± 0.03	4923.816 ± 191.34	1.1655
e	4	$0.02817^{+0.00083}_{-0.00087}$	$4.2142 \times 10^6\ ^{+1.2417\times 10^4}_{-1.3015\times 10^4}$	0.918 ± 0.039	5855.004 ± 248.742	1.4385
f	5	0.0371 ± 0.0011	$5.5502 \times 10^6 \pm 1.6456 \times 10^5$	1.045 ± 0.038	6665.01 ± 242.364	1.7138
g	6	0.0451 ± 0.0014	$6.7470 \times 10^6 \pm 2.0944 \times 10^5$	1.127 ± 0.041	7188.006 ± 261.498	1.9091
h	7	$0.063^{+0.027}_{-0.013}$	$9.4248 \times 10^6\ ^{+4.0392\times 10^6}_{-1.9448\times 10^6}$	0.755 ± 0.034	4815.39 ± 216.852	2.2433

Table 1: TRAPPIST-1 system parameters according to [1]. i: planet number counting outwardly from the star TRAPPIST-1, a: semi-major axis, r: radius of the planet, $\hat{a}_i = \ln(a_i/10^6\ \text{km})$, a and r are given in two different units ([AU], [km]) and ([$R_\oplus$], [km]), respectively.

with $N = 7$ (i.e., the maximum number of planets of the TRAPPIST-1 system) and β given as

$$\beta = \frac{j - \hat{a}_i}{w_p / 2\sqrt{2\ln(2)}}, \qquad (2)$$

for $j = 1, 1.01, 1.02, \ldots, 3$, with w_p the width (i.e., the full-width-at-half-maximum) of each Gaussian peak of the PDF, and α_i a scale factor. This approach was first introduced by Bohr and Olsen [9]. The scale factor α in equation (1) defines the magnitude of each peak of the PDF and was assigned to the radius of the specific planet ($\alpha_i = r_i$). With this the size of the planets is incorporated to determine the PDF, i.e., larger planets then contribute more to the overall multimodal PDF than smaller planets. The width of each peak w_p was set to such a parameter value that is was ensured that an optimum compromise between a too strong overlap of the Gaussian peaks on the one side and to small peaks on the other was realized. This was ensured with $w_p = 0.15$. The final multimodal PDF, $\rho(\hat{a})$, then represents a sum of Gaussian peaks located at the logarithmized planets' semi-major axis values ($\hat{a}$) and weighted by the individual radius value of the planet (α_i).

To quantify the correlation structure of $\rho(\hat{a})$, the autocorrelation function (ACF) of $\rho(\hat{a})$ was determined according to equations (3) and (4) given in [7]. The ACF properties correspond to the type and grade of the order (short- or long-range) of the input sequence. Finally, the frequency-dependent power spectral density (PSD) of the multimodal PDF $\rho(\hat{a})$ was determined by the periodogram method.

At present, the exact semi-major axis value of the exoplanet TRAPPIST-1h is known only with large uncertainity ($a = 0.063\ ^{+0.027}_{-0.013}$ AU). In an additional analysis, it was tested which a value in the range [0.05, 0.09] AU will maximize the long-range order of the orbital spacing. The maximum was determined by fitting an exponential function to the orbital spacing values while changing the a value for the planet 1h in the range given. The goodness-of-fit was then determined by the coefficient of determination (R^2) and the root-mean-square error (RMSE). The a value that maximized the R^2 and minimized the RMSE was chosen as the one to most likely representing the true value for this exoplanet.

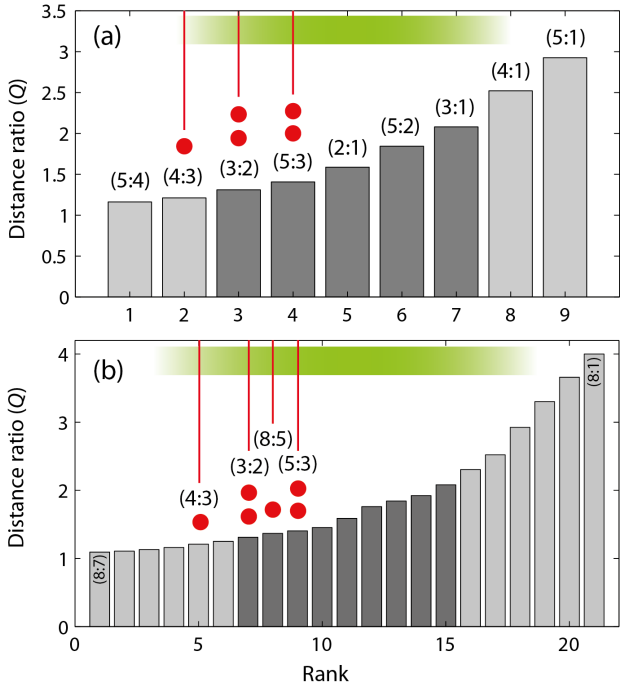

Fig. 1: Distance ratios Q with respect to the rank (given according to the period ratios q). The red dots and vertical lines mark the positions of the exoplanet's orbits according to the distance ratios. (a) Range of distance ratios as used by Aschwanden and McFadden [8]. (b) Range of distance ratios as used in the present study. The green bar marks the interval where it is most likely to find the distances ratios based on empirical data (according to [8]).

2.3 Analysis of harmonic orbital resonances

The methodology based on the recently published *harmonic orbit resonance model* by Aschwanden and McFadden [8] was employed for this analysis. The harmonic orbit resonance model states that the planetary system is best viewed as a self-organisation system where the orbital parameters evolve to attractor states in the sense of harmonical relations (the harmonic orbit resonance). Attracttor states of the orbits are realised when harmonical relations are reached, ensuring stability of the planetary system. The basic idea is that the distance ratios (Q) of semi-major axis values a are (i) not

Harmonic ratio ($H_{i+1} : H_i$)	Distance ratio (Q)	Period ratio (q)	Rank (#)
(8:7)	1.0931	1.1429	1
(8:5)	1.3680	1.6000	8
(8:3)	1.9230	2.6667	14
(8:1)	4.0000	8.0000	21
(7:6)	1.1082	1.1667	2
(7:5)	1.2515	1.4000	6
(7:4)	1.4522	1.7500	10
(7:3)	1.7592	2.3333	12
(7:2)	2.3052	3.5000	16
(7:1)	3.6593	7.0000	20
(6:5)	1.1292	1.2000	3
(6:1)	3.3019	6.0000	19
(5:4)	1.1604	1.2500	4
(5:3)	1.4057	1.6667	9
(5:2)	1.8420	2.5000	13
(5:1)	2.9240	5.0000	18
(4:3)	1.2114	1.3333	5
(4:1)	2.5198	4.0000	17
(3:2)	1.3104	1.5000	7
(3:1)	2.0801	3.0000	15
(2:1)	1.5874	2.0000	11

Table 2: Numerical values of the harmonic ratios, distance ratios and period ratios for all harmonic ratios in the interval (2 : 1) to (8 : 7). The rank of the harmonic ratios is given according to the period ratio values.

constant for a planetary system and (ii) show a quantization whereas only specific values are "allowed" according to

$$Q = \left(\frac{a_{i+1}}{a_i}\right) = \left(\frac{H_{i+1}}{H_i}\right)^{2/3}, \quad (1)$$

with H being harmonic numbers ($H = [1, 2, \ldots, M]$) that form harmonic ratios. Due to Kepler's third law, this equation leads automatically also to quantized orbital period ratios q:

$$q = \left(\frac{P_{i+1}}{P_i}\right) = \left(\frac{a_{i+1}}{a_i}\right)^{3/2} = Q^{3/2}. \quad (1)$$

For $M = 8$ (i.e., $H = [1, 2, \ldots, 8]$), the attractor states are realized by the harmonic ratios $Q = (H_{i+1}/H_i) = (8 : 7)$, $(8 : 5)$, $(8 : 3)$, $(8/1)$, $(7 : 6)$, $(7 : 5)$, $(7 : 3)$, $(7 : 2)$, $(7 : 1)$, $(6 : 5)$, $(6 : 1)$, $(5 : 4)$, $(5 : 3)$, $(5 : 2)$, $(5 : 1)$, $(4 : 3)$, $(4 : 1)$, $(3 : 2)$, $(3 : 1)$ and $(2 : 1)$. The associated numerical values of the distance and period ratios are given in Table 2. When sorted in ascending order of q, the attractor values of the distance ratios Q follow the function as shown in Figure 1. The most dominant ratios in a planetary system, according to Aschwanden and McFadden [8], are marked with a green bar.

3 Results

3.1 Orbital long-range order

As shown in Figure 2(c) the analysis of the semi-major axis values of TRAPPIST-1's planets b-h revealed an exponential function (or a quasi linear one when logarithmized values were used; Figure 2(d)). The parameter values for the exponential function $f(n) = \alpha \exp^{\beta n}$ were found to be (given as optimal value (95% confidence bound)): $\alpha = 4.086 \times 10^6$ $(3.85 \times 10^6, 4.321 \times 10^6)$, $\beta = 0.5936$ $(0.5398, 0.6475)$.

In an additional analysis, it was investigated if the fit with an exponential function related to the Titius-Bode law [12] in the form $f(n) = \alpha + \beta 2^n$ was better or worse at describing the data than the exponential function of type $f(n) = \alpha \exp^{\beta n}$ (with α and β free parameters), as also used by Naficy et al. [11] to describe the planetray orbit scaling. It was found (see Figures 4(a) and (b)) that the second exponential model fitted the data better than the first one (coefficient of determination (R^2: 0.9921 and 0.9944, respectively).

Figure 2(e) shows the calculated multimodal PDF. The ACF and the power spectrum are depicted in Figures 2(f) and 2(g), respectively. A clear peak of the spectrum of the multimodal PDF is evident with a center frequency of 3.47 $1/\hat{a}$, corresponding to a an orbital spacing regularity with a spacing of 0.288.

3.2 Prediction of the TRAPPIST-1h exoplanet position

Figure 3 depicts the results of the analysis investigating how the orbital position of the TRAPPIST-1h exoplanet has an effect on the long-range order. The "optimal" position (i.e., maximizing R^2 and minimizing RMSE) were found to be in the range $a = [0.060, 0.061$ AU].

3.3 Harmonic orbital resonances

The analysis with the *harmonic orbit resonance model* by Aschwanden and McFadden [8] revelaed that all exoplanets of the TRAPPIST-1 system occupy orbitals that are attractor states according to the harmonic orbital resonance model (see Figure 4(c)). The harmonic ratios describing the planetary system are found to be: $(H_{i+1}/H_i) = (4 : 3)$, $(3 : 2)$, $(8 : 5)$, and $(5 : 3)$. The ratios $(3 : 2)$, $(8 : 5)$, and $(5 : 3)$ are in the interval where the most dominant ratios are being expected according to Aschwanden and McFadden [8]. The ratios $(4 : 3)$ is at the border of this interval (see Figure 1).

4 Discussion and conclusion

The following conclusions can be drawn from the analysis conducted in the present study:

(i) The orbitals of the exoplanets of the TRAPPIST-1 planetary system exhibit a long-range order. This property is cleary visible in the linear periodicity of the multimodal PDF when lograithmizing the distances between the planets. The single peak in the power spectrum quantifies this characteristic.

(ii) The orbital postition of the TRAPPIST-1h exoplanet is most likely in the range of $a = [0.060, 0.061$ AU].

(iii) All exoplanets of the TRAPPIST-1 system occupy orbitals that are attractor states according to the harmonic orbital resonance model.

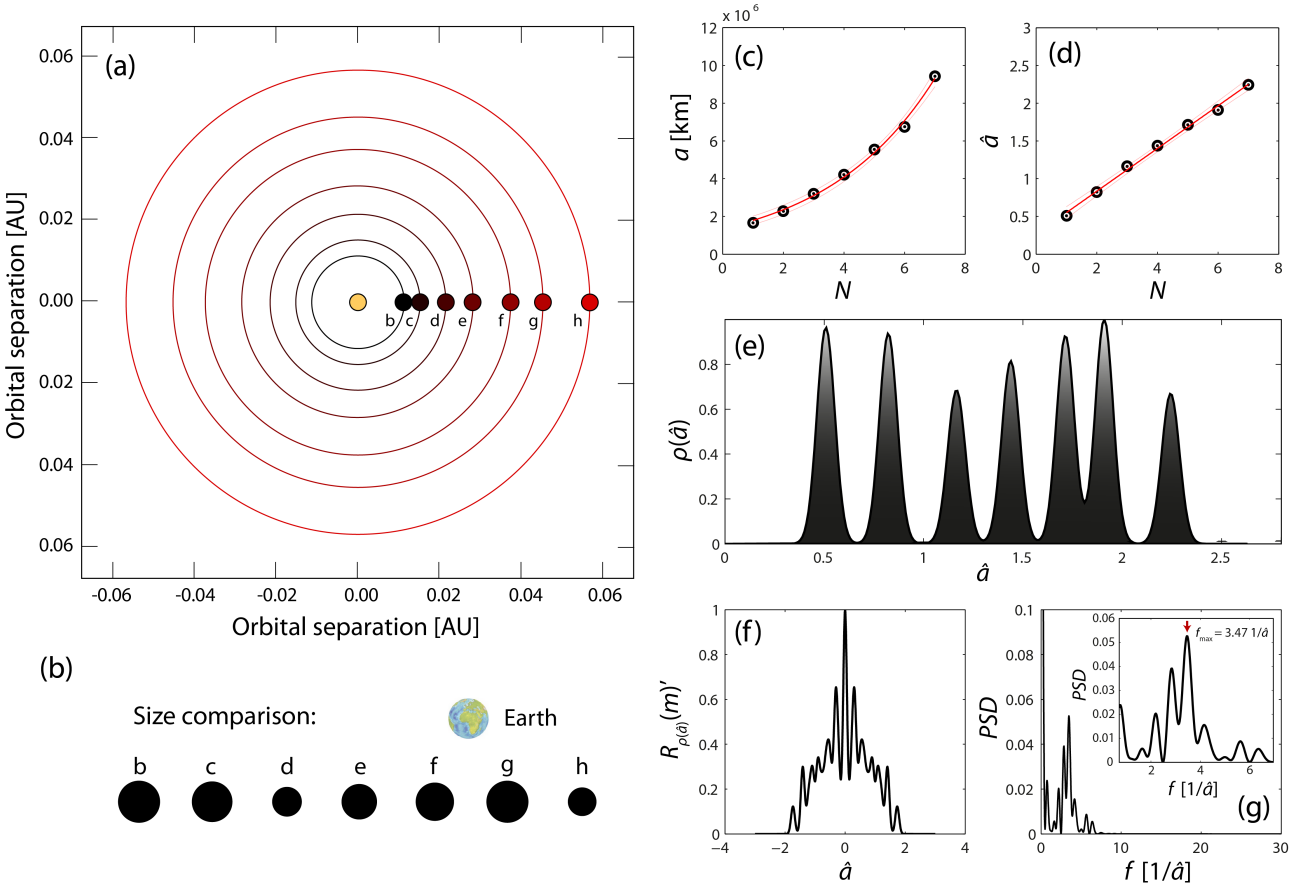

Fig. 2: (a) Diagram with the orbits of the exoplanets of TRAPPIST-1. (b) Comparison of the exoplanets' sizes with respect to the size of the Earth. (c, d) Semi-major axis values with respect to the rank (n), plotted in linear and logartihmic space, respectively. (e) Multimodal PDF of the seven exoplanets. (f) ACF and (f) power spectrum of the multimodal PDF

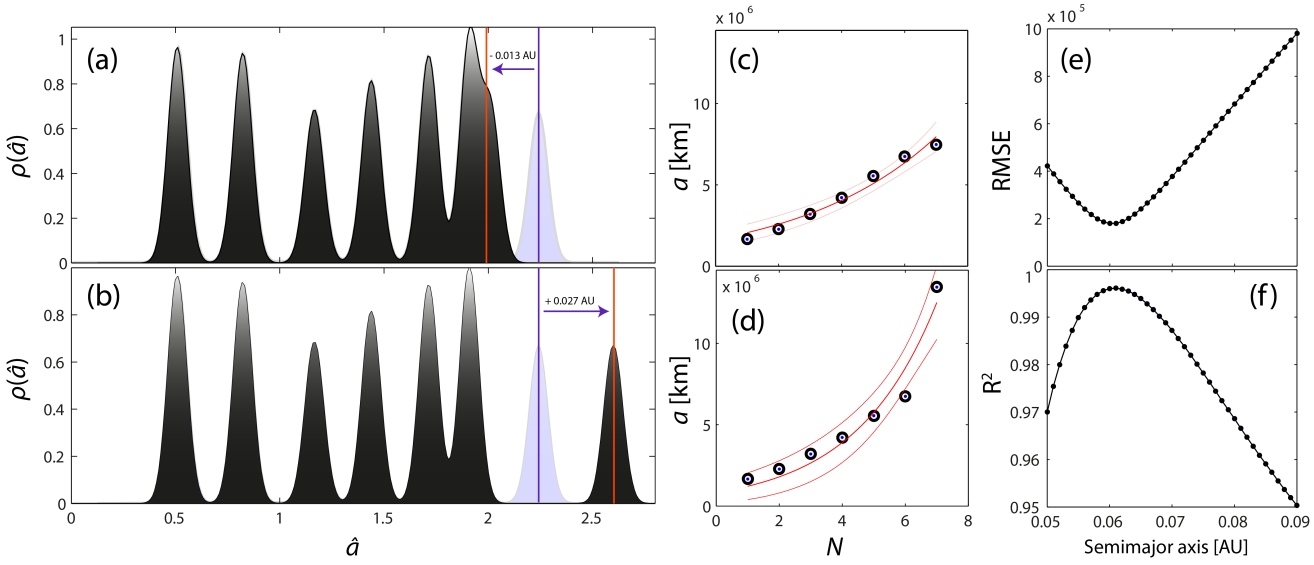

Fig. 3: (a, b) Multimodal PDFs $\rho(\hat{a})$ with different positions of the exoplanet TRAPPIST-1h. The corresponding scaling functions (a vs. rank (n)) are shown in (c) and (d), respectively. (e) R^2 vs. a. (f) RMSE vs. a.

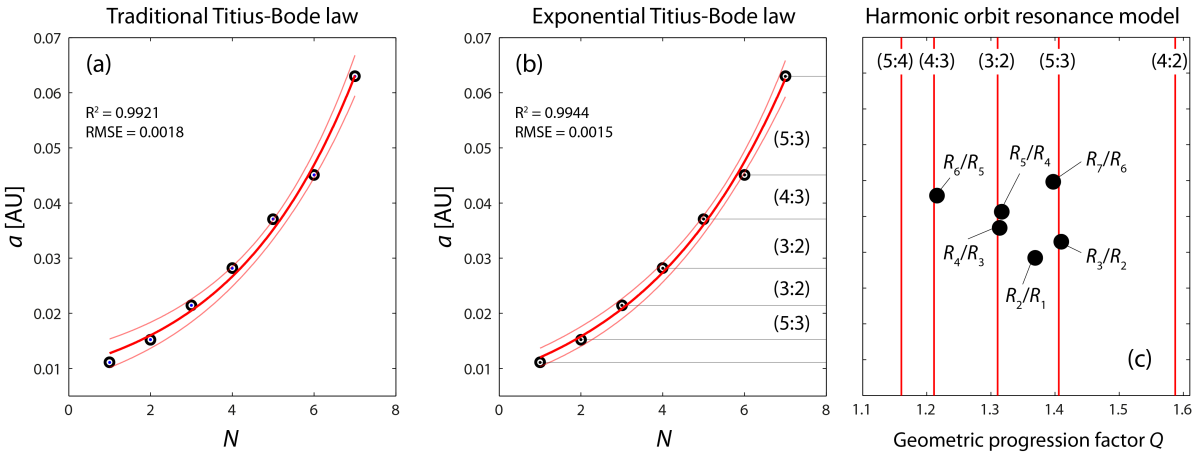

Fig. 4: Fitting of the semi-major axis values with two different types of exponential functions, i.e., (a) $f(n) = \alpha + \beta\, 2^n$ and (b) $f(n) = \alpha \exp^{\beta n}$. (c) Predicitons of the orbital positions according to the harmonic orbit resonance model, and the corresponding values of the TRAPPIST-1 exoplanetary system.

What is the physical mechanism causing this long-range order and the harmonic orbital resonances? A review of different approaches and models related to this question can be found in my previously published paper [7] as well as one recently published by Aschwanden and McFadden [8]. In my opinion, the most promising and interesting aproaches are those based on plasma physics [13–17], the concept of macroscopic quantization due to finite gravitational propagation speed [18], and the view that the solar system is a self-organising system with attractor states leading to harmonic orbit resonances [8].

In conclusion, the present analysis of the extrasolar planetary system TRAPPIST-1 reveals that the semi-major axis values of the planets follow (i) a long-range order and (ii) a quantization in accordance with the harmonic orbital resonance model. Furthermore, the analysis predicts that the exact position of the exoplanet TRAPPIST-1h is in the range of $a = [0.060, 0.061$ AU], slightly less then the determined mean semi-major axis value of 0.063 AU given by Gillon et al. [1].

References

1. Gillon M., Triaud A.H.M., Demory B.-O., Jehin E., Agol E., et al. Seven temperate terrestrial planets around the nearby ultracool dwarf star TRAPPIST-1. *Nature*, 2017, v. 542, 456–460.
2. Gillon M., Jehin E., Lederer S.M., Delrez L., et al. Temperate Earth-sized planets transiting a nearby ultracool dwarf star. *Nature*, 2016, v. 533, 221–224.
3. Mills S.M., Fabrycky D.C., Migaszewski C., Ford E.B., et al. A resonant chain of four transiting, sub-Neptune planets. *Nature*, 2016, v. 533, 509–512.
4. MacDonald M.G., Rogozzine D., Fabrycky D.C., Ford E.B., Holman M.J., et al. A dynamical analysis of the Kepler-80 system of five transiting planets. *The Astronomical Journal*, 2016, v. 152 (4), 105.
5. Man Hoi L. and Peale S.J. Dynamics and origin of the 2:1 orbital resonances of the GJ 876 planets. *The Astrophysical Journal*, 2002, v. 567 (1), 596–609.
6. Goździewski K. and Maciejewski A.J. Dynamical analysis of the orbital parameters of the HD 82943 planetary system. *The Astrophysical Journal*, 2001, v. 563 (1), L81.
7. Scholkmann F. A prediction of an additional planet of the extrasolar planetary system Kepler-62 based on the planetary distances' long-range order. *Progress in Physics*, 2013, v. 4, 85–89.
8. Aschwanden M.J. and McFadden L.A. Harmonic resonances of planet and moon orbits – From the Titius-Bode law to self-organizing systems *arXiv:1701.08181 [astro-ph.EP]*.
9. Bohr J. and Olsen K. Long-range order between the planets in the Solar system. *Monthly Notices of the Royal Astronomical Society*, 2010, v. 403, L59–L63.
10. Olsen K. and Bohr J. Pair-correlation analysis of HD 10180 reveals a possible planetary orbit at about 0.92 AU. 2010, arXiv: astro-ph.EP/1009.5507.
11. Naficy K., Ayubinia A. and Saeedi M. Exponential law as a more comp atible model to describe orbits of planetary systems. *Iranian Journal of Physics Research*, 2012, v. 12 (3), 25–31.
12. Jaki S. L. The early history of the Titius-Bode law. *American Journal of Physics*, 1972, v. 40 (7), 1014–1023
13. Wells D. R. Was the Titius-Bode series dictated by the minimum energy states of the generic solar plasma? *IEEE Transactions on Plasma Science*, 1990, v. 19 (1), 73–76.
14. Wells D. R. Titius-Bode and the helicity connection: a quantized field theory of protostar formation. *IEEE Transactions on Plasma Science*, 1989, v. 14 (6), 865–873.
15. Wells D. R. Quantization effects in the plasma universe. *IEEE Transactions on Plasma Science*, 1989, v. 17 (2), 270–281.
16. Wells D. R. Unification of gravitational, electrical, and strong forces by a virtual plasma theory. *IEEE Transactions on Plasma Science*, 1992, v. 20 (6), 939–943.
17. Livadiotis G., McComas D.J. Evidence of large-scale quantization in space plasmas. *Entropy*, 2013, v. 15, 1118–1134.
18. Giné J. On the origin of the gravitational quantization: The Titius–Bode law. *Chaos, Solitons & Fractals*, 2007, v. 32 (2), 362–369.

LETTERS TO PROGRESS IN PHYSICS

Introducing a Theory of Neutrosophic Evolution: Degrees of Evolution, Indeterminacy, and Involution

Florentin Smarandache
University of New Mexico, 705 Gurley Ave., Gallup, NM 87301, USA. E-mail: smarand@unm.edu

During the process of adaptation of a being (plant, animal, or human), to a new environment or conditions, the being partially evolves, partially devolves (degenerates), and partially is indeterminate i.e. neither evolving nor devolving, therefore unchanged (neutral), or the change is unclear, ambiguous, vague, as in neutrosophic logic. Thank to adaptation, one therefore has: evolution, involution, and indeterminacy (or neutrality), each one of these three neutrosophic components in some degree. The degrees of evolution/indeterminacy/involution are referred to both: the structure of the being (its body parts), and functionality of the being (functionality of each part, or inter-functionality of the parts among each other, or functionality of the being as a whole). We therefore introduce now for the first time the Neutrosophic Theory of Evolution, Involution, and Indeterminacy (or Neutrality).

1 Introduction

During the 2016–2017 winter, in December-January, I went to a cultural and scientific trip to Galápagos Archipelago, Ecuador, in the Pacific Ocean, and visited seven islands and islets: Mosquera, Isabela, Fernandina, Santiago, Sombrero Chino, Santa Cruz, and Rabida, in a cruise with Golondrina Ship. I had extensive discussions with our likeable guide, señor Milton Ulloa, about natural habitats and their transformations.

After seeing many animals and plants, that evolved differently from their ancestors that came from the continental land, I consulted, returning back to my University of New Mexico, various scientific literature about the life of animals and plants, their reproductions, and about multiple theories of evolutions. I used the online scientific databases that UNM Library has subscribed to, such as MathSciNet, Web of Science, EBSCO, Thomson Gale (Cengage), ProQuest, IEEE/IET Electronic Library, IEEE Xplore Digital Library etc., and DOAJ, Amazon Kindle, Google Play Books as well, doing searches for keywords related to origins of life, species, evolution, controversial ideas about evolution, adaptation and inadaptation, life curiosities, mutations, genetics, embryology, and so on.

My general conclusion was that each evolution theory had some degree of truth, some degree of indeterminacy, and some degree of untruth (as in neutrosophic logic), depending on the types of species, environment, timespan, and other hidden parameters that may exist.

And all these degrees are different from a species to another species, from an environment to another environment, from a timespan to another timespan, and in general from a parameter to another parameter.

By environment, one understands: geography, climate, prays and predators of that species, i.e. the whole ecosystem.

I have observed that the animals and plants (and even human beings) not only evolve, but also *devolve* (i.e. involve back, decline, atrophy, pass down, regress, degenerate). Some treats increase, other treats decrease, while others remains unchanged (neutrality).

One also sees: adaptation by physical or functional evolution of a body part, and physical or functional involution of another body part, while other body parts and functions remain unchanged. After evolution, a new process start, reevaluation, and so on.

In the society it looks that the most opportunistic (which is the fittest!) succeeds, not the smartest. And professional deformation signifies evolution (specialization in a narrow field), and involution (incapability of doing things in another field).

The paper is organized as follows: some information on taxonomy, species, a short list of theories of origin of life, another list of theories and ideas about evolution. Afterwards the main contribution of this paper, the *theory of neutrosophic evolution*, the dynamicity of species, several examples of evolution, involution, and indeterminacy (neutrality), neutrosophic selection, refined neutrosophic theory of evolution, and the paper ends with open questions on evolution/neutrality/involution.

2 Taxonomy

Let's recall several notions from classical biology.

The **taxonomy** is a classification, from a scientifically point of view, of the living things, and it classifies them into three categories: **species**, **genus**, and **family**.

3 Species

A **species** means a group of organisms, living in a specific area, sharing many characteristics, and able to reproduce with

each other.

In some cases, the distinction between a population subgroup to be a different species, or not, is unclear, as in the *Sorites Paradoxes* in the frame of *neutrosophy*: the frontier between <A> (where <A> can be a species, a genus, or a family), and <nonA> (which means that is not <A>) is vague, incomplete, ambiguous. Similarly, for the distinction between a series and its subseries.

4 Theories of origin of life

Louis Pasteur (1822–1895) developed in 1860 the theory of *precellular* (*prebiotic*) *evolution*, which says that life evolved from non-living chemical combinations that, over long time, arose spontaneously.

In the late 19th century a theory, called *abiogenesis*, promulgated that the living organisms originated from lifeless matter spontaneously, without any living parents' action.

Carl R. Woese (b. 1928) has proposed in 1970's that the *progenotes* were the very first living cells, but their biological specificity was small. The genes were considered probable (rather than identical) proteins.

John Burdon Sanderson Haldane (1872–1964) proposed in 1929 the *theory that the viruses were precursors to the living cells* [1].

John Bernal and A. G. Cairns-Smith stated in 1966 the *mineral theory*: that life evolved from inorganic crystals found in the clay, by natural selection [2].

According to the *little bags theory of evolution*, the life is considered as having evolved from organic chemicals that happened to get trapped in some tiny vesicles.

Eigen and Schuster, adepts of the *hypercycle theory*, asserted in 1977 that the precursors of single cells were these little bags, and their chemical reactions cycles were equivalent to the life's functionality [3].

Other theories about the origin of life have been proposed in the biology literature, such as: *primordial soup*, *dynamic state theory*, and *phenotype theory*, but they were later dismissed by experiments.

5 Theories and ideas about evolution

The theory of *fixism* says that species are fixed, they do not evolve or devolve, and therefore the today's species are identical to the past species.

Of course, the *creationism* is a fixism theory, from a religious point of view. Opposed to the fixism is the theory of *transformism*, antecedent to the evolutionary doctrine, in the pre-Darwinian period, which asserts that plants and animals are modified and transformed gradually from one species into another through many generations [22].

Jean Baptiste Pierre Antoine de Monet Lamarck (1749–1829), in 1801, ahead of Charles Darwin, is associated with the *theory of inheritance of acquired characteristics* (or *use-inheritance*), and even *of acquired habits*. Which is called *Lamarckism* or *Lamarckian Evolution*.

If an animal repeatedly stresses in the environment, its body part under stress will modify in order to overcome the environmental stress, and the modification will be transmitted to its offspring.

For example: the giraffe having a long neck in order to catch the tree leaves [4].

Herbert Spencer (1820–1903) used for the first time the term evolution in biology, showing that a population's gene pool changes from a generation to another generation, producing new species after a time [5].

Charles Darwin (1809–1882) introduced the natural selection, meaning that individuals that are more endowed with characteristics for reproduction and survival will prevail ("selection of the fittest"), while those less endowed would perish [6].

Darwin had also explained the structure similarities of leaving things in genera and families, due to the common descent of related species [7].

In his *gradualism* (or *phyletic gradualism*), Darwin said that species evolve slowly, rather than suddenly.

The adaptation of an organism means nervous response change, after being exposed to a permanent stimulus.

In the *modern gradualism*, from the genetic point of view, the beneficial genes of the individuals best adapted to the environment, will have a higher frequency into the population over a period of time, giving birth to a new species [8].

Herbert Spencer also coined the phrase survival of the fittest in 1864, that those individuals the best adapted to the environment are the most likely to survive and reproduce. Alfred Russel Wallace (1823–1913) coined in 1888 the terms *Darwinism* (individuals the most adapted to environment pass their characteristics to their offspring), and Darwinian fitness (the better adapted, the better surviving chance) [9].

One has upward evolution (*anagenesis*, coined by Alpheus Hyatt, 1838–1902, in 1889), as the progressive evolution of the species into another [10], and a *branching evolution* (*cladogenesis*, coined in 1953 by Sir Julian Sorell Huxley, 1887–1975), when the population diverges and new species evolve [11].

George John Romanes (1848–1894) coined the word *neo-Darwinism*, related to natural selection and the theory of genetics that explains the *synthetic theory of evolution*. What counts for the natural selection is the gene frequency in the population [12]. The Darwinism is put together with the paleontology, systematics, embryology, molecular biology, and genetics.

In the 19th century Gregor Johann Mendel (1822–1884) set the base of *genetics*, together with other scientists, among them Thomas Hunt Morgan (1866–1945).

The *Mendelism* is the study of heredity according to the chromosome theory: the living thing reproductive cells contain factors which transmit to their offspring particular characteristics [13].

August Weismann (1834-1914) in year 1892 enounced the germ plasm theory, saying that the offspring do not inherit the acquired characteristics of the parents [14].

Hugo de Vries (1848–1935) published a book in 1901 on *mutation theory*, considering that randomly genetic mutations may produce new forms of living things. Therefore, new species may occur suddenly [15].

Louis Antoine Marie Joseph Dollo (1857–1931) enunciated the *Dollo's principle* (*law* or *rule*) that evolution is irreversible, i.e. the lost functions and structures in species are not regained by future evolving species.

In the present, the *synergetic theory of evolution* considers that one has a natural or artificial multipolar selection, which occurs at all life levels, from the molecule to the ecosystem — not only at the population level.

But nowadays it has been discovered organisms that have re-evolved structured similar to those lost by their ancestors [16].

Life is... complicated!

The genetic assimilation (for *Baldwin Effect*, after James Mark Baldwin, 1861–1934) considered that an advantageous trait (or phenotype) may appear in several individuals of a population in response to the environmental cues, which would determine the gene responsible for the trait to spread through this population [17].

The British geneticist Sir Ronald A. Fisher (1890–1962) elaborated in 1930 the *evolutionary or directional determinism*, when a trait of individuals is preferred for the new generations (for example the largest grains to replant, chosen by farmers) [18].

The *theory of speciation* was associated with Ernst Mayr (b. 1904) and asserts that because of geographic isolation new species arise, that diverge genetically from the larger original population of sexually reproducing organisms. A subgroup becomes new species if its distinct characteristics allow it to survive and its genes do not mix with other species [19].

In the 20th century, Trofim Denisovitch Lysenko (1898–1976) revived the Lamarckism to the *Lysenkoism* school of genetics, proclaiming that the new characteristics acquired by parents will be passed on to the offspring [20].

Richard Goldschmidt (1878–1958) in 1940 has coined the terms of macroevolution, which means evolution from a long timespan (geological) perspective, and microevolution, which means evolution from a small timespan (a few generations) perspective with observable changes [1].

Sewall Wright (1889–1988), in the mid 20th century, developed the *founders effect of principle*, that in isolated places population arrived from the continent or from another island, becomes little by little distinct from its original place population. This is explained because the founders are few in number and therefore the genetic pool is smaller in diversity, whence their offspring are more similar in comparison to the offspring of the original place population.

The founders effect or principle is regarded as a particular case of the *genetic drift* (authored by the same biologist, Sewall Wright), which tells that the change in gene occurs by chance [21].

The mathematician John Maynard Smith has applied the game theory to animal behavior and in 1976 he stated the *evolutionary stable strategy* in a population. It means that, unless the environment changes, the best strategy will evolve, and persist for solving problems.

Other theories related to evolution such as: *punctuated equilibrium* (instantaneous evolution), *hopeful monsters*, and *saltation* (*quantum*) *speciation* (that new species suddenly occur; by Ernst Mayr) have been criticized by the majority of biologists.

6 Open research

By genetic engineering it is possible to make another combination of genes, within the same number of chromosomes. Thus, it is possible to mating a species with another closer species, but their offspring is sterile (the offspring cannot reproduce).

Despite the tremendous genetic engineering development in the last decades, there has not been possible to prove by experiments in the laboratory that: from an inorganic matter one can make organic matter that may reproduce and assimilate energy; nor was possible in the laboratory to transform a species into a new species that has a number of chromosomes different from the existent species.

7 Involution

According to several online dictionaries, **involution** means:

— Decay, retrogression or shrinkage in size; or return to a former state [Collins Dictionary of Medicine, Robert M. Youngson, 2005];

— Returning of an enlarged organ to normal size; or turning inward of the edges of a part; mental decline associated with advanced age (psychiatry) [Medical Dictionary for the Health Professions and Nursing, Farlex, 2012];

— Having rolled-up margins (for the plant organs) [Collins Dictionary of Biology, 3rd edition, W. G. Hale, V. A. Saunders, J. P. Margham, 2005];

— A retrograde change of the body or of an organ [Dorland's Medical Dictionary for Health Consumers, Saunders, an imprint of Elsevier, Inc., 2007];

— A progressive decline or degeneration of normal physiological functioning [The American Heritage, Houghton Mifflin Company, 2007].

8 Theory of Neutrosophic Evolution

During the process of adaptation of a being (plant, animal, or human) B, to a new environment η,

— B partially ***evolves***;

— B partially ***devolves*** (involves, regresses, degenerates);

— and B partially remains ***indeterminate*** which means *neutral* (unchanged), or ambigous — i.e. not sure if it is evolution or involution.

Any action has a reaction. We see, thank to adaptation: evolution, involution, and neutrality (indeterminacy), each one of these three *neutrosophic components* in some degree.

The degrees of evolution/indeterminacy/involution are referred to both: the **structure** of B (its body parts), and **functionality** of B (functionality of each part, or inter-functionality of the parts among each other, or functionality of B as a whole).

Adaptation to new environment conditions means **deadaptation** from the old environment conditions.

Evolution in one direction means involution in the opposite direction.

Loosing in one direction, one has to gain in another direction in order to survive (for equilibrium). And reciprocally.

A species, with respect to an environment, can be:

— in equilibrium, disequilibrium, or indetermination;

— stable, unstable, or indeterminate (ambiguous state);

— optimal, suboptimal, or indeterminate.

One therefore has a **Neutrosophic Theory of Evolution, Involution, and Indeterminacy** (neutrality, or fluctuation between Evolution and Involution). The evolution, the involution, and the indeterminate-evolution depend not only on natural selection, but also on many other factors such as: artificial selection, friends and enemies, bad luck or good luck, weather change, environment juncture etc.

9 Dynamicity of the species

If the species is in indeterminate (unclear, vague, ambiguous) state with respect to its environment, it tends to converge towards one extreme:

— either to equilibrium/stability/optimality, or to disequilibrium/instability/suboptimality with respect to an environment;

— therefore the species either rises up gradually or suddenly by mutation towards equilibrium/stability/optimality;

— or the species deeps down gradually or suddenly by mutation to disequilibrium/instability/suboptimality and perish.

The **attraction point** in this neutrosophic dynamic system is, of course, the state of equilibrium/stability/optimality. But even in this state, the species is not fixed, it may get, due to new conditions or accidents, to a degree of disequilibrium/instability/suboptimality, and from this new state again the struggle on the long way back of the species to its attraction point.

10 Several examples of evolution, involution, and indeterminacy (neutrality)

10.1 Cormorants example

Let's take the flightless cormorants (*Nannopterum harrisi*) in Galápagos Islands, their wings and tail have atrophied (hence **devolved**) due to their no need to fly (for they having no predators on the land), and because their permanent need to dive on near-shore bottom after fish, octopi, eels etc.

Their avian breastbone vanished (**involution**), since no flying muscles to support were needed.

But their neck got longer, their legs stronger, and their feet got huge webbed is order to catch fish underwater (**evolution**).

Yet, the flightless cormorants kept several of their ancestors' habits (functionality as a whole): make nests, hatch the eggs etc. (hence **neutrality**).

10.2 Cosmos example

The astronauts, in space, for extended period of time get accustomed to low or no gravity (**evolution**), but they lose bone density (**involution**). Yet other body parts do not change, or it has not been find out so far (**neutrality/indeterminacy**).

10.3 Example of evolution and involution

The whales **evolved** with respect to their teeth from pig-like teeth to cusped teeth. Afterwards, the whales **devolved** from cusped teeth back to conical teeth without cusps.

10.4 Penguin example

The Galápagos Penguin (Spheniscus mendiculus) evolved from the Humboldt Penguin by shrinking its size at 35 cm high (adaptation by involution) in order to be able to stay cool in the equatorial sun.

10.5 Frigate birds example

The Galápagos Frigate birds are birds that lost their ability to dive for food, since their feathers are not waterproof (**involution**), but they became masters of faster-and-maneuverable flying by stealing food from other birds, called kleptoparasite feeding (**evolution**).

10.6 Example of Darwin's finches

The 13 Galápagos species of Darwin's Finches manifest various degrees of evolution upon their beak, having different shapes and sizes for each species in order to gobble different types of foods (hence **evolution**):

— for cracking hard seeds, a thick beak (ground finch);

— for insects, flowers and cacti, a long and slim beak (another finch species).

Besides their beaks, the finches look similar, proving they came from a common ancestor (hence **neutrality**).

If one experiments, let's suppose one moves the thick-beak ground finches back to an environment with soft seeds, where it is not needed a thick beak, then the thick beak will atrophy and, in time, since it becomes hard for the finches to use the heavy beak, the thin-beak finches will prevail (hence **involution**).

10.7 El Niño example

Professor of ecology, ethology, and evolution Martin Wikelski, from the University of Illinois at Urbana-Champaign, has published in *Nature* a curious report, regarding data he and his team collected about marine iguanas since 1987. During the 1997–1998 El Niño, the marine algae died, and because the lack of food, on one of the Galápagos islands some marine iguanas shrank a quarter of their length and lost half of their weight (adaptation by **involution**).

After plentiful of food became available again, the marine iguanas grew back to their original length and weight (re-adaptation by **evolution**).

[J. Smith, J. Brown, The Incredible Shrinking Iguanas, in Ecuador & The Galápagos Islands, Moon Handbook, Avalon Travel, p. 325.]

10.8 Bat example

The bats are the only mammals capable of naturally flying, due to the fact that their forelimbs have developed into webbed wings (**evolution** by transformation). But navigating and foraging in the darkness, have caused their eyes' functionality to diminish (**involution**), yet the bats "see" with their ears (**evolution** by transformation) using the echolocation (or the bio sonar) in the following way: the bats emit sounds by mouth (one emitter), and their ears receive echoes (two receivers); the time delay (between emission and reception of the sound) and the relative intensity of the received sound give to the bats information about the distance, direction, size and type of animal in its environment.

10.9 Mole example

For the moles, mammals that live underground, their eyes and ears have degenerated and become minuscule since their functions are not much needed (hence adaptation by **involution**), yet their forelimbs became more powerful and their paws larger for better digging (adaptation by **evolution**).

11 Neutrosophic selection

Neutrosophic selection with respect to a population of a species means that over a specific timespan a percentage of its individuals evolve, another percentage of individuals devolve, and a third category of individuals do not change or their change is indeterminate (not knowing if it is evolution or involution). We may have a natural or artificial neutrosophic selection.

12 Refined Neutrosophic Theory of Evolution

Refined Neutrosophic Theory of Evolution is an extension of the neutrosophic theory of evolution, when the degrees of evolution/indeterminacy/involution are considered separately with respect to each body part, and with respect to each body part functionality, and with respect to the whole organism functionality.

13 Open questions on evolution/neutrality/involution

13.1. How to measure the degree of evolution, degree of involution, and degree of indeterminacy (neutrality) of a species in a given environment and a specific timespan?

13.2. How to compute the degree of similarity to ancestors, degree of dissimilarity to ancestors, and degree of indeterminate similarity-dissimilarity to ancestors?

13.3. Experimental Question. Let's suppose that a partial population of species S_1 moves from environment η_1 to a different environment η_2; after a while, a new species S_2 emerges by adaptation to η_2; then a partial population S_2 moves back from η_2 to η_1; will S_2 evolve back (actually devolve to S_1)?

13.4. Are all species needed by nature, or they arrived by accident?

14 Conclusion

We have introduced for the first time the concept of *Neutrosophic Theory of Evolution, Indeterminacy* (*or Neutrality*), *and Involution*.

For each being, during a long timespan, there is a process of partial evolution, partial indeterminacy or neutrality, and partial involution with respect to the being body parts and functionalities.

The function creates the organ. The lack of organ functioning, brings atrophy to the organ.

In order to survive, the being has to adapt. One has adaptation by evolution, or adaptation by involution — as many examples have been provided in this paper. The being partially evolves, partially devolves, and partially remains unchanged (fixed) or its process of evolution-involution is indeterminate. There are species partially adapted and partially struggling to adapt.

References

1. Barbieri M. The Semantic Theory of Evolution. Chur, Switzerland, 1985.
2. Cairns-Smith A.G. The Origin of Life and the Nature of Primitive Gene. *Journal of Theoretical Biology*, 1966, v. X, 53–88.
3. Eigen M. and Schuster P. The Hypercycle. A Principle of Natural Self-Organization. *Naturwissenschaften*, 1977, v. LXIV, 541–565.
4. Lamarck J.B. Zoological Philosophy. 1809.
5. Reader J. The Rise of Life. New York, 1988
6. Sober E. The Nature of Selection. Cambridge, MA, 1984.
7. Kohn D. The Darwinian Heritage. Princeton, NJ, 1985.

8. Eldredge N. Life Pulse: Episodes from the Story of the Fossil Record. New York, 1987.
9. Wallace A.R. Darwinism: An Exposition of the Theory of Natural Selection with Some of its Applications MacMillan, London, 1889.
10. Brown J. Biogeography. St. Louis, MO, 1983.
11. Delson E. Ancestors: The Hard Evidence. New York, 1985.
12. Bowler P. Evolution: The History of an Idea. Berkeley, California, 1984.
13. Olby R. The Origins of Mendelism. London-Chicago, 1985.
14. Weismann A. The Germ Plasm: A Theory of Heredity. London, 1893.
15. de Vries H. Mutationstheorie [Mutation Theory]. Leipzig. Veit und Co. 1901 & 1903.
16. Milner R. The Encyclopedia of Evolution: Humanity's Search for its Origins. New York, 1987.
17. Hitching F. The Neck of the Giraffe: Where Darwin Went Wrong. New Haven, Connecticut, 1987.
18. Eldredge N. Unfinished Synthesis. Oxfrd Univ. Press, Oxford, 1985.
19. Ereshefsky M. The Units of Evolution: Essays on the Nature of Species. Cambridge, Massachusetts, 1992.
20. Joravsky D. The Lysenko Affair. Cambridge, Massachusetts, 1970.
21. Magill F. Magill's Survey of Science: Life Science Series. Englewood Cliffs, NJ, 1991.
22. The Great Soviet Encyclopedia. 3rd Edition, The Gale Group, Inc., 2010.
23. Linfan Mao. Biological n-System with Global Stability. *International Conference on Applications of Mathematics in Topological Dynamics*, Section: "Physics, Biological and Chemical Systems", Kolkata, India, December 9–11, 2016.
24. Smarandache F. Galápagos sau Ținutul Broaștelor Țestoase Gigantice: Teoria Neutrosofică a Evoluției. Editura Agora, Sibiu, 2017.

On the Vacuum Induced Periodicities Inherent to Maxwell Equations

Fernando Ogiba
E-mail: fogiba@gmail.com

The hypothesis that the Planck's vacuum is inherent to all physical laws, given that it interact with massless elementary electrical charges, is examined exploring gauge invariance. It is then found that Compton's and de Broglie's periodicities, parameters of distinct vacuum induced fluctuations, are inherent to Maxwell equations.

Electromagnetic fields, in principle, are produced by electrical charges (and its movements), which are permanently actuated by the Planck's vacuum [1]. In this sense, it is expected that Maxwell's equations contain some (hidden) information about vacuum induced fluctuations.

The above hypothesis will be examined, firstly, considering the well-known redefinitions of the electromagnetic potentials that leaves the Maxwell equations unchanged, i.e.

$$\mathbf{A} \to \mathbf{A} + \nabla\chi, \quad \phi \to \phi - \partial_t\chi, \tag{1}$$

where χ is a scalar function (not as arbitrary as it may seem), together with the Lorenz condition (SI units)

$$c^{-2}\partial_t\phi + \nabla \cdot \mathbf{A} = 0, \tag{2}$$

which is not a condition (nor a gauge) but a physical law [2].

In order to preserve the local conservation law (2) under the redefinitions (1), χ must obey

$$\nabla^2\chi - c^{-2}\partial_{tt}\chi = 0, \tag{3}$$

as can be seen in the reference [3, p.$\dot{2}$39]. This wave equation (and the assumptions to get it) suggests that electrical charges – regardless of their ordinary translational motions – present *local* periodical space-time evolutions at the light speed c. It means that massless elementary electrical charges (MEECs), everywhere, incorporate the local space-time evolution of the incoming zero-point radiation (ZPR). Apart randomness, this interpretation agrees with the Schrödinger's *zitterbewegung* [4]; i.e., electrons describe random curvilinear paths (Compton's angular frequency) at the light speed.

Aiming to proof that the periodicity of the *local* Eq.(3) is indeed the Compton's one, the observed motion will be introduced through the simple (but rich in content) relation

$$\mathbf{A} = \left(\phi/c^2\right)\mathbf{v}, \tag{4}$$

which relates the potentials of a free charged particle moving with velocity $\mathbf{v}$, as can be verified from the corresponding current density $\mathbf{J} = \rho\mathbf{v}$, where ρ is charge density, together with

$$\nabla^2\mathbf{A} - c^{-2}\partial_{tt}\mathbf{A} = -\mu_o\mathbf{J}, \quad \nabla^2\phi - c^{-2}\partial_{tt}\phi = -\rho/\epsilon_o. \tag{5}$$

Following the same steps that led to Eq.(3), to preserve the form of Eq.(4) – relativistic energy-momentum relation (per unit charge) – under the redefinitions (1), χ must obey

$$\nabla\chi + c^{-2}\partial_t\chi = 0. \tag{6}$$

Assuming that the inferred periodicity of χ obeys the standard phase $\omega t - \mathbf{k} \cdot \mathbf{x}$, the Eq.(6) implies

$$-\mathbf{k} + (\omega/c^2)\mathbf{v} = 0, \tag{7}$$

from which we obtain the *improper* phase velocity

$$v_p = \omega/|\mathbf{k}| = c^2/v; \tag{8}$$

i.e., the phase velocity of the inherent de Broglie wave.

The above result implies that ω is the Compton's angular frequency ($\gamma m_o c^2/\hbar$), and $|\mathbf{k}|$ is the de Broglie wave number ($\gamma m_o v/\hbar$), where γ is the Lorentz factor [5].

Notice, the periodicity of the (co-moving) Eq.(3) is therefore $m_o c^2/\hbar$, as inferred in connection with *zitterbewegung*.

The improper nature of v_p and its close relation with inertia [6] are indicative of vibrations triggered by "imminent" violations of the radiation speed limit (ZPR absorbed-emitted by MEECs) when the ordinary motion takes place (quantum wave-packet), as suggested in the reference [5].

Keep the form of Eq.(4), considering the non-uniqueness of $\mathbf{A}$ and ϕ, is convenient for comparing $e\mathbf{A} = (e\phi/c^2)\mathbf{v}$, calculated in the domain d of the extended charge e producing the potentials, with the relativistic relation $\mathbf{p} = (E/c^2)\mathbf{v}$. It means admitting that $\mathbf{p} = [e\mathbf{A}]_d$ and $E = [e\phi]_d$. This, besides agreeing with the classical electron radius as well as with the canonical momentum of a charged particle in an external field, in the sense that $\mathbf{P} = e\mathbf{A}_{tot} = e\mathbf{A} + e\mathbf{A}_{ext} = m\mathbf{v} + e\mathbf{A}_{ext}$, implies that the mass E/c^2 is of electromagnetic origin [7].

References

1. de la Peña L., Cetto A. M., Hernandez A. V. The Emerging Quantum The Physics Behind Quantum Mechanics. Springer, 2015.
2. Jefimenko O. D. Presenting electromagnetic theory in accordance with the principle of causality. *European Journal of Physics*, 2004, v. 25, 287–296.
3. Jackson J. D. Classical Electrodynamics. 3rd ed., John Wiley and Sons Inc., 1999.
4. Dirac P. A. M. The Principles of Quantum Mechanics. 4ed. Oxford University Press, 1958.
5. Ogiba F. On the Quantum-relativistic Behavior of Moving Particles. *Progress in Physics*, 2016, v. 12, n. 4, 325–328.
6. Wignall J. W. G. De Broglie waves and the nature of mass. *Foundations of Physics*, 1985, v. 15, n. 2, 207–227.
7. Griffiths D.J. Electromagnetic Momentum. *American Journal of Physics*, 2012, v. 80, n. 7, 7–18.

The Journal on Advanced Studies in Theoretical and Experimental Physics, including Related Themes from Mathematics

PROGRESS IN PHYSICS

A quarterly issue scientific journal, registered with the Library of Congress (DC, USA). This journal is peer reviewed and included in the abstracting and indexing coverage of: Mathematical Reviews and MathSciNet (AMS, USA), DOAJ of Lund University (Sweden), Scientific Commons of the University of St. Gallen (Switzerland), Open-J-Gate (India), Referativnyi Zhurnal VINITI (Russia), etc.

Electronic version of this journal:
http://www.ptep-online.com

Postal Address

Department of Mathematics and Science,
University of New Mexico,
705 Gurley Ave., Gallup, NM 87301, USA

ISSN: 1555-5534 (print)
ISSN: 1555-5615 (online)

Standard Address Number: 297-5092
Printed in the United States of America

July 2017 **Vol. 13, Issue 3**

CONTENTS

Information for Authors

Progress in Physics has been created for rapid publications on advanced studies in theoretical and experimental physics, including related themes from mathematics and astronomy. All submitted papers should be professional, in good English, containing a brief review of a problem and obtained results.

All submissions should be designed in LaTeX format using *Progress in Physics* template. This template can be downloaded from *Progress in Physics* home page http://www.ptep-online.com

Preliminary, authors may submit papers in PDF format. If the paper is accepted, authors can manage LaTeXtyping. Do not send MS Word documents, please: we do not use this software, so unable to read this file format. Incorrectly formatted papers (i.e. not LaTeXwith the template) will not be accepted for publication. Those authors who are unable to prepare their submissions in LaTeXformat can apply to a third-party payable service for LaTeX typing. Our personnel work voluntarily. Authors must assist by conforming to this policy, to make the publication process as easy and fast as possible.

Abstract and the necessary information about author(s) should be included into the papers. To submit a paper, mail the file(s) to the Editor-in-Chief.

All submitted papers should be as brief as possible. Short articles are preferable. Large papers can also be considered. Letters related to the publications in the journal or to the events among the science community can be applied to the section *Letters to Progress in Physics*.

All that has been accepted for the online issue of *Progress in Physics* is printed in the paper version of the journal. To order printed issues, contact the Editors.

Consideration and review process does not require any payment from the side of the submitters. Nevertheless the authors of accepted papers are requested to pay the page charges. *Progress in Physics* is a non-profit/academic journal: money collected from the authors cover the cost of printing and distribution of the annual volumes of the journal along the major academic/university libraries of the world. (Look for the current author fee in the online version of *Progress in Physics*.)

The Curved Space is the Electrified Flat Space

Jamila Douari

Department of Science, University of North Florida, 1 UNF Drive 32224, Jacksonville, Florida, USA.
High Energy Section, The Abdus Salam International Center for Theoretical Physics, Trieste, Italy.
E-mail: jdouari@hotmail.com

The responsibility of the electric field E in the modification of the nature of the space is proved. We investigate the way the fundamental strings are related to super-gravity background of D5-branes; i.e. once the endpoints of the D-strings are electrified the flat space becomes curved. We study the electrified relative and overall transverse perturbations of fuzzy funnel solutions of intersecting (N, N_f)-strings and D5-branes in flat and super-gravity backgrounds respectively. As a result the perturbations have a discontinuity which corresponds to a zero phase shift realizing Polchinski's open string Neumann boundary condition. And once the electric field E is turned on in flat space these perturbations decrease and when E is close to the critical value $1/\lambda$ the perturbations disappear forever and the string coupling becomes strong. At this stage the space is considered curved and the electric field is responsible for this effect. This phenomenon is also enhanced by the behavior of the potential V associated to the perturbations Φ on the funnel solutions under the influence of the electric field. The potential goes too fast to $-\infty$ when E goes to the critical value $1/\lambda$ in flat space which looks like a kink to increase the velocity for Φ to disappear. But in curved space and close to the intersecting point we do not find any perturbation for all E and there is no effect of E on V and this is a sign to the absence of the perturbation effects in super-gravity background. This clarifies the existence of a relation between the electric field and the super-gravity background.

1 Introduction

The present work proves the fact that the flat space becomes curved because of the presence of the electric field. We use the non-Abelian Dirac-Born-Infeld (DBI) effective action for this study. Many results using this action have dealt with brane intersections and polarization [1–3, 5, 6, 18]. The study of brane intersections has given a realization of non-commutative geometry in the form of so-called fuzzy funnels [7–13]. In the context of time dependence in string theory from the effective D-brane action, we expect that the hyperplanes can fluctuate in shape and position as dynamical objects.

We deal with the branes intersection problem of (N, N_f)-strings with D5-branes in flat and curved spaces by treating the relative and overall transverse perturbations. And it will be devoted to extend the research begun in [9, 12, 13]. The duality of intersecting D1-D3 branes in the low energy effective theory in the presence of electric field is found to be broken in [11] but the duality of intersecting D1-D5 branes discussed in [12] is unbroken in the same theory with the electric field switched on which allows us to be more interested by the study of the intersecting D1-D5 branes.

We observe, in section 2, that the most lowest energy is gotten as the electric field E is approximately its critical value $1/\lambda$ ($\lambda = 2\pi\ell_s^2$ and ℓ_s the string length) and also as E is going to $1/\lambda$ the physical radius is going to the highest value and then D5-brane is getting bulky.

The analysis we give in sections 3 and 4 proves that the perturbations have a discontinuity which corresponds to zero phase shift and then the string is Polchinski's open string obeying Neumann boundary condition. Hence the endpoints lie on the hyperplane are still free to move in.

We also look for more effects of E on the perturbations and the associated potentials. The behavior of the perturbations in both backgrounds is as follows: in flat space (section 3), the perturbations are disappearing because of the presence of E and when $E \approx 1/\lambda$ we end by no perturbation and our system is stable; and in curved space (section 4) we did not get any perturbation for all E which means the presence of the super-gravity does not allow any perturbation to appear in the same way that E does in flat space.

The effect of E on the potentials associated to the perturbations in flat and curved spaces is the following: the potential is going down too fast to a very low amplitude minima $(-\infty)$ in flat space as E is going to its maxima, this is interpreted as inducing an increase in the velocity of the perturbation to disappear; and in curved space the effect of E on the potential is absent.

The comparison of the flat and curved cases leads us to say if E or super-gravity is present then the perturbations should be absent. This looks like E affects the flat background of D5-brane and transformed it to super-gravity background where the objects are stable. Consequently, we can think of E and super-gravity as dual.

It's known that in curved space the string coupling g_s is strong. And from our study the electric field E is fixed in terms of g_s by the relation $E = \frac{1}{\lambda}(1 + (N/N_f g_s)^2)^{-1/2}$. Then

if $E \approx 1/\lambda$ that means $N_f g_s \gg 1$ and g_s is strong. In this case the system should be described by Quantum Field Theory (QFT) in curved space where no perturbations show up. Hence our electric field is sending us to another theory such that our space is not flat any more.

The effect of the electric field is clear in this work. E increases the volume of D5-brane and decreases the low energy of the system and changes the nature of the background from flat to curved and tells us the system should now be studied in QFT in curved space.

We start the study by introducing D1⊥D5 branes and discussing the influence of the electric field on the low energy and the volume of D5-brane in section 2. We give the solutions of the linearized equations of motion of the relative transverse perturbations in flat space and we treat the effect of the electric field on the perturbations and the associated potentials in section 3. Then in section 4, we study the overall transverse perturbations and their associated potentials in zero and non-zero modes propagating on a dyonic string in the super-gravity background of the orthogonal D5-branes and we look for the effect of the electric field in this case. The discussion and conclusion are presented in section 5.

2 Intersecting D1 and D5 branes

Let's briefly review the non-abelian viewpoint of the (N, N_f)-strings which grow into D5-branes by using non-commutative coordinates [7, 15, 18]. The dual picture is the intersecting D5 and D1 branes such that (N, N_f)-strings can end on D5-branes, but they must act as sources of second Chern class or instanton number in the world volume theory of the D5-branes. Hence D5 world volume description is complicated because of the second chern term which is not vanishing. The most important feature of the intersecting D1-D5 branes is the fact that the duality of this system discussed in [12] in the low energy effective theory with the electric field switched on is unbroken.

In the present description, the fundamental N_f strings are introduced by adding a U(1) electric field denoted $F_{\tau\sigma} = EI_N$, with I_N the $N \times N$ identity matrix. In fact the electric field turns the N D-strings into a (N, N_f)-strings by dissolving the fundamental string degrees of freedom into the world volume.

For a fixed E we consider the quantization condition on the displacement $D = \frac{N_f}{N}$ such that

$$D \equiv \frac{1}{N}\frac{\delta S}{\delta E} = \frac{\lambda^2 T_1 E}{\sqrt{1-\lambda^2 E^2}}\,.$$

Then the electric field is expressed in terms of string coupling g_s and the number of fundamental strings N_f,

$$E = \frac{1}{\lambda}\left(1+\left(\frac{N}{N_f g_s}\right)^2\right)^{-1/2}. \tag{1}$$

The electric field is turned on and the system dyonic is described by the action

$$\begin{aligned} S &= -T_1 \int d^2\sigma \times \\ &\times STr\left[-\det\left(\eta_{ab} + \lambda F_{ab} \lambda\partial_a \Phi^j - \lambda\partial_b \Phi^i Q^{ij}\right)\right]^{\frac{1}{2}} \end{aligned} \tag{2}$$

with $i, j = 1, ..., 5$, $a, b = \tau, \sigma$ and using $T = 1/\lambda g_s$ such that $\lambda = 2\pi l_s^2$ with l_s is the string length, g_s is the string coupling and $Q_{ij} = \delta_{ij} + i\lambda[\Phi_i, \Phi_j]$. The funnel solution is given by suggesting the ansatz

$$\Phi_i(\sigma) = \mp \hat{R}(\sigma) G_i \tag{3}$$

$i = 1, ..., 5$, where $\hat{R}(\sigma)$ is the (positive) radial profile and G_i are the matrices constructed by Castelino, Lee and Taylor in [14]. We note that G_i are given by the totally symmetric n-fold tensor product of 4×4 Euclidean gamma matrices, such that $\frac{1}{2}[G^i, G^j]$ are generators of SO(5) rotations, and that the dimension of the matrices is related to the integer n by $N = (n+1)(n+2)(n+3)/6$. The funnel solution (3) has the following physical radius

$$R(\sigma) = \sqrt{c}\lambda \hat{R}(\sigma) \tag{4}$$

with c is the Casimir associated with the G_i matrices, given by $c = n(n+4)$, and the funnel solution is

$$\Phi_i(\sigma) = \pm \frac{R(\sigma)}{\lambda\sqrt{c}}\, G_i\,. \tag{5}$$

We compute the determinant in (2) and we obtain

$$S = -NT_1 \int d^2\sigma \sqrt{1-\lambda^2 E^2 + (R')^2}\left(1 + 4\,\frac{R^4}{c\lambda^2}\right). \tag{6}$$

This result only captures the leading large N contribution at each order in the expansion of the square root. Using the action (6), we can derive the lowest energy ξ_{min} as the electric field is present and $E \in]0, 1/\lambda[$, (the low energy in the case of intersecting D1-D5 branes when the electric field is absent was discussed in [15])

$$\begin{aligned} \xi = NT_1 \int d\sigma \Bigg[\Bigg(\sqrt{1-\lambda^2E^2} \mp R'\left(\frac{8R^4}{c\lambda^2} + \frac{16R^8}{c^2\lambda^4}\right)^{\frac{1}{2}}\Bigg)^2 + \\ + \left(R' \pm \sqrt{1-\lambda^2E^2}\left(\frac{8R^4}{c\lambda^2} + \frac{16R^8}{c^2\lambda^4}\right)^{\frac{1}{2}}\right)^2\Bigg]^{\frac{1}{2}} \end{aligned}$$

and

$$\xi_{min} = NT_1\sqrt{1-\lambda^2E^2}\int\left(1+\frac{4R^4}{c\lambda^2}\right)^2 d\sigma. \tag{7}$$

such that

$$R' = \mp\sqrt{1-\lambda^2E^2}\left(\frac{8R^4}{c\lambda^2} + \frac{16R^8}{c^2\lambda^4}\right)^{\frac{1}{2}}. \tag{8}$$

The lowest energy (7) can be rewritten in the following expression

$$\begin{aligned}\xi_{min} &= N_f g_s T_1 \frac{1-\lambda^2E^2}{\lambda E}\int_0^\infty d\sigma + \\ &+ \frac{6N}{c} T_5 \sqrt{1-\lambda^2E^2}\int_0^\infty \Omega_4 R^4 dR + \\ &+ NT_1\sqrt{1-\lambda^2E^2}\int_0^\infty dR - \Delta\xi.\end{aligned} \tag{9}$$

In this equation, $T_5 = T_1/(2\pi l_s)^4$ and we can interpret the four terms as follows; the first term is the energy of N_f strings and the second is the energy of $6N/c \approx n$ (for large N) D5-branes and the third is of N D-strings running out radially across D5-brane world volume and the last term is a binding energy

$$\begin{aligned}\Delta\xi &= 2NT_1\sqrt{1-\lambda^2E^2}\times \\ &\times \int_0^\infty du\, u^4\left(1+\frac{1}{2u^4}-\sqrt{1+\frac{1}{u^4}}\right) \\ &\approx 1.0102\, T_1 l_s N c^{\frac{1}{4}}\sqrt{1-\lambda^2E^2}.\end{aligned} \tag{10}$$

This equation shows that the lowest energy is gotten more lowest as the value of electric field is more important.

The equation (6) can be solved in the dyonic case by considering various limits. For small R, the physical radius of the fuzzy funnel solution (5) is found to be

$$R(\sigma) \approx \frac{\lambda\sqrt{c}}{2\sqrt{2}\sqrt{1-\lambda^2E^2}\sigma} \tag{11}$$

and for large R the solution is

$$R(\sigma) \approx \left(\frac{\lambda^2 c}{\sqrt{18}\sqrt{1-\lambda^2E^2}\sigma}\right)^{\frac{1}{3}} \tag{12}$$

with an upper bound on the electric field $E < 1/\lambda$ for both cases.

According to equations (11) and (12), we remark that as the higher order terms in the BI action would effect a transition from the universal small R behavior to the "harmonic" expansion at large R (σ goes to zero). The effect we get at this stage when the electric field is turned on is that R is going up faster as σ goes to zero once E reaches approximately $1/2\lambda$ as shown in Fig. 1, and we are on D5-brane. It looks like the electric field increases the velocity of the transition from strings to D5-branes world volume. Also we remark that D5 brane got highest radius once E close to its critical value.

The equations (9) and (12) give us the impression that the presence of the electric field is an important phenomena; it decreases the low energy and makes the D5-brane more voluminous.

In the following sections, we include a perturbation in the D5-brane configuration by simply adding lower and higher order symmetric polynomials in the G^i to the matrix configuration. We study the spatial perturbations of the moving D1-branes as the electric field is switched on.

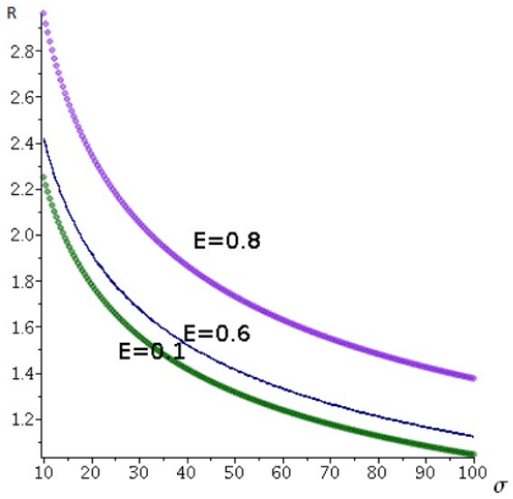

Fig. 1: Large radius.

3 Flat space

In this section, we examine the propagation of the perturbations on the fuzzy funnel by considering dyonic strings in flat background. We discuss the relative transverse perturbations which are transverse to the string, but parallel to the D5-brane world volume (i.e. along $X^{1,..,5}$). The overall transverse perturbations were studied in [13].

We give the relative transverse perturbations in the following form

$$\delta\phi^i(\sigma,t) = f^i(\sigma,t)I_N, \tag{13}$$

as zero mode with $i = 1,..,5$ and I_N the identity matrix. By inserting this perturbation into the full (N, N_f)-string action (2), together with the funnel (6) the action is found to be

$$\begin{aligned}S \approx -NT_1\int d^2\sigma\Big[&\left(1-\lambda^2E^2\right)A - \\ &-(1-\lambda E)\frac{\lambda^2}{2}\left(\dot{f}^i\right)^2 + \frac{(1+\lambda E)\lambda^2}{2A}\left(\partial_\sigma f^i\right)^2 + ...\Big]\end{aligned} \tag{14}$$

with

$$A = \left(1+\frac{4R(\sigma)^4}{c\lambda^2}\right)^2. \tag{15}$$

Then, in large and fixed n the equations of motion are

$$\left(\frac{1-\lambda E}{1+\lambda E}\left\{1+\frac{n^2\lambda^2}{16(1-\lambda^2E^2)^2\sigma^4}\right\}^2\partial_\tau^2 - \partial_\sigma^2\right)f^i = 0. \tag{16}$$

Let's suggest that

$$f^i = \Phi(\sigma)e^{-i\omega\tau}\delta x^i,$$

in the direction of δx^i with Φ is a function of σ and the equations of motion become

$$\left(-\frac{1-\lambda E}{1+\lambda E}\left(1+\frac{n^2\lambda^2}{16(1-\lambda^2E^2)^2\sigma^4}\right)^2 w^2-\partial_\sigma^2\right)\Phi = 0 \quad (17)$$

which can be rewritten as

$$\left(-\frac{1-\lambda E}{1+\lambda E}\left(\frac{n^2\lambda^2}{8(1-\lambda^2E^2)^2\sigma^4}+ \right.\right. \\ \left.\left.+\frac{n^4\lambda^4}{16^2(1-\lambda^2E^2)^4\sigma^8}\right)w^2-\partial_\sigma^2\right)\Phi = \frac{1-\lambda E}{1+\lambda E}\,w^2\,\Phi\,. \quad (18)$$

Since the equation looks complicated, we simplify the calculations by dealing with asymptotic analysis; we start by the system in small and then large σ limits.

3.1 Small σ region

In this region, we see that σ^8 dominates and the equation of motion is reduced to

$$\left(-\partial_\sigma^2+V(\sigma)\right)\Phi = \frac{1-\lambda E}{1+\lambda E}\,w^2\Phi \quad (19)$$

for each direction δx^i, with the potential

$$V(\sigma) = -\frac{w^2n^4\lambda^4}{16^2(1+\lambda E)^5(1-\lambda E)^3\sigma^8}\,. \quad (20)$$

The progress of this potential is shown in Fig. 2; when we are close to the D5-brane the potential is close to zero and once E is turned on it gets negative values until E is close to its maxima, we see this potential goes down too fast to a very low amplitude minima ($-\infty$). This phenomenon should have a physical meaning! This could be thought as a kink to increase the Φ's velocity to push the perturbation to disappear.

To solve (19), we consider the total differential on the perturbation. Let's denote $\partial_\sigma\Phi \equiv \Phi'$. Since Φ depends only on σ we find $\frac{d\Phi}{d\sigma} = \partial_\sigma\Phi$. We rewrite (19) in this form

$$\frac{1}{\Phi}\frac{d\Phi'}{d\sigma} = -w^2\left[\frac{n^4\lambda^4}{16^2(1+\lambda E)^5(1-\lambda E)^3\sigma^8}+1\right]. \quad (21)$$

An integral formula can be written as follows

$$\int_0^{\Phi'}\frac{d\Phi'}{\Phi} = -\int_0^{\sigma} w^2\left[\frac{n^4\lambda^4}{16^2(1+\lambda E)^5(1-\lambda E)^3\sigma^8}+1\right]d\sigma \quad (22)$$

which gives

$$\frac{\Phi'}{\Phi} = -w^2\left[-\frac{n^4\lambda^4}{16^2(1+\lambda E)^5(1-\lambda E)^3\times 7\sigma^7}+\sigma\right]+\alpha\,. \quad (23)$$

We integrate again the following

$$\int_0^{\Phi}\frac{d\Phi}{\Phi} = -\int_0^{\sigma} d\sigma\times \\ \times\left(w^2\left[-\frac{n^4\lambda^4}{16^2\,7(1+\lambda E)^5(1-\lambda E)^3\sigma^7}+\sigma\right]+\alpha\right). \quad (24)$$

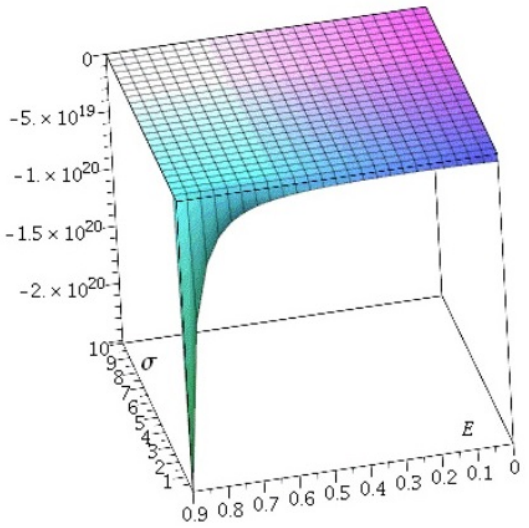

Fig. 2: Potential associated to the relative transverse perturbations in small region in flat space.

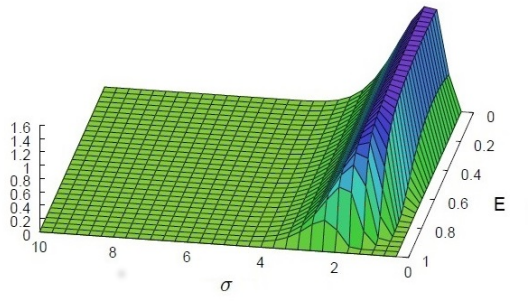

Fig. 3: Relative transverse perturbations in small region in flat space.

We get

$$\ln\Phi = -w^2\left[-\frac{n^4\lambda^4}{16^2\;42(1+\lambda E)^5(1-\lambda E)^3\sigma^6}+\frac{\sigma^2}{2}\right]+ \\ +\;\alpha\sigma+\beta \quad (25)$$

and the perturbation in small σ region is found to be

$$\Phi(\sigma) = \beta\, e^{-w^2\left[-\frac{n^4\lambda^4}{16^2\;42(1+\lambda E)^5(1-\lambda E)^3\sigma^6}+\frac{\sigma^2}{2}\right]+\alpha\sigma} \quad (26)$$

with β and α are constants.

We plot the progress of the obtained perturbation. First we consider the constants $\beta = 1 = \alpha$, then the small spatial coordinate in the interval $[0, 10]$ with the unit of $\lambda = 1$, $w = 1$ and $n \approx 10^3$ with the electric field in $[0, 1[$.

As shown in Fig. 3, close to D5-brane there is perturbation. We remark that as E goes up, the perturbation goes down. And when $E \approx 1/\lambda$ we observe no perturbation effects.

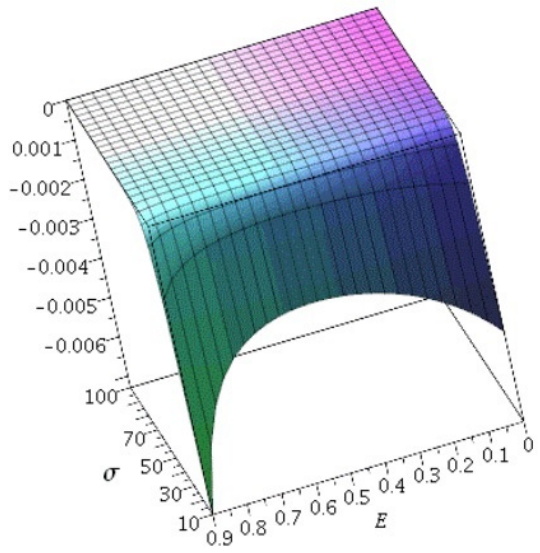

Fig. 4: Potential of relative transverse perturbations in large region in flat space.

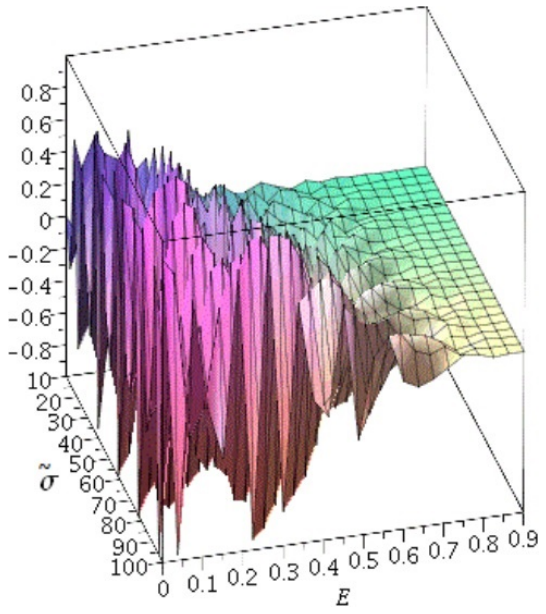

Fig. 5: Relative transverse perturbations in large region in flat space.

At this stage, according to (1) the string coupling gets strong $N_f g_s \gg 1$ which means the system background is changed. We know that with strong coupling the system should be in super-gravity background where the perturbations are no more. Consequently, the presence of E kills the perturbation and moves the system from flat to super-gravity background.

3.2 Large σ region

By considering large σ limit the equation of motion (18) becomes

$$\Big(-\partial_\sigma^2 + V(\sigma)\Big)\Phi = \frac{1-\lambda E}{1+\lambda E}\, w^2\Phi \tag{27}$$

with the potential

$$V(\sigma) = -\frac{w^2 n^2 \lambda^2}{8(1+\lambda E)^3(1-\lambda E)\sigma^4}\,. \tag{28}$$

By plotting the progress of this potential (Fig. 4) we remark that when σ goes faraway from the D5-brane the potential vanishes approximately for all values of the electric field. And close to D5-brane the potential gets negative values. The effect of E is very clear; as E goes up V slows down the decreasing until the medium of E, then V decreases too fast until its minimum value for E going up to its critical value.

Consequently, the electric field has the same effect on V in both regions of σ; as E goes to its maxima V goes to its minima.

To solve (27) we rewrite it in the following form

$$\left(\partial_{\tilde\sigma}^2 + \frac{\kappa^2}{\tilde\sigma^4} + 1\right)\Phi = 0, \tag{29}$$

with

$$\tilde\sigma = \sqrt{\frac{1-\lambda E}{1+\lambda E}}\, w\sigma \tag{30}$$

and

$$\kappa^2 = \frac{n^2\lambda^2}{8w^2(1+\lambda E)(1-\lambda E)^3}\,. \tag{31}$$

Eq. (29) is a Schrödinger equation for an attractive singular potential $\propto \tilde\sigma^{-4}$ and depends on the single coupling parameter κ with constant positive Schrödinger energy. The solution is then known by making the following coordinate change

$$\chi(\tilde\sigma) = \int_{\sqrt{\kappa}}^{\tilde\sigma} dy \sqrt{1+\frac{\kappa^2}{y^4}} \tag{32}$$

and

$$\Phi = \left(1+\frac{\kappa^2}{\tilde\sigma^4}\right)^{-\frac{1}{4}}\tilde\Phi. \tag{33}$$

Thus, (29) becomes

$$\Big(-\partial_\chi^2 + V(\chi)\Big)\tilde\Phi = 0 \tag{34}$$

with

$$V(\chi) = \frac{5\kappa^2}{\left(\tilde\sigma^2 + \frac{\kappa^2}{\tilde\sigma^2}\right)^3}\,. \tag{35}$$

Then, the perturbation is found to be

$$\Phi = \left(1+\frac{\kappa^2}{\tilde\sigma^4}\right)^{-\frac{1}{4}} e^{\pm i\chi(\tilde\sigma)} \tag{36}$$

which has the following limit; since we are in large σ region $\Phi \sim e^{\pm i\chi(\tilde{\sigma})}$. This is the asymptotic wave function in the region $\chi \to +\infty$, while around $\chi \sim 0$, i.e. $\tilde{\sigma} \sim \sqrt{\kappa}$ and $\sigma \sim n\lambda/2\sqrt{2}w^2(1-\lambda E)^2$, $\Phi \sim 2^{-\frac{1}{4}}$.

Owing to the plotting of the progress of this perturbation (Fig. 5), by considering the real part of the function, the perturbation solution is totally different from the one gotten in the small σ limit (26). Hence the perturbations have a discontinuity and the system is divided into two regions which implies Neumann boundary conditions and the end of an open string can move freely on the brane in the dyonic case, which means the end of a string on D5-brane can be seen as an electrically charged particle.

Fig. 5 shows that the perturbation is slowing down as E is turned on then starts to disappear once E reaches the value $1/2\lambda$. The perturbation disappears when E is too close to $1/\lambda$ for all values of σ. The effect of E is very surprising! The presence of E stops the perturbations.

No electric field means the intersecting point is in high perturbation. Then as E is turned on the perturbations decrease. When E is close to its critical value the perturbations are no more. They are killed by E. This phenomena matches very well with the fact that g_s becomes strong ($N_f g_s \gg 1$) at this point according to the relation (5) such that $E \approx 1/\lambda$. Consequently, we can suggest that the presence of the electric field changes the background of D-branes from flat to supergravity background (where the string coupling is strong).

4 Curved space

We extend the investigation of the intersecting D1-D5 branes to curved space. We consider again the presence of electric field and the resulting configuration is a bound state of fundamental strings and D-strings. Under these conditions the bosonic part of the effective action is the non-abelian BI action

$$\begin{aligned} S &= -T_1 \int d^2\sigma e^{-\phi} STr\Big[-\det\Big(P\left(G_{ab}+\right. \\ &\left. +G_{ai}\left(Q^{-1}-\delta\right)^{ij}G_{jb}+\lambda F_{ab}\right)\Big)\det Q^{ij}\Big]^{\frac{1}{2}} \end{aligned} \tag{37}$$

with T_1 the D1-brane tension, G the bulk metric, (for simplicity we set the Kalb-Ramond two form B to be zero), ϕ the dilaton and F the field strength, $a, b = \tau, \sigma$ and $i, j = 1, 2, 3, 4, 5$. Furthermore, P denotes the pullback of the bulk space time tensors to each of the brane world volume. The matrix Q is given by $Q^i_j = \delta^i_j + i\lambda\left[\phi^i, \phi^k\right]G_{kj}$, with ϕ^i are the transverse coordinates to the D1-branes.

We consider the super-gravity background and the metric of n D5-branes

$$\begin{aligned} ds^2 &= \frac{1}{\sqrt{h}}\eta_{\mu\nu}dx^\mu dx^\nu + \sqrt{h}\left(d\sigma^2+\sigma^2 d\Omega_3^2\right) \\ e^{-\phi} &= \sqrt{h} \\ h &= 1+\frac{L^2}{\sigma^2} \end{aligned} \tag{38}$$

with $\mu, \nu = \tau, \sigma$ and $L = nl_s^2 g_s$.

4.1 Zero mode

In our work we treat E as a variable to discuss its influence on the perturbations. We investigate the perturbations in the super-gravity background of an orthogonal 5-brane in the context of dyonic strings growing into D5-branes. The study is focused on overall transverse perturbations in the *zero mode*; $\delta\phi^i = f^i(\tau,\sigma)I$, $i = 6, 7, 8, 9$ and I is $N \times N$ identity matrix.

The action describing the perturbed intersecting D1-D5 branes in the super-gravity background is

$$\begin{aligned} S &\equiv -NT_1 e^{-\phi}\int d^2\sigma\Big[G_{\tau\tau}G_{\sigma\sigma}(1+\lambda E)- \\ &\quad -\frac{\lambda^2}{2}\left(1-\lambda^2E^2\right)G_{\sigma\sigma}G_{ii}(\dot{f}^i)^2+ \\ &\quad +\frac{\lambda^2}{2}\left(1+\lambda E\right)G_{\tau\tau}G_{ii}(f^i)'^2+\ldots\Big] \\ &\equiv -NT_1\int d^2\sigma\sqrt{h}\Big[1+\lambda E- \\ &\quad -\frac{\lambda^2\alpha_i}{2h}(1-\lambda^2E^2)(\dot{f}^i)^2+ \\ &\quad +\frac{\lambda^2\sqrt{h}\alpha_i}{2}(1+\lambda E)(f^i)'^2+\ldots\Big] \end{aligned} \tag{39}$$

where $h(\sigma) = e^{-2\phi} = 1+L^2/\sigma^2$, $\dot{f}^i = \partial_\tau f^i$, $(f^i)' = \partial_\sigma f^i$, $G_{\tau\tau} = h^{-1/2}G_{\sigma\sigma} = \sqrt{h}e^{-\phi}$ and $G_{ii} = \alpha_i$ with α_i some real numbers.

The equations of motion of the perturbations are found to be

$$\left(\frac{1-\lambda E}{h^{3/2}}\partial_\tau^2 - \partial_\sigma^2 + \frac{L^2}{h\sigma^3}\partial_\sigma\right)f^i = 0\,. \tag{40}$$

If we consider $\tilde{\sigma}^2 = \sigma^2 + L^2$ the equations of motion become

$$\left(\frac{1-\lambda E}{\sqrt{h}}\partial_\tau^2 - \partial_{\tilde{\sigma}}^2\right)f^i(\tilde{\sigma},t) = 0\,. \tag{41}$$

We define the perturbations as

$$f^i(\tilde{\sigma},t) = \Psi(\tilde{\sigma})\,e^{-iw\tau}\delta x^i \tag{42}$$

with δx^i ($i = 6, 7, 8, 9$) the direction of the perturbation and (41) becomes

$$\left(-w^2(1-\lambda E)\frac{\tilde{\sigma}}{\sqrt{\tilde{\sigma}^2-L^2}} - \partial_{\tilde{\sigma}}^2\right)\Psi = w^2(1-\lambda E)\Psi \tag{43}$$

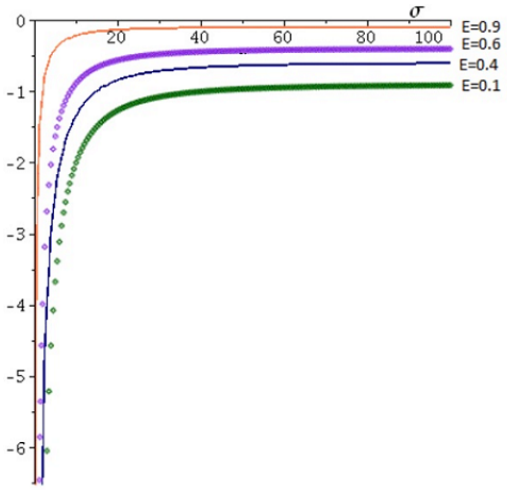

Fig. 6: Potential in curved space for zero mode.

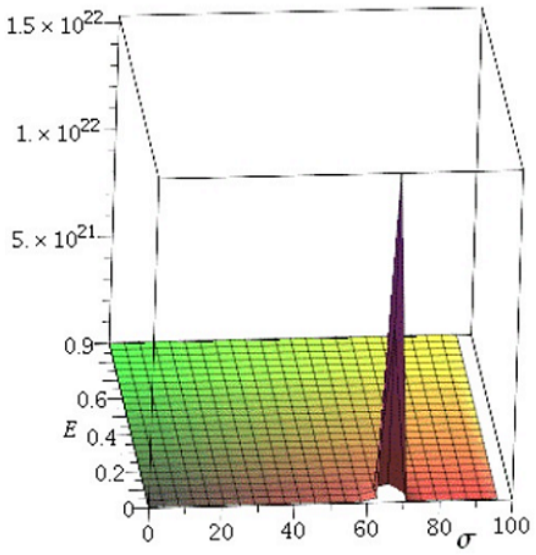

Fig. 7: Overall transverse perturbations in curved space for zero mode.

with the potential

$$V = -w^2(1-\lambda E)\,\frac{\tilde{\sigma}}{\sqrt{\tilde{\sigma}^2-L^2}} = -w^2(1-\lambda E)\,\frac{\sqrt{\sigma^2+L^2}}{\sigma}\,.$$

Fig. 6 shows the variation of the potential V in terms of σ. We remark approximately the absence of the potential for all large values of σ and V goes to zero as E goes to $1/\lambda$. When σ is too close to zero, in this case V is negative and goes down too quick for all E and the potential is not that low. In addition, in the curved space the effect of E is approximately absent.

Let's solve the differential equation (43). As we see this is Heun's equation and the solution is the perturbation

$$\begin{aligned}\Psi &= \left(-\tilde{\sigma}^2+L^2\right)\times\\ &\times\Big[\eta\,\mathrm{HeunC}\left(0,\frac{-1}{2},1,\frac{1}{4}\,w^2(1-\lambda E)L^2,\frac{1}{2}+\right.\\ &+\left.\frac{1}{4}\,(-L^2+L^2)w^2(1-\lambda E),\tilde{\sigma}^2/L^2\right)+\\ &+\beta\,\mathrm{HeunC}\left(0,\frac{1}{2},1,\frac{1}{4}\,w^2(1-\lambda E)L^2,\frac{1}{2}+\right.\\ &+\left.\frac{1}{4}\,(-L^2+L^2)w^2(1-\lambda E),\tilde{\sigma}^2/L^2\right)\Big]\tilde{\sigma}\end{aligned} \tag{44}$$

with η and β are constants.

We tried to plot the perturbation (44) for small region of σ (the radius of funnel solution is too large) and there is no perturbation in this region. The intersecting point is stable in super-gravity background even if the electric field is present.

Fig. 7 shows the variation of the perturbation in terms of the electric field E and the coordinate $\tilde{\sigma}$ in large region such that the radius of funnel solution is too small. We set $\lambda = 1$, $w = 1$ and $n = 10^2$. The perturbation is showing up as a peak for a while and for low electric field. In general we observe approximately no perturbation effects for all E in this case.

The important remark we obtain by comparing the influence of E on the perturbation in flat and curved spaces is that E kills the perturbation in flat space (Fig. 3, Fig. 5) and turns the string coupling to be strong and then the flat space in this case becomes curved when E reaches its critical value, but when the space is already curved the influence of E is absent. This observation leads us to think that E is strongly related in some way to the super-gravity background.

4.2 Non-zero modes

Let's now consider the *non-zero modes*, the perturbations can be written in the form

$$\delta\phi^m(\sigma,t) = \sum_{\ell=1}^{N-1}\psi^m_{i_1\ldots i_\ell}G^{i_1}\ldots G^{i_\ell}$$

and $\psi^m_{i_1\ldots i_\ell}$ are completely symmetric and traceless in the lower indices. We get two terms added to the action (39) to describe the present system $[\phi^i,\delta\phi^m]^2$ and $[\partial_\sigma\phi^i,\partial_t\delta\phi^m]^2$. Then in the equation of motion (40) these two terms $[\phi^i,[\phi^i,\delta\phi^m]]$ and $[\partial_\sigma\phi^i,[\partial_\sigma\phi^i,\partial_t^2\delta\phi^m]]$ appeared. We have $\phi^i = RG^i$ and by straightforward calculations we have

$$\begin{aligned}[G^i,[G^i,\delta\phi^m],] &= \sum_{\ell<N}^{N-1}\psi^m_{i_1\ldots i_\ell}[G^i,[G^i,G^{i_1}\ldots G^{i_\ell}]]\\ &= \sum_{\ell<N}^{N-1}\psi^m_{i_1\ldots i_\ell}\epsilon^{i_1\ldots i_\ell}G^{i_1}\ldots G^{i_\ell},\\ &= \sum_{\ell<N}^{N-1}4\ell(\ell+\beta)\,\delta\phi^m_\ell\end{aligned} \tag{45}$$

with $\epsilon^{i_1\cdots i_\ell}$ antisymmetric tensor and β a real number. To obtain a specific spherical harmonic on 4-sphere, we have

$$\begin{aligned}[\phi^i,[\phi^i,\delta\phi^m_\ell]] &= \frac{\ell(\ell+\beta)\lambda^2 c}{2(1-\lambda^2E^2)\sigma^2}\,\delta\phi^m_\ell,\\ [\partial_\sigma\phi^i,[\partial_\sigma\phi^i,\partial_t^2\delta\phi^m]] &= \frac{\ell(\ell+\beta)\lambda^2 c}{2(1-\lambda^2E^2)\sigma^4}\,\partial_t^2\delta\phi^m_\ell\,.\end{aligned} \tag{46}$$

Then for each mode we set $\delta\phi^m_\ell = f^m_\ell(\tilde\sigma)e^{-i\omega\tau}\delta x^m$ with f^m_ℓ some function for each mode. Then the equations of motion will be in this form

$$(-\partial^2_{\tilde\sigma} + V(\tilde\sigma))f^m_\ell(\tilde\sigma) = -w^2(1-\lambda E)f^m_\ell(\tilde\sigma) \tag{47}$$

with $V(\tilde\sigma) = V_1 + V_2 + V_3$ and

$$V_1 = -w^2(1-\lambda E)\,\frac{\tilde\sigma}{\sqrt{\tilde\sigma^2-L^2}} = -w^2(1-\lambda E)\,\frac{\sqrt{\sigma^2+L^2}}{\sigma} \tag{48}$$

$$V_2 = \frac{\ell(\ell+\beta)\lambda^2 c}{2(\tilde\sigma^2-L^2)} = \frac{\ell(\ell+\beta)\lambda^2 c}{2\sigma^2} \tag{49}$$

$$V_3 = \frac{\ell(\ell+\beta)\lambda^6 c w^2\alpha^i\alpha^m}{24(1-\lambda^2E^2)(\tilde\sigma^2-L^2)^2} = \frac{\ell(\ell+\beta)\lambda^6 c w^2\alpha^i\alpha^m}{24(1-\lambda^2E^2)\sigma^4}\,. \tag{50}$$

These expressions can be treated by taking into account the limits of σ such as σ goes to zero and the infinity.

For small σ, V_3 dominates and in large σ, $V_1 + V_2$ will dominate. From now on, it is clear that the system in the present background will get different potentials and perturbations from region to other which support the idea of Neumann boundary condition in super-gravity background.

We start by small σ region, and the plot of V_3 (Fig. 8) shows that if σ goes to zero then the potential goes to $+\infty$. Physically this behavior should mean something! This could be a sign to the absence of the perturbation effects and the influence of E is absent.

We remark that the electric field does not have any influence on the perturbations in non-zero mode at the presence of the super-gravity background.

Then the perturbation for each mode ℓ is gotten (see (51) at the top of the next page) with b_1 and b_2 are constants and $d = \ell(\ell+\beta)\lambda^6 n(n+1)\alpha^i\alpha^m w^2$. We tried to plot this function but noway we could not get any perturbation for the values $\lambda = 1$, $w = 1$ and for all E, $\ell > 4$ and $n > 1$ in the region $\sigma \in [0, 10]$.

Also the potential shows up with little values by comparison to the case of small region and for all E which means E does not change anything in the case of curved space.

Let's move to the large σ. As σ goes to infinity we see the potential goes to zero (Fig. 9) but when σ approaches the small σ region the potential goes up too quick and reaches the maximum value, approximately for all E. Then the electric field does not have influence on the behavior of the potential in curved space.

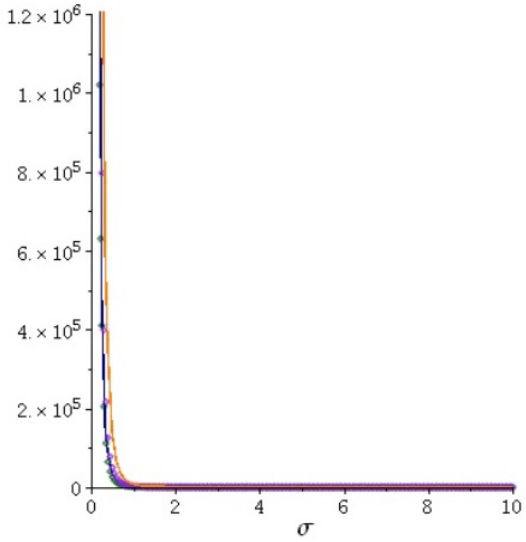

Fig. 8: Potential in curved space for non-zero mode for different values of E in small region.

The perturbation for each mode is (see (52)) with a_1 and a_2 are real constants. We tried to plot this function for all E, $\ell = 10$ and $n = 10^2$, and no perturbations appear which is consistent with the nature of space. Since the system is in super-gravity background, there is no perturbations then no influence of electric field.

5 Discussion and conclusion

In the low energy effective theory with the electric field E is switched on, we proved in [11] that the duality of intersecting D1-D3 branes is broken and in [12] the duality of intersecting D1-D5 branes is unbroken. Hence, it is interesting to know more about the effect of the electric field, and the intersecting D1-D5 branes looks more important as a system.

We consider the non-abelian Born-Infeld (BI) dynamics of the dyonic string such that the electric field E has a limited value. If we suppose there is no excitation on transverse directions then the action of D1-branes is

$$S = -NT_1\int d^2\sigma\,\sqrt{1-\lambda^2E^2}.$$

The limit of E attains a maximum value $E_{max} = 1/\lambda$ just as there is an upper limit for the velocity in special relativity. In fact, if E is constant, after T-duality along the direction of E the speed of the brane is precisely λE so that the upper limit on the electric field follows from the upper limit on the velocity. Hence if this critical value arises such as $E_{max} > 1/\lambda$ the action ceases to make physical sense and the system becomes unstable. Since the string effectively carries electric charges of equal sign at each of its endpoints, as E increases the charges start to repel each other and stretch the string. For

$$
\begin{aligned}
f_\ell^m = b_1\,\mathrm{HeunT}&\left(\frac{-3\,2^{1/3}d\left(-1+\lambda^2E^2\right)(-1+\lambda E)}{\lambda^2\left(-d\left(-1+\lambda^2E^2\right)\right)^{4/3}},0,\frac{\frac{1}{2}d\lambda^2L^2\left(-1+\lambda^2E^2\right)2^{2/3}}{\left(-d\left(-1+\lambda^2E^2\right)\right)^{2/3}},\frac{12^{1/3}\left(-6d\left(-1+\lambda^2E^2\right)\right)^{1/6}\lambda\tilde{\sigma}}{6}\right)\\
&\exp\left(-\frac{\frac{1}{24}\lambda^3\tilde{\sigma}\left(\frac{2}{3}\sqrt{-6d\left(-1+\lambda^2E^2\right)}\tilde{\sigma}^2\left(-d\left(-1+\lambda^2E^2\right)\right)^{2/3}+dL^2 2^{2/3}12^{1/3}\left(-6\left(-1+\lambda^2E^2\right)\right)^{1/6}\left(-1+\lambda^2E^2\right)\right)}{\left(-d\left(-1+\lambda^2E^2\right)\right)^{2/3}}\right)\\
+b_2\,\mathrm{HeunT}&\left(\frac{-3\,2^{1/3}d\left(-1+\lambda^2E^2\right)(-1+\lambda E)}{\lambda^2\left(-d\left(-1+\lambda^2E^2\right)\right)^{4/3}},0,\frac{\frac{1}{2}d\lambda^2L^2\left(-1+\lambda^2E^2\right)2^{2/3}}{-d\left(-1+\lambda^2E^2\right)^{2/3}},-\frac{12^{1/3}\left(-6d\left(-1+\lambda^2E^2\right)\right)^{1/6}\lambda\tilde{\sigma}}{6}\right)\\
&\exp\left(\frac{\frac{1}{24}\lambda^3\tilde{\sigma}\left(\frac{2}{3}\sqrt{-6d\left(-1+\lambda^2E^2\right)}\tilde{\sigma}^2\left(-d\left(-1+\lambda^2E^2\right)\right)^{2/3}+dL^2 2^{2/3}12^{1/3}\left(-6d\left(-1+\lambda^2E^2\right)\right)^{1/6}\left(-1+\lambda^2E^2\right)\right)}{\left(-d\left(-1+\lambda^2E^2\right)\right)^{2/3}}\right)
\end{aligned}
\tag{51}
$$

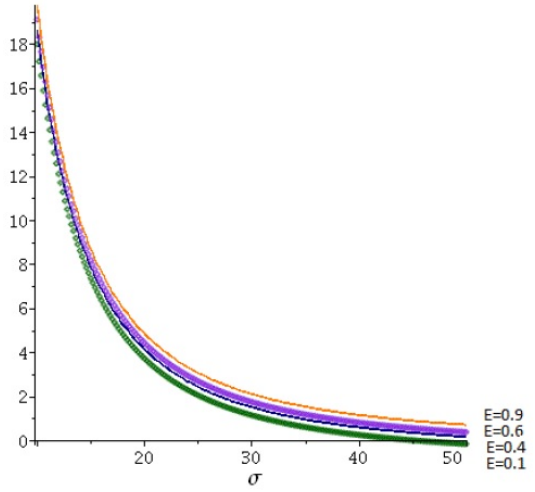

Fig. 9: Potential in curved space for non-zero modes in large region.

E larger than the critical value, the string tension T_1 can no longer hold the strings together.

In this context, we have treated in this project in particular the perturbations of a set of (N, N_f)-strings ending on a collection of n orthogonal D5-branes in lowest energy world volume theory. The fundamental strings ending on an orthogonal D5-branes act as an electric point sources in the world volume theory of D5-brane and the perturbations in both flat and curved spaces were studied from this point of view.

We showed in section 2 that the semi-infinite fuzzy funnel is a minimum energy configuration by imposing singular boundary conditions that have interesting physical interpretation in terms of D-brane geometries. And to consider the lowest energy effective theory the electric field should be present. We found the lowest energy

$$
\begin{aligned}
\xi_{min} &= N_f g_s T_1 \frac{1-\lambda^2E^2}{\lambda E}\int_0^\infty d\sigma+\\
&+\frac{6N}{c}T_5\sqrt{1-\lambda^2E^2}\int_0^\infty \Omega_4 R^4 dR+\\
&+NT_1\sqrt{1-\lambda^2E^2}\int_0^\infty dR-\\
&-1.0102\,T_1 l_s N c^{\frac{1}{4}}\sqrt{1-\lambda^2E^2}
\end{aligned}
$$

by considering E switched on in the low energy effective theory. The energy of intersecting D1-D5 branes is found to be a sum of four parts depending on the electric field E and all these energies are decreasing as E goes to $1/\lambda$. The first is for N_f fundamental strings extending orthogonally away from the D5-branes and the second for the n D5-branes and the third for the N D-strings extending out radially in D5-branes and the fourth is the binding energy.

In this theory, the transition between the universal behavior at small radius of the funnel solution and the harmonic behavior at large one in terms of electric field is mentioned too. When the electric field is turned on the physical radius of the fuzzy funnel solution $R(\sigma) \approx (\lambda^2 c/\sqrt{18}\sqrt{1-\lambda^2E^2}\sigma)^{\frac{1}{3}}$ is going up faster as σ goes to zero (the intersecting point) and E reaches approximately $1/2\lambda$ which looks like the electric field increases the velocity of the transition from strings to D5-branes world volume. Then D5-branes get highest radius once E is close to $1/\lambda$ which interprets the increasing of the volume of the D5-branes under the effect of the electric field (Fig. 1).

In section 3, we have investigated the relative transverse perturbations of the funnel solutions of the intersecting D1-D5 branes in flat space and the associated potentials in terms of the electric field $E \in]0, 1/\lambda[$ and the spatial coordinate σ. We find that too close to the intersecting point the potential is

$$
\begin{aligned}
f_\ell^m = \quad & a_1 \,\text{HeunC}\left(0, \frac{\sqrt{2w^2L^4(\lambda E-1)+L^2-4\lambda^2 cl(l+\beta)}}{2L}, -2, \frac{w^2L^2(\lambda E-1)}{8}, \frac{5}{4}-\frac{w^2L^2(\lambda E-1)}{8},\right. \\
& \left.\frac{2\tilde{\sigma}^2-2\tilde{\sigma}\sqrt{\tilde{\sigma}^2-L^2}-L^2}{L^2}\right)\left(\sqrt{\tilde{\sigma}^2-L^2}+\tilde{\sigma}\right)^{\frac{L-\sqrt{2w^2L^4(\lambda E-1)+L^2-4\lambda^2 cl(l+\beta)}}{2L}} \\
& +a_2 \,\text{HeunC}\left(0, -\frac{\sqrt{2w^2L^4(\lambda E-1)+L^2-4\lambda^2 cl(l+\beta)}}{2L}, -2, \frac{w^2L^2(\lambda E-1)}{8}, \frac{5}{4}-\frac{w^2L^2(\lambda E-1)}{8},\right. \\
& \left.\frac{2\tilde{\sigma}^2-2\tilde{\sigma}\sqrt{\tilde{\sigma}^2-L^2}-L^2}{L^2}\right)\left(\sqrt{\tilde{\sigma}^2-L^2}+\tilde{\sigma}\right)^{\frac{L+\sqrt{2w^2L^4(\lambda E-1)+L^2-4\lambda^2 cl(l+\beta)}}{2L}}
\end{aligned}
\tag{52}
$$

close to zero and once E is turned on it gets negative values until E is close to its maxima, we see this potential goes down too fast to a very low amplitude minima $-\infty$ (Figs. 2,4) and away from the intersecting point there is approximately no potential for all E. This is interpreted as inducing an increase in the velocity of the perturbation to disappear at the intersecting point toward the D5-brane world volume. Figs. 3,5 show that when E goes to its maxima there is no perturbation effects. Hence the presence of E kills in general the perturbations. At this stage, according to (1) the string coupling starts to get strong which means the system background is changing.

In curved space, we have studied the same system by looking for the effect of electric field on the perturbations and the associated potentials in zero (Figs. 6,7) and non zero-modes (Figs. 8,9) of the overall transverse perturbations in section 4. It was surprisingly that too close to the intersecting point; i.e. at large physical radius of D5-brane, we could not find any perturbation and also there is approximately no influence of E on potentials. The effect of E appears only when we are too far away from the intersecting point where the radius is too small and still E makes the perturbations to disappear on the strings. In general we do not see the influence of E in curved space.

The main and very important feature we got from this investigation is the following; the presence of electric field flux on the strings changes the background of the system. We proved explicitly that when the coupling is going to be strong which means E goes to its critical value we should move to QFT to describe the system where no perturbations exist. In curved space the influence of the electric field appears for too small radius of funnel solution which means for large spatial coordinate σ of strings and this phenomena decreases from zero mode to non-zero modes but when the radius is important as σ goes to zero there is no effect of E. By contrast in the case of flat space that was very clear when E is turned on the perturbations change their behavior in general. E forces them to disappear as it is close to the critical value and in meantime the string coupling is getting strong.

The string coupling is strong means $N_f g_s \gg 1$ and $g_s \approx N/N_f$ since $E \approx 1/\lambda$ which is the critical value and if the electric field exceeds this value the system will be non-physical phenomena as discussed above and to be out of this problem we should choose another theory to describe our system.

In the case of weak coupling $N_f g_s \ll 1$ the electric field will be approximately $E \approx N_f g_s/\lambda N$ and the condition matches our perturbative phenomena $E \in [0, 1/\lambda[$. We mention here that if E goes to zero then $N_f g_s$ does too which means the number of fundamental strings decreases and simply the endpoints of the strings loose their electric charges and vice-versa.

In curved space, we can say the electric field E has no effect on the intersecting point. We can connect then the phenomena to the electric field E and the string coupling g_s such as E and g_s are connected by the relation (5). We see that once E is turned on and goes up g_s is getting stronger. At the critical point, E reaches its maxima and g_s is strong then the space should become curved. Hence we can remark at this stage that the effect of E looks like it transforms the flat space to curved one. In this context we can say there is a one-to-one map between the super-gravity background and the electric field that we should look for!

Acknowledgements

The author would like to thank the Abdus Salam International Center for Theoretical Physics, Trieste, for the invitation and the hospitality during the stage in which this paper was done.

Received on February 18, 2017

References

1. Polchinski J. Tasi Lectures on D-branes. arXiv: hep-th/9611050; Leigh R. *Modern Physics Letters A*, 1989, v. 4, 2767.
2. Callan C. G. and Maldacena J. M. *Nuclear Physics B*, 1998, v. 513, 198. arXiv: hep-th/9708147; Bhattacharyya R. and Douari J. *Journal of High Energy Physics*, 2005, v. 12, 012.

3. Brecher D., *Physics Letters B*, 1998, v. 442, 117; Cook P., De Mello Koch R. and Murugan J. *Physics Review D*, 2003, v. 68, 126007. arXiv: hep-th/9804180. arXiv: hep-th/0306250; Constable N. R., Myers R. C. and Tafjord O. *Physics Review D*, 2000, v. 61, 106009. arXiv: hep-th/9911136.
4. Lee S., Peet A. and Thorlacius L. *Nuclear Physics B*, 1998, v. 514, 161. arXiv: hep-th/9710097; Kastor D. and Traschen J. *Physics Review D*, 1999, v. 61, 024034. arXiv: hep-th/9906237.
5. Constable N. R., Myers R. C., Tafjord O. *Physics Review D*, 2000, v. 61, 106009. arXiv: hep-th/9911136; Myers R. C. *Classical Quantum Gravity*, 2003, v. 20, S347–S372. arXiv: hep-th/0303072.
6. Gibbons G. W. *Nuclear Physics B*, 1998, v. 514, 603. arXiv: hep-th/9709027; Howe P. S., Lambert N. D. and West P. C. *Nuclear Physics B*, 1998, v. 515, 203. arXiv: hep-th/9709014; Banks T., Fischler W., Shenker S. H. and Susskind L. *Physics Review D*, 1997, v. 55, 5112. arXiv: hepth/9610043; Kabat D. and Taylor W. *Advances in Theoretical and Mathematical Physics*, 1998, v. 2, 181. arXiv: hep-th/9711078; Rey S. arXiv: hep-th/9711081; Myers R. C. *Journal of High Energy Physics*, 1999, v. 9912, 022. arXiv: hep-th/9910053.
7. Constable N. R., Myers R. C. and Tafjord O. *Physics Review D*, 2000, v. 61, 106009. arXiv: hep-th/9911136.
8. Bhattacharyya R. and De Mello Koch R. arXiv: hep-th/0508131; Papageorgakis C., Ramgoolam S., Toumbas N. arXiv: hep-th/0510144; Papageorgakis C., Ramgoolam S. *International Journal of Modern Physics A*, 2006, v. 21. arXiv: hep-th/0603239.
9. Douari J. *Physics Letters B*, 2007, v. 644, 83–87. arXiv: hep-th/0603037.
10. Thomas S., Ward J. *Journal of High Energy Physics*, 2006, v. 0611, 019. arXiv: hep-th/0602071; *Physics Review D*, 2005, v. 72, 083519. arXiv: hep-th/0504226v3.
11. Bhattacharyya R. and Douari J. *Journal of High Energy Physics*, 2005, v. 12, 012.
12. Douari J. *Physics Letters B*, 2007, v. 656, 233–242. arXiv: hep-th/0610156.
13. Douari J. *Nuclear Physics B*, 2009, v. 808, 592–612. arXiv: hep-th/0803.0065.
14. Castelino J., Lee S. and Taylor W. *Nuclear Physics B*, 1998, v. 526, 334. arXiv: hep-th/9712105.
15. Constable N. R., Myers R. C., Tafjord O. *Journal of High Energy Physics*, 2001, v. 0106, 023. arXiv: hep-th/0102080.
16. Gibbons G. W. *Nuclear Physics B*, 1998, v. 514, 603–639. arXiv: hep-th/9709027.
17. Tseytlin A. A. *Nuclear Physics B*, 1997, v. 501, 41. arXiv: hep-th/9701125; Tseytlin A. A. arXiv: hep-th/9908105; Myers R. C. *Journal of High Energy Physics*, 1999, v. 9912, 022. arXiv: hep-th/9910053.
18. Lee S., Peet A. and Thorlacius L. *Nuclear Physics B*, 1998, v. 514, 161. arXiv: hep-th/9710097; Constable N. R., Myers R. C. and Tafjord O. *Physics Review D*, 2000, v. 61, 106009. arXiv: hep-th/9911136.
19. Grosse H., Klimcik C. and Presnajder P. *Communications in Mathematical Physics*, 1996, v. 180, 429. arXiv: hep-th/9602115.
20. Savvidy K. G. and Savvidy G. K. *Nuclear Physics B*, 1999, v. 561, 117–124. arXiv: hep-th/9902023.

Configuration Mixing in Particle Decay and Reaction

Elsayed K. Elmaghraby

Experimental Nuclear Physics Department, Nuclear Research Center, Atomic Energy Authority, Cairo 13759, Egypt.
E-mail: e.m.k.elmaghraby@gmail.com

Recent controversy on the existence (versus non-existence) of variability in the observation of decay rate can be settled by considering mixing in decay configuration. Variability in decay rate was investigated based on the available information of beta decay rate data, solar neutrino flux, and energy distribution. Full systematic analysis of the oscillatory behavior was carried out. Based on the zero threshold energy for neutrino absorption in beta emitters, a model for configuration mixing between two distinct beta disintegration modes β^{ν}-disintegration (electron from neutrino interaction) and the β^{-}-disintegration (electron from natural decay) was proposed. The phenomenon of variability in beta decay rate was related to the possible exothermic neutrino absorption by unstable nuclei which, in principle, should include the whole range of flux energies involving flux with energy below the ^{71}Ga threshold at 0.23 MeV. These two disintegration modes occur independently and model for their apparent mixing rate was proposed. The configuration mixing between the two modes cause depletion of radioactive nuclei which is subject to change with seasonal solar neutrino variability. Ability to detect this variability was found to be dependent on the Q-value of the β^{ν} disintegration and detection instrument setup. Value of neutrino cross section, weighted by the ratio between β^{ν} and β^{-} detection efficiencies, was found to be in the range 10^{-44} to 10^{-36} cm^2. For experiments that uses the end point to determine the neutrino mass, interference due to mixing should be taken into account.

1 Introduction

Anomalous behavior in radioisotopes activity was reported by several scientists, they considered it as influence of solar proximity and activity. Several scientist are in favor of the influence of solar activity/distance on the decay rate. Early results of Alburger et al. [3] are based on normalizing the count rate ratio of ^{32}Si/^{32}P decay rate. Siegert et al. [34] had reported oscillatory behavior of ^{226}Ra, ^{152}Eu, and ^{154}Eu. Jenkins et al. [44] had studied these cases and reported several new data and measurements. Most investigator had reported seasonal relation between oscillatory behavior and the earth's position with respect to its sun's orbit; referring to the neutrino influence to the decay process.

Several other scientists oppose the connection between sun and the phenomenon. In one of the oppose thoughts, scientists may consider the rare neutrino events in experiments like Ice Cube and Sudbury Neutrino Observatory [2]; yet, the energy threshold of there detection system may not fall below ^{71}Ga border at 0.233 MeV (3.5-5 MeV for electron scattering [7], 1.44 MeV for $d(\nu_e, e)pp$ interaction.) In all measurements, no relation between half-life and the existence of this phenomenon was reported. Several other oppose reports, based on measurements by different techniques, were published, see Refs. [5, 8, 10, 11, 29].

In the present work, full systematic analysis and treatment of the oscillatory behavior was performed in order to reconcile these viewpoints. Based on the zero threshold energy for neutrino absorption beta emitters, a model for configuration mixing between distinct β^{ν}-disintegration (the electrons from neutrino interaction) and the β^{-}-disintegration (the electrons from natural decay) was proposed.

2 Model for analysis

The majority of solar neutrino are with electron flavor associated with proton burn-up processes ($\phi_{\nu_e,pp} = 6{\pm}0.8{\times}10^{10}$ cm^{-1}s^{-1}) with maximum energy around 0.41 MeV [1]. During solar flares protons stimulates production of pions / muons; π^+ (π^-) decays into $\nu_\mu(\overline{\nu}_\mu)$ with μ^+ (μ^-), later partners decay and emit ν_e ($\overline{\nu}_e$) together with $\overline{\nu}_\mu$ (ν_μ) [30] total flux is of order 10^9 cm^{-2}s^{-1} and has energy up to 10 MeV.

Rare reaction of neutrino with stable isotopes is attributed to its small coupling with $W^{\pm}$ and Z^0 bosons, and higher threshold of reaction kinematics. Coupling with Z^0 may be not appreciated due to non-existence of flavor changing neutral currents. If happened, an electron neutrino in the vicinity of the nucleus couples with a W boson emitting a β^{ν} and induces beta transformation in the nucleus. Threshold energy of neutrino capture in ^{37}Cl is about 0.813 MeV compared to 0.233 MeV in ^{61}Ga, these isotopes are used as monitor for ^{8}Be neutrinos. Radioactive isotopes, on the other hand, have excess energy to deliver due to positive Q-values as illustrated in Table 1. Hence, one can conclude that the solar influence on the *apparent* decay rate is associated mixing of specific mode of *disintegration* in consequence of neutrino capture in nuclei with the natural disintegration rate. The apparent decay rate of radioactive isotopes, λ' may be split into two terms; a term for usual disintegration of the nucleus labelled

λ_d and a terms for neutrino interaction. Presumably, neutral current will contribute to scattering only. β^--decay rate is proportional to the matrix element of the decay, $|M_d|^2$ while the reaction terms are associated with matrix elements of neutrino interaction with charged current, $|M_{\nu W^\pm}|^2$.

$$N(t)\lambda' = N(t)\lambda_d + N(t)\sum_{\text{flavors}} \phi_\nu(t) N_N \left\langle K_{\beta^\nu}(Q)\right\rangle \sigma_{\nu n} \quad (1)$$

The summation is taken over all possible neutrino flavors. Here, N(t) is the number of nuclei at time t, $\langle K(Q)\rangle$ is the factor representing the modification of nucleon properties in the nuclear medium, which can be investigated by nucleon induced nuclear reactions [12, 13]; $\langle K(Q)\rangle$ depends on the Q-value of the reaction and the state of the nucleus upon interaction. The in-medium neutrino cross section σ_ν can replace $\langle K(Q)\rangle\,\sigma_{\nu n}$.

The flux would be altered with the change in earth to sun distance R. Hence the time varying function is inversely proportional to the area of a sphere centered at sun. The radius vector has the form

$$R = a\frac{1-\epsilon^2}{1+\epsilon\cos(\theta)}, \quad \theta \approx \omega t. \quad (2)$$

Where ϵ is the eccentricity of earth's orbit (now, 0.0167 [35]) and the cosine argument is the angle relative to the distance of closest approach (2-4 January) in which value equals to $R = a(1-\epsilon)$. $\omega = 2\pi/T_\omega$ is the average orbital velocity, and T_ω is the duration of earth's years in days. The approximate sign is introduced because earth's spend much more time at larger distance from the sun than in the near distances. Assuming that the average flux ($\phi_\nu^{(0)}$) occurs at time t_0 during the revolution around the sun, the flux at any other time will be

$$\phi_\nu(t) = \phi_\nu^{(0)} F(t), \quad (3)$$

$$F(t) = \frac{(1+\epsilon\cos(\omega t))^2}{(1+\epsilon\cos(\omega t_0))^2}. \quad (4)$$

Here, $\phi_\nu^{(0)}$ is the average flux of neutrinos reaching earth's surface (about 6.65×10^{10} cm^{-2}s^{-1} as average of all sun's producing routes [37], in which only 2.3×10^6 cm^{-2}s^{-1} are from ^{8}Be. Comparison between $F(t)$ (taking $t_0 = 0$) and normalized seasonal variation of ^{8}Be neutrons (data taken from Yoo et al. [46] and normalised to its yearly average) is represented in Fig. 1. $F(t)$ gives the averaged trend of Yoo et al. data within the experimental uncertainty of measurement.

For simplicity, and due to nature of available data of being related to oscillatory behavior, effect of cosmological neutrinos will be disregarded. Additionally, non-predominant radioactive isotopes should have the neutrino-induced beta disintegration of contribution much smaller than that of the β^--decay; hence, λ_d can be replaced by the laboratory decay constant, λ, with good precision. The apparent decay rate for specific interaction current can be described by the formulae

$$\lambda' \Rightarrow \lambda + \phi_\nu^{(0)} N_N \sigma_\nu F(t). \quad (5)$$

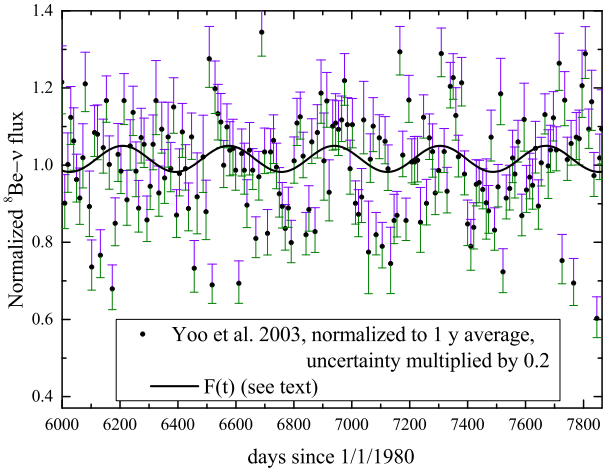

Fig. 1: Normalized measurements of ^{8}Be neutrino variation by Yoo et al. [46] in comparison with predictions of $F(t)$ function in Eq. 4.

Where, $\phi_\nu^{(0)}$, N_N, and $\sigma_\nu = \langle K\rangle\sigma_{\nu n}$ are related to the considered current and the disintegrated nucleus. Differential nuclear decay rate is simply described by the rate equation $dN(t)/dt = -N(t)\lambda'$. Upon integration, the number of survived nuclei become

$$\begin{aligned} N(t) =& N(0)\exp\left(-\lambda t - \mu\left(1+\frac{\epsilon^2}{2}\right)t\right)\times \\ & \exp\left(-2\epsilon\mu\left(1+\frac{\epsilon}{4}\cos(\omega t)\right)\sin(\omega t)\right), \quad (6) \\ \mu =& \frac{\phi_\nu^{(0)} N_N \sigma_\nu}{\omega\,(1+\epsilon\cos(\omega t_0))^2}. \end{aligned}$$

The first exponential represent the *depletion* of nuclei with neutrino interaction together with the radioactive decay. The second exponential can be represented as

$$1 + \sum_{i=1} \frac{(-1)^i}{i!}\left(2\epsilon\mu\left(1+\frac{\epsilon}{4}\cos(\omega t)\right)\sin(\omega t)\right)^i. \quad (7)$$

The value of $2\epsilon\mu << 1$; hence, only the first term in the summation is effective. I.e.,

$$N(t) = e^{-\lambda t - \mu\left(1+\frac{\epsilon^2}{2}\right)t}\left(N(0) - A\left(1+\frac{\epsilon}{4}\cos(\omega t)\right)\sin(\omega t)\right), \quad (8)$$

which reveal seasonal variability. The amplitude of the oscillation is $A = 2\,N(0)\,\epsilon\,\mu$ with the depletion factor $\exp\big(-\lambda t - \mu\left(1+\frac{\epsilon^2}{2}\right)t\big)$; depletion factor reaches unity for long-lived isotopes with relative short-term measurements.

The method of normalization of data, mentioned in context, is intended to remove the effect of isotope decay rate and give the residual of neutrino interaction. So, when normalized to 1, the normalized fraction (proportional to decay rate or detector count) becomes

$$\overline{N(t)} = \left(1 - Ae^{-\lambda t}e^{-\mu\left(1+\frac{\epsilon^2}{2}\right)t}\left(1+\frac{\epsilon}{4}\cos(\omega t)\right)\sin(\omega t)\right). \quad (9)$$

Similarly, for normalization of the ratio between two isotope 1 and 2,

$$\overline{N_{1/2}(t)} \approx 1 - 2\frac{N_1(0)}{N_2(0)} e^{-(\lambda_1-\lambda_2)t} e^{-(\mu_1-\mu_2)\left(1+\frac{\epsilon^2}{2}\right)t} \times \frac{\epsilon\mu_1\left(1+\frac{\epsilon}{4}\cos(\omega t)\right)\sin(\omega t)}{1-2\epsilon\mu_2\left(1+\frac{\epsilon}{4}\cos(\omega t)\right)\sin(\omega t)}. \quad (10)$$

Which is not a complete sinusoidal variation. The amplitude and depletion factors in case of two activity ratio becomes

$$A_{1/2} = 2\frac{N_1(0)}{N_2(0)}\frac{\epsilon\mu_1}{1-2\epsilon\mu_2} e^{-(\lambda_1-\lambda_2)t} e^{-(\mu_1-\mu_2)\left(1+\frac{\epsilon^2}{2}\right)t}. \quad (11)$$

This depletion term can be ignored if both isotopes have comparable half-life and mass.

3 Discussion

Normalized oscillatory data, were collected for the decay of isotopes given in Table 1. Because we need to have a starting point, data retrieved relative to 1 Jan. 1980. The time shift, t_0, was obtained using least square fitting of every data set with Eq. 9 by shifting time with free parameter–say t_1. Results are illustrated in Table 1 in which a shift of -120±14(1σ-stat.) ± 5(1σ-syst.) days was found; i.e. the average flux received on earth from the sun occurs around end of October (or, alternatively, May first.) This is consistent with data given in measurement of ^{8}Be neutrino variation by Yoo et al. [46].

Before going further in the discussion, we must apprehend measurement techniques and circumstance of each experiment. The correlation between earth sun distance and decay rate for ^{32}Si and ^{226}Ra was reported by Jenkins et al. [17] based on Alburger et al. [3] and Siegert et al. [34]; those measurements are based on the β spectrum measurements. Alburger and coworkers used end-window gas-flow proportional counter system and a liquid/plastic scintillation detectors and Siegert and coworkers used both 4π ionization chamber and Ge and Si semiconductor detectors with reference to ionization chamber measurements. Same group of Ref. [17] and others in later work [24] had measured the ^{54}Mn using the 834.8 keVγ-line during 2 years without significant seasonal variation, they only report a connection with solar storm. Similar results appeared after solar flare [16]. Variation of ^{36}Cl decay rate was reported by BNL group [18] using Geiger-Müller counter and in PTB-2014 measurements [22] using the triple-to-double coincidence ratio liquid scintillation counting system. PTB-2014 detection system excluded the idea of time varying decay rate while the BNL measurements prove the phenomenon. Power spectrum analysis [15, 18, 20, 26, 40, 43] reveal several spectral frequencies especially at 1 y^{-1}. Some explanations of seasonal variation of decay rate were related to decoherence in gravitational field [36] and internal sun modes [42]. An experiment was performed for ^{222}Rn decay in controlled environment showed dependence on the angular emission of gamma ray [39] and daily behavior [9, 19, 44]; however Bellotti et al. [9] excluded the sun influenced decay rate in support with their earlier work [8]. Ware et al. [45] returned the variation to change in the pressure of counting chamber during the seasonal variation.

Opposition to the connection between sun's and the variability phenomenon of apparent decay rate came out as a consequence of measurements, as well. No significant deviations from exponential decay are observed in Cassini spacecraft power production due to the decay of ^{238}Pu [11]. Bellotti et al. [8] studied decay of ^{40}K, ^{137}Cs and ^{232}Th using NaI and Ge detectors with no significant effect of earth-sun distance. Same results had been reported by Alexeyev et al. [5] in the alpha decay of ^{214}Po measured by α-particle absorption. However, Stancil et al. [38] detected seasonal variation in the gamma transition in ^{214}Po due to ^{214}Bi decay in radium chain. Others [4] had reported seasonal variation in life time of ^{214}Po. Recently, Pommé et al. [29] re-performed measurements in several laboratories by all possible measurement techniques including ionisation chamber, HPGe detector, silicon detector, proportional counter, anti-coincidence counting, triple-to-double coincidence, liquid scintillation, CsI(Tl) spectrometer, internal gas counting. They returned the phenomenon to lower stability of instruments. Bikit et al [10] investigated the ^{3}H decay rate by measured by liquid scintillation and related the fluctuation of the high-energy tail of the beta spectrum to instrumental instability.

The techniques of measurements is different among these two parties. Among all measurements given above, all techniques that are based on detecting β-radiation, or combined β-γ-radiation coming from its daughter, had signaled variability. Which can be explained as a consequence of the mixing between β^{ν} and β^{-} disintegrations. In such case, both terms in Eq. 5 are effective and the apparent decay rate should be influenced by solar proximity and activity. On the other hand, techniques that uses specific decay parameter such as specific γ-line from $\beta^{\pm}$- or α-decay may not be able to recorded any variability because the oscillatory part of configuration mixing in Eq. 5 is not operative. With pure α-emitters like ^{241}Am and ^{226}Ra, the mixing oscillatory term will change sign and time shift of half-period may appear. In accordance to Siegert et al. [34] results, time shift of a half period in the fluctuation measured between $4\pi\gamma$-ionization chamber measurement of ^{226}Ra and measurements of ^{152,154}Eu by GeLi semiconductor detectors was found. Hence, both parties concluded existence or non-existence of the phenomenon based on their technique of measuring it. Each team draw the correct picture of his viewpoint; that is determined by whether the mixing part of Eqs. 5 and 9 were taken into account or not.

The β^{ν} energy spectrum should, in principle, reflects the energy distribution of neutrino and the structure of residual nucleus. In β^{ν}-decay, all energy of neutrino plus the major contribution of mass access (Q-value) is transferred to the

Table 1: Data of seasonal variability of radioactive disintegration. Unit of $\xi\sigma_\nu$ is cm^2, Q-value is calculated from AME2003 atomic mass evaluation [6] in the unit of MeV; t_1 is the time shift in days.

Isotope	Ref	A $\times 10^4$	$-t_1$	$\xi\sigma_\nu \times 10^{41}$	Q	E_{th}
^{3}H	[21,27]	5.29 ± 2 ± 6	-10 ± 30	1.8 ± 0.4 ± 2 ×10^{-6}	0.0186	0
^{3}H	[14]	38.4 ± 0.8 ± 35	138 ± 1	13 ± 0.1 ± 12×10^{-6}	0.0186	0
^{32}Si	[3]	10.8 ± 2 ± 5	109 ± 12	1.15 ± 0.01 ± 0.5×10^{-3}	0.2243	0
^{32}Si/^{36}Cl	[3,15,17]	15.8 ± 0.67 ± 7	126 ± 5			
^{36}Cl	[18]	19 ± 0.9 ± 10	160 ± 5	4.52 ± 0.01 ± 2.4	0.7097	0
^{152}Eu	[31,32,41]	8.4 ± 0.3 ± 2	113 ± 3	3.51 ± 0.01 ± 0.79	1.8197	0
^{154}Eu	[31,32,41]	8.5 ± 0.4 ± 3	121 ± 2	8.7 ± 0.004 ± 3	1.9688	0
^{214}Bi	[38]	31 ± 2 ± 17	119 ± 6	39.7 ± 0.02 ± 22	3.2701	0
^{214}Bi	[38]	30 ± 2 ± 12	118 ± 5	38.5 ± 0.02 ± 15	3.2701	0
^{85}Kr	[32,41]	7.2 ± 0.35 ± 1.5	113 ± 3		0.687	0
^{90}Sr	[32,41]	8.8 ± 0.4 ± 2	121 ± 3		0.546	0
^{108}Ag	[32,41]	8.6 ± 0.3 ± 2	126 ± 2		1.76	0
^{133}Ba	[32,41]	6.18 ± 0.6 ± 4	119 ± 5		-2.061	2.061
^{226}Ra	[15,17]	10.1 ± 0.3 ± 3	105 ± 20	83 ± 0.02 ± 20×10^{-3}	diverse	
^{226}Ra	[34]	11.9 ± 0.2 ± 2	125 ± 2	99 ± 0.01 ± 20×10^{-3}	diverse	

beta particle. The higher the Q-value, the higher the energy of the emitted β^ν. This is another source of disagreement among both teams supporting and declining the phenomenon. Observation of the phenomenon is determined by the ability of their system to detect β^ν or the specific γ-transition or mass loss subsequent the disintegration. Detection volume, in general, is selective to a band of radiation energy. Ionization chamber detects gamma radiation and fraction of beta radiation above few hundreds eV [31]. Additionally, higher energy of β^ν have higher value of detection efficiency. Counting of β^ν, and β^-, and/or their corresponding γ-ray from nuclei, have different efficiencies due to difference in energy distribution and end-point(c.f. [33]); literally, β^ν has no end-point. Hence, each count rate must be related to its efficiency; i.e. the amplitude of the variation must be modified by a ratio–say ξ–between β^ν counting efficiency and β^- counting efficiency; which depends on the β^ν energy and the measurement setup. If variation occurs, it would be reflected on the counting rate. The value of $\xi\sigma_\nu$ represent a weighted cross section and it was calculated as a whole in Table 1.

The amplitude of the variability was obtained from each dataset by fitting using Eq. 9; results are represented in Table 1. The value of $N(0)$ (alternatively, mass or activity) was found for ^{3}H (assuming 1-20 g of ^3H_2O as for PTB measurements catalogue of activity standards [25]), ^{32}Si (0.0477 g of $^{32}SiO_2$ [3]), ^{36}Cl(0.4 μCi [22]), ^{152}Eu (40 MBq [31,32,41]), ^{154}Eu (2.5 MBq [31,32,41]), and ^{214}Bi(2 μCi [38]), see Table 1. Mass, activity, and/or number of decaying atoms were not reported for other datasets. Then, the value ($\xi\sigma_\nu$) are calculated only for the said isotopes. A plot for the variation of $\xi\sigma_\nu$ with Q-value is represented in Fig. 2. The known limit of

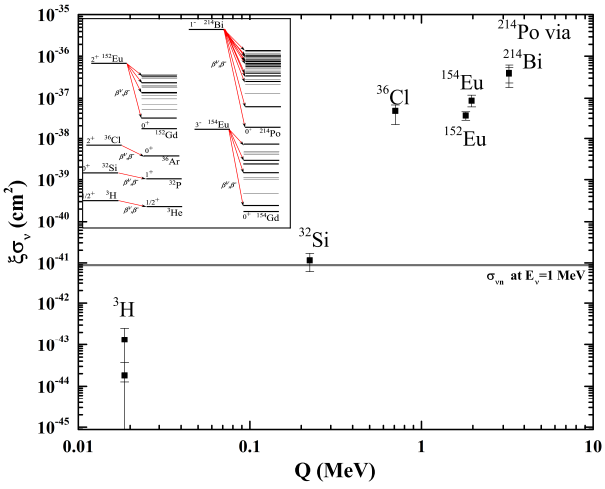

Fig. 2: Value of the reduced cross section $\xi\sigma_\nu$ in the unit of cm^2 in correlation with the Q-value of the possible β^ν-disintegration. Line represent the value of $\sigma_{\nu n}$=0.881×10^{-38} $E_\nu(GeV)$ cm^2 at E_ν=1 MeV. Insert: possible disintegration probabilities of represented isotopes to levels in daughter nuclei.

ν_e-neutron cross section is $\sigma_{\nu n}$= 0.881×10^{-38} $E_\nu(GeV)$ cm^2 which is represented by the line in Fig. 2 for electron neutrino with E_ν=1 MeV considering $\xi = 1$. The increase of $\xi\sigma_\nu$ with Q-value confirms the mentioned hypothesis of existence of instrumental setting participation in the detection of the variability of apparent decay rate.

In the insert of Fig. 2, decay schemes of said isotopes are represented. The β^ν spectrum is expected to have definite spectrum corresponding to direct transition to levels in daugh-

ter nuclei in similarity to neutrinoless double beta decay; one of the possible broadening that could occur is due to original energy distribution of neutrinos. Sensitive detector like KATRINE [23] can be used to detect such energy distribution in ^{3}H; fortunately, neutrinoless double beta decay cannot occur in case of ^{3}H without fission of the whole nucleus. Disintegration of ^{3}H, ^{32}Si and ^{36}Cl have single possible transition for both β^{ν} and β^{-} decays. The maximum energy of β^{ν}-^{3}H decay is expected to be 0.42 MeV with $\xi\sigma_{\nu} = 1.82 \pm 0.4$ stat. ± 2 syst. $\times 10^{-44}$ cm^{2} as calculated from Pomme et al. [27] data, and 13.2 ± 0.1 stat. $\pm$ 11 syst. $\times 10^{-44}$ cm^{2} as calculated from Falkenberg [14] data. Systematic uncertainties are mostly related to unknown mass of the material. The BNL data of ^{226}Ra and other data of radium had been evaluated but was not represented in Fig. 2. ^{226}Ra has threshold for β^{ν} decay of 0.641 MeV, its daughters have possible beta decay probability, that is why variability can be observed [15,17,31,32,34,41]. The phenomenon disappeared when α-detection system is used [28].

4 Conclusion

Rare mixed configuration between neutrino induced beta disintegration and natural beta disintegration may exists. These two distinct classes of beta decay could, in principle, explain the variation of apparent decay rate of radioactive isotopes with sun proximity. The circumstances of detection and instrumental ability determine whether to detect pure natural disintegration or the mixed mode. Configuration mixing between β^{ν} and β^{-} is, presumably, happen among all existing β^{-} emitters. The mixing in configuration of decay and reaction can be extended to all particles and nuclei. It must be taken into account in the in high precision measurements of neutrino mass. Mixing may be of significance for nucleosynthesis in astronomical object.

Received on April 26, 2017

References

1. Abdurashitov J. N., Gavrin V. N., Gorbachev V. V., Gurkina P. P., Ibragimova T. V., Kalikhov A. V., Khairnasov N. G., Knodel T. V., Mirmov I. N., Shikhin A. A., Veretenkin E. P., Yants V. E., Zatsepin G. T., Bowles T. J., Elliott S. R., Teasdale W. A., Nico J. S., Cleveland B. T. and Wilkerson J. F. Measurement of the Solar Neutrino Capture Rate With Gallium Metal: III. Results for the 2002-2007 Data-Taking Period. *Physical Review C*, 2009, v. 80, 015807.
2. Aharmim B. et al. Determination of the ν_e and Total ^{8}B Solar Neutrino Fluxes Using the Sudbury Neutrino Observatory Phase I Data Set. *Physical Review C*, 2007, v. 75, 045502.
3. Alburger D., Harbottle G. and Norton E. Half-Life of ^{32}Si. *Earth and Planetary Science Letters*, 1986, v. 78 (2-3), 168–176.
4. Alexeyev E. N., Gavrilyuk Y. M., Gangapshev A. M., Kazalov V. V., Kuzminov V. V., Panasenko S. I. and Ratkevich S. S. Results of a Search for Daily and Annual Variations of the ^{214}Po Half-Life at the Two Year Observation Period. *Physics of Particles and Nuclei*, 2016, v. 47, 986–994.
5. Alexeyev E., Alekseenko V., Gavriljuk J., Gangapshev A., Gezhaev A., Kazalov V., Kuzminov V., Panasenko S., Ratkevich S. and Yakimenko S. Experimental Test of the Time Stability of the Half-Life of Alpha-Decay ^{214}Po Nuclei. *Astroparticle Physics*, 2013, v. 46, 23–28.
6. Audi G., Wapstra A. H. and Thibault C. The AME2003 Atomic Mass Evaluation: (II). Tables, Graphs and References. *Nuclear Physics*, 2003, v. A729, 337.
7. Bellini G. et al. Measurement of the Solar ^{8}B Neutrino Rate With a Liquid Scintillator Target and 3 MeV Energy Threshold in the Borexino Detector. *Physical Review D*, 2010, v. 82, 033006.
8. Bellotti E., Broggini C., Carlo G. D., Laubenstein M. and Menegazzo, R. Search for Correlations Between Solar Flares and Decay Rate of Radioactive Nuclei. *Physics Letters*, 2013, v. B720, 116–119.
9. Bellotti E., Broggini C., Carlo G. D., Laubenstein M. and Menegazzo R. Precise Measurement of the ^{222}Rn Half-Life: A Probe to Monitor the Stability of Radioactivity. *Physics Letters*, 2015, v. B743, 526– 530.
10. Bikit K., Nikolov J., Bikit I., Mrda D., Todorovic N., Forkapic S., Slivka J., and Veskovic M. Reinvestigation of the Irregularities in the ^{3}H decay. *Astroparticle Physics*, 2013, v. 47, 38–44.
11. Cooper P. S. Searching for Modifications to the Exponential Radioactive Decay Law with the Cassini Spacecraft. *Astroparticle Physics*, 2009, v. 31(4), 267–269.
12. Elmaghraby E. K. PHASE-OTI: A pre-equilibrium model code for nuclear reactions calculations. *Computer Physics Communications*, 2009, v. 180, 1694–1699.
13. Elmaghraby E. K. Initial exciton configuration in (p,n) pre-equilibrium emission reactions. *Physical Review C*, 2008, v. 78, 014601.
14. Falkenberg E. D. Radioactive decay caused by neutrinos? *Apeiron*, 2001, v. 8 (2), 32.
15. Javorsek II D., Sturrock P., Lasenby R., Lasenby A., Buncher J., Fischbach E., Gruenwald J., Hoft A., Horan T., Jenkins J., Kerford J., Lee R., Longman A., Mattes J., Morreale B., Morris D., Mudry R., Newport J., O'Keefe D., Petrelli M., Silver M., Stewart C. and Terry B. Power Spectrum Analyses of Nuclear Decay Rates. *Astroparticle Physics*, 2010, v. 34 (3), 173–178.
16. Jenkins J. H. and Fischbach E. Perturbation of Nuclear Decay Rates During the Solar Flare of 2006 December 13. *Astroparticle Physics*, 2009, v. 31 (6), 407–411.
17. Jenkins J. H., Fischbach E., Buncher J. B., Gruenwald J. T., Krause D. E. and Mattes J. J. Evidence of Correlations Between Nuclear Decay Rates and Earth-Sun Distance. *Astroparticle Physics*, 2009, v. 32 (1), 42–46.
18. Jenkins J. H., Herminghuysen K. R., Blue T. E., Fischbach E., Javorsek II D., Kauffman A. C., Mundy D. W., Sturrock P. A. and Talnagi J. W. Additional Experimental Evidence for a Solar Influence on Nuclear Decay Rates. *Astroparticle Physics*, 2012, v. 37, 81–88.
19. Jenkins J. H., Mundy D. W. and Fischbach E. Analysis of Environmental Influences in Nuclear Half-Life Measurements Exhibiting Time-Dependent Decay Rates. *Nuclear Instruments and Methods in Physics Research A*, 2010, v. 620 (2-3), 332–342.
20. Jenkins J., Fischbach E., Javorsek II D., Lee R. and Sturrock P. Concerning the Time Dependence of The Decay Rate of ^{137}Cs. *Applied Radiation and Isotopes*, 2013, v. 74, 50–55.
21. Kossert K., Broda R., Cassette P., Ratel G. and Zimmerman B. Uncertainty Determination for Activity Measurements by Means of the TDCR Method and the CIEMAT/NIST Efficiency Tracing Technique. *Metrologia*, 2015, v. 52 (3), S172.
22. Kossert K. and Nahle O. J. Long-Term Measurements of ^{36}Cl to Investigate Potential Solar Influence on the Decay Rate. *Astroparticle Physics*, 2014, v. 55, 33–36.
23. Mertens S. Status of the KATRIN Experiment and Prospects to Search for keV-Mass Sterile Neutrinos in Tritium β-decay. *Physics Procedia*, 2015, v. 61, 267–273.

24. Mohsinally T., Fancher S., Czerny M., Fischbach E., Gruenwald J., Heim J., Jenkins J., Nistor J. and O'Keefe D. Evidence for Correlations Between Fluctuations in ^{54}Mn Decay Rates and Solar Storms. *Astroparticle Physics*, 2016, v. 75, 29–37.
25. NIST. SRM 4927F - Hydrogen-3 water radioactivity standard. Accessed 3 Feb 2017, 2017.
26. O'Keefe D., Morreale B. L., Lee R. H., Buncher J. B., Jenkins J. H., Fischbach E., Gruenwald T., Javorsek II D. and Sturrock P. A. Spectral Content of ^{22}Na/^{44}Ti Decay Data: Implications for a Solar Influence. *Astrophysics and Space Science*, 2013, v. 344 (2), 297–303.
27. Pomme S., Stroh H., Paepen J., Ammel R. V., Marouli M., Altzitzoglou T., Hult M., Kossert K., Nahle O., Schrader H., Juget F., Bailat C., Nedjadi Y., Bochud F., Buchillier T., Michotte C., Courte S., van Rooy M. W., van Staden M. J., Lubbe J., Simpson B. R. S., Fazio A., Felice P. D., Jackson T. W., Wyngaardt W. M. V., Reinhard M. I., Golya J., Bourke S., Roy T., Galea R., Keightley J. D., Ferreira K. M., Collins S. M., Ceccatelli A., Verheyen L., Bruggeman M., Vodenik B., Korun M., Chisté V., and Amiot M.-N. On Decay Constants and Orbital Distance to the Sun—Part II: Beta Minus Decay. *Metrologia*, 2017, v. 54 (1), 19.
28. Pomme S., Stroh H., Paepen J., Ammel R. V., Marouli M., Altzitzoglou T., Hult M., Kossert K., Nahle O., Schrader H., Juget F., Bailat C., Nedjadi Y., Bochud F., Buchillier T., Michotte C., Courte S., van Rooy M. W., van Staden M. J., Lubbe J., Simpson B. R. S., Fazio A., Felice P. D., Jackson T. W., Wyngaardt W. M. V., Reinhard M. I., Golya J., Bourke S., Roy T., Galea R., Keightley J. D., Ferreira K. M., Collins S. M., Ceccatelli A., Verheyen L., Bruggeman M., Vodenik B., Korun M., Chisté V., and Amiot M.-N. On Decay Constants and Orbital Distance to the Sun—Part I: Alpha Decay. *Metrologia*, 2017, v. 54 (1), 1.
29. Pommé S., Stroh H., Paepen J., Ammel R. V., Marouli M., Altzitzoglou T., Hult M., Kossert K., Nähle O., Schrader H., Juget F., Bailat C., Nedjadi Y., Bochud F., Buchillier T., Michotte C., Courte S., van Rooy M., van Staden M., Lubbe J., Simpson B., Fazio A., Felice P. D., Jackson T., Wyngaardt W. V., Reinhard M., Golya J., Bourke S., Roy T., Galea R., Keightley J., Ferreira K., Collins S., Ceccatelli A., Unterweger M., Fitzgerald R., Bergeron D., Pibida L., Verheyen L., Bruggeman M., Vodenik B., Korun M., Chiste V. and Amiot M.-N. Evidence Against Solar Influence on Nuclear Decay Constants. *Physics Letters*, 2016, v. B761, 281–286.
30. Ryazhskaya O., Volkova L. and Zatsepin, G. Neutrinos from Solar Flares at the Earth. *Nuclear Physics - Proceedings Supplements* 2002, v. B110, 358–360.
31. Schrader H. Ionization Chambers. *Metrologia*, 2007,v. 44 (4), S53–S66.
32. Schrader H. Half-Life Measurements of Long-Lived Radionuclides-New Data Analysis and Systematic Effects. *Applied Radiation and Isotopes*, 2010 v 68 (7-8), 1583–1590.
33. Schrader H. Calibration and Consistency of Results of an Ionization-Chamber Secondary Standard Measuring System for Activity. *Applied Radiation and Isotopes*, 2000, v. 52 (3), 325–334.
34. Siegert H., Schrader H. and Schatzig U. Half-Life Measurements of Europium Radionuclides and the Long-Term Stability of Detectors. *Applied Radiation and Isotopes*, 1998, v. 49 (9-11) 1397–1401.
35. Simon J. L., Bretagnon P., Chapront J., Chapront-Touze M., Francou G. and Laskar J. Numerical Expressions for Precession Formulae and Mean Elements for the Moon and the Planets. *Astronomy and Astrophysics*, 1994, v. 282, 663–683.
36. Singleton D., Inan N. and Chiao R. Y. Neutrino Induced Decoherence and Variation in Nuclear Decay Rates. *Physics Letters*, 2015, v. A379 (12-13), 941– 946.
37. Soler F., Froggatt C. and Muheim F. Neutrinos in Particle Physics, Astrophysics and Cosmology. Scottish Graduate Series. Taylor & Francis, 2008.
38. Stancil D. D., Yegen S. B., Dickey D. A. and Gould C. R. Search for Possible Solar Influences in Ra-226 Decays. *Results in Physics*, 2017, v. 7, 385–406.
39. Steinitz G., Kotlarsky P. and Piatibratova O. Observations of the Relationship Between Directionality and Decay Rate of Radon in a Confined Experiment. *The European Physical Journal Special Topics*, 2015, v. 224 (4), 731–740.
40. Sturrock P. A., Buncher J. B., Fischbach E., Gruenwald J. T., Javorsek II D., Jenkins J. H., Lee R. H., Mattes J. J. and Newport J. R. Power Spectrum Analysis of Physikalisch-Technische Bundesanstalt Decay-Rate Data: Evidence for Solar Rotational Modulation. *Solar Physics*, 2010, v. 267 (2), 251–265.
41. Sturrock P. A., Fischbach E., and Jenkins J. Analysis of Beta-Decay Rates for Ag-108, Ba-133, Eu-152, Eu-154, Kr-85, Ra-226, and Sr-90, Measured at the Physikalisch-Technische Bundesanstalt from 1990 to 1996. *The Astrophysical Journal*, 2014, v. 794 (1), 42.
42. Sturrock P., Bertello L., Fischbach E., Javorsek II D., Jenkins J., Kosovichev A. and Parkhomov A. An Analysis of Apparent R-Mode Oscillations in Solar Activity, the Solar Diameter, the Solar Neutrino Flux, and Nuclear Decay Rates, with Implications concerning the Sun's Internal Structure and Rotation, and Neutrino Processes. *Astroparticle Physics*, 2013, v. 42, 62–69.
43. Sturrock P., Parkhomov A., Fischbach E. and Jenkins J. Power Spectrum Analysis of LMSU (Lomonosov Moscow State University) Nuclear Decay-Rate Data: Further Indication of R-Mode Oscillations in an Inner Solar Tachocline. *Astroparticle Physics*, 2012, v. 35 (11), 755–758.
44. Sturrock P., Steinitz G., Fischbach E., Parkhomov A. and Scargle J. Analysis of Beta-Decay Data Acquired at the Physikalisch-Technische Bundesanstalt: Evidence of a Solar Influence. *Astroparticle Physics*, 2016, v. 84, 8–14.
45. Ware M. J., Bergeson S. D., Ellsworth J. E., Groesbeck M., Hansen J. E., Pace D. and Peatross J. Instrument for Precision Long-Term β-Decay Rate Measurements. *Review of Scientific Instruments*. 2015, v. 86 (7), 073505.
46. Yoo J. et al. Search for Periodic Modulations of the Solar Neutrino Flux in Super-Kamiokande-I. *Physical Review D*, 2003, v. 68, 092002.

Are Energy and Space-time Expanding Together?

Jacques Consiglio
52, Chemin de Labarthe. 31600 Labastidette. France. E-mail: Jacques.Consiglio@gmail.com

Assuming the universe has permanent critical density gives energy non-conservation, a linear increase of the universe total energy as a function of time. It enables to compute the universe densities of matter, dark matter, and dark energy as distinct effects of a unique source, where dark matter is stress. We show coherence with the Schwarzschild and the Schwarzschild-de Sitter solutions from which we compute the term Λ as geometrical effect of expansion. In this context, we show that MOND is consequence of the universe expansion and compute its parameter value and time evolution.

1 Introduction

This paper follows [1], where we find that energy "is" the universe expansion, and complements the analysis. But here we proceed from side-thinking: The next theory of gravity, if any, will have to recover the Einstein field equations (EFE). Therefore correlations between quantities considered independent in general relativity (GR), are instructive as to the object and contents of a better theory. Then in order to find new correlations we shall rely on a) the geometry of existing EFE solutions, and b) one coincidence which is critical density.

1.1 Coincidences

According to the Planck mission (PM) 2015 results [10], it seems that the universe has critical density:

$$\rho_T = \frac{3\,H^2}{8\pi\,G}\,, \tag{1}$$

where G is Newton's constant, and H the Hubble parameter. Note, with respect to [1], that we compute ρ_T from (1) instead of the total dark fields density. Taking $H = 1/T$, where T is the universe age and the distance to the cosmological event horizon $R_U = c\,T$, it also reads:

$$2\,G = \frac{R_U\,c^2}{M_T}\,, \tag{2}$$

where $M_T\,c^2$ is the total energy of the observed universe. Then (1-2) uncovers a symmetry of the Schwarzschild solution:

$$\frac{R_s}{r} = \frac{R_U\,M}{M_T\,r}\,, \tag{3}$$

where gravity is the interaction of all energies of the observed universe; that is to say Mach's principle. But (1) also reads:

$$M_T c^2 = \frac{P_p\,T}{2}\,, \tag{4}$$

which means that the energy of the observed universe grows linearly according to half the Planck power $P_p = c^5/G$. We see that the same equation (1) takes 4 forms which can be given very large significance ranging from the simplest system (3) to cosmology (4) and the absence of a big bang.
Now take the Bekenstein-Hawking area-entropy law:

$$S = \frac{K\,A\,c^3}{4\,G\,\hbar}\,, \tag{5}$$

which states that the entropy S associated with an event horizon is its area A divided by $4G$ [2] [3] (where K and $\hbar$ are Boltzmann and the reduced Planck constants respectively). It also applies to the de Sitter cosmological event horizon [4] seen at R_U:

$$S = \frac{4\pi\,K\,R_U^2\,c^3}{4\,G\,\hbar}\,. \tag{6}$$

Now injecting (1) in (6) gives:

$$\frac{\hbar}{K} \times \frac{S}{M_T\,c^2} = 2\pi\,T\,, \tag{7}$$

which means that the ratio between entropy S and energy $M_T\,c^2$ at any given epoch, "is cosmic time" – or the opposite, entropy is accumulation of action in the manner of an old de Broglie conjecture about the physical significance of $h\,S = K\,A$ which associates an action A and an entropy S to any piece of energy.

Using GR the probability for the "coincidence" (1) to be observed is about zero, there is not even a theoretical reason for the order of magnitude to ever come out; secondly (2) and (7) establish a simple, clear, and unexpected quantitative fit between gravity, cosmic time, energy, and entropy – where energy is not supposed to be. So maybe this is a big deal and we shall assume that (1) is not a coincidence but a law of nature ruling the universe expansion together with its energy.

Consider now the FLRW metric with a positive cosmological term and homogeneous density - that is to say the ΛCDM model. Assuming that (1) is not just a coincidence implies that it is valid at any epoch; then using (4) since the FLRW metric describes a simple 4-ball, we can slice it with 4-spheres centered at the origin, of radius r and thickness $2\,l_p$ (both along the light cone), and each slice adds an identical energy increment M_p, the non-reduced Planck mass, and it looks like the universe is a Planck power space-time generator.

The visible matter field exists "now" at the surface of the 4-sphere while M_T, as defined from R_U, is causal and occupies the light cone. Then a geometrical ratio exists between the two quantities, which evolve together. Simple integration gives $2\pi^2$ the 4-sphere surface coefficient and removing the "surface" we get the total dark field density ρ_D:

$$\rho_D = \rho_T \times \frac{2\pi^2}{1+2\pi^2} = 8.98 \times 10^{-27}\,\mathrm{kg\,m^{-3}}\,, \qquad (8)$$

which agrees with PM results. The difference $\rho_V = \rho_T - \rho_D$ is the visible matter density and represents 4.82% of the total density ρ_T where the PM found 4.86 (8)%.

So, computing matter density ρ_V from geometry and (1) is totally abnormal in GR; we can even say irrelevant. But at the opposite, if those quantities *and others* are calculable, GR is incomplete and we can even say that it misses a fundamental point. In the remainder of this paper we shall analyze the consequences of (1) and (8) and check if nature agrees.

1.2 Premises

Noether's theorem is the basis of conservation laws; it is used to evaluate energy conservation, and it works perfectly in quantum field theory. In GR, an area in which energy is assumed constant is defined by physical rods and clocks.

But how do we measure the rod? Essentially by decree of conservation. We define a-priori what a meter is and the postulate is that a rod does not evolve; up to now, there is no experimental results which is recognized to require any change to this postulate. But we cannot physically compare rods between distinct epochs. Even though GR studies the transfers of clocks and rods between distinct space-time locations, it assumes that no hidden source comes to expand its energy – and this is what (2) states: G is assumed constant, then the total energy M_T evolves in proportion of R_U, and we measure that the observable universe radius $R_U = c\,T$ grows.

It can be interpreted in different manners and we have to choose one that can be logically understood and requires minimal hypothesis. In the next sections we shall proceed from the four premises hereafter which were chosen appropriately, explaining how (2) physically works; we shall then use three EFE solutions to show coherence with existing theory and unexplained experimental data. Premises are:

P1: The universe proceeds from the FLRW metric with cosmological term $\Lambda > 0$.

P2: The observable matter field (particles) rests at the surface of a 4-sphere.

P3: A mechanism exists inflating the 4-sphere and expanding masses and energy; both effects are simultaneous.

P4: The metric expansion includes inflation of the 4-sphere radius and a reduction of particles wavelengths; energy condenses permanently and progressively.

Those premises are easily justified:

- P1 agree with the best verified model, and
- P2 is direct consequences of the "coincidences".
- P3 and P4 must be taken together; the feed mechanism in P3 could be just the radial expansion of a 4-ball in a preexisting 4-dimensional space filled with constant energy density. The sphere expands and masses increase reducing wavelengths; this is permanent and progressive condensation, hence P4.

2 The dark fields and the expansions

2.1 Expansion in the Schwarzschild solution

We first use the Schwarzschild solution to study the effects of (2) and expansion at different heights in the gravitational pit of a central mass M (the basic test case) and assume the system far away from other gravitational sources. With respect to (2), M_T is variable in time but constant in space ($M_T \sim T$), so M is also variable in time. At the opposite since gravitation is a retarded interaction, the metric in r is retarded and the Schwarzschild solution must be modified accordingly. Hence, using P3-P4, r and M (or R_s) expand; with respect to [1], introducing new ad-hoc parameters α, β to separate the effects of energy and space expansion, we write from (2):

$$\frac{R_s}{r} = \frac{R_U\,M}{M_T\,r} \to \frac{R_U\,M}{M_T\,r} \times \frac{1-\alpha\,Hr/c}{1+\beta\,Hr/c}\,. \qquad (9)$$

Gravitation is retarded; a signal goes from M to r. Hence the correction at the numerator of (9) denotes that when the signal was emitted the mass M was lesser than expected in GR. Secondly, the additional delay we introduce comes from expansion. Then at the denominator, r "looks" advanced because the signal dilutes more than with a static r, and we expect $\beta = 1$. Second order limited development yields:

$$\frac{R_U\,M}{M_T\,r} \to \frac{R_U\,M}{M_T\,r} - (\alpha+\beta)\,\frac{M}{M_T} + \beta(\alpha+\beta)\,\frac{M\,r}{M_T\,R_U}\,. \qquad (10)$$

Now examine this expression:

- The first term is nominal and now corresponds to a static field.
- The middle term cannot be seen negligible since it addresses identically all masses of the universe. It must be integrated to M_T, giving -1 *which is the flat metric and it denotes its production*; from (8), $\alpha + \beta = 2\pi^2$.
- Therefore the right hand term must also be integrated to M_T giving $H\,r/c$, or a cosmological term $H\,c$ with unit of acceleration; and we find $\beta = 1$.

Note that we use a limited development in r so we cannot integrate to R_U, but we can still integrate to M_T as the middle term of (10) requires. Overall, after integration to M_T we get:

$$\frac{2\,G\,M}{r\,c^2} = \frac{R_U\,M}{M_T\,r} \to \frac{2\,G\,M}{r\,c^2} - 1 + \frac{r}{R_U}. \tag{11}$$

We shall now analyze this modified solution and show that the two new terms correspond to dark energy (DE) and dark matter (DM) – meaning exactly.

2.2 Dark energy and dark matter

The limited development above corresponds to a unique field that we split in three non-independent components. In [1], we analyzed the relations between the two new components; we showed that considering the first as an energy field X and the second as stress leads to:

$$M_{se(R)}\,c^2 = \frac{1}{2}\int_0^R \left(4\pi\,\rho_X\,r^2\right)(H_R\,c\,r)\;dr = \frac{3}{8}\,M_{X(R)}\,c^2\,,$$

where $M_{X(R)}$ is the energy of the field X in a 3-sphere of radius $R \ll R_U$, while $M_{se(R)}\,c^2$ is the stress given by the acceleration $H\,c$, which is equivalent to a potential $H\,c\,r$. (Note that in the integral energy is given by acceleration, then kinetic energy $p^2/2m$; thus the factor 1/2.) Therefore:

$$\frac{M_{se(R)}}{M_{X(R)}} = \frac{3}{8} = 0.375\,, \tag{12}$$

which agrees with the ratio of DM to DE given by the PM:

$$\frac{\Omega_C}{\Omega_{DE}} = \frac{0.2589}{0.6911} = 0.3746\,, \tag{13}$$

and, since M_{se} is stress, identification is trivial; X is dark energy which creates stress interpreted as dark matter. Now we solve the system of equations and coincidences:

$$\rho_D = 2\pi^2\,\rho_V = \frac{2\pi^2}{2\pi^2+1}\,\rho_T = \frac{11}{8}\,\rho_{DE} = \frac{11}{3}\,\rho_C\,. \tag{14}$$

It leaves no freedom or randomness in cosmological energies. In GR theory, those energy densities give four distinct effects:

- ρ_{DE} provides with a *decreasing* repelling force at the origin of expansion and then of the flat metric.
- ρ_C is stress due to the same repelling force; in the EFE stress comes in the stress-energy tensor, like mass, and then this result agrees with the ΛCDM model.
- ρ_V lies at the 4-sphere surface and non-homogeneity creates deviations to the flat metric.
- ρ_T is their sum and has critical density.

Each density finds its appropriate places in the EFE, and we can use M_T and R_U to replace G in the equations; we could compute $\Lambda = 8\pi\,G\,\rho_{DE}$ but we shall deduce it differently.

2.3 Λ and the CDM

In recent papers, [5–7] P. Marquet formally showed that a varying cosmological term restores in the EFE a conserved energy-momentum *true tensor* of matter and gravity with a massive source:

$$G^{\alpha\beta} = \frac{8\pi\,G}{c^4}\left[(T^{\alpha\beta})_{\text{matter}} + (t^{\alpha\beta})_{\text{gravity}}\right], \tag{15}$$

Here $(t^{\alpha\beta})_{\text{gravity}}$ includes a background field tensor which persists in the absence of matter:

$$(t_\beta^{\ \alpha})_{background} = \frac{c^3}{8\pi\,G}\,\delta_\beta^{\ \alpha}(\Xi/2)\,, \tag{16}$$

where $\Xi/2$ is the variation of cosmological constant Λ. As a result the de Sitter-Schwarzschild metric is slightly modified:

$$1 - \frac{R_s}{r} - \frac{\Lambda\,r^2}{3} \to 1 - \frac{R_s}{r} - \frac{\Lambda+\delta\Lambda}{3}\,r^2\,,$$

which we identify term to term with (11). But recall that the factor 1/3 in this metric is given by integration, it is then irrelevant for a correspondence with a derivative. We also introduce a parameter k to solve:

$$k\,\Lambda + k\,\delta\Lambda \leftrightarrow -1 + \frac{r}{R_U}\,, \tag{17}$$

which means that since Λ is a constant, integration to RU is now possible and will give the flat metric like in (11); then:

$$-k\,\Lambda\int_0^{R_U} r^2 dr = 1 \to k\,\Lambda = \frac{1}{3\,R_U^3}\,. \tag{18}$$

Then for any r we have $k\,\delta\Lambda(r) = -1/r^2$. Integrating the last term to the full solid angle (as stress), multiplying by 1/2 for kinetic energy and identifying with $H\,r/c$ gives:

$$\frac{1}{2}\int 4\pi\,k\,\delta\Lambda(r)\,r^2\,dr = \int 2\pi\,k\,dr = \frac{H\,r}{c}$$

$$\to k = \frac{H}{2\pi\,c} = \frac{1}{2\pi\,R_U}\,, \tag{19}$$

where k is also the ratio entropy/energy on the right-hand side of (7). Here it links the expansion of R_U (∼ energy) to that of DE (∼ Λ) through $2\pi\,R_U$. Now we have completed the correspondence and using (18) and (19) we get:

$$\Lambda = \frac{2\pi\,c}{3\,H\,R_U^3} = \frac{2\pi}{3\,R_U^2} = 1.229\times10^{-52}\,\text{m}^{-2}\,. \tag{20}$$

The standard ΛCDM estimate is:

$$\Lambda \approx 1.19\times10^{-52}\,\text{m}^{-2}\,, \tag{21}$$

and then our reasoning on energy expansion is appropriate. But we found that the dark field has a unique source since

$\rho_{DE} \to \rho_{DM}$; then extending the source unicity to ρ_V explains the difference between (20) and (21) as the share of dark energy invested at the surface, its share of ρ_V. Picking Λ in (20) and following the ratios in (8) and (14):

$$\frac{\Lambda}{1+\frac{1}{2\pi^2}\times\frac{8}{11}} = 1.185\times10^{-52}\,\mathrm{m}^{-2}\,, \tag{22}$$

which is well within precision of (21); here the complimentary 3/11 of ρ_V comes from stress (12) in agreement with (8) where ρ_V is the surface.

3 The classical field

As shown in [1], using the Bohr hydrogen model (or inspecting the Dirac equation), we find the effects of $H\,c/2\pi$ when elementary particles mass increase linearly in time, and abusively computing with respect to a fixed frame:

$$\frac{da_0}{dt} = \frac{H\,c}{2\pi\,\nu}\,, \tag{23}$$

where a_0 is the Bohr radius and ν the electron pulsation ($E = h\,\nu$). In quantum theory, distances like a_0 are quantized as the inverse of mass, but in gravity the classical force is given by a product of masses, which doubles the effect. Then in the very weak gravitational field the acceleration $H\,c$ gives measurable effects in the form of anomalous acceleration; in circular orbit it will be:

$$a_{Hc} = \frac{H\,c}{2\,\pi} = 1.10\times10^{-10}\,\mathrm{m\,s}^{-2}\,, \tag{24}$$

like in (7) and (19). Then Newton's theory is no more the weak field limit of GR as it also needs $R_U \to \infty$. Now a_{Hc} is in range with Milgrom's modified Newton dynamics (MOND) limit acceleration [8, 9], which estimate is:

$$a_0 = 1.20\,(\pm0.2)\times10^{-10}\,\mathrm{m\,s}^{-2}\,. \tag{25}$$

Then we shall recover MOND in the weak field/circular orbit problem. In the modified Schwarzschild solution in (11), the term $H\,c$ denotes that the classical potential is permanently becoming steeper. Then a_{Hc} has specific direction; it just amplifies the local Newton acceleration. The simple sum gives:

$$A = \frac{G\,M}{r^2} + a_{Hc}\,. \tag{26}$$

Applying a force to an object in free fall gives reaction, so denoting A_N the Newton acceleration we can write:

$$A_N\left(1+\frac{a}{A_N}\right) \Rightarrow -a\,, \tag{27}$$

where $-a$ corresponds to the effect of inertia, as a reaction to a non-gravitational acceleration a when A_N and a are parallel. *In GR this equation is given by the field transformation in weak accelerations.* Now denoting A_{eff} the effective acceleration in circular orbit we have $A_{eff} \Rightarrow 0$; meaning that it is A_{eff} that transforms the field, and not A_N. Then in order to link A_N, A_{Eff} and A_{Hc}, we must write:

$$A_N = \frac{f}{m} = A_{eff}\left(1+\frac{a_{Hc}}{A_{eff}}\right)^{-1}\,, \tag{28}$$

where, since (27) defines the field transformation, the denominator of the right-hand side formally removes a_{Hc} from A_{eff} and then recovers the Newton force. *This equation is MOND simple interpolation function; needless to list the wide range of astrophysical data it fits*. It is then a formal approximation of the modified Schwarzschild solution in (11). QED.

4 The Hubble parameter and accelerated expansion

The parameters $\alpha = 2\pi^2 - 1$ and $\beta = 1$ in (9), which values are deduced reasoning on (10), show that the contribution of space expansion to the metric is trivial ($\beta = 1$), and the contribution of mass expansion is $1/2\pi^2$. Therefore the observable r, which depends on *massive* clocks and rulers, expands more than simple space expansion. Then we can approximate the metric state at distance r from the observer with:

$$d\tau(r)^2 \approx d\tau(0)^2 \times \left(\frac{2\pi^2}{2\pi^2+\frac{R_U-r}{R_U}}\right)^2\,. \tag{29}$$

Therefore, measurements of the Hubble parameter from the CMB spectrum ($r \to R_U$) will give a value different from and larger than $H = 1/T$; we find:

$$H = \frac{1}{T} \to H^0_{CMB} = \frac{2\pi^2\,H}{2\pi^2+1} = 67.53\,\mathrm{km/s/Mpc}\,, \tag{30}$$

which agrees with the PM results:

$$H^0_{CMB} = 67.74 \pm 0.46\,\mathrm{km/s/Mpc}\,.$$

Eq. (29) gives other measurable effects:

- When measuring H^0 from baryon acoustic oscillations (BAO) for which T is also close to zero, the same discrepancy appears, $H^0_{BAO} \approx H^0_{CMB}$, as shown in [10].
- At the opposite, $H = 1/T = 71.1$ km/s/Mpc is compatible with most recent Hubble space telescope data [11] taken from SN1A (73.24 ± 1.73 km/s/Mpc, currently valid at $\sim 2-3\sigma$), for which $r \to 0$.
- A simple plot shows that the denominator of (29) permanently gives the illusion of accelerating expansion.

Last, the symmetry in (1) is:

$$\lambda\,R_U = const\,, \tag{31}$$

where λ is the Compton wavelength of any piece of energy. Taking the universe mass and $\lambda_T = h/M_T\,c$ yields:

$$\lambda_T\,\frac{T}{2} = l_p\,t_p\,,$$

where l_p and t_p are the non-reduced Planck length and time respectively. It gives immediate significance to those units as they define the symmetry of the field expansion versus condensation. It denotes an inversion between spaces and times which reads:

$$\frac{T}{t_p} = \frac{2\,l_p}{\lambda_T}\,, \tag{32}$$

and a similar equation also applies to any mass. Hence the energy scales corresponding to l_p and t_p are epoch-relative like clocks and rulers, and also other Planck units (M_p, P_p). It just means that the laws of nature are constant but that the scale at which they apply vary in time.

It makes a big difference when thinking of quantum gravity which is expected to solve the big bang problem, because (32) is a symmetry linking the expansions of space-time and energy in a non-linear manner. To show this, from (32) and since energies increase, we find that at any given epoch:

$$R_U = c\,T_0 \int t_p/t\,, \tag{33}$$

where the quantum of time t_p replaces dt, and T_0 is a constant. Integration gives a logarithm which implies that the universe radius as observed from loopback time at any epoch, but assuming energy conservation, starts with inflation.

5 Conclusion

Overall, we found 9 strong correlations (*) giving distinct numerical results agreeing with unexplained experimental data in several domains of cosmology and astrophysics. We also find inflation for which a quantitative fit is out of reach, and the illusion of accelerating expansion. All come from a single assumption, a limited development, and classical solutions of the Einstein field equations.

The correlations above are totally irrelevant in GR, and also in QFT, but nature agrees at all scales. Hence the answer to the title is positive, and then GR and QFT miss the most important point which is that the expansion of space-time is identical to the expansion of energy. That is to say that space-time and energy are the same phenomenon. Importantly, all correlations are geometrical and all calculus use as input only one parameter, namely the universe age T, and natural constants G and c; then the next theory uses geometry and has no free parameters.

Acknowledgements

Many thanks to Patrick Marquet for interesting discussions and for pointing to his results.

Received on April 29, 2017

*With (1), (8), (12–13), (19), (20), (23), (24–25), (28), and (30).

References

1. Consiglio J. Energy is the Expansion. *Progress in Physics*, 2017, v. 13 (2), 102–105.
2. Bekenstein J. D. Black Holes and Entropy. *Phys. Rev. D*, 1973, v. 7, 2333.
3. Hawking S. W. Particle Creation by Black Holes. *Commun. Math. Phys.*, 1975, v. 43, 199.
4. Gibbons G. W. and Hawking S. W. Cosmological Event Horizons, Thermodynamics, and Particle Creation. *Phys. Rev.* , 1977, v. D 15, 2738.
5. Marquet P. The Gravitational Field : A New Approach. *Progress in Physics*, 2013, v. 3, 62–66.
6. Marquet P. Vacuum Background Field in General Relativity. *Progress in Physics*, 2016, v. 12, 314–316.
7. Marquet P. Some Insights on the Nature of the Vacuum Background Field in General Relativity. *Progress in Physics*, 2016, v. 12, 366–367.
8. Milgrom M. A Modification of the Newtonian Dynamics as a Possible Alternative to the Hidden Mass Hypothesis. *Astrophysical Journal*, 1983, v. 270, 365–370.
9. Milgrom M. MOND Theory. arXiv: astro-ph/1404.7661v2.
10. The Plank Collaboration. Planck 2015 Results. I. Overview of Products and Scientific Results. arXiv: astro-ph/1502.01582.
11. Riess A. G., Macri L. M., Hoffmann S. L., Scolnic D., Casertano S., Filippenko A. V., Tucker B. E., Reid M. J., Jones D. O. A 2.4% Determination of the Local Value of the Hubble Constant. arXiv: astro-ph/1604.01424.

Using the SALI Method to Distinguish Chaotic and Regular Orbits in Barred Galaxies with the LP-VIcode Program

Lucas Antonio Caritá[1,2,3], Irapuan Rodrigues[2], Ivânio Puerari[3] and Luiz Eduardo Camargo Aranha Schiavo[2]

[1]Instituto Federal de Educação, Ciência e Tecnologia de São Paulo, IFSP, São José dos Campos, Brasil.
[2]Universidade do Vale do Paraíba, UNIVAP, São José dos Campos, Brasil.
[3]Instituto Nacional de Astrofísica, Óptica y Electrónica, INAOE, Puebla, México.

The Smaller Alignment Index (SALI) is a new mathematical tool for chaos detection in the phase space of Hamiltonian Dynamical Systems. With temporal behavior very specific to movements ordered or chaotic, the SALI method is very efficient in distinguishing between chaotic and regular movements. In this work, this method will be applied in the study of stellar orbits immersed in a gravitational potential of barred galaxies, once the motion of a test particle, in a rotating barred galaxy model is given by a Hamiltonian function. Using an analytical potential representative of a galaxy with bar (two degrees of freedom), we integrate some orbits and apply SALI in order to verify their stabilities. In this paper, we will discuss a few cases illustrating the trajectories of chaotic and regular orbits accompanied by the graph containing the behavior of SALI. All calculations and integrations were performed with the LP-VIcode program.

1 Introduction

One of the schemes more used to classify galaxies according to their morphology was proposed by Edwin Powell Hubble. Basically, the Hubble fork separates galaxies in two types: regular spirals (S) and barred spirals (SB). The galaxy bar, spiral arms and even galactic rings are structures that can be interpreted as disturbance to axisymmetric potential of the galactic disk.

In this work, we study the nature of some orbits immersed in analytical potentials with two degrees of freedom representing barred galaxies. In order to do this, we applied the Smaller Alignment Index (SALI) [9–13], which is a mathematical tool for distinguishing regular and chaotic motions in the phase space of Hamiltonian Dynamical Systems in analytical gravitational potentials. It is possible because the motion of a test particle in a rotating barred galaxy model is given by a Hamiltonian function.

The orbits integration and the SALI calculation were performed using the LP-VIcode program [2]. The LP-VIcode is a fully operational code in Fortran 77 that calculates efficiently 10 chaos indicators for dynamic systems, regardless of the number of dimensions, where SALI is one of them. To construct our barred galaxies models, two different sets of parameters were extracted from the paper of Manos and Athanassoula [5].

The main purpose of this paper is to show some regular and chaotic orbits, where the stability study was done using the SALI method. Such orbits were taken immersed in a mathematical model for the gravitational potential that simulates a barred galaxy in a system with two degrees of freedom.

2 Methodology

2.1 The SALI method

Considering a Hamiltonian flow (N degrees of freedom), an orbit in the $2N$-dimensional phase space with initial condition $P(0) = (x_1(0), \cdots, x_{2N}(0))$ and two different initial deviation vectors from the initial point $P(0)$, $w_1(t)$ and $w_2(t)$, we define the Smaller Alignment Index (SALI) by:

$$\mathrm{SALI}(t) = \min\{||\widehat{w}_1(t) + \widehat{w}_2(t)||, ||\widehat{w}_1(t) - \widehat{w}_2(t)||\} \quad (1)$$

where $\widehat{w}_i(t) = w_i(t)/||w_i(t)||$ for $i \in \{1, 2\}$.

In the case of chaotic orbits, SALI(t) falls exponentially to zero as follows:

$$\mathrm{SALI}(t) \propto e^{-(L_1 - L_2)t} \quad (2)$$

where L_1 and L_2 are the biggest Lyapunov Exponents.

When the behavior is ordered, SALI oscillates in non-zero values, that is:

$$\mathrm{SALI}(t) \approx \text{constant} > 0,\ t \longrightarrow \infty\,. \quad (3)$$

Therefore, there is a clear distinction between orderly and chaotic behavior using this method.

2.2 Gravitational potential of a barred galaxy

We apply the SALI method in the study of stellar orbits immersed in a gravitational potential of barred galaxies, once the movement of a test particle in a rotating three-dimensional model of a barred galaxy is given by the Hamiltonian:

$$\begin{aligned} &H(x, y, z, p_x, p_y, p_z) = \\ &= \left(p_x^2 + p_y^2 + p_z^2\right) + \Phi_T(x, y, z) + \Omega_b(x p_y - y p_x) \end{aligned} \quad (4)$$

where the bar rotates around z; x and y contain respectively the major and minor axes of the galactic bar, Φ_T is the gravitational potential (which will be described later), and Ω_b represents the standard angular velocity of the bar.

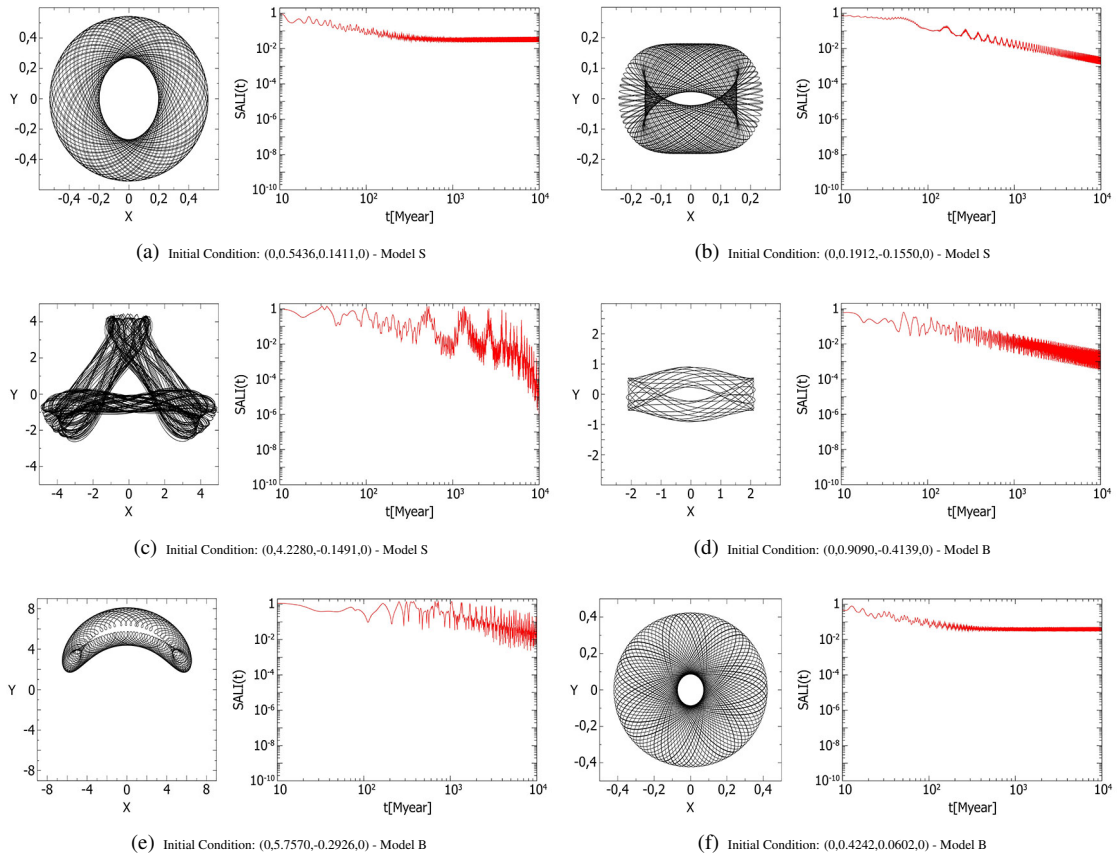

(a) Initial Condition: (0,0.5436,0.1411,0) - Model S

(b) Initial Condition: (0,0.1912,-0.1550,0) - Model S

(c) Initial Condition: (0,4.2280,-0.1491,0) - Model S

(d) Initial Condition: (0,0.9090,-0.4139,0) - Model B

(e) Initial Condition: (0,5.7570,-0.2926,0) - Model B

(f) Initial Condition: (0,0.4242,0.0602,0) - Model B

Fig. 1: Six orbits, each one with its SALI diagram. All orbits were integrated up to 10,000 Myr. Only the first 500 Myr were plotted in (a), (b), (d) and (f), for clarity.

For this Hamiltonian, the corresponding equations of motion and the corresponding variational equations that govern the evolution of a deviation vector can be found in [4]. With such equations it is possible to follow the temporal evolution of a moving particle immersed in the potential Φ_T, as well as verify if this orbit is chaotic or regular, following the evolution of deviation vectors by the SALI method.

In this work, the total potential Φ_T is composed by three components, representing the galactic bulge, disk and bar:

$$\Phi_T = \Phi_{Bulge} + \Phi_{Disk} + \Phi_{Bar} \,. \tag{5}$$

We represent the bulge by the Plummer Model [8]

$$\Phi_{Bulge} = -\frac{GM_S}{\sqrt{x^2 + y^2 + z^2 + \epsilon_S^2}} \,, \tag{6}$$

where ϵ_S is the length scale and M_S is the bulge mass.

We represent the disk by the Miyamoto-Nagai Model [6]

$$\Phi_{Disk} = -\frac{GM_D}{\sqrt{x^2 + y^2 + (A + \sqrt{z^2 + B^2})^2}} \tag{7}$$

where A and B are respectively the radial and vertical scale lengths, and M_D is the disk mass.

We represent the bar by the Ferrers Model [3]. In this model, the density in given by

$$\begin{cases} \rho_B(x,y,z) = \rho_c \left(1 - m^2\right)^2 \,, & m < 1 \\ \\ \rho_B(x,y,z) = 0 \,, & m \geq 1 \end{cases} \tag{8}$$

where the central density is

$$\rho_c = \frac{105}{32\pi} \frac{GM_B}{abc} \,,$$

M_B is the bar mass and

$$m^2 = \frac{x^2}{a^2} + \frac{y^2}{b^2} + \frac{z^2}{c^2} \,,$$

where $a > b > c > 0$ are the semi-axes of the ellipsoid which represents the bar.

The potential created by the galactic bar is calculated with the Poisson equation (see [1]):

$$\Phi_{Bar} = -\pi\, G\, abc\, \frac{\rho_c}{3} \int_\lambda^\infty \frac{du}{\Delta(u)} \left(1 - m^2(u)\right)^3 \tag{9}$$

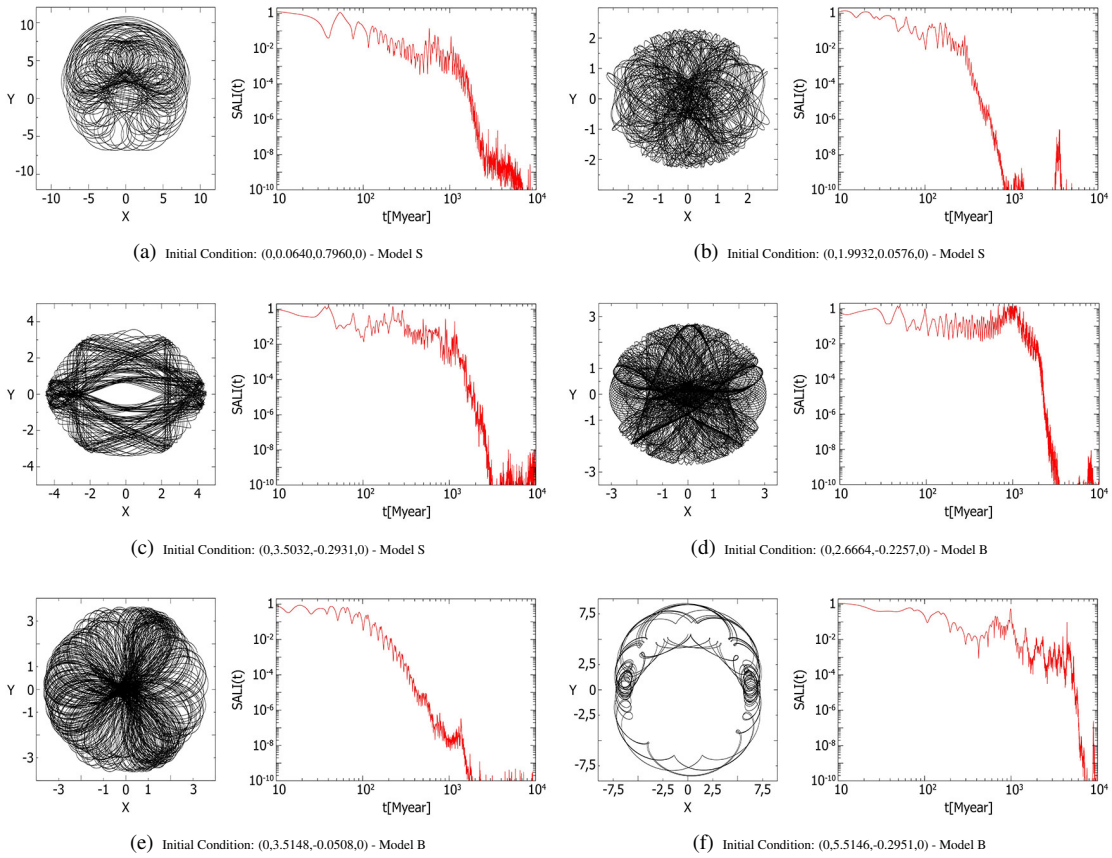

(a) Initial Condition: (0,0.0640,0.7960,0) - Model S

(b) Initial Condition: (0,1.9932,0.0576,0) - Model S

(c) Initial Condition: (0,3.5032,-0.2931,0) - Model S

(d) Initial Condition: (0,2.6664,-0.2257,0) - Model B

(e) Initial Condition: (0,3.5148,-0.0508,0) - Model B

(f) Initial Condition: (0,5.5146,-0.2951,0) - Model B

Fig. 2: The SALI graphics has both axes in logarithmic scale. All orbits were integrated into 10,000 Myr. Only the first 5,000 Myr were plotted in (b), for clarity.

where

$$m^2(u) = \frac{x^2}{a^2+u} + \frac{y^2}{b^2+u} + \frac{z^2}{c^2+u},$$

$$\Delta^2(u) = (a^2+u)(b^2+u)(c^2+u)$$

and λ is the positive solution of $m^2(\lambda) = 1$ for the region outside the bar ($m \geq 1$) and $\lambda = 0$ for the region inside the bar ($m < 1$).

2.3 The LP-VIcode program with minor adjustments

To perform the orbits integrations and the SALI calculation, we used the LP-VIcode program [2], which is an operational code in Fortran 77 that calculates efficiently 10 chaos indicators for dynamical systems, including SALI.

In this program, the user must provide the expressions of the potential as well the expressions of motion and variational equations. However, the general structure of motion and variational equations previously written in the main program, take into account only a static reference frame, and it is known that in order to model the galactic bar potential, it is necessary to consider a coordinate system that rotates along with the bar.

In this context, considering Ω_b the bar angular velocity, our reference frame should also rotate with angular velocity Ω_b. This affects the motion and variational equations since, as can be seen in [4], they depend on Ω_b. In order to solve this problem, adjustments were made to the main program to include the rotation in the coordinate system with the same angular velocity of the bar.

2.4 Parameters sets

We used the two parameter sets shown in Table 1 for the potential model, taken from the paper by Manos & Athanassoula [5]. The model units adopted are: 1 kpc for length, 10^3 km s^{-1} for velocity, 10^3 km s^{-1} kpc^{-1} for angular velocity, 1 Myr for time, and $2 \times 10^{11}\, M_{solar}$ for mass. The universal gravitational constant G will always be considered 1 and the total mass $G(M_S + M_D + M_B)$ will be always equal to 1.

2.5 Initial conditions

We emphasize that in this paper we study orbits with two degrees of freedom. In order to do that, we consider $z = 0$ and $p_z = 0$ in the three-dimensional Hamiltonian (4).

Table 1: Parameter Sets and the Bars Co-rotation.

	M_S	ϵ_S	M_D	A	B	M_B	a	b	c	Ω_b	CR
Model S	0.08	0.4	0.82	3.0	1.0	0.1	6.0	1.5	0.6	0.054	6.04
Model B	0.08	0.4	0.82	3.0	1.0	0.1	6.0	3.0	0.6	0.054	6.06

The effective potential, which is the sum of the gravitational potential with the potential generated by the repulsive centrifugal force, is given by:

$$\Phi_{eff}(\mathbf{x}) = \Phi_T(\mathbf{x}) - \frac{1}{2}|\Omega \times \mathbf{x}|^2 . \tag{10}$$

Written like that, this potential represents a rotating system.

The quantity

$$E_J = \frac{1}{2}|\mathbf{v}|^2 + \Phi_{eff}(\mathbf{x}) \tag{11}$$

is called Jacobi Energy and is conserved in the rotating system.

The curve given by $\Phi_{eff}(0, y, 0) = E_J$ is called Zero Velocity Curve and provides a good demarcation for the choice of initial conditions, since there is only possibility of orbits when $\Phi_{eff} \leq E_J$, in other words, below this curve (see [1]).

Therefore, we generated some random initial conditions initially taking a value to y_0 less than the highest possible value of y for a given energy E_J, taking $x_0 = 0$ and $v_{y_0} = 0$. This done, we could calculate v_x as follows:

$$E_J = \frac{1}{2}\left(v_{x_0}^2 + v_{y_0}^2\right) + \Phi_{eff} = \frac{1}{2}v_{x_0}^2 + \Phi_{eff} \tag{12}$$

and this implies

$$v_{x_0} = \pm\sqrt{2(E_J - \Phi_{eff})} . \tag{13}$$

Then we constructed initial conditions $(x_0, y_0, v_{x_0}, v_{y_0})$ to integrate the orbits. As $x_0 = 0$ and $v_{y_0} = 0$, the launched orbits will always be initially over the y axis and will have initial velocity only in the x direction.

Notice that we have two possible velocities from equation (13): one negative and one positive. We decided to take y_0 always positive, so that when v_{x_0} is positive, the orbits are prograde (orbits that rotate in the same direction of the bar) and when v_{x_0} is negative, the orbits are retrograde (orbits that rotate in the opposite direction of the bar).

3 Results

In our computational calculations, we consider SALI $< 10^{-8}$ close enough to zero to consider the movement chaotic.

3.1 Regular orbits

In Fig. 1 we show 6 different orbits, each one with its SALI diagram, from where we can identify them as regular orbits, as explained in section 2.1.

3.2 Chaotic orbits

Fig. 2 shows a sample of 6 chaotic orbits, identified by their SALI indexes that goes to zero after some time, as discussed in section 2.1.

4 Conclusion

In this study, we were able to reproduce a mathematical modeling of the gravitational potential of a barred galaxy and, in order to verify the stability of the orbits within, we applied the SALI method. We were able to prove the SALI efficiency in distinguishing regular or chaotic orbits. In fact, this method offers an easily observable distinction between chaotic and regular behavior.

We also perceive the LP-VIcode efficiency, which proved to be extremely competent in the orbits integration and study of stability with SALI. To make an adjustment in the variational and motion equations programmed in the LP-VIcode, we insert an adaptation in the main code to take into account a rotating system.

Therefore, we conclude that we were successful in calculating these orbits and confirm the SALI method as a new important tool in the study of stellar orbits stability.

Acknowledgements

We acknowledge the Brazilian agencies FAPESP, CAPES and CNPq (200906-2015-1), as well as the Mexican agency CONACyT (CB-2014-240426) for supporting this work. Our sincere thanks to Dr. Pfenniger, who kindly provided us with his Fortran 77 implementation of the Ferrers bar potential. All the numerical work was developed using the Hipercubo Cluster resources (FINEP 01.10.0661-00, FAPESP 2011/13250-0 and FAPESP 2013/17247-9) at IP&D–UNIVAP.

Received on May 12, 2017

References

1. Binney J. and Tremaine S. Galactic Dynamics, 2nd ed. Princeton University Press, 2008.
2. Carpintero D. D., Maffione N. and Darriba L. LP-VIcode: a program to compute a suite of variational chaos indicators. *Astronomy and Computing*, 2014, v. 5, 19–27. DOI: 10.1016/j.ascom.2014.04.001.
3. Ferrers N. M. On the potential of ellipsoids, ellipsoidal shells, elliptic laminae and elliptic rings, of variables densities. *Quarterly Journal of Pure and Applied Mathematics*, 1877, v. 14, 1–22.
4. Manos T. A Study of Hamiltonian Dynamics with Applications to Models of Barred Galaxies. PhD Thesis in Mathematics, Université de Provence and University of Patras, 2008.

5. Manos T. and Athanassoula E. Regular and chaotic orbits in barred galaxies – I. Applying the SALI/GALI method to explore their distribution in several models. *Monthly Notices of the Royal Astronomical Society*, 2011, v. 415, 629–642. DOI: 10.1111/j.1365-2966.2011.18734.x.

6. Miyamoto M. and Nagai R. Three-dimensional models for the distribution of mass in galaxies. *Astronomical Society of Japan*, 1975, v. 27, 533–543.

7. Pfenniger D. The 3D dynamics of barred galaxies. *Astronomy and Astrophysics*, 1984, v. 134, 373–386. ISSN: 0004-6361.

8. Plummer H. C. On the problem of distribution in globular star clusters. *Notices of the Royal Astronomical Society*, 1911, v. 71, 460–470. DOI: 10.1093/mnras/71.5.460.

9. Skokos Ch. Alignment indices: a new, simple method for determining the ordered or chaotic nature of orbits. *Journal of Physics: Mathematical and General*, 2001, v. 34, 10029–10043. DOI: 10.1088/0305-4470/34/47/309.

10. Skokos Ch., Antonopoulos Ch., Bountis T. C. and Vrahatis M. N. Smaller alignment index (SALI): Determining the ordered or chaotic nature of orbits in conservative dynamical systems. In Gomez G., Lo M. W., Masdemont J. J., eds. Proceedings of the Conference Libration Point Orbits and Applications, World Scientific, 2002, 653–664. DOI: 10.1142/9789812704849_0030.

11. Skokos Ch., Antonopoulos Ch., Bountis T. C. and Vrahatis M. N. How does the Smaller Alignment Index (SALI) distinguish order from chaos? *Prog. Theor. Phys. Supp.*, 2003, v. 150, 439–443. DOI: 10.1143/PTPS.150.439.

12. Skokos Ch., Antonopoulos Ch., Bountis T. C. and Vrahatis M. N. Detecting order and chaos in Hamiltonian systems by the SALI method. *J. Phys. A*, 2004, v. 37, 6269–6284. DOI: 10.1088/0305-4470/37/24/006.

13. Skokos Ch. and Bountis T. C. Complex Hamiltonian Dynamics. Springer, 2012.

A New Perspective for Kinetic Theory and Heat Capacity

Kent W. Mayhew

68 Pineglen Cres., Ottawa, Ontario, K2G 0G8, Canada. E-mail: Kent.Mayhew@gmail.com

The currently accepted kinetic theory considers that a gas' kinetic energy is purely translational and then applies equipartition/degrees of freedom. In order for accepted theory to match known empirical finding, numerous exceptions have been proposed. By redefining the gas' kinetic energy as translational plus rotational, an alternative explanation for kinetic theory is obtained, resulting in a theory that is a better fit with empirical findings. Moreover, exceptions are no longer required to explain known heat capacities. Other plausible implications are discussed.

1 Introduction

The conceptualization of a gaseous system's kinematics originated in the writings of the 19th century greats. In 1875, Maxwell [1] expressed surprise at the ratio of energies (translational, rotational and/or vibrational) all being equal. Boltzmann's work on statistical ensembles reinforced the current acceptance of law of equipartition with a gas's energy being equally distributed among all of its degrees of freedom [2–3]. The net result being that the accepted mean energy for each independent quadratic term being $kT/2$.

The accepted empirically verified value for the energy of a /textitN molecule monatomic gas is $kT/2$ with its isometric molar heat capacity (C_v) being ($3R/2$). An implication is that a monatomic gas only possesses translational energy [4–5]. The reasoning for this exception is that the radius of a monatomic gas is so small that its rotational energy remains negligible, hence its energy contribution is simply ignored.

Mathematically speaking equipartition based kinetic theory states that a molecule with n'' atoms has $3n''$ degrees of freedom (f) [5–6] i.e.:

$$f = 3n''. \tag{1}$$

This leads to the isometric molar heat capacity (C_v) for large polyatomic molecules:

$$C_v = \frac{3}{2} n'' R. \tag{2}$$

Interestingly, the theoretical expected heat capacity for N diatomic molecules is $7NkT/2$. This is the summation of the following three energies a) three translational degrees, i.e. $3NkT/2$. b) three rotational degrees of freedom, however since the moment of inertia about the internuclear axis is vanishing small w.r.t. other moments, then it is excluded, i.e. NkT. c) Vibrational energy, i.e. NkT. This implies a molar heat capacity C_v =$7NkT/2$ = 29.3 J/(mol*K). However, empirical findings indicate that the isometric molar heat capacity for a diatomic gas is actually 20.8 J/(mol*K), which equates to $5RT/2$ [6]. This discrepancy for diatomic gases certainly allows one to question the precise validity of accepted kinetic theory! In 1875 Maxwell noted that since atoms have internal parts then this discrepancy maybe worse than we believe [7].

Various explanations for equipartition's failure in describing heat capacities have been proposed. Boltzmann suggested that the gases might not be in thermal equilibrium [8]. Planck [9] followed by Einstein and Stern [10] argued the possibility of zero-point harmonic oscillator. More recently Dahl [11] has shown that a zero point oscillator to be illusionary. Lord Kelvin [12–13] realized that equipartition maybe wrongly derived. The debate was somewhat ended by Einstein claiming that equipartition's failure demonstrated the need for quantum theory [14–15]. Heat capacities of gases have been studied throughout the 20th century [16–19] with significantly more complex models being developed [20–21].

It becomes a goal of this paper to clearly show that an alternative kinetic theory/model exists. A simple theory that correlates better with empirical findings without relying on exceptions while correlating with quantum theory.

2 Kinetic theory and heat capacity simplified

Consider wall molecules 1 through 8, in Fig. 1. The total mean energy along the x-axis of a vibrating wall molecule is

$$\overline{E}_x = kT. \tag{3}$$

Half of a wall molecule's mean energy would be kinetic energy, and half would be potential energy. Thus, the mean kinetic energy along the x-axis, remains

$$\overline{E}_x = \frac{kT}{2}. \tag{4}$$

In equilibrium, the mean kinetic energy of a wall molecule, as defined by equation (4) equals the mean kinetic energy of the gas molecule along the same x-axis. Herein, the wall in the y-z plane acts as a massive pump, pumping its mean kinetic energy along the x-axis onto the much smaller gas molecules.

In equilibrium each gas molecule will have received a component of kinetic energy along each orthogonal axis. Although there are six possible directions, at any given instant, a gas molecule can only have components of motion along three directions, i.e. it cannot be moving along both the positive and negative x-axis at the same time. Therefore, the total kinetic energy of the N molecule gas is defined by

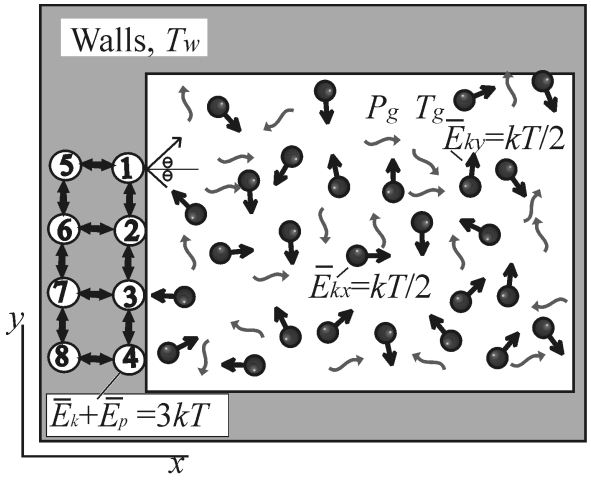

Fig. 1: Ideal monoatomic gas at pressure P_g and temperature T_g sourrounded by walls at temperature $T_w = T_g$. Gas molecules have no vibrational energy.

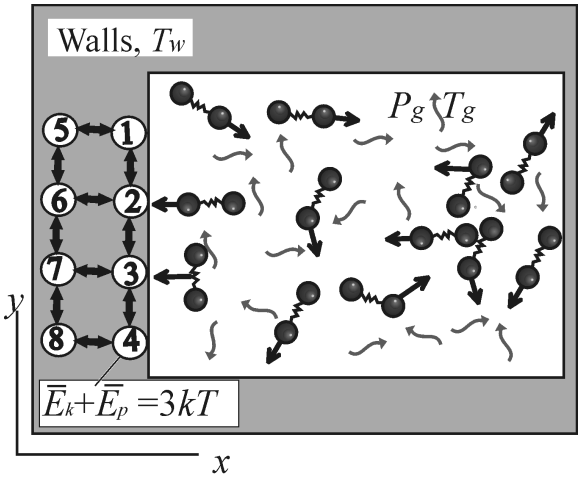

Fig. 2: Ideal diatomic gas at pressure P_g and temperature T_g sourrounded by walls at temperature $T_w = T_g$. Gas molecules have vibrational energy.

equation (4) i.e. $3NkT/2$. Up to this point we remain in agreement with accepted theory.

Consider that you hit a tennis ball with a suitable racquet. If the ball impacts the racquet's face at a 90 degree angle, then the ball will have significant translational energy in comparison to any rotational energy. Conversely, if the ball impacts the racquet at an acute angle, although the same force is imparted onto that ball, the ball's rotational energy can be significant in comparison to its translational energy. The point being, in real life both the translational and rotational energy, are due to the same impact.

Now reconsider kinetic theory. Understandably, momentum transfer between both the wall's and gas' molecules result in energy exchanges between the massive wall and small gas molecules. Moreover, the exact nature of the impact will vary, even though the exchanged mean energy is constant.

Case 1: Imagine that a monatomic gas molecule collides head on with a wall molecule, e.g. the gas molecule hitting wall molecule no. 3 in Fig. 1. Herein, the gas molecule might only exchange translational energy with the wall, resulting in the gas molecule's mean kinetic energy being purely translational, and defined by equation (4).

Case 2: Imagine that a monatomic gas molecule strikes wall molecule no. 1 at an acute angle. The gas molecule would obtain both rotational and translational energy from the impact such that the total resultant mean energy of the gas molecule would be the same as it was in Case 1, i.e. defined by equation (4).

Case 3: Imagine a rotating and translating monatomic gas molecule striking the wall. Both the rotational and translational energies will be passed onto the wall molecule. Since the wall molecule is bound to its neighbors, it cannot rotate hence both energies can only result in vibrational energy of the wall molecules along its three orthogonal axis.

After numerous wall impacts, our model predicts that an N molecule monatomic gas will have a total kinetic energy (translational plus rotational) defined by

$$E_{kT(t,r)} = \frac{3}{2} NkT. \tag{5}$$

Fig. 2 illustrates a system of diatomic gas molecules in a container. The wall molecules still pass the same mean kinetic energy onto the diatomic gas molecule's center of mass with each collision. Therefore the diatomic gas' kinetic energy is defined by equation (5). The diatomic gas molecule's vibrational energy would be related to the absorption and emission of its surrounding blackbody/thermal radiation. Therefore, the mean x-axis vibrational energy within a diatomic gas molecule remains defined by equation (3) and the total mean energy for a diatomic gas molecule becomes defined by

$$\overline{E}_{tot} = \overline{E}_{kT(t,r)} + \overline{E}_v = \frac{3}{2} kT + kT = \frac{5}{2} kT. \tag{6}$$

Therefore the total energy for an N molecule diatomic gas becomes

$$E_{tot} = E_{kT(t,r)} + E_v = \frac{3}{2} NkT + NkT = \frac{5}{2} NkT. \tag{7}$$

For an N molecule triatomic gas:

$$E_{tot} = E_{kT(t,r)} + E_v = \frac{3}{2} NkT + 2NkT = \frac{7}{2} NkT, \tag{8}$$

n'' signifies the polyatomic number. Therefore for N molecules of n''-polyatomic gas, the vibrational energy is

$$E_v = (n'' - 1)NkT. \tag{9}$$

Therefore, the total energy for a polyatomic gas molecule is:

$$E_{tot} = E_{kT(t,r)} + E_v = \frac{3}{2} NkT + (n'' - 1) NkT = \left(n'' + \frac{1}{2}\right) NkT. \quad (10)$$

Dividing both sides by temperature and rewriting in terms of per mole (N=6.02 × 10^{23}) then equation (10) becomes:

$$\frac{E_{tot}}{T} = nk\left(n'' + \frac{1}{2}\right) = R\left(n'' + \frac{1}{2}\right). \quad (11)$$

For most temperature regimes, the heat capacity of gases remains fairly constant, hence equation (11) can be rewritten in terms of the isometric molar heat capacity (C_v), i.e.

$$C_v = R\left(n'' + \frac{1}{2}\right). \quad (12)$$

The difference between molar isobaric heat capacity (C_p) and molar isometric heat capacity (C_v) for gases is the ideal gas constant (R) [see equation (15)]. Therefore, a gas's isobaric heat capacity C_p becomes

$$C_p = R\left(n'' + \frac{1}{2}\right) + R = R\left(n'' + \frac{3}{2}\right). \quad (13)$$

The adiabatic index is the ratio of heat capacities, i.e. dividing equation (13) by equation (12) gives the adiabatic index

$$\gamma = \frac{C_p}{C_v} = \frac{\left(n'' + \frac{3}{2}\right)}{\left(n'' + \frac{1}{2}\right)}. \quad (14)$$

Table 1 shows the accepted isometric and isobaric molar heat capacities for various substances for $0 > n'' > 27$. These values were calculated using data (specific heats) from an engineering table (Rolle [22]) that is shown in Table 2. Note: Engineer's use specific heats (per mass), physicists and chemists prefer heat capacity (per mole).

In Fig. 3, both our theoretical molar isometric and isobaric [equations (12) and (13)] heat capacities are plotted against the number of atoms (n'') in each molecule. The accepted empirically determined values for heat capacities versus n'' (from Table 1) are also plotted. The traditional theoretical values for molar heat capacities [eq. (2)] are also plotted.

The theory/model proposed herein remains a better fit to empirical findings for all polyatomic molecules. Importantly, it does not rely upon the exceptions that plague the traditionally accepted degrees of freedom based kinetic theory.

Interestingly, there is a discrepancy, between our model and empirical known values for $4 < n'' < 9$. Moreover, the slope of our theoretical values visually remains close to the slope of empirically determined values for $n'' > 8$. Furthermore, hydrogen peroxide (H_2O_2, C_v= 37.8, n'' = 4) and acetylene (C_2H_2, n'' = 4, C_v= 35.7) are linear bent molecules and good fit, while pyramidal ammonia (NH_3, n'' = 4, C_v = 27.34) is not. Could the gas molecule's shape influence how it absorbs surrounding thermal radiation, hence its vibrational energy?

Table 2 shows the accepted adiabatic index versus our theoretical adiabatic index for most of the same substances shown in Table 1. Our theoretical adiabatic index compares rather well with the accepted empirical based values, especially for low $n'' < 4$ and high $n'' > 11$, as is clearly seen in Fig. 4. Although not 100% perfect, this new theory/model certainly warrants due consideration by others.

3 Kinetic theory and thermal equilibrium

Kinetic theory holds because the walls act as massive energy pumps, i.e. gas molecules take on the wall's energy with every gas-wall collision. For sufficiently dilute gases, this remains the dominant method of energy exchange. Mayhew [23–24] has asserted that inter-gas molecular collisions tend to obey conservation of momentum, rather than adhere to kinetic theory. Therefore, when inter-gas collisions dominate over gas-wall collisions, then kinetic theory, the ideal gas law, Avogadro's hypothesis, Maxwell's velocities etc. all can start to lose their precise validity.

It is accepted that there are changes to heat capacity in and around dissociation temperatures. Firstly, at such high temperatures, the pressure tends to be high; hence the inter-gas collisions may dominate. This author believes that this actually helps explain why kinetic theory falters in polytropic stars, wherein high-density gases collide in a condensed matter fashion hence one must use polytropic solutions. Secondly, at high temperatures a system's thermal energy density is no longer proportional to temperature, i.e. a blast furnace's thermal energy density is proportional to T^4 [22].

Blackbody radiation describes the radiation within an enclosure. For an open system and/or none blackbody, the thermal radiation surrounding the gas molecules may be better to considered. Herein thermal radiation means radiation that is readily absorbed and radiated by condensed matter and/or polyatomic gases, resulting in both intramolecular and intermolecular vibrations.

For a system of dilute polyatomic gas e.g. Fig. 2, thermal equilibrium requires that all of the following three states remain related to the same temperature (T):

1. The walls are in thermal equilibrium with the enclosed blackbody/thermal radiation.
2. The gas' translational plus rotational energy is in mechanical equilibrium with the molecular vibrations of the walls.
3. The gas' vibrational energies are in thermal equilibrium with the enclosed blackbody/thermal radiation.

Imagine that a system of dilute polyatomic gas is taken to remote outer space, and that the walls are magically re-

Table 1: Accepted isometric and isobaric heat capacities versus theoretical i.e. empirical findings versus Eqn. (12), Eqn. (13), as well as Eqn. (2). Note: Accepted heat capacities were calculated from the engineer's specific heats in Table 2 (Rolle [22]), exception being H_2O_2 which was taken from Giguere [19].

Substance		n''	Accepted C_v [J/mol*K]	Eqn. (12) C_v [J/mol*K]	Accepted C_p [J/mol*K]	Eqn. (13) C_p [J/mol*K]	Eqn. (2) C_v [J/mol*K]
Helium	He	1	12.48	12.47	20.80	20.78	
Neon	Ne	1	12.47	12.47	20.79	20.78	
Argon	Ar	1	12.46	12.47	20.81	20.78	
Xenon	Xe	1	12.47	12.47	20.58	20.78	
Hydrogen	H_2	2	20.52	20.78	28.83	29.09	
Nitrogen	N_2	2	20.82	20.78	29.14	29.09	
Oxygen	O_2	2	21.02	20.78	29.34	29.09	
Nitric oxide	NO	2	21.55	20.78	29.86	29.09	
Water vapor	H_2O	3	25.26	29.09	33.58	37.40	37.40
Carbon dioxide	CO_2	3	28.83	29.09	37.14	37.40	37.40
Sulfur dioxide	SO_2	3	31.46	29.09	39.78	37.40	37.40
Hydrogen peroxide	H_2O_2	4	37.4	37.73	46.05	45.71	49.86
Ammonia	NH_3	4	27.37	37.40	35.70	45.71	49.86
Methane	CH_4	5	27.4	45.71	35.72	54.0	62.33
Ethylene	C_2H_4	6	35.24	54.02	43.54	62.33	74.79
Ethane	C_2H_6	8	44.35	70.64	52.65	78.95	99.72
Propylene	C_3H_6	9	53.82	78.95	63.92	87.26	112.19
Propane	C_3H_8	11	65.18	95.57	73.51	103.88	137.12
Benzene	C_6H_6	12	73.50	103.88	81.63	112.19	149.58
Isobutene	C_4H_8	12	77.09	103.88	85.68	112.19	149.58
n-Butane	C_4H_{10}	14	89.10	120.50	97.42	128.81	174.51
Isobutane	C_4H_{10}	14	88.52	120.50	96.84	128.81	174.51
n-Pentane	C_5H_{12}	17	111.91	145.43	120.20	153.74	211.91
Isopentane	C_5H_{12}	17	111.69	145.43	119.99	153.74	211.91
n-Hexane	C_6H_{14}	20	134.78	170.36	143.06	178.67	249.30
n-Heptane	C_7H_{16}	23	157.62	195.29	165.94	203.60	286.70
Octane	C_8H_{18}	26	180.60	220.22	188.83	228.53	324.09

moved and the gas disperses. Spreading at the speed of light the blackbody/thermal radiation density decreases faster than the density of slower moving gas molecules. As the radiation density decreases, the rate at which polyatomic gaseous molecules absorbs blackbody/thermal radiation decreases in time. Hence their vibrational energy decreases although their mean velocity remains constant. Now place a thermometer in the expanding wall-less gas, what will it read? Traditional kinetic theory claims that the temperature will be the same because the gas molecule's velocity remains constant i.e. temperature is only associated with the system's kinematics [2–3]. However, without walls the blackbody/thermal radiation decouples from thermal equilibrium i.e. the mean velocity of the gas molecules are associated with one temperature, but the radiation density is no longer associated with that temperature. This bodes the question: What is the real temperature? Of course this means accepting that the thermometer not only exchanges kinetic energy with the gas molecules, but it also exchanges blackbody/thermal radiation with its surroundings.

The above is another reason that this author hypothesizes that kinetic theory can falter in systems without walls. The

Table 2: Engineer's accepted adiabatic index compared to theoretical: Eqn. (14). Note: Data in first six columns after Rolle [22]. Rolle's reference: J.F. Masi, Trans. ASME, 76:1067 (October, 1954): National Source of Standards (U.S.) Circ. 500, Feb. 1952; Selected Values of Properties of Hydrocarbons and Related Compounds, American Petroleum Institute Research Project 44, Thermodynamic Research Center, Texas, A&M University, College Station, Texas.

Substance		n''	Molar mass [g/mol]	Engineer's R [J/kg*K)]	Engineer's C_p [kJ/mol*K)]	Engineer's C_v [kJ/mol*K)]	Accepted adiabatic index(γ)	Theoretical index (γ) Eqn. (14)
Helium	He	1	4.00	2079	5.196	3.117	1.67	1.67
Neon	Ne	1	20.18	412	1.030	0.618	1.67	1.67
Argon	Ar	1	39.94	208	0.521	0.312	1.67	1.67
Xenon	Xe	1	131.30	63	0.1568	0.095	1.67	1.67
Hydrogen	H_2	2	2.02	4124	14.302	10.178	1.41	1.4
Nitrogen	N_2	2	28.02	297	1.040	0.743	1.4	1.4
Oxygen	O_2	2	32.00	260	0.917	0.657	1.4	1.4
Nitric oxide	NO	2	30.01	277	0.995	0.718	1.39	1.4
Water vapor	H_2O	3	18.02	462	1.864	1.402	1.33	1.29
Carbon dioxide	CO_2	3	44.01	189	0.844	0.655	1.29	1.29
Sulfur dioxide	SO_2	3	64.07	130	0.621	0.491	1.26	1.29
Ammonia	NH_3	4	17.03	488	2.096	1.607	1.30	1.22
Methane	CH_4	5	16.04	519	2.227	1.708	1.30	1.18
Ethylene	C_2H_4	6	28.05	297	1.552	1.256	1.24	1.15
Ethane	C_2H_6	8	30.07	277	1.751	1.475	1.19	1.12
Propylene	C_3H_6	9	42.08	198	1.519	1.279	1.19	1.11
Propane	C_3H_8	11	44.10	189	1.667	1.478	1.13	1.09
Benzene	C_6H_6	12	78.11	106	1.045	0.939	1.11	1.08
Isobutene	C_4H_8	12	56.11	148	1.527	1.374	1.11	1.08
n-Butane	C_4H_{10}	14	58.12	143	1.676	1.533	1.09	1.07
Isobutane	C_4H_{10}	14	58.12	143	1.666	1.523	1.09	1.07
n-Pentane	C_5H_{12}	17	72.15	115	1.666	1.551	1.07	1.06
Isopentane	C_5H_{12}	17	72.15	115	1.663	1.548	1.07	1.06
n-Hexane	C_6H_{14}	20	86.18	96	1.660	1.564	1.06	1.05
n-Heptane	C_7H_{16}	23	100.20	83	1.656	1.573	1.05	1.04
Octane	C_8H_{18}	26	114.23	73	1.653	1.581	1.05	1.04

other reason kinetic theory may falter without walls is that wall-gas interactions no longer exist, hence kinetic theory's complete virtues may be limited to systems with walls [24–25] i.e. experimental systems.

4 Discussion of other implications

This author [24–25] has hypothesized that blackbody/thermal radiation within a system has a temperature associated with it. So although the total energy associated with radiation often is infinitesimally small in comparison to the total energy associated with the kinematics of matter, the idea that blackbody radiation has a temperature associated with it, should no longer be ignored. In other words, even a vacuum can have a temperature, although it has no matter and comparatively speaking only contains a minute amount of energy.

Pressure is traditionally envisioned as being solely due to change in translational energy i.e. "every molecule that impinges and rebounds exerts an impulse equal to the difference in its momenta before and after impact" [pg. 32, 20]. Interestingly, the analysis given herein does alter such explanations just because the rotational energy plus the translational energy of the gas molecules now combine to exert pressure. Moreover, consider the tennis ball impacting a wall. Ask

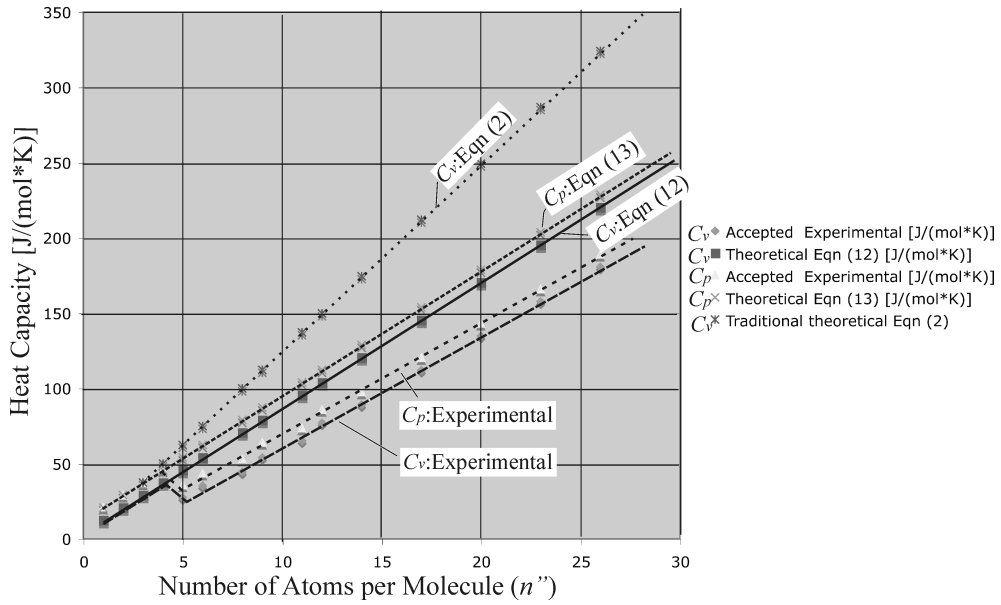

Fig. 3: Theoretical molar heat capacity based on our theoretical equations (12) and (13) versus empirical values, plus the traditional theoretical isometric molar heat capacity plot [based upon degrees of freedom, equation (2)].

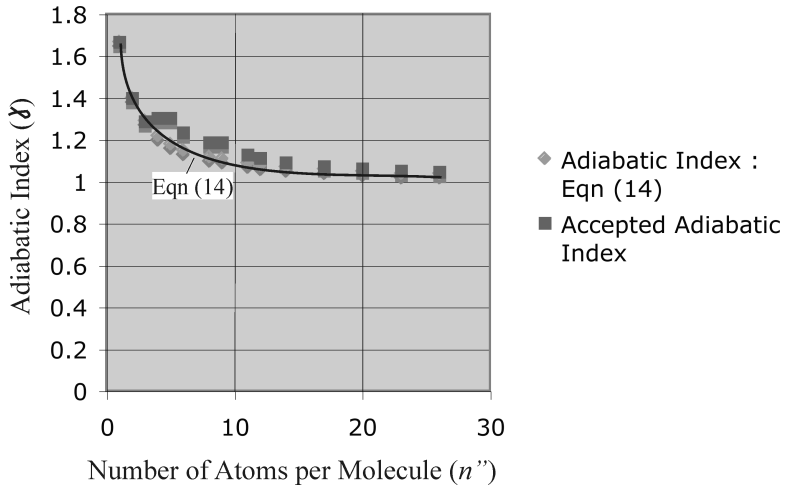

Fig. 4: Theoretical adiabatic index [eq. (14)] versus number of atoms (solid line). Adiabatic index data points based upon engineering table for gases.

yourself: Are not both the rotational and translational energy of that ball exchanged with the wall. So why would a gas molecule behave any differently? Just because wall molecules are bound i.e. cannot rotate, does not mean that they don't exchange rotational energy/momentum with an impacting gas! The gas' mean translational velocity ($mv^2/2$) can no longer be simply equated in terms of Boltzmann's constant ($kT/2$). This has consequences to fundaments such as Maxwell's velocity distributions for gases. In our analysis, the magnitude of translational energy compared to rotational energy is not defined beyond that they add up to and equal, the summation of the walls molecule's kinetic energies! Since the gas' total kinetic energy remains the same, then most of what is known in quantum theorem still applies with the change being how a gas' kinetic energy is expressed.

Consider the hypothesis that rotational energy of a gas is frozen out at low temperatures [26]. This is like claiming that gas molecules never impact a wall at acute angles, when in a cold environment. This author thinks in terms of thermal energy being energy that results in both intermolecular and intramolecular vibrations within condensed matter. Just consider the blackbody radiation curve for 3 K, whose peak is located at wavelength of 1 mm. Compare this to 300 K, where the radiation curves' peak occurs in the infrared spec-

trum, wavelength equals 10 micrometers. Accepting that the majority of thermal energy is in the infrared then this author also believes that somewhere between 3 K and 300 K, a system's thermal energy density will no longer proportional to temperature i.e. probably aroound 100 K. Perhaps it is the gas' vibrational energy that is frozen out? Understandably, at low temperatures the blackbody/thermal radiation within the system may be such that it does not provide enough thermal energy (infrared) for measurable gas vibration. However, this should equally apply to the system's walls, unless the walls have more thermal energy relative to the gas i.e. apparatus considerations? This is conjecture, as remains the current notion that rotational energies are frozen out.

For gases the accepted difference between molar isobaric heat capacity and molar isometric heat capacity is the ideal gas constant (R). Accordingly [2–3]:

$$C_p - C_v = R. \tag{15}$$

The difference in heat capacities is obviously independent of the type of gas. This implies that the difference depends upon the system's surroundings and not the experimental system, nor its contents. This fits this author's assertion that "the ideal gas constant is the molar ability of a gas to do work per degree Kelvin" [27]. This is based upon the realization that work is required by expanding systems to upwardly displace our atmosphere's weight, i.e. an expanding system does such work, which becomes irreversibly lost into the surrounding Earth's atmosphere. The lost work being [24, 28–29]

$$W_{lost} = P_{atm}\, dV. \tag{16}$$

This does not mean that the atmosphere is always upwardly displaced, rather that the energy lost by an expanding system is defined by equation (17). This lost energy can be associated with a potential energy increase of the atmosphere, or a regional pressure increase. Note: A regional pressure increase will result in either a volume increase, or viscous dissipation i.e. heat created = lost work. This requires the acceptance that the atmosphere has mass and resides in a gravitational field. It is no different than realizing that an expanding system at the bottom of an ocean, i.e. a nucleating bubble, must displace the weight of the ocean plus atmosphere. Accordingly, any expanding system here on Earth's surface must expend energy/work to displace our atmosphere's weight and such lost work, is immediately or eventually lost into the surrounding atmosphere. Accepting this then allows one to question our understanding of entropy [24, 29].

5 Conclusions

Kinetic theory has been reconstructed with the understanding that a gas' kinetic energy has both translational and rotational components that are obtained from the wall molecule's kinetic energy. Therefore, the gas' translational plus rotational energies along each of the x, y and z-axis, are added and equated to the wall molecules' kinetic energy along the identical three axes. No knowledge pertaining to the magnitudes of the gas' rotational energy versus translational energy is claimed. This is then added to the gas' internal energy e.g. vibrational energy, in order to determine the gas' total energy.

The empirically known heat capacity and adiabatic index for all gases are clearly a better fit to this new theory/model, when compared to accepted theory. The fit for monatomic through triatomic gases is exceptional, without any reliance upon traditionally accepted exceptions! Moreover, our model treats all polyatomic molecules in the same manner as condensed matter.

Seemingly, Lord Kelvin's assertion that equipartition was wrongly derived, may have been right after all. Accepting that the traditional degrees of freedom in equipartition theory may be mathematical conjecture rather than constructive reasoning will cause some displeasure. Certainly, one could argue that what is said herein is really just an adjustment to our understanding. Even so, it will alter how pressure is perceived that being due to the gas molecules' momenta from both rotation and translation, which is imparted onto a surface. Ditto for the consideration of a gas' energy in quantum theory.

The consequence of a polyatomic gas' thermal vibrations being related to its surrounding thermal radiation may alter our conceptualization of temperature, i.e. a vacuum now has a temperature. The notion that rotation in cold gases is frozen out was also questioned. Perhaps it is a case that the thermal energy density does not remain proportional to temperature, as T approaches 0, which also is the case for very high temperature gases.

The difference between isobaric and isometric heat capacity is gas independent. This fits well with this author's assertion that lost work represents the energy lost by an expanding system into the surrounding atmosphere. Interestingly, for a mole of gas molecules this lost work can be related to the ideal gas constant.

To some, the combining of a gas' rotational and translational energy may seem like a minor alteration, however the significance to the various realms of science maybe shattering. Not only may this help put to rest more than a century of speculations, it also may alter the way that thermodynamics is envisioned. If accepted it actually opens the door for a simpler new thermodynamics vested in constructive logic, rather than mathematical conjecture.

A thanks goes out to Chifu E. Ndikilar for his helpful preliminary comments, as well as both Dmitri Rabounski and Andreas Ries for their insights in finalizing the paper.

6 Example calculations

1. Table 1 for $n'' = 3$; our theoretical values:
   [equation (12)]: I.e. $C_v = \frac{7}{2}R = \frac{7}{2}$ 8.31 J/(mol*K)
   = 29.09 J/(mol*K).

[eq. (13)]: I.e. $C_p = \frac{9}{2}R = \frac{9}{2}$ 8.31 J/(mol*K) = 37.40 J/(mol*K).
For n''=3, traditional accepted theoretical value is equation (2): I.e. $C_v = \frac{9}{2}R = \frac{9}{2}$ 8.31 J/(mol*K) = 37.40 J/(mol*K).

2. Table 2, for $n'' = 3$. Accepted adiabatic index (γ) for carbon dioxide ($n'' = 3$) based upon engineering data [22] is $\gamma = 0.844/0.655 = 1.29$. Our theoretical adiabatic index (γ) is equation (14): I.e.

$$\gamma = \frac{\frac{9}{2}}{\frac{7}{2}} = 1.29.$$

Submitted on June 16, 2017

References

1. Maxwell J.C. *J. Chem. Soc.* (London), 1875, 28, 493–508; [facsimile published in Mary Jo Nye, The Question of the Atom (Los Angeles: Tomash 1984)].
2. Reif, F. Fundamentals of Statistical and Thermal Physics. McGraw-Hill, New York, 1965.
3. Carey V. Statistical Thermodynamics and Microscale Thermophysics. Cambridge University press 1999.
4. Kundt A, and Warburg E. Ueber die specifische Wärme des Quecksilbergases (On the specific heat of mercury gas). *Ann. Phys.*, 1876, 157, 353–369.
5. Goldstein H. Classical Mechanics (2nd. ed.). Addison-Wesley, 1980.
6. Wüller A., Lehrbuch der Experimentalphysik (Textbook of Experimental Physics). Leipzig, Teubner. Vol. 2, 507 ff, (1896).
7. Maxwell J.C. (1890). On the Dynamical Evidence of the Molecular Constitution of Bodies. In WD Niven. The Scientific Papers of James Clerk Maxwell. Cambridge University Press. Vol.2, pp.418–438. A lecture delivered by Prof. Maxwell at the Chemical Society on 18 February 1875.
8. Boltzmann L. On certain Questions of the Theory of Gases. *Nature*, 1895, v. 51(1322), 413–415.
9. Planck M. On the Law of the Energy Distribution in the Normal Spectrum. *Ann. Phys.*, 1901, v. 4(553), 1–11.
10. Einstein A. and Stern O. Einige Argumente Fur die Annahme einer molekularen Agitation beim absoluten Nullpunkt (Some Arguments for the Assumption of Molecular Agitation at Absolute Zero). *Ann. Phys.*, 1913, v. 40(551) 551–560.
11. Dahl J.P. On the Einstein–Stern model of rotational heat capacities. *J. Chem. Phys.*, 1998, v. 109, 10688.
12. Thomson W. (1904). Baltimore Lectures. Baltimore: Johns Hopkins University Press. Sec. 27. Re-issued in 1987 by MIT Press as Kelvin's Baltimore Lectures and Modern Theoretical Physics: Historical and Philosophical Perspectives. (Robert Kargon and Peter Achinstein, editors).
13. Rayleigh J.W.S. The Law of Partition of Kinetic Energy. *Phil. Mag.*, 1900, v. 49, 98–118.
14. Pais A. Subtle is the Lord. Oxford University Press. Oxford UK 1982.
15. Hermann Armin (1971). The Genesis of Quantum Theory (1899–1913) (original title: Frühgeschichte der Quantentheorie (1899–1913), translated by Claude W. Nash ed.), Cambridge, MA.
16. Masi J.F., Petkof B. *J. Res. Natl. Bur. Stand.*, 1952, v. 48(3), 179–187.
17. Scott R.B., Mellors J.W. *J. Res. Natl. Bur. Stand.*, 1945, v. 34, 243–248.
18. Prydz R., Goodwin R.D. *J. Res. Natl. Bur. Stand.*, 1970, v. 74A(5), 661–665.
19. Giguere P.A. Heat capacities for water-hydrogen peroxide systems between 25 and 60. *J. Chem. Eng. Data*, 1962, v. 7(4), 526–527.
20. Chapman S., Cowling T.G. The mathematical theory of non-uniform gases, third edition. Cambridge University Press 1970.
21. Wu L., White C., Scanlon T.J., Reese J.M. and Zhang Y. A kinetic model of the Boltzmann equation for non-vibrating polyatomic gases. *J. Fluid Mechanics*, 2015, v. 763, 24–50.
22. Rolle K.C. Thermodynamics and Heat Power 4th edition. Maxwell Macmillian Canada, 1993.
23. Mayhew K. Latent heat and critical temperature: A unique perspective. *Phys. Essays*, 2013, v. 26(4), 604–611.
24. Mayhew K. Changing our Perspective: Part 1: A New Thermodynamics (Self-published 2015) Available at http://www.newthermodynamics.com and https://createspace.com/5277845
25. Mayhew K. Improving our thermodynamic perspective. *Phys. Essays*, 2011, v. 24(3), 338–344.
26. Levin K., Fetter, A., Stampur-Kurn, D. Ultracold Bosonic and Fermonic gases. Elsevier Press Oxford UK (2012).
27. Mayhew K., A new thermodynamics. *IJRDO*, Vol. 2 Issue 1, 45 (2016) (Note: Concerning this paper: Publication has numerous equations wrong and journal did not care. Please see http://www.newthermodynamics.com/ijrdojournaljan2016.pdf)
28. Mayhew K. Second law and lost work. *Phys. Essays*, 2015, v. 28(1), 152–155.
29. Mayhew K. Entropy: an ill-conceived mathematical contrivance? *Phys. Essays*, 2015, v. 28(3), 352–357.

Exotic Matter: A New Perspective

Patrick Marquet
18 avenue du Président Wilson, 62100 Calais, France
E-mail: patrick.marquet6@wanadoo.fr

In this paper we suggest a possible theoretical way to produce negative energy that is required to allow hyperfast interstellar travels. The term "Exotic Matter" was first coined by K. Thorne and M. Morris to identify a material endowed with such energy in their famous traversable space-time wormhole theory. This possibility relies on the wave-particle dualism theory that was originally predicted by L. de Broglie and later confirmed by electrons scattering experiments. In some circumstances, an electron interacting with a specific dispersive and refracting medium, has its velocity direction opposite to that of the phase velocity of its associated wave. However, it is here shown that a positron placed in the same material exhibits a negative mass. Generalizing the obtained equations leads to an energy density tensor which is de facto negative. This tensor can be used to adequately fit in various "shortcut theories" without violating the energy conditions.

Introduction

Introduction In this paper we show that it is possible to obtain a negative energy provided the associated proper particle's mass is variable. The basis for this study starts with the associated wave that was originally detected on electrons diffraction experiments [1]. In some circumstances, L. de Broglie showed that a particular homogeneous refractive and dispersive material may cause the tunnelling particle to reverse its velocity with respect to its wave phase propagating velocity [2]. In this case, and under the assumption that the proper mass of the particle is subject to a ultra high frequency vibration synchronized with the wave frequency, it is formally shown that an anti-particle exhibits a negative mass (energy). This energy could be extracted to sustain for example the space-time wormhole, set forth by K. Thorne and M. Morris [3, 4]. To be physically viable, it is well known that it requires a so-called exotic matter endowed with a negative energy density which violates all energy conditions [5]. However, if the exotic matter threading the inner throat of the wormhole is likened to the specific dispersive material wherein circulates a stream of antiparticles, our model doesnot conflict with classical physics restrictions and can be fully applied.

Notations

In this paper we will use a set of orthonormal vector basis denoted by $\{e_0, e_a\}$, where the space-time indices are $a, b = 0, 1, 2, 3$, while the spatial indices are $\mu, \nu = 1, 2, 3$. The space-time signature is $\{-2\}$.

1 Proper mass variation

1.1 Phase velocity and group velocity

It is well known that the classical wave with a frequency n

$$\psi = a(n) \exp\left[2\pi i(\nu t - \boldsymbol{kr})\right] \tag{1}$$

propagates along the direction given by the unit vector $\boldsymbol{N}$. Here $\boldsymbol{k}$ is the 3-wave vector, $\boldsymbol{kr} = \phi$ is the wave spatial phase, and n is the refractive index of the medium. Equation (1) is a solution of the wave propagation equation

$$\Delta\psi = \frac{1}{w^2}\,\frac{\partial^2\psi}{c^2\partial t^2}\,, \tag{1bis}$$

where w is the wave phase velocity of the wave moving in a dispersive medium whose refractive index is $n(\nu)$ generally depending of the coordinates, and which is defined by:

$$\frac{1}{w} = \frac{n(\nu)}{c}\,. \tag{2}$$

In our study, the medium is assumed to be homogeneous but it can be anisotropic and ir will depend on the fequency ν. In this material, the phase ϕ of the wave is progressing along the given direction with a separation given by a distance

$$\lambda = \frac{w}{\nu} = \frac{c}{n\nu} \tag{2bis}$$

called the wavelength. Consider now the superposition of two stationary waves along the x-axis having each close frequencies $\nu' = \nu + \delta\nu$ and close velocities $w' = w + (dw/d\nu)\delta\nu$, so that their superposition can be expressed by:

$$\sin 2\pi\left(\nu t - \frac{\nu x}{w}\right) + \sin 2\pi\left(\nu' t - \frac{\nu' x}{w'}\right) =$$
$$= 2\sin 2\pi\left(\nu t - \frac{\nu x}{w}\right)\cos 2\pi\left[\delta\left(\frac{\nu}{2}\right)t - x\,\frac{d}{d\nu}\,\frac{\nu}{w}\,\delta\frac{\nu}{2}\right].$$

The resulting wave displays a wave packet (or beat) that varies along with the so-called group velocity ($\mathbf{v} = v^\mu$):

$$\frac{1}{\mathbf{v}_g} = \frac{d}{d\nu}\,\frac{\nu}{w}\,. \tag{3}$$

The wave mechanics shows that the momentum 3-vector of an electron of a rest mass m_0 (in vacuum) is given by the de Broglie relation

$$\boldsymbol{p} = m_0 \mathbf{v} = \frac{h}{\lambda}\,. \tag{4}$$

which completes the Einstein relation $E = h\nu$.

1.2 The plane wave spinor

Since we deal here with a spin 1/2-fermion, we must introduce the four components wave function Ψ_A expressed with the non local 4×4 Dirac trace free matrices γ_a (capital latin spinor indices are $A = B = 1, 2, 3, 0$). They display here the following real components [8]:

$$\gamma_0 = \begin{pmatrix} 0 & 0 & 0 & -1 \\ 0 & 0 & -1 & 0 \\ 0 & 1 & 0 & 0 \\ 1 & 0 & 0 & 0 \end{pmatrix}, \quad \gamma_1 = \begin{pmatrix} 0 & 0 & 0 & -1 \\ 0 & 0 & 1 & 0 \\ 0 & 1 & 0 & 0 \\ -1 & 0 & 0 & 0 \end{pmatrix},$$

$$\gamma_2 = \begin{pmatrix} 1 & 0 & 0 & 0 \\ 0 & 1 & 0 & 0 \\ 0 & 0 & -1 & 0 \\ 0 & 0 & 0 & -1 \end{pmatrix}, \quad \gamma_3 = \begin{pmatrix} 0 & 0 & -1 & 0 \\ 0 & 0 & 0 & -1 \\ -1 & 0 & 0 & 0 \\ 0 & -1 & 0 & 0 \end{pmatrix}.$$

These matrices are said standard representation as opposed for example to the Majorana representation. Moreover, they verify

$$\gamma_a \gamma_b + \gamma_b \gamma_a = -2\eta_{ab}\mathbf{I} \tag{5}$$

where η_{ab} is the Minkowski tensor and $\mathbf{I}$ is the unit matrix. In what follows, Λ^* is the complex conjugate of an arbitrary matrix Λ, ${}^{\mathrm{T}}\Lambda$ is the transpose of Λ, and $\tilde{\Lambda}$ is the classical adjoint of Λ.

Introducing now the Hermitean matrix $\beta = i\gamma_0$

$$\beta = \begin{pmatrix} 0 & 0 & 0 & -i \\ 0 & 0 & -i & 0 \\ 0 & i & 0 & 0 \\ i & 0 & 0 & 0 \end{pmatrix},$$

which verifies $\beta^2 = \mathbf{I}$, we derive the important relation

$$\beta\, \gamma_a \beta^{-1} = -\tilde{\gamma}_a \tag{5bis}$$

with β and the spinor Ψ, we form the Dirac conjugate [9]

$${}^{\circ}\Psi = t\, \tilde{\Psi} \beta\,, \tag{5ter}$$

where t is the time orientation. or the electron, the Dirac equation is written as

$$[W - (m_0)_{\mathrm{elec}}\, c]\, \Psi = 0\,, \tag{6}$$

where $W = \gamma^a{}_B{}^A\, \partial_a$ is the Dirac operator and it is customary to omit the spinor indices A, B by simply writing $\gamma_a = \gamma_a{}^a{}_B$ so that this operator becomes $\gamma^a \partial_a$, or in the slash notation (Feynman), $\not{\partial}_a$. The monochromatic wave associated with the electron can be approximated to a plane wave spinor without loss of generality [10]:

$$\Psi_A = a\,(x^a) \exp 2\pi i\,(p_a x^a)\,, \tag{6bis}$$

where

$$p_a x^a = Et - p_\mu x^\mu. \tag{6ter}$$

The 4-vector p_a is the 4-momentum of the electron . The spinor "amplitude" $a(x^a)$ satisfies the Dirac equation

$$[\gamma^a (p_a)_{\mathrm{elec}}]\, a = [(m_0)_{\mathrm{elec}}\, c]\, a \tag{7}$$

where the operator $[\gamma^a (p_a)_{\mathrm{elec}}]$ is here substituted to the Dirac operator $\gamma^a \partial_a$. We now re-write (6)bis as

$$\Psi = a(x^a) \exp(2\pi i/h)\, \phi\,, \tag{7bis}$$

where the global phase is $\phi = h[\nu - (\alpha x + \beta y + \gamma z)/\lambda]\, t$ (here α, β, γ are the direction cosines). The energy and momentum of the electron located at x^a are then related with the wave phase by:

$$E = \partial_t\, \phi\,, \quad \boldsymbol{p} = -\mathrm{grad}\, \phi\,. \tag{7ter}$$

Now, if the electron moves at a velocity $\mathbf{v} = \beta c$ within a slight variation $\beta, \beta + \delta\beta$, corresponding to the frequency interval $\nu, \nu + \delta\nu$, w and ν are functions of β. The wave phase velocity (in vacuum) can be expressed as $w = c^2/\mathbf{v} = c/\beta$ and since $\nu = (1/h)\, m_0 c^2/\sqrt{1 - \beta^2}$, it is easy to infer that:

$$\mathbf{v}_g = \frac{d\nu}{d\beta} \frac{1}{\frac{d}{d\beta}\frac{\nu}{w}} = \beta c = \mathbf{v}\,. \tag{8}$$

The group velocity $\mathbf{v}_g$ of the wave packet associated with the electron of rest mass m_0, coincides with its velocity $\mathbf{v}$. The group velocity is thus also expressed by the Hamiltonian form $\mathbf{v}_g = \partial E/\partial \boldsymbol{k}$ which corresponds to the particle's velocity $\mathbf{v} = \partial E/\partial \boldsymbol{p}$. Recalling (2) and (2)bis to as $1/w = n(\nu)/c$, $\lambda = w/n\nu$, we easily infer the Rayleigh's formulae [11]:

$$\frac{1}{\mathbf{v}_g} = \frac{1}{c} \frac{\partial n\nu}{\partial \nu} = \frac{\partial \left(\frac{1}{\lambda}\right)}{\partial \nu}\,. \tag{9}$$

1.3 Making the electron vibrate

In the framework of the special theory of relativity, the proper frequency ν_0 of a plane monochromatic wave is transformed as

$$\nu = \frac{\nu_0}{\sqrt{1 - \mathbf{v}^2/c^2}}\,. \tag{10}$$

Constraint A: We assume that the electron is subject to an ultra high stationary vibration having a proper frequency ν_0.

When moving at the velocity $\mathbf{v}$, this frequency is known to transform according to:

$$\nu_e = \nu_0 \sqrt{1 - \mathbf{v}^2/c^2}\,. \tag{11}$$

We clearly see that its frequency ν_e differs from that of its associated wave denoted here by ν.

If $\boldsymbol{N}$ is the unit vector normal to the associated wave phase, the electron subject to the frequency $\nu_0 = m_0c^2/h$ has traveled a distance $d\boldsymbol{N}$ during a time interval dt, so that we may define an electronic phase ϕ_e which has changed by:

$$d\phi_e = h\nu_0 \sqrt{(1 - \mathbf{v}^2/c^2)}\, dt = m_0c^2 \sqrt{(1 - \mathbf{v}^2/c^2)}\, dt. \quad (12)$$

Simultaneously, the corresponding wave phase variation is

$$d\phi = \partial_t\phi dt + \partial_{\boldsymbol{N}}\phi d\boldsymbol{N} = (\partial_t\phi + \mathbf{v}\,\mathrm{grad}\,\phi)\, dt \quad (12)\text{bis}$$

and by analogy to the classical formula (7)ter, one may write

$$\boldsymbol{p} = -\mathrm{grad}\,\phi = \frac{m_0\mathbf{v}}{\sqrt{1 - \mathbf{v}^2/c^2}}, \quad E = \partial_t\phi = \frac{m_0c^2}{\sqrt{1 - \mathbf{v}^2/c^2}}$$

so we find

$$d\phi = \left[\frac{m_0c^2}{\sqrt{1 - \mathbf{v}^2/c^2}} - \frac{m_0\mathbf{v}^2}{\sqrt{1 - \mathbf{v}^2/c^2}}\right] dt. \quad (13)$$

Constraint B: We set the following phase synchronization:

$$d\phi = d\phi_e\,, \quad (14)$$

which leads to:

$$\left[\frac{m_0c^2}{\sqrt{1 - \mathbf{v}^2/c^2}} - \frac{m_0\mathbf{v}^2}{\sqrt{1 - \mathbf{v}^2/c^2}}\right] dt = \\ = \left[m_0c^2 \sqrt{1 - \mathbf{v}^2/c^2}\right] dt\,. \quad (15)$$

Dividing through by dt , we retrieve the famous Planck-Laue equation

$$\frac{m_0c^2}{\sqrt{1 - \mathbf{v}^2/c^2}} = m_0c^2 \sqrt{1 - \mathbf{v}^2/c^2} + \frac{m_0\mathbf{v}^2}{\sqrt{1 - \mathbf{v}^2/c^2}}, \quad (15)\text{bis}$$

which holds provided the proper mass is slightly variable. (see proof in Appendix A). In the frameworks of our postulate, the ultra high frequency vibration imparted to the electron can be viewed as apparently reflecting its stationary mass variation which is likened to a fluctuation.

From now on, ${}^\sharp m_0$ will denote the variable rest mass of the electron so that the Planck-Laue relation becomes:

$${}^\sharp E = \frac{{}^\sharp m_0c^2}{\sqrt{1 - \mathbf{v}^2/c^2}} = \\ = {}^\sharp m_0c^2 \sqrt{1 - \mathbf{v}^2/c^2} + \frac{{}^\sharp m_0v^2}{\sqrt{1 - \mathbf{v}^2/c^2}}\,. \quad (15)\text{ter}$$

This formulae will be required to determine the explicit form of the dispersive material which is the key point of our theory.

2 Exotic matter

2.1 Dynamics in a refracting material

Let us first recall the relativistic form of the Doppler formulae:

$$\nu_0 = \frac{\nu\,(1 - \mathbf{v}/w)}{\sqrt{1 - \mathbf{v}^2/c^2}}\,, \quad (16)$$

where as before, ν_0 is the wave's frequency in the frame attached to the electron. With the latter equation and taking into account the classical Planck relation $E = h\nu$, we find

$$E = \frac{E_0\sqrt{1 - \mathbf{v}^2/c^2}}{1 - \mathbf{v}/w}\,. \quad (17)$$

However, inspection shows that the usual equation

$$E = \frac{E_0}{\sqrt{1 - \mathbf{v}^2/c^2}} \quad (18)$$

holds only if

$$1 - \frac{\mathbf{v}}{w} = 1 - \frac{\mathbf{v}^2}{c^2} \quad (19)$$

which implies

$$w\,\mathbf{v} = c^2. \quad (20)$$

The latter relation is satisfied provided we set

$${}^\sharp E = \frac{{}^\sharp m_0c^2}{\sqrt{1 - \mathbf{v}^2/c^2}}\,, \quad (21)$$

$${}^\sharp \boldsymbol{p} = \frac{{}^\sharp m_0\mathbf{v}}{\sqrt{1 - \mathbf{v}^2/c^2}}\,. \quad (22)$$

Constraint C: ${}^\sharp E$ depends on a specific dispersive and refracting material through which the electron is tunnelling.

Let us define this influence by a function $Q(n)$ where n is the refractive index of the material. Note: The variation of the proper mass is independent on $Q(n)$. Equation (21) is modified to as

$${}^\sharp E = \frac{{}^\sharp m_0c^2}{\sqrt{1 - \mathbf{v}^2/c^2}} + Q(n) \quad (23)$$

from which Eq. (22) can be expressed as:

$${}^\sharp \boldsymbol{p} = \frac{{}^\sharp m_0\mathbf{v}}{\sqrt{1 - \mathbf{v}^2/c^2}} = \frac{\mathbf{v}\left[{}^\sharp E - Q(n)\right]}{c^2}\,. \quad (24)$$

Now taking into account the Doppler formulae (16), and the Planck-Laue relation (15)ter, we find

$${}^\sharp E - \frac{\mathbf{v}^2\left[{}^\sharp E - Q(n)\right]}{c^2} = {}^\sharp E\left(1 - \frac{\mathbf{v}}{w}\right) \quad (25)$$

wherefrom is inferred

$$Q(n) = {}^\sharp E\left(1 - \frac{c^2}{w\,\mathbf{v}}\right) = h\nu\left(1 - \frac{c^2}{w\,\mathbf{v}}\right) \tag{26}$$

and with the Rayleigh formulae (4), we eventually obtain the explicit form of $Q(n)$:

$$Q(n) = {}^\sharp E\left[1 - \frac{n\partial(n\nu)}{\partial\nu}\right]. \tag{27}$$

2.2 Specific dispersive material

Depending on the nature of the dispersive material, thus its index (n), it is well known that the tunelling electron's 3-velocity $\boldsymbol{v}$ can be directed either in the direction of the associated wave phase velocity w or in the opposite direction. The electron then moves backward through the specific material.

Let $\boldsymbol{N}$ be the 3-unit vector directed to the wave phase direction (chosen positive) so that the wave number is given by:

$$\boldsymbol{k} = \frac{\boldsymbol{N}h}{\lambda}\,. \tag{28}$$

By applying the Rayleigh formulae (4) to this particular case where $\boldsymbol{v}$ is opposite to the wave phase propagation, we have $\boldsymbol{v} < 0$. Hence, from $Q(n) = {}^\sharp E\,(1 - c^2/w\,\boldsymbol{v})$, we find

$${}^\sharp E - Q(n) = \frac{{}^\sharp E c^2}{w\,\mathbf{v}} \tag{29}$$

which is negative.

Then, with $\boldsymbol{p} = {}^\sharp m_0\mathbf{v}/\sqrt{1 - \mathbf{v}^2/c^2}$, we infer from (24):

$$\frac{{}^\sharp m_0}{\sqrt{1 - \mathbf{v}^2/c^2}} = \frac{{}^\sharp E - Q(n)}{c^2}\,. \tag{29bis}$$

In order to maintain the variable proper mass $\sharp m_0$ positive i.e.

$${}^\sharp m_0 = \sqrt{(1 - \mathbf{v}^2/c^2)}\;\frac{{}^\sharp E}{w\,\mathbf{v}} > 0 \tag{30}$$

we must have necessarily: $\boldsymbol{p} = -\boldsymbol{k}$.

2.3 Matching the exotic matter definition

Now consider a stream of electrons and positrons placed in the specific material whose respective associated wave (positive) direction is given by the same unit vector $\boldsymbol{N}$ (i.e. $w > 0$). From the Dirac theory, we kwnow that the electron momentum 3-vector $\boldsymbol{p}_{\text{elec}}$ and that of the positron momentum 3-vector p pos are opposed. (See proof in Appendix B). Therefore we have here $\boldsymbol{p}_{\text{pos}} = \boldsymbol{k}$, however the dispersive material yet imposes $\boldsymbol{v}_{\text{pos}} < 0$, hence, we are led to the fundamental conclusion:

A positron moving at the backward velocity $\mathbf{v}_{\text{pos}}$ through the specific dispersive refracting material defined above and subject to Constraints A, B and C, will exhibit a negative mass given by:

$$({}^\sharp m_0)_{\text{pos}} = \sqrt{1 - \mathbf{v}_{\text{pos}}^2/c^2}\;\frac{{}^\sharp E}{w\,\mathbf{v}} < 0\,, \tag{30bis}$$

where ${}^\sharp E - Q(n) = {}^\sharp E c^2/\mathbf{v}_{\text{pos}}\,w) < 0$ in accordance with Eq. (29).

Let us write the mass (30)bis as:

$$({}^\sharp m_0)_{\text{pos}} = \int ({}^\sharp\rho_0)_{\text{pos}}\,\sqrt{-g}\,dV, \tag{31}$$

where $({}^\sharp\rho_0)_{\text{pos}}$ is the variable proper density of the positronic massive flow. The integral is performed over the 3-volume V delimiting the variable proper mass $({}^\sharp m_0)_{\text{pos}}$ boundary. We then readily infer the familiar form of the energy density tensor in the static case

$$({}^\sharp T_0^0)_{\text{pos}} = ({}^\sharp\rho_0)_{\text{pos}}\,c^2, \tag{32}$$

which is de facto negative.

So, within the scheme of the wave-particle picture, we have been able to give a consistent picture of what could be the united conditions to reach our goal :

The so-called "exotic matter" required to assemble a space-time distortion can be provided by the negative energy extracted from a stream of vibrating antifermions interacting with a specific dispersive refracting material adequately engineered.

3 Concluding remarks

Without going into details of a sound engineering, we have here only scratched the surface of a basic theory describing the ability of a system composed of antiparticles to interact with a specific refracting and dispersive material in order to exhibit a dynamical negative mass.

Thus, our approach mainly relies on de Broglie's theory which has been verified for the electron.

Upon Constraints A, B, and C, we might as well consider other heavier particles such as the antiproton to produce negative energy.

Once these conditions are fulfilled, the concept of hyperfast interstellar tracel is viable if one can "handle" routinely antimatter, and envision a sufficient amount of negative energy density. These orders of magnitude are beyond the scope of this text.

Without any doubt, some advanced civilizations have already long mastered the negative energy obtained by this process, to achieve superluminal travels as described by space-time warp drive theories [12–14].

For us, a huge research work is still ahead, but if we have contributed to open a small door, then the challenge is widely available for physicists.

Appendix A: The Planck-Laue relation

The Planck-Laue relation is a relativistic equation which has been derived when the proper mass is assumed to sligthly fluctuate. This proper mass is here denoted by ${}^\sharp m_0$. Under this circumstance, the relativistic dynamics of ${}^\sharp m_0$ can now be extended as follows.

We first write the Lagrange function for an observer who see the particle moving at he velocity $\boldsymbol{v}$

$$L = -\,{}^\sharp m_0 c^2 \sqrt{1 - \boldsymbol{v}^2/c^2}$$

so that the least action principle applied to this function is still expressed by

$$\delta \int_{t_0}^{t_1} L dt = \delta \int_{t_0}^{t_1} -\,{}^\sharp m_0 c^2 \sqrt{1 - \boldsymbol{v}^2/c^2} \; = 0\,.$$

From this principle the equations of motion

$$\frac{d}{dt}\left(\frac{\partial L}{\partial \dot{x}_a}\right) = \frac{\partial L}{\partial x_a}\,, \qquad \dot{x}_a = \frac{dx_a}{dt},$$

are inferred, which lead to

$$\frac{d\,{}^\sharp \boldsymbol{p}}{dt} = -\,c^2 \sqrt{1 - \boldsymbol{v}^2/c^2}\,\operatorname{grad}{}^\sharp m_0 \tag{A.1}$$

(since ${}^\sharp m_0$ is now variable). Hence, by differentiating the relativistic relation ${}^\sharp E^2/c^2 = {}^\sharp p^2 + {}^\sharp m_0^2 c^2$, we obtain

$$\frac{d\,{}^\sharp E}{dt} = c^2 \sqrt{1 - \boldsymbol{v}^2/c^2}\,\frac{\partial\,{}^\sharp m_0}{\partial t}\,. \tag{A.2}$$

Combining (A.1) and (A.2) readily gives

$$\frac{d\,{}^\sharp E}{dt} - \boldsymbol{v}\frac{d\,{}^\sharp \boldsymbol{p}}{dt} = c^2 \sqrt{1 - \boldsymbol{v}^2/c^2}\,\frac{d\,{}^\sharp m_0}{dt}\,, \tag{A.3}$$

where $d\,{}^\sharp m_0/dt = \partial\,{}^\sharp m_0/\partial t + \operatorname{grad}{}^\sharp m_0$ is the variation of the mass in the course of its motion. On the other hand, we have

$$\begin{aligned}\frac{d\,({}^\sharp \boldsymbol{p}\cdot\boldsymbol{v})}{dt} &= \frac{\boldsymbol{v}\cdot d\,{}^\sharp \boldsymbol{p}}{dt} + {}^\sharp m_0 c^2 \frac{(\boldsymbol{v}/c)\,d(\boldsymbol{v}/c)\,dt}{\sqrt{1 - \boldsymbol{v}^2/c^2}} = \\ &= \boldsymbol{v}\frac{d\,{}^\sharp \boldsymbol{p}}{dt} - {}^\sharp m_0 c^2 \frac{d}{dt}\left(1 - \boldsymbol{v}^2/c^2\right)\end{aligned} \tag{A.4}$$

i.e.

$$\begin{aligned}&\frac{d}{dt}\left[\,{}^\sharp m_0 c^2 \sqrt{1 - \boldsymbol{v}^2/c^2}\,\right] = \\ &= c^2 \sqrt{1 - \boldsymbol{v}^2/c^2}\,\frac{d\,{}^\sharp m_0}{dt} + {}^\sharp m_0 c^2 \frac{d}{dt}\sqrt{1 - \boldsymbol{v}^2/c^2}\end{aligned}$$

hence (A.3) can be re-written as

$$\frac{d}{dt}\left[\,{}^\sharp E - \boldsymbol{v}\cdot{}^\sharp \boldsymbol{p} - {}^\sharp m_0 c^2 \sqrt{1 - \boldsymbol{v}^2/c^2}\,\right] = 0 \tag{A.5}$$

which is satisfied when the particle is at rest, that is: $\boldsymbol{v} = 0 \Rightarrow {}^\sharp E_0 = {}^\sharp m_0 c^2$. Therefore, we must always have:

$${}^\sharp E = \frac{{}^\sharp m_0 c^2}{\sqrt{1 - \boldsymbol{v}^2/c^2}} = {}^\sharp m_0 c^2 \sqrt{1 - \boldsymbol{v}^2/c^2} + \frac{{}^\sharp m_0 \boldsymbol{v}^2}{\sqrt{1 - \boldsymbol{v}^2/c^2}}\,. \tag{A.6}$$

It is important to note that this variable (proper) mass, ${}^\sharp m_0$, is purely intrinsic, i.e. its motion is unaffected.

Equation (A.6) is known as the Planck-Laue formula.

Appendix B: Dirac currents

Let us consider the real Dirac current as

$$J^a = i\,({}^\circ\Psi\,\gamma^a\,\Psi) = (J^a)\,1 - (J^a)\,2\,,$$

where

$$(J^a)\,1 = i\,{}^\circ\Psi_A\,\gamma^{aA}_B\,\Psi^B, \quad (J^a)\,2 = i\,\Psi^B\,\gamma^{aA}_B\,{}^\circ\Psi_A\,.$$

The charge conjugate of J^a is first calculated

$$[(J^a)\,1]^{(\mathrm{C})} = i\,\Psi^*_A\,\gamma^{aA}_B\,\Psi^{*B} = i\,t\,{}^{\mathrm{T}}\Psi_A\,\beta^A_B\,\gamma^{aB}_C\,\Psi^{*C}$$

i.e.

$$[(J^a)\,1]^{(\mathrm{C})} = i\,t\,\Psi^A\,{}^{\mathrm{T}}\beta^B_A\,{}^{\mathrm{T}}\gamma^{aC}_B\,{}^{\mathrm{T}}\Psi^{*C}.$$

From the antisymmetry of β, and remembering that the γ^a are here *real*, we have

$${}^{\mathrm{T}}\gamma^a\,{}^{\mathrm{T}}\beta = -\,\tilde{\gamma}^a\beta = \beta\gamma^a$$

from which we infer

$$[(J^a)\,1]^{(\mathrm{C})} = i\,t\,\Psi^A\,\gamma^{aB}_A\,\beta^C_B\,{}^\circ\tilde{\Psi}_C = i\,\Psi^A\,\gamma^{aB}_A\,{}^\circ\Psi_B$$

hence, we see that

$$[(J^a)\,1]^{(\mathrm{C})} = (J^a)\,2$$

and similarly

$$[(J^a)\,2]^{(\mathrm{C})} = (J^a)\,1$$

therefore, we obtain the most important relation:

$$-(J^a)^{(\mathrm{C})} = J^a \tag{B.1}$$

The Dirac current orientation is opposed to that of its Dirac conjugate [15]. The Dirac conjugate ${}^\circ\Psi$ of the plane wave spinor (6)bis is here:

$${}^\circ\Psi = {}^\circ a\,\exp -2\pi i\,(p_a\,x^a)\,. \tag{B.2}$$

With the Dirac conjugate spinor amplitude ${}^\circ a = a^*\,\gamma^0$, that is equivalent to (5)ter, we first set the normalization condition:

$${}^\circ a\,a = m_0 c\,. \tag{B.3}$$

Besides, the Dirac equation reads:

$$(\gamma^a p_a)^\circ\,a = m_0 c\,{}^\circ a\,. \tag{B.4}$$

Due to the property of $(\gamma^a)^2$, Equations (7) and (B.4) are both satisfied for:

$$(p_a)^2 = (m_0 c)^2. \tag{B.5}$$

Multiplying now Equation (7) on the left with $^\circ a$, we obtain with (B.2) and (B.5)

$$(^\circ a\, \gamma^a\, a)\, p_a = (m_0 c)^2 = (p_a)^2 \tag{B.6}$$

from which we infer:

$$^\circ a\, \gamma^a\, a = p^a. \tag{B.7}$$

The Dirac current density vector $J^a = {}^\circ\Psi\, \gamma^a\, \Psi$ will here yield

$$J^a = {}^\circ a\, \gamma^a\, a = p^a \tag{B.8}$$

with

$$p^a = m_0 c^2 + p^\mu \tag{B.9}$$

([16]: compare with formulae (23.6) there).

From the charge conjugate $\Psi^{(C)}$ corresponding to the positron plane spinor, we define the Dirac current for the positron $(J^a)^{(C)}$. However, it was shown that $(J^a)^{(C)} = -J^a$. Therefore, assuming that $(m_0)_{\text{elec}} = (m_0)_{\text{posit}}$ in vacuum, we must then have

$$(J^\mu)^{(C)} = (p^\mu)_{\text{posit}} = -(p^\mu)_{\text{elect}}\,. \tag{B.10}$$

This clearly means that in vacuum, $\mathbf{v}_{\text{posit}} = -\mathbf{v}_{\text{elect}}$.

Submitted on May 15, 2017

References

1. Davisson C.J., Germer L.H. The Diffraction of electrons by a crystal of Nickel. *Proc. of the National Acad. of Sci. of the USA*, 1 April 1928, v. 14, no. 4, 317–322.
2. de Broglie L. Etude du mouvement des particules dans un milieu réfringent. *Ann. Inst. Henri Poincaré*, 1973, v. XVIII, no. 2, 89–98.
3. Morris M., Thorne K. Wormholes in spacetime and their use for interstellar travel. *Am. J. Phys.*, 1988, v. 56, 395.
4. Morris M., Thorne K., Yurtzever U. *Phys. Rev. Letters*, 1988, v. 61, 1446.
5. Hawking S.W., Ellis G.F.R. The Large Scale Structure of Space-Time. Cambridge University Press, 1987.
6. Kramer D., Stephani H., Hertl E., MacCallum M. Exact Solutions of Einstein's Field Equations. Cambridge University Press, 1979.
7. Marquet P. A space-time wormhole sustained by the electromagnetic field. *The Abraham Zelmanov Journal*, 2011, v. 4, 92–107.
8. Lichnérowicz A. Champs spinoriels et propagateurs en Relativité Générale. *Bulletin. Soc. Mathématique de France*, 1964, t. 92. p. 11 à 100.
9. Moret-Bailly F. Le champ neutrinique en Relativité Générale. *Ann. Institut Henri Poincaré*, sec. A: 1966, v. 4, 301–355.
10. Marquet P. On the physical nature of the de Broglie wave. *Progress in Physics*, 2016, v. 12, issue 4, 318–322.
11. de Broglie L. Eléments de la théorie des quanta et de la mécanique ondulatoire. Gauthier-Villars, Paris, 1959.
12. Alcubierre M. The Warp Drive: hyper fast travel within General Relativity. *Class. Quantum Gravity*, 1994, v. 11, L73–L77.
13. Natario J. Warp Drive with zero expansion. *Class. Quantum Gravity*, 2002, v. 19 , no. 6, 1157–1165.
14. Krasnikov S. The quantum inequalities do not forbid spacetime shortcuts. arXiv: gr-qc/020705.
15. Lichnérowicz A. Champ de Dirac, champ du neutrino et transformations C, P, T sur un espace courbe. *Ann. Institut Henri Poincaré*, sec. A: 1964, v. 3, p.233–290.
16. Beretevski V.L., Lifshitz E., Pitayevski L. Electrodynamique Quantique. Edition Mir, Moscow, 1973.

Testing 5D Gravity with LIGO for Space Polarization by Scalar Field

T. X. Zhang

Department of Physics, Alabama A & M University, Normal, Alabama 35762
E-mail: tianxi.zhang@aamu.edu

Whether LIGO detectors can directly detect the scalar field dark energy and thus test the five-dimensional (5D) gravity or not is examined analytically in terms of the author previously well-developed 5D fully covariant theory of gravitation with a scalar field. It is shown that an object with some thousand kilograms (e.g. 4700 kg), if electrically charged up to some ten kilovolts (e.g. 40 kV), can polarize the space or vacuum by the scalar field dark energy of the charged object and thus be able to extend the optical path length of a laser beam that travels through one LIGO arm with some hundred reflections (e.g. 280) by approximately 4×10^{-19} m (or the space-polarization strain of 10^{-22}), which is the amount of 4 times greater than that to be detected by the LIGO detectors. Switching on and off the power to the object, we can carry out tests of this 5D gravity by examining whether the converging laser beams become out of phase and thus the interference pattern varies or not. We can also apply a harmonically varying voltage with a frequency, e.g. 100 Hz, to charge the object and thus produce a varying optical length difference in the specific frequency range of LIGO detectors. Therefore, being added a highly charged sphere into the experimental setup, LIGO, which has recently detected first ever the gravitational waves from binary black hole mergers, can directly examine the existence of the scalar field dark energy of 5D gravity in a ground-base experiment. This study provides a design criterion for this new approach and experiment of discovering dark energy as well as testing 5D gravity.

1 Introduction

The observed acceleration of the present universe is generally attributed to the existence of dark energy throughout the universe [1-2]. A direct detection of the dark energy, whose true nature remains elusive, has become one of the most important issues in the modern astrophysics and cosmology since the discovery of acceleration of the universe. Two commonly accepted candidates of dark energy are the cosmological constant and the quintessence. Unlike the cosmological constant, which Albert Einstein first introduced into his general theory of relativity in order for the universe to be static, the quintessence is a scalar field Φ that varies throughout spacetime and has been modeled in various theories of gravitation such as the four-dimensional (4D) Brans-Dicke scalar-tensor gravity [3] and the five-dimensional (5D) Kaluza-Klein scalar-vector-tensor gravity (shortened by 5D gravity) [4-6].

The scalar field of 5D gravity, which has been recently related to the Higgs field of 4D particle physics in[7], were theoretically shown to be capable of polarizing the space or vacuum [8-9] and thus able to extend the optical path length of a laser beam that travels through the polarized vacuum. The vacuum polarization by a scalar field has been studied in the Schwarzschild spacetime [10] , in a waveguide [11], in the de Sitter spacetime with the presence of global monopole [12], and in a homogeneous space with an invariant metric [13]. Recently, the author, in terms of his 5D fully covariant theory of gravitation, has quantitatively determined the dielectric constant of the polarized vacuum in accordance with the charge-mass ratio of a charged object [14].

In this paper, we will further analytically demonstrate that the vacuum polarization by the scalar field dark energy of 5D gravity can increase the relative optical path length (i.e. the strain) above a factor of 10^{-22} and therefore can be directly detected via the extremely accurate LIGO detectors that have recently detected first ever the gravitational waves from the binary black hole merger as declared in [15]. We will use a harmonic voltage to charge the object, which leads to a varying optical length difference in the frequency range of the LIGO detection. A positive result of detecting the scalar field dark energy by LIGO will provide a fundamental test of 5D gravity.

2 5D gravity and vacuum polarization by scalar field dark energy

2.1 5D gravity with scalar field and field solution

A 5D gravity is a Kaluza-Klein theory that unifies the 4D Einsteinian general relativity (GR) and Maxwellian electromagnetism (EM). Without a scalar field (i.e. $\Phi = 1$), the 5D unification is trivial because, in the (4+1) split form, it is identical to GR and EM. With a scalar field, however, a 5D gravity can lead to a sequence of new effects such as the space or vacuum polarization [8-9, 14], electric redshift [16], gravitational field shielding [17-18], gravitationless black hole [19], modified neutron star mass-radius relation [20], and so on. A 5D gravity with the Friedmann-Lemaitre-Robertson-Walker (FLRW) metric of the universe modifies the Friedmann equa-

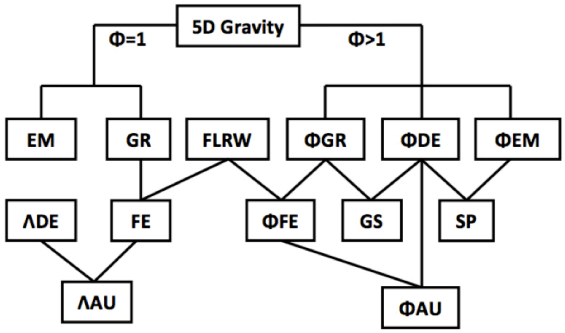

Fig. 1: Characteristics of 5D gravity with and without a scalar field dark energy (ΦDE). Without a scalar field (i.e. $\Phi = 1$), 5D gravity just trivially unifies the 4D Einsteinian general relativity (GR) and Maxwellian electromagnetism (EM). Combining with the Friedmann-Lemaitre-Robertson-Walker (FLRW) metric of 4D spacetime, the field equation given in GR derives the Friedmann equation (FE) that governs the dynamic and development of the universe. Including the cosmological constant dark energy (ΛDE), FE explains the acceleration of the universe (ΛAU). With a scalar field (i.e. $\Phi > 1$), 5D gravity modifies the general relativity (ΦGR) and electromagnetism (ΦEM) through the scalar field dark energy (ΦDE). These modifications lead to a sequence of new effects such as the space or vacuum polarization (SP) and the gravitational field shielding (GS). Combining with the FLRW metric of 4D spcatime, ΦGR derives a modified Friedmann equation (ΦFE), which can also explain the acceleration of the universe (ΦAU) but due to the scalar field dark energy (ΦDE). The space polarization (SP) or the effect on light by the ΦDE of 5D gravity can be significant enough for the accurate LIGO detectors to detect.

tion with a scalar field, which plays the role of dark energy and explains the acceleration of the universe [21-23]. These new effects are results of the scalar field that modulates both gravitational and electromagnetic fields as shown in the (4+1) split form of the 5D field equation or as seen in the field solutions [14, 24]. Figure 1 shows the characteristics of a 5D gravity with and without a scalar field dark energy and its role to the cosmology.

The metric of 5D spactime is usually given by [25]:

$$\bar{g}_{\alpha\beta} = \begin{pmatrix} g_{\mu\nu} + q^2\Phi^2 A_\mu A_\nu & q\Phi^2 A_\nu \\ q\Phi^2 A_\mu & \Phi^2 \end{pmatrix} \tag{1}$$

where α and β are the subscripts for the 5D coordinates, running through 0 - 4; μ and ν are the subscripts for the 4D coordinates, running through 0 - 3; $g_{\mu\nu}$ is the metric of 4D spacetime; A_μ is the standard 4D electromagnetic potential; Φ is the scalar field, which is an effectively massless 4D scalar; q is a scale constant defined by $q = 2\sqrt{G}$ with G the gravitational constant. The fifth dimension is compact [26]. In isotropic coordinates, the line element ds^2 of 4D spacetime can be represented according to the metric as [27]

$$ds^2 = -g_{\mu\nu}dx^\mu dx^\nu$$

$$ds^2 = -e^\nu dt^2 + e^\lambda\left(dr^2 + r^2 d\theta^2 + r^2\sin^2\theta d\phi^2\right), \tag{2}$$

where e^λ and e^ν are the metric $rr-$ and $tt-$components as functions of the radial distance r. Then, the exact static spherically symmetric solution of gravitational, electromagnetic, and scalar fields of a charged body is given by [24]

$$e^\lambda = \left(1 - \frac{B^2}{r^2}\right)^2 \Psi^{-2}, \tag{3}$$

$$e^\nu = \Psi^2\Phi^{-2}, \tag{4}$$

$$H_{01} = -H_{10} = -\frac{Q}{r^2}e^{(\nu-\lambda)/2}, \tag{5}$$

$$\Phi^2 = a_1\Psi^{p_1} + a_2\Psi^{p_2}, \tag{6}$$

where the function Ψ is defined by

$$\Psi = \left(\frac{r-B}{r+B}\right)^{C/2B}, \tag{7}$$

and the seven constants (K, p_1, p_2, B, C, a_1, and a_2) are constrained by the following five relations:

$$K = 4(4B^2 - C^2)C^{-2}, \tag{8}$$

$$a_1 + a_2 = 1, \tag{9}$$

$$p_1 = 1 + \sqrt{1+K}, \tag{10}$$

$$p_2 = 1 - \sqrt{1+K}, \tag{11}$$

$$Q^2 = -a_1 a_2 C^2(1+K)G^{-1}. \tag{12}$$

Here H_{01} and H_{10} are non-zero components of the effective 4D electromagnetic field $H_{\mu\nu} \equiv \phi^3 F_{\mu\nu}$ with $F_{\mu\nu} = \partial_\nu A_\mu - \partial_\mu A_\nu$. At $r \to \infty$, the limits of e^λ, e^ν, and Φ are the unity. The parameter Q denotes the electric charge. It is obvious that the above 5D solution of the fields includes two independent constants.

In a traditional 5D gravity, one usually assumes or hypothetically forms the fifteenth component ($\bar{T}^{44}$) of the 5D energy-momentum tensor by including an undetermined parameter called scalar charge S, e.g. $\bar{T}^{44} = S\rho$ as done by [24] with ρ the density of matter. Since it lacks of any measurement and short of any observational support, the undetermined parameter makes all results obtained from the traditional 5D gravity to be non-decisive and hence non-conclusive in comparison with other theories of gravitation, observations, and experiments. Describing the matter to be also covariant in the 5D spacetime as the fields are, however, this author analytically derived the fifteenth component of the 5D energy-momentum tensor without assuming any unknown parameter ([14] and references therein such as the early studies by the author [28-29]),

$$\bar{T}^{44} = \frac{\rho\alpha^2}{\Phi^2\sqrt{\Phi^2+\alpha^2}}, \tag{13}$$

where α is a non-dimensional constant (or charge-mass ratio) defined by

$$\alpha = \frac{Q}{2\sqrt{G}M}, \tag{14}$$

with M the mass of matter, and therefore analytically determined all the constants in the solution as follows

$$K = 8, \quad p_1 = 4, \quad p_2 = -2, \tag{15}$$

$$a_1 = -\alpha^2, \quad a_2 = 1 + \alpha^2, \tag{16}$$

$$C = \frac{2GM}{3c^2\sqrt{1+\alpha^2}}, \quad B = \frac{GM}{c^2\sqrt{3(1+\alpha^2)}}. \tag{17}$$

Here the cgs or Gaussian unit system is adapted. This set of constants is the simplest and most elegant, because of $K = 8$ that leads to p_1 and p_2 to be whole numbers, for the solution to be non-trivial. Therefore, according to this solution with the constants obtained, the gravitational, electromagnetic, and scalar fields of a charged spherically symmetric object are completely determined from the charge and mass of the object.

In the Einstein frame, this field solution simply reduces to the Schwarzschild solution of the Einsteinian general relativity when matter is neutral and fields are weak [14,17]. This guarantees that the fundamental tests of the Einsteinian general relativity in the case of weak fields are also the tests of this 5D gravity. In the case of strong fields, especially when matter is electrically charged, however, the results obtained from this 5D gravity are significantly different from the Einsteinian general relativity. These new strong field effects include the space polarization [8, 14], electric redshift [16], gravitational field shielding [17-18], and so on. At $\Phi = 1$, the 5D gravity is trivially equivalent to GR and EM, where the Reissner-Nordstrom solution determines the standard GR metric of a charged, massive particle [30-31]. The solution of this 5D gravity Eq. (3) is obtained at $\Phi \neq 1$ and thus cannot be limited to the Reissner-Nordstrom solution for a charged, massive particle. But when fields are weak and matter is weakly charged, the effect of the scalar field on both gravitational and electromagnetic fields are negligible.

2.2 Vacuum polarization by scalar field

In terms of this 5D gravity and the field solution obtained, the electric field of a charged body can be defined as

$$E \equiv H_{10} = -H_{01} = \frac{Q}{r^2} e^{(\nu-\lambda)/2}, \tag{18}$$

and then the dielectric constant (or relative permittivity) ϵ_r of the vacuum that is polarized by the scalar field can be determined by

$$\epsilon_r \equiv \frac{E_C}{E} = e^{(\lambda-\nu)/2} = \left(1 - \frac{B^2}{r^2}\right)\Phi\Psi^{-2}, \tag{19}$$

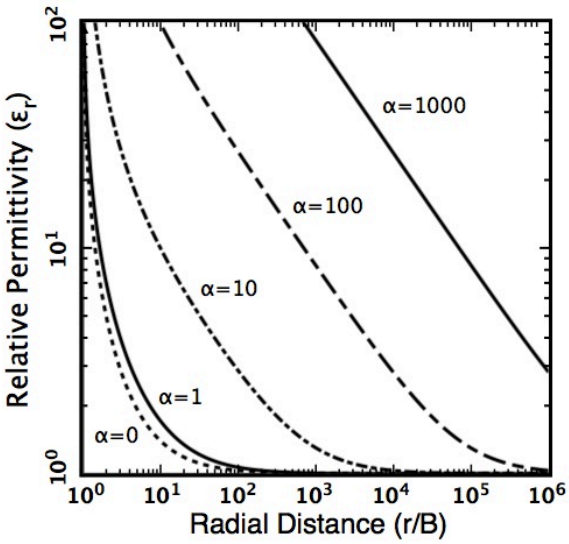

Fig. 2: The relative permittivity ϵ_r or the electric field ratio E_C/E versus the normalized radial distance r/B for a charged object with α = 0, 1, 10, 100, 1000, respectively.

where $E_C = Q/r^2$ is the Coulomb electric field of the charged object. To see how significant the space or vacuum polarization is, we plot, in Figure 2, the relative permittivity ϵ_r as a function of the normalized radial distance r/B for a charged object with five different charge-mass ratios α = 0, 1, 10, 100, 1000.

The result indicates that the electric field of the charged object asymptotically approaches the Coulomb electric field (i.e. $\epsilon_r \to 1$), when r is getting larger ($r \gg B$) or approaches infinity. When r becomes small, however, the electric field significantly deviates from the Coulomb electric field (i.e. $\epsilon_r \gg 1$) due to the vacuum space to be extensively polarized by the strong scalar field. When r tends to B, the relative permittivity approaches infinity and the electric field becomes weaker and weaker as compared with the strength of the Coulomb electric field, especially when the object is highly charged. In the limit case of $\epsilon_r = \infty$, the vacuum space is completely polarized by the extremely strong scalar field. It should be noted that a big deviation at $r \sim B$ still exists even if the object is weakly charged ($\alpha \ll 1$) or neutral. The deviation increases as the charge increases. For instance, at $\alpha = 100$ and $r/B = 10^3$, the electric field is only 10% of the Coulomb electric field. The electric field is significantly weakened as compared with the strength of the Coulomb electric field and the vacuum space is greatly polarized, especially when the object is highly charged.

Only for a massive, compact and charged object, we can have a B not to be too small in comparison with its radius and can see a significant polarization of the vacuum. For a lab-sized object, the polarization of the vacuum can only be extremely weak. Figure 3 plots the deviation of the rel-

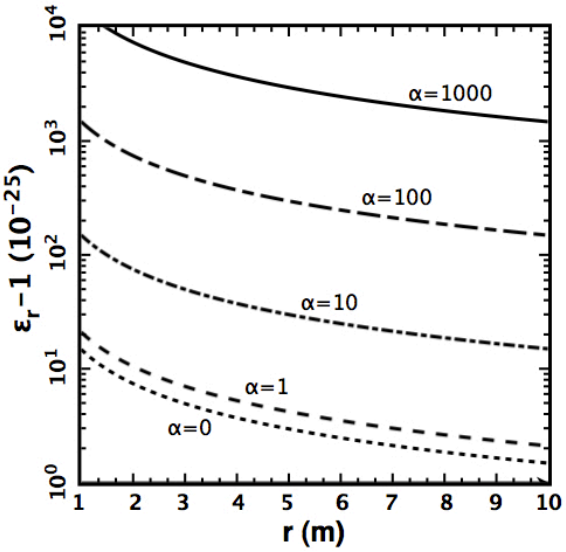

Fig. 3: The change of the relative permittivity $\epsilon_r - 1$ or the change of relative electric field $(E_c - E)/E$ versus the radial distance r for a charged object with mass of 1000-kg and charge-mass ratio $\alpha = 0$, 1, 10, 100, 1000, respectively.

ative permittivity of the vacuum from the unity, $\epsilon_r - 1$, due to the polarization as a function of the radial distance r for a charged object with mass of 1000 kilograms and charge in a range of $\alpha = 0 - 1000$. It is seen that, because the fields of a non-massive object are too weak, the polarization of the vacuum by the scalar field dark energy of 5D gravity is very very small and thus extremely difficult to be detected in laboratory, except for us to have an extremely accurate detector with an appropriate approach. In the following section, we will examine whether the LIGO detectors can detect such small vacuum polarization or not. The answer as shown in the next section is positive when the charge-mass ratio of the charged body is much greater than 1.

3 Can LIGO detect the scalar field dark energy?

In accordance with the relative permittivity determined above, we can find the refractive index of the vacuum that is polarized by the scalar field of 5D gravity as,

$$n \equiv \sqrt{\epsilon_r} = e^{(\lambda-\nu)/4}. \tag{20}$$

For the non-polarized vaccum, we have $n = 1$ and $\epsilon_r = 1$. Substituting Eqs. (3) and (4) into Eq. (20), we have

$$n = \Phi^{1/2}\Psi^{-1}\left(1 - \frac{B^2}{r^2}\right)^{1/2}. \tag{21}$$

In the case of weak fields, we can obtain the change of the refractive index for the polarized vacuum as,

$$\delta n = n - 1 \simeq \frac{\sqrt{1+\alpha^2}\, GM}{c^2 r}, \tag{22}$$

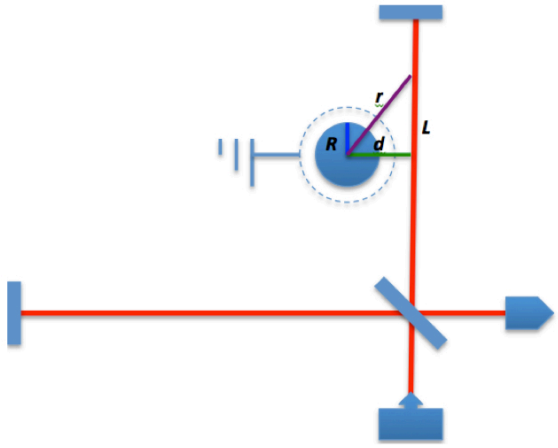

Fig. 4: A schematic diagram for LIGO with a charged object to detect the scalar field dark energy of 5D gravity. When we place a highly charged object, whose strong electromagnetic fields are shielded by a conductor shell that is grounded, nearby one path of the LIGO laser beams. The space surrounding the charged object and the vacuum travelled through by the laser beam back and forth are polarized by the scalar field of the charged object. This polarization extends the optical path length of the laser beam to be significant enough for the accurate LIGO to detect the scalar field dark energy.

When $\alpha \gg 1$, δn is about linearly increasing with α. Then, the change of the optical path length of the polarized space or vacuum can be obtained by the following path line integration

$$\delta l = \int_C \delta n\, ds. \tag{23}$$

To quantitatively estimate the polarization, we consider a metal (e.g. copper) sphere with radius $R = 0.5$ m. From the mass density of copper $\rho = 9 \times 10^3$ kg/m^3, we can find the mass of the sphere to be $M = 4\pi\rho R^3/3 \sim 4.7 \times 10^3$ kg. Now, if the sphere is electrically charged up to $V = 10^5$ V, we can also calculate the charge Q and charge-mass ratio α of the sphere as $Q = 4\pi\epsilon_0 RV \sim 5.6 \times 10^{-6}$C $= 1.7 \times 10^4$ esu and $\alpha \sim 7$, respectively. Then, from Eq. (22), we can find the change of the refractive index in the space surrounding the charged sphere to be $\delta n = 1.2 \times 10^{-23}$. Here, we have chosen as an example the radial distance to be 4 radii of the object, i.e. $r = 2$ m. This result indicates that the scalar field of the charged object can extend the optical path length relatively by $\sim 1.2 \times 10^{-23}$ m for each meter, which is significant enough for the accurate LIGO detectors to detect.

Now, we suggest to place this charged object into the LIGO system nearby the middle of the path of one of the two perpendicular arms or laser beams (Figure 4). Then, the variation of the optical path length due to the space polarization by the scalar field dark energy can be estimated by,

$$\Delta L = (N+1)\int_{-L/2}^{L/2} \delta n\, ds$$

$$\Delta L = \frac{(N+1)\sqrt{1+\alpha^2}\,GM}{c^2} \ln \frac{L+\sqrt{L^2+4d^2}}{-L+\sqrt{L^2+4d^2}}, \qquad (24)$$

where N is the number of reflections of the laser beam, L is the geometric length of the arm, d is the minimum distance from the center of the charged object to the laser beam, and s is the coordinate of position to be integrated along the path from $-L/2$ to $L/2$. For the LIGO working parameters, we can choose $N = 280$ and $L = 4$ km. The distance can be chosen again as 4 radii of the charged object, i.e. $d = 2$ m. Then, we can obtain that the optical length of the 4 km path of the LIGO laser beam with 280 times reflections is increased due to the space polarization by $\Delta L \sim 10^{-18}$ m, about the amount of one order higher than that being detectable by LIGO. Similarly to the gravitational-wave strain defined in [15], we can define a strain for the space polarization by scalar field, h, as the change of the optical length dividing by the length of the LIGO arm L,

$$h \equiv \frac{\Delta L}{L} \simeq \frac{2(N+1)\sqrt{1+\alpha^2}\,GM}{c^2 L} \ln \frac{L}{d}. \qquad (25)$$

Here, we have approximate the expression or Eq. (24) by considering $d \ll L$. For $\alpha \gg 1$, we have that the strain is proportional to the charge Q but independent of the mass M.

$$h \simeq \frac{(N+1)\sqrt{G}\,Q}{c^2 L} \ln \frac{L}{d} \propto Q. \qquad (26)$$

Here, the cgs units are adapted since we have used Eq. (14).

To see the charge dependence, we plot in Figure 5 the increase of the optical path length as a function of the voltage of the charged object. The result indicates that the extension of the optical path length remains a constant as the mass is fixed when the object is weakly charged ($V < 500$ V) and linearly increases with the voltage when the object is highly charged. For instance, when $V = 40$ kV, the charged object can cause the optical path length of one laser beam in a LIGO arm with 280 times reflections to extend up to about $\Delta L \sim 4 \times 10^{-19}$ m (or the strain $h \sim 10^{-22}$), which is the amount of 4 times greater than that to be detectable by the LIGO detectors [15]. For LIGO to detect the scalar field dark energy or to test the 5D gravity, we can switch on and off the power to the object and check whether the converging laser beams become out of phase and thus the interference pattern varies or not. In addition, to have a timely varying optical length difference in a specific range of 20-2000 Hz that LIGO can measure, we consider a harmonically varying voltage or power to charge the sphere, $V(t) = V_0 \sin(2\pi f t)$, with $V_0 = 10^5$ V and $f = 100$ Hz. Figure 6 plots the the varying optical length change between two laser beams as a function of time. Therefore, the accurate LIGO detectors that have recently detected first ever the gravitational waves from a binary black hole merger are capable to be detectors and testers for the scalar field dark energy of 5D gravity. This study provides a creative approach for LIGO to detect the vacuum polarization by the scalar field

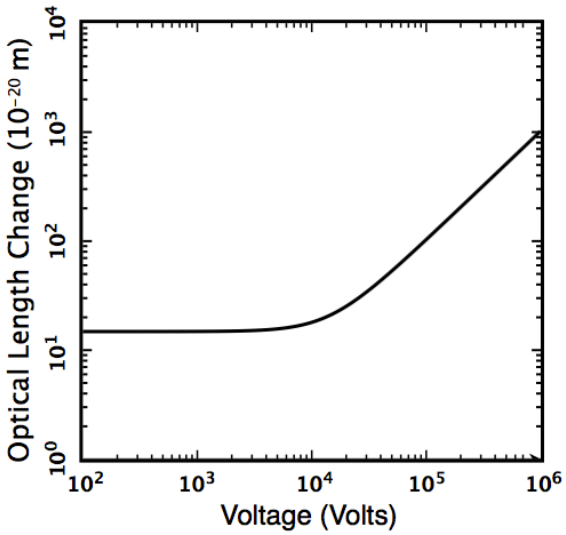

Fig. 5: Space polarization by the scalar field dark energy of 5D gravity. The increase of the optical path length of a laser beam in one LIGO arm that is polarized by a charged object is plotted as a function of the voltage applied to the object. In the case of the object to be only weakly charged ($V < 500$ V), the extension of the optical path length remains a constant as the mass is fixed. When the object is highly charged, however, the optical path length linearly increases with the voltage. At $V = 40$ kV, the charged object can extend the optical path length of one laser beam in a LIGO arm with 280 times reflections up to about $\Delta L \sim 4 \times 10^{-19}$ m (or the strain $h \sim 10^{-22}$), about one order higher than that to be detected by LIGO.

of 5D gravity, a candidate of dark energy that drives the universe in its accelerating expansion. It should be noted that this paper only focuses on the variation in optical length due to the vacuum polarization by the scalar field. To include the variation in optical length due to other fields, we need compute it based on the full solution of all fields. This leaves for future study.

4 Discussions and conclusions

LIGO uses the interference pattern where the beams combine to determine if the optical length down the two laser arms is changing. Possible physical causes for the change of the optical length down the two laser beams can be various sources such as seismic disturbances, gravitational waves from binary black hole mergers, space polarizations by scalar field, and so on. When a gravitational wave passes through the interferometer, the spacetime in the local area is altered, disturbed, and curved. This results in an effective change in the optical length of one or both of the laser beams, which is estimated by $\Delta L(t) = h(t)L$, where $h(t)$ is the gravitational-wave strain amplitude projected onto the detector [15]. The advanced LIGO detectors can have sensitive responses to a strain of $h(t) \sim 10^{-21} - 10^{-23}$. This change of the optical length causes the light currently very slightly out of phase with the incom-

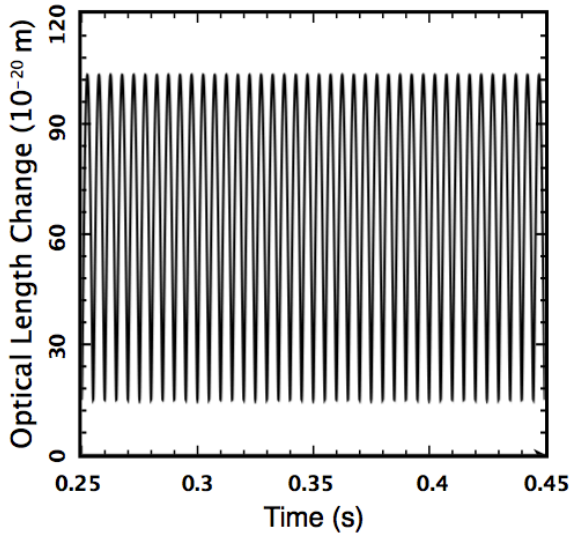

Fig. 6: The optical length difference between the two laser beams is plotted as a function of time when a 100-Hz harmonically varying voltage is applied to charge the sphere. LIGO detectors that have detected the gravitational waves from binary black hole mergers can measure the varying optical length change.

ing light and thus varies the interference pattern. The effective optical length change due to the spacetime disturbances and distortions by the passing of gravitational waves is calculated from the solution of the deviating geodesics equation with a gravitational wave from a binary black hole merger. For the space polarization by scalar field, as analyzed in this paper, we calculate the change of the optical length in accordance with the solution of the deviating index refraction. Seismic disturbances can also result in the converging laser beams being out of phase.

As a consequence, we have in terms of a 5D gravity found that a some-thousand-kilogram (e.g., 4700 kg) sphere electrically charged to some ten kilovolts (e.g. 40 kV) can polarize the vacuum by its scalar field dark energy and thus extend the optical path length of a laser beam that travels through one LIGO arm with some hundred (e.g. 280) reflections by approximately 4×10^{-19} m (or the strain of $h \sim 10^{-22}$), which is the amount of 4 times greater than that to be detected by the LIGO detectors. Switching on and off the power to the object allows to check whether the LIGO detectors can detect the scalar field dark energy and thus test the 5D gravity or not. For a harmonic voltage with frequency, e.g. 100 Hz, we have a varying optical length difference between the two laser beams in the frequency range of the LIGO detection. Therefore, being added a highly charged sphere into the experimental setup, LIGO, which has recently detected first ever the gravitational waves from the binary black hole merger, may directly discover first ever the scalar field dark energy of 5D gravity. This study also provides a design criterion for a new approach and experiment of discovering dark energy.

Acknowledgement

This work was partially supported by the NSF/REU programs (Grant #: PHY-1263253, PHY-1559870) at Alabama A & M University.

Submitted on June 20, 2017

References

1. Riess A.G. et al. Observational evidence from supernovae for an accelerating universe and a cosmological constant. *Astronomical Journal*, 1998, v. 116, 1009–1038.
2. Perlmutter S. et al. Measurements of Ω and Λ from 42 high-redshift supernovae. *The Astrophysical Journal*, 1999, v. 517, 565—586.
3. Brans C.H., Dicke R.H. Mach's principle and a relativistic theory of gravitation. *Physical Review*, 1961, v. 124, 925–935.
4. Kaluza T. On the problem of unity in physics. *Sitz. Preuss. Akad. Wiss. (Phys. Math.)*, 1921, K1, 966–972.
5. Klein O. Quantum theory and five–dimensional theory of relativity. *Zeitschrift fur Physik*, 1926a, v. 37, 895–906.
6. Klein O. The atomicity of electricity as a quantum theory law. *Nature*, 1926b, v. 118, 516–516.
7. Wesson P.S. The scalar field of 5D gravity and the Higgs field of 4D particle physics: A possible connection, *eprint arXiv:1003.2476*, 2010, arXiv: 1003.2476.
8. Nodvik J.S. Suppression of singularities by the g55 field with mass and classical vacuum polarization in a classical Kaluza-Klein theory. *Physical Review Letters*, 1985, v. 55, 2519-2522.
9. Dragilev V.M. Vacuum polarization of a scalar field in anisotropic multidimensional cosmology. *Theoretical and Mathematical Physics*, 1990, v. 84, 887–893.
10. Frolov V.P., Zelnikov A.I. Vacuum polarization by a massive scalar field in Schwarzschild spacetime. *Physics Letters*, 1982, v. B115, 372–374.
11. Rodrigues R.B., Svaiter N.F. Vacuum fluctuations of a scalar field in a rectangular waveguide. *Physica A: Statistical Mechanics and Its Applications*, 2003, v. 328, 466–492.
12. Bezerra de Mello E.R. Vacuum polarization by a scalar field in de Sitter spacetime in the presence of a global monopole. *Gravitation and Cosmology*, 2010, v. 16, 92–104.
13. Breev A.I. Scalar field vacuum polarization on homogenous spaces with an invariant metric. *Theoretical and Mathematical Physics*, 2014, v. 178, 59–75.

14. Zhang T.X. The 5D fully-covariant theory of gravitation and its astrophysical applications. *Galaxies*, 2015, v. 3, 18–53.

15. Abbott B.P. et al. Observation of gravitational waves from a binary black hole merger. *Physical Review Letters*, 2016, v. 116, id. 061102.

16. Zhang T.X. Electric redshift and quasar. *The Astrophysical Journal Letters*, 2006, v. 636, L61–L63.

17. Zhang T.X. Gravitational field shielding and supernova explosions. *The Astrophysical Journal Letters*, 2010, v. 725, L117–L120.

18. Zhang B.J., Zhang T.X., Guggilla P., Dokhanian M. Gravitational field shielding by a scalar field. *Progress in Physics*, 2013, v. 1, 69–73.

19. Zhang T.X. Gravitationless black holes. *Astrophysics and Space Science*, 2011, v. 334, 311–316.

20. Zhang B.J., Zhang T.X., Guggilla P., Dokhanian M. Neutron star mass-radius relation with gravitational field shielding by a scalar field. *Research in Astronomy and Astrophysics*, 2013a, v. 13, 571–578.

21. Dvali G., Turner S. Dark energy as a modification of the Friedmann equation. *arXiv: astro-ph/0301510*, 2003.

22. Jadhav M. Five-dimensional fully covariant Kaluza-Klein cosmology with scalar field dark energy. *PhD Thesis* (Advisor: T. X. Zhang), 2013, Alabama A & M University

23. Sharif M., Khanum F. Kaluza-Klein cosmology with modified holographic dark energy. *General Relativity and Gravitation*, 2011, v. 43, 2885-2894.

24. Chodos A., Detweiler S. Spherically symmetric solutions in five dimensional general relativity. *General Relativity and Gravitation*, 1982, v. 14, 879–890.

25. Overduin J.M., Wesson P.S. Kaluza-Klein gravity. *Physics Reports*, 1997, v. 283, 303–378.

26. Souriau J.M. Five-Dimensional Relativity. *Nuovo Cimento*, 1963, v. 30, 565-578

27. Weinberg S. Gravitation and Cosmology, Wiley: New York, 1980.

28. Zhang T.X. Static spherically symmetric solution of Kaluza-Klein theory with scalar field and its experimental examination. *Thesis* (Advisor: Z.T. Yang), Yunnan University, 1987.

29. Zhang T.X. Kaluza-Klein theory with five-dimenally complete covariance. *Journal of Jiangxi University: Natural Science*, 1993, v. 17, 63–70.

30. Reissner H. Über die Eigengravitation des elektrischen Fields nach der Einsteinschen Theorie. *Annalen der Physik (in German)*, 1916, v. 355, 106–120.

31. Nordström G. On the Energy of the Gravitational Field in Einstein's Theory. *Koninkljke Nederlandsche Akaddemie van Wetenschappen Proceedings*, 1918, v. 20, 1238–1245.

The Journal on Advanced Studies in Theoretical and Experimental Physics, including Related Themes from Mathematics

PROGRESS IN PHYSICS

A quarterly issue scientific journal, registered with the Library of Congress (DC, USA). This journal is peer reviewed and included in the abstracting and indexing coverage of: Mathematical Reviews and MathSciNet (AMS, USA), DOAJ of Lund University (Sweden), Scientific Commons of the University of St. Gallen (Switzerland), Open-J-Gate (India), Referativnyi Zhurnal VINITI (Russia), etc.

Electronic version of this journal:
http://www.ptep-online.com

Postal Address

Department of Mathematics and Science,
University of New Mexico,
705 Gurley Ave., Gallup, NM 87301, USA

ISSN: 1555-5534 (print)
ISSN: 1555-5615 (online)

Standard Address Number: 297-5092
Printed in the United States of America

October 2017 **Vol. 13, Issue 4**

CONTENTS

Information for Authors

Progress in Physics has been created for rapid publications on advanced studies in theoretical and experimental physics, including related themes from mathematics and astronomy. All submitted papers should be professional, in good English, containing a brief review of a problem and obtained results.

All submissions should be designed in LaTeX format using *Progress in Physics* template. This template can be downloaded from *Progress in Physics* home page http://www.ptep-online.com

Preliminary, authors may submit papers in PDF format. If the paper is accepted, authors can manage LaTeXtyping. Do not send MS Word documents, please: we do not use this software, so unable to read this file format. Incorrectly formatted papers (i.e. not LaTeXwith the template) will not be accepted for publication. Those authors who are unable to prepare their submissions in LaTeXformat can apply to a third-party payable service for LaTeX typing. Our personnel work voluntarily. Authors must assist by conforming to this policy, to make the publication process as easy and fast as possible.

Abstract and the necessary information about author(s) should be included into the papers. To submit a paper, mail the file(s) to the Editor-in-Chief.

All submitted papers should be as brief as possible. Short articles are preferable. Large papers can also be considered. Letters related to the publications in the journal or to the events among the science community can be applied to the section *Letters to Progress in Physics*.

All that has been accepted for the online issue of *Progress in Physics* is printed in the paper version of the journal. To order printed issues, contact the Editors.

Authors retain their rights to use their papers published in *Progress in Physics* as a whole or any part of it in any other publications and in any way they see fit. This copyright agreement shall remain valid even if the authors transfer copyright of their published papers to another party.

Electronic copies of all papers published in *Progress in Physics* are available for free download, copying, and re-distribution, according to the copyright agreement printed on the titlepage of each issue of the journal. This copyright agreement follows the *Budapest Open Initiative* and the *Creative Commons Attribution-Noncommercial-No Derivative Works 2.5 License* declaring that electronic copies of such books and journals should always be accessed for reading, download, and copying for any person, and free of charge.

Consideration and review process does not require any payment from the side of the submitters. Nevertheless the authors of accepted papers are requested to pay the page charges. *Progress in Physics* is a non-profit/academic journal: money collected from the authors cover the cost of printing and distribution of the annual volumes of the journal along the major academic/university libraries of the world. (Look for the current author fee in the online version of *Progress in Physics*.)

Scale-Invariant Models of Natural Oscillations in Chain Systems and Their Cosmological Significance

Hartmut Müller

E-mail: hm@interscalar.com

In this paper we review scale-invariant models of natural oscillations in chain systems of harmonic quantum oscillators and derive measurable consequences. Basic model claims are verified in terms of fundamental particles, the cosmic microwave background and the solar system. The cosmological significance of some model statements is discussed.

Introduction

In the last 40 years many studies [1] were published which show that scale invariance (scaling) is a widely distributed phenomenon discovered in high energy physics [2–4], seismology [5, 6], biology [7–9] and stochastic processes of various nature [10].

As a property of power laws, scale invariance can be generated by very different mechanisms. The origin of power law relations and efforts to observe and validate them is a topic of research in many fields of science. However, the universality of scaling may have a mathematical origin that does not depend on the actual mechanism of manifestation.

In [11] we have shown that scale invariance is a fundamental property of natural oscillations in chain systems of similar harmonic oscillators. In [12] we applied this model on chain systems of harmonic quantum oscillators. In the case of a chain of protons as fundamental oscillators, particle rest masses coincide with the eigenstates of the system. This is valid not only for hadrons, but for mesons and leptons as well. Because of scale invariance, chains of electrons produce similar sets of natural frequencies.

In [13] Andreas Ries has shown that the complete description of elementary particle masses by the model of oscillations in chain systems is only possible if considering both, chains of protons and electrons. Furthermore, in [14] he was able to show that this model allows the prediction of the most abundant isotope for a given chemical element.

The core claims of scale-invariant models do not depend on the selection of the fundamental oscillator. Therefore, the rest mass of the fundamental oscillator can be even smaller than the electron mass. Consequently, all elementary particles can be interpreted as eigenstates in a chain system of harmonic quantum oscillators, in which the rest mass of each single oscillator goes to zero. This is how the transition of massless to massive states can be explained [15].

In [16] we have shown that scale-invariant models of natural oscillations in chain systems of protons also describe the mass distribution of large celestial bodies in the solar system.

The intention of this article is an adjustment of the basic claims of our model and an additional verification on fundamental particles, the cosmic microwave background and the solar system. Furthermore, we discuss the cosmological significance of some model claims.

1 Methods

Kyril Dombrowski [17] mentioned that oscillating systems – having the peculiarity to change their own parameters because of interactions inside the systems – have a tendency to reach a stable state where the individual oscillator frequencies are interrelated by specific numbers – namely minima of the rational number density on the number line.

Viktor and Maria Panchelyuga [18] showed that resonance phenomena appear more easily if they belong to maxima in the distribution of rational numbers, while maxima in the distribution of irrational numbers correspond with a high stability of the system, minimal interaction between parts of the system and minimal interaction with the surroundings.

In [11] we have shown that in the case of harmonic oscillations in chain systems, the set of natural frequencies is isomorphic to a discrete set of natural logarithms whose values are rational numbers.

Each real number (rational or irrational) has a biunique representation as a simple continued fraction. In addition, any rational number can be represented as a finite continued fraction and any finite continued fraction represents a rational number [19].

Consequently, the set of natural frequencies of a chain system of harmonic oscillators corresponds with a set of finite continued fractions $\mathcal{F}$, which are natural logarithms:

$$\ln(\omega_{jk}/\omega_{00}) = n_{j0} + \cfrac{z}{n_{j1} + \cfrac{z}{n_{j2} + \ddots + \cfrac{z}{n_{jk}}}} = [z, n_{j0}; n_{j1}, n_{j2}, \ldots, n_{jk}] = \mathcal{F}, \tag{1}$$

where ω_{jk} is the set of angular frequencies and ω_{00} is the fundamental frequency of the set. The denominators are integer numbers: $n_{j0}, n_{j1}, n_{j2}, \ldots, n_{jk} \in \mathrm{Z}$, the cardinality $j \in \mathrm{N}$ of the set and the number $k \in \mathrm{N}$ of layers are finite. In the canonical form, the numerator z is equal 1.

However, by means of the Euler equivalent transformation [20] every continued fraction with partial numerators

$z \neq 1$ can be changed into a continued fraction in the canonical form with $z = 1$.

Therefore, we will call the set $\mathcal{F}$ of finite continued fractions (1) with $z = 1$ the "Fundamental Fractal" of natural frequencies in chain systems of harmonic oscillators.

For rational exponents the natural exponential function is transcendental [21]. Therefore, $\mathcal{F}$ is a set of transcendental numbers that is isomorphic to the set of rational numbers represented by finite continued fractions. The function of isomorphism is the natural logarithm.

It seems that this transcendence and consequently the irrationality of $\mathcal{F}$ provides the high stability of the oscillating chain system because it avoids resonance interaction between the elements of the system.

2 Projections of the Fundamental Fractal

All elements of the continued fractions $\mathcal{F}$ are integers and can therefore be represented as unique products of prime factors. Consequently, we can distinguish classes of finite continued fractions (classes of rational numbers) in dependency on the divisibility of the numerators and denominators by prime numbers, as we have shown in [11]. Based on this, different projections of $\mathcal{F}$ can be studied.

Figure 1 demonstrates the formation of the canonical projection ($z = 1$). Each vertical line represents a rational number that is the logarithm of a natural frequency of a chain system of harmonic oscillators.

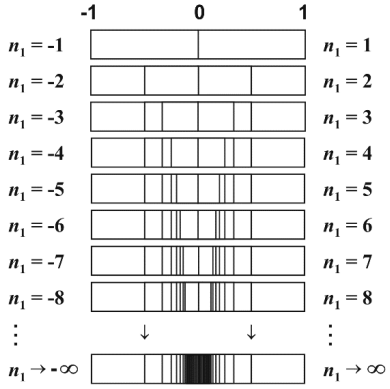

Fig. 1: The formation of the canonical projection ($z = 1$) of the $\mathcal{F}$ on the first layer $k = 1$ (natural logarithmic representation).

The distribution density increases hyperbolically with $|n_{j1}|$. In the range $1 < |n_{j1}| < 2$ the distribution density is minimum. Figure 2 shows that for finite continued fractions (1), ranges of high distribution density (nodes) arise near reciprocal integers $1, 1/2, 1/3, 1/4, \ldots$ which are the attractor points of the distribution.

All the denominators of the continued fractions $\mathcal{F}$ are (positive and negative) integers. Therefore, the canonical projection is logarithmically symmetric, as figures 3 and 4 show.

Fig. 2: The canonical projection of the $\mathcal{F}$ in the range $0 \leqslant |n_{j0}| \leqslant 1$ for $k = 2$ (natural logarithmic representation).

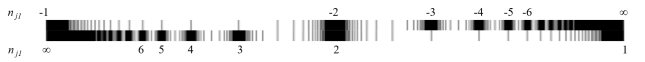

Fig. 3: The canonical projection of the $\mathcal{F}$ in the range $1 \leqslant |n_{j1}| < \infty$ for $k = 2$ (natural logarithmic representation).

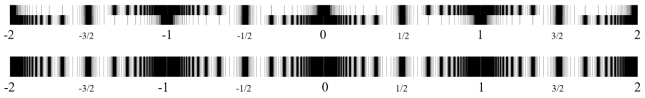

Fig. 4: The canonical projection of the $\mathcal{F}$ in the range $-2 \leqslant S \leqslant 2$ for $k = 2$ (natural logarithmic representation).

In the following we investigate continued fractions (1) which meet the Markov [22] convergence condition $|n| \geqslant |z|+1$.

Figure 5 illustrates different projections generated by continued fractions (1) with denominators divisible by $2, 3, 4, \ldots$ and the corresponding numerators $z = 1, 2, 3, \ldots$

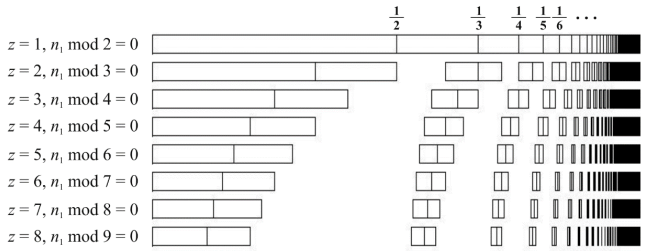

Fig. 5: Different projections generated by continued fractions (1) with denominators divisible by $2, 3, 4, \ldots$ and corresponding numerators $z = 1, 2, 3, \ldots$.

Figure 5 shows the nodes on the first layer $j = 1$ and also the borders of the node ranges, so the gaps are clearly visible. The borders of the gaps are determined by the alternating continued fractions $[z, 0; z+1, -z-1, z+1, -z-1, \ldots] = 1$ and $[z, 0; z-1, -z+1, z-1, -z+1, \ldots] = -1$, for $z \geqslant 1$.

Denominators that are divisible by 3 with $z = 2$ build the class of continued fractions (1) that generates the projection with the smallest gaps. These gaps remain empty even if the number of layers k increases infinitely.

In the 2/3-projection, free links n_{j0} of the continued fractions (1) that are divisible by 3 designate the main nodes, denominators divisible by 3 designate subnodes while all the other denominators designate the borders of gaps (see Figure 6 and 7).

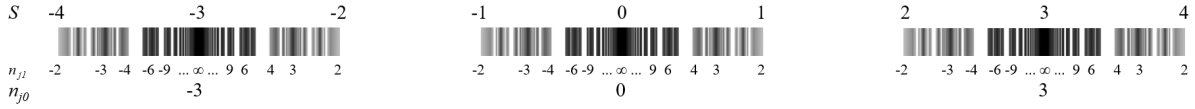

Fig. 6: The 2/3-projection of (1) with $z = 2$, divisible by 3 $|n_{j0}| = 3l$, ($l = 0, 1, 2, \dots$) and denominators divisible by 3 $|n_{jk}| = 3d$, ($d = 1, 2, \dots$) in the range of $-4 \leqslant \mathcal{F} \leqslant 4$).

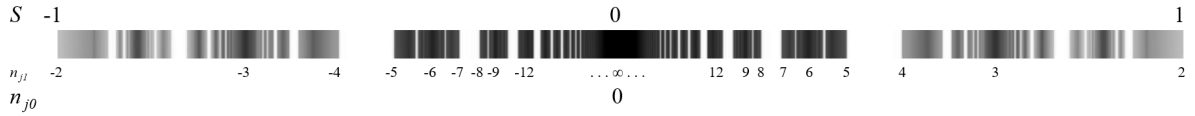

Fig. 7: The same 2/3-projection like in fig. 6, but in the range of $-1 \leqslant \mathcal{F} \leqslant 1$.

In [23] we have shown that in the 2/3-projection, ranges of gaps are connected with stochastic properties of natural oscillations in chain systems of protons. In the current paper we apply the canonical projection only.

3 Harmonic Scaling

Based on (1), we can now calculate the complete set ω_{jk} of natural angular frequencies of a chain system of similar harmonic oscillators, if the fundamental frequency ω_{00} or any other natural frequency of the set ω_{jk} is known:

$$\omega_{jk} = \omega_{00} \exp(\mathcal{F}) . \tag{2}$$

Here and in the following, $\mathcal{F}$ is considered in its canonical projection with $z = 1$. The natural angular oscillation period τ is defined as the reciprocal of the angular frequency:

$$\tau_{jk} = 1/\omega_{jk} . \tag{3}$$

The complete set of natural angular scale oscillation periods:

$$\tau_{jk} = \tau_{00} \exp(\mathcal{F}) . \tag{4}$$

In [12] we have shown that our model (1) can be applied also in the case of natural oscillations in chain systems of harmonic quantum oscillators where the oscillation energy E depends only on the frequency ($\hbar$ being the Planck constant):

$$E_{jk} = \hbar\omega_{jk} . \tag{5}$$

Consequently, the natural frequency set and the corresponding set of natural energies are isomorphic, so that chain systems of harmonic quantum oscillators generate discrete exponential energy series:

$$E_{jk} = E_{00} \exp(\mathcal{F}) , \tag{6}$$

where $E_{00} = \hbar\omega_{00}$ is the fundamental energy. Because of the mass-energy equivalence,

$$m_{jk} = E_{jk}/c^2 \tag{7}$$

the set of natural energies and the corresponding set of natural masses are isomorphic, so that chain systems of harmonic quantum oscillators generate discrete exponential series of masses:

$$m_{jk} = m_{00} \exp(\mathcal{F}) , \tag{8}$$

where $m_{00} = \omega_{00} \cdot \hbar/c^2$ is the fundamental mass.

Finally, the set of natural frequencies corresponds to an isomorphic set of natural wavelengths (c being the speed of light in vacuum),

$$\lambda_{jk} = c/\omega_{jk} \tag{9}$$

so that chain systems of harmonic quantum oscillators generate discrete exponential series of natural wavelengths:

$$\lambda_{jk} = \lambda_{00} \exp(\mathcal{F}) , \tag{10}$$

where $\lambda_{00} = c/\omega_{00}$ is the fundamental wavelength.

As a consequence of (3) and (9), the set of natural wavelengths and the set of natural oscillation periods in chain systems of harmonic quantum oscillators coincide with an isomorphic set of natural velocities:

$$v_{jk} = \lambda_{jk}/\tau_{jk} . \tag{11}$$

Therefore, chain systems of harmonic quantum oscillators generate discrete exponential series of natural velocities as well:

$$v_{jk} = v_{00} \exp(\mathcal{F}) , \tag{12}$$

where the fundamental velocity $v_{00} = c$ is the speed of light in a vacuum.

In relation to the anticipated harmonic exponential series of wavelengths, velocities, energies and masses as a consequence of harmonic oscillations in chain systems, we propose the term "harmonic scaling".

The natural exponential function of a real argument x is the unique nontrivial function that is its own derivative

$$\frac{d}{dx} e^x = e^x$$

and therefore its own anti-derivative as well. Because of the self-similarity of the natural exponential function regarding its derivatives, any real number, being the result of a measurement, can be thought of as a natural logarithm or as the logarithm of a logarithm. Therefore, harmonic scaling is not

limited to exponentiation, but can be extended to tetration, pentation and other hyperoperations as well. In this case we will use the term "hyperscaling".

4 Harmonic Scaling of Fundamental Particles

In [12] we have shown that physical properties of fundamental particles, for example the proton-to-electron mass ratio or the vector boson-to-electron mass ratio, can be derived from eigenstates in chain systems of harmonic quantum oscillators.

In fact, the natural logarithm of the proton/neutron to electron mass ratio is close to [7; 2] and the logarithm of the W/Z-boson to proton mass ratio is near [4; 2], so we can assume the equation:

$$\ln(m_{wz}/m_{pn}) = \ln(m_{pn}/m_e) - 3\,.$$

Consequently, the logarithm of the W/Z-boson to electron mass ratio is $4\frac{1}{2} + 7\frac{1}{2} = 12$:

$$\ln(m_{wz}/m_e) = 12\,,$$

where m_e, m_{pn}, m_{wz}, are the electron, proton/neutron and W/Z-boson rest masses. As table 1 shows, fundamental particle rest mass ratios correspond to attractor nodes of $\mathcal{F}$. Here and in the following we consider the continued fractions (1) in the canonical form, with the numerator $z = 1$ and write them in square brackets.

Table 1: Fundamental particle rest masses and the corresponding attractor nodes of $\mathcal{F}$, with the electron mass as fundamental. Data taken from Particle Data Group.

particle	particle rest mass m, MeV/c^2	$\mathcal{F}$	$\ln(m/m_e)$	$\ln(m/m_e)-\mathcal{F}$
H-boson	125090 ± 240	[12;2]	12.408	-0.092
Z-boson	91187.6 ± 2.1	[12;∞]	12.092	0.092
W-boson	80385 ± 15	[12;∞]	11.966	-0.034
neutron	939.565379 ± 0.000021	[7;2]	7.517	0.017
proton	938.272046 ± 0.000021	[7;2]	7.515	0.015
electron	$0.510998928 \pm 0.000000011$	[0;∞]	0.000	0.000

As table 1 shows, the logarithms of fundamental particle mass ratios are close to integer or half values that are rational numbers with the smallest possible numerators and denominators.

However, the natural logarithm of the W/Z-boson to proton mass ratio is not exactly 4.5, but between $11.966 - 7.515 = 4.451$ and $12.092 - 7.515 = 4.577$ that approximates $\exp(3/2) = 4.4817$. Thus, the properties of fundamental particle masses (table 1) also support our model of hyperscaling.

5 Fundamental Metrology and Planck Units

The electron and the proton are exceptionally stable and therefore accessible anywhere in the universe. Their lifespan tops everything that is measurable, exceeding 10^{29} years for protons and 10^{28} years for electrons [24]. In the framework of the standard theory of particle physics, the electron is stable because it is the least massive particle with non-zero electric charge. Its decay would violate charge conservation [25]. The proton is stable, because it is the lightest baryon and the baryon number is conserved as well. Therefore, the proton-to-electron mass ratio can be understood as a fundamental physical constant.

These unique properties of electrons and protons predestinate their physical characteristics as fundamental units. Table 2 shows the basic set of electron and proton units that can be considered as a fundamental metrology (c is the speed of light in a vacuum, $\hbar$ is the Planck constant, k_B is the Boltzmann constant).

Table 2: The basic set of physical properties of the electron and proton. Data taken from Particle Data Group. Frequencies, oscillation periods, temperatures and the proton wavelength are calculated.

property	electron	proton
mass m	$9.10938356(11) \cdot 10^{-31}$ kg	$1.672621898(21) \cdot 10^{-27}$ kg
energy $E = mc^2$	0.5109989461(31) MeV	938.2720813(58) MeV
angular frequency $\omega = E/\hbar$	$7.76344071 \cdot 10^{20}$ Hz	$1.42548624 \cdot 10^{24}$ Hz
oscillation period $\tau = 1/\omega$	$1.28808867 \cdot 10^{-21}$ s	$7.01515 \cdot 10^{-25}$ s
wavelength $\lambda = c/\omega$	$3.8615926764(18) \cdot 10^{-13}$ m	$2.1030891 \cdot 10^{-16}$ m
temperature $T = mc^2/k_B$	$5.9298 \cdot 10^{9}$ K	$1.08881 \cdot 10^{13}$ m

In [15] we have shown that the Planck scale corresponds to a main attractor node of $\mathcal{F}$ and consequently, Planck units [26] are completely compatible with the fundamental metrology (tab. 2).

Originally proposed in 1899 by Max Planck, these units are also known as natural units, because the origin of their definition comes only from properties of nature and not from any human construct.

Max Planck wrote [27] that these units, "regardless of any particular bodies or substances, retain their importance for all times and for all cultures, including alien and non-human, and can therefore be called natural units of measurement". Planck units are based only on the properties of space-time.

In fact, the logarithm of the Planck-to-proton mass ration is near the node [44; ∞] of the $\mathcal{F}$:

$$\ln\left(\frac{m_{\text{Planck}}}{m_{\text{proton}}}\right) = \ln\left(\frac{2.17647 \cdot 10^{-8}}{1.6726219 \cdot 10^{-27}}\right) = 44.012. \qquad (13)$$

This fact does not only support our model (1), but allows us to derive the proton rest mass from the fundamental physical constants c, $\hbar$, G:

$$m_{\text{proton}} = \exp(-44)(\hbar c/G)^{1/2}\,. \qquad (14)$$

In 1899, Max Planck noted that with his discovery of the quantum of action, sufficient fundamental constants were now

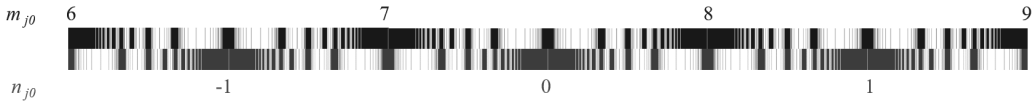

Fig. 8: The correspondence between electron-calibrated attractor nodes $[m_{j0}]$ and proton-calibrated attractor nodes $[n_{j0}]$ of $\mathcal{F}$ in its canonical projection.

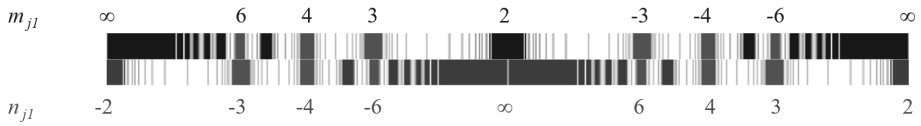

Fig. 9: The correspondence of electron-calibrated subnodes $[m_{j0}; m_{j1}]$ to proton-calibrated subnodes $[n_{j0}; n_{j1}]$ on the first layer of $\mathcal{F}$ in the canonical projection.

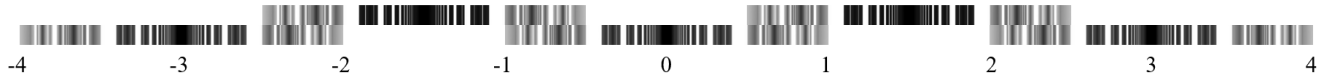

Fig. 10: The correspondence of the electron-calibrated $\mathcal{F}$ (above) to the proton-calibrated $\mathcal{F}$ (below) in the 2/3-projection.

known to define universal units for length, time, mass, and temperature.

This equation (14) may well be of cosmological significance, because it means that the values of proton and the electron rest masses are equally fundamental properties of space-time as are the speed of light, the Planck constant and the gravitational constant.

6 Cosmic Microwave Background

CMB data is critical to cosmology since any proposed model of the universe must explain this radiation. Within our model, the CMB can be understood as an eigenstate in a chain system of oscillating protons, because the black body temperature of the CMB corresponds to the main attractor node $[-29; \infty]$ of the $\mathcal{F}$ calibrated on the proton temperature (table 2):

$$\ln\left(\frac{T_{\mathrm{CMB}}}{T_{\mathrm{proton}}}\right) = \ln\left(\frac{2.726\,\mathrm{K}}{1.08881 \cdot 10^{13}\,\mathrm{K}}\right) = -29.016. \qquad (15)$$

7 Global Scaling

We hypothesise that harmonic scaling is a global phenomenon and continues in all scales, following the fundamental fractal (1) that is calibrated by this fundamental metrology (table 2). This hypothesis we have called 'Global Scaling' [23].

8 Calibration of the Fundamental Fractal

Table 1 shows that the natural logarithm of the proton-to-electron mass ratio is approximately 7.5 and consequently, the $\mathcal{F}$ calibrated on the proton will be shifted by 7.5 logarithmic units relative to the $\mathcal{F}$ calibrated on the electron. Figure 8 demonstrates this situation in the canonical projection.

As a consequence, all integer logarithms ($n_{j1} = \infty$) of the proton $\mathcal{F}$ correspond to half logarithms ($m_{j1} = \pm 2$) of the electron $\mathcal{F}$ and vice versa. In addition, the Diophantine equation (18) describes the correspondence of proton-calibrated subnodes $[n_{j0}; n_{j1}]$ with electron-calibrated subnodes $[m_{j0}; m_{j1}]$ on the first layer $k = 1$ of $\mathcal{F}$:

$$\frac{1}{n_{j1}} + \frac{1}{m_{j1}} = \frac{1}{2}\,. \qquad (16)$$

Only three pairs (n_{j1}, m_{j1}) of integers are solutions to this equation: (4, 4), (3, 6) and (6, 3). Figure 9 demonstrates this correspondence.

In fact, if a process property corresponds to a half logarithm ($m_{j1} = \pm 2$) of the electron calibrated $\mathcal{F}$ it also corresponds to an integer logarithm ($n_{j1} = \infty$) of the proton calibrated $\mathcal{F}$. Consequently, we must treat half logarithms and integer logarithms with equal (highest) priority. Furthermore, subnodes that satisfy the equation (16) are of high significance because the subnodes $m_{j1} = \pm 3$, $m_{j1} = \pm 4$ and $m_{j1} = \pm 6$ of the electron $\mathcal{F}$ coincide with the subnodes $n_{j1} = \pm 6$, $n_{j1} = \pm 4$ and $n_{j1} = \pm 3$ of the proton $\mathcal{F}$. It is likely that this correspondence amplifies the attractor effect of these subnodes.

As figure 10 shows, in the 2/3-projection, the electron-based $\mathcal{F}$ (above) fills the empty intervals $3l + 1 \leqslant S \leqslant 3l + 2$ ($l = 0, 1, 2, \dots$) in the proton-based $\mathcal{F}$ (below). Furthermore, in the intervals $3l + 1/2 \leqslant S \leqslant 3l + 1$ ($l = 0, 1, 2, \dots$) the proton $\mathcal{F}$ overlaps with the electron $\mathcal{F}$. In the 2/3-projection, the subnodes $[2, n_{j0}; 3, -6]$ and $[2, n_{j0}; -3, 6]$ in the logarithmic center of the overlapping area are the only nodes that are common to both the proton-based and electron-based $\mathcal{F}$.

In [23] we have applied the 2/3-projection on the Solar system. In the following, we will test our hypothesis of global scaling on the Solar system applying the canonical projection.

9 Applying Global Scaling on the Solar System

In 2010 we have shown [16] that the masses of large celestial bodies in the Solar system continue the scale-invariant sequence of fundamental particle rest masses (see table 1), corresponding with main attractor nodes of the fundamental fractal (1).

If we consider the Solar system as still evolving – at least in terms of small body collisions and matter exchanges with neighbouring systems – the expected attractor effect of nodes suggests applying $\mathcal{F}$ for the prediction of evolutionary trends.

Yet, the existence of stable orbits and large celestial bodies with stable rotation periods suggests testing our hypothesis of global scaling on the Solar system. Let us begin with the most noticeable examples.

The Sun

The current amount of the Solar mass supports our hypothesis of global scaling, because it corresponds to a main attractor node of the electron-calibrated $\mathcal{F}$ (8). In fact, the natural logarithm of the Sun-to-electron mass ratio is close to an integer number:

$$\ln\left(\frac{M_{\text{Sun}}}{m_{\text{electron}}}\right) = \ln\left(\frac{1.9884 \cdot 10^{30}\ \text{kg}}{9.10938356 \cdot 10^{-31}\ \text{kg}}\right) = 138.936.$$

Also, the Solar radius corresponds to a main attractor node of the electron $\mathcal{F}$ (10):

$$\ln\left(\frac{R_{\text{Sun}}}{\lambda_{\text{electron}}}\right) = \ln\left(\frac{6.96407 \cdot 10^{8}\ \text{m}}{3.8615926764 \cdot 10^{-13}\ \text{m}}\right) = 48.945.$$

The Solar sidereal rotation period is in between $\tau_{\min} = 24.5$ days at the equator and $\tau_{\max} = 34.4$ days at the poles. The canonical projection of the electron $\mathcal{F}$ (4) shows that the Solar rotation period varies between the main attractor node $[63; \infty]$ and its nearest significant subnode $[63; -3]$:

$$\ln\left(\frac{\tau_{\max}}{\tau_{\text{electron}}}\right) = \ln\left(\frac{34.4 \cdot 86164\ \text{s}}{1.28808867 \cdot 10^{-21}\ \text{s}}\right) = 63.003\,,$$

$$\ln\left(\frac{\tau_{\min}}{\tau_{\text{electron}}}\right) = \ln\left(\frac{24.5 \cdot 86164\ \text{s}}{1.28808867 \cdot 10^{-21}\ \text{s}}\right) = 62.664\,.$$

Jupiter

Let's start with Jupiter's body mass:

$$\ln\left(\frac{M_{\text{Jupiter}}}{m_{\text{electron}}}\right) = \ln\left(\frac{1.8986 \cdot 10^{27}\ \text{kg}}{9.10938356 \cdot 10^{-31}\ \text{kg}}\right) = 131.981$$

we can see that the Jupiter body mass corresponds to the main attractor node $[132; \infty]$ of the electron $\mathcal{F}$ (8) and within our model, the body mass of Jupiter M_{Jupiter} can be calculated from the Solar Mass M_{Sun}, by simply dividing it seven times by the Euler number $e = 2.71828\ldots$:

$$M_{\text{Jupiter}} = \frac{M_{\text{Sun}}}{\exp(7)}\,. \tag{17}$$

Jupiter's body radius corresponds to the significant subnode $[47; -3]$ of the electron $\mathcal{F}$ (10):

$$\ln\left(\frac{R_{\text{Jupiter}}}{\lambda_{\text{electron}}}\right) = \ln\left(\frac{7.1492 \cdot 10^{7}\ \text{m}}{3.8615926764 \cdot 10^{-13}\ \text{m}}\right) = 46.668\,.$$

The sidereal rotation period of Jupiter is 9.925 hours and corresponds with the main attractor node $[66; \infty]$ of the proton $\mathcal{F}$ (4):

$$\ln\left(\frac{\tau_{\text{Jupiter}}}{\tau_{\text{proton}}}\right) = \ln\left(\frac{9.925 \cdot 3600\ s}{7.01515 \cdot 10^{-25}\ s}\right) = 66.100\,.$$

In contrast to rotation as angular movement, the location of a celestial body in the Solar system in orbital movement changes permanently. Furthermore, in the case of non-zero eccentricity, the angular velocity of orbital movement is not constant. Therefore, we expect that the orbital periods coincide with attractor nodes of the $\mathcal{F}$ (4) with the electron oscillation period $2\pi\tau_e$ as the fundamental. For example, Jupiter's orbital period of 4332.59 days fulfils the conditions of global scaling very precisely:

$$\ln\left(\frac{T_{\text{Jupiter}}}{2\pi\tau_{\text{electron}}}\right) = \ln\left(\frac{4332.59 \cdot 86164\ \text{s}}{8.0932998 \cdot 10^{-21}\ \text{s}}\right) = 66.001.$$

When the logarithm of the sidereal rotation period of Jupiter slows down to $[66; \infty]$, the orbital-to-rotation period ratio of Jupiter can be described by the equation:

$$\frac{T_{\text{Jupiter}}}{\tau_{\text{Jupiter}}} = 2\pi\frac{\tau_{\text{electron}}}{\tau_{\text{proton}}}\,. \tag{18}$$

The orbital velocity of Jupiter is between $v_{\min} = 12.44$ and $v_{\max} = 13.72$ km/s. This velocity clearly approximates the main attractor node $[-10; \infty]$ of the $\mathcal{F}$ calibrated on the speed of light (12):

$$\ln\left(\frac{v_{\max}}{c}\right) = \ln\left(\frac{13720\ \text{m/s}}{299792458\ \text{m/s}}\right) = -9.992,$$

$$\ln\left(\frac{v_{\min}}{c}\right) = \ln\left(\frac{12440\ \text{m/s}}{299792458\ \text{m/s}}\right) = -10.090.$$

Consequently, the orbital distance of Jupiter between Perihelion = 4.95029 and Aphelion = 5.45492 astronomical units approximates the main attractor node $[56; \infty]$ of the electron-calibrated $\mathcal{F}$ (10):

$$\ln\left(\frac{A_{\text{Jupiter}}}{\lambda_{\text{electron}}}\right) = \ln\left(\frac{5.45492 \cdot 149597870700\ \text{m}}{3.8615926764 \cdot 10^{-13}\ \text{m}}\right) = 56.011,$$

$$\ln\left(\frac{P_{\text{Jupiter}}}{\lambda_{\text{electron}}}\right) = \ln\left(\frac{4.95029 \cdot 149597870700\ \text{m}}{3.8615926764 \cdot 10^{-13}\ \text{m}}\right) = 55.914.$$

By the way, the masses of Jupiter's largest moons fulfil the condition of global scaling as well. For example, the body

mass of Ganymede fits perfectly with the main node $[115; \infty]$ of the proton $\mathcal{F}$ (8):

$$\ln\left(\frac{M_{\text{Ganymede}}}{m_{\text{proton}}}\right) = \ln\left(\frac{1.4819 \cdot 10^{23}\ \text{kg}}{1.672621 \cdot 10^{-27}\ \text{kg}}\right) = 115.009.$$

On the other hand, the body mass of Io corresponds with the significant subnode [114; 2]:

$$\ln\left(\frac{M_{\text{Io}}}{m_{\text{proton}}}\right) = \ln\left(\frac{8.9319 \cdot 10^{22}\ \text{kg}}{1.672621 \cdot 10^{-27}\ \text{kg}}\right) = 114.502.$$

Venus

The morning star is another impressive example of global scaling. Like the Sun or Jupiter, the body mass of Venus corresponds to a main attractor node of the electron $\mathcal{F}$ (8):

$$\ln\left(\frac{M_{\text{Venus}}}{m_{\text{electron}}}\right) = \ln\left(\frac{4.8675 \cdot 10^{24}\ \text{kg}}{9.10938356 \cdot 10^{-31}\ \text{kg}}\right) = 126.015.$$

Although the rotation of Venus is reverse, its rotation period of 5816.66728 hours fits perfectly with the main attractor node $[65; \infty]$ of the electron calibrated $\mathcal{F}$ (4):

$$\ln\left(\frac{\tau_{\text{Venus}}}{\tau_{\text{electron}}}\right) = \ln\left(\frac{5816.66728 \cdot 3600\ \text{s}}{1.28808867 \cdot 10^{-21}\ \text{s}}\right) = 64.958.$$

The sidereal orbital period of Venus of 224.701 days fulfils the condition of global scaling as well:

$$\ln\left(\frac{T_{\text{Venus}}}{2\pi\tau_{\text{electron}}}\right) = \ln\left(\frac{224.701 \cdot 86164\ \text{s}}{2\pi \cdot 1.28808867 \cdot 10^{-21}\ \text{s}}\right) = 63.042.$$

The orbital velocity of Venus ($v_{\min} = 34.79$ and $v_{\max} = 35.26$ km/s) corresponds well to the main attractor node $[-9; \infty]$ of the speed of light calibrated $\mathcal{F}$ (12):

$$\ln\left(\frac{v_{\max}}{c}\right) = \ln\left(\frac{35260\ \text{m/s}}{299792458\ \text{m/s}}\right) = -9.048,$$

$$\ln\left(\frac{v_{\min}}{c}\right) = \ln\left(\frac{34790\ \text{m/s}}{299792458\ \text{m/s}}\right) = -9.062.$$

The orbital distance of Venus (Perihelion=0.71844 and Aphelion = 0.728213 astronomical units) corresponds precisely to the main attractor node $[54; \infty]$ of the electron calibrated $\mathcal{F}$ (10):

$$\ln\left(\frac{A_{\text{Venus}}}{\lambda_{\text{electron}}}\right) = \ln\left(\frac{0.728213 \cdot 149597870700\ \text{m}}{3.8615926764 \cdot 10^{-13}\ \text{m}}\right) = 53.997,$$

$$\ln\left(\frac{P_{\text{Venus}}}{\lambda_{\text{electron}}}\right) = \ln\left(\frac{0.718440 \cdot 149597870700\ \text{m}}{3.8615926764 \cdot 10^{-13}\ \text{m}}\right) = 53.984.$$

The current body radius of Venus corresponds with the subnode [44; 5] of the electron $\mathcal{F}$ (10):

$$\ln\left(\frac{R_{\text{Venus}}}{\lambda_{\text{electron}}}\right) = \ln\left(\frac{6.053 \cdot 10^{6}\ \text{m}}{3.8615926764 \cdot 10^{-13}\ \text{m}}\right) = 44.199.$$

However, its vicinity to the significant subnode [44; 4] gives reason to expect that Venus is still growing.

Mars

Again, the body mass of Mars corresponds to a main attractor node of the electron $\mathcal{F}$ (8):

$$\ln\left(\frac{M_{\text{Mars}}}{m_{\text{electron}}}\right) = \ln\left(\frac{6.4171 \cdot 10^{23}\ \text{kg}}{9.10938356 \cdot 10^{-31}\ \text{kg}}\right) = 123.989.$$

The sidereal rotation period of Mars is 24.62278 hours and coincides perfectly to the main node $[67; \infty]$ of the proton $\mathcal{F}$ (4):

$$\ln\left(\frac{\tau_{\text{Mars}}}{\tau_{\text{proton}}}\right) = \ln\left(\frac{24.62278 \cdot 3600\ \text{s}}{7.01515 \cdot 10^{-25}\ \text{s}}\right) = 67.008.$$

The orbital velocity of Mars is between 21.97 and 26.50 km/s, approximating the subnode $[-9; -2]$ of the speed of light calibrated $\mathcal{F}$ (12):

$$\ln\left(\frac{v_{\max}}{c}\right) = \ln\left(\frac{26500\ \text{m/s}}{299792458\ \text{m/s}}\right) = -9.334,$$

$$\ln\left(\frac{v_{\min}}{c}\right) = \ln\left(\frac{21970\ \text{m/s}}{299792458\ \text{m/s}}\right) = -9.521.$$

In addition, the orbital period of Mars 686.971 days meets precisely the condition of global scaling:

$$\ln\left(\frac{T_{\text{Mars}}}{2\pi\tau_{\text{electron}}}\right) = \ln\left(\frac{686.971 \cdot 86164\ \text{s}}{2\pi \cdot 1.28808867 \cdot 10^{-21}\ \text{s}}\right) = 65.997.$$

The orbital distance of Mars (Perihelion = 1.3814 and Aphelion = 1.6660 astronomical units) approximates the significant subnode [55; −4] of the electron $\mathcal{F}$ (10):

$$\ln\left(\frac{A_{\text{Mars}}}{\lambda_{\text{electron}}}\right) = \ln\left(\frac{1.6660 \cdot 149597870700\ \text{m}}{3.8615926764 \cdot 10^{-13}\ \text{m}}\right) = 54.825,$$

$$\ln\left(\frac{P_{\text{Mars}}}{\lambda_{\text{electron}}}\right) = \ln\left(\frac{1.3814 \cdot 149597870700\ \text{m}}{3.8615926764 \cdot 10^{-13}\ \text{m}}\right) = 54.637.$$

The current body radius of Mars is close to the significant subnode [44; −3] of the $\mathcal{F}$ (10):

$$\ln\left(\frac{R_{\text{Mars}}}{\lambda_{\text{electron}}}\right) = \ln\left(\frac{3.396 \cdot 10^{6}\ \text{m}}{3.8615926764 \cdot 10^{-13}\ \text{m}}\right) = 43.621.$$

It is therefore likely that Mars, too, is still growing. From this point of view, the large Martian canyon (Valles Marineris) can be interpreted as a sign of crustal swelling [28].

Earth

The current mass of the Earth corresponds to the significant subnode [126; 4] of the electron $\mathcal{F}$ (8):

$$\ln\left(\frac{M_{\text{Earth}}}{m_{\text{electron}}}\right) = \ln\left(\frac{5.97237 \cdot 10^{24}\ \text{kg}}{9.10938356 \cdot 10^{-31}\ \text{kg}}\right) = 126.220.$$

Hence, we can expect that the Earth is slightly increasing its mass.

The body radius of the Earth approximates precisely the significant subnode [44; 4] of the electron $\mathcal{F}$ (10):

$$\ln\left(\frac{R_{\text{Earth equator}}}{\lambda_{\text{electron}}}\right) = \ln\left(\frac{6.378 \cdot 10^3 \text{ m}}{3.8615926764 \cdot 10^{-13} \text{ m}}\right) = 44.251,$$

$$\ln\left(\frac{R_{\text{Earth pole}}}{\lambda_{\text{electron}}}\right) = \ln\left(\frac{6.357 \cdot 10^3 \text{ m}}{3.8615926764 \cdot 10^{-13} \text{ m}}\right) = 44.248.$$

The sidereal rotation period of the Earth is 23.93444 hours and is located very close to the main node [67; ∞] in the proton $\mathcal{F}$ (4):

$$\ln\left(\frac{\tau_{\text{Earth}}}{\tau_{\text{proton}}}\right) = \ln\left(\frac{23.93444 \cdot 3600 \text{ s}}{7.01515 \cdot 10^{-25} \text{ s}}\right) = 66.980,$$

Therefore, we can expect that the rotation period of the Earth is also slightly increasing. Empirical studies [29] confirm the correlation between body mass and rotation period.

Earth's orbital period of 365.256363 days is close to the main attractor node [71] of the proton-based $\mathcal{F}$ (4):

$$\ln\left(\frac{T_{\text{Earth}}}{2\pi\tau_{\text{proton}}}\right) = \ln\left(\frac{365.256363 \cdot 86164 \text{ s}}{2\pi \cdot 7.01515 \cdot 10^{-25} \text{ s}}\right) = 71.043.$$

Earth's orbital velocity is between $v_{\min} = 29.29$ and $v_{\max} = 30.29$ km/s, approximating the significant subnode [−9; 4] of the speed of light-based $\mathcal{F}$ (12):

$$\ln\left(\frac{v_{\max}}{c}\right) = \ln\left(\frac{30290 \text{ m/s}}{299792458 \text{ m/s}}\right) = -9.200,$$

$$\ln\left(\frac{v_{\min}}{c}\right) = \ln\left(\frac{29290 \text{ m/s}}{299792458 \text{ m/s}}\right) = -9.234,$$

The orbital distance of the Earth (Perihelion = 0.9832687 and Aphelion = 1.01673 astronomical units) corresponds to the significant subnode [54; 3] of the electron-based $\mathcal{F}$ (10):

$$\ln\left(\frac{A_{\text{Earth}}}{\lambda_{\text{electron}}}\right) = \ln\left(\frac{1.0167300 \cdot 149597870700 \text{ m}}{3.8615926764 \cdot 10^{-13} \text{ m}}\right) = 54.331,$$

$$\ln\left(\frac{P_{\text{Earth}}}{\lambda_{\text{electron}}}\right) = \ln\left(\frac{0.9832687 \cdot 149597870700 \text{ m}}{3.8615926764 \cdot 10^{-13} \text{ m}}\right) = 54.297.$$

Mercury

Mercury's body mass is close to the significant subnode [123; 3] of the electron $\mathcal{F}$ (8):

$$\ln\left(\frac{M_{\text{Mercury}}}{m_{\text{electron}}}\right) = \ln\left(\frac{3.3011 \cdot 10^{23} \text{ kg}}{9.10938356 \cdot 10^{-31} \text{ kg}}\right) = 123.324.$$

Its body radius is close to the significant subnode [43; 3] of the electron $\mathcal{F}$ (10):

$$\ln\left(\frac{R_{\text{Mercury}}}{\lambda_{\text{electron}}}\right) = \ln\left(\frac{2.44 \cdot 10^3 \text{ m}}{3.8615926764 \cdot 10^{-13} \text{ m}}\right) = 43.290.$$

So we can expect that Mercury is slightly increasing its mass and size. The sidereal rotation period of Mercury is 1407.5 hours and corresponds to the main attractor node [71; ∞] of the proton $\mathcal{F}$ (4):

$$\ln\left(\frac{\tau_{\text{Mercury}}}{\tau_{\text{proton}}}\right) = \ln\left(\frac{1407.5 \cdot 3600 \text{ s}}{7.01515 \cdot 10^{-25} \text{ s}}\right) = 71.054.$$

The sidereal orbital period of Mercury of 87.9691 days is close to the main attractor node [62; ∞] of the electron $\mathcal{F}$ (4):

$$\ln\left(\frac{T_{\text{Mercury}}}{2\pi\tau_{\text{electron}}}\right) = \ln\left(\frac{87.9691 \cdot 86164 \text{ s}}{2\pi \cdot 1.28808867 \cdot 10^{-21} \text{ s}}\right) = 62.104.$$

The orbital velocity of Mercury oscillates between the main attractor node [−9; ∞] and the significant subnode [−9; 2] of the speed of light calibrated $\mathcal{F}$ (12):

$$\ln\left(\frac{v_{\max}}{c}\right) = \ln\left(\frac{58980 \text{ m/s}}{299792458 \text{ m/s}}\right) = -8.534,$$

$$\ln\left(\frac{v_{\min}}{c}\right) = \ln\left(\frac{38860 \text{ m/s}}{299792458 \text{ m/s}}\right) = -8.951.$$

Mercury's Aphelion corresponds to the main attractor node [61; ∞] of the proton calibrated $\mathcal{F}$ (10):

$$\ln\left(\frac{A_{\text{Mercury}}}{\lambda_{\text{proton}}}\right) = \ln\left(\frac{0.466697 \cdot 149597870700 \text{ m}}{2.1030891 \cdot 10^{-16} \text{ m}}\right) = 61.067.$$

Saturn

Saturn's body mass is close to the significant subnode [131; −4] of the electron calibrated $\mathcal{F}$ (8),

$$\ln\left(\frac{M_{\text{Saturn}}}{m_{\text{electron}}}\right) = \ln\left(\frac{5.6836 \cdot 10^{23} \text{ kg}}{9.10938356 \cdot 10^{-31} \text{ kg}}\right) = 130.776$$

so we suspect that Saturn is actually losing mass and that its ring system is part of the loss process.

The sidereal rotation period of Saturn is 10.55 hours and corresponds to the significant subnode [59; −3] of the electron $\mathcal{F}$ (4):

$$\ln\left(\frac{\tau_{\text{Saturn}}}{\tau_{\text{electron}}}\right) = \ln\left(\frac{10.55 \cdot 3600 \text{ s}}{1.28808867 \cdot 10^{-21} \text{ s}}\right) = 58.646.$$

Therefore, we may expect that Saturn is slightly slowing down its rotation. The orbital period of Saturn of 10759.22 days corresponds to the main attractor node [67; ∞] of the electron $\mathcal{F}$ (4):

$$\ln\left(\frac{T_{\text{Saturn}}}{2\pi\tau_{\text{electron}}}\right) = \ln\left(\frac{10759.22 \cdot 86164 \text{ s}}{2\pi \cdot 1.28808867 \cdot 10^{-21} \text{ s}}\right) = 66.911.$$

Therefore, we may predict that Saturn is slightly increasing its orbit.

The current orbital velocity of Saturn is between 9.09 and 10.18 km/s, approximating the significant subnode $[-10; 3]$ of the speed of light calibrated $\mathcal{F}$ (12):

$$\ln\left(\frac{v_{\max}}{c}\right) = \ln\left(\frac{10180\ \text{m/s}}{299792458\ \text{m/s}}\right) = -10.290,$$

$$\ln\left(\frac{v_{\min}}{c}\right) = \ln\left(\frac{9090\ \text{m/s}}{299792458\ \text{m/s}}\right) = -10.404.$$

The orbital distance of Saturn is between Perihelion = 9.024 and Aphelion=10.086 astronomical units, oscillating between the significant subnodes $[57; -2]$ and $[57; -3]$ of the electron $\mathcal{F}$ (10):

$$\ln\left(\frac{A_{\text{Saturn}}}{\lambda_{\text{electron}}}\right) = \ln\left(\frac{10.086 \cdot 149597870700\ \text{m}}{3.8615926764 \cdot 10^{-13}\ \text{m}}\right) = 56.625,$$

$$\ln\left(\frac{P_{\text{Saturn}}}{\lambda_{\text{electron}}}\right) = \ln\left(\frac{9.024 \cdot 149597870700\ \text{m}}{3.8615926764 \cdot 10^{-13}\ \text{m}}\right) = 56.514.$$

Saturn's equatorial body radius is very close to the significant subnode $[46; 2]$ of the electron $\mathcal{F}$ (10):

$$\ln\left(\frac{R_{\text{Saturn}}}{\lambda_{\text{electron}}}\right) = \ln\left(\frac{6.0268 \cdot 10^{7}\ \text{m}}{3.8615926764 \cdot 10^{-13}\ \text{m}}\right) = 46.497$$

and consequently, to the main attractor node $[54; \infty]$ of the proton $\mathcal{F}$ (10) as well:

$$\ln\left(\frac{R_{\text{Saturn}}}{\lambda_{\text{proton}}}\right) = \ln\left(\frac{6.0268 \cdot 10^{7}\ \text{m}}{2.1030891 \cdot 10^{-16}\ \text{m}}\right) = 54.012.$$

Furthermore, Titan's body mass is near the main node $[115; \infty]$ of the proton $\mathcal{F}$ (8):

$$\ln\left(\frac{M_{\text{Titan}}}{m_{\text{proton}}}\right) = \ln\left(\frac{1.3452 \cdot 10^{23}\ \text{kg}}{1.672621 \cdot 10^{-27}\ \text{kg}}\right) = 114.912.$$

Uranus

To reach the nearby main attractor node $[129; \infty]$ of the electron-based $\mathcal{F}$ (8), Uranus must increase its body mass by approx. 1/10 logarithmic units:

$$\ln\left(\frac{M_{\text{Uranus}}}{m_{\text{electron}}}\right) = \ln\left(\frac{8.681 \cdot 10^{25}\ \text{kg}}{9.10938356 \cdot 10^{-31}\ \text{kg}}\right) = 128.897.$$

The orbital period of Uranus of 30688.5 days corresponds to the main attractor node $[68; \infty]$ of the electron-based $\mathcal{F}$ (4):

$$\ln\left(\frac{T_{\text{Uranus}}}{2\pi\tau_{\text{electron}}}\right) = \ln\left(\frac{30688.5 \cdot 86164\ \text{s}}{2\pi \cdot 1.28808867 \cdot 10^{-21}\ \text{s}}\right) = 67.959,$$

Like Neptune, the body radius of Uranus is close to the significant subnode $[46; -3]$ of the electron $\mathcal{F}$ (10):

$$\ln\left(\frac{R_{\text{Uranus}}}{\lambda_{\text{electron}}}\right) = \ln\left(\frac{2.5559 \cdot 10^{7}\ \text{m}}{3.8615926764 \cdot 10^{-13}\ \text{m}}\right) = 45.639.$$

We may therefore expect that Uranus, like Neptune, is slightly swelling.

The orbital distance of Uranus (Perihelion = 18.33 and Aphelion = 20.11 astronomical units) approximates the significant subnode $[57; 4]$ of the electron $\mathcal{F}$ (10):

$$\ln\left(\frac{A_{\text{Uranus}}}{\lambda_{\text{electron}}}\right) = \ln\left(\frac{20.11 \cdot 149597870700\ \text{m}}{3.8615926764 \cdot 10^{-13}\ \text{m}}\right) = 57.315,$$

$$\ln\left(\frac{P_{\text{Uranus}}}{\lambda_{\text{electron}}}\right) = \ln\left(\frac{18.33 \cdot 149597870700\ \text{m}}{3.8615926764 \cdot 10^{-13}\ \text{m}}\right) = 57.223.$$

The orbital velocity of Uranus is between 6.49 and 7.11 km/s, approximating the significant subnode $[-11; 3]$ of the speed of light calibrated $\mathcal{F}$ (12):

$$\ln\left(\frac{v_{\max}}{c}\right) = \ln\left(\frac{7110\ \text{m/s}}{299792458\ \text{m/s}}\right) = -10.741,$$

$$\ln\left(\frac{v_{\min}}{c}\right) = \ln\left(\frac{6490\ \text{m/s}}{299792458\ \text{m/s}}\right) = -10.649.$$

The sidereal rotation period of Uranus is 17.24 hours and corresponds to the significant subnode $[67; -3]$ of the proton $\mathcal{F}$ (4):

$$\ln\left(\frac{\tau_{\text{Uranus}}}{\tau_{\text{proton}}}\right) = \ln\left(\frac{17.24 \cdot 3600\ \text{s}}{7.01515 \cdot 10^{-25}\ \text{s}}\right) = 66.652.$$

Therefore,we can expect that Uranus is slightly slowing down its rotation.

Neptune

Neptune's body mass corresponds to the main attractor node $[129; \infty]$ of the electron calibrated $\mathcal{F}$ (8):

$$\ln\left(\frac{M_{\text{Neptune}}}{m_{\text{electron}}}\right) = \ln\left(\frac{1.0243 \cdot 10^{26}\ \text{kg}}{9.10938356 \cdot 10^{-31}\ \text{kg}}\right) = 129.062.$$

The sidereal rotation period of Neptune is 16.11 hours and coincides perfectly with the main attractor node $[59; \infty]$ of the electron-calibrated $\mathcal{F}$ (4):

$$\ln\left(\frac{\tau_{\text{Neptune}}}{\tau_{\text{electron}}}\right) = \ln\left(\frac{16.11 \cdot 3600\ \text{s}}{1.28808867 \cdot 10^{-21}\ \text{s}}\right) = 59.069.$$

The orbital velocity of Neptune is between 5.37 and 5.50 km/s, close to the main node $[-11; \infty]$ of the speed of light calibrated $\mathcal{F}$ (12):

$$\ln\left(\frac{v_{\max}}{c}\right) = \ln\left(\frac{5500\ \text{m/s}}{299792458\ \text{m/s}}\right) = -10.930,$$

$$\ln\left(\frac{v_{\min}}{c}\right) = \ln\left(\frac{5370\ \text{m/s}}{299792458\ \text{m/s}}\right) = -10.906.$$

Neptune's current orbital distance (Perihelion = 29.81 and Aphelion = 30.33 astronomical units) corresponds to the significant subnode [58; −4] of the electron-calibrated $\mathcal{F}$ (10):

$$\ln\left(\frac{A_{\text{Neptune}}}{\lambda_{\text{electron}}}\right) = \ln\left(\frac{30.33 \cdot 149597870700\ \text{m}}{3.8615926764 \cdot 10^{-13}\ \text{m}}\right) = 57.726,$$

$$\ln\left(\frac{P_{\text{Neptune}}}{\lambda_{\text{electron}}}\right) = \ln\left(\frac{29.81 \cdot 149597870700\ \text{m}}{3.8615926764 \cdot 10^{-13}\ \text{m}}\right) = 57.709.$$

Because of the assumed attractor effect of the main node [−11; ∞] of the $\mathcal{F}$ (12), we can expect that the logarithm of Neptune's orbital velocity should decrease by nearly 1/10. At the same time, the logarithm of Neptune's orbital distance should increase by almost 1/20 due to the attractor effect of the significant subnode [58; −4] of the $\mathcal{F}$ (10). This trend forecast agrees with the Kepler laws: for circular Solar orbits, the orbital velocity of a planet changes with the square root of its orbital distance.

In addition, Neptune's orbital period of 60182 days is close to the significant subnode [69; −3] of the electron $\mathcal{F}$ (4):

$$\ln\left(\frac{T_{\text{Neptune}}}{2\pi\tau_{\text{electron}}}\right) = \ln\left(\frac{60182 \cdot 86164\ \text{s}}{2\pi \cdot 1.28808867 \cdot 10^{-21}\ \text{s}}\right) = 68.632.$$

This value supports our trend estimation that Neptune's orbit is slightly growing.

The current body radius of Neptune is close to the significant subnode [46; −3] of $\mathcal{F}$ (10):

$$\ln\left(\frac{R_{\text{Neptune}}}{\lambda_{\text{electron}}}\right) = \ln\left(\frac{2.4764 \cdot 10^{7}\ \text{m}}{3.8615926764 \cdot 10^{-13}\ \text{m}}\right) = 45.607.$$

And so, we can expect that Neptune is still swelling.

Pluto

Although Pluto is no longer considered a planet, its body mass corresponds well with the main attractor node [120; ∞] of the electron $\mathcal{F}$ (8):

$$\ln\left(\frac{M_{\text{Pluto}}}{m_{\text{electron}}}\right) = \ln\left(\frac{1.305 \cdot 10^{22}\ \text{kg}}{9.10938356 \cdot 10^{-31}\ \text{kg}}\right) = 120.094.$$

The orbital period of Pluto of 90560 days corresponds to the main attractor node [69; ∞] of the electron $\mathcal{F}$ (4):

$$\ln\left(\frac{T_{\text{Pluto}}}{2\pi\tau_{\text{electron}}}\right) = \ln\left(\frac{90560 \cdot 86164\ \text{s}}{2\pi \cdot 1.28808867 \cdot 10^{-21}\ \text{s}}\right) = 69.044.$$

The sidereal rotation period of Pluto is 152.87496 hours and corresponds to the significant subnode [61; 3] of the electron-calibrated $\mathcal{F}$ (4):

$$\ln\left(\frac{\tau_{\text{Pluto}}}{\tau_{\text{electron}}}\right) = \ln\left(\frac{152.87496 \cdot 3600\ \text{s}}{1.28808867 \cdot 10^{-21}\ \text{s}}\right) = 61.319.$$

Therefore, we can expect that Pluto is slightly slowing down in its rotation.

The orbital velocity of Pluto oscillates between 3.71 and 6.10 km/s, approximating the main attractor node [−11; ∞] of the speed of light calibrated $\mathcal{F}$ (12):

$$\ln\left(\frac{v_{\max}}{c}\right) = \ln\left(\frac{6100\ \text{m/s}}{299792458\ \text{m/s}}\right) = -10.803,$$

$$\ln\left(\frac{v_{\min}}{c}\right) = \ln\left(\frac{3710\ \text{m/s}}{299792458\ \text{m/s}}\right) = -11.300.$$

The orbital distance of Pluto (Perihelion = 29.656 and Aphelion = 49.319 astronomical units) approximates the main attractor node [58; ∞] of the electron-calibrated $\mathcal{F}$ (10):

$$\ln\left(\frac{A_{\text{Pluto}}}{\lambda_{\text{electron}}}\right) = \ln\left(\frac{49.319 \cdot 149597870700\ \text{m}}{3.8615926764 \cdot 10^{-13}\ \text{m}}\right) = 58.212,$$

$$\ln\left(\frac{P_{\text{Pluto}}}{\lambda_{\text{electron}}}\right) = \ln\left(\frac{29.656 \cdot 149597870700\ \text{m}}{3.8615926764 \cdot 10^{-13}\ \text{m}}\right) = 57.704.$$

The body radius of Pluto 1187 ± 7 km is close to the significant subnode [42; 2] of the electron-calibrated $\mathcal{F}$ (10),

$$\ln\left(\frac{R_{\text{Pluto}}}{\lambda_{\text{electron}}}\right) = \ln\left(\frac{1187 \cdot 10^{6}\ \text{m}}{3.8615926764 \cdot 10^{-13}\ \text{m}}\right) = 42.570,$$

which is also close to the main attractor node [50; ∞] of the proton-calibrated $\mathcal{F}$ (10):

$$\ln\left(\frac{R_{\text{Pluto}}}{\lambda_{\text{proton}}}\right) = \ln\left(\frac{1187 \cdot 10^{6}\ \text{m}}{2.1030891 \cdot 10^{-16}\ \text{m}}\right) = 50.085.$$

Hence, we can expect that Pluto is slightly shrinking. This prognosis matches with new findings of surface-atmosphere interactions and mass wasting processes [30] on Pluto.

By the way, also Charon's body mass fits with the main node [118; ∞] of the electron $\mathcal{F}$ (8):

$$\ln\left(\frac{M_{\text{Charon}}}{m_{\text{electron}}}\right) = \ln\left(\frac{1.587 \cdot 10^{21}\ \text{kg}}{9.10938356 \cdot 10^{-31}\ \text{kg}}\right) = 117.944.$$

In conclusion, table 3 gives an overview of the current positions in the electron calibrated $\mathcal{F}$ (4), (8), (10), and (12) of the Sun and the planets (including Pluto) regarding their masses, sizes, rotation, orbital distances, periods and velocities.

Table 3 shows that our model (1) allows to see a connection between the stability of the Solar system and the stability of electron and proton. Jupiter, Neptune, Venus and Pluto occupy mostly main attractor nodes of the electron calibrated fundamental fractal $\mathcal{F}$ and therefore they can be understood as electron determined factors of stability in the Solar system. It is interesting that also the Sun occupies main nodes of the electron $\mathcal{F}$. Considering the coincidence of half logarithms in the electron $\mathcal{F}$ with integer logarithms (main attractor nodes) of the proton $\mathcal{F}$, the stability of Earth's rotation and orbit seems connected with the stability of the proton. Furthermore, Earth's mass and radius occupy the subnode $n_1 = 4$ that is maximum distant from any main attractor node of the $\mathcal{F}$. This position could be connected with some optimum of flexibility, if we consider the main nodes as islands of stability.

Table 3: The current positions in the electron calibrated $\mathcal{F}$ (4), (8), (10) and (12) of the largest bodies regarding their masses, sizes, rotation, orbital distances, periods and velocities. In the cases of large eccentricity*, the logarithmically average position is indicated.

celestial body	mass in $\mathcal{F}$ (8)	radius in $\mathcal{F}$ (10)	rotation period in $\mathcal{F}$ (4)	orbital period in in $\mathcal{F}$ (4)	orbital distance in $\mathcal{F}$ (10)	orbital velocity in $\mathcal{F}$ (12)
Sun	[139; ∞]	[49; ∞]	[63; ∞]			
Jupiter	[132; ∞]	[47; −3]	[58; 2]	[66; ∞]	[56; ∞]	[−10; ∞]
Saturn	[131;−4]	[46; 2]	[59; −3]	[67; ∞]	[56; 2]	[−10; −3]
Neptune	[129; ∞]	[46; -3]	[59; ∞]	[69; −3]	[58; −4]	[−11; ∞]
Uranus	[129; ∞]	[46; -3]	[59; 6]	[68; ∞]	[57; 4]	[−11; 3]
Earth	[126; 4]	[44; 4]	[59; 2]	[63; 2]	[54; 3]	[−9; −4]
Venus	[126; ∞]	[44; 4]	[65; ∞]	[63; ∞]	[54; ∞]	[-9; ∞]
Mars	[124; ∞]	[44; −3]	[59; 2]	[64; 6]	[55; −4]	[−9; −2]
Mercury	[123; 3]	[43; 3]	[63; 2]	[62; 6]	[53; 3]*	[−9; 3]*
Pluto	[120; ∞]	[42; 2]	[61; 3]	[69; ∞]	[58; ∞]*	[−11; ∞]*

Resume

Properties of fundamental particles, for example the proton-to-electron mass ratio or the vector boson-to-electron mass ratio (table 1), support our scale-invariant model (1) of eigenstates in chain systems of harmonic quantum oscillators and have allowed us to derive the proton rest mass from fundamental physical constants (14). In addition, the cosmic microwave background can be interpreted as an eigenstate of a chain system of oscillating protons (15).

In our scale-invariant model, physical properties of celestial bodies such as mass, size, rotation and orbital period can be understood as macroscopic quantized eigenstates of chain systems of oscillating protons and electrons. This understanding can be applied to evolutionary trend prognosis of the Solar system but may be of cosmological significance as well. Conceivably, the observable exponential expansion of the universe is a consequence of the scale-invariance of the fundamental fractal (1).

Acknowledgements

The author is grateful to Viktor Panchelyuga for valuable discussions and support.

Submitted on July 18, 2017

References

1. Barenblatt G. I. Scaling. Cambridge University Press, 2003.
2. Feynman R. P. Very High-Energy Collisions of Hadrons. *Phys. Rev. Lett.*, 1969, 23, 1415.
3. Kolombet V. Macroscopic fluctuations, masses of particles and discrete space-time. *Biofizika*, 1992, v. 36, 492–499 (in Russian).
4. Tatischeff B. Fractals and log-periodic corrections applied to masses and energy levels of several nuclei. arXiv:1107.1976v1 [physics.gen-ph] 11 Jul 2011.
5. Gutenberg B., Richter C. F., Seismicity of the Earth and Associated Phenomena, 2nd ed. Princeton, N.J., Princeton University Press, 1954.
6. Corral A. Universal local versus unified global scaling laws in the statistics of seismicity. arXiv:cond-mat/0402555 v1 23 Feb 2004.
7. Čislenko L. L. The Structure of the Fauna and Flora in connection with the sizes of the organisms. Moscow, 1981 (in Russian).
8. Schmidt-Nielsen K. Scaling. Why is the animal size so important? Cambridge University Press, 1984.
9. Zhirmunsky A. V., Kuzmin V. I. Critical levels in developmental processes of biological systems. Moscow, Nauka, 1982 (in Russian).
10. Shnoll S. E. Changes in the fine structure of stochastic distributions as a consequence of space-time fluctuations. arxiv.org/ftp/physics/papers/0602/0602017.
11. Müller H. Fractal Scaling Models of Resonant Oscillations in Chain Systems of Harmonic Oscillators. *Progress in Physics*, 2009, issue 2, 72–76.
12. Müller H. Fractal Scaling Models of Natural Oscillations in Chain Systems and the Mass Distribution of Particles. *Progress in Physics*, 2010, issue 3, 61–66.
13. Ries A. Bipolar Model of Oscillations in a Chain System for Elementary Particle Masses. *Progress in Physics*, 2012, issue 4, 20–28.
14. Ries A. Qualitative Prediction of Isotope Abundances with the Bipolar Model of Oscillations in a Chain System. *Progress in Physics*, 2015, issue 11, 183–186.
15. Müller H. Emergence of Particle Masses in Fractal Scaling Models of Matter. *Progress in Physics*, 2012, issue 4, 44–47.
16. Müller H. Fractal scaling models of natural oscillations in chain systems and the mass distribution of the celestial bodies in the Solar System. *Progress in Physics*, 2010, issue 3, 61–66.
    Müller H. Scaling of body masses and orbital periods in the Solar system as consequence of gravity interaction elasticity. Abstracts of the XII. International Conference on Gravitation, Astrophysics and Cosmology, dedicated to the centenary of Einstein's General Relativity theory. Moscow, PFUR, 2015.
17. Dombrowski K. I. Rational numbers distribution and resonance. *Progress in Physics*, 2005, v. 1, 65–67.
18. Panchelyuga V. A., Panchelyuga M. S. Resonance and Fractals on the Real Numbers Set. *Progress in Physics*, 2012, issue 4, 48–53.
19. Khintchine A. Ya. Continued fractions. University of Chicago Press, Chicago, 1964.
20. Skorobogatko V. Ya. The Theory of Branched Continued Fractions and mathematical Applications. Moscow, Nauka, 1983.
21. Hilbert D. Über die Transcendenz der Zahlen e und π. *Mathematische Annalen*, 1893, 43, 216–219.
22. Markov A. A. Selected work on the continued fraction theory and theory of functions which are minimum divergent from zero. Moscow – Leningrad, 1948 (In Russian).
23. Müller H. Scaling as Fundamental Property of Natural Oscillations and the Fractal Structure of Space-Time. Foundations of Physics and Geometry. Peoples Friendship University of Russia, 2008 (in Russian).
24. Olive K. A. et al. (Particle Data Group), *Chin. Phys. C.*, 2016, v. 38, 090001.
25. Steinberg R. I. et al. Experimental test of charge conservation and the stability of the electron. *Physical Review D*, 1999, 61 (2), 2582–2586.
26. Astrophysical constants. Particle Data Group, pdg.lbl.gov
27. Max Planck. Über Irreversible Strahlungsvorgänge. In: *Sitzungsbericht der Königlich Preußischen Akademie der Wissenschaften*, 1899, vol. 1, 479–480.
28. Lin An. Structural analysis of the Valles Marineris fault zone: Possible evidence for large-scale strike-slip faulting on Mars. *Lithosphere*, 2012, 4 (4), 286–330.
29. Gizachew Tiruneh. Explaining Planetary-Rotation Periods Using an Inductive Method. arXiv: 0906.3531 [astro-ph.SR]
30. Stern S. A. et al. The Pluto system: Initial results from its exploration by New Horizons. *Science*, 2015, 350 (6258), 249–352; arXiv:1510.07704.

Notes on Extended Lorentz Transformations for Superluminal Reference Frames

Yaroslav I. Grushka

Institute of Mathematics NAS of Ukraine. 3, Tereschenkivska st., Kyiv, 01601, Ukraine. E-mail: grushka@imath.kiev.ua

The present paper is devoted to the analysis of different versions of extended Lorentz transformations, proposed for reference frames moving with the velocity, greater then the velocity of light. In particular we point out some errors of individual authors in this field.

This work is connected with the theory of tachyon movement. Research in this direction were initiated in the papers [1, 2] more than 50 years ago. Then, in the papers of E. Recami, V. Olkhovsky and R. Goldoni [3–5], the *extended Lorentz transformations* for reference frames, moving with the velocity, greater then the velocity of light c were proposed. Latter the above extended Lorentz transformations were rediscovered in [6, 7]. The ideas of E. Recami, V. Olkhovsky and R. Goldoni are still relevant in our time. In particular B. Cox and J. Hill published in [7] a new and elegant way to deduce the formulas of E. Recami, V. Olkhovsky and R. Goldoni's extended Lorentz transformations. Also in paper [8] the extended Lorentz transformations are obtained for the case, where the space of geometrical coordinates may be any real Hilbert space of any dimension, including infinity. Application of the E. Recami, V. Olkhovsky and R. Goldoni's extended Lorentz transformations to the problem of spinless tachyon localization can be found in [9].

In the paper [10] author tries to obtain several variants of new extended superluminal Lorentz transformations, different from transforms obtained by E. Recami, V. Olkhovsky and R. Goldoni. It should be emphasized, that the paper [10], together with incorrect statements, contains also valuable new results. For example, nonlinear extended Lorentz transformations, proposed in [10], may be applied in the theory of kinematic changeable sets [11] for construction some interesting examples or counterexamples. Now we focus on errors, committed by the author of [10].

At first view, the coordinate transformations (3)–(4) and (9)–(10) from [10] look like as new. But, actually, the formulas (3)–(4) and (9)–(10) from [10] are some, not quite correct, representations for well-known classical Lorentz transformations. Hence, these transformations can not be coordinate transformations for reference frames moving with the superluminal velocity.

For example, let us analyze in details the transformations (3)–(4) from [10] for the case of one space dimension:

$$x' = \gamma(v)\,(x - vf(v)t) \tag{a}$$

$$t' = \gamma(v)\left(t - \frac{vf(v)x}{c^2}\right), \tag{b}$$

where (x, t) are the space-time coordinates of any point in the fixed reference frame $\mathfrak{l}$ and (x', t') are the space-time coordinates of this point in the moving frame $\mathfrak{l}'$.

According to [10], the function $f(v)$ may be any real function, satisfying the following conditions:

1. $f(v) > 0$, $v \in \mathbb{R}$ and $f(0) = 1$;
2. $f(v)$ is even (that is $f(-v) = f(v)$, $v \in \mathbb{R}$);

   The multiplier $\gamma(v)$ in (a)–(b) is connected with the function f by the formula,

$$\gamma(v) = \left(1 - \frac{v^2 f^2(v)}{c^2}\right)^{-1/2}.$$

   Thus, the following condition must be satisfied:
3. The transformations (a)–(b) are defined for such values $v \in \mathbb{R}$, for which the inequality $|v|\, f(v) < c$ is performed.

   In the paper [10], the parameter v is treated as the velocity of the moving reference frame $\mathfrak{l}'$. Thus, to include the subluminal diapason into the set of "allowed velocities", we may apply following condition:
4. $vf(v) < c$ for $0 < v < c$.

Note, that the condition 4 is not strictly necessary, and in the analysis of the transformations (a)–(b) we take into account only the conditions 1–3.

According to the paper [10], the parameter v in transformations (a)–(b) is the velocity of the moving reference frame $\mathfrak{l}'$. But now we are going to prove that the last statement is not true. For this purpose we calculate the inverse transform to (a)–(b), by means of solving the system (a)–(b) relatively the variables (x, t):

$$x = \gamma(v)\,(x' + vf(v)t') \tag{c}$$

$$t = \gamma(v)\left(t' + \frac{vf(v)x'}{c^2}\right). \tag{d}$$

The origin of the moving reference frame $\mathfrak{l}'$ at any fixed time point τ has the coordinates $(0, \tau)$ in the frame $\mathfrak{l}'$, and, according to the transformations (c)–(d), it has the coordinates $(\gamma(v)vf(v)\tau,\ \gamma(v)\tau)$ in the frame $\mathfrak{l}$. Consequently, the origin of the moving frame $\mathfrak{l}'$ will overpass the distance $\gamma(v)vf(v)\tau$ during the time interval $[\,0,\ \gamma(v)\tau\,]$ (where we select any $\tau \neq 0$). Hence, the velocity u of the moving reference frame $\mathfrak{l}'$ is equal to the following value:

$$u = \frac{\gamma(v)vf(v)\tau}{\gamma(v)\tau} = vf(v),$$

which is not v. Thus, the parameter v in (a)–(b) is expressed via the actual velocity u of the reference frame $\mathfrak{l}'$ by means of the formula, $v = \frac{u}{f(v)}$. And the substitution of the value $\frac{u}{f(v)}$ instead of v into transformations (a)–(b) leads to the classical Lorentz transformations.

Hence, we have seen, that *the formulas* (a)–(b) *(or the formulas* (3)–(4) *from* [10]*) are one of the representations for classical Lorentz transformations, and the actual velocity $u = vf(v)$ of the moving reference frame, according to the condition 3, can not exceed the velocity of light*.

Also, it should be noted, that the transformations (a)–(b) (or (3)–(4) from [10]) are preserving the Lorentz-Minkowski pseudo-metric:

$$\mathsf{M}_c(t, x) = x^2 - c^2t^2$$

in the Minkowski space-time over real axis $x \in \mathbb{R}$. But *any bijective linear operator in the Minkowski space-time, preserving the Lorentz-Minkowski pseudo-metric, belongs to the general Lorentz group* [12]*, and it can not be coordinate transform for superluminal reference frame*.

The coordinate transformations (9)–(10) from [10], according to the author requirements, also are preserving the Lorentz-Minkowski pseudo-metric in the Minkowski space-time over $\mathbb{R}^3$. Therefore *they also can not be coordinate transformations for superluminal reference frames*. And they can be analyzed in details by a similar way as the transformations (3)–(4) from [10].

Submitted on July 25, 2017

References

1. O.-M. P. Bilaniuk, V.K. Deshpande, E.C.G. Sudarshan. "Meta" Relativity. *American Journal of Physics*, 1962, v. 30 (10), 718–723.
2. O.-M. P. Bilaniuk, E.C.G. Sudarshan. Particles beyond the Light Barrier. *Physics Today*, 1969, v. 22 (5), 43–51.
3. E. Recami, V.S. Olkhovsky. About Lorentz transformations and tachyons. *Lettere al Nuovo Cimento*, 1971, v. 1 (4), 165–168.
4. E. Recami, R. Mignani. More about Lorentz transformations and tachyons. *Lettere al Nuovo Cimento*, 1972, v. 4 (4), 144–152.
5. R. Goldoni. Faster-than-light inertial frames, interacting tachyons and tadpoles. *Lettere al Nuovo Cimento*, 1972, v. 5 (6), 495–502.
6. S.Yu. Medvedev On the Possibility of Broadening Special Relativity Theory Beyond Light Barrier. *Uzhhorod University Scientific Herald. Ser. Phys*, 2005, no. 18, 7–15 (in Ukrainian).
7. James M. Hill, Barry J. Cox. Einstein's special relativity beyond the speed of light. *Proc. of the Royal Society A*, 2012, v. 468 (2148), 4174–4192.
8. Ya.I. Grushka. Tachyon Generalization for Lorentz Transforms. *Methods of Functional Analysis and Topology*, 2013, v. 20 (2), 127–145.
9. Michele Mantegna. Revisiting Barry Cox and James Hill's theory of superluminal motion: a possible solution to the problem of spinless tachyon localization. *Proc. of the Royal Society A*, 2015, v. 471 (2175), 20140541.
10. Dara Faroughy. Extended Linear and Nonlinear Lorentz Transformations and Superluminality. *Advances in High Energy Physics*, 2013, article ID 760916, 20 pages.
11. Grushka Ya.I. Existence criteria for universal coordinate transforms in kinematic changeable sets. *Bukovinian Mathematical Journal*, 2014, v. 2 (2-3), 59-71, (In Ukrainian, English translation is available at https://www.researchgate.net/publication/270647695).
12. M. A. Naimark, Linear Representations of the Lorentz Group. *International Series of Monographs in Pure and Applied Mathematics*, v. 63 (XIV), 1964.

On Time Dilation, Space Contraction, and the Question of Relativistic Mass

Pierre A. Millette

E-mail: PierreAMillette@alumni.uottawa.ca, Ottawa, Canada

In this paper, we revisit the question of relativistic mass to clarify the meaning of this concept within special relativity, and consider time dilation and length contraction in more detail. We see that "length contraction" is a misnomer and that it should really be named "space contraction" to avoid confusion, and demonstrate the complementary nature of time dilation and space contraction. We see that relativistic mass is dependent on the difference in velocity v between an object's proper frame of reference that is at rest with the object and the frame of reference from which it is observed. We show that the inertial mass of a body is its proper mass while the relativistic mass m^* is in effect an effective mass. We find that relativistic mass results from dealing with dynamic equations in local time t in a frame of reference moving with respect to the object of interest, instead of the invariant proper time τ in the frame of reference at rest with the object. The results obtained are in agreement with the Elastodynamics of the Spacetime Continuum.

1 Introduction

The concept of relativistic mass has been a part of special relativistic physics since it was first introduced by Einstein [1, 2] and explored by the early relativists (see for example [3, 4]). Other terminology is also used for relativistic mass, representing the users' perspective on the concept. For example, Aharoni [5] refers to it as the "relative mass", while Dixon [6] refers to it as "apparent mass". Oas [7] and Okun [10] provide good overviews on the development of the historical use of the concept of relativistic mass. Oas [8] has prepared a bibliography of published works where the concept is used and where it is ignored.

There is no consensus in the physics community on the validity and use of the concept of relativistic mass. Some consider relativistic mass to represent an actual increase in the inertial mass of a body [12]. However, there have been objections raised against this interpretation (see Taylor and Wheeler [14], Okun [9–11], Oas [7]). The situation seems to arise from confusion on the meaning of the special relativistic dynamics equations. In this paper, we revisit the question of relativistic mass to clarify the meaning of this concept within special relativity, in light of the Elastodynamics of the Spacetime Continuum (*STCED*) [18, 19].

2 Relativistic mass depends on the frame of reference

The relativistic mass m^* is given by

$$m^* = \gamma m_0 \,, \tag{1}$$

where

$$\gamma = \frac{1}{(1-\beta^2)^{1/2}} \,, \tag{2}$$

$\beta = v/c$ and m_0 is the rest-mass or proper mass which is an invariant. Some authors [11] suggest that rest-mass should be denoted as m as this is the real measure of inertial mass. The relativistic mass of an object corresponds to the total energy of an object (invariant proper mass plus kinetic energy). The first point to note is that the relativistic mass is the same as the proper mass in the frame of reference at rest with the object, *i.e.* $m^* = m_0$ for $v = 0$. In any other frame of reference in motion with velocity v with respect to the object, the relativistic mass will depend on v according to (1).

For example, when the relativistic mass of a cosmic ray particle is measured[†] in an earth lab, it depends on the speed of the particle measured with respect to the earth lab. Similarly for a particle in a particle accelerator, where its speed is measured with respect to the earth lab. The relativistic mass of the cosmic ray particle measured from say a space station in orbit around the earth or a spaceship in transit in space would depend on the speed of the particle measured with respect to the space station or the spaceship respectively.

We thus see that relativistic mass is an effect similar to length contraction and time dilation in that it is dependent on the difference in velocity v between the object's frame of reference and the frame of reference from which it is measured. Observers in different moving frames will measure different relativistic masses of an object as there is no absolute frame of reference with respect to which an object's speed can be measured.

3 Time dilation and space contraction

To further understand this conclusion, we need to look into time dilation and length contraction in more detail. These special relativistic concepts are often misunderstood by physicists. Many consider these changes to be actual physical changes, taking the Lorentz-Fitzgerald contraction and the time dilation effect to be real.

[†] what is measured is the energy of the particle, not its mass.

For example, John Bell in [15] relates the problem of the thread tied between two spaceships and whether the thread will break at relativistic speeds due to length contraction. He insists that it will – he relates how "[a] distinguished experimental physicist refused to accept that the thread would break, and regarded my assertion, that indeed it would, as a personal misinterpretation of special relativity". Bell appealed to the CERN Theory Division for arbitration, and was dismayed that a clear consensus agreed that the thread would not break, as indeed is correct. As the number of special relativistic "paradoxes" attest, many physicists, scientists and engineers have similar misunderstandings, not clearly understanding the concepts.

This situation arises due to not realizing that v is the difference in velocity between an object's frame of reference and the frame of reference from which it is measured, not an absolute velocity, as discussed in the previous section 2. In a nutshell, time dilation and length contraction are apparent effects. In the frame of reference at rest with an object that is moving at relativistic speeds with respect to another frame of reference, there is no length contraction or time dilation.

The proper time in the frame of reference at rest with the object is the physical time, and the length of the object in the frame of reference at rest with the object is the physical length – there is no time dilation or length contraction. These are observed in other frames of reference moving with respect to that object and are only apparent dilations or contractions perceived in those frames only. Indeed, observers in frames of reference moving at different speeds with respect to the object of interest will see *different* time dilations and length contractions. These cannot all be correct – hence time dilation and length contraction are apparent, not real.

This can be demonstrated to be the case from physical considerations, and in so doing, we clarify further the nature of length contraction. Petkov [13] provides graphically a physical explanation of time dilation and length contraction, based on Minkowski's 1908 paper [16] where the latter first introduced the concept of a four-dimensional spacetime and the description of particles in that spacetime as worldlines. Worldlines of particles at rest are vertical straight lines in a *space*−*ct* diagram, while particles moving at a constant velocity v are oblique lines and accelerated particles are curved lines.

The basic physical reason for these effects can be seen from the special relativistic line element (using x to represent the direction of propagation and $c = 1$)

$$d\tau^2 = dt^2 - dx^2 \,. \tag{3}$$

One sees that for a particle at rest, the vertical straight line in a *space*−*ct* diagram is equivalent to

$$d\tau^2 = dt^2 \,, \tag{4}$$

which is the only case where the time t is equivalent to the proper time τ (in the object's frame of reference). In all other cases, in particular for the oblique line in the case of constant velocity v, (3) applies and there is a mixing of space x and time t, resulting in the perceived special relativistic effects observed in a frame of reference moving at speed v with respect to the object of interest.

Loedel diagrams [17], a variation on *space*−*ct* diagrams allowing to display the Lorentz transformation graphically, are used to demonstrate graphically length contraction, time dilation and other special relativistic effects in problems that involve two frames of reference. Figs. 1 and 2, adapted from Petkov's Figs. 4.18 [12, p. 86], and 4.20 [12, p. 91] respectively, and Sartori's Fig. 5.15 [17, p. 160], provide a graphical view of the physical explanation of time dilation and length contraction respectively.

From Fig. 1, we see that $\Delta t' > \Delta t$ as expected – the moving observer sees time interval $\Delta t'$ of the observed object to be dilated, while the observed object's time interval Δt is actually the physical proper time interval $\Delta\tau$. From Fig. 2, we see that space distance measurements, *i.e.* space intervals, $\Delta x' < \Delta x$ as expected – the moving observer sees space interval $\Delta x'$ of the observed object to be contracted, while the observed object's space interval Δx is actually the proper space interval.

This provides a physical explanation for length contraction as a manifestation of the reality of a particle's extended worldline, where the cross-section measured by an observer moving relative to it (*i.e.* at an oblique line in the *space*−*ct* diagram), creates the difference in perceived length between a body in its rest frame and a frame in movement, as seen in

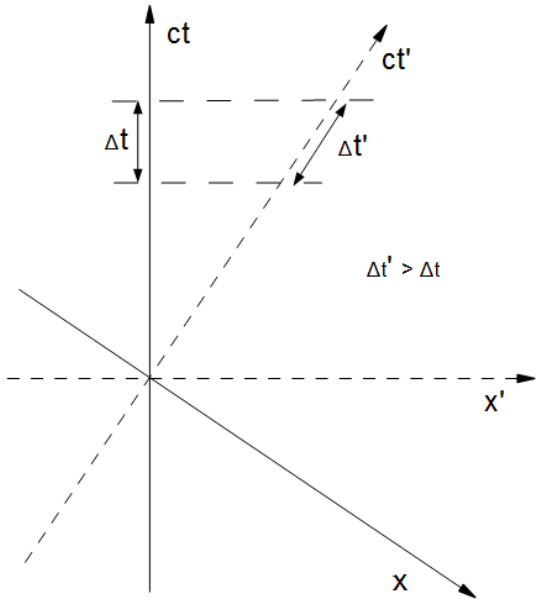

Fig. 1: Physical explanation of time dilation in a Loedel *space*−*ct* diagram

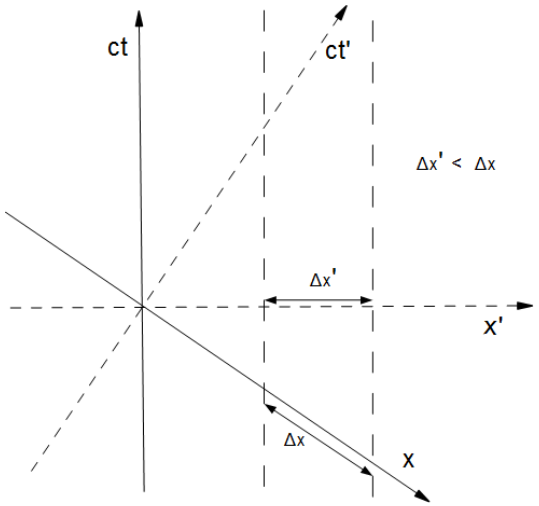

Fig. 2: Physical explanation of length contraction in a Loedel *space–ct* diagram

Fig. 2. It is important to understand that space itself is perceived to be contracted, not just objects in space. As seen in *STCED* [18], objects are not independent of spacetime, but are themselves deformations of spacetime, and are as such perceived to be contracted as space itself is. In actual practice, this phenomenon should be called *space contraction*, to avoid confusion, and demonstrate the complementary nature of time dilation and space contraction.

Thus we see that apparent time dilation and space contraction are perfectly valid physical results of Special Relativity, and there is nothing anomalous about them. Proper consideration of these phenomena eliminates the so-called paradoxes of Special Relativity as demonstrated by various authors, see for example [12, 14, 17]. We now explore the question of relativistic mass, which we first considered in section 2, in light of these considerations.

4 Relativistic mass as an effective mass

In this section, we show that the inertial mass of a body is its proper mass while the relativistic mass m^* is in effect an effective mass or, as Dixon [6] refers to it, an apparent mass. An effective mass is often introduced in dynamic equations in various fields of physics. An effective mass is not an actual mass – it represents a quantity of energy that behaves in dynamic equations similar to a mass. Using the effective mass, we can write the energy E as the sum of the proper mass and the kinetic energy K of the body, which is typically written as

$$E = m^* c^2 = m_0 c^2 + K \tag{5}$$

to give

$$K = (\gamma - 1)\, m_0 c^2 . \tag{6}$$

In reality, the energy relation in special relativity is quadratic, given by

$$E^2 = m_0^2 c^4 + p^2 c^2 , \tag{7}$$

where p is the momentum. Making use of the effective mass (1) allows us to obtain a linear expression from (7), starting from

$$m^{*2} c^4 = \gamma^2 m_0^2 c^4 = m_0^2 c^4 + p^2 c^2 , \tag{8}$$

which becomes

$$pc = \sqrt{\gamma^2 - 1}\, m_0 c^2 \tag{9}$$

or

$$pc = \beta\gamma m_0 c^2 = \frac{v}{c}\, \gamma m_0 c^2 = \frac{v}{c}\, E . \tag{10}$$

Then

$$p = m^* v . \tag{11}$$

As [12, p. 112] shows, the γ factor corresponds to the derivative of time with respect to proper time, *i.e.*

$$\frac{\mathrm{d}t}{\mathrm{d}\tau} = \frac{1}{(1-\beta^2)^{1/2}} = \gamma , \tag{12}$$

such that the velocity with respect to the proper time, u, is given by

$$u = \gamma v . \tag{13}$$

Hence using (13) in (11) yields the correct special relativistic relation

$$p = m_0 u , \tag{14}$$

which again shows that m^* in (11) is an effective mass when dealing with dynamic equations in the local time t instead of the invariant proper time τ. It is easy to see that differentiating (14) with respect to proper time results in a force law that obeys Newton's law with the proper mass acting as the inertial mass.

Hence we find that relativistic mass results from dealing with mass in local time t in a frame of reference moving with respect to the object of interest, instead of the invariant proper time τ in the frame of reference at rest with the object, and, from that perspective, is an effect similar to space contraction and time dilation seen in section 3. We see that the rest-mass m_0 should really be referred to as the proper mass, to avoid any confusion about the invariant mass of a body.

Relativistic mass is not apparent as time dilation and space contraction are, but rather is a measure of energy that depends on the relative speed v between two frames of reference, and is not an intrinsic property of an object as there is no absolute frame of reference to measure an object's speed against. The relativistic mass energy $m^* c^2$ is actually the total energy of an object (proper mass plus kinetic energy) measured with respect to a given frame of reference and is not a mass *per se* as mass is a relativistic invariant, *i.e.* a four-dimensional scalar, while energy is the fourth component of a four-vector.

5 Relativistic mass and *STCED*

In *STCED*, the proper mass corresponds to the invariant longitudinal volume dilatation given by [19, p. 32]

$$\rho c^2 = 4\kappa_0\,\varepsilon \tag{15}$$

which is equivalent to the inertial mass. The constant κ_0 is the spacetime bulk modulus and ε is the spacetime volume dilatation. Clearly, the longitudinal volume dilatation does not increase with velocity as it is an invariant. The result (14) is as expected from *STCED*.

For a spacetime volume element, the apparent space contraction in the direction of motion will be cancelled out by the apparent time dilation, *i.e.* the γ factors will cancel out. Thus the volume dilatation ε and the proper mass density ρ of (15) remain unchanged from the perspective of all frames of reference.

The only quantity that is impacted by the observer's frame of reference is the kinetic energy K or alternatively the quantity pc. In the frame of reference at rest with the object (which we can call the proper frame of reference), the kinetic energy $K = 0$ as seen from (6), while $pc = 0$ as seen from (9). The relativistic mass of an object is an effective mass defined to correspond to the total energy of an object (invariant proper mass plus kinetic energy) as observed from the perspective of another frame of reference. It does not represent an increase in the proper mass of an object, which as we have seen in section 4, corresponds to the inertial mass of the object.

6 Discussion and conclusion

In this paper, we have revisited the question of relativistic mass to clarify the meaning of this concept within special relativity. We have also considered time dilation and length contraction in more detail to help clarify the concept of relativistic mass. We have seen that "length contraction" is a misnomer and that it should really be named "space contraction" to avoid confusion, and demonstrate the complementary nature of time dilation and space contraction.

We have seen that relativistic mass is dependent on the difference in velocity v between an object's proper frame of reference that is at rest with the object and the frame of reference from which it is observed. We showed that the inertial mass of a body is its proper mass while the relativistic mass m^* is in effect an effective mass. We showed that relativistic mass results from dealing with dynamic equations in local time t in a frame of reference moving with respect to the object of interest, instead of the invariant proper time τ in the frame of reference at rest with the object. The results obtained are in agreement with the Elastodynamics of the Spacetime Continuum.

Received on August 30, 2017

References

1. Einstein A. Zur Electrodynamik bewegter Körper. *Annalen der Physik*, 1905, vol. 17. English translation (On the Electrodynamics of Moving Bodies) reprinted in Lorentz H. A., Einstein A., Minkowski H, and Weyl H. The Principle of Relativity: A Collection of Original Memoirs on the Special and General Theory of Relativity. Dover Publications, New York, 1952, pp. 37–65.
2. Einstein A. Ist die Trägheit eines Körpers von seinem Energiegehalt abhängig? *Annalen der Physik*, 1905, vol. 17. English translation (Does the Inertia of a Body Depend upon its Energy-Content?) reprinted in Lorentz H. A., Einstein A., Minkowski H, and Weyl H. The Principle of Relativity: A Collection of Original Memoirs on the Special and General Theory of Relativity. Dover Publications, New York, 1952, pp. 69–71.
3. Tolman R. C. Relativity, Thermodynamics and Cosmology. Dover Publications, New York, (1934) 1987, pp. 42–58.
4. Torretti R. Relativity and Geometry. Dover Publications, New York, (1984) 1996, pp. 107–113.
5. Aharoni J. The Special Theory of Relativity, 2nd rev. ed. Dover Publications, New York, (1965) 1985, ch. 5.
6. Dixon W. G. Special Relativity: The Foundation of Macroscopic Physics. Cambridge University Press, Cambridge, 1982, ch. 3.
7. Oas G. On the Abuse and Use of Relativistic Mass. arXiv: physics.ed-ph/0504110v2.
8. Oas G. On the Use of Relativistic Mass in Various Published Works. arXiv: physics.ed-ph/0504111.
9. Okun L. B. The Concept of Mass. *Physics Today*, 1989, v. 42 (6), 31–36.
10. Okun L. B. The Einstein Formula: $E_0 = mc^2$. "Isn't the Lord Laughing?". *Physics–Uspekhi*, 2008, v. 51 (5), 513–527. arXiv: physics.hist-ph/0808.0437.
11. Okun L. B. Energy and Mass in Relativity Theory. World Scientific, New Jersey, 2009.
12. Petkov V. Relativity and the Nature of Spacetime, 2nd ed. Springer, New York, 2009, pp. 77–102, 111–114.
13. Petkov V. Inertia and Gravitation: From Aristotle's Natural Motion to Geodesic Worldlines in Curved Spacetime. Minkowski Institute Press, Montreal, 2012, pp. 78–82.
14. Taylor E. F., Wheeler J. A. Spacetime Physics: Introduction to Special Relativity, 2nd ed. Freeman, New York, 1992, pp. 250–251.
15. Bell J. S. How to Teach Special Relativity. *Progress in Scientific Culture*, 1976, v. 1 (2). Reprinted in Bell J. S. Speakable and Unspeakable in Quantum Mechanics. Cambridge University Press, Cambridge, 1987, pp. 67–80.
16. Minkowski H. Space and Time. 80*th Assembly of German Natural Scientists and Physicians*. Cologne, 21 September 1908. English translation reprinted in Lorentz H. A., Einstein A., Minkowski H, and Weyl H. The Principle of Relativity: A Collection of Original Memoirs on the Special and General Theory of Relativity. Dover Publications, New York, 1952, pp. 73–91.
17. Sartori L. Understanding Relativity: A Simplified Approach to Einstein's Theories. University of California Press, Berkley, 1996, pp. 151–201.
18. Millette P. A. Elastodynamics of the Spacetime Continuum. *The Abraham Zelmanov Journal*, 2012, v. 5, 221–277.
19. Millette P. A. Elastodynamics of the Spacetime Continuum: A Spacetime Physics Theory of Gravitation, Electromagnetism and Quantum Physics. American Research Press, Rehoboth, NM, 2017.

Global Scaling as Heuristic Model for Search of Additional Planets in the Solar System

Hartmut Müller

E-mail: hm@interscalar.com

In this paper we apply scale-invariant models of natural oscillations in chain systems of harmonic quantum oscillators to search for additional planets in the Solar System and discuss the heuristic significance of those models in terms of our hypothesis of global scaling.

Introduction

In the last 8 years the heuristic significance of scale invariance (scaling) was demonstrated in various fields of physical research. In [1] we have shown that scale invariance is a fundamental property of natural oscillations in chain systems of similar harmonic oscillators. In [2] we applied this model on chain systems of harmonic quantum oscillators and could show that particle rest masses coincide with the eigenstates of the system. This is valid not only for hadrons, but for mesons and leptons as well. Andreas Ries [3] demonstrated that this model allows for the prediction of the most abundant isotope of a given chemical element. The interpretation of the Planck mass as eigenstate in a chain system of oscillating protons has allowed us to derive the proton rest mass from fundamental physical constants [4]. There we have proposed a new interpretation of the cosmic microwave background as a stable eigenstate of a chain system of oscillating protons.

Scale-invariant models of natural oscillations in chain systems of protons also give a good description of the mass distribution of large celestial bodies in the Solar System [5]. Physical properties of celestial bodies such as mass, size, rotation and orbital period can be understood as macroscopic quantized eigenstates of chain systems of oscillating protons and electrons [4]. This understanding can be applied to an evolutionary trend prognosis of the Solar System but may be of cosmological significance as well.

In this paper we apply our hypothesis of global scaling [4] to the search for additional planets in the Solar System.

Methods

In [1] we have shown that the set of natural frequencies of a chain system of harmonic oscillators coincides with a set of finite continued fractions $\mathcal{F}$, which are natural logarithms:

$$\ln(\omega_{jk}/\omega_{00}) = n_{j0} + \cfrac{z}{n_{j1} + \cfrac{z}{n_{j2} + \ddots + \cfrac{z}{n_{jk}}}} = [z, n_{j0}; n_{j1}, n_{j2}, \ldots, n_{jk}] = \mathcal{F}, \quad (1)$$

where ω_{jk} is the set of angular frequencies and ω_{00} is the fundamental frequency of the set. The denominators are integer numbers: $n_{j0}, n_{j1}, n_{j2}, \ldots, n_{jk} \in \mathrm{Z}$, the cardinality $j \in \mathrm{N}$ of the set and the number $k \in \mathrm{N}$ of layers are finite. In the canonical form, the numerator z is equal 1.

Any finite continued fraction represents a rational number [6]. Therefore, all frequencies ω_{jk} in (1) are irrational, because for rational exponents the natural exponential function is transcendental [7]. This circumstance presumably provides for the high stability of the oscillating chain system because it avoids resonance interaction between the elements of the system [8].

In the case of harmonic quantum oscillators, the continued fraction (1) defines not only a fractal set of natural angular frequencies ω_{jk} and oscillation periods $\tau_{jk} = 1/\omega_{jk}$ of the chain system, but also fractal sets of natural energies $E_{jk} = \hbar \cdot \omega_{jk}$ and masses $m_{jk} = E_{jk}/c^2$ which correspond with the eigenstates of the system. For this reason, we have called the continued fraction (1) the "fundamental fractal" of eigenstates in chain systems of harmonic quantum oscillators [4].

The electron and the proton are exceptionally stable quantum oscillators and therefore the proton-to-electron rest mass ratio can be understood as a fundamental physical constant.

We hypothesize the cosmological significance of scale invariance based on the fundamental fractal $\mathcal{F}$ (1) that is calibrated by the physical characteristics of the electron and the proton. This hypothesis we have called 'global scaling' [9].

Results

In [4] we have shown that the masses of the largest bodies in the Solar System correlate with main attractor nodes of the $\mathcal{F}$ (1), supporting our hypothesis of global scaling as forming factor of the Solar System.

For example, the natural logarithm of the Sun-to-electron mass ratio is close to an integer number:

$$\ln(M_{\mathrm{Sun}}/m_{\mathrm{electron}}) =$$

$$= \ln(1.9884 \cdot 10^{30}\mathrm{kg}/9.10938356 \cdot 10^{-31}\mathrm{kg}) = 138.936$$

This is also valid for Jupiter's body mass:

$$\ln\left(M_{\mathrm{Jupiter}}/m_{\mathrm{electron}}\right) =$$

$$= \ln(1.8986 \cdot 10^{27}\mathrm{kg}/9.10938356 \cdot 10^{-31}\mathrm{kg}) = 131.981$$

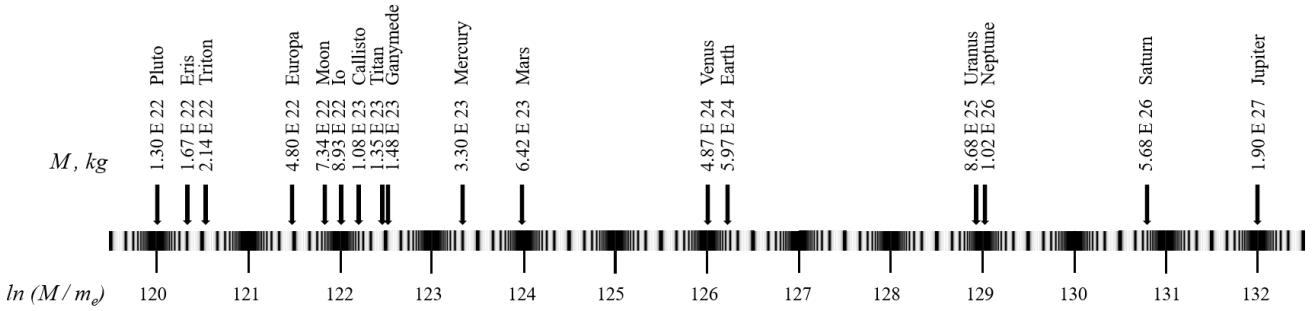

Fig. 1: The mass distribution of planets, heaviest planetoids and moons along the electron-calibrated fundamental fractal $\mathcal{F}$ (1). The nodes [130], [128], [127], [125], [123] and [121] are vacant.

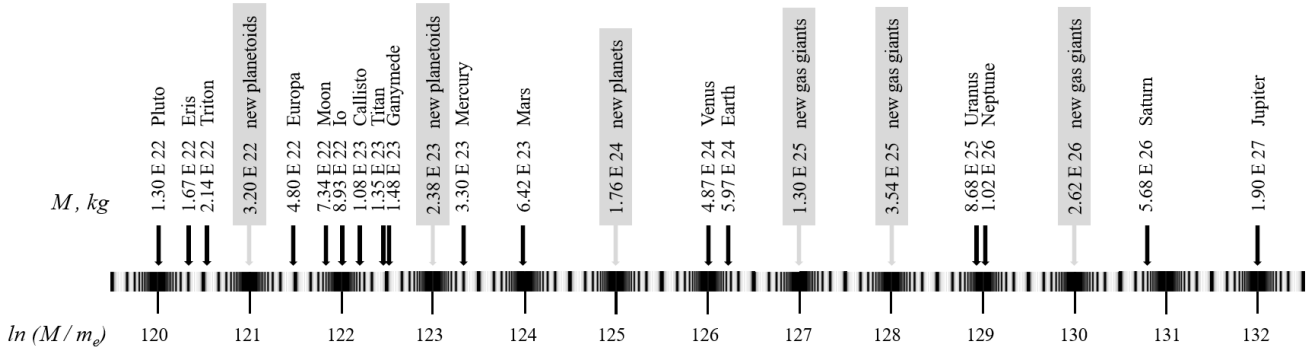

Fig. 2: This copy of fig. 1 shows the mass ranges of hypothetical planetoids, planets and gas giants which could occupy the vacant nodes [130], [128], [127], [125], [123] and [121] of the electron-calibrated fundamental fractal $\mathcal{F}$ (1).

And for Venus as well:

$$\ln\left(M_{\text{Venus}}/m_{\text{electron}}\right) =$$

$$= \ln(4.8675)\cdot 10^{24}\text{kg}/9.10938356\cdot 10^{-31}\text{kg}) = 126.015$$

Table 1 gives an overview of the body masses of the planets and heaviest planetoids and their positions in the fundamental fractal $\mathcal{F}$ (1).

The electron rest mass $m_e = 9.10938356\cdot 10^{-31}$ kg [10].

Table 1 shows that the body masses of Jupiter, Neptune, Uranus, Venus, Mars, Pluto, Charon and Haumea coincide with main attractor nodes (integer logarithms) of the electron-calibrated $\mathcal{F}$ (1). This also applies to the Sun. Figure 1 shows the mass distribution of planets, heaviest planetoids and moons along the electron-calibrated fundamental fractal $\mathcal{F}$ (1). The nodes [130], [128], [127], [125], [123], [121] are vacant.

The vacant nodes [121] and [123] indicate that in the mass ranges of 2 to $4\cdot 10^{22}$ kg and in the range of 2 to $3\cdot 10^{23}$ kg there should be planetoids still to be discovered. Furthermore, we may expect new planets in the range of 1 to $2\cdot 10^{24}$ kg. The probability of new gas giants in the Solar System is also very high, because of the wide vacant mass ranges of 1 to $5\cdot 10^{25}$ kg and of 2 to $3\cdot 10^{26}$ kg. Figure 2 shows the distribution of these hypothetical bodies on the fundamental fractal $\mathcal{F}$ (1).

Conclusion

The discovery of new gas giants, planets and planetoids with the properties predicted above would be an important confirmation of our hypothesis of global scaling as a forming factor of the Solar System. Already in 2010 [5] we calculated the masses of some of these hypothetical bodies and in 2015 [11, 12] we estimated their orbital elements.

Our calculations correspond well with the hypothesis of Batygin and Brown [13] about a new gas giant called “planet 9” and with the hypothesis of Volk and Malhotra [14] about an unknown Mars-to-Earth mass “planet 10” beyond Pluto.

Based on the vacancies in the fundamental fractal $\mathcal{F}$ (1), we hypothesize the existence of at least two unknown giant planets (see fig. 2). It is likely that they are gas giants. However, this conclusion cannot be made based on the estimation of their masses only, but requires an additional estimation of their radii, which should correspond with vacant positions in the fundamental fractal $\mathcal{F}$ (1) that is calibrated by the proton

Table 1: The logarithms of the body-to-electron mass ratio for the Sun, the planets, the heaviest planetoids (P) and the corresponding positions in the fundamental fractal $\mathcal{F}$ (1).

celestial body	**body mass m, kg**	**ln (m/m_e)**	$\mathcal{F}$
Sun	$1.9884 \cdot 10^{30}$	138.936	[139; ∞]
Jupiter	$1.8986 \cdot 10^{27}$	131.981	[132; ∞]
Saturn	$5.6836 \cdot 10^{26}$	130.776	[131; -4]
Neptune	$1.0243 \cdot 10^{26}$	129.062	[129; ∞]
Uranus	$8.681 \cdot 10^{25}$	128.897	[129; ∞]
Earth	$5.97237 \cdot 10^{24}$	126.220	[126; 4]
Venus	$4.8675 \cdot 10^{24}$	126.015	[126; ∞]
Mars	$6.4171 \cdot 10^{23}$	123.989	[124; ∞]
Mercury	$3.3011 \cdot 10^{23}$	123.324	[123; 3]
Eris (P)	$1.67 \cdot 10^{22}$	120.341	[120; 3]
Pluto (P)	$1.305 \cdot 10^{22}$	120.094	[120; ∞]
Haumea (P)	$4.006 \cdot 10^{21}$	118.913	[119; ∞]
Charon (P)	$1.587 \cdot 10^{21}$	117.944	[118; ∞]

and electron wavelengths.

Acknowledgements

The author is grateful to Viktor Panchelyuga for valuable discussions.

Received on September 9, 2017

References

1. Müller H. Fractal Scaling Models of Resonant Oscillations in Chain Systems of Harmonic Oscillators. *Progress in Physics*, 2009, vol. 2, 72–76.
2. Müller H. Fractal Scaling Models of Natural Oscillations in Chain Systems and the Mass Distribution of Particles. *Progress in Physics*, 2010, vol. 3, 61–66.
3. Ries A. Qualitative Prediction of Isotope Abundances with the Bipolar Model of Oscillations in a Chain System. *Progress in Physics*, 2015, vol. 11, 183–186.
4. Müller H. Scale-Invariant Models of Natural Oscillations in Chain Systems and their Cosmological Significance. *Progress in Physics*, 2017, vol. 4, 187–197.
5. Müller H. Fractal scaling models of natural oscillations in chain systems and the mass distribution of the celestial bodies in the Solar System. *Progress in Physics*, 2010, vol. 3, 61–66.
6. Khintchine A. Ya. Continued fractions. University of Chicago Press, Chicago 1964.
7. Hilbert D. Über die Transcendenz der Zahlen e und π. *Mathematische Annalen*, 1893, 43, 216–219.
8. Panchelyuga V. A., Panchelyuga M. S. Resonance and Fractals on the Real Numbers Set. *Progress in Physics*, October 2012, vol. 4, 48–53.
9. Müller H. Scaling as Fundamental Property of Natural Oscillations and the Fractal Structure of Space-Time. Foundations of Physics and Geometry. Peoples Friendship University of Russia, 2008 (in Russian).
10. Olive K. A. et al. (Particle Data Group), *Chin. Phys. C.* 38, 090001, 2016.
11. Müller H. Scaling of body masses and orbital periods in the Solar System. *Progress in Physics*, 2015, vol. 11, 133–135.
12. Müller H. Scaling of body masses and orbital periods in the Solar system as consequence of gravity interaction elasticity. Abstracts of the XII. International Conference on Gravitation, Astrophysics and Cosmology, dedicated to the centenary of Einstein's General Relativity theory. Moscow, PFUR, 2015.
13. Batygin K., Brown M.E. Evidence for a distant giant planet in the Solar System. *The Astronomical Journal*, 151/22, February 2016.
14. Volk K., Malhotra R. The curiously warped mean plane of the Kuiper belt. arXiv:1704.02444v2 [astro-ph.EP], 19 June 2017.

LETTERS TO PROGRESS IN PHYSICS

Discovered "Angel Particle", which is Both Matter and Antimatter, as a New Experimental Proof of Unmatter

Florentin Smarandache and Dmitri Rabounski

Department of Mathematics and Science, University of New Mexico, 705 Gurley Avenue, Gallup, NM 87301, USA
E-mails: smarand@unm.edu, rabounski@ptep-online.com

"Angel particle" bearing properties of both particles and anti-particles, which was recently discovered by the Stanford team of experimental physicists, is usually associated with Majorana fermions (predicted in 1937 by Ettore Majorana). In this message we point out that particles bearing properties of both matter and anti-matter were as well predicted without any connexion with particle physics, but on the basis of pure mathematics, namely — neutrosophic logic which is a generalization of fuzzy and intuitionistic fuzzy logics in mathematics.

Recently, a group of experimental physicists conducted by Prof. Shoucheng Zhang, in Stanford University, claimed about discovery of the particles that bear properties of both particles and anti-particles. The press-release [1] was issued on July 20, one day before the official publication [2].

Shoucheng Zhang told [1, 2] that the idea itself rose up from Ettore Majorana who in 1937 suggested that within the class of fermions a particle may exist which bear properties of particle and anti-particle in the same time. Such hypothetic particles are now know as "Majorana fermions".

In their experiment, the Stanford team used the following experimental setup. Two stacked films — the top film made of superconductor and the bottom film made of magnetic insulator — were stored together in a cooled down vacuum box. And an electrical current was sent through this "sandwich". Using a magnet mounted over the stackled films, the speed of the electrons in the film was able to be modifying. Varying the magnet's properties, the experimentalists registered Majorana particles which appeared in pairs in the electron flow but deviated from the electrons (so they were able to be registered separately). The experimentalists referred to the supposed new particle as "Angel particle" (meaning that, as well as angels are neither male nor female, the supposed particle is neither matter nor anti-matter).

Shoucheng Zhang also declared the importance of this discovery because, he thinks, the particles bearing properties of matter and anti-matter in the same time shows a fantastic perspective for computer industry and machinery.

In this background, we should note that particles bearing properties of matter and anti-matter were as well theoretically predicted being non-connected with particle physics, but only on the basis of pure mathematics. This is a series of works [3–8] based on neutrosophic logic (one of the multi-valued modern logics, a part of mathematics) authored by Florentin Smarandache.

So, following the neutrosophic logics, "between an entity <A> and its opposite <AntiA> there exist intermediate entities <NeutA> which are neither <A> nor <AntiA> [...] Thus, between "matter" and "antimatter" there must exist something which is neither matter nor antimatter, let's call it UNMATTER" [3]. Expanding this theory, a new type of matter — "unmatter" — was predicted.

Now, this theoretical study based on pure mathematics, elucidates that was discovered by the Stanford team conducted by Shoucheng Zhang. This fact shows that not only particle physics but also pure mathematics can make essential predictions that may change the wirld of science and techniques.

Submitted on September 18, 2017

References

1. Chui G. An experiment proposed by Stanford theorists finds evidence for the Majorana fermion, a particle that's its own antiparticle. *Stanford News Service*, 20 July 2017, http://news.stanford.edu/press/view/15528
2. He Q. L., Pan L., Stern A. L. et al. Chiral Majorana fermion modes in a quantum anomalous Hall insulator–superconductor structure. *Science*, 21 Jul 2017, v. 357, issue 6348, 294–299.
3. Smarandache F. A new form of matter — unmatter, composed of particles and anti-particles. *Progress in Physics*, 2005, v. 1, issue 1, 9–11.
4. Smarandache F. Verifying unmatter by experiments, more types of unmatter, and a Quantum Chromodynamics formula. *Progress in Physics*, 2005, v. 1, issue 2, 113–116.
5. Smarandache F. Unmatter entities inside nuclei, predicted by the Brightsen nucleon cluster model. *Progress in Physics*, 2006, v. 2, issue 1, 14–18.
6. Rabounski D., Smarandache F., Borissova L. Neutrosophic Methods in General Relativity. Hexis Publishers, Phoenix (Arizona), 2005.
7. Goldfain E. and Smarandache F. On emergent physics, "unparticles" and exotic "unmatter" states. *Progress in Physics*, 2008, v. 4, issue 4, 10–15.
8. Smarandache F. Unmatter plasma discovered. *Progress in Physics*, 2015, v. 11, issue 3, 246.

Vacuum Polarization by Scalar Field of Bose-Einstein Condensates and Experimental Design with Laser Interferences

B. J. Zhang[1], T. X. Zhang[2]

[1]Department of Electrical Engineering, University of Alabama in Huntsville, Huntsville, AL 35899. E-mail: bojunzhang333@gmail.com
[2]Department of Physics, Alabama A & M University, Normal, AL 35762. E-mail: tianxi.zhang@aamu.edu

In a five-dimensional gravitational theory (or 5D gravity), a scalar field is usually included to couple with the gravitational and electromagnetic fields, which are directly originated from or generated by the mass and electric charge of matter, respectively. Theoretical analyses have shown that the scalar field of 5D gravity can polarize the space (or vacuum) and shield gravity (or flatten spacetime), especially when the object that generates the fields is extremely compact, massive, and/or highly charged. Recently, the scalar field of 5D gravity has been directly connected to the Higgs field of 4D particle physics, so that it dramatically relates to the Ginzburg-Landau scalar field of Bose-Einstein condensates associated with superconductors and/or superfluids. Therefore, the scalar field effect on the properties of light and the weight of objects may be detectable in a laboratory of low temperature physics. In this study, we first analyze the index of refraction of the space or vacuum that is polarized by scalar field. We then explore approaches of detection and design experiments to test the space polarization or the effect of scalar field on light as well as the equivalence or connection between the scalar field of 5D gravity and that of 4D particle physics.

1 Introduction

In contrast to the vector field of electromagnetism and the tensor field of gravitation, a scalar field is a field that has no direction. Up to now, many physical phenomena are explained with the physics of scalar fields such as the cosmic inflation [1-2], dark matter [3-4], dark energy [5-6], particle mass generation [7-9], particle creation [10], gravitational field shielding [11-12], space or vacuum polarization [13-15], and so on. In the particle physics, the Higgs field, which generates masses of particles such as leptons and bosons, is a scalar field associated with particles of spin zero. In the 5D gravity, the gravitational and electromagnetic fields are coupled with a scalar field. Theoretical analyses have shown that the scalar field of 5D gravity can polarize the space or vacuum [13-15] and shield the gravity or flatten the spacetime [11-12,16-17], especially when the object of the fields is extremely compact, massive, and/or highly charged.

The scalar field of the 5D gravity has a direct relation or connection to the Higgs scalar field of the 4D particle physics [18]. The Higgs boson or Higgs particle is an elementary particle initially theorized in 1964 [7-9] and tentatively discovered to exist by the Large Hadron Collider at CERN [19]. This tentative discovery confirmed the existence of the Higgs scalar field, which led to the Nobel Prize of physics in 2013 to be awarded to Peter W. Higgs and Francois Englert. The Higgs mechanism is a process for particles to gain masses from the interaction with the Higgs scalar field. It describes the superconductivity of vacuum according to the Ginzburg-Landau model of the Bose-Einstein condensates.

Therefore, the scalar field of the 5D gravity can be considered as a type of Higgs scalar field of 4D particle physics. The latter can be considered as a type of Ginzburg-Landau scalar field of the Bose-Einstein condensates [20-21]. Then, that the scalar field of the 5D gravity can shield the gravitational field (or flatten the spacetime) and polarize the space or vacuum must imply that the Ginzburg-Landau scalar field of superconductors and superfluids in the state of Bose-Einstein condensates can also shield the gravitational field (or flatten the spacetime) and polarize the space or vacuum.

In fact, the experiment conducted about two decades ago had indeed shown that a rotating type-II ceramic superconductor disk at low temperature could have a moderate ($\sim$2 – 3%) shielding effect against the Earth gravitational field [22]. The experiment conducted later for a static testing with the shielding effect of $\sim$0.4% [23]. Recently, we have explained these measurements as the gravitational field shielding [12] by the Ginzburg-Landau scalar field of Bose–Einstein condensates associated with the type II ceramic superconductor disk according to the 5D fully covariant gravity developed by Zhang [11,15,24].

In this paper, we will focus on the vacuum polarization by scalar field and its testing. We will explore some possible approaches and further design viable experiment setups to test the space or vacuum polarization by the scalar field (*i.e.* the effect of scalar field on light). We will, at first, apply the fully covariant 5D gravity with a scalar field that was developed by Zhang [11,15] and references therein to formulate the index of refraction in the vacuum that is polarized by the scalar field of this 5D gravity. Then, we will employ the Ginzburg-Landau scalar field generated by the Bose-Einstein condensates of superconductors and superfluids to replace or add the scalar field of the 5D gravity. Finally, we will design

an experiment setup of laser light interferences that may detect the vacuum polarization by the Ginzburg-Landau scalar field and thus test Zhang's theory of vacuum polarization by scalar field as well as Wesson's equivalence and connection between the scalar field of 5D gravity and the scalar field of 4D particle physics.

2 Index of refraction of the vacuum polarized by the scalar field

According to the 5D fully covariant gravity with a scalar field [15] and references therein, we can determine the index of refraction of the vacuum that is polarized by the scalar field as

$$n \equiv \sqrt{\epsilon_r} = \Phi^{3/2} \exp\left(\frac{\lambda - \nu}{4}\right). \quad (1)$$

Here, Φ is the scalar field and the functions, e^{λ} and e^{ν}, are the $rr-$ and $tt-$components of the 4D spacetime metric. Both the scalar field and the metric components are completely determined according to the exact field solution obtained by Zhang [15] and references therein without any unknown parameter.

For objects in labs and the Earth itself, the fields of 5D gravity are weak, so that we can approximately represent $\Phi \sim 1 + \delta\Phi$, $e^{\lambda} \sim 1$, and $e^{\nu} \sim 1$. Then, the index of refraction in the vacuum that is polarized by scalar fields reduces to

$$n = 1 + \frac{3}{2} \sum \delta\Phi = 1 + \frac{3}{2} \left(\delta\Phi_{5D} + \delta\Phi_{GL}\right). \quad (2)$$

Here, Σ refers to the summation of contributions from all kinds of scalar fields, including the scalar fields of the 5D gravity from the Earth and any other charged objects and the Ginzburg-Landau scalar fields of the 4D particle physics from the Bose-Einstein condensates associated with superconductors and superfluids.

According to Zhang's fully covariant 5D gravity [15] and references therein such as [11,24], the scalar field of a charged object with charge Q and mass M is given by,

$$\delta\Phi_{5D} = \frac{2GM(1 + 3\alpha^2)}{3\sqrt{1 + \alpha^2}c^2} \frac{1}{r}, \quad (3)$$

where

$$\alpha = \frac{Q}{2\sqrt{G}M} \quad (4)$$

is a constant in cgs units, G is the gravitational constant, c is the light speed in free space, and r is the radial distance from the object. Considering an object with mass of 600 kg and charge of 0.01 C, we have $\alpha \sim 10^5$ and $\delta\Phi_{5D} \sim 10^{-19}$ at 1 m radial distance. For Earth, we have $\alpha \sim 0$ and $\delta\Phi_{5D} \sim 5 \times 10^{-10}$ on the surface. Therefore, via Earth or a charged object in labs, the scalar field of the 5D gravity is negligibly weak, *i.e.* $\delta\Phi_{5D} \sim 0$, and the effect on the vacuum polarization may be extremely difficult to detect. A new study by Zhang [25] has theoretically shown that the space or vacuum polarization by the scalar field of 5D gravity generated by a highly charged object may be directly detected by the extremely accurate Laser Interferometer Gravitational-Wave Observatory (LIGO), which has recently detected first ever the gravitational waves from a binary black hole merger as claimed in [26].

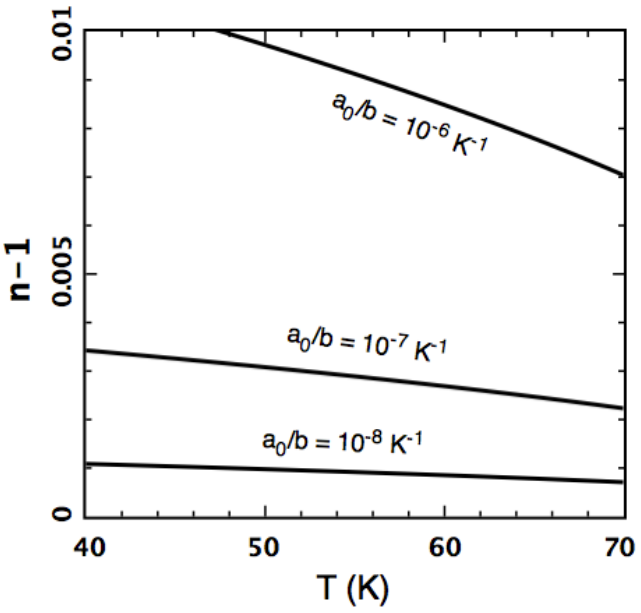

Fig. 1: The change for the index of refraction of the vacuum $(n - 1)$ versus the temperature of the superconductor (T). The vacuum is polarized by the Ginzburg-Landau scalar field of Bose-Einstein condensates associated with a type II superconductor whose transition temperature is $T_c = 92$ K. Three lines correspond to three cases for the ratio of the two phenomenological constants to be $a_0/b = 10^{-8}, 10^{-7}, 10^{-6}$ K, respectively.

The Ginzburg-Landau scalar field of Bose-Einstein condensates associated with superconductors and superfluids can be expressed as [20-21,27],

$$\delta\Phi_{GL} = \sqrt{-\frac{a_0}{b}(T - T_c)}, \quad (5)$$

where a_0 and b are the phenomenological constants, T is the temperature, and T_c is the transition temperature. A type II superconductor, if its Ginzburg-Landau scalar field can produce a few percent (*e.g.* $2 - 3\%$) weight loss for a sample as experimentally shown by [22-23], can also polarize the vacuum by increasing the index of refraction about a detectable percentage. For a quantitative study, we plot in Fig. 1 the index of refraction in the vacuum that is polarized by the Ginzburg-Landau scalar field of Bose-Einstein condensates associated with a type II superconductor as a function of the temperature of the superconductor. In this plot, we have chosen the values $T_c = 92$ K and $a_0/b = 10^{-8}, 10^{-7}, 10^{-6}$ K^{-1} as done in [12].

It is seen that due to the polarization the index of refrac-

tion of the vacuum can be increased by $\sim 0.1 - 1\%$ for the ratio of the phenomenological constants to be in a range of $a_0/b = 10^{-8} - 10^{-6}\ \mathrm{K}^{-1}$, which could lead to $\sim 2 - 3\%$ weight loss for a sample as shown in [12]. This significant increase of the index of refraction should be detectable in an optical experiment. In the following section, we design an experiment to test this scalar field effect on light or space polarization here predicted according to Zhang's 5D fully covariant gravity and Wesson's scalar field equivalence or connection between the 5D gravity and the 4D particle physics. Superfluids, though the transition temperature is lower but if the ratio of phenomenological constants is higher, can also generate a significant scalar field to polarize the vacuum.

3 Experimental design and prediction

A laser light beam that has passed through a spatial filter can be separated into two beams by a beam separator. These two laser light beams once reflected by two mirrors into the same region will interfere. If the difference of their optical distances travelled by the two beams is a factor of a whole number of the light wavelength, the interference is constructive otherwise the interference is destructive. A bright and dark pattern of interference is formed in the interference region. Now, if one of the two laser light beams passes through the space or vacuum that is polarized by scalar fields, then the interference pattern will be changed. This is because the space polarization lengthens the optical length of the path of the light beam.

The interference pattern will change from bright to dark or dark to bright, if the extra optical distance traveled for the beam that has passed through the space or vacuum polarized by scalar fields is given by

$$(n-1)\,D = \left(m + \frac{1}{2}\right)\lambda\,, \tag{6}$$

where n is the index of refraction of the space or vacuum that is polarized by the scalar field and its relation to the scalar field is given by (1) or (2); D is the dimension of the object that produces the scalar field; $m+1$ is the number of shifting the interference pattern from bright to dark (only one shift from bright to dark if $m = 0$); and λ is the wavelength of the laser light. The interference pattern does not change, if the extra optical distance is a whole number of the light wavelength, *i.e.* $(n-1)\,D = m\lambda$.

To polarize the space or vacuum that one of the two laser light beams travels through, we can place or put an electrically charged object, a type II ceramic superconductor disk, or a superfluid torus near the path of the beam (Fig. 2). Of course, we can put all of them together to enhance the total scalar field. Two superconductor disks can also double the effect. In these cases, the parameter D in (6) can be roughly estimated as the diameter of the charged object, superconductor disk, or superfluid torus.

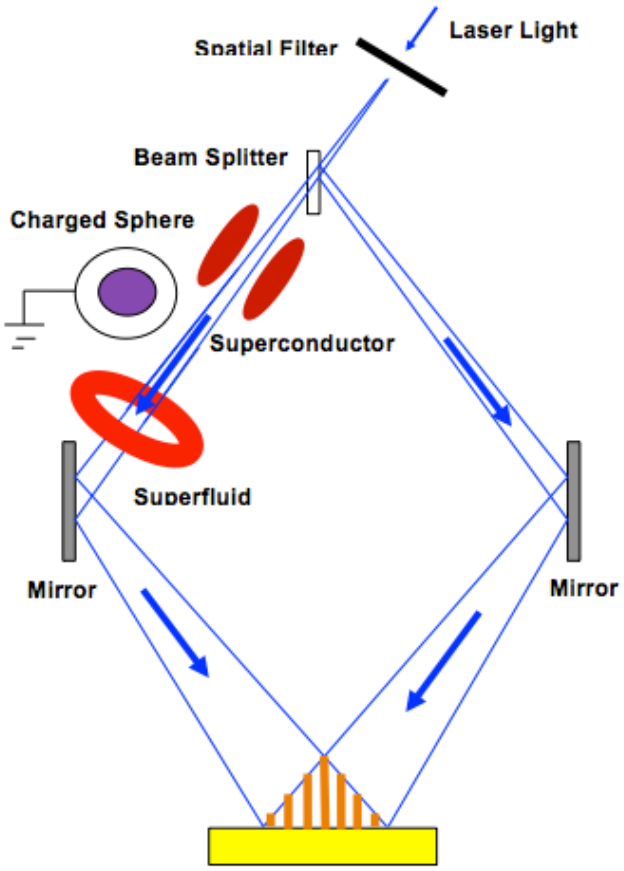

Fig. 2: A schematic diagram for the experimental setup to test the vacuum polarization by scalar field. A laser light that passes a spatial filter can be separated into two beams by a beam separator. The two beams once reflected by two mirrors into the same region will interfere and produce a bright-dark interference pattern. When the space or vacuum for the path of one beam is polarized by the scalar field generated by charged objects, superconductor disks, and/or superfluid toruses, the interference pattern will be varied or shifted. Therefore, the detection of any variation or shifting of the interference pattern will test the theory for the vacuum polarization by scalar field and the equivalence or connection for the scalar fields of 5D gravity and 4D particle physics.

As pointed out above, since it is not enough compact, massive, and/or highly charged, an object in labs cannot generate a significant scalar field to polarize the space or vacuum up to a detectable level, but except for LIGO [25-26]. The extra optical distance that a charged object can produce is $(n-1)\,D = 3/2\,\delta\Phi_{5\mathrm{D}}D \sim 10^{-19}$, which is too small in comparison with the wavelength of light. Therefore, a charged object cannot lead to a measurable shifting of the interference pattern. The scalar field of 5D gravity due to the Earth can neither vary the interference pattern, because it evenly affects both the beams of laser light.

To see how significant for a type II ceramic supercon-

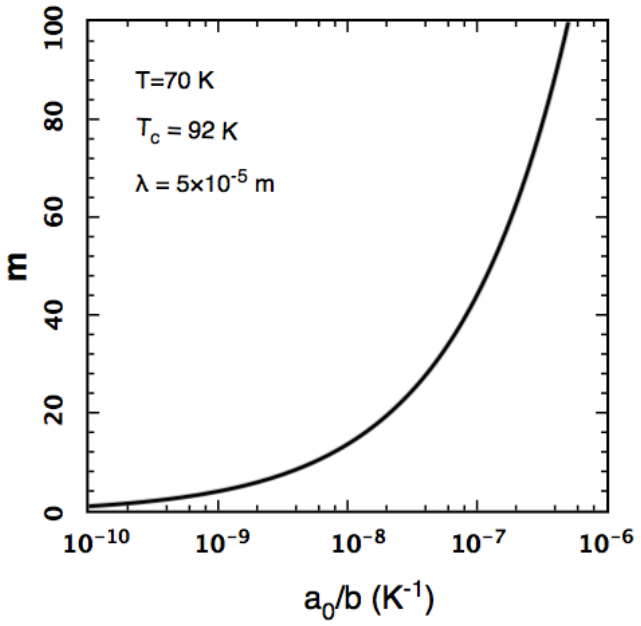

Fig. 3: The number of shifting the interference pattern from bright to dark, m, versus the ratio of the phenomenological constants, a_0/b. The temperature and transition temperature of the conductor are chosen as = 70 K and T_c = 92 K, respectvely.

ductor disk to vary the interference pattern, we plot in Fig. 3 the number of shift, m, as a function of the ratio of the phenomenological constants, a_0/b, according to (6) with (2) and (5). Here, we have chosen $D = 0.11$ m, $T_c = 92$ K, and $T = 70$ K according to the previous laboratory experiment [22] and analytical study [12]. The wavelength is chosen as a blue light with $\lambda \sim 5 \times 10^{-5}$ m. It is seen that the Ginzburg-Landau scalar field of Bose-Einstein condensates associated with a type II ceramic superconductor disk can lead to a significant shifting of the interference pattern. This varying of interference pattern is detectable only needing the ratio of the phenomenological constants to be greater than about 10^{-10} K^{-1}. Therefore, the effect of scalar field on light (or the space polarization) should be much more easily detected than the effect of scalar field on weight (or the gravitational field shielding).

4 Discussions and conclusions

We have investigated the vacuum polarization by the Ginzburg-Landau scalar field of Bose-Einstein condensates associated with superconductors and superfluids. First, we have formulated the index of refraction of the vacuum that is polarized by the scalar field according to Zhang's 5D fully covariant gravity and Wesson's equivalence or connection of scalar fields between 5D gravity and 4D particle physics. Then, we have designed an experimental setup with laser light interferences to detect the effect of scalar field on light and hence the vacuum polarization by the Ginzburg-Landau scalar field. Via this study, we have seen that the Ginzburg-Landau scalar field of Bose-Einstein condensates associated with a type II ceramic superconductor disk can cause a significant and thus detectable shifting of the laser light interference pattern. The ratio of the phenomenological constants can be much smaller than that for a detectable weight loss of a sample. Therefore, we have provided a possible approach and experimental setup for detecting the effect of scalar field on light in labs. In future, we will implement the design to conduct the experiment and perform the testing.

Acknowledgements

The author (B.J.Z.) is grateful for the support of educations in physics and engineering from Vanderbilt University, Georgia State University, and University of Alabama in Huntsville. He is especially appreciating very much for Dr. A. Kozhanov from Georgia State University and Dr. P. Reardon from University of Alabama in Huntsville for their great supervisions on his graduate study for Masters of Physics (2015) and Masters of Electrical Engineering in the concentration of optics (2017). He also thanks Dr. P. Guggilla, Dr. M. Edwards, and Dr. M. Aggarwal from Alabama A & M University for their support. This work was partially supported by the NSF/REU programs (Grant #: PHY-1263253, PHY-1559870) at Alabama A & M University.

Received on September 16, 2017

References

1. Guth A. Inflationary universe: A possible solution to the horizon and flatness problems. *Physical Review D*, 1981, v. 23, 347–356.
2. Watson G. S. An explosion of inflationary cosmology. arXiv: astro-ph/0005003.
3. Baldeschi M. R., Gelmini G. B., Ruffini R. On massive femions and bosons in galactic halos. *Physics Letters B*, 1983, v. 122, 221–224.
4. Matos T., Urena-Lepez L. A. Quintessence abd scalar dark matter in the universe. *Classical and Quantum Gravity*, 2000, v. 17, L75–L81.
5. Ratra B., Peebles P. J. E. Cosmological consequences of a rolling homogeneous scalar field. *Physical Review D*, 1988, v. 37, 3406–3427.
6. Sahni V. The cosmological constant problem and quintessence. *Classical and Quantum Gravity*, 2002, v. 19, 3435–3448.
7. Higgs P. W. Broken symmetries, massless particles and gauge fields. *Physics Letters*, 1964, v. 12, 132–133.
8. Higgs P. W. Broken symmetries and the masses of gauge bosons. *Physical Review Letters*, 1964, v. 13, 508–509.
9. Englert F., Brout R. Broken symmetry and the mass of gauge vector mesons. *Physical Review Letters*, 1964, v. 13, 321–323.
10. Sahni V., Habib S. Does inflationary particle production suggest $\Omega_m <$ 1. *Physical Review Letters*, 1998, v. 81, 1766–1769.
11. Zhang T. X. Gravitational field shielding and supernova explosions. *The Astrophysical Journal Letters*, 2010, v. 725, L117–L120.
12. Zhang B. J., Zhang T. X., Guggilla P., Dokhanian M. Gravitational field shielding by scalar field and type II superconductors. *Progress in Physics*, 2013, v. 1, 69–73.
13. Nodvik J. S. Suppression of singularities by the g^{55} field with mass and classical vacuum polarization in a classical Kaluza-Klein theory. *Physical Review Letters*, 1985, v. 55, L2519–L2522.

14. Dragilev V. M. Vacuum polarization of a scalar field in anisotropic multidimensional cosmology. *Theoretical Mathematics in Physics*, 1990, v. 84, 887–893.

15. Zhang T. X. The 5D fully-covariant theory of gravitation and its astrophysical application, *Galaxies*, 2014, v. 3, 18–51.

16. Zhang B. J., Zhang T. X., Guggilla P., Dokhanian M. Neutron star mass-radius relation with gravitational field shielding by a scalar field. *Research in Astronomy and Astrophysics*, 2013, v. 13, 571–578.

17. Zhang T. X. Gravitationless black holes. *Astrophysics and Space Science*, 2011, v. 334, 311–316.

18. Wesson P. S. The scalar field of 5D gravity and the Higgs field of 4D particle physics: A possible connection. arXiv:1003.2476.

19. Cho A. The discovery of the Higgs boson. *Science*, 2012, v. 338, 1524–1525.

20. Ginzburg V. I., Landau L. D. On the theory of superconductivity. *Zh. Eksp. Teor. Fiz.*, 1950, v. 20, 1064–1082.

21. Cyrot M. Ginzburg-Landau theory for superconductors. *Reports on Progress in Physics*, 1973, v. 36, 103–158.

22. Podkletnov E., Nieminen R. A possibility of gravitational force shielding by bulk $YBa_2Cu_3O_{7-x}$. *Physica C*, 1992, v. 203, 441–444.

23. Li N., Noever D., Robertson T., Koczer R., Brantley W. Static test for a gravitational force coupled to type II YBCO superconductor. *Physica C*, 1997, v. 281, 260–267.

24. Zhang T. X. Electric redshift and quasar. *The Astrophysical Journal Letters*, 2006, v. 636, L61–L63.

25. Zhang T. X. Testing 5D Gravity for Space Polarization by Scalar field with LIGO. *Progress in Physics*, 2017, v. 13, 180–186.

26. Abbott B. P. *et al.* Observation of gravitational waves from a binary black hole merger. *Physical Review Letters*, 2016, v. 116, id.061102.

27. Robertson G. A. Manipulating the vacuum scalar field with superconductor: A search for exotic material. *AIP Conference Proceedings*, 2005, v. 746, 1371–1378.

On the Question of Acceleration in Special Relativity

Pierre A. Millette

E-mail: PierreAMillette@alumni.uottawa.ca, Ottawa, Canada

In this paper, we consider the question of the impact of acceleration in special relativity. Some physicists claim that acceleration does not matter in special relativity based on the Clock Hypothesis. We find that the experimental support of the Clock Hypothesis usually provided by the Mössbauer spectroscopy experiment of Kündig [5] and the muon experiment of Bailey *et al* [2] is questionable at best. We consider the case for the impact of acceleration in special relativity and derive an expression for the time dilation in an accelerated frame of reference, based on the equivalence principle of general relativity. We also derive an expression for space contraction in an accelerated frame of reference. We note that the presence of acceleration in a frame of reference provides a means of determining the motion of that frame of reference as acceleration can be easily detected compared to constant velocity which cannot. We discuss the "twin paradox" of special relativity and note that this is not truly a special relativity problem for there is no way to avoid acceleration. We note that because of time dilation in accelerated frames of reference, the astronaut will age less than its earth-bound twin, but only during periods of acceleration.

1 Introduction

In a recent paper [1], we showed that time dilation and space contraction in inertial reference frames, that is unaccelerated reference frames moving at a constant velocity, are apparent effects perceived in a frame of reference moving with respect to an object of interest. The real physical time and length are in the frame of reference at rest with the object, and in that frame, there is no time dilation or space contraction as $v = 0$ (and acceleration $a = 0$). This is seen clearly in Fig. 1 where a time dilation is perceived in the frame of reference moving at speed v with respect to the object of interest ($\Delta t'$), while there is no dilation in the object's frame of reference (Δt).

This result would seem to be at odds with the often quoted experimental tests of special relativity confirming time dilation and length contraction. But if we consider, for example, Bailey *et al*'s muon experiment [2], we find that there is no contradiction with the experimental observations: a perceived time dilation is observed in the Earth's laboratory frame of reference while the muon, in its frame of reference has no time dilation – note that no measurements were carried out in the muon's frame of reference in the Bailey experiment.

Careful examination of experimental tests of special relativity also often reveals the presence of acceleration in the experiments, contrary to the conditions under which special relativity applies. The question of how to deal with acceleration in special relativity underlies many of the analytical and experimental conundrums encountered in the theory and is investigated in more details in this paper.

2 Measuring the impact of acceleration in special relativity

The theory of special relativity applies to unaccelerated (constant velocity) frames of reference, known as inertial frames of reference, in a four-dimensional Minkowski spacetime [3], of which the three-dimensional Euclidean space is a subspace. When the Lorentz-Fitzgerald contraction was first introduced, it was considered to be a real physical effect in Euclidean space to account for the null results of the Michelson-Morley experiment. Einstein derived length contraction and time dilation as effects originating in special relativity. These depend on the velocity of the frame of reference with respect to which an object is being observed, not the object's velocity

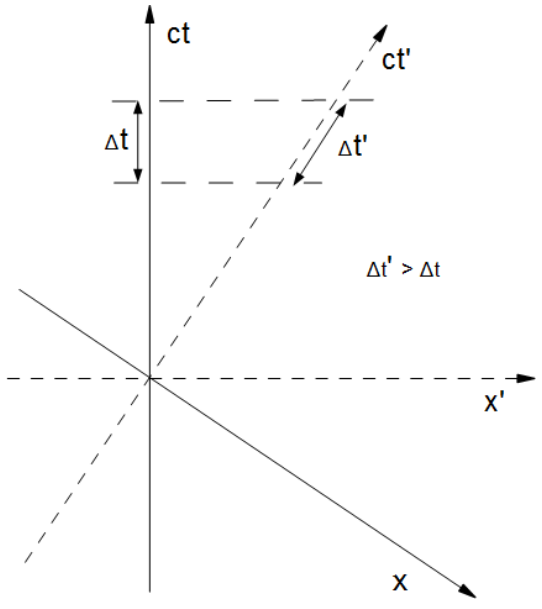

Fig. 1: Physical explanation of time dilation in a Loedel *space–ct* diagram

which can only be relative to another frame of reference, as there is no absolute frame of reference against which to measure the object's velocity. Indeed, if time dilation and length contraction were real effects in special relativity, this would be equivalent to saying that there is an absolute frame of reference against which it is possible to measure an object's velocity, contrary to the theory.

Increasingly, special relativity has been applied to accelerated frames of reference for which the theory does not apply. Some physicists claim that acceleration does not matter in special relativity and that it has no impact on its results, but there are many indications that this is not the case. The Clock Hypothesis (or Postulate) is used to justify the use of accelerated frames in special relativity: "when a clock is accelerated, the effect of motion on the rate of the clock is no more than that associated with its instantaneous velocity – the acceleration adds nothing" [4, p. 9], and further postulates that if the Clock Hypothesis applies to a clock, " then the clock's proper time will be proportional to the Minkowski distance along its worldline" [4, p. 95] as required.

Two experimental confirmations of the Clock Hypothesis are usually given. The postulate is claimed to have been shown to be true for accelerations of $\sim 10^{16} g$ in a Mössbauer spectroscopy experiment by Kündig [5] and of $\sim 10^{18} g$ in Bailey *et al*'s muon experiment [2], which uses rotational motion of particles to generate the acceleration – one obtains the quoted acceleration for a particle velocity close to the speed of light. However, a close examination of these experiments shows that they don't quite provide the experimental confirmation they are purported to give.

Kholmetskii *et al* [6] reviewed and corrected the processing of Kündig's experimental data and obtained an appreciable difference of the relative energy shift $\Delta E/E$ between emission and absorption resonant lines from the predicted relativistic time dilation $\Delta E/E = -v^2/2c^2$ (to order c^{-2}), where v is the tangential velocity of the resonant radiation absorber. Writing the relative energy shift as $\Delta E/E = -k\, v^2/c^2$, they found that $k = 0.596 \pm 0.006$ instead of $k = 0.5$ as predicted by special relativity and Kündig's original reported result of $k = 0.5003 \pm 0.006$. They then performed a similar Mössbauer spectroscopy experiment [7] with two absorbers with a substantially different isomer shift to be able to correct the Mössbauer data for vibrations in the rotor system at various rotational frequencies. They obtained a value of $k = 0.68 \pm 0.03$, a value similar to $2/3$. Since then Kholmetskii and others [8–12] have performed additional experimental and theoretical work to try to explain the difference, but the issue remains unresolved at this time, and is a clear indication that acceleration is not compatible with special relativity.

In their experiment of the measurement of the lifetime of positive and negative muons in a circular orbit, Bailey *et al* [2] obtained lifetimes of high-speed muons which they then reduced to a mean proper lifetime at rest, assuming that special relativity holds in their accelerated muon experimental setup. This experiment was carried out at CERN's second Muon Storage Ring (MSR) [13, 14] which stores relativistic muons in a ring in a uniform magnetic field. The MSR was specifically designed to carry out muon $(g-2)$ precession experiments (g is the Landé g-factor) with muons of momentum $3.094\,\mathrm{GeV}/c$ corresponding to a γ-factor of 29.3 (effective relativistic mass [1]), so that the electrons emitted from muon decay in the lab frame were very nearly parallel to the muon momentum. The decay times of the emitted electrons were measured in shower counters inside the ring to a high precision, and the muon lifetimes in the laboratory frame were calculated by fitting the experimental decay electron time spectrum to a six-parameter exponential decay modulated by the muon spin precession frequency, using the maximum likelihood method – one of the six parameters is the muon relativistic lifetime.

It is important to note that the decay electrons would be ejected at the instantaneous velocity of the muon ($0.9994c$ from the $\gamma = 29.3$ factor) tangential to the muon's orbit. Thus the ejected electron moves at the constant velocity of ejection to the shower counter and acceleration does not play a role. Even though the muons are accelerated, the detected electrons are not, and the experiment is not a test of the Clock Hypothesis under acceleration as claimed. There is thus no way of knowing the impact of acceleration from the experimental results as acceleration is non-existent in the detection and measurement process.

It should also be noted that Hafele *et al* [17] in their time dilation "twin paradox" experiment applied a correction for centripetal acceleration to their experimental results. in addition to a gravitational time dilation correction, to obtain results in agreement with Lorentz time dilation. The effect of acceleration cannot be disregarded in that experiment. This will be considered in more details in section 4. We thus find that the experimental support of the Clock Hypothesis is questionable at best.

3 The case for the impact of acceleration in special relativity

Having determined that there is little experimental support for the validity of the Clock Hypothesis in accelerated frames of reference in special relativity, we consider the case for the impact of acceleration in special relativity. Einstein developed general relativity to deal with accelerated frames of reference – if acceleration can be used in special relativity, why bother to develop a more general theory of relativity? Inspection of an accelerated worldline in a Minkowski *space-ct* diagram shows that indeed there is no basis for the Clock Hypothesis, as seen in Fig. 2. The accelerated worldline suffers an increasing rate of time dilation, somewhat like gravitational time dilation where increasing height in the gravitational potential results in increasing time dilation.

This brings to mind Einstein's equivalence principle in-

troduced in the analysis of accelerated frames of reference in general relativity. The simplest formulation of this principle states that on a local scale, the physical effects of a gravitational field are indistinguishable from the physical effects of an accelerated frame of reference [15] (*i.e.* an accelerated frame of reference is locally equivalent to a gravitational field). Hence, as displayed graphically for the accelerated worldline in the Minkowski *space-ct* diagram of Fig. 2, an accelerated frame of reference undergoes time dilation similar to gravitational time dilation [15]. Indeed, assuming that acceleration has no impact in special relativity cannot be correct as it violates the equivalence principle of general relativity.

We explore the connection between gravitational time dilation and the time dilation in an accelerated frame of reference in greater details. Gravitational time dilation can be derived starting from the Schwarzschild metric with signature (+ - - -) [16, p. 40]

$$c^2 d\tau^2 = \left(1 - \frac{2GM}{rc^2}\right) c^2 dt^2 - \left(1 - \frac{2GM}{rc^2}\right)^{-1} dr^2 - \\ - r^2 \left(d\theta^2 + \sin^2\theta\, d\varphi^2\right), \tag{1}$$

where τ is the proper time, (r, θ, φ, t) are the spherical polar coordinates including time, G is the gravitational constant, M is the mass of the earth and c is the speed of light in vacuo. The gravitational time dilation is obtained from the dt^2 term to give

$$\Delta t = \left(1 - \frac{2GM}{rc^2}\right)^{-\frac{1}{2}} \Delta t_0\,, \tag{2}$$

where Δt_0 is the undilated (proper) time interval and Δt is the dilated time interval in the earth's gravitational field. This can be rewritten as

$$\Delta t = \left(1 - \frac{2GMr}{r^2c^2}\right)^{-\frac{1}{2}} \Delta t_0\,, \tag{3}$$

where the term GM/r^2 is an acceleration a equal to g for $r = R$, the earth's radius, and finally

$$\Delta t = \left(1 - \frac{2ar}{c^2}\right)^{-\frac{1}{2}} \Delta t_0\,. \tag{4}$$

By the equivalence principle, this is also the time dilation in an accelerated frame of reference. For small accelerations, using the first few terms of the Taylor expansion, this time dilation expression can be written as

$$\Delta t \simeq \left(1 + \frac{ar}{c^2}\right) \Delta t_0\,. \tag{5}$$

The impact of acceleration on time dilation for small acceleration will usually be small due to the c^{-2} dependency.

We note in particular the expressions for centripetal acceleration $a = v^2/r$ in the case of circular motion

$$\Delta t = \left(1 - \frac{2v^2}{c^2}\right)^{-\frac{1}{2}} \Delta t_0\,, \tag{6}$$

which becomes for small accelerations, again using the first few terms of the Taylor expansion,

$$\Delta t \simeq \left(1 + \frac{v^2}{c^2}\right) \Delta t_0\,. \tag{7}$$

In this case, the impact can be significant, of the same order as the relativistic Lorentz time dilation. Hence there is no doubt that accelerated frames of reference also undergo time dilation compared to unaccelerated (inertial) frames of reference.

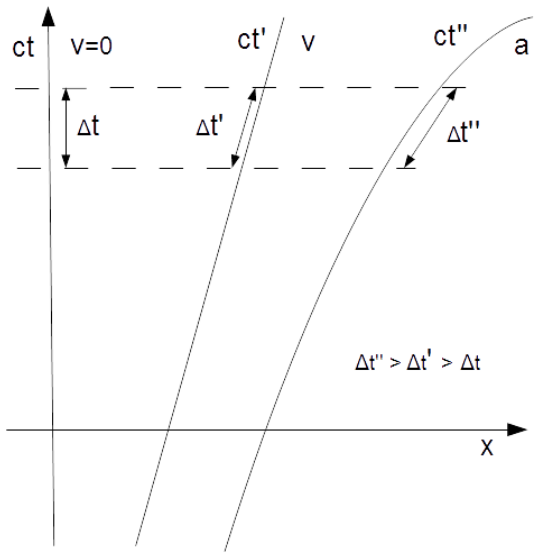

Fig. 2: Physical explanation of an accelerated worldline in a Minkowski *space–ct* diagram

4 The consequences of acceleration in special relativity

The presence of acceleration in a frame of reference provides a means of determining the motion of that frame of reference as acceleration can be easily detected compared to constant velocity which cannot. Whereas in an inertial frame of reference there is no way of determining one's velocity, this limitation disappears in accelerated frames of reference.

Physical time dilation due to acceleration is a reality, as is physical space contraction, which, from (1), is seen to have the inverse of the functional form of (4), to give the acceleration space contraction relation

$$\Delta x = \left(1 - \frac{2ar}{c^2}\right)^{\frac{1}{2}} \Delta x_0 \tag{8}$$

which for small accelerations, using the first few terms of the Taylor expansion, becomes

$$\Delta x \simeq \left(1 - \frac{ar}{c^2}\right) \Delta x_0\,. \tag{9}$$

Till now, we have not discussed the so-called "twin paradox" of special relativity. This is not truly a paradox for there is no way to avoid acceleration in the problem and it is thus not a special relativity problem. Assume that by some miracle we have twins moving at constant velocity with respect to one another from departure to return with no acceleration and that they are able to compare their age. It is important to notice that in their inertial frames of reference, both proper times $d\tau$, the one in the frame of reference at rest with the earth, and the one in the frame of reference at rest with the spaceship, are equal to the physical time in both the frame of reference at rest with the earth and the frame of reference at rest with the spaceship. From the earth, it looks like the spaceship's time is dilated, and from the spaceship, it looks like the earth's time is dilated. It doesn't matter as the time dilation in one location as seen from the other location is apparent as seen in [1]. When the spaceship comes back to earth, the twins would see that indeed they have the same age.

The problem can be recast in a simpler fashion. Suppose instead of the earth and a spaceship, we have two spaceships moving at constant relativistic speed with respect to one another from start to finish with no acceleration, and that the twins are able to compare their age at the start and the finish. One spaceship moves slowly because of engine problems, while the other moves at relativistic speeds. The resolution would be as described in the previous paragraph: the twins would see that indeed they have the same age at the finish.

The complication in this problem is that forces have to be applied to accelerate the spaceship, then decelerate it to turn around, accelerate it again and finally decelerate it when it comes back to the earth. The problem then needs to be treated using accelerated frames of reference for those periods on the spaceship. As we have seen in section 3, because of time dilation in accelerated frames of reference, the astronaut will age less than its earth-bound twin, but only during periods of acceleration. During periods of unaccelerated constant velocity travel, there will be no differential aging between the twins. However, the earth-bound twin is itself in an accelerated frame of reference the whole time, so its time will also be dilated. The details of who is older and younger will depend on the details of the acceleration periods, with the earth-bound twin's time dilation depending on (2) and (6), and the spaceship-bound twin's time dilation depending on (4).

Comparing how these findings line up with the results of Hafele's circumglobal experiment [17, 18], it is important to note that Hafele's experiment was done the whole time in a non-inertial accelerated frame of reference. Its results were corrected for gravitational time dilation and centripetal acceleration time dilation, the latter correction clearly showing that acceleration has an impact on special relativity. The centripetal acceleration time dilation correction used by Hafele *et al* [17] is similar to (6). One side effect of the experiment being conducted in gravitational and accelerated frames of reference is that it was possible to determine their motion, contrary to special relativity. The Lorentz time dilation would then become a real effect in this purported test of the "twin paradox". There was no symmetry in the relative motions that would have seen the plane stationary and the earth moving given that gravitational and centripetal accelerations clearly showed who was moving and at what velocity.

5 Discussion and conclusion

In this paper, we have considered the question of the impact of acceleration in special relativity. Some physicists claim that acceleration does not matter in special relativity – this view is part of the Clock Hypothesis which is used to justify the use of accelerated frames in special relativity. We have found that the experimental support of the Clock Hypothesis usually provided by the Mössbauer spectroscopy experiment of Kündig [5] and the muon experiment of Bailey *et al* [2] is questionable at best.

We have considered the case for the impact of acceleration in special relativity and have derived an expression for the time dilation in an accelerated frame of reference, based on the equivalence principle of general relativity. We have also derived an expression for space contraction in an accelerated frame of reference.

As a consequence, we have noted that the presence of acceleration in a frame of reference provides a means of determining the motion of that frame of reference as acceleration can be easily detected compared to constant velocity which cannot – whereas in an inertial frame of reference there is no way of determining one's velocity, this limitation disappears in accelerated frames of reference.

We have discussed the "twin paradox" of special relativity and have noted that this is not truly a paradox for there is no way to avoid acceleration in the problem and it is thus not a special relativity problem. We have noted that because of time dilation in accelerated frames of reference, the astronaut will age less than its earth-bound twin, but only during periods of acceleration, while during periods of unaccelerated constant velocity travel, there will be no differential aging between the twins. However, as the earth-bound twin is itself in an accelerated frame of reference the whole time, the details of who is older and who is younger will depend on the details of the acceleration periods of both twins. Finally we have reviewed how these findings line up with the results of Hafele's circumglobal experiment [17, 18] and find no contradiction.

Received on September 28, 2017

References

1. Millette P. A. On Time Dilation, Space Contraction and the Question of Relativistic Mass. *Progress in Physics*, 2017, v. 13, 200–203.
2. Bailey J., Borer K., Combley F., Drumm H., Krienen F., Lange F., Picasso E., von Ruden W., Farley F. J. M., Field, J. H., Flegel, W., Hattersley P. M. Measurements of Relativistic Time Dilatation for Positive and Negative Muons in a Circular Orbit. *Nature*, 1977, v. 268, 301–305.

3. Minkowski H. Space and Time. 80th *Assembly of German Natural Scientists and Physicians*. Cologne, 21 September 1908. English translation reprinted in Lorentz H. A., Einstein A., Minkowski H, and Weyl H. The Principle of Relativity: A Collection of Original Memoirs on the Special and General Theory of Relativity. Dover Publications, New York, 1952, pp. 73–91.
4. Brown H. Physical Relativity: Spacetime Structure from a Dynamical Perspective. Oxford University Press, Oxford, 2005.
5. Kündig W. *Phys. Rev.*, 1963, v. 129, 2371.
6. Kholmetskii A. L., Yarman T. and Missevitch O. V. Kündig's Experiment on the Transverse Doppler Shift Re-analyzed. *Phys. Scr.*, 2008, v. 77, 035302–035306.
7. Kholmetskii A. L., Yarman T., Missevitch O. V. and Rogozev B. I. A Mössbauer Experiment in a Rotating System on the Second-order Doppler Shift: Confirmation of the Corrected Result by Kündig. *Phys. Scr.*, 2009, v. 79, 065007.
8. Kholmetskii A. L., Yarman T., Missevitch O. V. and Rogozev B. I. Mössbauer Experiments in a Rotating System on the Time Dilation Effect. *Int. J. Phys. Sci.*, 2011, v. 6, 84–92.
9. Yarman T., Kholmetskii A. L., Arik M., Akku, B., Öktem Y., Susam A., Missevitch O. V. Novel Mössbauer Experiment in a Rotating System and the Extra Energy Shift Between Emission and Absorption Lines. arXiv: physics.gen-ph/1503.05853.
10. Yarman T., Kholmetskii A. L., Arik M. Mössbauer Experiments in a Rotating System: Recent Errors and Novel Interpretation. *The European Physical Journal Plus*, 2015, v. 130, 191.
11. Corda C. The Mössbauer Rotor Experiment and the General Theory of Relativity. arXiv: gr-qc/1602.04212.
12. Kholmetskii A. L., Yarman T., Yarman O., Arik M. Unabridged Response to "The Mössbauer Rotor Experiment and the General Theory of Relativity" by C. Corda: General Relativity Cannot Supply an Answer to the Extra Time Dilation in Rotor Mössbauer Experiments. arXiv: physics.gen-ph/1610.04219.
13. Combley F., Farley F. J. M., and Picasso E. The CERN Muon $(g-2)$ Experiments. *Physics Reports (Review Section of Physics Letters)*, 1981, v. 68 (2), 93–119.
14. Miller J. P., de Rafael E., and Roberts B. L. Muon $(g-2)$: Experiment and Theory. *Rep. Prog. Phys.*, 2007, v. 70, 7953–881.
15. Nolan P.J. The Fundamentals of the Theory of Relativity. Farmingdale State College, New York, pp. 7-2, 7-13.
16. Ciufolini I. and Wheeler J. A. Gravitation and Inertia. Princeton University Press, Princeton, NJ, 1995.
17. Hafele J. C. and Keating R. E. Around-the-World Atomic Clocks: Predicted Relativistic Time Gains. *Science*, 1972, v. 177, 166–168.
18. Hafele J. C. and Keating R. E. Around-the-World Atomic Clocks: Observed Relativistic Time Gains. *Science*, 1972, v. 177, 168–170.

Theorem of Non-Returning and Time Irreversibility of Tachyon Kinematics

Yaroslav I. Grushka
Institute of Mathematics NAS of Ukraine, 3, Tereschenkivska st., 01601, Kyiv, Ukraine.
E-mail: grushka@imath.kiev.ua

Using the recently developed mathematical apparatus of the theory of universal kinematic sets, we prove that the hypothesis of the existence of material objects and inertial reference frames moving with superluminal velocities in the general case does not lead to the violation of the principle of causality, that is, to a possibility of the returning to the own past. This result is obtained as the corollary of the abstract theorem on irreversibility, which gives the sufficient condition of time irreversibility for universal kinematic sets.

1 Introduction

Subject of constructing the theory of super-light movement, had been posed in the papers [1, 2] more than 50 years ago. Despite the fact that on today tachyons (ie objects moving at a velocity greater than the velocity of light) are not experimentally detected, this subject remains being actual.

It is well known that among physicists it is popular the belief that the hypothesis of the existence of tachyons leads to temporal paradoxes, connected with the possibility of changing the own past. Conditions of appearing these time paradoxes were carefully analyzed in [3]. It should be noted, that in [3] superluminal motion is allowed only for particles or signals whereas superluminal motion for reference frames is forbidden. This fact does not give the possibility to bind the own time with tachyon particle, and, therefore to determine real direction of motion of the particle. In the paper [4] for tachyon particles the own reference frames are axiomatically introduced only for the case of one space dimension. Such approach allows to determine real direction of motion of the tachyon particle by more correct way, and so to obtain more precise results.

In particular, in the paper [4] it was shown, that the hypothesis of existence of material objects, moving with the velocity, greater than the velocity of light, does not lead to formal possibility of returning to the own past in general. Meanwhile in the papers of E. Recami, V. Olkhovsky and R. Goldoni [5–7], and and later in the papers of S. Medvedev [8] as well as J. Hill and B. Cox [9] the generalized Lorentz transforms for superluminal reference frames are deduced in the case of three-dimension space of geometric variables. In the paper [10] it was proven, that the above generalized Lorentz transforms may be easy introduced for the more general case of arbitrary (in particular infinity) dimension of the space of geometric variables.

Further, in [11], using theory of kinematic changeable sets, on the basis of the transformations [10], the mathematically strict models of kinematics, allowing the superluminal motion for particles as well as for inertial reference frames, had been constructed. Thus, the tachyon kinematics in the sense of E.Recami, V. Olkhovsky and R. Goldoni are surely mathematically strict objects. But, these kinematics are impossible to analyze on the subject of time irreversibility (that is on existence the formal possibility of returning to the own past), using the results of the paper [4], because in [4] complete, multidimensional superluminal reference frames are missing.

Moreover, it can be proved, that the axiom "AxSameFuture" from [4, subsection 2.1] for these tachyon kinematics is not satisfied. The paper [12] [1] is based on more general mathematical apparatus in comparison with the paper [4], namely on mathematical apparatus of the theory of kinematic changeable sets. In [12] the strict definitions of time reversibility and time irreversibility for universal kinematics were given, moreover in this paper it was proven, that all tachyon kinematics, constructed in the paper [11], are time reversible in principle. In connection with the last fact the following question arises:

Is it possible to build the certainly time-irreversible universal kinematics, which allows for reference frames moving with any speed other than the speed of light, using the generalized Lorentz-Poincare transformations in terms of E. Recami, V. Olkhovsky and R. Goldoni?

In the present paper we prove the abstract theorem on non-returning for universal kinematics and, using this theorem, we give the positive answer on the last question.

For further understanding of this paper the main concepts and denotation system of the theories of changeable sets, kinematic sets and universal kinematics, are needed. These theories were developed in [11, 13–17]. Some of these papers were published in Ukrainian. That is why, for the convenience of readers, main results of these papers were "converted" into English and collected in the preprint [18], where one can find the most complete and detailed explanation of these theories. Hence, we refer to [18] all readers who are not familiar with the essential concepts. So, during citation of needed main results we sometimes will give the dual reference of these results (in one of the papers [11, 13–17] as well as in [18]).

[1] Note, that main results of the paper [12] were announced in [19].

2 Elementary-time states and changeable systems of universal kinematics

Definition 1. *Let $\mathcal{F}$ be any universal kinematics* [1], *$\mathfrak{l} \in \mathcal{L}k(\mathcal{F})$ be any reference frame of $\mathcal{F}$ and $\omega \in \mathbb{B}\mathfrak{s}(\mathfrak{l})$ be any elementary-time state in the reference frame $\mathfrak{l}$. The set*

$$\omega^{\{\mathfrak{l},\mathcal{F}\}} = \{(\mathfrak{m}, \langle ! \ \mathfrak{m} \leftarrow \mathfrak{l}\rangle\, \omega) \mid \mathfrak{m} \in \mathcal{L}k(\mathcal{F})\}$$

(where (x, y) is the ordered pair, composed of x and y) is called by ***elementary-time state of the universal kinematics*** *$\mathcal{F}$, generated by ω in the reference frame $\mathfrak{l}$.*

Remark 1. In the case, where the universal kinematics $\mathcal{F}$ is known in advance, we use the abbreviated denotation $\omega^{\{\mathfrak{l}\}}$ instead of the denotation $\omega^{\{\mathfrak{l},\mathcal{F}\}}$.

Assertion 1. *Let $\mathcal{F}$ be any universal kinematics and $\mathfrak{l}, \mathfrak{m} \in \mathcal{L}k(\mathcal{F})$. Then for arbitrary elementary-time states $\omega \in \mathbb{B}\mathfrak{s}(\mathfrak{l})$ and $\omega_1 \in \mathbb{B}\mathfrak{s}(\mathfrak{m})$ the following assertions are equivalent:*
1) $\omega^{\{\mathfrak{l}\}} = \omega_1^{\{\mathfrak{m}\}}$; 2) $\omega_1 = \langle ! \ \mathfrak{m} \leftarrow \mathfrak{l}\rangle\, \omega$.

Proof. **1.** First, we prove, that statement 2) leads to the statement 1). Consider any $\omega \in \mathbb{B}\mathfrak{s}(\mathfrak{l})$ and $\omega_1 \in \mathbb{B}\mathfrak{s}(\mathfrak{m})$ such that $\omega_1 = \langle ! \ \mathfrak{m} \leftarrow \mathfrak{l}\rangle\, \omega$. Applying Definition 1 and [18, Property 1.12.1(3)] [2], we deduce

$$\begin{aligned}\omega_1^{\{\mathfrak{m}\}} &= \{(\mathfrak{p}, \langle ! \ \mathfrak{p} \leftarrow \mathfrak{m}\rangle\, \omega_1) \mid \mathfrak{p} \in \mathcal{L}k(\mathcal{F})\} = \\ &= \{(\mathfrak{p}, \langle ! \ \mathfrak{p} \leftarrow \mathfrak{m}\rangle\, \langle ! \ \mathfrak{m} \leftarrow \mathfrak{l}\rangle\, \omega) \mid \mathfrak{p} \in \mathcal{L}k(\mathcal{F})\} = \\ &= \{(\mathfrak{p}, \langle ! \ \mathfrak{p} \leftarrow \mathfrak{l}\rangle\, \omega) \mid \mathfrak{p} \in \mathcal{L}k(\mathcal{F})\} = \omega^{\{\mathfrak{l}\}}.\end{aligned}$$

2. Inversely, suppose, that $\omega \in \mathbb{B}\mathfrak{s}(\mathfrak{l})$, $\omega_1 \in \mathbb{B}\mathfrak{s}(\mathfrak{m})$ and $\omega^{\{\mathfrak{l}\}} = \omega_1^{\{\mathfrak{m}\}}$. Then, by Definition 1, we have

$$\begin{aligned}\{(\mathfrak{p}, \langle ! \ \mathfrak{p} \leftarrow \mathfrak{l}\rangle\, \omega) \mid \mathfrak{p} \in \mathcal{L}k(\mathcal{F})\} = \\ = \{(\mathfrak{p}, \langle ! \ \mathfrak{p} \leftarrow \mathfrak{m}\rangle\, \omega_1) \mid \mathfrak{p} \in \mathcal{L}k(\mathcal{F})\}. \quad (1)\end{aligned}$$

According to [18, Property 1.12.1(1)], we have, $\langle ! \ \mathfrak{l} \leftarrow \mathfrak{l}\rangle\, \omega = \omega$. Hence, in accordance with (1), for element $(\mathfrak{l}, \omega) = (\mathfrak{l}, \langle ! \ \mathfrak{l} \leftarrow \mathfrak{l}\rangle\, \omega) \in \{(\mathfrak{p}, \langle ! \ \mathfrak{p} \leftarrow \mathfrak{l}\rangle\, \omega) \mid \mathfrak{p} \in \mathcal{L}k(\mathcal{F})\}$ we obtain the correlation, $(\mathfrak{l}, \omega) \in \{(\mathfrak{p}, \langle ! \ \mathfrak{p} \leftarrow \mathfrak{m}\rangle\, \omega_1) \mid \mathfrak{p} \in \mathcal{L}k(\mathcal{F})\}$. Therefore, there exists the reference frame $\mathfrak{p}_0 \in \mathcal{L}k(\mathcal{F})$ such that $(\mathfrak{l}, \omega) = (\mathfrak{p}_0, \langle ! \ \mathfrak{p}_0 \leftarrow \mathfrak{m}\rangle\, \omega_1)$. Hence we deduce $\mathfrak{l} = \mathfrak{p}_0$, as well $\omega = \langle ! \ \mathfrak{p}_0 \leftarrow \mathfrak{m}\rangle\, \omega_1 = \langle ! \ \mathfrak{l} \leftarrow \mathfrak{m}\rangle\, \omega_1$. So, based on [18, Properties 1.12.1(1,3)], we conclude, $\omega_1 = \langle ! \ \mathfrak{m} \leftarrow \mathfrak{m}\rangle\, \omega_1 = \langle ! \ \mathfrak{m} \leftarrow \mathfrak{l}\rangle\, \langle ! \ \mathfrak{l} \leftarrow \mathfrak{m}\rangle\, \omega_1 = \langle ! \ \mathfrak{m} \leftarrow \mathfrak{l}\rangle\, \omega$. □

The next corollary follows from Assertion 1.

Corollary 1. *Let $\mathcal{F}$ be any universal kinematics. Then for every $\mathfrak{l}, \mathfrak{m} \in \mathcal{L}k(\mathcal{F})$ and $\omega \in \mathbb{B}\mathfrak{s}(\mathfrak{l})$ the following equality holds:*

$$\omega^{\{\mathfrak{l}\}} = (\langle ! \ \mathfrak{m} \leftarrow \mathfrak{l}\rangle\, \omega)^{\{\mathfrak{m}\}}.$$

[1] Definition of universal kinematics can be found in [11, page 89] or [18, page 156].

[2] Reference to Property 1.12.1(3) means reference to the item 3 from the group of properties "Properties 1.12.1".

Assertion 2. *Let $\mathcal{F}$ be any universal kinematics. Then the set*

$$\mathbb{B}\mathfrak{s}[\mathfrak{l}, \mathcal{F}] = \left\{\omega^{\{\mathfrak{l},\mathcal{F}\}} \mid \omega \in \mathbb{B}\mathfrak{s}(\mathfrak{l})\right\} \quad (2)$$

does not depend of the reference frame $\mathfrak{l} \in \mathcal{L}k(\mathcal{F})$ (ie $\forall \mathfrak{l}, \mathfrak{m} \in \mathcal{L}k(\mathcal{F})$ $\mathbb{B}\mathfrak{s}[\mathfrak{l}, \mathcal{F}] = \mathbb{B}\mathfrak{s}[\mathfrak{m}, \mathcal{F}]$).

Proof. Consider arbitrary $\mathfrak{l}, \mathfrak{m} \in \mathcal{L}k(\mathcal{F})$. Using Corollary 1, we have

$$\begin{aligned}\mathbb{B}\mathfrak{s}[\mathfrak{l}, \mathcal{F}] = \left\{\omega^{\{\mathfrak{l}\}} \mid \omega \in \mathbb{B}\mathfrak{s}(\mathfrak{l})\right\} = \\ = \left\{(\langle ! \ \mathfrak{m} \leftarrow \mathfrak{l}\rangle\, \omega)^{\{\mathfrak{m}\}} \mid \omega \in \mathbb{B}\mathfrak{s}(\mathfrak{l})\right\}.\end{aligned}$$

Hence, according to [18, Corollary 1.12.6], we obtain

$$\begin{aligned}\mathbb{B}\mathfrak{s}[\mathfrak{l}, \mathcal{F}] = \left\{(\langle ! \ \mathfrak{m} \leftarrow \mathfrak{l}\rangle\, \omega)^{\{\mathfrak{m}\}} \mid \omega \in \mathbb{B}\mathfrak{s}(\mathfrak{l})\right\} = \\ = \left\{\omega_1^{\{\mathfrak{m}\}} \mid \omega_1 \in \mathbb{B}\mathfrak{s}(\mathfrak{m})\right\} = \mathbb{B}\mathfrak{s}[\mathfrak{m}, \mathcal{F}].\end{aligned}$$ □

Definition 2. *Let $\mathcal{F}$ be any universal kinematics.*

1. *The set $\mathbb{B}\mathfrak{s}(\mathcal{F}) = \mathbb{B}\mathfrak{s}[\mathfrak{l}, \mathcal{F}]$ $(\forall \mathfrak{l} \in \mathcal{L}k(\mathcal{F}))$ is called by the set of all elementary-time states of $\mathcal{F}$.*

2. *Any subset $\widehat{\mathbf{A}} \subseteq \mathbb{B}\mathfrak{s}(\mathcal{F})$ is called by the (common)* ***changeable system of the universal kinematics*** *$\mathcal{F}$.*

Assertion 3. *Let $\mathcal{F}$ be any universal kinematics and $\mathfrak{l} \in \mathcal{L}k(\mathcal{F})$ be any reference frame of $\mathcal{F}$. Then for every element $\hat{\omega} \in \mathbb{B}\mathfrak{s}(\mathcal{F})$ only one element $\omega_0 \in \mathbb{B}\mathfrak{s}(\mathfrak{l})$ exists such, that $\hat{\omega} = \omega_0^{\{\mathfrak{l}\}}$.*

Proof. Consider any $\mathfrak{l} \in \mathcal{L}k(\mathcal{F})$ and $\hat{\omega} \in \mathbb{B}\mathfrak{s}(\mathcal{F})$. By Definition 2 and Assertion 2 (formula (2)), we have

$$\mathbb{B}\mathfrak{s}(\mathcal{F}) = \mathbb{B}\mathfrak{s}[\mathfrak{l}, \mathcal{F}] = \left\{\omega^{\{\mathfrak{l}\}} \mid \omega \in \mathbb{B}\mathfrak{s}(\mathfrak{l})\right\}.$$

So, since $\hat{\omega} \in \mathbb{B}\mathfrak{s}(\mathcal{F})$, the element $\omega_0 \in \mathbb{B}\mathfrak{s}(\mathfrak{l})$ must exist such that the following equality is performed:

$$\hat{\omega} = \omega_0^{\{\mathfrak{l}\}}. \quad (3)$$

Let us prove that such element ω_0 is unique. Assume that $\hat{\omega} = \omega_1^{\{\mathfrak{l}\}}$, where $\omega_1 \in \mathbb{B}\mathfrak{s}(\mathfrak{l})$. Then, from the equality (3) we deduce, $\omega_0^{\{\mathfrak{l}\}} = \omega_1^{\{\mathfrak{l}\}}$. Hence, according to Assertion 1 and [18, Property 1.12.1(1)], we obtain, $\omega_1 = \langle ! \ \mathfrak{l} \leftarrow \mathfrak{l}\rangle\, \omega_0 = \omega_0$. □

Definition 3. *Let $\mathcal{F}$ be any universal kinematics, $\hat{\omega} \in \mathbb{B}\mathfrak{s}(\mathcal{F})$ be any elementary-time state of $\mathcal{F}$ and $\mathfrak{l} \in \mathcal{L}k(\mathcal{F})$ be any reference frame of $\mathcal{F}$. Elementary-time state $\omega \in \mathbb{B}\mathfrak{s}(\mathfrak{l})$ is named by* ***image*** *of elementary-time state $\hat{\omega}$* ***in the reference frame*** *$\mathfrak{l}$ if and only if $\hat{\omega} = \omega^{\{\mathfrak{l}\}}$.*

In accordance with Assertion 3, every elementary-time state $\hat{\omega} \in \mathbb{B}\mathfrak{s}(\mathcal{F})$ always has only one image in any reference frame $\mathfrak{l} \in \mathcal{L}k(\mathcal{F})$. Image of elementary-time state $\hat{\omega} \in \mathbb{B}\mathfrak{s}(\mathcal{F})$ in the reference frame $\mathfrak{l} \in \mathcal{L}k(\mathcal{Z})$ will be denoted via $\hat{\omega}_{\{\mathfrak{l},\mathcal{F}\}}$ (in the cases, where the universal kinematics $\mathcal{F}$ is known in advance, we use the abbreviated denotation $\hat{\omega}_{\{\mathfrak{l}\}}$).

Thus, according to Definition 3, for arbitrary $\hat{\omega} \in \mathbb{B}\mathfrak{s}(\mathcal{F})$ the following equality holds:

$$(\hat{\omega}_{\{\mathfrak{l}\}})^{\{\mathfrak{l}\}} = \hat{\omega}. \tag{4}$$

From the other hand, if for any reference frame $\mathfrak{l} \in \mathcal{L}k(\mathcal{F})$ and any fixed elementary-time state $\omega \in \mathbb{B}\mathfrak{s}(\mathfrak{l})$, we denote $\hat{\omega} := \omega^{\{\mathfrak{l}\}}$, then by Definition 3, we will receive, $\omega = \hat{\omega}_{\{\mathfrak{l}\}}$. Therefore we have:

$$\left(\omega^{\{\mathfrak{l}\}}\right)_{\{\mathfrak{l}\}} = \omega \quad (\forall \mathfrak{l} \in \mathcal{L}k(\mathcal{F})\ \forall \omega \in \mathbb{B}\mathfrak{s}(\mathfrak{l})). \tag{5}$$

From equalities (4) and (5) we deduce the following corollary:

Corollary 2. *Let $\mathcal{F}$ be any universal kinematics and $\mathfrak{l} \in \mathcal{L}k(\mathcal{F})$ be any reference frame of $\mathcal{F}$. Then:*

1. *The mapping $(\cdot)^{\{\mathfrak{l}\}}$ is bijection from $\mathbb{B}\mathfrak{s}(\mathfrak{l})$ onto $\mathbb{B}\mathfrak{s}(\mathcal{F})$.*
2. *The mapping $(\cdot)_{\{\mathfrak{l}\}}$ is bijection from $\mathbb{B}\mathfrak{s}(\mathcal{F})$ onto $\mathbb{B}\mathfrak{s}(\mathfrak{l})$.*
3. *The mapping $(\cdot)_{\{\mathfrak{l}\}}$ is inverse to the mapping $(\cdot)^{\{\mathfrak{l}\}}$.*

Assertion 4. *Let $\mathcal{F}$ be any universal kinematics and $\mathfrak{l}, \mathfrak{m} \in \mathcal{L}k(\mathcal{F})$ be any reference frames $\mathcal{F}$. Then the following statements are performed:*

1. For every $\hat{\omega} \in \mathbb{B}\mathfrak{s}(\mathcal{F})$ the equality $\hat{\omega}_{\{\mathfrak{m}\}} = \langle ! \ \mathfrak{m} \leftarrow \mathfrak{l} \rangle \hat{\omega}_{\{\mathfrak{l}\}}$ holds.

2. For each $\omega \in \mathbb{B}\mathfrak{s}(\mathfrak{l})$ the equality $\left(\omega^{\{\mathfrak{l}\}}\right)_{\{\mathfrak{m}\}} = \langle ! \ \mathfrak{m} \leftarrow \mathfrak{l} \rangle \omega$ is true.

Proof. 1) Chose any $\hat{\omega} \in \mathbb{B}\mathfrak{s}(\mathcal{F})$. Applying Corollary 1 to the elementary-time state $\hat{\omega}_{\{\mathfrak{l}\}} \in \mathbb{B}\mathfrak{s}(\mathfrak{l})$ and using equality (4), we obtain

$$(\langle ! \ \mathfrak{m} \leftarrow \mathfrak{l} \rangle \hat{\omega}_{\{\mathfrak{l}\}})^{\{\mathfrak{m}\}} = (\hat{\omega}_{\{\mathfrak{l}\}})^{\{\mathfrak{l}\}} = \hat{\omega}.$$

Thence, using equality (5), we have

$$\hat{\omega}_{\{\mathfrak{m}\}} = \left((\langle ! \ \mathfrak{m} \leftarrow \mathfrak{l} \rangle \hat{\omega}_{\{\mathfrak{l}\}})^{\{\mathfrak{m}\}}\right)_{\{\mathfrak{m}\}} = \langle ! \ \mathfrak{m} \leftarrow \mathfrak{l} \rangle \hat{\omega}_{\{\mathfrak{l}\}}.$$

2) Consider any $\omega \in \mathbb{B}\mathfrak{s}(\mathfrak{l})$. Applying Corollary 1 as well as equality (5), we deliver

$$\left(\omega^{\{\mathfrak{l}\}}\right)_{\{\mathfrak{m}\}} = \left((\langle ! \ \mathfrak{m} \leftarrow \mathfrak{l} \rangle \omega)^{\{\mathfrak{m}\}}\right)_{\{\mathfrak{m}\}} = \langle ! \ \mathfrak{m} \leftarrow \mathfrak{l} \rangle \omega. \qquad \square$$

Let $\mathcal{F}$ be any universal kinematics. The set $\widehat{\mathbf{A}}_{\{\mathfrak{l},\mathcal{F}\}} = \left\{\hat{\omega}_{\{\mathfrak{l},\mathcal{F}\}} \mid \hat{\omega} \in \widehat{\mathbf{A}}\right\}$ is called ***image of changeable system*** $\widehat{\mathbf{A}} \subseteq \mathbb{B}\mathfrak{s}(\mathcal{F})$ in the reference frame $\mathfrak{l} \in \mathcal{L}k(\mathcal{F})$.

Any changeable system $A \subseteq \mathbb{B}\mathfrak{s}(\mathfrak{l})$ in the reference frame $\mathfrak{l} \in \mathcal{L}k(\mathcal{F})$ always generates the (common) changeable system $A^{\{\mathfrak{l},\mathcal{F}\}} := \left\{\omega^{\{\mathfrak{l},\mathcal{F}\}} \mid \omega \in A\right\} \subseteq \mathbb{B}\mathfrak{s}(\mathcal{F})$.

Remark 2. In the cases, where universal kinematics $\mathcal{F}$ is known in advance, we use the abbreviated denotations $\widehat{\mathbf{A}}_{\{\mathfrak{l}\}}$ and $A^{\{\mathfrak{l}\}}$ instead of $\widehat{\mathbf{A}}_{\{\mathfrak{l},\mathcal{F}\}}$ and $A^{\{\mathfrak{l},\mathcal{F}\}}$ (correspondingly).

Applying equalities (4) and (5), we obtain the equalities:

$$\left(\widehat{\mathbf{A}}_{\{\mathfrak{l}\}}\right)^{\{\mathfrak{l}\}} = \widehat{\mathbf{A}} \quad \text{and} \quad \left(A^{\{\mathfrak{l}\}}\right)_{\{\mathfrak{l}\}} = A$$

(for arbitrary universal kinematics $\mathcal{F}$, reference frame $\mathfrak{l} \in \mathcal{L}k(\mathcal{F})$ and changeable systems $\widehat{\mathbf{A}} \subseteq \mathbb{B}\mathfrak{s}(\mathcal{F})$ as well $A \subseteq \mathbb{B}\mathfrak{s}(\mathfrak{l})$).

3 Chain paths of universal kinematics and definition of time irreversibility

Definition 4. *Let $\mathcal{F}$ be any universal kinematics. Changeable system $\widehat{\mathbf{A}} \subseteq \mathbb{B}\mathfrak{s}(\mathcal{F})$ is called **piecewise chain** changeable system if and only if there exist the sequences of changeable systems $\widehat{\mathbf{A}}_1, \cdots, \widehat{\mathbf{A}}_n \subseteq \mathbb{B}\mathfrak{s}(\mathcal{F})$ and reference frames $\mathfrak{l}_1, \cdots, \mathfrak{l}_n \in \mathcal{L}k(\mathcal{F})$ ($n \in \mathbb{N}$) satisfying the following conditions:*

(a) $\left(\widehat{\mathbf{A}}_k\right)_{\{\mathfrak{l}_k\}} \in \mathbb{L}l(\mathfrak{l}_k) \quad \left(\forall k \in \overline{1,n}\right)$,[1] *where definition of set $\mathbb{L}l(\mathfrak{l}_k) = \mathbb{L}l((\mathfrak{l}_k)^{\wedge})$ can be found in* [18, pages 63, 88, 156]*;*

(b) $\bigcup_{k=1}^{n} \widehat{\mathbf{A}}_k = \widehat{\mathbf{A}}$,

and, moreover, in the case $n \geq 2$ the following additional conditions are satisfied:

(c) $\widehat{\mathbf{A}}_k \cap \widehat{\mathbf{A}}_{k+1} \neq \emptyset \ \left(\forall k \in \overline{1,n-1}\right)$;

(d) *For each $k \in \overline{1,n-1}$ and arbitrary $\omega_1 \in \left(\widehat{\mathbf{A}}_k \setminus \widehat{\mathbf{A}}_{k+1}\right)_{\{\mathfrak{l}_k\}}$, $\omega_2 \in \left(\widehat{\mathbf{A}}_k \cap \widehat{\mathbf{A}}_{k+1}\right)_{\{\mathfrak{l}_k\}}$ the inequality $\mathsf{tm}(\omega_1) <_{\mathfrak{l}_k} \mathsf{tm}(\omega_2)$ holds.*

(e) *For every $k \in \overline{2,n}$ and arbitrary $\omega_1 \in \left(\widehat{\mathbf{A}}_{k-1} \cap \widehat{\mathbf{A}}_k\right)_{\{\mathfrak{l}_k\}}$, $\omega_2 \in \left(\widehat{\mathbf{A}}_k \setminus \widehat{\mathbf{A}}_{k-1}\right)_{\{\mathfrak{l}_k\}}$ the inequality $\mathsf{tm}(\omega_1) <_{\mathfrak{l}_k} \mathsf{tm}(\omega_2)$ is performed.*

*In this case the ordered composition $\mathscr{A} = \left(\widehat{\mathbf{A}}, \left(\widehat{\mathbf{A}}_1, \mathfrak{l}_1\right), \cdots, \left(\widehat{\mathbf{A}}_n, \mathfrak{l}_n\right)\right)$ will be named by the **chain path** of universal kinematics $\mathcal{F}$.*

Definition 5. *Let $\mathcal{F}$ be any universal kinematics.*

(a) *Changeable system $A \subseteq \mathbb{B}\mathfrak{s}(\mathfrak{l})$ is refereed to as **geometrically-stationary** in the reference frame $\mathfrak{l} \in \mathcal{L}k(\mathcal{F})$ if and only if $A \in \mathbb{L}l(\mathfrak{l})$ and for arbitrary $\omega_1, \omega_2 \in A$ the equality $\mathsf{bs}\left(\mathbf{Q}^{\langle \mathfrak{l} \rangle}(\omega_1)\right) = \mathsf{bs}\left(\mathbf{Q}^{\langle \mathfrak{l} \rangle}(\omega_2)\right)$ holds.*

(b) *The set of all geometrically-stationary changeable systems in the reference frame $\mathfrak{l}$ is denoted via $\mathbb{L}g(\mathfrak{l}, \mathcal{F})$. In the cases, where the universal kinematics $\mathcal{F}$ is known in advance, we use the abbreviated denotation $\mathbb{L}g(\mathfrak{l})$.*

(c) *The chain path $\mathscr{A} = \left(\widehat{\mathbf{A}}, \left(\widehat{\mathbf{A}}_1, \mathfrak{l}_1\right), \cdots, \left(\widehat{\mathbf{A}}_n, \mathfrak{l}_n\right)\right)$ in $\mathcal{F}$ ($n \in \mathbb{N}$) is called by **piecewise geometrically-stationary** if and only if $\forall k \in \overline{1,n}\ \left(\widehat{\mathbf{A}}_k\right)_{\{\mathfrak{l}_k\}} \in \mathbb{L}g(\mathfrak{l}_k)$.*

From the physical point of view piecewise geometrically-stationary chain path may be interpreted as process of "vagrancy" of observer (or some material particle or signal), which moves by means of "jumping" from previous reference frame to the next frame with a finite number of times.

Definition 6. *Let $\mathcal{F}$ be any universal kinematics and let $\mathscr{A} = \left(\widehat{\mathbf{A}}, \left(\widehat{\mathbf{A}}_1, \mathfrak{l}_1\right), \cdots, \left(\widehat{\mathbf{A}}_n, \mathfrak{l}_n\right)\right)$ be arbitrary chain path in $\mathcal{F}$.*

[1] Further we denote via $\overline{m,n}$ ($m, n \in \mathbb{N}$, $m \leq n$) the set $\overline{m,n} = \{m, \cdots, n\}$.

1. *Element* $\hat{\omega}_s \in \mathbb{B}\mathfrak{s}(\mathcal{F})$ *is called by* ***start*** *element of the path* $\mathscr{A}$*, if and only if* $\hat{\omega}_s \in \widehat{\mathbf{A}}_1$ *and for every* $\hat{\omega} \in \widehat{\mathbf{A}}_1$ *the inequality* $\mathsf{tm}\left((\hat{\omega}_s)_{\{\mathfrak{l}_1\}}\right) \leq_{\mathfrak{l}_1} \mathsf{tm}\left((\hat{\omega})_{\{\mathfrak{l}_1\}}\right)$ *is performed.*
2. *Element* $\hat{\omega}_f \in \mathbb{B}\mathfrak{s}(\mathcal{F})$ *is called by* ***final*** *element of the path* $\mathscr{A}$*, if and only if* $\hat{\omega}_f \in \widehat{\mathbf{A}}_n$ *and for every* $\hat{\omega} \in \widehat{\mathbf{A}}_n$ *the inequality* $\mathsf{tm}\left((\hat{\omega})_{\{\mathfrak{l}_n\}}\right) \leq_{\mathfrak{l}_n} \mathsf{tm}\left(\left(\hat{\omega}_f\right)_{\{\mathfrak{l}_n\}}\right)$ *holds.*
3. *The chain path* $\mathscr{A}$*, which owns (at least one) start element and (at least one) final element, is called by* ***closed****.*

Assertion 5. *Any chain path* $\mathscr{A}$ *of arbitrary universal kinematics* $\mathcal{F}$ *can not have more, than one start element and more, than one final element.*

Proof. **(a)** Let $\hat{\omega}_s$, $\hat{\omega}_x$ be two start elements of the chain path $\mathscr{A} = \left(\widehat{\mathbf{A}}, \left(\widehat{\mathbf{A}}_1, \mathfrak{l}_1\right), \cdots, \left(\widehat{\mathbf{A}}_n, \mathfrak{l}_n\right)\right)$. Then, by Definition 6, we have $\hat{\omega}_s, \hat{\omega}_x \in \widehat{\mathbf{A}}_1$, $\mathsf{tm}\left((\hat{\omega}_s)_{\{\mathfrak{l}_1\}}\right) \leq_{\mathfrak{l}_1} \mathsf{tm}\left((\hat{\omega}_x)_{\{\mathfrak{l}_1\}}\right)$ and $\mathsf{tm}\left((\hat{\omega}_x)_{\{\mathfrak{l}_1\}}\right) \leq_{\mathfrak{l}_1} \mathsf{tm}\left((\hat{\omega}_s)_{\{\mathfrak{l}_1\}}\right)$. Therefore we get

$$\mathsf{tm}\left((\hat{\omega}_s)_{\{\mathfrak{l}_1\}}\right) = \mathsf{tm}\left((\hat{\omega}_x)_{\{\mathfrak{l}_1\}}\right). \tag{6}$$

Since $\hat{\omega}_s, \hat{\omega}_x \in \widehat{\mathbf{A}}_1$, then $(\hat{\omega}_s)_{\{\mathfrak{l}_1\}}, (\hat{\omega}_x)_{\{\mathfrak{l}_1\}} \in \left(\widehat{\mathbf{A}}_1\right)_{\{\mathfrak{l}_1\}}$, where, in accordance with Definition 4 (subitem (a)), we have, $\left(\widehat{\mathbf{A}}_1\right)_{\{\mathfrak{l}_1\}} \in \mathbb{L}l(\mathfrak{l}_1)$. That is, according to [18, Assertion 1.7.5 (item 1)], $\left(\widehat{\mathbf{A}}_1\right)_{\{\mathfrak{l}_1\}}$ is a function from $\mathbf{Tm}(\mathfrak{l}_1)$ into $\mathfrak{Bs}(\mathfrak{l}_1)$. So, using equality $\omega = (\mathsf{tm}(\omega), \mathsf{bs}(\omega))$ $(\omega \in \mathbb{B}\mathfrak{s}(\mathfrak{l}_1))$ as well as formula (6), we obtain

$$\begin{aligned}\mathsf{bs}\left((\hat{\omega}_s)_{\{\mathfrak{l}_1\}}\right) &= \left(\widehat{\mathbf{A}}_1\right)_{\{\mathfrak{l}_1\}}\left(\mathsf{tm}\left((\hat{\omega}_s)_{\{\mathfrak{l}_1\}}\right)\right) = \\ &= \left(\widehat{\mathbf{A}}_1\right)_{\{\mathfrak{l}_1\}}\left(\mathsf{tm}\left((\hat{\omega}_x)_{\{\mathfrak{l}_1\}}\right)\right) = \mathsf{bs}\left((\hat{\omega}_x)_{\{\mathfrak{l}_1\}}\right).\end{aligned}$$

Using the last equality and equality (6), we deduce, $(\hat{\omega}_s)_{\{\mathfrak{l}_1\}} = \left(\mathsf{tm}\left((\hat{\omega}_s)_{\{\mathfrak{l}_1\}}\right), \mathsf{bs}\left((\hat{\omega}_s)_{\{\mathfrak{l}_1\}}\right)\right) = \left(\mathsf{tm}\left((\hat{\omega}_x)_{\{\mathfrak{l}_1\}}\right), \mathsf{bs}\left((\hat{\omega}_x)_{\{\mathfrak{l}_1\}}\right)\right) = (\hat{\omega}_x)_{\{\mathfrak{l}_1\}}$. Hence, according to formula (4), we deliver $\hat{\omega}_s = \left((\hat{\omega}_s)_{\{\mathfrak{l}_1\}}\right)^{\{\mathfrak{l}_1\}} = \left((\hat{\omega}_x)_{\{\mathfrak{l}_1\}}\right)^{\{\mathfrak{l}_1\}} = \hat{\omega}_x$.

(c) Similarly it can be proven that the chain path $\mathscr{A}$ can not have more, than one final element. □

Further the start element of the chain path $\mathscr{A}$ of the universal kinematics $\mathcal{F}$ will be denoted via $\mathsf{po}(\mathscr{A}, \mathcal{F})$, or via $\mathsf{po}(\mathscr{A})$. The final element of the chain path $\mathscr{A}$ will be denoted via $\mathsf{ki}(\mathscr{A}, \mathcal{F})$, or via $\mathsf{ki}(\mathscr{A})$. Where the denotations $\mathsf{po}(\mathscr{A})$ and $\mathsf{ki}(\mathscr{A})$ are used in the cases when they do not cause misunderstanding. Thus, for every closed chain path $\mathscr{A}$ both start and final elements ($\mathsf{po}(\mathscr{A})$ and $\mathsf{ki}(\mathscr{A})$) always exist.

Definition 7. *Closed chain path* $\mathscr{A}$ *of universal kinematics* $\mathcal{F}$ *is refereed to as* ***geometrically-cyclic*** *in the reference frame* $\mathfrak{l} \in \mathcal{L}k(\mathcal{F})$ *if and only if* $\mathsf{bs}\left(\mathbf{Q}^{\langle\mathfrak{l}\rangle}\left(\mathsf{po}(\mathscr{A})_{\{\mathfrak{l}\}}\right)\right) = \mathsf{bs}\left(\mathbf{Q}^{\langle\mathfrak{l}\rangle}\left(\mathsf{ki}(\mathscr{A})_{\{\mathfrak{l}\}}\right)\right)$.

Definition 8. *Universal kinematics* $\mathcal{F}$ *is called* ***time irreversible*** *if and only if for every reference frame* $\mathfrak{l} \in \mathcal{L}k(\mathcal{F})$ *and for each chain path* $\mathscr{A}$*, geometrically-cyclic in the frame* $\mathfrak{l}$ *and piecewise geometrically-stationary in* $\mathcal{F}$*, it is performed the inequality* $\mathsf{tm}\left(\mathsf{po}(\mathscr{A})_{\{\mathfrak{l}\}}\right) \leq_{\mathfrak{l}} \mathsf{tm}\left(\mathsf{ki}(\mathscr{A})_{\{\mathfrak{l}\}}\right)$.

Universal kinematics $\mathcal{F}$ *is called* ***time reversible*** *if and only if it is not time irreversible.*

The physical sense of time irreversibility notion is that in time irreversible kinematics there is not any process or object which returns to the begin of the own path at the past, moving by means of "jumping" from previous reference frame to the next frame. So, there are not temporal paradoxes in these kinematics.

4 Direction of time between reference frames of universal kinematics

For formulation main theorem we need some notions, connected with direction of time between reference frames.

Definition 9. *Let* $\mathcal{F}$ *be any universal kinematics.*

1. *We say that reference frame* $\mathfrak{m} \in \mathcal{L}k(\mathcal{F})$ *is* ***time-nonnegative*** *relatively the reference frame* $\mathfrak{l} \in \mathcal{L}k(\mathcal{F})$ *(in the universal kinematics* $\mathcal{F}$*) (denotation is* $\mathfrak{m} \Uparrow_{\mathcal{F}} \mathfrak{l}$*) if and only if for arbitrary* $\mathrm{w}_1, \mathrm{w}_2 \in \mathbb{M}k(\mathfrak{l})$ *such that* $\mathsf{bs}(\mathrm{w}_1) = \mathsf{bs}(\mathrm{w}_2)$ *and* $\mathsf{tm}(\mathrm{w}_1) \leq_{\mathfrak{l}} \mathsf{tm}(\mathrm{w}_2)$ *it is performed the inequality,* $\mathsf{tm}([\mathfrak{m} \leftarrow \mathfrak{l}]\,\mathrm{w}_1) \leq_{\mathfrak{m}} \mathsf{tm}([\mathfrak{m} \leftarrow \mathfrak{l}]\,\mathrm{w}_2)$.
2. *We say that reference frame* $\mathfrak{m} \in \mathcal{L}k(\mathcal{F})$ *is* ***time-positive*** *in* $\mathcal{F}$ *relatively the reference frame* $\mathfrak{l} \in \mathcal{L}k(\mathcal{F})$ *(denotation is* $\mathfrak{m} \Uparrow^{+}_{\mathcal{F}} \mathfrak{l}$*) if and only if for arbitrary* $\mathrm{w}_1, \mathrm{w}_2 \in \mathbb{M}k(\mathfrak{l})$ *such that* $\mathsf{bs}(\mathrm{w}_1) = \mathsf{bs}(\mathrm{w}_2)$ *and* $\mathsf{tm}(\mathrm{w}_1) <_{\mathfrak{l}} \mathsf{tm}(\mathrm{w}_2)$ *it is performed the inequality,* $\mathsf{tm}([\mathfrak{m} \leftarrow \mathfrak{l}]\,\mathrm{w}_1) <_{\mathfrak{m}} \mathsf{tm}([\mathfrak{m} \leftarrow \mathfrak{l}]\,\mathrm{w}_2)$.
3. *We say that reference frame* $\mathfrak{m} \in \mathcal{L}k(\mathcal{F})$ *is* ***time-nonpositive*** *in* $\mathcal{F}$ *relatively the reference frame* $\mathfrak{l} \in \mathcal{L}k(\mathcal{F})$ *(denotation is* $\mathfrak{m} \Downarrow_{\mathcal{F}} \mathfrak{l}$*) if and only if for arbitrary* $\mathrm{w}_1, \mathrm{w}_2 \in \mathbb{M}k(\mathfrak{l})$ *such that* $\mathsf{bs}(\mathrm{w}_1) = \mathsf{bs}(\mathrm{w}_2)$ *and* $\mathsf{tm}(\mathrm{w}_1) \leq_{\mathfrak{l}} \mathsf{tm}(\mathrm{w}_2)$ *it is performed the inequality,* $\mathsf{tm}([\mathfrak{m} \leftarrow \mathfrak{l}]\,\mathrm{w}_1) \geq_{\mathfrak{m}} \mathsf{tm}([\mathfrak{m} \leftarrow \mathfrak{l}]\,\mathrm{w}_2)$.
4. *We say that reference frame* $\mathfrak{m} \in \mathcal{L}k(\mathcal{F})$ *is* ***time-negative*** *in* $\mathcal{F}$ *relatively the reference frame* $\mathfrak{l} \in \mathcal{L}k(\mathcal{F})$ *(denotation is* $\mathfrak{m} \Downarrow^{-}_{\mathcal{F}} \mathfrak{l}$*) if and only if for arbitrary* $\mathrm{w}_1, \mathrm{w}_2 \in \mathbb{M}k(\mathfrak{l})$ *such that* $\mathsf{bs}(\mathrm{w}_1) = \mathsf{bs}(\mathrm{w}_2)$ *and* $\mathsf{tm}(\mathrm{w}_1) <_{\mathfrak{l}} \mathsf{tm}(\mathrm{w}_2)$ *it is performed the inequality,* $\mathsf{tm}([\mathfrak{m} \leftarrow \mathfrak{l}]\,\mathrm{w}_1) >_{\mathfrak{m}} \mathsf{tm}([\mathfrak{m} \leftarrow \mathfrak{l}]\,\mathrm{w}_2)$.
5. *The universal kinematics* $\mathcal{F}$ *is named by* ***weakly time-positive*** *if and only if there exist at least one reference frame* $\mathfrak{l}_0 \in \mathcal{L}k(\mathcal{F})$ *such that the correlation* $\mathfrak{l}_0 \Uparrow^{+}_{\mathcal{F}} \mathfrak{l}$ *holds for every reference frame* $\mathfrak{l} \in \mathcal{L}k(\mathcal{F})$.

Remark 3. Apart from weak time-positivity we can introduce other, more strong, form of time-positivity. We say that universal kinematics $\mathcal{F}$ is **time-positive** if and only if for arbitrary reference frames $\mathfrak{l}, \mathfrak{m} \in \mathcal{L}k(\mathcal{F})$ the correlation $\mathfrak{l} \Uparrow^{+}_{\mathcal{F}} \mathfrak{m}$

holds. It is not hard to prove that every kinematics of kind $\mathcal{F} = \mathfrak{UP}(\mathfrak{H}, \mathcal{B}, c)$ (connected with classical special relativity and introduced in [11] and [18, Section 24]) is time-positive.

Assertion 6. *For arbitrary reference frames $\mathfrak{l}, \mathfrak{m} \in \mathcal{L}k(\mathcal{F})$ of any universal kinematics $\mathcal{F}$ the following statements are performed.*

1) If $\mathfrak{m} \Uparrow^{+}_{\mathcal{F}} \mathfrak{l}$, then $\mathfrak{m} \Uparrow_{\mathcal{F}} \mathfrak{l}$.

2) If $\mathfrak{m} \Downarrow^{-}_{\mathcal{F}} \mathfrak{l}$, then $\mathfrak{m} \Downarrow_{\mathcal{F}} \mathfrak{l}$.

Proof. **1)** Indeed, let $\mathfrak{l}, \mathfrak{m} \in \mathcal{L}k(\mathcal{F})$ and $\mathfrak{m} \Uparrow^{+}_{\mathcal{F}} \mathfrak{l}$. Then for every $\mathrm{w}_1, \mathrm{w}_2 \in \mathbb{M}k(\mathfrak{l})$ such, that $\mathsf{bs}(\mathrm{w}_1) = \mathsf{bs}(\mathrm{w}_2)$ and $\mathsf{tm}(\mathrm{w}_1) \leq_{\mathfrak{l}} \mathsf{tm}(\mathrm{w}_2)$, we deduce the following:

(a) In the case $\mathsf{tm}(\mathrm{w}_1) <_{\mathfrak{l}} \mathsf{tm}(\mathrm{w}_2)$, by Definition 9, item 2, we get, $\mathsf{tm}([\mathfrak{m} \leftarrow \mathfrak{l}]\,\mathrm{w}_1) <_{\mathfrak{m}} \mathsf{tm}([\mathfrak{m} \leftarrow \mathfrak{l}]\,\mathrm{w}_2)$.

(b) In the case $\mathsf{tm}(\mathrm{w}_1) = \mathsf{tm}(\mathrm{w}_2)$, we have $\mathrm{w}_1 = (\mathsf{tm}(\mathrm{w}_1), \mathsf{bs}(\mathrm{w}_1)) = (\mathsf{tm}(\mathrm{w}_2), \mathsf{bs}(\mathrm{w}_2)) = \mathrm{w}_2$, and so $\mathsf{tm}([\mathfrak{m} \leftarrow \mathfrak{l}]\,\mathrm{w}_1) = \mathsf{tm}([\mathfrak{m} \leftarrow \mathfrak{l}]\,\mathrm{w}_2)$.

2) Second item of this Assertion can be proven similarly. □

5 Theorem of Non-Returning

Theorem 1. *Any weakly time-positive universal kinematics $\mathcal{F}$ is time irreversible.*

To prove Theorem 1 we need a few auxiliary assertions.

Assertion 7. *Let $\widehat{\mathbf{A}} \subseteq \mathbb{B}\mathfrak{s}(\mathcal{F})$ be changeable system of universal kinematics $\mathcal{F}$ such, that $\widehat{\mathbf{A}}_{\{\mathfrak{l}_0\}} \in \mathbb{L}g(\mathfrak{l}_0)$ for some reference frame $\mathfrak{l}_0 \in \mathcal{L}k(\mathcal{F})$. Let $\mathfrak{l} \in \mathcal{L}k(\mathcal{F})$ be reference frame, satisfying condition $\mathfrak{l} \Uparrow_{\mathcal{F}} \mathfrak{l}_0$.*

Then for arbitrary $\hat{\omega}_1, \hat{\omega}_2 \in \widehat{\mathbf{A}}$ the inequality $\mathsf{tm}\left((\hat{\omega}_1)_{\{\mathfrak{l}_0\}}\right) \leq_{\mathfrak{l}_0} \mathsf{tm}\left((\hat{\omega}_2)_{\{\mathfrak{l}_0\}}\right)$ assures the the inequality $\mathsf{tm}\left((\hat{\omega}_1)_{\{\mathfrak{l}\}}\right) \leq_{\mathfrak{l}} \mathsf{tm}\left((\hat{\omega}_2)_{\{\mathfrak{l}\}}\right)$.

Proof. Suppose that, under conditions of the assertion, we have $\hat{\omega}_1, \hat{\omega}_2 \in \widehat{\mathbf{A}}$ and $\mathsf{tm}\left((\hat{\omega}_1)_{\{\mathfrak{l}_0\}}\right) \leq_{\mathfrak{l}_0} \mathsf{tm}\left((\hat{\omega}_2)_{\{\mathfrak{l}_0\}}\right)$. According to Definition of Minkowski coordinates (see [11, formula (2)] or [18, formula (2.3)]), we have $\mathsf{tm}(\omega) = \mathsf{tm}\left(\mathbf{Q}^{\langle \mathfrak{l}_0 \rangle}(\omega)\right)$ $(\forall\, \omega \in \mathbb{B}\mathfrak{s}(\mathfrak{l}_0))$. So, we get

$$\mathsf{tm}\left(\mathbf{Q}^{\langle \mathfrak{l}_0 \rangle}\left((\hat{\omega}_1)_{\{\mathfrak{l}_0\}}\right)\right) \leq_{\mathfrak{l}_0} \mathsf{tm}\left(\mathbf{Q}^{\langle \mathfrak{l}_0 \rangle}\left((\hat{\omega}_2)_{\{\mathfrak{l}_0\}}\right)\right). \tag{7}$$

Since $(\hat{\omega}_1)_{\{\mathfrak{l}_0\}}, (\hat{\omega}_2)_{\{\mathfrak{l}_0\}} \in \widehat{\mathbf{A}}_{\{\mathfrak{l}_0\}}$ (where $\widehat{\mathbf{A}}_{\{\mathfrak{l}_0\}} \in \mathbb{L}g(\mathfrak{l}_0)$) then, by Definition 5 (items (a),(b)), we have

$$\mathsf{bs}\left(\mathbf{Q}^{\langle \mathfrak{l}_0 \rangle}\left((\hat{\omega}_1)_{\{\mathfrak{l}_0\}}\right)\right) = \mathsf{bs}\left(\mathbf{Q}^{\langle \mathfrak{l}_0 \rangle}\left((\hat{\omega}_2)_{\{\mathfrak{l}_0\}}\right)\right). \tag{8}$$

Taking into account that $\mathfrak{l} \Uparrow_{\mathcal{F}} \mathfrak{l}_0$ and using Definition 9 (item 1) as well as formulas (7), (8), we get the inequality:

$$\mathsf{tm}\left([\mathfrak{l} \leftarrow \mathfrak{l}_0]\,\mathbf{Q}^{\langle \mathfrak{l}_0 \rangle}\left((\hat{\omega}_1)_{\{\mathfrak{l}_0\}}\right)\right) \leq_{\mathfrak{l}} \mathsf{tm}\left([\mathfrak{l} \leftarrow \mathfrak{l}_0]\,\mathbf{Q}^{\langle \mathfrak{l}_0 \rangle}\left((\hat{\omega}_2)_{\{\mathfrak{l}_0\}}\right)\right).$$

Thence, using [18, formula (3.2)], we obtain

$$\mathsf{tm}\left(\mathbf{Q}^{\langle \mathfrak{l} \rangle}\left(\langle ! \; \mathfrak{l} \leftarrow \mathfrak{l}_0 \rangle\,(\hat{\omega}_1)_{\{\mathfrak{l}_0\}}\right)\right) \leq_{\mathfrak{l}} \leq_{\mathfrak{l}} \mathsf{tm}\left(\mathbf{Q}^{\langle \mathfrak{l} \rangle}\left(\langle ! \; \mathfrak{l} \leftarrow \mathfrak{l}_0 \rangle\,(\hat{\omega}_2)_{\{\mathfrak{l}_0\}}\right)\right).$$

Applying the last inequality as well as Assertion 4, we deduce the inequality:

$$\mathsf{tm}\left(\mathbf{Q}^{\langle \mathfrak{l} \rangle}\left((\hat{\omega}_1)_{\{\mathfrak{l}\}}\right)\right) \leq_{\mathfrak{l}} \mathsf{tm}\left(\mathbf{Q}^{\langle \mathfrak{l} \rangle}\left((\hat{\omega}_2)_{\{\mathfrak{l}\}}\right)\right). \tag{9}$$

According to Definition of Minkowski coordinates (see [11, formula (2)] or [18, formula (2.3)]), for every $\omega \in \mathbb{B}\mathfrak{s}(\mathfrak{l})$ we have the equality $\mathsf{tm}\left(\mathbf{Q}^{\langle \mathfrak{l} \rangle}(\omega)\right) = \mathsf{tm}(\omega)$. That is why from the inequality (9) it follows the desired inequality $\mathsf{tm}\left((\hat{\omega}_1)_{\{\mathfrak{l}\}}\right) \leq_{\mathfrak{l}} \mathsf{tm}\left((\hat{\omega}_2)_{\{\mathfrak{l}\}}\right)$. □

Assertion 8. *Let, $\mathscr{A} = \left(\widehat{\mathbf{A}}, \left(\widehat{\mathbf{A}}_1, \mathfrak{l}_1\right), \cdots, \left(\widehat{\mathbf{A}}_n, \mathfrak{l}_n\right)\right)$ $(n \in \mathbb{N})$ be closed, piecewise geometrically-stationary chain path of universal kinematics $\mathcal{F}$ and $\mathfrak{l} \in \mathcal{L}k(\mathcal{F})$ be reference frame such that $\mathfrak{l} \Uparrow_{\mathcal{F}} \mathfrak{l}_i$ for every $i \in \overline{1,n}$. Then for arbitrary $\hat{\omega} \in \widehat{\mathbf{A}}$ the following inequality holds:*

$$\mathsf{tm}\left(\mathsf{po}(\mathscr{A})_{\{\mathfrak{l}\}}\right) \leq_{\mathfrak{l}} \mathsf{tm}(\hat{\omega}_{\{\mathfrak{l}\}}) \leq_{\mathfrak{l}} \mathsf{tm}\left(\mathsf{ki}(\mathscr{A})_{\{\mathfrak{l}\}}\right). \tag{10}$$

Proof. Let $\mathcal{F}$ be universal kinematics and $\mathscr{A} = \left(\widehat{\mathbf{A}}, \left(\widehat{\mathbf{A}}_1, \mathfrak{l}_1\right), \cdots, \left(\widehat{\mathbf{A}}_n, \mathfrak{l}_n\right)\right)$ $(n \in \mathbb{N})$ be closed, piecewise geometrically-stationary chain path of $\mathcal{F}$. Let, $\mathfrak{l} \in \mathcal{L}k(\mathcal{F})$ be reference frame such that $\mathfrak{l} \Uparrow_{\mathcal{F}} \mathfrak{l}_i$ $(\forall\, i \in \overline{1,n})$.

1) First we prove that for any $\hat{\omega} \in \widehat{\mathbf{A}}$ it holds the inequality:

$$\mathsf{tm}\left(\mathsf{po}(\mathscr{A})_{\{\mathfrak{l}\}}\right) \leq_{\mathfrak{l}} \mathsf{tm}(\hat{\omega}_{\{\mathfrak{l}\}}). \tag{11}$$

By Definition 4 (item (b)), $\widehat{\mathbf{A}} = \bigcup_{k=1}^{n} \widehat{\mathbf{A}}_k$. So, it is sufficient to prove the inequality (11) for the cases $\hat{\omega} \in \widehat{\mathbf{A}}_k$ $(k \in \overline{1,n})$.

1.a) First we prove the inequality (11) for $\hat{\omega} \in \widehat{\mathbf{A}}_1$. According to Definition 6 (item 1), for $\hat{\omega} \in \widehat{\mathbf{A}}_1$ we obtain that $\mathsf{po}(\mathscr{A}) \in \widehat{\mathbf{A}}_1$ and

$$\mathsf{tm}\left(\mathsf{po}(\mathscr{A})_{\{\mathfrak{l}_1\}}\right) \leq_{\mathfrak{l}_1} \mathsf{tm}(\hat{\omega}_{\{\mathfrak{l}_1\}}). \tag{12}$$

According to the above, we have $\hat{\omega} \in \widehat{\mathbf{A}}_1$ and $\mathsf{po}(\mathscr{A}) \in \widehat{\mathbf{A}}_1$. Moreover, by Definition 5 (item (c)), we get, $\left(\widehat{\mathbf{A}}_1\right)_{\{\mathfrak{l}_1\}} \in \mathbb{L}g(\mathfrak{l}_1)$. By conditions of Assertion, we have, $\mathfrak{l} \Uparrow_{\mathcal{F}} \mathfrak{l}_1$. So, in accordance with Assertion 7, the correlation (12) stipulates the inequality $\mathsf{tm}\left(\mathsf{po}(\mathscr{A})_{\{\mathfrak{l}\}}\right) \leq_{\mathfrak{l}} \mathsf{tm}(\hat{\omega}_{\{\mathfrak{l}\}})$. Hence, in the case $\hat{\omega} \in \widehat{\mathbf{A}}_1$, the inequality (11) has been proven. Moreover, the last inequality has been proven for all $\hat{\omega} \in \widehat{\mathbf{A}}$ in the case $n = 1$. So, further we consider, that $n > 1$.

1.b) Assume, that inequality (11) is performed for all $\hat{\omega} \in \widehat{\mathbf{A}}_{k-1}$, where $k \in \overline{2,n}$. And, let us prove, that then this inequality is true for each $\hat{\omega} \in \widehat{\mathbf{A}}_k$.

In the case $\hat{\omega} \in \widehat{\mathbf{A}}_k \cap \widehat{\mathbf{A}}_{k-1}$ the inequality (11) is true in accordance with inductive hypothesis. Hence, it remains to

prove the last inequality for every $\hat{\omega} \in \widehat{\mathbf{A}}_k \setminus \widehat{\mathbf{A}}_{k-1}$. According to item (c) of Definition 4, we have $\widehat{\mathbf{A}}_k \cap \widehat{\mathbf{A}}_{k-1} \neq \emptyset$. Hence, at least one element $\hat{\eta} \in \widehat{\mathbf{A}}_k \cap \widehat{\mathbf{A}}_{k-1}$ exists. Since,

$$\hat{\eta} \in \widehat{\mathbf{A}}_k \cap \widehat{\mathbf{A}}_{k-1} \quad \text{and} \quad \hat{\omega} \in \widehat{\mathbf{A}}_k \setminus \widehat{\mathbf{A}}_{k-1}, \tag{13}$$

then we get $\hat{\eta}_{\{\mathfrak{l}_k\}} \in \left(\widehat{\mathbf{A}}_k \cap \widehat{\mathbf{A}}_{k-1}\right)_{\{\mathfrak{l}_k\}}$, $\hat{\omega}_{\{\mathfrak{l}_k\}} \in \left(\widehat{\mathbf{A}}_k \setminus \widehat{\mathbf{A}}_{k-1}\right)_{\{\mathfrak{l}_k\}}$. Therefore, according to item (e) of Definition 4, we deliver

$$\mathsf{tm}\left(\hat{\eta}_{\{\mathfrak{l}_k\}}\right) \leq_{\mathfrak{l}_k} \mathsf{tm}\left(\hat{\omega}_{\{\mathfrak{l}_k\}}\right). \tag{14}$$

According to (13), we have $\hat{\eta}$, $\hat{\omega} \in \widehat{\mathbf{A}}_k$, where, by item (c) of Definition 5, $\left(\widehat{\mathbf{A}}_k\right)_{\{\mathfrak{l}_k\}} \in \mathbb{L}g\left(\mathfrak{l}_k\right)$. Since $\mathfrak{l} \Uparrow_{\mathcal{F}} \mathfrak{l}_k$, then taking into account inequality (14) and Assertion 7 we deduce

$$\mathsf{tm}\left(\hat{\eta}_{\{\mathfrak{l}\}}\right) \leq_{\mathfrak{l}} \mathsf{tm}\left(\hat{\omega}_{\{\mathfrak{l}\}}\right). \tag{15}$$

According to (13), we have $\hat{\eta} \in \widehat{\mathbf{A}}_{k-1}$. So, by inductive hypothesis, we deliver

$$\mathsf{tm}\left(\mathsf{po}\left(\mathscr{A}\right)_{\{\mathfrak{l}\}}\right) \leq_{\mathfrak{l}} \mathsf{tm}\left(\hat{\eta}_{\{\mathfrak{l}\}}\right). \tag{16}$$

Inequalities (15) and (16) assure inequality (11).

Thus, by Principle of mathematical induction, inequality (11) is true for arbitrary $\hat{\omega} \in \bigcup_{k=1}^{n} \widehat{\mathbf{A}}_k = \widehat{\mathbf{A}}$.

2) Now we are aiming to prove, that for any $\hat{\omega} \in \widehat{\mathbf{A}}$ it holds the inequality:

$$\mathsf{tm}\left(\hat{\omega}_{\{\mathfrak{l}\}}\right) \leq_{\mathfrak{l}} \mathsf{tm}\left(\mathsf{ki}\left(\mathscr{A}\right)_{\{\mathfrak{l}\}}\right). \tag{17}$$

2.a) First we prove the inequality (17) for $\omega \in \widehat{\mathbf{A}}_n$. According to Definition 6 (item 2), for $\hat{\omega} \in \widehat{\mathbf{A}}_n$ we obtain that $\mathsf{ki}\left(\mathscr{A}\right) \in \widehat{\mathbf{A}}_n$ and

$$\mathsf{tm}\left(\hat{\omega}_{\{\mathfrak{l}_n\}}\right) \leq_{\mathfrak{l}_n} \mathsf{tm}\left(\mathsf{ki}\left(\mathscr{A}\right)_{\{\mathfrak{l}_n\}}\right). \tag{18}$$

According to the above, we have $\hat{\omega} \in \widehat{\mathbf{A}}_n$ and $\mathsf{ki}\left(\mathscr{A}\right) \in \widehat{\mathbf{A}}_n$. Moreover, by Definition 5 (item (c)), we get $\left(\widehat{\mathbf{A}}_n\right)_{\{\mathfrak{l}_n\}} \in \mathbb{L}g\left(\mathfrak{l}_n\right)$. By conditions of Assertion, we have $\mathfrak{l} \Uparrow_{\mathcal{F}} \mathfrak{l}_n$. So, in accordance with Assertion 7, the correlation (18) stipulates the inequality (17). Hence, in the case $\hat{\omega} \in \widehat{\mathbf{A}}_n$, the inequality (17) is proven. Moreover, the last inequality is proven for all $\hat{\omega} \in \widehat{\mathbf{A}}$ in the case $n = 1$. So, further we consider, that $n > 1$.

2.b) Assume, that inequality (17) is performed for all $\hat{\omega} \in \widehat{\mathbf{A}}_{k+1}$, where $k \in \overline{1, n-1}$. And, let us prove, that then this inequality is true for each $\hat{\omega} \in \widehat{\mathbf{A}}_k$.

In the case $\omega \in \widehat{\mathbf{A}}_k \cap \widehat{\mathbf{A}}_{k+1}$ the inequality (17) is true in accordance with inductive hypothesis. Hence, it remains to prove the last inequality for every $\hat{\omega} \in \widehat{\mathbf{A}}_k \setminus \widehat{\mathbf{A}}_{k+1}$. According to item (c) of Definition 4, we have $\widehat{\mathbf{A}}_k \cap \widehat{\mathbf{A}}_{k+1} \neq \emptyset$. Hence, at least one element $\hat{\eta} \in \widehat{\mathbf{A}}_k \cap \widehat{\mathbf{A}}_{k+1}$ exists. Taking into account that

$$\hat{\eta} \in \widehat{\mathbf{A}}_k \cap \widehat{\mathbf{A}}_{k+1} \quad \text{and} \quad \hat{\omega} \in \widehat{\mathbf{A}}_k \setminus \widehat{\mathbf{A}}_{k+1}, \tag{19}$$

we get $\hat{\eta}_{\{\mathfrak{l}_k\}} \in \left(\widehat{\mathbf{A}}_k \cap \widehat{\mathbf{A}}_{k+1}\right)_{\{\mathfrak{l}_k\}}$, $\hat{\omega}_{\{\mathfrak{l}_k\}} \in \left(\widehat{\mathbf{A}}_k \setminus \widehat{\mathbf{A}}_{k+1}\right)_{\{\mathfrak{l}_k\}}$. Therefore, according to item (d) of Definition 4, we deliver

$$\mathsf{tm}\left(\hat{\omega}_{\{\mathfrak{l}_k\}}\right) \leq_{\mathfrak{l}_k} \mathsf{tm}\left(\hat{\eta}_{\{\mathfrak{l}_k\}}\right). \tag{20}$$

According to (19), we have $\hat{\eta}$, $\hat{\omega} \in \widehat{\mathbf{A}}_k$, where $\left(\widehat{\mathbf{A}}_k\right)_{\{\mathfrak{l}_k\}} \in \mathbb{L}g\left(\mathfrak{l}_k\right)$ by item (c) of Definition 5. Since $\mathfrak{l} \Uparrow_{\mathcal{F}} \mathfrak{l}_k$ then, taking into account inequality (20) and Assertion 7, we deduce

$$\mathsf{tm}\left(\hat{\omega}_{\{\mathfrak{l}\}}\right) \leq_{\mathfrak{l}} \mathsf{tm}\left(\hat{\eta}_{\{\mathfrak{l}\}}\right). \tag{21}$$

According to (19), we have $\hat{\eta} \in \widehat{\mathbf{A}}_{k+1}$. So, by inductive hypothesis, we deliver

$$\mathsf{tm}\left(\hat{\eta}_{\{\mathfrak{l}\}}\right) \leq_{\mathfrak{l}} \mathsf{tm}\left(\mathsf{ki}\left(\mathscr{A}\right)_{\{\mathfrak{l}\}}\right). \tag{22}$$

Inequalities (21) and (22) assure inequality (17). Thus, by Principle of mathematical induction, inequality (17) is true for arbitrary $\hat{\omega} \in \bigcup_{k=1}^{n} \widehat{\mathbf{A}}_k = \widehat{\mathbf{A}}$.

Inequality (10) follows from (11) and (17). □

Proof of Theorem 1. Let $\mathcal{F}$ be weakly time-positive universal kinematics. Then, by Definition 9, there exists the reference frame $\mathfrak{l}_0 \in \mathcal{L}k\left(\mathcal{F}\right)$ such that

$$\forall\, \mathfrak{m} \in \mathcal{L}k\left(\mathcal{F}\right) \quad \mathfrak{l}_0 \Uparrow^{+}_{\mathcal{F}} \mathfrak{m}. \tag{23}$$

Let $\mathscr{A} = \left(\widehat{\mathbf{A}}, \left(\widehat{\mathbf{A}}_1, \mathfrak{l}_1\right), \cdots, \left(\widehat{\mathbf{A}}_n, \mathfrak{l}_n\right)\right)$ $(n \in \mathbb{N})$ be piecewise geometrically-stationary chain path in $\mathcal{F}$ and, moreover, $\mathscr{A}$ is geometrically-cyclic relatively some reference frame $\mathfrak{l} \in \mathcal{L}k\left(\mathcal{F}\right)$. By Definition 7, $\mathscr{A}$ is closed chain path. According to Assertion 6, correlation (23) leads to the correlation $\mathfrak{l}_0 \Uparrow_{\mathcal{F}} \mathfrak{l}_k$ $(\forall k \in \overline{1, n})$. Hence, applying Assertion 8, we ensure

$$\mathsf{tm}\left(\mathsf{po}\left(\mathscr{A}\right)_{\{\mathfrak{l}_0\}}\right) \leq_{\mathfrak{l}_0} \mathsf{tm}\left(\mathsf{ki}\left(\mathscr{A}\right)_{\{\mathfrak{l}_0\}}\right). \tag{24}$$

Assume, that $\mathsf{tm}\left(\mathsf{ki}\left(\mathscr{A}\right)_{\{\mathfrak{l}\}}\right) <_{\mathfrak{l}} \mathsf{tm}\left(\mathsf{po}\left(\mathscr{A}\right)_{\{\mathfrak{l}\}}\right)$. Then, by Definition of Minkowski coordinates (see [11, formula (2)] or [18, formula (2.3)]), we obtain

$$\mathsf{tm}\left(\mathbf{Q}^{\langle\mathfrak{l}\rangle}\left(\mathsf{ki}\left(\mathscr{A}\right)_{\{\mathfrak{l}\}}\right)\right) <_{\mathfrak{l}} \mathsf{tm}\left(\mathbf{Q}^{\langle\mathfrak{l}\rangle}\left(\mathsf{po}\left(\mathscr{A}\right)_{\{\mathfrak{l}\}}\right)\right). \tag{25}$$

Since the path $\mathscr{A}$ is geometrically-cyclic relatively the reference frame $\mathfrak{l}$, then, by Definition 7, we have

$$\mathsf{bs}\left(\mathbf{Q}^{\langle\mathfrak{l}\rangle}\left(\mathsf{po}\left(\mathscr{A}\right)_{\{\mathfrak{l}\}}\right)\right) = \mathsf{bs}\left(\mathbf{Q}^{\langle\mathfrak{l}\rangle}\left(\mathsf{ki}\left(\mathscr{A}\right)_{\{\mathfrak{l}\}}\right)\right). \tag{26}$$

Since (in accordance with (23)) $\mathfrak{l}_0 \Uparrow^{+}_{\mathcal{F}} \mathfrak{l}$, then, by Definition 9 (item 2), from the correlations (25), and (26), we get the inequality:

$$\mathsf{tm}\left([\mathfrak{l}_0 \leftarrow \mathfrak{l}]\,\mathbf{Q}^{\langle\mathfrak{l}\rangle}\left(\mathsf{ki}\left(\mathscr{A}\right)_{\{\mathfrak{l}\}}\right)\right) <_{\mathfrak{l}_0} <_{\mathfrak{l}_0} \mathsf{tm}\left([\mathfrak{l}_0 \leftarrow \mathfrak{l}]\,\mathbf{Q}^{\langle\mathfrak{l}\rangle}\left(\mathsf{po}\left(\mathscr{A}\right)_{\{\mathfrak{l}\}}\right)\right).$$

Thence, using [18, formula (3.2)] , we deduce the inequality:

$$\mathsf{tm}\left(\mathbf{Q}^{\langle \mathfrak{l}_0\rangle}\left(\langle !\ \mathfrak{l}_0 \leftarrow \mathfrak{l}\rangle\, \mathsf{ki}\,(\mathscr{A})_{\{\mathfrak{l}\}}\right)\right) <_{\mathfrak{l}_0} <_{\mathfrak{l}_0} \mathsf{tm}\left(\mathbf{Q}^{\langle \mathfrak{l}_0\rangle}\left(\langle !\ \mathfrak{l}_0 \leftarrow \mathfrak{l}\rangle\, \mathsf{po}\,(\mathscr{A})_{\{\mathfrak{l}\}}\right)\right).$$

Taking into account Assertion 4, the last inequality can be reduced to the form, $\mathsf{tm}\left(\mathbf{Q}^{\langle \mathfrak{l}_0\rangle}\left(\mathsf{ki}\,(\mathscr{A})_{\{\mathfrak{l}_0\}}\right)\right) <_{\mathfrak{l}_0} \mathsf{tm}\left(\mathbf{Q}^{\langle \mathfrak{l}_0\rangle}\left(\mathsf{po}\,(\mathscr{A})_{\{\mathfrak{l}_0\}}\right)\right)$, and, by Definition of Minkowski coordinates (see [11, formula (2)] or [18, formula (2.3)])), we assure

$$\mathsf{tm}\left(\mathsf{ki}\,(\mathscr{A})_{\{\mathfrak{l}_0\}}\right) <_{\mathfrak{l}_0} \mathsf{tm}\left(\mathsf{po}\,(\mathscr{A})_{\{\mathfrak{l}_0\}}\right).$$

But, the last inequality contradicts to the correlation (24). Therefore, hypothesis affirming, that $\mathsf{tm}\left(\mathsf{ki}\,(\mathscr{A})_{\{\mathfrak{l}\}}\right) <_{\mathfrak{l}} \mathsf{tm}\left(\mathsf{po}\,(\mathscr{A})_{\{\mathfrak{l}\}}\right)$ is false. Consequently we have

$$\mathsf{tm}\left(\mathsf{po}\,(\mathscr{A})_{\{\mathfrak{l}\}}\right) \leq_{\mathfrak{l}} \mathsf{tm}\left(\mathsf{ki}\,(\mathscr{A})_{\{\mathfrak{l}\}}\right). \tag{27}$$

Thus, for each reference frame $\mathfrak{l} \in \mathcal{L}k\,(\mathcal{F})$ and for each chain path $\mathscr{A}$, geometrically-cyclic in the frame $\mathfrak{l}$ and piecewise geometrically-stationary in $\mathcal{F}$, it holds the inequality (27). So, by Definition 8, kinematics $\mathcal{F}$ is time irreversible, which must be proved. □

6 Certainly time irreversibility. Strengthened version of theorem of non-returning

Recall, that in the papers [17, Definition 6], [18, Definition 3.25.2] the notion of equivalence of universal kinematics relatively coordinate transform had been introduced. According to these papers, we denote equivalent relatively coordinate transform kinematics $\mathcal{F}_1$ and $\mathcal{F}_2$ via $\mathcal{F}_1\,[\equiv]\,\mathcal{F}_2$.

Definition 10. *We say that universal kinematics $\mathcal{F}$ is **certainly time irreversible** if and only if arbitrary universal kinematics $\mathcal{F}_1$ such, that $\mathcal{F}\,[\equiv]\,\mathcal{F}_1$ is time irreversible. In the opposite case we will say that universal kinematics $\mathcal{F}$ is **conditionally time reversible**.*

Since, according to [17, Assertion 3] (see also [18, Assertion 3.25.1]), for each universal kinematics $\mathcal{F}$ it is fulfilled the correlation $\mathcal{F}\,[\equiv]\,\mathcal{F}$, then we receive the following Corollary from Definition 10:

Corollary 3. *Any certainly time irreversible universal kinematics $\mathcal{F}$ is time irreversible.*

The physical sense of certain time irreversibility notion is that in certainly time irreversible kinematics temporal paradoxes are impossible basically, that is there is not potential possibility to affect the own past by means of "traveling" and "jumping" between reference frames. Whereas, in time irreversible, but conditionally time reversible kinematics such potential possibility exists, but it is not realized in the scenario of evolution, acting in this kinematics.

Assertion 9. *Let universal kinematics $\mathcal{F}$ be weakly time-positive. Then every universal kinematics $\mathcal{F}_1$ such that $\mathcal{F}_1\,[\equiv]\,\mathcal{F}$ is weakly time-positive also.*

Proof. Let $\mathcal{F}$ be weakly time-positive universal kinematics and $\mathcal{F}_1\,[\equiv]\,\mathcal{F}$. Recall, that in [18, Definition 3.27.3] for every reference frame $\mathfrak{m} \in \mathcal{L}k\,(\mathcal{F})$ it was introduced the reference frame $\mathfrak{m}\downarrow_{\mathcal{F}_1}$, related with $\mathfrak{m}$ in the universal kinematics $\mathcal{F}_1$:

$$\mathfrak{m}\downarrow_{\mathcal{F}_1} := \mathbf{lk}_{\mathsf{ind}(\mathfrak{m})}\,(\mathcal{F}_1). \tag{28}$$

Since kinematics $\mathcal{F}$ is weakly time-positive then, by Definition 9, the reference frame $\mathfrak{l}_0 \in \mathcal{L}k\,(\mathcal{F})$ exists such that for each reference frame $\mathfrak{l} \in \mathcal{L}k\,(\mathcal{F})$ the correlation $\mathfrak{l}_0 \Uparrow^{+}_{\mathcal{F}} \mathfrak{l}$ holds. Denote:

$$\mathfrak{l}^{(1)}_0 := \mathfrak{l}_0\downarrow_{\mathcal{F}_1}.$$

Let us consider any reference frame $\mathfrak{l}^{(1)} \in \mathcal{L}k\,(\mathcal{F}_1)$. Denote: $\mathfrak{l} := \mathfrak{l}^{(1)}\downarrow_{\mathcal{F}} \in \mathcal{L}k\,(\mathcal{F})$. Then, according to [18, Properties 3.27.1] and formula (28), we have

$$\mathfrak{l}^{(1)} = \mathfrak{l}\downarrow_{\mathcal{F}_1} = \mathbf{lk}_{\mathsf{ind}(\mathfrak{l})}\,(\mathcal{F}_1).$$

Hence, taking into account [18, Definition 3.25.2 (item 2)], formula (28) and [18, Property 3.25.1(1)], we get

$$\begin{aligned}\mathbb{M}k\left(\mathfrak{l}^{(1)}_0;\mathcal{F}_1\right) &= \mathbb{M}k\left(\mathbf{lk}_{\mathsf{ind}(\mathfrak{l}_0)}\,(\mathcal{F}_1);\mathcal{F}_1\right) = \\ &= \mathbb{M}k\left(\mathbf{lk}_{\mathsf{ind}(\mathfrak{l}_0)}\,(\mathcal{F});\mathcal{F}\right) = \mathbb{M}k\left(\mathfrak{l}_0;\mathcal{F}\right); \\ \mathbb{M}k\left(\mathfrak{l}^{(1)};\mathcal{F}_1\right) &= \mathbb{M}k\left(\mathfrak{l};\mathcal{F}\right).\end{aligned} \tag{29}$$

Similarly applying [18, Definition 3.25.2 (item 2)] we ensure the equalities:

$$\mathbb{T}\mathbf{m}\left(\mathfrak{l}^{(1)}_0\right) = \mathbb{T}\mathbf{m}\left(\mathfrak{l}_0\right); \quad \mathbb{T}\mathbf{m}\left(\mathfrak{l}^{(1)}\right) = \mathbb{T}\mathbf{m}\left(\mathfrak{l}\right) \tag{30}$$

(where (in accordance with [18, Subsection 6.3]) $\mathbb{T}\mathbf{m}(\mathfrak{m}) = (\mathbf{Tm}\,(\mathfrak{m}), \leq_{\mathfrak{m}})$ $(\forall\, \mathfrak{m} \in \mathcal{L}k\,(\mathcal{F}) \cup \mathcal{L}k\,(\mathcal{F}_1)))$. Moreover, according to [18, Property 3.25.1(1) and Definition 3.25.2 (item 3)], we obtain

$$\begin{aligned}[\mathfrak{l}_0 \leftarrow \mathfrak{l}, \mathcal{F}] &= [\mathbf{lk}_{\mathsf{ind}(\mathfrak{l}_0)}\,(\mathcal{F}) \leftarrow \mathbf{lk}_{\mathsf{ind}(\mathfrak{l})}\,(\mathcal{F}), \mathcal{F}] = \\ &= [\mathbf{lk}_{\mathsf{ind}(\mathfrak{l}_0)}\,(\mathcal{F}_1) \leftarrow \mathbf{lk}_{\mathsf{ind}(\mathfrak{l})}\,(\mathcal{F}_1), \mathcal{F}_1] = \\ &= [\mathfrak{l}_0\downarrow_{\mathcal{F}_1} \leftarrow \mathfrak{l}\downarrow_{\mathcal{F}_1}, \mathcal{F}_1] = \left[\mathfrak{l}^{(1)}_0 \leftarrow \mathfrak{l}^{(1)}, \mathcal{F}_1\right].\end{aligned} \tag{31}$$

Taking into account (29), let us consider any elements $\mathrm{w}_1, \mathrm{w}_2 \in \mathbb{M}k\left(\mathfrak{l}^{(1)};\mathcal{F}_1\right) = \mathbb{M}k\left(\mathfrak{l};\mathcal{F}\right)$ such that $\mathsf{bs}\,(\mathrm{w}_1) = \mathsf{bs}\,(\mathrm{w}_2)$ and $\mathsf{tm}\,(\mathrm{w}_1) <_{\mathfrak{l}^{(1)}} \mathsf{tm}\,(\mathrm{w}_2)$. Then, in accordance with (30), we obtain the inequality $\mathsf{tm}\,(\mathrm{w}_1) <_{\mathfrak{l}} \mathsf{tm}\,(\mathrm{w}_2)$. Since (as it was mentioned before) $\mathfrak{l}_0 \Uparrow^{+}_{\mathcal{F}} \mathfrak{l}$, then, by Definition 9 (item 2), we obtain the inequality $\mathsf{tm}\,([\mathfrak{l}_0 \leftarrow \mathfrak{l}, \mathcal{F}]\,\mathrm{w}_1) <_{\mathfrak{l}_0} \mathsf{tm}\,([\mathfrak{l}_0 \leftarrow \mathfrak{l}, \mathcal{F}]\,\mathrm{w}_2)$. Thence, using (31) and (30), we ensure the inequality, $\mathsf{tm}\left(\left[\mathfrak{l}^{(1)}_0 \leftarrow \mathfrak{l}^{(1)}, \mathcal{F}_1\right]\mathrm{w}_1\right) <_{\mathfrak{l}^{(1)}_0} \mathsf{tm}\left(\left[\mathfrak{l}^{(1)}_0 \leftarrow \mathfrak{l}^{(1)}, \mathcal{F}_1\right]\mathrm{w}_2\right)$. By Definition 9 (item 2), taking into account the arbitrariness of

choice elements $\mathrm{w}_1, \mathrm{w}_2 \in \mathbb{M}k\left(\mathfrak{l}^{(1)}; \mathcal{F}_1\right)$ such, that $\mathsf{bs}(\mathrm{w}_1) = \mathsf{bs}(\mathrm{w}_2)$ and $\mathsf{tm}(\mathrm{w}_1) <_{\mathfrak{l}^{(1)}} \mathsf{tm}(\mathrm{w}_2)$, we obtain the correlation $\mathfrak{l}_0^{(1)} \Uparrow^{+}_{\mathcal{F}_1} \mathfrak{l}^{(1)}$ (for every reference frame $\mathfrak{l}^{(1)} \in \mathcal{L}k(\mathcal{F}_1)$). Hence, by Definition 9, kinematics $\mathcal{F}_1$ is weakly time-positive. □

Applying Assertion 9 as well as Theorem 1, we obtain the following (strengthened) variant of Theorem of Non-Returning:

Theorem 2. *Any weakly time-positive universal kinematics $\mathcal{F}$ is **certainly** time irreversible.*

7 Example of certainly time irreversible tachyon kinematics

In this section we build the certainly time-irreversible universal kinematics, which allows for reference frames moving with any speed other than the speed of light, using the generalized Lorentz-Poincare transformations in terms of E. Recami, V. Olkhovsky and R. Goldoni.

Let $(\mathfrak{H}, \|\cdot\|, \langle\cdot,\cdot\rangle)$ be a Hilbert space over the real field such, that $\dim(\mathfrak{H}) \geq 1$, where $\dim(\mathfrak{H})$ is dimension of the space $\mathfrak{H}$. Emphasize, that the condition $\dim(\mathfrak{H}) \geq 1$ should be interpreted in a way that the space $\mathfrak{H}$ may be infinite-dimensional. Let $\mathcal{L}(\mathfrak{H})$ be the space of (homogeneous) linear continuous operators over the space $\mathfrak{H}$. Denote by $\mathcal{L}^{\times}(\mathfrak{H})$ the space of all operators of affine transformations over the space $\mathfrak{H}$, that is $\mathcal{L}^{\times}(\mathfrak{H}) = \{\mathbf{A}_{[\mathbf{a}]} \,|\, \mathbf{A} \in \mathcal{L}(\mathfrak{H}),\, \mathbf{a} \in \mathfrak{H}\}$, where $\mathbf{A}_{[\mathbf{a}]}x = \mathbf{A}x + \mathbf{a}$, $x \in \mathfrak{H}$. The ***Minkowski space*** over the Hilbert space $\mathfrak{H}$ is defined as the Hilbert space $\mathcal{M}(\mathfrak{H}) = \mathbb{R} \times \mathfrak{H} = \{(t, x) \,|\, t \in \mathbb{R},\ x \in \mathfrak{H}\}$, equipped by the inner product and norm: $\langle \mathrm{w}_1, \mathrm{w}_2\rangle = \langle \mathrm{w}_1, \mathrm{w}_2\rangle_{\mathcal{M}(\mathfrak{H})} = t_1 t_2 + \langle x_1, x_2\rangle$, $\|\mathrm{w}_1\| = \|\mathrm{w}_1\|_{\mathcal{M}(\mathfrak{H})} = \left(t_1^2 + \|x_1\|^2\right)^{1/2}$ (where $\mathrm{w}_i = (t_i, x_i) \in \mathcal{M}(\mathfrak{H})$, $i \in \{1, 2\}$) ([10, 18]). In the space $\mathcal{M}(\mathfrak{H})$ we select the next subspaces: $\mathfrak{H}_0 := \{(t, \mathbf{0}) \,|\, t \in \mathbb{R}\}$, $\mathfrak{H}_1 := \{(0, x) \,|\, x \in \mathfrak{H}\}$ with $\mathbf{0}$ being zero vector. Then, $\mathcal{M}(\mathfrak{H}) = \mathfrak{H}_0 \oplus \mathfrak{H}_1$, where $\oplus$ means the orthogonal sum of subspaces. Denote: $\mathbf{e}_0 := (1, \mathbf{0}) \in \mathcal{M}(\mathfrak{H})$. Introduce the orthogonal projectors on the subspaces $\mathfrak{H}_1$ and $\mathfrak{H}_0$:

$$\mathbf{X}\mathrm{w} = (0, x) \in \mathfrak{H}_1;\ \widehat{\mathbf{T}}\mathrm{w} = (t, \mathbf{0}) = \mathcal{T}(\mathrm{w})\,\mathbf{e}_0 \in \mathfrak{H}_0,$$
$$\text{where } \mathcal{T}(\mathrm{w}) = t \quad (\mathrm{w} = (t, x) \in \mathcal{M}(\mathfrak{H})).$$

Let $\mathbf{B}_1(\mathfrak{H}_1)$ be the unit sphere in the space $\mathfrak{H}_1$ ($\mathbf{B}_1(\mathfrak{H}_1) = \{x \in \mathfrak{H}_1 \,|\, \|x\| = 1\}$). Any vector $\mathbf{n} \in \mathbf{B}_1(\mathfrak{H}_1)$ generates the following orthogonal projectors, acting in $\mathcal{M}(\mathfrak{H})$:

$$\mathbf{X}_1[\mathbf{n}]\,\mathrm{w} = \langle \mathbf{n}, \mathrm{w}\rangle\,\mathbf{n} \quad (\mathrm{w} \in \mathcal{M}(\mathfrak{H}));$$
$$\mathbf{X}_1^{\perp}[\mathbf{n}] = \mathbf{X} - \mathbf{X}_1[\mathbf{n}].$$

Recall, that an operator $U \in \mathcal{L}(\mathfrak{H})$ is referred to as ***unitary*** on $\mathfrak{H}$, if and only if $\exists\, U^{-1} \in \mathcal{L}(\mathfrak{H})$ and $\forall\, x \in \mathfrak{H}\ \|Ux\| = \|x\|$. Let $\mathfrak{U}(\mathfrak{H}_1)$ be the set of all ***unitary*** operators over the space $\mathfrak{H}_1$.

Fix some real number c such, that $0 < c < \infty$. Denote:

$$\mathfrak{P}\mathfrak{T}^{\mp}_{\mathsf{fin}}(\mathfrak{H}, c) := \left\{ \mathbf{W}_{\lambda,c}[s, \mathbf{n}, J; \mathbf{a}] \;\middle|\; \begin{array}{l} \lambda \in [0, \infty) \setminus \{c\}, \\ s = \mathrm{sign}(c - \lambda), \\ J \in \mathfrak{U}(\mathfrak{H}_1),\ \mathbf{n} \in \mathbf{B}_1(\mathfrak{H}_1), \\ \mathbf{a} \in \mathcal{M}(\mathfrak{H}) \end{array} \right\}, \tag{32}$$

where $\mathbf{W}_{\lambda,c}[s, \mathbf{n}, J; \mathbf{a}] \in \mathcal{L}^{\times}(\mathcal{M}(\mathfrak{H}))$ ($\lambda \in [0, \infty) \setminus \{c\}$, $s \in \{-1, 1\}$, $J \in \mathfrak{U}(\mathfrak{H}_1)$, $\mathbf{n} \in \mathbf{B}_1(\mathfrak{H}_1)$, $\mathbf{a} \in \mathcal{M}(\mathfrak{H})$) are operators of generalized Lorentz-Poincare Transformations in the sense of E. Recami, V. Olkhovsky and R. Goldoni, introduced in [10, 11, 18]:

$$\mathbf{W}_{\lambda,c}[s, \mathbf{n}, J; \mathbf{a}]\mathrm{w} = \mathbf{W}_{\lambda,c}[s, \mathbf{n}, J](\mathrm{w} + \mathbf{a}), \quad \text{where}$$
$$\mathbf{W}_{\lambda,c}[s, \mathbf{n}, J]\mathrm{w} = \frac{\left(s\mathcal{T}(\mathrm{w}) - \frac{\lambda}{c^2}\langle \mathbf{n}, \mathrm{w}\rangle\right)}{\sqrt{\left|1 - \frac{\lambda^2}{c^2}\right|}}\mathbf{e}_0 +$$
$$+ J\left(\frac{\lambda\mathcal{T}(\mathrm{w}) - s\langle \mathbf{n}, \mathrm{w}\rangle}{\sqrt{\left|1 - \frac{\lambda^2}{c^2}\right|}}\mathbf{n} + \mathbf{X}_1^{\perp}[\mathbf{n}]\,\mathrm{w}\right). \tag{33}$$

According to [18, 20], every operator of kind $\mathbf{W}_{\lambda,c}[s, \mathbf{n}, J; \mathbf{a}]$ belongs to $\mathbf{Pk}(\mathfrak{H})$, where $\mathbf{Pk}(\mathfrak{H})$ is the set of all operators $\mathbf{S} \in \mathcal{L}^{\times}(\mathcal{M}(\mathfrak{H}))$, which have the continuous inverse operator $\mathbf{S}^{-1} \in \mathcal{L}^{\times}(\mathcal{M}(\mathfrak{H}))$. Using results of the papers [18, 20], we can calculate the operators, inverse to the operators of kind $\mathbf{W}_{\lambda,c}[s, \mathbf{n}, J]$ and $\mathbf{W}_{\lambda,c}[s, \mathbf{n}, J; \mathbf{a}]$.

Lemma 1. *For arbitrary $c \in (0, \infty)$, $\lambda \in [0, \infty) \setminus \{c\}$, $s \in \{-1, 1\}$, $J \in \mathfrak{U}(\mathfrak{H}_1)$ and $\mathbf{n} \in \mathbf{B}_1(\mathfrak{H}_1)$ the following equality holds:*

$$\left(\mathbf{W}_{\lambda,c}[s, \mathbf{n}, J]\right)^{-1} =$$
$$= \mathbf{W}_{\lambda,c}\left[s\,\mathrm{sign}(c - \lambda), \mathrm{sign}(c - \lambda)J\mathbf{n}, J^{-1}\right]. \tag{34}$$

Proof. Consider arbitrary $0 < c < \infty$, $\lambda \in [0, \infty) \setminus \{c\}$, $s \in \{-1, 1\}$, $J \in \mathfrak{U}(\mathfrak{H}_1)$ and $\mathbf{n} \in \mathbf{B}_1(\mathfrak{H}_1)$. According to [10, page 143] or [18, formula (2.86)], operator $\mathbf{W}_{\lambda,c}[s, \mathbf{n}, J]$ may be represented in the form:

$$\mathbf{W}_{\lambda,c}[s, \mathbf{n}, J] = \mathbf{U}_{\theta,c}[s, \mathbf{n}, J], \tag{35}$$

where

$$\theta = \frac{1 - \frac{\lambda}{c}}{\sqrt{\left|1 - \frac{\lambda^2}{c^2}\right|}} \quad \left(\lambda = c\frac{1 - \theta|\theta|}{1 + \theta|\theta|}\right),\ -1 \leq \theta \leq 1.$$

Hence, according to [20, Corollary 5.1] or [18, Corollary 2.18.3], we obtain, that $\left(\mathbf{W}_{\lambda,c}[s, \mathbf{n}, J]\right)^{-1} \in \mathcal{L}(\mathcal{M}(\mathfrak{H}))$, and moreover:

$$\left(\mathbf{W}_{\lambda,c}[s, \mathbf{n}, J]\right)^{-1} = \left(\mathbf{U}_{\theta,c}[s, \mathbf{n}, J]\right)^{-1} =$$
$$= \mathbf{U}_{\theta^s,c}\left[s_\theta, s_\theta J\mathbf{n}, J^{-1}\right], \tag{36}$$
$$\text{where } s_\theta = \mathfrak{S}(s, \theta) = \begin{cases} 1, & s, \theta > 0 \\ -1, & s < 0 \text{ or } \theta < 0. \end{cases}$$

In the case $s = 1$ we have, $s_\theta = \operatorname{sign}\theta = \operatorname{sign}\left(\frac{1-\frac{\lambda}{c}}{\sqrt{\left|1-\frac{\lambda^2}{c^2}\right|}}\right) = \operatorname{sign}(c-\lambda)$. Hence, in this case, using (36) and (35), we obtain

$$\begin{aligned}(\mathbf{W}_{\lambda,c}[s,\mathbf{n},J])^{-1} &= \mathbf{U}_{\theta,c}\left[s_\theta, s_\theta J\mathbf{n}, J^{-1}\right] = \\ &= \mathbf{W}_{\lambda,c}\left[s_\theta, s_\theta J\mathbf{n}, J^{-1}\right] = \\ &= \mathbf{W}_{\lambda,c}\left[\operatorname{sign}(c-\lambda), \operatorname{sign}(c-\lambda)J\mathbf{n}, J^{-1}\right] \quad (s=1). \quad (37)\end{aligned}$$

Now we consider the case $s = -1$ $(\theta^s = \theta^{-1})$. Applying (36) and [18, formula (2.90)], in this case we deduce

$$\begin{aligned}(\mathbf{W}_{\lambda,c}[s,\mathbf{n},J])^{-1} &= \mathbf{U}_{\theta^{-1},c}\left[s_\theta, s_\theta J\mathbf{n}, J^{-1}\right] = \\ &= \mathbf{U}_{\theta,c}\left[s_\theta \operatorname{sign}\theta, -s_\theta(\operatorname{sign}\theta)J\mathbf{n}, J^{-1}\right] = \\ &= \mathbf{U}_{\theta,c}\left[-\operatorname{sign}\theta, (\operatorname{sign}\theta)J\mathbf{n}, J^{-1}\right] = \\ &= \mathbf{U}_{\theta,c}\left[-\operatorname{sign}(c-\lambda), \operatorname{sign}(c-\lambda)J\mathbf{n}, J^{-1}\right] = \\ &= \mathbf{W}_{\lambda,c}\left[-\operatorname{sign}(c-\lambda), \operatorname{sign}(c-\lambda)J\mathbf{n}, J^{-1}\right] \\ &\qquad (s=-1). \quad (38)\end{aligned}$$

Taking into account (37) and (38) in the both cases we obtain (34). □

Using Lemma 1, we obtain the following corollary.

Corollary 4. *For arbitrary $c \in (0,\infty)$, $\lambda \in [0,\infty)\setminus\{c\}$, $s \in \{-1,1\}$, $J \in \mathfrak{U}(\mathfrak{H}_1)$, $\mathbf{n} \in \mathbf{B}_1(\mathfrak{H}_1)$ and $\mathbf{a} \in \mathcal{M}(\mathfrak{H})$ the following equality is fulfilled:*

$$\begin{aligned}&(\mathbf{W}_{\lambda,c}[s,\mathbf{n},J;\mathbf{a}])^{-1}\,\mathrm{w} = \\ &\quad = \mathbf{W}_{\lambda,c}\left[s\operatorname{sign}(c-\lambda), \operatorname{sign}(c-\lambda)J\mathbf{n}, J^{-1}\right]\mathrm{w} - \mathbf{a} \\ &\qquad\qquad (\mathrm{w} \in \mathcal{M}(\mathfrak{H})).\end{aligned}$$

Let $\mathcal{B}$ be any base changeable set such, that $\mathfrak{Bs}(\mathcal{B}) \subseteq \mathfrak{H}$ and $\mathbb{T}\mathbf{m}(\mathcal{B}) = (\mathbb{R}, \leq)$, where $\leq$ is the standard order in the field of real numbers $\mathbb{R}$. Denote:

$$\mathfrak{UPT}^{\mp}_{\mathsf{fin}}(\mathfrak{H},\mathcal{B},c) := \mathfrak{Ru}\left(\mathfrak{PT}^{\mp}_{\mathsf{fin}}(\mathfrak{H},c), \mathcal{B};\ \mathfrak{H}\right), \quad (39)$$

where the denotation $\mathfrak{Ru}(\cdot,\cdot;\cdot)$ is introduced in [11], [18, page 166]. From [18, Assertion 2.17.5] it follows, that in the case $\dim(\mathfrak{H}) = 3$ universal kinematics $\mathfrak{UPT}^{\mp}_{\mathsf{fin}}(\mathfrak{H},\mathcal{B},c)$ may be considered as tachyon extension of kinematics of classical special relativity, which allows for reference frames moving with arbitrary speed other than the speed of light.

According to [18, Property 3.23.1(1)], the set $\mathcal{L}k\left(\mathfrak{UPT}^{\mp}_{\mathsf{fin}}(\mathfrak{H},\mathcal{B},c)\right)$ of all reference frames of universal kinematics $\mathfrak{UPT}^{\mp}_{\mathsf{fin}}(\mathfrak{H},\mathcal{B},c)$, defined by (39), can be represented in the form:

$$\begin{aligned}&\mathcal{L}k\left(\mathfrak{UPT}^{\mp}_{\mathsf{fin}}(\mathfrak{H},\mathcal{B},c)\right) = \\ &\quad = \left\{(\mathbf{U}, \mathbf{U}[\mathcal{B}, \mathbb{T}\mathbf{m}(\mathcal{B})]) \mid \mathbf{U} \in \mathfrak{PT}^{\mp}_{\mathsf{fin}}(\mathfrak{H},c)\right\} = \\ &\quad = \left\{(\mathbf{U}, \mathbf{U}[\mathcal{B}]) \mid \mathbf{U} \in \mathfrak{PT}^{\mp}_{\mathsf{fin}}(\mathfrak{H},c)\right\}. \quad (40)\end{aligned}$$

In accordance with [18, Corollary 2.19.5], subclass of operators

$$\begin{aligned}&\mathfrak{P}_+(\mathfrak{H},c) = \\ &\quad = \left\{\mathbf{W}_{\lambda,c}[s,\mathbf{n},J;\mathbf{a}] \;\middle|\; \begin{array}{l}\lambda \in [0,c),\ s=1,\\ J \in \mathfrak{U}(\mathfrak{H}_1),\\ \mathbf{n} \in \mathbf{B}_1(\mathfrak{H}_1),\ \mathbf{a} \in \mathcal{M}(\mathfrak{H})\end{array}\right\} \subseteq \\ &\qquad\qquad \subseteq \mathfrak{PT}^{\mp}_{\mathsf{fin}}(\mathfrak{H},c)\end{aligned}$$

is group of operators over the space $\mathcal{M}(\mathfrak{H})$. So, the identity operator $\mathbb{I}_{\mathcal{M}(\mathfrak{H})}\mathrm{w} = \mathrm{w}$ $(\forall \mathrm{w} \in \mathcal{M}(\mathfrak{H}))$ belongs to the class $\mathfrak{PT}^{\mp}_{\mathsf{fin}}(\mathfrak{H},c)$. Hence, in accordance with (40), we may define the following reference frame:

$$\begin{aligned}\mathfrak{I}_{0,\mathcal{B}} &:= (\mathbb{I}_{\mathcal{M}(\mathfrak{H})}, \mathbb{I}_{\mathcal{M}(\mathfrak{H})}[\mathcal{B}]) = \\ &= (\mathbb{I}_{\mathcal{M}(\mathfrak{H})}, \mathcal{B}) \in \mathcal{L}k\left(\mathfrak{UPT}^{\mp}_{\mathsf{fin}}(\mathfrak{H},\mathcal{B},c)\right) \quad (41)\end{aligned}$$

(recall, that, according to [18, Remark 1.11.3], $\mathbb{I}_{\mathcal{M}(\mathfrak{H})}[\mathcal{B}] = \mathcal{B}$).

Lemma 2. *For each reference frame $\mathfrak{I} \in \mathcal{L}k\left(\mathfrak{UPT}^{\mp}_{\mathsf{fin}}(\mathfrak{H},\mathcal{B},c)\right)$ the following correlation holds:*

$$\mathfrak{I}_{0,\mathcal{B}} \Uparrow^{+}_{\mathfrak{UPT}^{\mp}_{\mathsf{fin}}(\mathfrak{H},\mathcal{B},c)} \mathfrak{I}.$$

Proof. Consider any reference frame $\mathfrak{I} \in \mathcal{L}k(\mathfrak{UPT}^{\mp}(\mathfrak{H},\mathcal{B},c))$. According to (40) and (32), frame $\mathfrak{I}$ can be represented in the form:

$$\mathfrak{I} = (\mathbf{U}, \mathbf{U}[\mathcal{B}]), \quad \text{where} \quad (42)$$

$$\begin{aligned}\mathbf{U} = \mathbf{W}_{\lambda,c}[&\operatorname{sign}(c-\lambda), \mathbf{n}, J; \mathbf{a}], \quad (43)\\ &0 \leq \lambda < +\infty,\ \lambda \neq c,\\ &\mathbf{n} \in \mathbf{B}_1(\mathfrak{H}_1),\ J \in \mathfrak{U}(\mathfrak{H}_1),\ \mathbf{a} \in \mathcal{M}(\mathfrak{H}).\end{aligned}$$

Applying [18, Properties 3.23.1(3,4,7)] as well (42), (43), (41) and Corollary 4 we obtain

$$\begin{aligned}\mathbb{T}\mathbf{m}(\mathfrak{I}) &= \mathbb{T}\mathbf{m}(\mathfrak{I}_{0,\mathcal{B}}) = \mathbb{T}\mathbf{m}(\mathcal{B}) = (\mathbb{R},\leq); \quad (44)\\ \mathbb{M}k(\mathfrak{I}) &= \mathbb{M}k(\mathfrak{I}_{0,\mathcal{B}}) = \mathbf{Tm}(\mathcal{B}) \times \mathfrak{H} = \\ &= \mathbb{R} \times \mathfrak{H} = \mathcal{M}(\mathfrak{H});\\ [\mathfrak{I}_{0,\mathcal{B}} \leftarrow \mathfrak{I}]\,\mathrm{w} &= \mathbb{I}_{\mathcal{M}(\mathfrak{H})}\mathbf{U}^{-1}\mathrm{w} = \\ &= (\mathbf{W}_{\lambda,c}[\operatorname{sign}(c-\lambda), \mathbf{n}, J; \mathbf{a}])^{-1}\,\mathrm{w} = \\ &= \mathbf{W}_{\lambda,c}\left[(\operatorname{sign}(c-\lambda))^2, \operatorname{sign}(c-\lambda)J\mathbf{n}, J^{-1}\right]\mathrm{w} - \mathbf{a} = \\ &= \mathbf{W}_{\lambda,c}\left[1, \operatorname{sign}(c-\lambda)J\mathbf{n}, J^{-1}\right]\mathrm{w} - \mathbf{a} \quad (45)\\ &\qquad (\mathrm{w} \in \mathbb{M}k(\mathfrak{I}) = \mathcal{M}(\mathfrak{H})).\end{aligned}$$

Now we consider any $\mathrm{w}_1, \mathrm{w}_2 \in \mathbb{M}k(\mathfrak{I}) = \mathcal{M}(\mathfrak{H})$ such that $\mathsf{bs}(\mathrm{w}_1) = \mathsf{bs}(\mathrm{w}_2)$ and $\mathsf{tm}(\mathrm{w}_1) <_{\mathfrak{I}} \mathsf{tm}(\mathrm{w}_2)$. According to (44), inequality $\mathsf{tm}(\mathrm{w}_1) <_{\mathfrak{I}} \mathsf{tm}(\mathrm{w}_2)$ is equivalent to the inequality $\mathsf{tm}(\mathrm{w}_1) < \mathsf{tm}(\mathrm{w}_2)$. From the equality $\mathsf{bs}(\mathrm{w}_1) = \mathsf{bs}(\mathrm{w}_2)$ it

follows that

$$\begin{aligned}\mathbf{X}(\mathrm{w}_2-\mathrm{w}_1)=\\ =\mathbf{X}(\mathsf{tm}(\mathrm{w}_2)-\mathsf{tm}(\mathrm{w}_1),\mathsf{bs}(\mathrm{w}_2)-\mathsf{bs}(\mathrm{w}_1))=\\ =(0,\mathsf{bs}(\mathrm{w}_2)-\mathsf{bs}(\mathrm{w}_1))=\mathbf{0}.\end{aligned}$$

Thence, using (45) and (33) we deduce

$$\begin{aligned}\mathsf{tm}\left(\left[\mathrm{I}_{0,\mathcal{B}}\leftarrow\mathfrak{l}\right]\mathrm{w}_2\right)-\mathsf{tm}\left(\left[\mathrm{I}_{0,\mathcal{B}}\leftarrow\mathfrak{l}\right]\mathrm{w}_1\right)=\\ =\mathsf{tm}\left(\left[\mathrm{I}_{0,\mathcal{B}}\leftarrow\mathfrak{l}\right]\mathrm{w}_2-\left[\mathrm{I}_{0,\mathcal{B}}\leftarrow\mathfrak{l}\right]\mathrm{w}_1\right)=\\ =\mathsf{tm}\left(\mathbf{W}_{\lambda,c}\left[1,\mathrm{sign}(c-\lambda)J\mathbf{n},J^{-1}\right]\mathrm{w}_2-\right.\\ \left.-\mathbf{W}_{\lambda,c}\left[1,\mathrm{sign}(c-\lambda)J\mathbf{n},J^{-1}\right]\mathrm{w}_1\right)=\\ =\mathsf{tm}\left(\mathbf{W}_{\lambda,c}\left[1,\mathrm{sign}(c-\lambda)J\mathbf{n},J^{-1}\right](\mathrm{w}_2-\mathrm{w}_1)\right)=\\ =\mathcal{T}\left(\mathbf{W}_{\lambda,c}\left[1,\mathrm{sign}(c-\lambda)J\mathbf{n},J^{-1}\right](\mathrm{w}_2-\mathrm{w}_1)\right)=\\ =\frac{\mathcal{T}(\mathrm{w}_2-\mathrm{w}_1)-\frac{\lambda}{c^2}\left\langle\mathrm{sign}(c-\lambda)J\mathbf{n},\mathrm{w}_2-\mathrm{w}_1\right\rangle}{\sqrt{\left|1-\frac{\lambda^2}{c^2}\right|}}=\\ =\frac{\mathcal{T}(\mathrm{w}_2-\mathrm{w}_1)-\frac{\lambda}{c^2}\left\langle\mathrm{sign}(c-\lambda)\mathbf{X}J\mathbf{n},\mathrm{w}_2-\mathrm{w}_1\right\rangle}{\sqrt{\left|1-\frac{\lambda^2}{c^2}\right|}}=\\ =\frac{\mathcal{T}(\mathrm{w}_2-\mathrm{w}_1)-\frac{\lambda}{c^2}\left\langle\mathrm{sign}(c-\lambda)J\mathbf{n},\mathbf{X}(\mathrm{w}_2-\mathrm{w}_1)\right\rangle}{\sqrt{\left|1-\frac{\lambda^2}{c^2}\right|}}=\\ =\frac{\mathcal{T}(\mathrm{w}_2-\mathrm{w}_1)}{\sqrt{\left|1-\frac{\lambda^2}{c^2}\right|}}=\frac{\mathcal{T}(\mathrm{w}_2)-\mathcal{T}(\mathrm{w}_1)}{\sqrt{\left|1-\frac{\lambda^2}{c^2}\right|}}>0\end{aligned}$$

Therefore, $\mathsf{tm}\left(\left[\mathrm{I}_{0,\mathcal{B}}\leftarrow\mathfrak{l}\right]\mathrm{w}_1\right)<\mathsf{tm}\left(\left[\mathrm{I}_{0,\mathcal{B}}\leftarrow\mathfrak{l}\right]\mathrm{w}_2\right)$, ie, according to (44), we have, $\mathsf{tm}\left(\left[\mathrm{I}_{0,\mathcal{B}}\leftarrow\mathfrak{l}\right]\mathrm{w}_1\right)<_{\mathrm{I}_{0,\mathcal{B}}}\mathsf{tm}\left(\left[\mathrm{I}_{0,\mathcal{B}}\leftarrow\mathfrak{l}\right]\mathrm{w}_2\right)$. Thus, for arbitrary $\mathrm{w}_1,\mathrm{w}_2\in\mathbb{M}k(\mathfrak{l})=\mathcal{M}(\mathfrak{H})$ such, that $\mathsf{bs}(\mathrm{w}_1)=\mathsf{bs}(\mathrm{w}_2)$ and $\mathsf{tm}(\mathrm{w}_1)<_{\mathfrak{l}}\mathsf{tm}(\mathrm{w}_2)$ it is true the inequality $\mathsf{tm}\left(\left[\mathrm{I}_{0,\mathcal{B}}\leftarrow\mathfrak{l}\right]\mathrm{w}_1\right)<_{\mathrm{I}_{0,\mathcal{B}}}\mathsf{tm}\left(\left[\mathrm{I}_{0,\mathcal{B}}\leftarrow\mathfrak{l}\right]\mathrm{w}_2\right)$. And, taking into account Definition 9 (item 2), we have seen, that $\mathrm{I}_{0,\mathcal{B}}\Uparrow^{+}_{\mathfrak{UPT}^{\mp}_{\mathsf{fin}}(\mathfrak{H},\mathcal{B},c)}\mathfrak{l}$. □

Corollary 5. *Every universal kinematics of kind* $\mathfrak{UPT}^{\mp}_{\mathsf{fin}}(\mathfrak{H},\mathcal{B},c)$ *$(0<c<\infty)$ is certainly time irreversible.*

Proof. According to Lemma 2 and Definition 9 (item 5), kinematics of kind $\mathfrak{UPT}^{\mp}_{\mathsf{fin}}(\mathfrak{H},\mathcal{B},c)$ $(0<c<\infty)$ is weakly time-positive. Hence, by Theorem 2, kinematics $\mathfrak{UPT}^{\mp}_{\mathsf{fin}}(\mathfrak{H},\mathcal{B},c)$ is certainly time irreversible. □

Remark 4. Kinematics of kind $\mathfrak{UPT}^{\mp}_{\mathsf{fin}}(\mathfrak{H},\mathcal{B},c)$ $(0<c<\infty)$ is weakly time-positive, but it is not time-positive. Similarly to Lemma 2 it can be proved, that for any (superluminal) reference frame of kind:

$$\begin{aligned}\mathfrak{l}=(\mathbf{U},\mathbf{U}[\mathcal{B}])\in\mathcal{L}k\left(\mathfrak{UPT}^{\mp}_{\mathsf{fin}}(\mathfrak{H},\mathcal{B},c)\right),\quad\text{where}\\ \mathbf{U}=\mathbf{W}_{\lambda,c}\left[\mathrm{sign}(c-\lambda),\mathbf{n},J;\mathbf{a}\right]=\mathbf{W}_{\lambda,c}\left[-1,\mathbf{n},J;\mathbf{a}\right],\\ c<\lambda<+\infty,\ \mathbf{n}\in\mathbf{B}_1(\mathfrak{H}_1),\ J\in\mathfrak{U}(\mathfrak{H}_1),\ \mathbf{a}\in\mathcal{M}(\mathfrak{H})\end{aligned}$$

the correlation $\mathfrak{l}\Downarrow^{-}_{\mathfrak{UPT}^{\mp}_{\mathsf{fin}}(\mathfrak{H},\mathcal{B},c)}\mathrm{I}_{0,\mathcal{B}}$ is true despite the fact that $\mathrm{I}_{0,\mathcal{B}}\Uparrow^{+}_{\mathfrak{UPT}^{\mp}_{\mathsf{fin}}(\mathfrak{H},\mathcal{B},c)}\mathfrak{l}$ (according to Lemma 2).

Remark 5. It is easy to see that the binary relation $\Uparrow^{+}_{\mathcal{F}}$ is reflexive on the set $\mathcal{L}k(\mathcal{F})$ of all reference frames of arbitrary universal kinematics $\mathcal{F}$. From Remark 4 it follows that in the general case this relation is not symmetric. Using the results of [10, Section 7, paragraph 4] it can be proven that this relation is not transitive in the general case.

8 On the physical interpretation of main result

The aim of this section is to explain main Theorem 2 in the physical language. We can imagine, that any universal kinematics $\mathcal{F}$ is some abstract "world", which not necessarily coincides with the our. In every such "world" $\mathcal{F}$ there exists the fixed for this "world" set of reference frames $\mathcal{L}k(\mathcal{F})$. We reach the agreement that for any reference frame $\mathfrak{l}\in\mathcal{L}k(\mathcal{F})$ the arrows of the clock, fixed in the frame $\mathfrak{l}$ are rotating clockwise relatively the frame $\mathfrak{l}$. We say, that the reference frame $\mathfrak{m}\in\mathcal{L}k(\mathcal{F})$ is time-positive relatively the reference frame $\mathfrak{l}\in\mathcal{L}k(\mathcal{F})$ (ie $\mathfrak{m}\Uparrow^{+}_{\mathcal{F}}\mathfrak{l}$) if and only if the observer in the reference frame $\mathfrak{m}$ (fixed relatively $\mathfrak{m}$) observes that the arrows of the clock, fixed in the frame $\mathfrak{l}$ are rotating clockwise in the frame $\mathfrak{m}$ as well (cf. Definition 9, item 2). We abandon the physical question, how can the observer in $\mathfrak{m}$ "see" the clock, fixed in the other frame $\mathfrak{l}$. From the mathematical point of view, the possibility of observation the clock, attached to another reference frame, is guaranteed by existence of universal coordinate transform between every two reference frames (see definition of universal kinematics in [11,18]). According to Remark 5, the binary relation $\Uparrow^{+}_{\mathcal{F}}$ always is reflexive, but, in the general case, it is not symmetric and is not transitive on the set $\mathcal{L}k(\mathcal{F})$ of all reference frames of the "world" $\mathcal{F}$.

We also suppose, that in the "world" $\mathcal{F}$ the interframe voyagers can exist. Such voyagers may move from one reference frame to the another frame, passing near them (similarly as, standing near the tram track, we can jump into the tram, passing near us).

From the physical point of view Theorem 2 asserts, that *if in the "world" $\mathcal{F}$ there exists at least one reference frame $\mathfrak{l}_0\in\mathcal{L}k(\mathcal{F})$, which is time-positive relatively the every frame $\mathfrak{l}\in\mathcal{L}k(\mathcal{F})$, then in this "world" the temporal paradoxes, connected with the possibility of the returning to the own past are impossible*. This means, that any interframe voyager, starting in some reference frame $\mathfrak{l}$ in some fixed point x can not finish its travel in the frame $\mathfrak{l}$ and in the point x at the past time.

9 Conclusions

1. According to Corollary 5, kinematics of kind $\mathfrak{UPT}^{\mp}_{\mathsf{fin}}(\mathfrak{H},\mathcal{B},c)$ (in the case $\dim(\mathfrak{H})=3$) gives the example of certainly time-irreversible tachyon extension of kinematics of classical special relativity, which

allows for reference frames moving with arbitrary velocity other than the velocity of light. Thus, the main conclusion of Theorem 2 is the following:

In the general case the hypothesis of existence of material objects and inertial reference frames, moving with the velocity, greater than the velocity of light, does not lead to temporal paradoxes, connected with existence of formal possibility of returning to the own past.

2. In [9] authors have deduced two variants of generalized superluminal Lorentz transforms for the case, when two inertial frames are moving along the common x-axis:

$$t' = \frac{t - \frac{vx}{c^2}}{\sqrt{\left(\frac{v}{c}\right)^2 - 1}},\ x' = \frac{x - vt}{\sqrt{\left(\frac{v}{c}\right)^2 - 1}},\ \begin{matrix} y' = y, \\ z' = z, \end{matrix} \qquad (46)$$

where $v \in \mathbb{R}$, $|v| > c$ (see [9, formula (3.16)]) and:

$$t' = \frac{-t + \frac{vx}{c^2}}{\sqrt{\left(\frac{v}{c}\right)^2 - 1}},\ x' = \frac{-x + vt}{\sqrt{\left(\frac{v}{c}\right)^2 - 1}},\ \begin{matrix} y' = y, \\ z' = z \end{matrix} \qquad (47)$$

(see [9, formula (3.18)]). Transforms (46) are particular cases of the transforms of kind (33) for the case, where $\dim(\mathfrak{H}) = 3$, $\lambda > c$ and $s = 1$, whereas transforms (47) belong to the transforms of kind (33) for the case, where $\dim(\mathfrak{H}) = 3$, $\lambda > c$ and $s = -1$. If we chose in (33) the value $s = 1$ for subluminal as well as superluminal diapason, we obtain the class of operators $\mathfrak{PT}_+(\mathfrak{H}, c)$, defined in [13, 18] and based on this class of operators universal kinematics of kind $\mathfrak{UPT}(\mathfrak{H}, \mathcal{B}, c)$. According to results, announced in [19] and published in [12], this kinematics is conditionally time reversible [1]. But, if we chose in (33) the value $s = 1$ for subluminal diapason and value $s = -1$ for superluminal diapason, we reach the class of operators $\mathfrak{PT}^{\mp}_{\mathsf{fin}}(\mathfrak{H}, c)$, defined in (32) and based on this class of operators universal kinematics of kind $\mathfrak{UPT}^{\mp}_{\mathsf{fin}}(\mathfrak{H}, \mathcal{B}, c)$. According to Corollary 5, kinematics $\mathfrak{UPT}^{\mp}_{\mathsf{fin}}(\mathfrak{H}, \mathcal{B}, c)$ is certainly time irreversible. Thus we can formulate the following conclusion, concerning two variants of superluminal Lorentz transforms, deduced in [9]:

From the standpoint of time-irreversibility, transforms (47) or [9, formula (3.18)] are more suitable for representation of the tachyon continuation of Einstein's special theory of relativity than (46) or [9, formula (3.16)].

Main results of this paper had been announced in [19].

Received on September 19, 2017

[1] In fact, class of operators $\mathfrak{PT}_+(\mathfrak{H}, c)$ contains apart from operators of kind (33) (with $s = 1$) also operators, corresponding tachyon inertial reference frames with infinite velocities. However, using results of the paper [12], it is not hard to deduce that the "subkinematics" of kinematics $\mathfrak{UPT}(\mathfrak{H}, \mathcal{B}, c)$, which includes only all reference frames from $\mathfrak{UPT}(\mathfrak{H}, \mathcal{B}, c)$ with finite velocities, also is conditionally time reversible.

References

1. Bilaniuk O.-M. P., Deshpande V.K., Sudarshan E.C.G. "Meta" Relativity. *American Journal of Physics*, 1962. v. 30, no. 10, 718–723.
2. Bilaniuk O.-M. P. , Sudarshan E.C.G. Particles beyond the light barrier. *Physics Today*, 1969, v. 22, no. 5, 43–51.
3. V.I. Ilyashevytch, S.Y. Medvedev. Tachyon acausal loops. *Uzhhorod University Scientific Herald. Series Physics*, 2010, no. 27, 103-111 (in Ukrainian).
4. Andréka H., Madarász J.X., Németi I., Stannett M., Székely G. Faster than light motion does not imply time travel. *Classical and Quantum Gravity*, 2014, v. 31, no. 9, 095005.
5. Recami E., Olkhovsky V.S. About Lorentz transformations and tachyons. *Lettere al Nuovo Cimento*, 1971, v. 1, no. 4, 165–168.
6. Goldoni R. Faster-than-light inertial frames, interacting tachyons and tadpoles. *Lettere al Nuovo Cimento*, 1972, v. 5, no. 6, 495–502.
7. Recami E. Classical Tachyons and Possible Applications. *Riv. Nuovo Cimento*, 1986, v. 9, s. 3, no. 6, 1–178.
8. Medvedev S.Yu. On the possibility of broadening special relativity theory beyond light barrier. *Uzhhorod University Scientific Herald. Ser. Phys.*, 2005, no. 18, 7–15 (in Ukrainian).
9. Hill J.M., Cox B.J. Einstein's special relativity beyond the speed of light. *Proc. of the Royal Society A*, 2012, v. 468, no. 2148, 4174–4192.
10. Grushka Ya.I. Tachyon generalization for lorentz transforms. *Methods of Functional Analysis and Topology*, 2013, v. 20, no. 2, 127–145.
11. Grushka Ya.I. Kinematic changeable sets with given universal coordinate transform. *Proceedings of Institute of Mathematics NAS of Ukraine (Zb. Pr. Inst. Mat. NAN Ukr.)*, 2015, v. 12, no. 1, 74–118 (in Ukrainian).
12. Grushka Ya.I. On time reversibility of tachyon kinematics. *Proceedings of Institute of Mathematics NAS of Ukraine (Zb. Pr. Inst. Mat. NAN Ukr.)*, 2016, v. 13, no. 2, 125–174 (in Ukrainian).
13. Grushka Ya.I. Changeable sets and their application for the construction of tachyon kinematics. *Proceedings of Institute of Mathematics NAS of Ukraine (Zb. Pr. Inst. Mat. NAN Ukr.)*, 2014, v. 11, no. 1, 192–227 (in Ukrainian).
14. Grushka Ya.I. Existence criteria for universal coordinate transforms in kinematic changeable sets. *Bukovinian Mathematical Journal*, 2014, v. 2, no. 2-3, 59–71 (in Ukrainian).
15. Grushka Ya.I. Abstract concept of changeable set. Preprint: arXiv:1207.3751v1, (2012), 54 p.
16. Grushka Ya.I. Coordinate transforms in kinematic changeable sets. *Reports of the National Academy of Sciences of Ukraine*, 2015, no. 3, 24–31, (in Ukrainian).
17. Grushka Ya.I. Evolutionary extensions of kinematic sets and universal kinematics. *Proceedings of Institute of Mathematics NAS of Ukraine (Zb. Pr. Inst. Mat. NAN Ukr.)*, 2015, v. 12, no. 2, 139–204 (in Ukrainian).
18. Grushka Ya.I. Draft introduction to abstract kinematics. (Version 2.0). Preprint: viXra: 1701.0523v2, (2017), 208 p.
19. Grushka Ya.I. On time irreversibility of universal kinematics. *Reports of the National Academy of Sciences of Ukraine*, 2016, no. 7, 14–21, (in Ukrainian).
20. Grushka Ya.I. Algebraic properties of tachyon lorentz transforms. *Proceedings of Institute of Mathematics NAS of Ukraine (Zb. Pr. Inst. Mat. NAN Ukr.)*, 2013, v. 10, no. 2, 138–169 (in Ukrainian).

Chain Systems of Harmonic Quantum Oscillators as a Fractal Model of Matter and Global Scaling in Biophysics

Hartmut Müller

E-mail: hm@interscalar.com

In this paper we introduce chain systems of harmonic quantum oscillators as a fractal model of matter and apply it to the analysis of frequency ranges of cyclical biological processes. The heuristic significance of global scaling in biophysics and medicine is discussed.

Introduction

Normal matter is formed by nucleons and electrons because they are exceptionally stable. Their lifespan tops everything that is measurable, exceeding 10^{29} years for the proton and 10^{28} years for the electron [1]. The proton-to-electron mass ratio is approximately 1836, so that the mass contribution of the proton to normal matter is very high, for example in the hydrogen atom (protium) it is $1 - 1/1836 \approx 99.95$ percent. Consequently, the mass contribution of the electron is only 0.05 percent. In heavier atoms which contain neutrons, the electron contribution to atomic mass is even smaller.

In addition, protons and neutrons have similar rest masses (the difference being only 0.14 percent) which allows us to interpret the proton and the neutron as similar quantum oscillators with regard to their rest masses. the framework of the standard particle model [2], protons and neutrons are baryons, with the proton connecting to a lower quantum energy level and a much more stable state than the neutron.

Therefore, in [3] we have introduced a fractal model of matter as a chain system of oscillating protons. In [4] we have shown that scale invariance is a fundamental property of this model. As a consequence of this scale invariance, chain systems of oscillating electrons produce similar series of eigenstates so that the proton model mass can be derived from the electron rest mass and vice versa. Furthermore, the interpretation of the Planck mass as an eigenstate in a chain system of oscillating protons has allowed us to derive the proton rest mass from fundamental physical constants [5].

Scale-invariant models of natural oscillations in chain systems of protons also provide a good description of the mass distribution of large celestial bodies in the Solar System [6]. Physical properties of celestial bodies such as mass, size, rotation and orbital period can be understood as macroscopic quantized eigenstates in chain systems of oscillating protons and electrons [7]. This understanding can be applied to an evolutionary trend prognosis of the Solar System but may be of cosmological significance as well. In [8] we have calculated the model masses of unknown planets in the Solar System.

In this paper we apply our fractal model of matter as a chain system of oscillating protons and our hypothesis of global scaling [7] to the domain of biophysics, especially to the analysis of frequency ranges of cyclical biological processes.

Methods

In [4] we have shown that the set of natural frequencies of a chain system of harmonic oscillators coincides with a set of finite continued fractions $\mathcal{F}$, which are natural logarithms:

$$\ln(\omega_{jk}/\omega_{00}) = n_{j0} + \cfrac{z}{n_{j1} + \cfrac{z}{n_{j2} + \ddots + \cfrac{z}{n_{jk}}}} = [z, n_{j0}; n_{j1}, n_{j2}, \ldots, n_{jk}] = \mathcal{F}, \quad (1)$$

where ω_{jk} is the set of angular frequencies and ω_{00} is the fundamental frequency of the set. The denominators are integer: $n_{j0}, n_{j1}, n_{j2}, \ldots, n_{jk} \in \mathrm{Z}$, the cardinality $j \in \mathrm{N}$ of the set and the number $k \in \mathrm{N}$ of layers are finite. In the canonical form, the numerator z is equal 1.

Any finite continued fraction represents a rational number [9]. Therefore, all frequencies ω_{jk} in (1) are irrational, because for rational exponents the natural exponential function is transcendental [10]. This circumstance presumably provides for the high stability of the oscillating chain system because it avoids resonance interaction between the elements of the system [11].

In the case of harmonic quantum oscillators, the continued fraction (1) defines not only a fractal set of natural angular frequencies ω_{jk} and oscillation periods $\tau_{jk} = 1/\omega_{jk}$ of the chain system, but also fractal sets of natural energies $E_{jk} = \hbar \cdot \omega_{jk}$ and masses $m_{jk} = E_{jk}/c^2$ which correspond with the eigenstates of the system. For this reason, we have called the continued fraction (1) the "fundamental fractal" of eigenstates in chain systems of harmonic quantum oscillators [4].

We hypothesize the scale invariance based on the fundamental fractal $\mathcal{F}$ (1) , calibrated by the properties of the proton and electron, is a universal characteristic of matter. This hypothesis we have called 'global scaling' [7].

In order to test global scaling on frequencies of cyclical biological processes we must calculate the natural logarithm of the process-to-proton frequency ratio. The proton angular frequency is $\omega_p = m_p c^2/\hbar = 1.425486 \cdot 10^{24}$ Hz,

Table 1: Frequency ranges of some cyclical biological processes and the corresponding attractor nodes of the fundamental fractal $\mathcal{F}$ (1), with the proton frequency $\omega_p = 1.425486 \cdot 10^{24}$ Hz as fundamental.

cyclic process of human physiology	**frequency range ω, Hz**	**ln (ω/ω_p)**	$\mathcal{F}$
adult relaxed breathing [13]	0.22..0.27	−57.13.. − 56.94	$[-57;\infty]$
adult relaxed heart rate [14]	0.83..1.5	−55.80.. − 55.21	$[-55;-2]$
brain activity delta	0.15..3	−57.52.. − 54.52	$[-57;-2]..[-54;-2]$
brain activity theta [12]	3..8	−54.52.. − 53.53	$[-54;-2]..[-54;2]$
brain activity alpha	8..13	−53.53.. − 53.06	$[-53;-2]..[-53;\infty]$
brain activity beta	14..34	−52.97.. − 52.06	$[-53;\infty]..[-52;\infty]$
brain activity gamma	35..250	−52.05.. − 50.10	$[-52;\infty]..[-50;\infty]$
muscle vibration [15]	22..24	−52.53.. − 52.44	$[-52;-2]$
flicker fusion threshold [16]	60..120	−51.52.. − 50.83	$[-51;-2]..[-51;\infty]$
newborn baby cry [17]	400..500	−49.62.. − 49.41	$[-49;-2]$
threshold of hearing [18, 19]	1900..2100	−40.55.. − 40.45	$[-40;-2]$

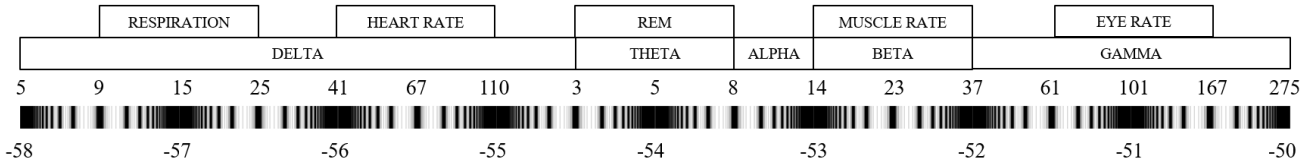

Fig. 1: Distribution (logarithmic representation) of frequency ranges (positive numbers) of human brain wave activity and other cyclical biological processes in the canonical projection of the fundamental fractal $\mathcal{F}$ (1) with the proton angular frequency $\omega_p = 1.42548624 \cdot 10^{24}$ Hz as fundamental. Negative numbers are logarithms and denote attractor nodes. Data taken from table 1.

where $m_p = 1.672621 \cdot 10^{-27}$ kg [1] is the proton rest mass, $\hbar$ is the Planck constant, c is the speed of light in vacuum. In the canonical form ($z = 1$), nodes of the fundamental fractal $\mathcal{F}$ (1) concur with integer and half logarithms.

For example, the frequency range of the theta electrical brain activity (theta waves, oscillatory pattern in electroencephalographic signals) is between 3 and 8 Hz [12] and the natural logarithm of the theta-to-proton frequency ratio is between $[-54;-2]$ and $[-54;2]$ approximating the main node $[54;\infty]$ of the proton calibrated fundamental fractal $\mathcal{F}$ (1):

$$\ln\left(\frac{\omega_{\max\, theta}}{\omega_{\text{proton}}}\right) = \ln\left(\frac{8\,\text{Hz}}{1.425486 \cdot 10^{24}\,\text{Hz}}\right) = -53.53,$$

$$\ln\left(\frac{\omega_{\min\, theta}}{\omega_{\text{proton}}}\right) = \ln\left(\frac{3\,\text{Hz}}{1.425486 \cdot 10^{24}\,\text{Hz}}\right) = -54.52.$$

Results

Table 1 shows the logarithms of frequency ranges of some cyclical biological processes and the corresponding attractor nodes (integer and half logarithms) of the fundamental fractal $\mathcal{F}$ (1).

Figure 1 shows the distribution (in logarithmic representation) of frequency ranges of brain wave activity and other cyclical processes of human physiology in the fundamental fractal $\mathcal{F}$ (1) with the proton angular frequency $\omega_p = 1.42548624 \cdot 10^{24}$ Hz as fundamental. Negative numbers are logarithms and denote attractor nodes. Positive numbers are frequencies, given in cycles per minute within the delta-range, and given in Hz within the theta, alpha, beta and gamma ranges.

Although the analyzed processes are of very high complexity, figure 1 shows that the frequency ranges of electrical brain activity (oscillatory patterns in electroencephalographic signals) and of other cyclical biological processes correspond with attractor nodes of the fundamental fractal $\mathcal{F}$ (1). This fact supports our hypothesis of global scaling.

Conclusion

Frequency ranges of electrical brain activity and of some other cyclical biological processes coincide well with the proton calibrated fundamental fractal $\mathcal{F}$ (1) which would indicate that these cycles may have a subatomic origin. It should also be considered that the frequency ranges of electrical brain activity are common to most mammalian species [20, 21].

The accordance of the brain wave frequency ranges with the proton calibrated fundamental fractal $\mathcal{F}$ (1) not only sup-

ports our hypothesis of global scaling, but also suggests an understanding of the biological organism as an oscillating chain system. This view could be of medical significance as well.

Scale invariance as a property of biological processes is well studied [22, 23] and it is not an exclusive characteristic of adult physiology. For example, the heart rate and the respiratory cycle of the fetus are related in the same way as in the adult [24]. Perhaps even the Weber-Fechner law – "intensity of sensation is proportional to the logarithm of stimulation" [25] – can be understood as a consequence of scale invariance in chain systems of cyclical biological processes.

Furthermore, global scaling suggests that the electrical brain activity continues beyond the known gamma range, because higher frequency processes like voice and hearing have to be brain-controlled as well. It is likely that traditional methods of electroencephalographic signal analysis are unable to separate high frequency patterns because of their very low amplitude. However, global scaling allows us to calculate the frequency ranges of such ultra-gamma activity (for which we propose the name "epsilon"). The frequency ranges of this very dynamic "epsilon" activity should be between $\omega_p \exp(-50) = 275$ Hz and $\omega_p \exp(-49) = 747$ Hz.

Acknowledgements

The author is grateful to Viktor Panchelyuga and Leili Khosravi for valuable discussions.

Received on September 19, 2017

References

1. Olive K.A. et al. (Particle Data Group), *Chin. Phys. C*, 2016, v. 38, 090001.
2. Patrignani C. et al. (Particle Data Group), *Chin. Phys. C*, 2016, v. 40, 100001.
3. Müller H. Fractal Scaling Models of Natural Oscillations in Chain Systems and the Mass Distribution of Particles. *Progress in Physics*, 2010, v. 3, 61–66.
4. Müller H. Fractal Scaling Models of Resonant Oscillations in Chain Systems of Harmonic Oscillators. *Progress in Physics*, 2009, v. 2, 72–76.
5. Müller H. Emergence of Particle Masses in Fractal Scaling Models of Matter. *Progress in Physics*, 2012, v. 4, 44–47.
6. Müller H. Fractal scaling models of natural oscillations in chain systems and the mass distribution of the celestial bodies in the Solar System. *Progress in Physics*, 2010, v. 3, 61–66.
7. Müller H. Scale-Invariant Models of Natural Oscillations in Chain Systems and their Cosmological Significance. *Progress in Physics*, 2017, v. 4, 187–197.
8. Müller H. Global Scaling as Heuristic Model for Search of Additional Planets in the Solar System.
9. Khintchine A. Ya. Continued fractions. University of Chicago Press, Chicago 1964.
10. Hilbert D. Über die Transcendenz der Zahlen e und π. *Mathematische Annalen*, 1893, v. 43, 216–219.
11. Panchelyuga V.A., Panchelyuga M. S. Resonance and Fractals on the Real Numbers Set. *Progress in Physics*, October 2012, v. 4, 48–53.
12. Tesche C.D., Karhu J. Theta oscillations index human hippocampal activation during a working memory task. *PNAS*, 2000, v. 97(2).
13. Ganong's Review of Medical Physiology (23 ed.) p. 600.
14. Spodick D.H. Survey of selected cardiologists for an operational definition of normal sinus heart rate. *The American Journal of Cardiology*. 1993, v. 72(5), 487–88.
15. Schaefer L.V. et al. Synchronization of muscular oscillations between two subjects during isometric interaction. *European Journal Trans Myology. Basic Appl. Myol.* 2014, v. 24(3), 195–202.
16. Davis J. Humans perceive flicker artefacts at 500 Hz, Sci Rep, Wiley, 5, 7861, PMC 4314649, 1986.
17. Lei G. et al. Pitch Analysis of Infant Crying. *National Journal of Digital Content Technology and its Applications*. 2013, v. 7(6).
18. Carhart, R. Clinical application of bone conduction audiometry. *Archives of Otolaryngology*, 1950, v. 51, 798–808.
19. Homma K., Shizmu Y., Puria, S. Ossicular resonance modes of the human middle ear for bone and air conduction. *Journal of the Acoustical Society of America*, 2009, v. 125, 968–979.
20. Sainsbury R.S., Heynen A., Montoya C.P. Behavioral correlates of hippocampal type 2 theta in the rat. *Physiol Behav.* 1987, v. 39(4), 513–519. PMID 3575499
21. Stewart M., Fox S.E. Hippocampal theta activity in monkeys. *Brain Res.* 1991, v. 538(1), 59–63. PMID 2018932
22. Barenblatt G.I. Scaling. Cambridge University Press, 2003.
23. Schmidt-Nielsen K., Scaling. Why is the animal size so important? Cambridge University Press, 1984.
24. Breathing and control of heart rate. *British Medical Journal*, 16.12.1978.
25. Fechner G.T. Elemente der Psychophysik, Band 2, Leipzig: Breitkopf und Härtel, 1860.

LETTERS TO PROGRESS IN PHYSICS

A Comment on "Can the One-way Speed of Light be Used for Detection of Violations of the Relativity Principle?"

Joseph Catania
E-mail: jcatania1@verizon.net

I show in this Letter that Spavieri et. al.'s clock transport delay calculations are incorrectly determined because of a sign error. Thus, the results of Roland De Witte (1991) should be considered significant.

1 Details

Assume for simplicity that what Spavieri et. al. [1] mean by $\mathbf{u}(t)$ is, a velocity of constant magnitude u, with a varying direction, yielding a total effective absolute velocity $\mathbf{V} \simeq \mathbf{v} + \mathbf{u}(t)$. Spavieri et. al.'s Equation (5) is reproduced here for convenience,

$$\delta\tau \simeq \frac{dt}{\gamma_V} - \frac{dt}{\gamma_v} \simeq \frac{(v^2 - V^2)\,dt}{2c^2} = -\frac{\mathbf{v}\cdot\mathbf{u}(t)\,dt}{c^2}\,. \qquad \text{(S5)}$$

Notice that Equation (6),

$$\Delta\tau = -\frac{1}{c^2}\int_A^B \mathbf{v}\cdot\mathbf{u}(t)\,dt = -\frac{L}{c^2}\,v\,(\cos\theta_A - \cos\theta_B) \qquad \text{(S6)}$$

is supposedly the integral of (5). Referring to Fig. 1 in [1] the projection of $\mathbf{u}(t)$ on $\mathbf{v}$ is $-u\cdot\cos(\pi/2-\theta) = -u\cdot\sin\theta$ and $|\,\mathbf{u}(t)\,| = L\omega = L\cdot\frac{d\theta}{dt}$ giving,

$$\Delta\tau = -\frac{1}{c^2}\int_A^B \mathbf{v}\cdot\mathbf{u}(t)\,dt = -\frac{L}{c^2}\,v\int_A^B -\sin\theta\cdot\frac{\mathrm{d}\theta}{\mathrm{dt}}\,dt =$$

$$= -\frac{L}{c^2}\,v\,(\cos\theta_B - \cos\theta_A). \qquad \text{(C1)}$$

Thus, Spavieri et. al. does not correctly calculate $\Delta\tau$, a quantity which they call clock transport delay (CTD). A simple sign check on $\delta\tau$ in (S5) and $\Delta\tau$ in (S6) shows they aren't the same. $|\,\mathbf{V}\,| < |\,\mathbf{v}\,|$ thus (S5) is positive, whereas since $-[\cos 0 - \cos(0 - d\theta)]$ is negtive, (S6) is negative. Replacing (C1) with (S6), the signs now agree.

2 Comments

The De Witte effect is given by,

$$t_{OB} - t_{OA} = \frac{L}{c^2}\,v\,(\cos\theta_B - \cos\theta_A) \qquad \text{(C2)}$$

and shows a decreasing effect as θ increases or decreases from its alignment with v (which we take as $\theta = 0$). Eqs. (C1) and (S5) show an increasing effect, whereas (S6), which is evidentally a harmonized version of (S5), shows a decreasing effect. So (S6), which supports Spavieri et. al.'s thesis, that the De Witte Effect is merely due to slow clock transport, is incorrect due to a sign error. The result is that if Spavieri et. al. is to be taken seriously the effect measured by De Witte will be due to twice what is derived in [1, 2, 4], which derivations do not ignore Fresnel drag. For instance Spavieri et. al's Equation (4) would be modified to,

$$\bar{t}_{OA} - \bar{t}_{OB} = \Delta\tau + \frac{L}{c^2}\,v\,(\cos\theta_A - \cos\theta_B) =$$

$$= \frac{2L}{c^2}\,v\,(\cos\theta_A - \cos\theta_B). \qquad \text{(C3)}$$

It must be noted at this point that Spavieri et. al. cites [5] (ref. 16 at the end of §3 in [1]) in which they claim that CTD is equivalent to Einstein Synchronization (ES). Unfortunately, the derivation in [5] §2 is riddled with error. For example Eq. (2) should be $t = \frac{h}{w}$ instead of $t = \frac{h}{\Delta w}$ and Eq. (6) should be $t_1 = \frac{\gamma h}{c-v}$ instead of $t_1 = \frac{h}{c-v}$. Thus, CTD and ES agree in [5] up to second order only after a harmonization.

3 Comments on synchronization

The discussion in [1] on clock transport time delay would seem to be completely spurious. An Einstein clock synchronization (ES) performed from O to A will guarantee synchronization throughout rotation about O. Such a vacuum synchronization will give the same result no matter whether the clock is at A, B or any other point as long as the laboratory frame path length is the same. This is guaranteed by the constant propagation velocity of light in the ether and the Lorentz transformation (LT), as shown by Maxwell's luminiferous ether theory and confirmed by two-way speed of light measurements in vacuo. Thus, Einstein's 'On the Electrodynamics of Moving Bodies' is based on ether theoretical dogma, as any treatment needs to be in order to be predictive.

Consider the case where the lab frame is moving at velocity v wrt the ether and the dielectric rod in this frame is rotating at constant velocity u. By ES any clock at rest wrt O can be synchronized to O and all such clocks at distance L wrt O have the same synchronization. Any clock at velocity u and distance L wrt O has the same synchronization wrt O. Therefore, if A is synchronized with O it will remain synchronized.

According to [1] the CTD, due to time dilation as clock A moves slowly due to Earth's rotation, can be calculated from [1] using,

$$\frac{1}{\gamma_0} - \frac{1}{\gamma_0} = 0. \tag{C6}$$

since in the frame of the rotating clocks they have no relative velocity wrt each other. They do have relative velocity wrt each other in the ether frame but that leads to (C1) and (C3) instead of (S6). Since no measurements are made from the ether frame but are made from the frame of the atomic clocks we must refer synchronization to this frame, as LT teaches that the two synchronizations aren't the same. LT also guarantees that the time dilation effects of CTD are the same for the signal propagation time on De Witte's cable as they are for the measuring clocks, negating relative effect between the two.

Alternatively, since the CTD of A wrt to O equals, by symmetry the CTD of O wrt A, they must cancel. This is an example of The Clock Paradox and ensures that no dissynchronization will occur between O and A, as opposed to what is taught in [1].

One might also ask, How do we ascribe CTD as the cause of De Witte's effect in the vacuum case when there is no De Witte Effect in the vacuum? Too, in De Witte's Experiment [3] when the North-South signal and the South-North signal are subtracted any biases or dissynchronizations would cancel. Additionally, if De Witte's results could be ascribed to clock transport delay it would still obtain that a measurement of velocity wrt the ether had been made in contradiction to SR canon.

4 Closing comments

Using the sidereal rotation period of Earth,

$$\omega \simeq \frac{2\pi}{86164.1}\ \mathrm{s}^{-1} \simeq 7.3 \cdot 10^{-5}\ \mathrm{s}^{-1} \tag{C4}$$

and,

$$dt = \frac{L}{c} = 5 \cdot 10^{-6}\ \mathrm{s}; \quad u(t) = L\omega \simeq 0.11\ \mathrm{m/s} \tag{C5}$$

from (C2) and [3] the absolute motion velocity is,

$$v = \frac{\left(14 \cdot 10^{-9}\right)\left(9 \cdot 10^{16}\right)\left(\cos 0 - \cos \frac{\pi}{2}\right)}{1500} = 8.4 \cdot 10^{5}\ \mathrm{m/s}.$$

[As an aside, this absolute motion velocity of 840 km/s is larger than those stated in [3] for the De Witte Experiment, larger than Earth's velocity wrt the Cosmic Microwave Background and larger than most author's estimates. Also, since the declinations of De Witte's cable and the absolute motion vector of Earth wrt vacuum are estimated to be as much as about 25° apart we should expect a velocity from 840-930 km/s. Note that this result is stated with some reservation (see below).]

Some have expressed the belief [1, 4] that Fresnel drag may not be acting in certain cases where a refractive material is known to be present. Fresnel drag is a dogmatic phenomenon equivalent to the LT with excellent experimental confirmation. It shouldn't be possible to turn physics on or off like a light switch, it is always present with refractive materials but the effect is not always correctly anticipated formally. In fact according to detailed calculations by the author, De Witte cannot be explained by a predictive ether-based formalism (Michelson-Lorentz formalism) with a final transformation to the lab frame. Such calculations, be they for one-way, two-way, with or without refractive media, always return results which speak of no unusual effects. Thus the Roland De Witte Effect remains a mystery.

Submitted on October 4, 2017

References

1. Spavieri G., et. al. Can the one-way speed of light be used for detection of violations of the relativity principle? *Phys. Lett. A*, 2012, v.376, 795–797.
2. Cahill R. T., Brotherton D. Experimental investigation of the Fresnel drag effect in RF coaxial cables. *Prog. Phys.*, 2011, v.7, issue 1, 43.
3. Cahill R. T. The Roland De Witte 1991 Experiment. *Prog. Phys.*, 2006, v.2, issue 3, 60–65.
4. Cahill R. T. One-way speed of light measurements without clock synchronisation. *Prog. Phys.*, 2012, v.8, issue 3, 43–45.
5. Cavalleri G., Spinelli G. Problems of synchronization in Special Relativity and possible links with stochastic electrodynamics. *Found. Phys.*, 1983, v.13, 1221.

Progress in Physics is an American scientific journal on advanced studies in physics, registered with the Library of Congress (DC, USA): ISSN 1555-5534 (print version) and ISSN 1555-5615 (online version). The journal is peer reviewed and listed in the abstracting and indexing coverage of: Mathematical Reviews of the AMS (USA), DOAJ of Lund University (Sweden), Scientific Commons of the University of St.Gallen (Switzerland), Open-J-Gate (India), Referential Journal of VINITI (Russia), etc. Progress in Physics is an open-access journal published and distributed in accordance with the Budapest Open Initiative: this means that the electronic copies of both full-size version of the journal and the individual papers published therein will always be acessed for reading, download, and copying for any user free of charge. The journal is issued quarterly (four volumes per year).

Electronic version of this journal: http://www.ptep-online.com

Postal address:
Department of Mathematics and Science, University of New Mexico,
705 Gurley Avenue, Gallup, NM 87301, USA